[redacted] Desk,

SEP 16 1998

SANDIA REPORT

SAND98-0049 · UC-721
Unlimited Release
Printed September 1998

SAND--98-0049

Analysis of Hydraulic Tests of the Culebra and Magenta Dolomites and Dewey Lake Redbeds Conducted at the Waste Isolation Pilot Plant Site

Richard L. Beauheim, Gregory J. Ruskauff

Prepared by
Sandia National Laboratories
Albuquerque, New Mexico 87185 and Livermore, California 94550

Sandia is a multiprogram laboratory operated by Sandia Corporation, a Lockheed Martin Company, for the United States Department of Energy under Contract DE-AC04-94AL85000.

Sandia National Laboratories

Issued by Sandia National Laboratories, operated for the United States Department of Energy by Sandia Corporation.

Available to DOE and DOE contractors from
Office of Scientific and Technical Information
P.O. Box 62
Oak Ridge, TN 37831

Prices available from (615) 576-8401, FTS 626-8401

Available to the public from
National Technical Information Service
U.S. Department of Commerce
5285 Port Royal Rd
Springfield, VA 22161

NTIS price codes
Printed copy: A11
Microfiche copy: A01

SAND98-0049
Unlimited Release
Printed September 1998

Analysis of Hydraulic Tests of the Culebra and Magenta Dolomites and Dewey Lake Redbeds Conducted at the Waste Isolation Pilot Plant Site

Richard L. Beauheim
Geohydrology Department 6115
Sandia National Laboratories
P.O. Box 5800
Albuquerque, NM 87185-0735

Gregory J. Ruskauff
Duke Engineering & Services, Inc.
1650 University Boulevard NE, Suite 300
Albuquerque, NM 87102-1732

ABSTRACT

This report completes documentation of hydraulic-test interpretations used as input to the Compliance Certification Application for the Waste Isolation Pilot Plant (WIPP). Interpretations are presented for 21 tests of the Culebra Dolomite Member of the Rustler Formation conducted at 15 well locations near the WIPP site, one test of the Magenta Member, and one test of the Dewey Lake Redbeds. Single-well pumping tests were conducted in the Culebra at H-19b2, WQSP-4, WQSP-5, and WQSP-6. Slug tests were conducted at H-10b, WIPP-27, and WIPP-28. Multiwell pumping tests were conducted on the H-2, H-6, H-7, H-9, H-11, and H-19 hydropads, where well spacings vary between 36 and 141 ft (11 and 43 m). Interpretable responses to pumping tests at H-9, P-14, WQSP-1, and WQSP-2 were monitored at wells 1,295 to 11,125 ft (395 to 3,390 m) away. The transmissivity of the Culebra ranges from approximately 4 x 10^{-2} to 2 x 10^{3} ft^2/d (4 x 10^{-8} to 2 x 10^{-3} m^2/s) at the tested locations. The Culebra behaves hydraulically as a double-porosity medium at nine of the locations, where open fractures are thought to dominate hydraulic responses. The slug-test data from WIPP-27 and WIPP-28 are inadequate for differentiation of single- from double-porosity behavior. At the four locations where the Culebra transmissivity is 1.2 ft^2/d (1.3 x 10^{-6} m^2/s) or lower, the Culebra responds as a single-porosity medium. Culebra storativity was found to range from 4.7 x 10^{-6} to 6.4 x 10^{-3}. The ratio of maximum to minimum Culebra transmissivity was found to be 1.6 or lower at three tested locations, reflecting little to no hydraulic anisotropy although transport anisotropy determined from tracer tests is significant. Hydraulic boundaries or other evidence of heterogeneity in hydraulic properties were indicated by the responses observed during testing at seven of the high-transmissivity, double-porosity locations. The transmissivity of the Magenta at H-19b1 is 0.38 ft^2/d (4.1 x 10^{-7} m^2/s), the highest value yet encountered on the WIPP site. However, as at all other locations where both the Culebra and Magenta have been tested, the transmissivity of the Magenta is much lower than that of the Culebra at H-19. The transmissivity of a saturated fractured zone within the upper Dewey Lake Redbeds at WQSP-6A, 0.44 mile (0.71 km) southwest of the WIPP disposal panels, is estimated to be approximately 360 ft^2/d (3.9 x 10^{-4} m^2/s). This zone of saturation appears to extend south of WQSP-6A, but not to the northeast over the disposal panels.

ACKNOWLEDGMENTS

The authors wish to thank the many field crews responsible for carrying out the tests discussed in this report. We also wish to thank Randy Roberts, Al Lappin, and Levy Kroitoru for their helpful reviews. Bob Jones' assistance with manuscript preparation is especially appreciated.

CONTENTS

Tables

Figures

1. INTRODUCTION

This report presents interpretations of hydraulic tests conducted at 15 well locations in the vicinity of the Waste Isolation Pilot Plant (WIPP) in southeastern New Mexico (Figure 1-1) between 1980 and 1996. The WIPP is a U.S. Department of Energy (DOE) facility to demonstrate safe disposal of transuranic wastes arising from the nation's defense programs. The WIPP repository lies within bedded halite of the Salado Formation, 2,155 ft (655 m) below ground surface. The tests reported herein were, with two exceptions, conducted in the Culebra Dolomite Member of the Rustler Formation, which overlies the Salado Formation (Figure 1-2). The remaining tests were conducted in the Magenta Member of the Rustler and in the overlying formation, the Dewey Lake Redbeds. This report completes the documentation of hydraulic-test interpretations used as input to the WIPP Compliance Certification Application (US DOE, 1996).

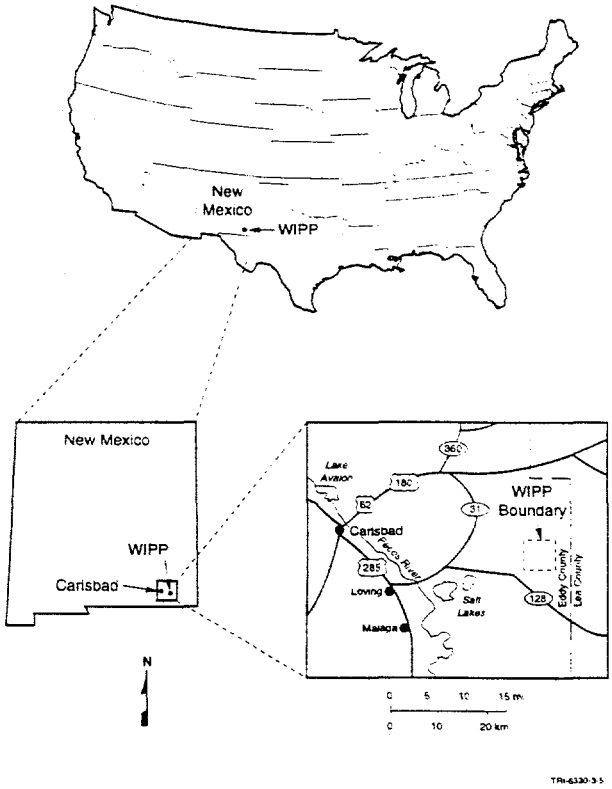

Figure 1-1. Location of the Waste Isolation Pilot Plant.

The Culebra is the most transmissive water-saturated unit overlying the WIPP repository and, as such, represents a possible pathway for transport of radionuclides to the accessible environment if the repository is ever breached through inadvertent human intrusion. As part of the characterization of the WIPP site, extensive testing of the Culebra has been performed at 43 well locations to determine its hydraulic and, in some cases, transport characteristics. The Magenta is typically one or more orders of magnitude less transmissive than the Culebra at any given location and, consequently, has been tested less extensively than the Culebra. Data are now available for the Magenta from 15 well locations. The Dewey Lake Redbeds have not been found to be saturated over most of the WIPP site. The test reported herein was performed in the first well on the WIPP site completed to an unambiguously saturated portion of the Dewey Lake.

The tests of the Culebra discussed in this report include multiwell (interference) pumping tests conducted at hydropads H-2, H-6, H-7, H-9, H-11, and H-19, and at test wells P-14, WQSP-1, and WQSP-2, and from single-well hydraulic tests conducted in wells H-10b, H-19b2, WIPP-27, WIPP-28, WQSP-4, WQSP-5, and WQSP-6 (Figure 1-3). Interpretations of a slug test of the Magenta conducted in well H-19b1 and of a single-well

System	Series	Group	Formation	Member	Approximate Thickness* (m ft)	
Quaternary	Recent		Surficial Deposits		3	10
	Pleistocene		Mescalero Caliche		10	30
			Gatuña			
Triassic		Dockum	Undivided		3	10
Permian	Ochoan		Dewey Lake Redbeds		150	500
			Rustler	Forty-niner	18	60
				Magenta	7	24
				Tamarisk	26	85
				Culebra Dolomite	7	24
				unnamed	37	120
			Salado		600	2000
			Castile		400	1300
	Guadalupian	Delaware Mountain	Bell Canyon		310	1000
			Cherry Canyon		335	1100
			Brushy Canyon		550	1800

* At center of WIPP site.

Figure 1-2. WIPP area stratigraphic column.

pumping test of the Dewey Lake Redbeds conducted in well WQSP-6A are also included. INTERA, Inc. (now Duke Engineering & Services, Inc., Austin, TX) conducted the tests at H-7, H-11, H-19, P-14, and the WQSP wells under the technical direction of Sandia National Laboratories (Albuquerque, NM), Hydro Geo Chem, Inc. (Tucson, AZ) was responsible for the design and performance of the tests at H-2, H-6, and H-9, and the US Geological Survey (USGS) conducted the tests at H-10b, WIPP-27, and WIPP-28.

The analyses presented herein were performed under the Sandia National Laboratories WIPP Quality Assurance Program Description, Revision R (on file in the Sandia WIPP Central Files [SWCF] under WPO#37209), and the following Quality Assurance Procedures (QAPs):

- QAP 6-2 (Preparing, Reviewing, and Approving Technical Information Documents);
- QAP 9-1 (QA Requirements for Conducting Analyses);
- QAP 17-1 (WIPP Quality Assurance Records Source Requirements);
- QAP 19-1 (WIPP Computer Software Requirements); and
- QAP 20-2 (Preparing, Reviewing, and Approving Scientific Notebooks).

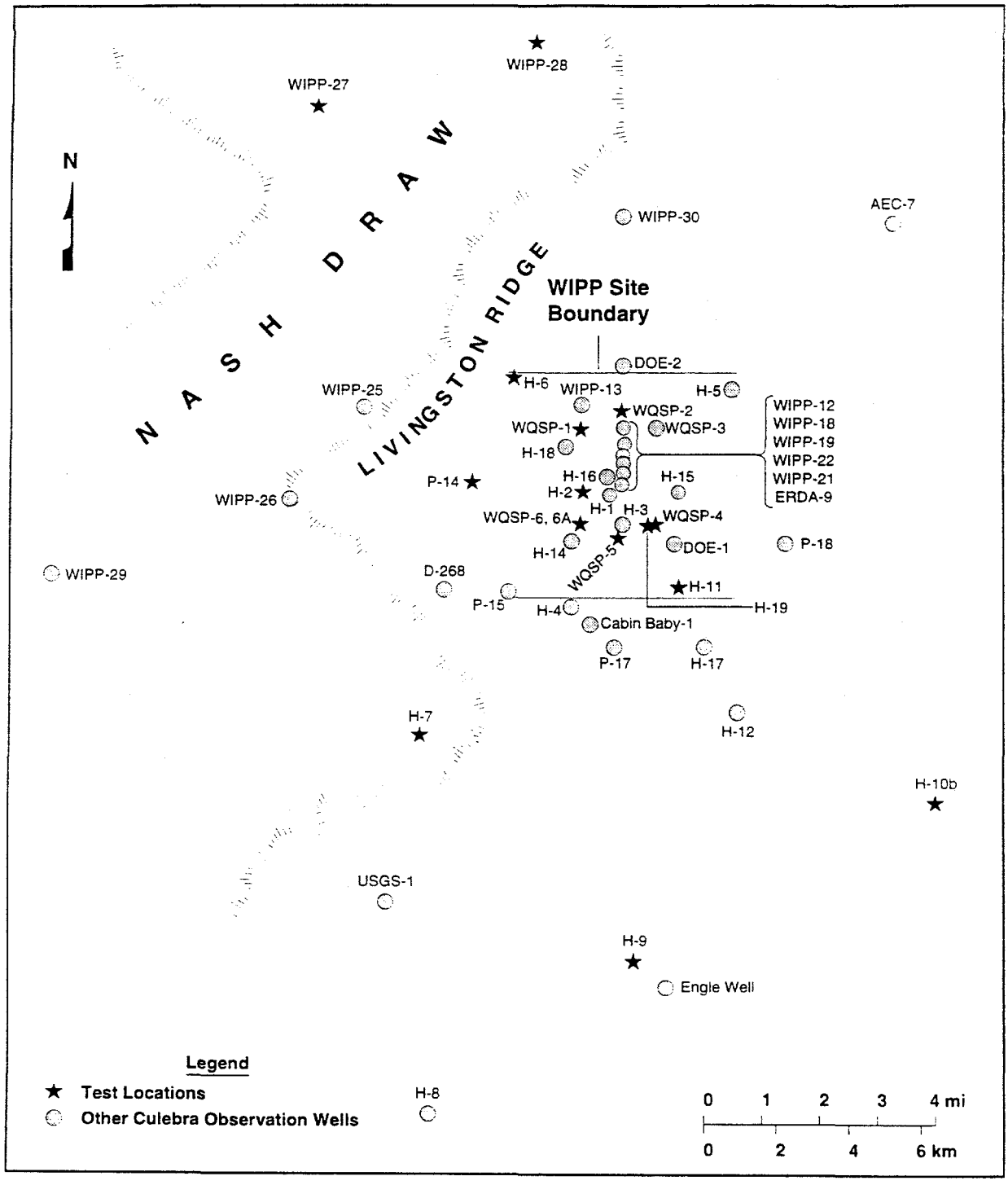

Figure 1-3. Locations of wells and hydropads in the vicinity of the WIPP Site.

This page intentionally left blank

2. HYDROGEOLOGIC SETTING

The WIPP site is located in the northern part of the Delaware Basin in southeastern New Mexico (Figure 1-1). Geologic investigations have concentrated on the upper seven formations typically found in the area, which are, in ascending order, the Bell Canyon Formation, the Castile Formation, the Salado Formation, the Rustler Formation, the Dewey Lake Redbeds, the Dockum Group, and the Gatuña Formation (Figure 1-2). All of these formations are of Permian age, except for the Dockum Group, which is of Triassic age, and the Gatuña, which is a Quaternary deposit.

The Rustler Formation comprises five members, which are, in ascending order, an unnamed lower member, the Culebra Dolomite Member, the Tamarisk Member, the Magenta Member, and the Forty-niner Member. The Culebra is the most transmissive member of the Rustler Formation and, as such, is considered to be the most important pathway for groundwater transport of radionuclides that may escape from the WIPP facility through inadvertent human intrusion to reach the accessible environment. Therefore, the vast majority of hydrologic testing performed at the WIPP site has investigated the hydraulic properties of the Culebra.

The Culebra is a laminated to thinly bedded, locally argillaceous dolomite with abundant open and gypsum-filled fractures and vugs. Holt (1997) divides the Culebra into four units. The uppermost unit, CU-1, is typically ten ft (3.0 m) thick and consists of massively bedded, well-indurated, microcrystalline dolomite. Most fractures in CU-1 are bedding-plane separations, and CU-1 tends to be less fractured than the lower units. CU-2 averages approximately five ft (1.6 m) thick and consists of an intensely fractured packbreccia with locally abundant vugs. CU-3 is typically four ft (1.2 m) thick, is thinly laminated to very thinly bedded, exhibits soft-sediment deformation, and is highly fractured between vugs. CU-4 averages approximately five ft (1.6 m) thick and has an undulatory contact with the underlying claystone of the unnamed lower member. It contains vugs up to three inches (8 cm) in diameter, some of which have collapsed. The lower contact of CU-4 is very undulatory and the lower part of CU-4 tends to be brecciated where undulations of the lower contact are most severe. The transmissivity of the Culebra varies over at least six orders of magnitude in the vicinity of the WIPP site (Mercer, 1983). Beauheim and Holt (1990) relate much of this variability to a combination of percentage of fractures (and other pores) filled by gypsum and depth of burial. The Culebra is overlain by anhydrite (or gypsum) of the Tamarisk Member of the Rustler.

A total of 74 wells have been completed to the Culebra at 48 locations in the vicinity of the WIPP site (Figure 1-3). Among the test sites reported herein, the Culebra ranges in thickness from 22 ft (6.7 m) at wells H-2b and P-14 to 37 ft (11.3 m) at H-7 (Mercer, 1983). The top of the unit is found at elevations from 2,329 ft (710 m) above mean sea level (amsl) at well H-10b to 2,927 ft (892 m) amsl at wells H-7b1 and WIPP-28 (Mercer, 1983; Gonzales, 1989). The depth to the top of the Culebra ranges from 237 ft (72 m) at H-7b1 to 1,360 ft (415 m) at H-10b (Mercer, 1983). The general dip of the unit is eastward. The hydraulic head in the Culebra generally decreases from north to south. Steady-state freshwater heads estimated by Cauffman et al. (1990) range from 2,978 to 3,078 ft (908 to 938 m) amsl at H-9b and WIPP-27, respectively.

The Magenta is a silty, gypsiferous, laminated dolomite ranging in thickness from approxi-

mately 19 to 28 ft (5.8 to 8.5 m) at the WIPP site (Mercer, 1983). The Magenta is underlain and overlain by anhydrite (or gypsum) of the Tamarisk and Forty-niner Members, respectively. At the test site reported herein, well H-19b1, the Magenta lies between 626 and 650 ft (191 and 198 m) below ground surface (BGS), or from 2,767 to 2,791 ft (843 to 851 m) amsl. The Magenta had been previously tested at 15 locations, with transmissivities on the WIPP site ranging from 1×10^{-3} ft^2/d (1×10^{-9} m^2/s) (DOE-2; Beauheim, 1986) to 3×10^{-1} ft^2/d (3×10^{-7} m^2/s) (H-6a; Dennehy, 1982). At all testing locations outside of Nash Draw, the transmissivity of the Magenta has been found to be one or more orders of magnitude lower than that of the Culebra. The hydraulic head in the Magenta generally decreases from east to west. Steady-state freshwater heads across the WIPP site shown in Beauheim and Holt (1990) range from 3,058 to 3,164 ft (932 to 964 m) amsl at H-6a and H-5a, respectively.

The Dewey Lake Redbeds consist of clastic sedimentary rocks ranging in thickness from approximately 200 to 530 ft (61 to 162 m) on the WIPP site (Mercer, 1983). At the WIPP Air-Intake Shaft (AIS), the Dewey Lake is approximately 476 ft (145 m) thick. At the AIS, Holt and Powers (1990) divide the Dewey Lake into a lower 20% consisting mostly of siltstones and mudstones and an upper 80% consisting mostly of thinly laminated to cross-laminated sandstones and siltstones. Abundant fractures are found throughout both units. Within the upper unit, Holt and Powers (1990) noted that a cement change occurs 126 ft (38.4 m) below the top of the unit. Above this depth, they found the rock to be poorly indurated, weakly cemented with carbonate, and locally moist, with fractures either open or filled with carbonate. Below this depth, they found the rock to be well cemented (probably with anhydrite), hard, and dry, with all fractures filled with gypsum.

No water table or zones of saturation in the Dewey Lake have been identified in holes drilled in the central and northern portions of the WIPP site, although "moist" cuttings have been logged in some holes drilled using compressed air as the circulation medium, such as H-1, H-2, and H-3 (Mercer and Orr, 1979). Water was detected in the Dewey Lake in holes drilled near the southern WIPP boundary, such as P-9 (on the H-11 hydropad), P-15, P-17 (Jones, 1978), and, more recently, WQSP-6 and WQSP-6A. Video logging of WQSP-6A has shown the water to be associated with open fractures at the base of the poorly cemented upper portion of the Dewey Lake. Similar unsaturated fractures were the cause of lost circulation while drilling with brine in hole H-3d.

3. TEST AND OBSERVATION WELLS

Many of the wells discussed in this report lie on multiwell "hydropads." Most of the hydropads comprise "a", "b", and "c" wells and are similar in general completion. The "a" wells at each hydropad were originally completed to the Magenta and (except for H-2a at the time of the test reported herein, and for H-7a) have been recompleted through the Culebra. In each of the "a" wells now open to the Culebra, a production-injection packer (PIP) isolates that zone from the Magenta. The "b" wells are completed to the Culebra. At the H-2 and H-7 hydropads, second "b" wells, H-2b2 and H-7b2, are screened to the Culebra. The H-11 hydropad comprises four "b" wells and the H-19 hydropad comprises seven "b" wells, all completed solely to the Culebra. The "c" wells were originally completed across the Rustler-Salado contact. The casing was then perforated across the Culebra interval and a bridge plug was set below the perforations to isolate the Culebra from the open downhole interval. Locations of individual wells and hydropads are shown in Figure 1-3. Additional information about each of the test and observation wells is presented below.

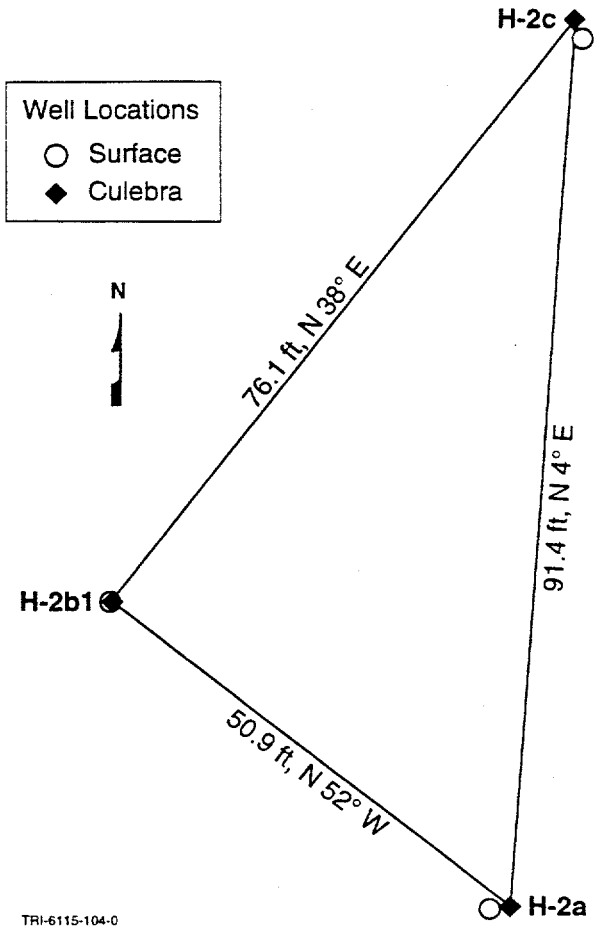

Figure 3-1. Relative locations of wells on the H-2 hydropad.

3.1 H-2 Hydropad

The H-2 hydropad is located in the northwest quarter of Section 29, Township 22 south, Range 31 east, approximately 2/3 mile (1.1 km) southwest of the WIPP construction and salt-handling shaft. Well locations on the H-2 hydropad are shown in Figure 3-1. Data on the original completions of wells H-2a, H-2b (later referred to as H-2b1), and H-2c, summarized below, are provided by Mercer and Orr (1979). Recompletion information about H-2a and basic data about the construction of H-2b2, both of which occurred after the test at the H-2 hydropad reported herein, are found in Hydro Geo Chem, Inc. (1985).

At the time of the testing reported herein, the H-2 hydropad comprised a 3-well array constructed in January and February 1977: H-2a, H-2b, and H-2c. Well H-2a was drilled to 513 ft (156.4 m) BGS in the Forty-niner Member, and cased with 6.625-inch (16.8-cm) casing to 511 ft (155.8 m) BGS. A 4.75-inch (12.1-cm) core hole was drilled through the Magenta to a total depth of 563 ft (171.6 m) BGS. Well H-2b was drilled to 611 ft (186.2 m) BGS in the Tamarisk Member and cased with 6.625-inch (16.8-cm) casing to 609 ft (185.6 m) BGS. A 4.75-inch (12.1-cm) core hole was drilled to a total depth of 661 ft (201.5 m) BGS, encountering

the Culebra from 623 to 645 ft (189.9 to 196.6 m) BGS (Mercer, 1983). In April 1977, the casing was perforated with three 0.5-inch (1.3-cm) jet shots/ft from 510 to 538 ft (155.4 to 164.0 m) BGS, opposite the Magenta. In May 1977, a PIP was installed on 2.375-inch (6.0-cm) tubing at a depth of 578 ft (176.2 m) BGS to isolate the Culebra from the Magenta. Hole H-2c was first drilled to 743 ft (226.5 m) BGS in the unnamed lower member of the Rustler and cased with 6.625-inch (16.8-cm) casing to 742 ft (226.2 m) BGS. A 4.75-inch (12.1-cm) core hole was then drilled to a total depth of 795 ft (242.3 m) BGS, crossing the Rustler-Salado contact at 764 ft (232.9 m) BGS. The casing was perforated with three 0.5-inch (1.3-cm) jet shots/ft from 624 to 652 ft (190.2 to 198.7 m) BGS to provide communication with the Culebra and a bridge plug was set at 731 ft (222.8 m) BGS in March 1977.

For the 1980-81 recirculating tracer test (Hydro Geo Chem, Inc., 1986) and 1981 pumping test, the PIP in H-2b was removed and replaced with a tracer-injection assembly. This assembly included a PIP set from 599.5 to 605.0 ft (182.7 to 184.4 m) BGS on 1.25-inch (3.2-cm) galvanized pipe, with a tailpipe consisting of 2.875-inch (7.3-cm) tubing, slotted from 632.5 to 633.2 ft (192.8 to 193.0 m) BGS, set to 633.7 ft (193.2 m) BGS. In H-2c, an additional bridge plug was set in the well perforations below the Culebra from 646 to 651 ft (196.9 to 198.4 m) BGS, and a PIP was set from 612.5 to 618.0 ft (186.7 to 188.4 m) BGS on 1.25-inch (3.2-cm) galvanized pipe. The pipe continued below the PIP, terminating in a standing valve at 633.0 ft (192.9 m) BGS. This configuration allowed pumping with a pump-jack assembly. These well completions are illustrated in Figure 3-2.

3.2 H-6 Hydropad

The H-6 hydropad is located in the northwest quarter of Section 18, Township 22 south, Range 31 east, near the northwest corner of the WIPP site. The three wells (Figure 3-3) at the H-6 hydropad, H-6a, H-6b, and H-6c, were drilled and completed in June and July 1978. Basic data on the original completions of the H-6 wells are provided by Dennehy (1982). Information on the recompletion of wells H-6a and H-6c is stored in the SWCF under WPO#21712.

Well H-6a was originally completed with 5.5-inch (14.0-cm) casing cemented from ground surface to 475 ft (144.8 m) BGS, and a 4.75-inch (12.1-cm) open hole to a total depth of 525 ft (160.0 m) BGS. The Magenta was encountered between 492 and 511 ft (150.0 and 155.8 m) BGS. In January 1981, the well was re-entered and drilled and cored to a 4.75-inch (12.1-cm) diameter to a new total depth of 640 ft (195.1 m) BGS, penetrating the Culebra between estimated depths of 604 and 627 ft (184.1 and 191.1 m) BGS. A PIP on 2.375-inch (6.0-cm) tubing was installed in the Tamarisk anhydrite to separate Culebra and Magenta waters. Well H-6b is completed with 5.5-inch (14.0-cm) casing cemented from ground surface to 590 ft (179.8 m) BGS, and a 4.75-inch (12.1-cm) open hole to the total depth of 640 ft (195.1 m) BGS. The Culebra was encountered between 604 and 627 ft (184.1 and 191.1 m) BGS. Well H-6c is completed with 5.5-inch (14.0-cm) casing cemented to a depth of 699 ft (213.1 m) BGS, and a 4.75-inch (12.1-cm) open hole to the total depth of 741 ft (225.9 m) BGS. The Rustler-Salado contact was encountered at 721 ft (219.8 m) BGS. In January 1981, the casing in H-6c was perforated using four 15/32-inch (1.2-cm) bullets/ft from 604 to 631 ft (184.1 to 192.3 m) BGS to provide communication with the Culebra, and a bridge plug was set at 641 ft (195.4 m) BGS to

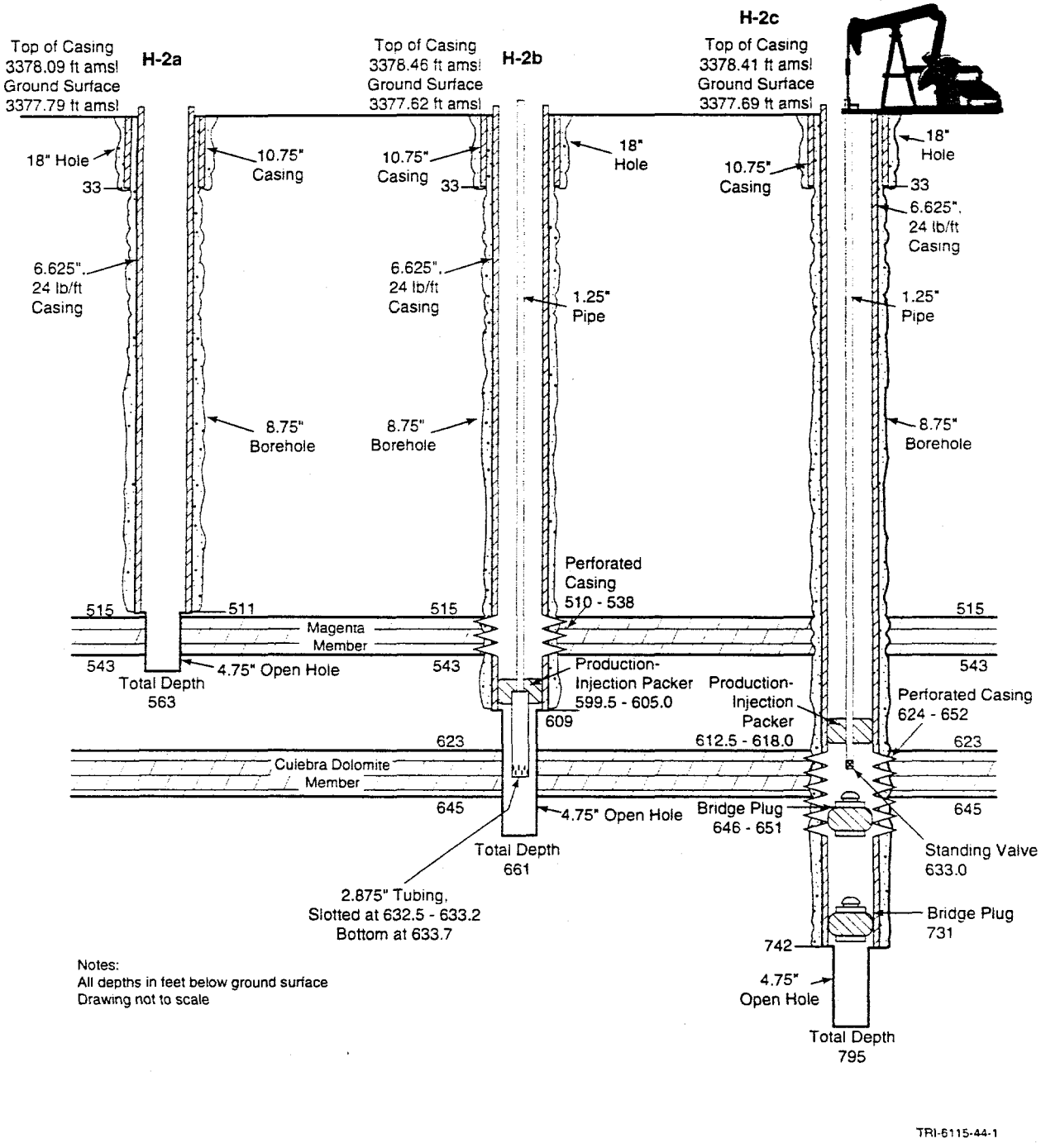

Figure 3-2. Configurations of H-2 wells during the 1981 pumping test.

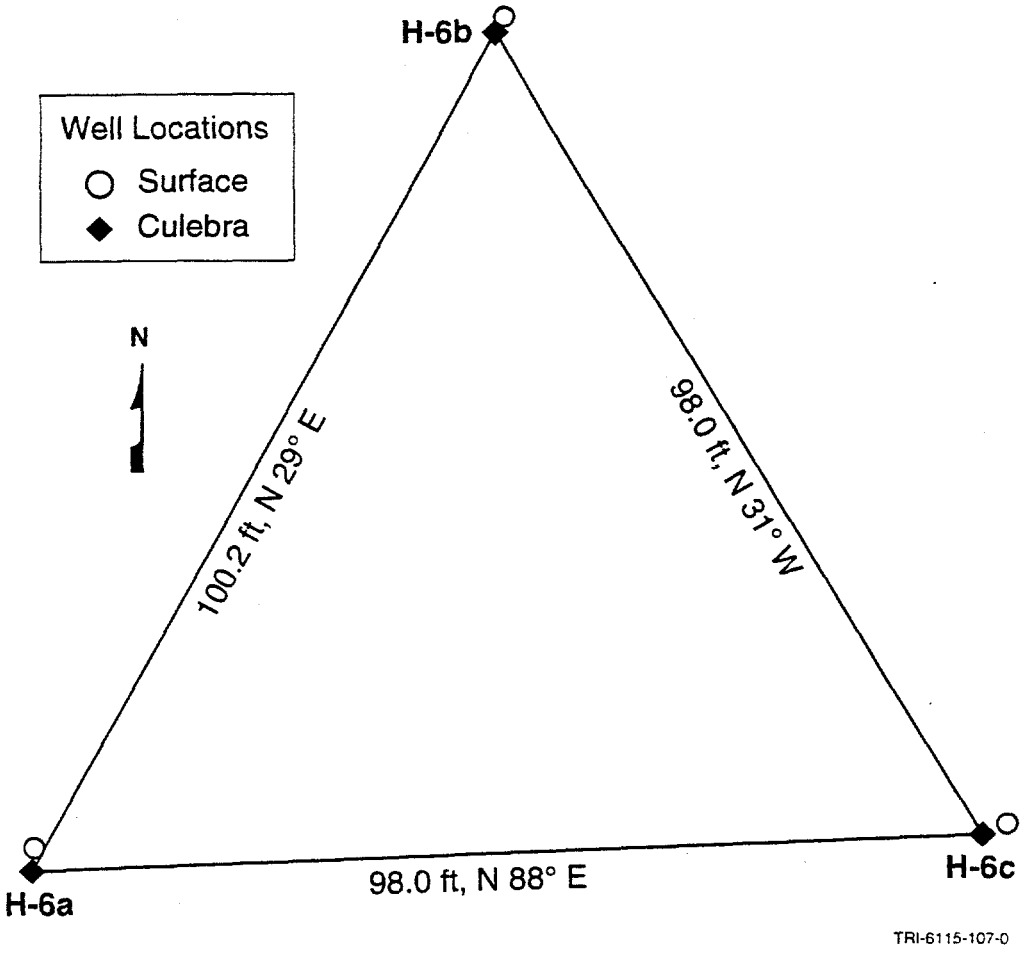

Figure 3-3. Relative locations of wells on the H-6 hydropad.

isolate the Culebra from the underlying open-hole portion of the well. The well configurations at the time of the testing discussed in this report are shown in Figure 3-4.

3.3 H-7 Hydropad

The H-7 hydropad is located near the center of Section 14, Township 23 south, Range 30 east, approximately 2.9 miles (4.7 km) southwest of the WIPP site. The hydropad configuration comprises four wells in a diamond pattern, with approximately 100 ft (30 m) separating each well except for H-7a and H-7b2, which are on opposite ends of the diamond (Figure 3-5). Basic data on the original completions of wells H-7a, H-7b (later referred to as H-7b1), and H-7c, constructed in September 1979, are provided by Drellack and Wells (1982a). Basic data on well H-7b2, constructed in September 1983, are presented by Hydro Geo Chem, Inc. (1985).

Well H-7a is completed with 7-inch (17.8-cm) casing to 109 ft (33.2 m) BGS, below which a 6.125-inch (15.6-cm) open borehole extends to a total depth of 154 ft (46.9 m) BGS, encountering the Magenta between approximately 117 and 140 ft (36 and 43 m) BGS. Well H-7b1 contains 7-inch (17.8-cm) casing installed to 230 ft (70.1 m) BGS. Below that, the well is a 6.125-inch (15.6-cm) open hole to its total depth of 286 ft (87.2 m) BGS, with the Culebra reported to lie between 237 and 274 ft (72.2 and 83.5 m) BGS. Well H-7c was originally drilled and completed with 356 ft (108.5 m) of 7-inch (17.8-cm) casing into the

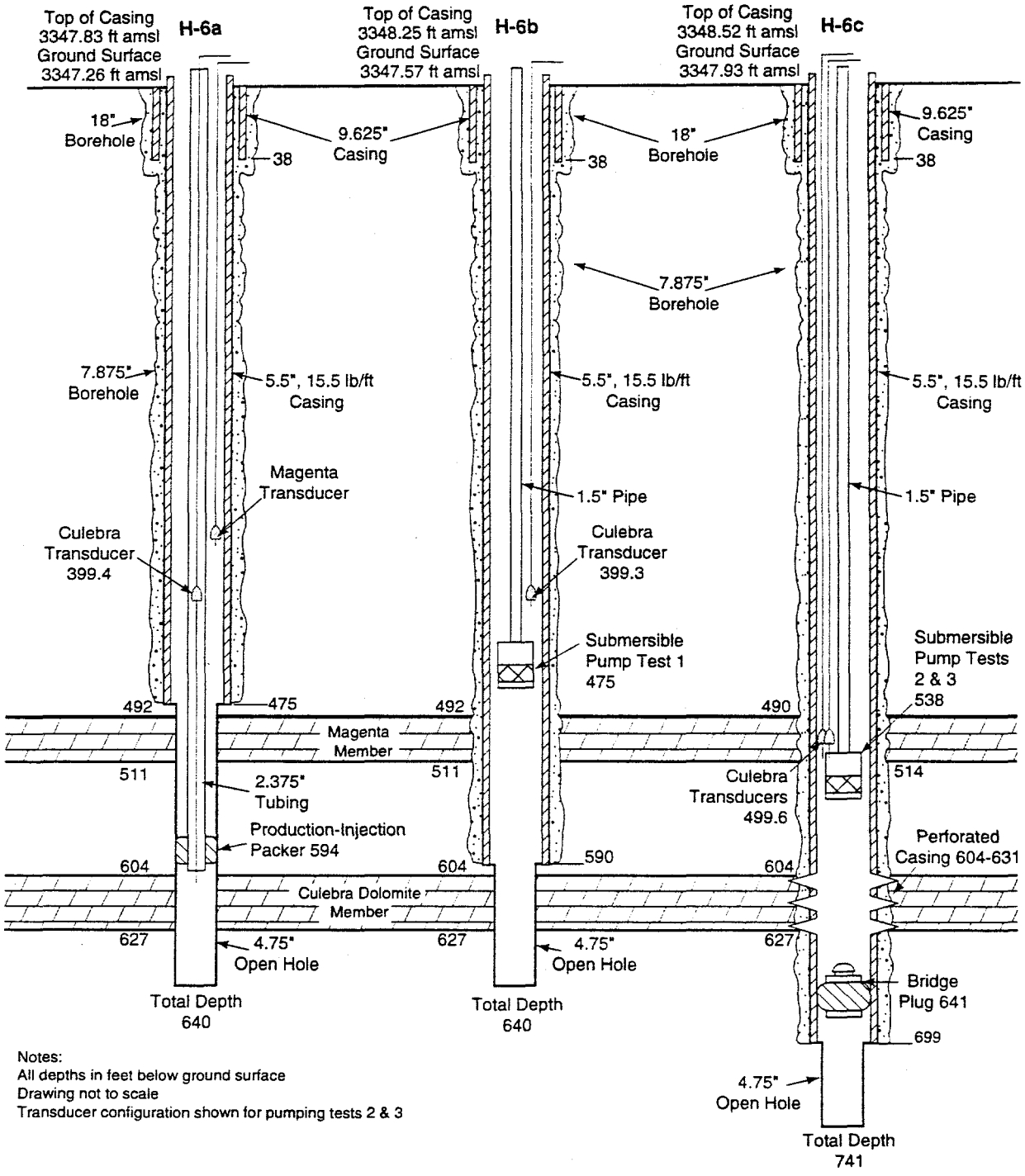

Figure 3-4. Configurations of H-6 wells during the 1981 pumping tests.

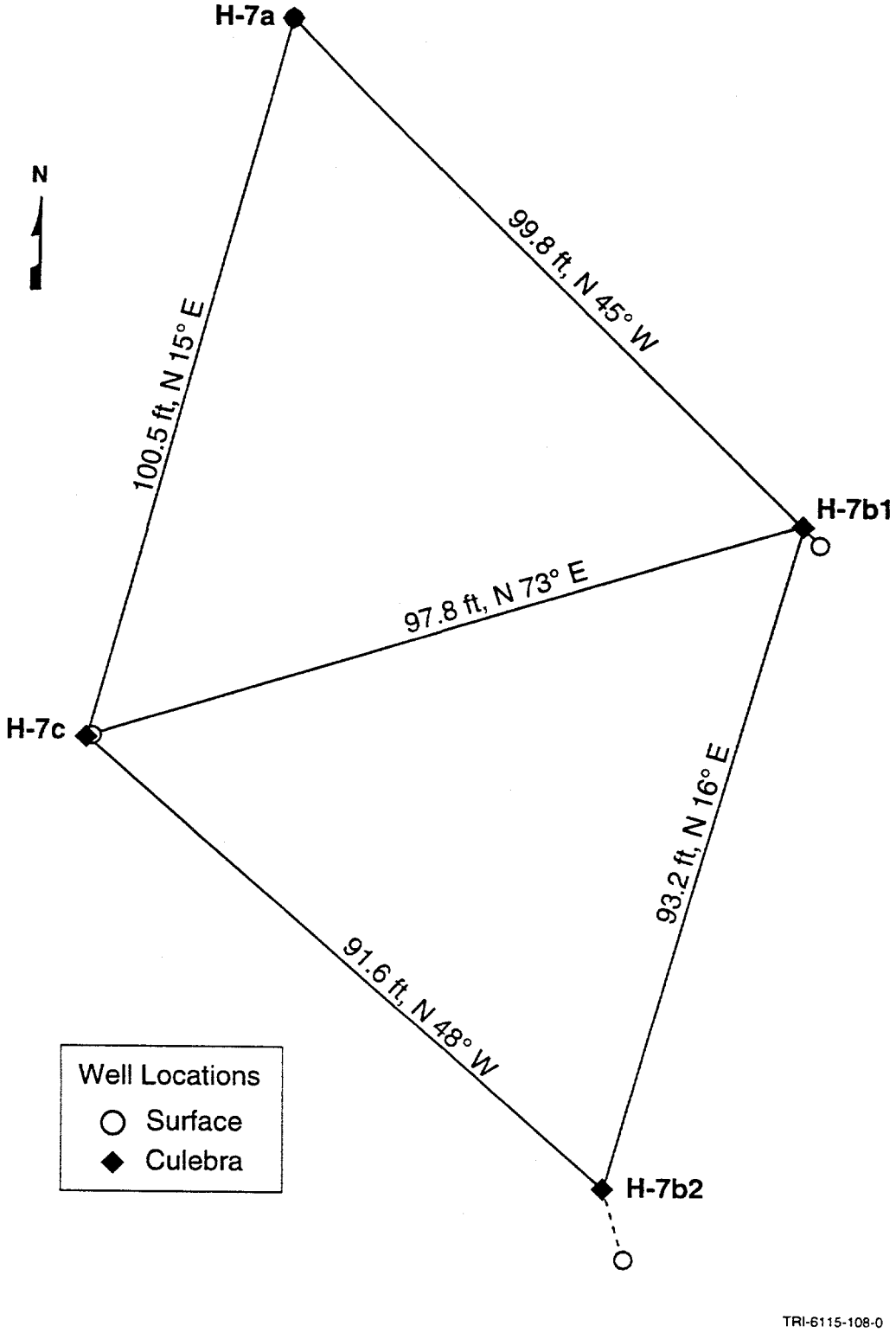

Figure 3-5. Relative locations of wells on the H-7 hydropad.

lower Rustler, with a 6.125-inch (15.6-cm) open borehole to 420 ft (128.0 m) BGS across the Rustler-Salado contact. The casing was subsequently perforated at the Culebra between 238 and 274 ft (72.5 and 83.5 m) BGS, and a bridge plug was installed at about 305 ft (93.0 m) BGS to separate the Culebra and Rustler-Salado contact zone. H-7b2 was drilled to 233 ft (71.0 m) BGS and cased with 7-inch (17.8-cm) casing to 230 ft (70.1 m) BGS. A 6.125-inch (15.6-cm) hole was cored and reamed to a total depth of 295 ft (89.9 m) BGS. The hole was backfilled with pea gravel to 268 ft (81.7 m) BGS, and a 3-inch (7.6-cm) stainless steel well screen was set from approximately 232 to 263 ft (71 to 80 m) BGS. Well construction details are shown on Figure 3-6.

3.4 H-9 Hydropad

Hydropad H-9 is located seven miles (11 km) south of the southern WIPP boundary in the northwest quarter of Section 4, Township 24 south, Range 31 east. The three wells (Figure 3-7) at the H-9 hydropad, H-9a, H-9b, and H-9c, were drilled and completed

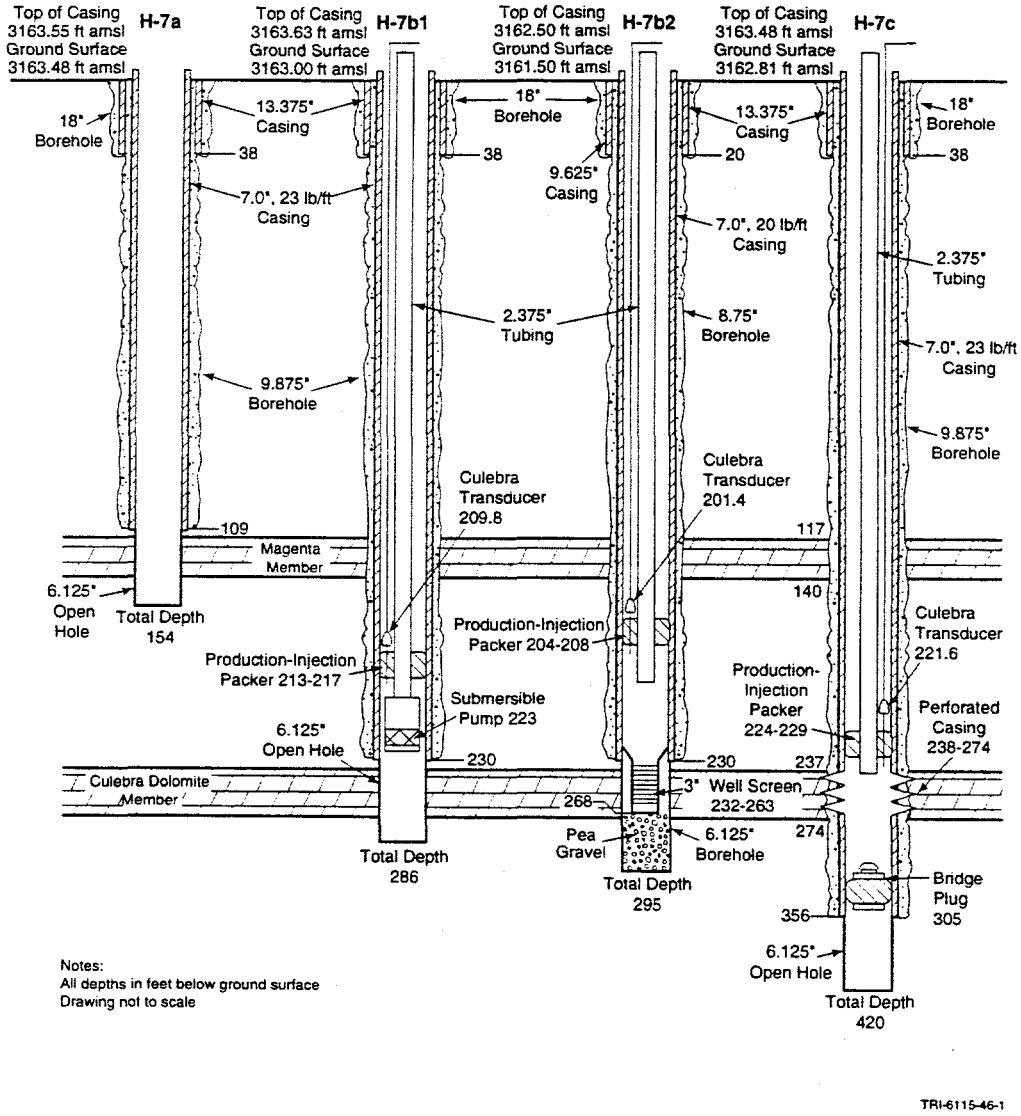

Figure 3-6. Configurations of H-7 wells during the 1986 pumping test.

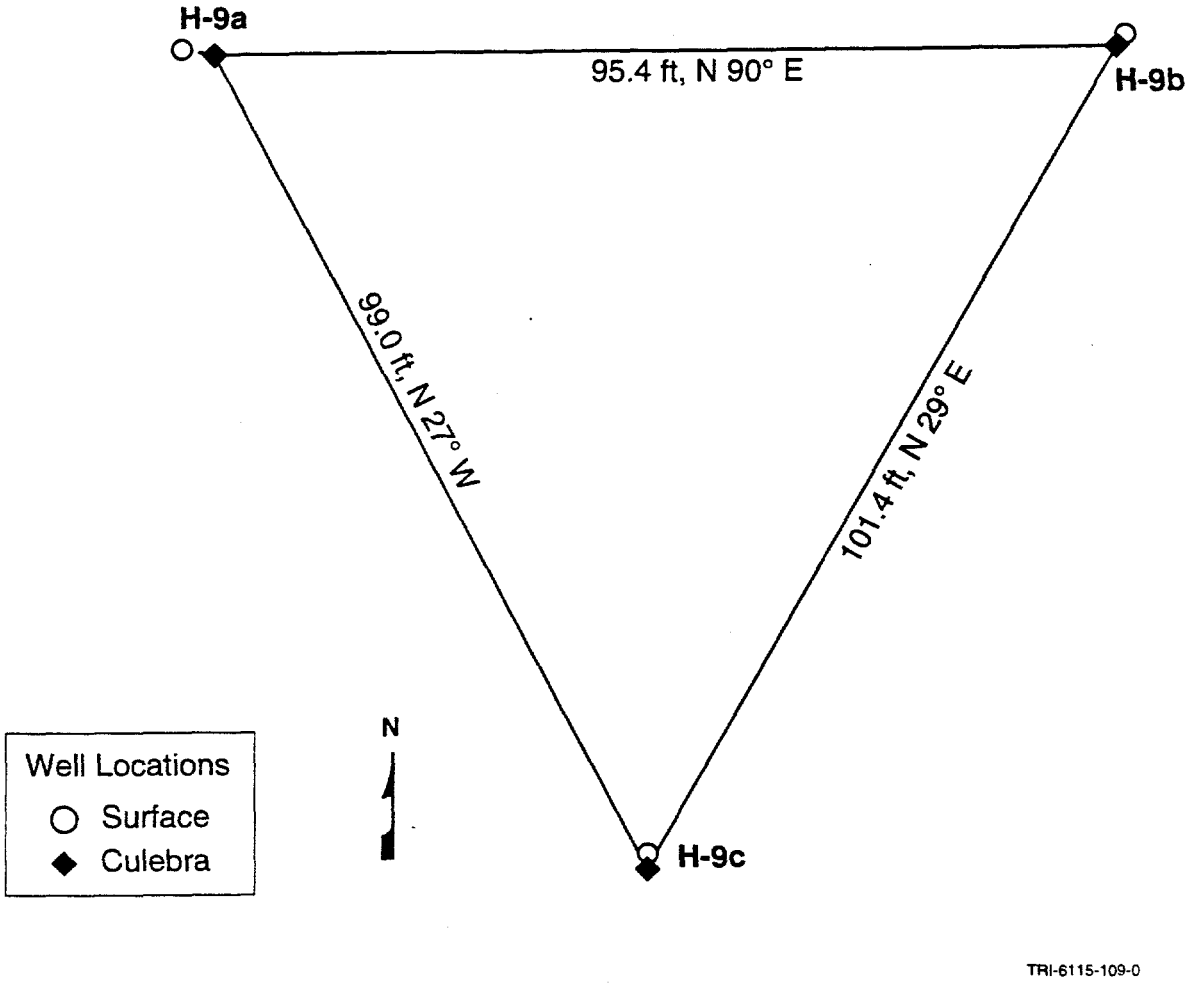

Figure 3-7. Relative locations of wells on the H-9 hydropad.

between July and September 1979. Basic data on the original completions of the H-9 wells are provided by Drellack and Wells (1982b). Information on the recompletion of well H-9a is given in Hydro Geo Chem, Inc. (1985). Information on the recompletion of well H-9c is given in INTERA Technologies, Inc. and Hydro Geo Chem, Inc. (1985).

Well H-9a was originally completed with 7-inch (17.8-cm) casing cemented from ground surface to 510 ft (155.4 m) BGS, and a 6.125-inch (15.6-cm) open hole to a total depth of 559 ft (170.4 m) BGS. The Magenta was encountered between 521 and 548 ft (158.8 and 167.0 m) BGS. In July 1983, the well was re-entered and drilled and cored to a 4.75-inch (12.1-cm) diameter to a new total depth of 692 ft (210.9 m) BGS, penetrating the Culebra between estimated depths of 647 and 677 ft (197.2 and 206.3 m) BGS. A PIP on 2.375-inch (6.0-cm) tubing was installed in the Tamarisk anhydrite at 633 ft (192.9 m) BGS to separate Culebra and Magenta waters. Well H-9b is completed with 7-inch (17.8-cm) casing cemented from ground surface to 638 ft (194.5 m) BGS, and a 6.125-inch (15.6-cm) open hole to the total depth of 708 ft (215.8 m) BGS. The Culebra was encountered between 642 and 671 ft (195.7 and 204.5 m) BGS. Well H-9c is completed with 7-inch (17.8-cm) casing cemented to a depth

of 783 ft (238.7 m) BGS, and a 6.125-inch (15.6-cm) open hole to the total depth of 816 ft (248.7 m) BGS. The Rustler-Salado contact was encountered at 791 ft (241.1 m) BGS. The casing in H-9c was perforated across the Culebra (647 to 677 ft [197.2 to 206.3 m] BGS) to provide communication with the Culebra, and a bridge plug at 712 ft (217.0 m) BGS isolates the Culebra from the underlying open-hole portion of the well. The H-9 well configurations at the time of the 1983 pumping tests are shown in Figure 3-8.

During the third H-9 pumping test, water-level responses were monitored in a privately owned stock well known as the Engle well, located 4,115 ft (1,255 m) southeast of H-9c (Figure 1-3). The Engle well has a total depth of approximately 683 ft (208 m), and is cased with 7-inch (17.8-cm) casing from approximately 648 ft (198 m) BGS to the surface (Beauheim, 1987c). The open hole through the Culebra, which lies between 659 and 681 ft (200.9 and 207.6 m) BGS, appears to have been drilled to a 7-inch (17.8-cm) diameter, although a caliper log indicates that it has washed out or caved to an average diameter of approximately 7.4 inches (18.8 cm). The configuration of the Engle well during the third H-9 pumping test is shown in Figure 3-9.

3.5 Well H-10b

Well H-10b was constructed on the H-10 hydropad, located approximately 5.3 miles (8.6 km) southeast of the southeastern corner of the WIPP boundary, in the southeast quarter of Section 4, Township 23 south, Range 32 east. The hydropad comprises three wells drilled in August and October 1979. Basic data on H-10b are provided by Wells and Drellack (1983). Well H-10b was drilled and reamed to 1,346 ft (410.3 m) BGS, after which 7-inch (17.8-cm) casing was cemented from ground surface to that depth. A 6.125-inch (15.6-cm) hole was then cored and reamed to 1,398 ft (426.1 m) BGS, encountering the Culebra between 1,357 and 1,386 ft (413.6 and 422.5 m) BGS. For the slug testing in H-10b, a 5.625-inch (14.3-cm) PIP was set on 2.375-inch (6.0-cm) tubing at 1,276.9 ft (389.2 m) BGS (Richey, 1986). The configuration of H-10b at the time of testing is illustrated in Figure 3-10.

3.6 H-11 Hydropad

The H-11 hydropad is located in the southeastern portion of the WIPP site in the southeast quarter of Section 33, Township 22 south, Range 31 east. Three of the four wells at the H-11 hydropad (Figure 3-11), H-11b1, H-11b2, and H-11b3, were drilled and completed between August 1983 and January 1984. The fourth well, H-11b4, was drilled and completed in February and March 1988. Basic data on the H-11 wells, summarized below, are provided by Mercer (1990).

The first three H-11 wells were completed in a similar fashion. A 4.75-inch (12.1-cm) hole was drilled from ground surface to the desired total depth in the upper portion of the unnamed lower member of the Rustler. The hole was then reamed to a diameter of 7.875 inches (20.0 cm) down to the casing point, which was intended to be in the lower Tamarisk, and 5.5-inch (14.0-cm) casing was set and cemented in the hole. The portion of the hole below the casing was then cleaned by running a 4.75-inch (12.1-cm) bit to the bottom and circulating water to the surface. Review of caliper and video logs performed since Mercer's (1990) report indicates that all three holes were mistakenly reamed into the Culebra, that the casing in H-11b1 also extends into the Culebra, and that some of the reported depths to the top and bottom of Culebra are in error. To counteract sloughing of the unnamed lower member, H-11b1, H-11b2, and H-11b3 were re-entered in December 1995 and cleaned to total depth

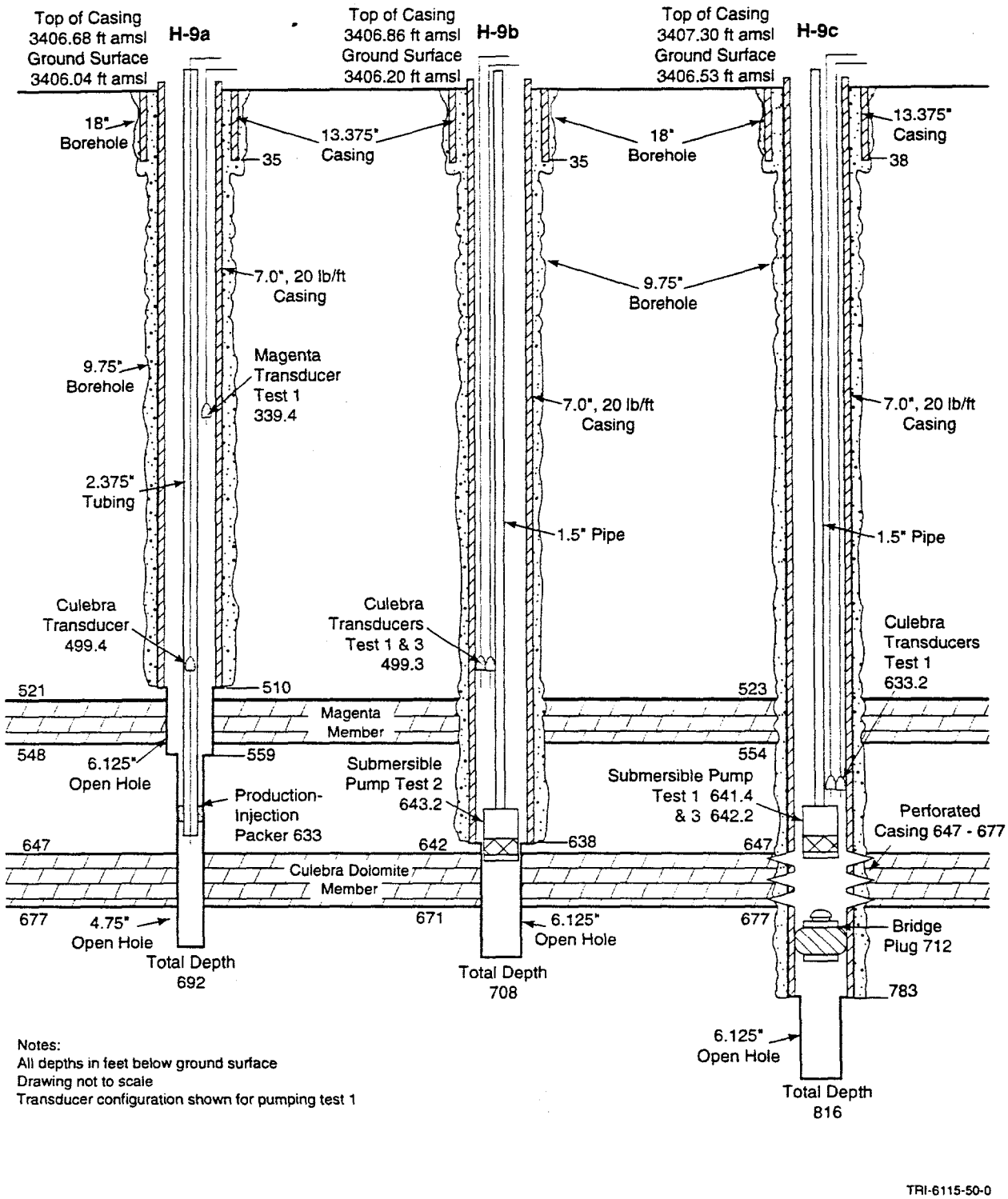

Figure 3-8. Configurations of H-9 wells during the 1983 pumping tests.

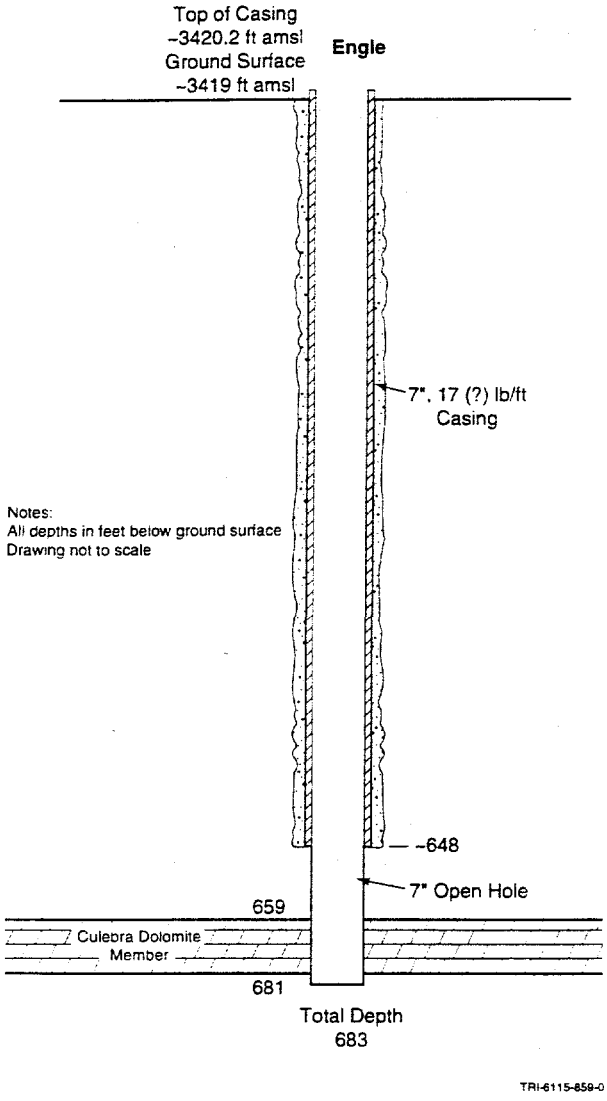

Figure 3-9. Configuration of the Engle well during H-9 pumping test #3.

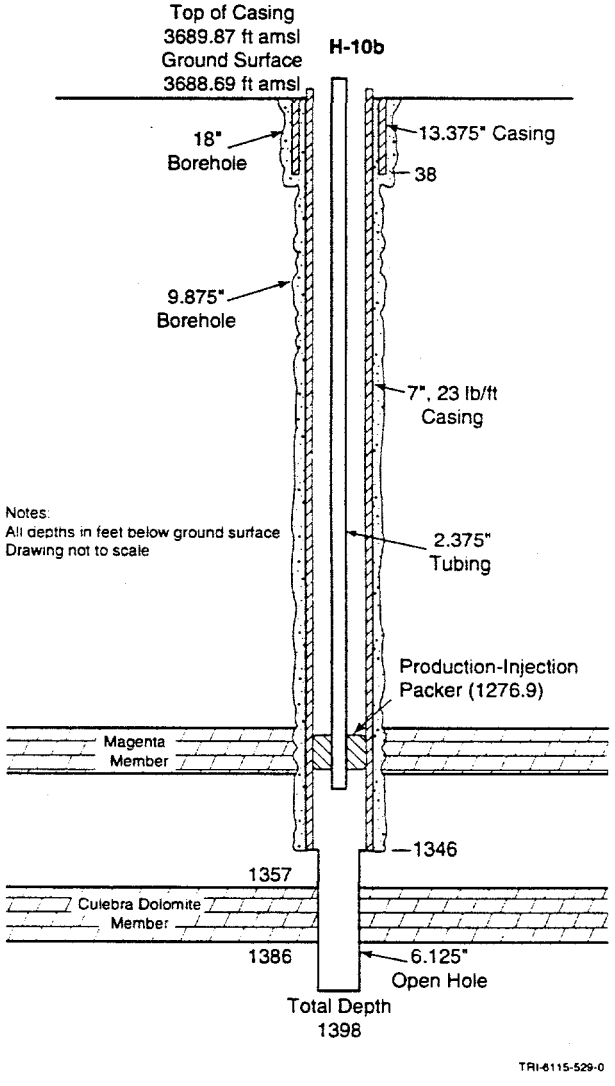

Figure 3-10. Configuration of H-10b during the 1980 slug tests.

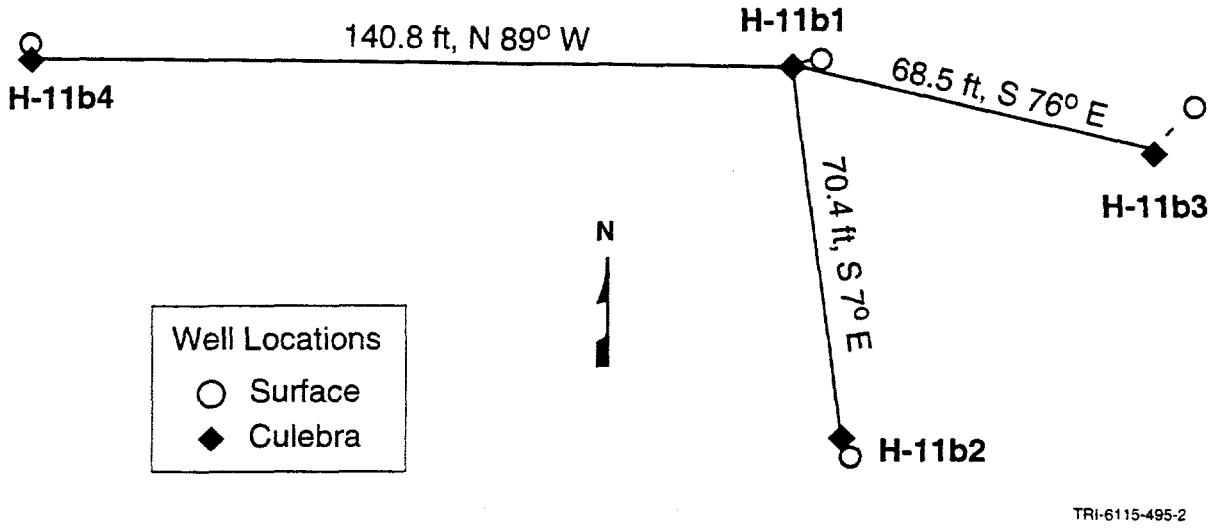

Figure 3-11. Relative locations of wells on the H-11 hydropad.

using a 4.625-inch (11.7-cm) bit. Twenty-ft (6.1-m) lengths of 4.5-inch (11.4-cm) outside diameter (O.D.) PVC pipe were then set at the bottom of each well to prevent further sloughing.

Well H-11b4 was constructed differently. A 7.875-inch (20.0-cm) hole was drilled and reamed to approximately 715 ft (218 m) BGS in the lower Tamarisk, after which 5.5-inch (14.0-cm) casing was set and cemented. The hole was then deepened to 765 ft (233.2 m) BGS by coring and reaming to a diameter of 4.75 inches (12.1 cm) into the upper portion of the unnamed lower member of the Rustler. Recent video logs show that the Culebra was encountered between 723 and 748 ft (220.4 and 228.0 m) BGS, making it two ft (0.6 m) thicker than reported by Mercer (1990). Figure 3-12 shows the H-11 well configurations based on the latest data.

3.7 H-19 Hydropad

The H-19 hydropad is located in the southeastern portion of the WIPP site in the southwest quarter of Section 28, Township 22 south, Range 31 east. The wells at the H-19 hydropad were all drilled and completed between February and August 1995. The locations of the wells on the hydropad are shown in Figure 3-13. Basic data on the H-19 wells, summarized below, are provided by Mercer et al. (1998).

The first well to be drilled on the H-19 hydropad was H-19b1 in February and March 1995. H-19b1 was cored through the Magenta to a depth of 651.6 ft (198.6 m) BGS at a diameter of 4.875 inches (12.4 cm). After the testing discussed in this report was completed, the hole was deepened to 732.6 ft (223.3 m) BGS at the same diameter. While reaming the hole to a diameter of 12.25 inches (31.1 cm), the drilling string separated in the hole. The bit and drilling collars could not be recovered and the hole was subsequently abandoned. The configuration of H-19b1 at the time the Magenta was tested is shown in Figure 3-14.

H-19b0 was drilled in March and April 1995 as the replacement well for H-19b1. The well is cased to a depth of 731.9 ft (223.1 m) BGS in the lower Tamarisk with 9.12-inch (23.2-cm) O.D. (8.42-inch [21.4-cm] I.D.) fiberglass

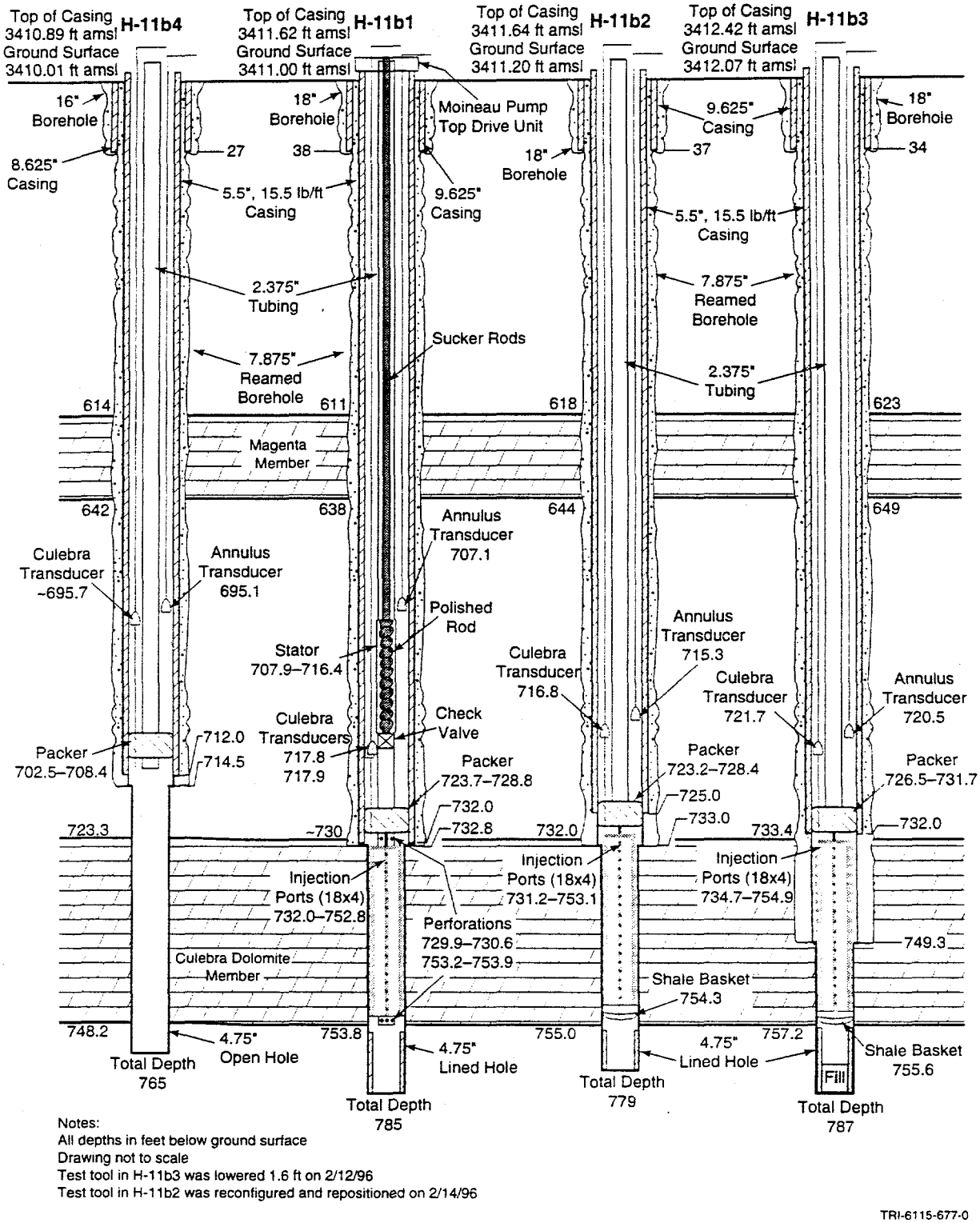

Figure 3-12. Configurations of H-11 wells at the start of the 1996 tracer/pumping test.

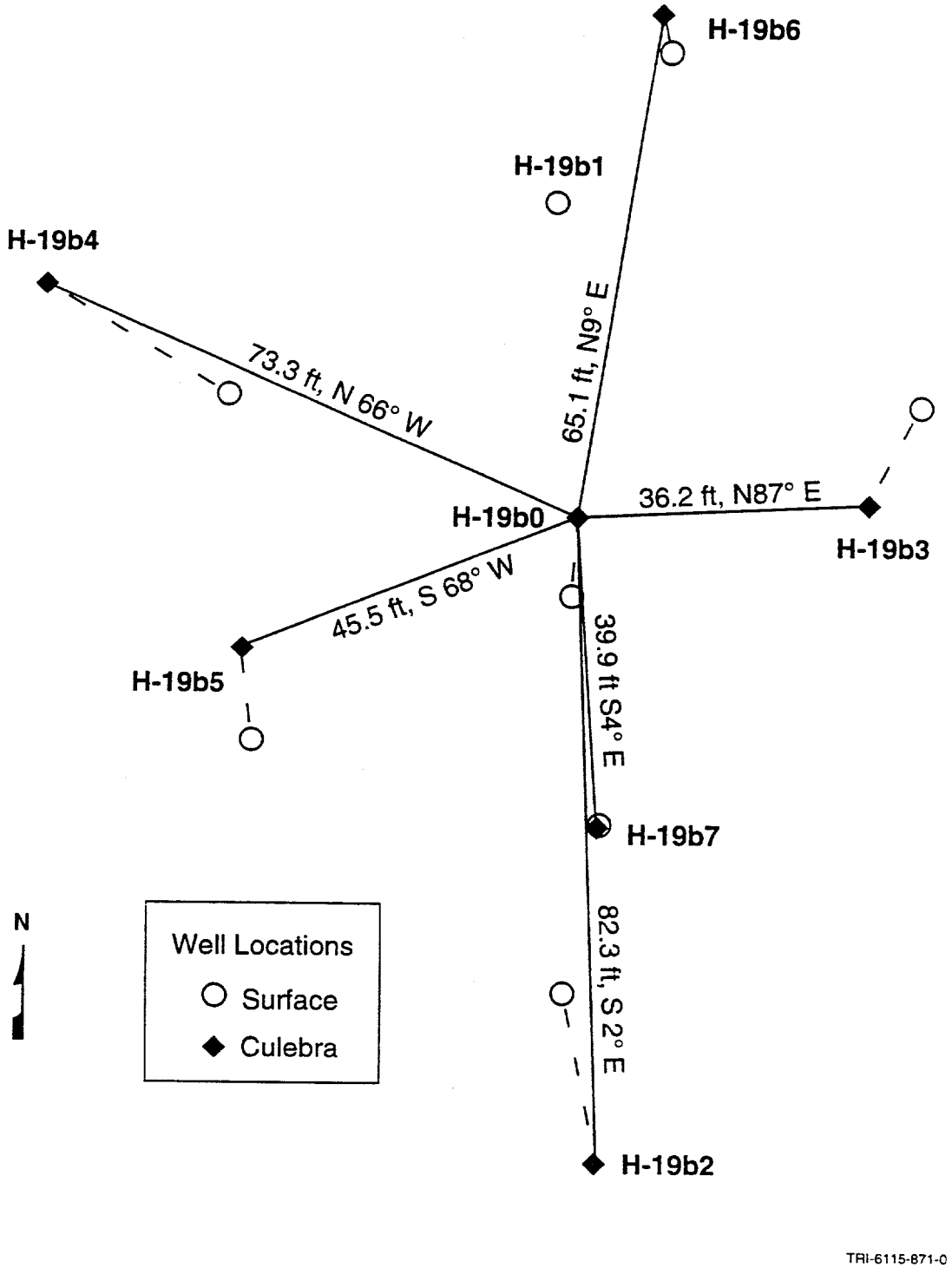

Figure 3-13. Relative locations of wells on the H-19 hydropad.

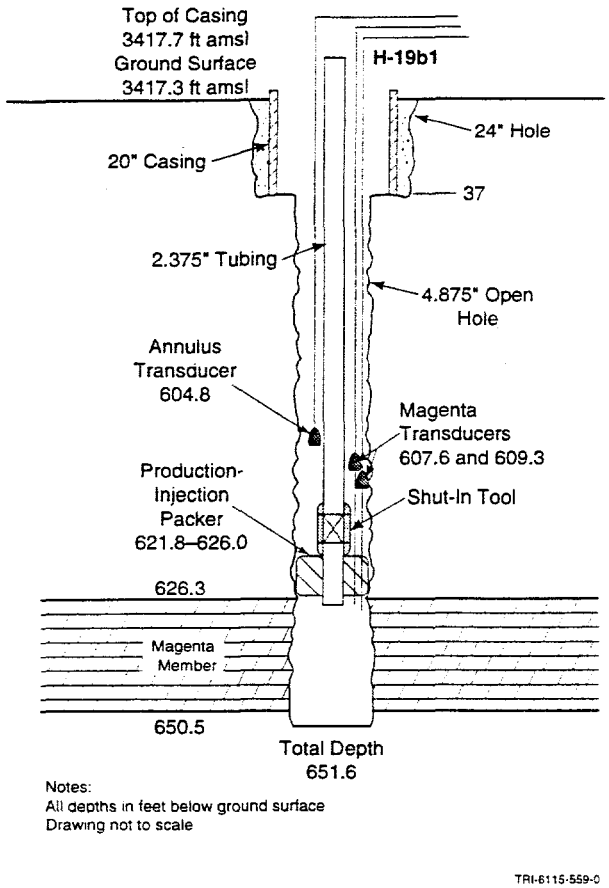

Figure 3-14. Configuration of H-19b1 during drillstem and slug tests of the Magenta.

casing. After casing, an approximately 8-inch (20.3-cm) diameter core hole was drilled to a total depth of 778.7 ft (237.3 m) BGS. Wells H-19b2 through H-19b7 were drilled between April and August 1995. Those six wells are cased with 7-inch (17.8-cm) O.D. (6.38-inch [16.2-cm] I.D.) fiberglass casing to the lower Tamarisk and were cored and reamed to diameters of approximately 5.9 inches (15.0 cm) to depths approximately 20 ft (6 m) below the Culebra. To stop sloughing of clay from the unnamed lower member into the holes, a 20-ft (6.1-m) length of 5.5-inch (14.0-cm) O.D. PVC pipe was set in the bottom of each well.

The H-19b2 well-development pumping test was performed before the PVC pipe was installed in the well. The configuration of H-19b2 during that test is shown in Figure 3-15. The configurations of H-19b0, H-19b3, H-19b5, and H-19b7 during the H-19 tracer/pumping test are shown in Figure 3-16. The configurations of H-19b2, H-19b4, and H-19b6 during that test are shown in Figure 3-17.

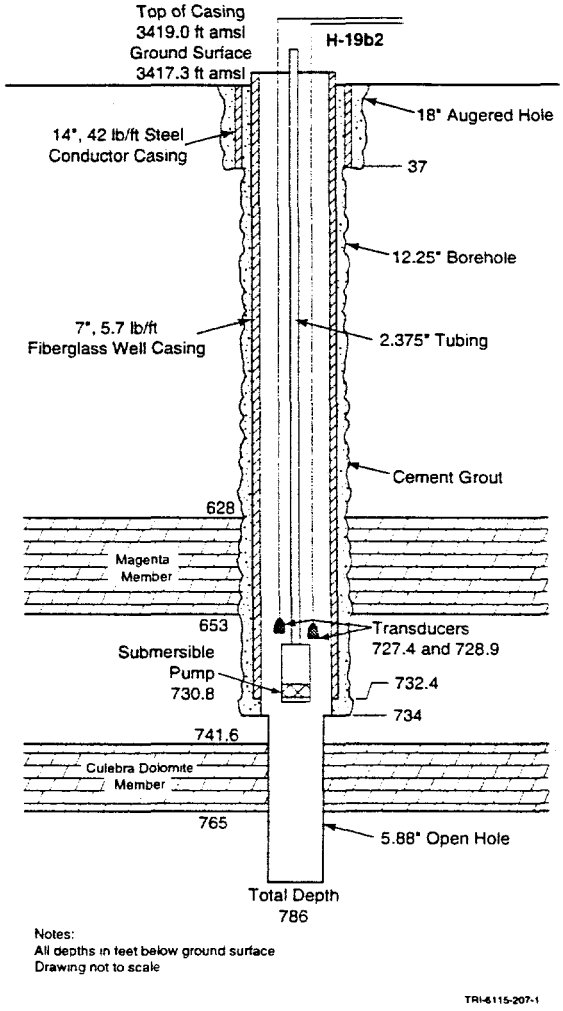

Figure 3-15. Configuration of H-19b2 during the well-development pumping test.

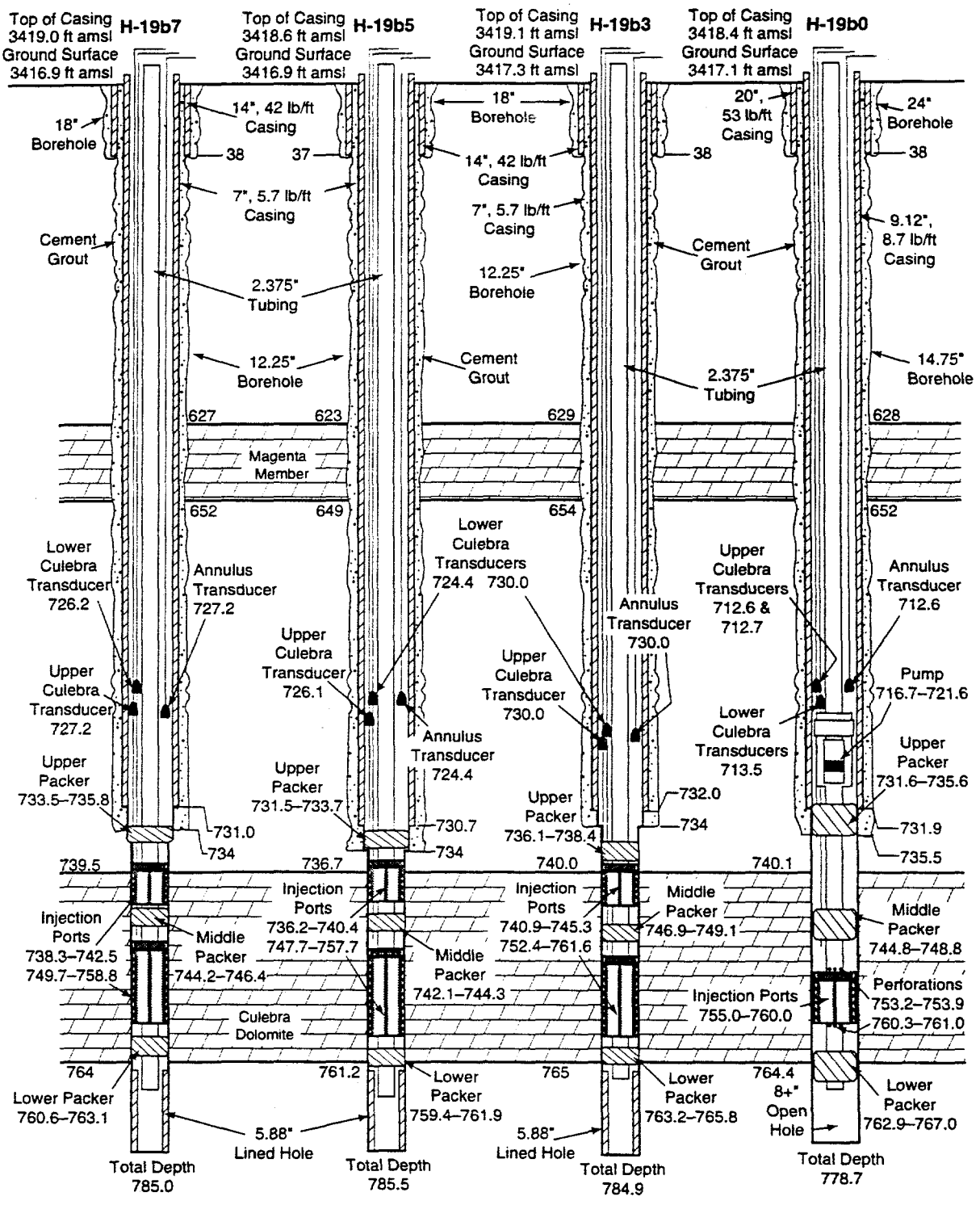

Figure 3-16. Configurations of H-19b0, H-19b3, H-19b5, and H-19b7 during the 1995-96 tracer/pumping test.

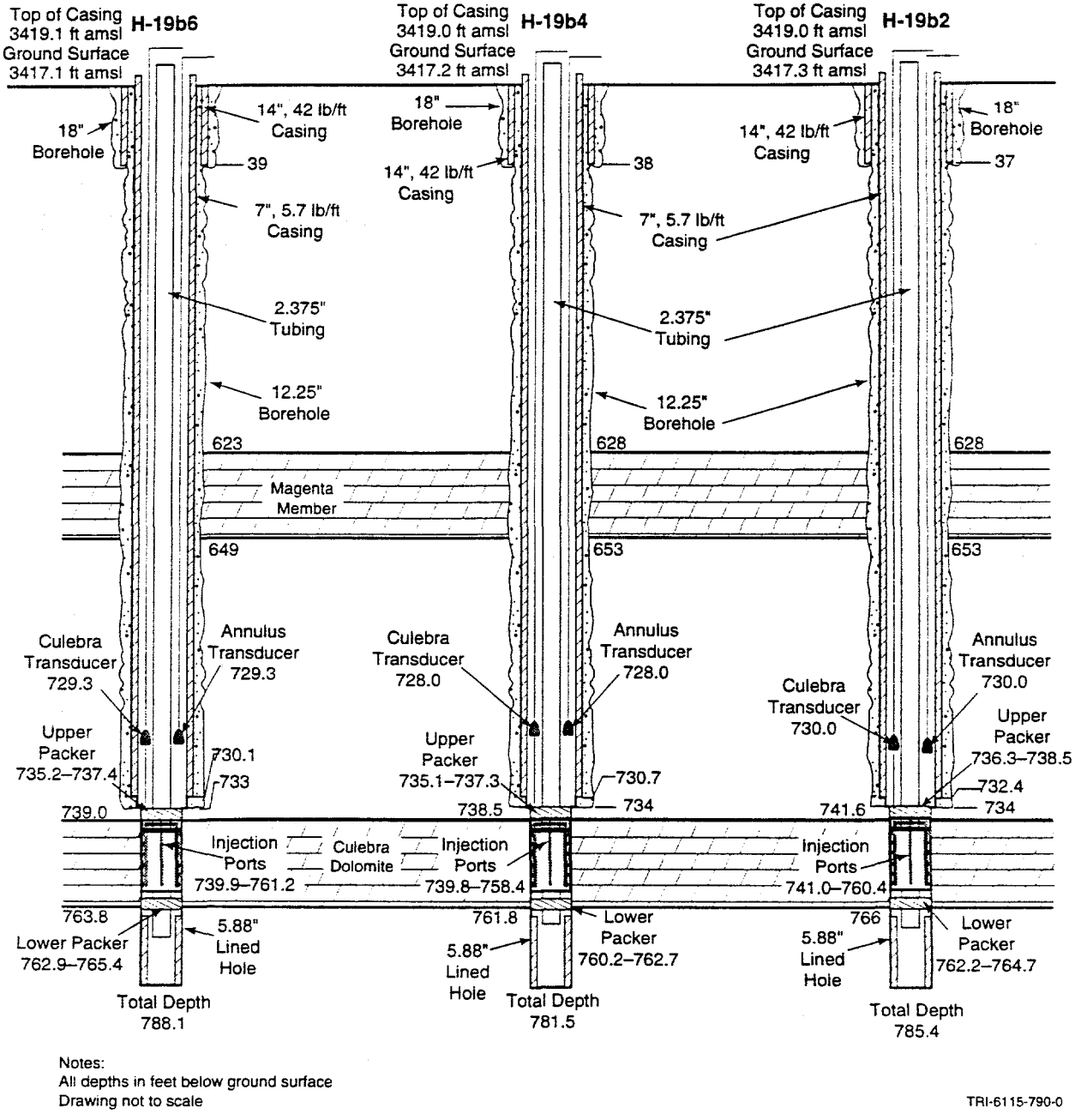

Figure 3-17. Configurations of H-19b2, H-19b4, and H-19b6 during the 1995-96 tracer/ pumping test.

3.8 Well P-14

Well P-14 is located in the southwest quarter of Section 24, Township 22 south, Range 30 east, approximately 0.9 mile (1.4 km) west of the WIPP site boundary. The well was drilled in September and October 1976 as part of a 21-well exploratory drilling and sampling program conducted by the Department of Energy to evaluate the potash mineral resources of the WIPP site (Jones, 1978). Basic data on the construction and completion of well P-14, summarized below, are presented in Mercer and Orr (1979).

After setting surface casing, a 7.875-inch (20.0-cm) borehole was rotary drilled through the Rustler Formation into the upper Salado to a depth of 784 ft (239.0 m) BGS. The borehole was cased with 4.5-inch (11.4-cm) casing cemented to a depth of 775 ft (236.2 m) BGS. A 4-inch (10.2-cm) borehole was then drilled and cored to a total depth of 1,545 ft (470.9 m) BGS and plugged back to 759 ft (231.3 m) BGS with cement. In January 1977, P-14 was perforated with three 0.5-inch (1.3-cm) jet shots/ft across the Rustler-Salado contact from 676 to 700 ft (206.0 to 213.4 m) BGS. A PIP was installed between the Rustler-Salado contact and the Culebra. The casing was perforated with three 0.5-inch (1.3-cm) jet shots/ft from 573 to 601 ft (174.7 to 183.2 m) BGS in March 1977, encompassing the Culebra which lies from 573 to 595 ft (174.7 to 181.4 m) BGS.

Subsequent bailing and pumping tests of the well produced inconclusive results. In February 1989, the casing was reperforated using four 15/32-inch (1.2-cm) bullets/ft from 573 to 601 ft (174.7 to 183.2 m) BGS, after which the well was acidized to improve communication with the Culebra (Stensrud et al., 1990). Shortly thereafter, a pumping test was conducted with wells D-268, DOE-2, H-2b2, H-6b, H-18, WIPP-13, WIPP-25, and WIPP-26 being used for water-level monitoring. Figure 3-18 shows the locations of these wells relative to P-14. Figure 3-19 shows the completion of well P-14 and Figures 3-4, 3-20, and 3-21 show the completions of H-6b, D-268, and WIPP-25, respectively, the monitoring wells that responded to the pumping at P-14. Well-completion information for D-268 and WIPP-25 is presented in Beauheim et al. (1991) and Sandia National Laboratories and U.S. Geological Survey (1979a), respectively.

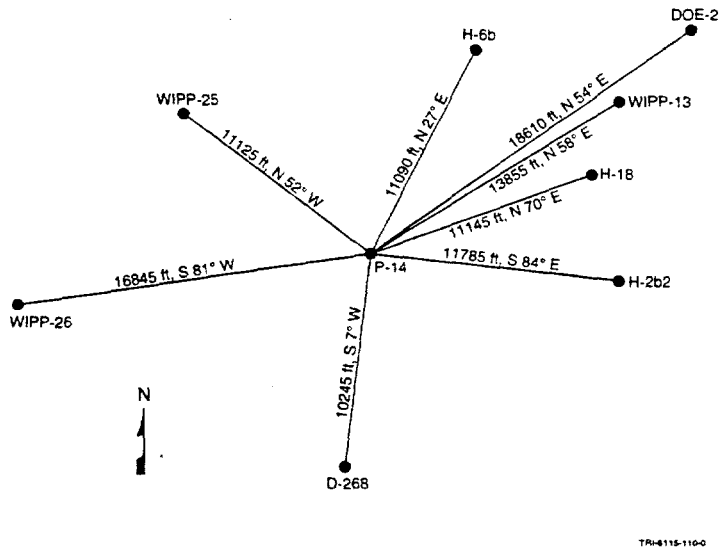

Figure 3-18. Relative locations of wells monitored during the P-14 pumping test.

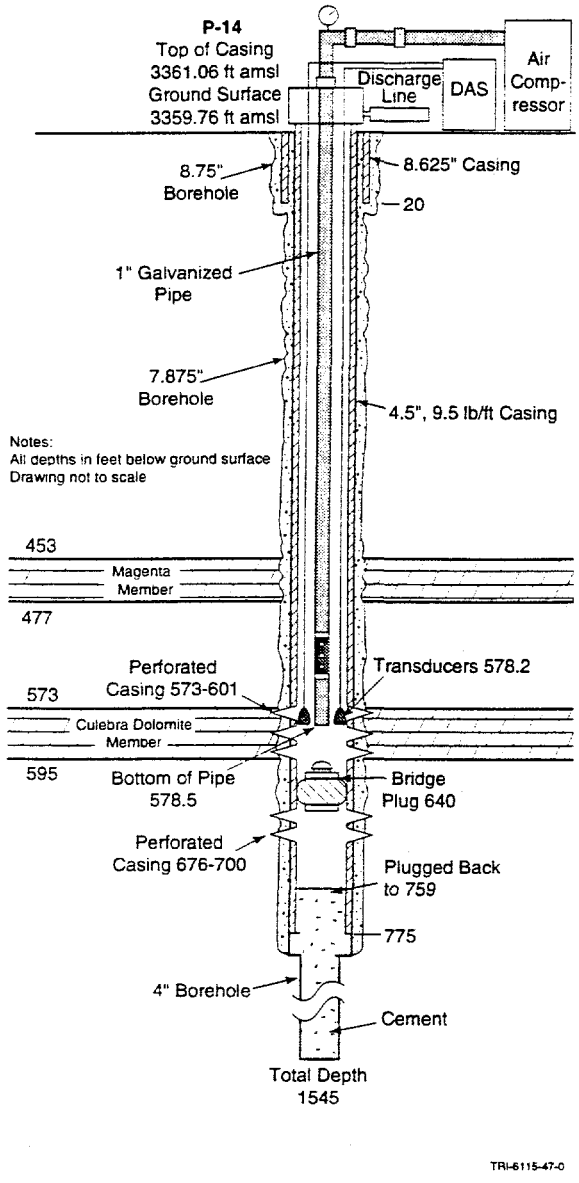

Figure 3-19. Configuration of P-14 during the air-lift pumping test.

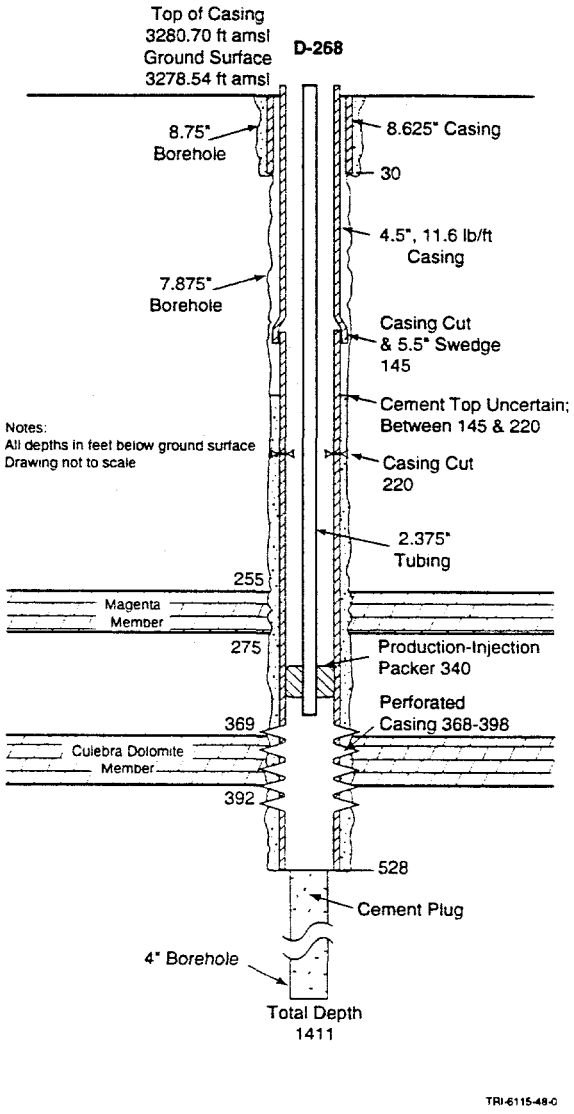

Figure 3-20. Configuration of D-268 during the P-14 pumping test.

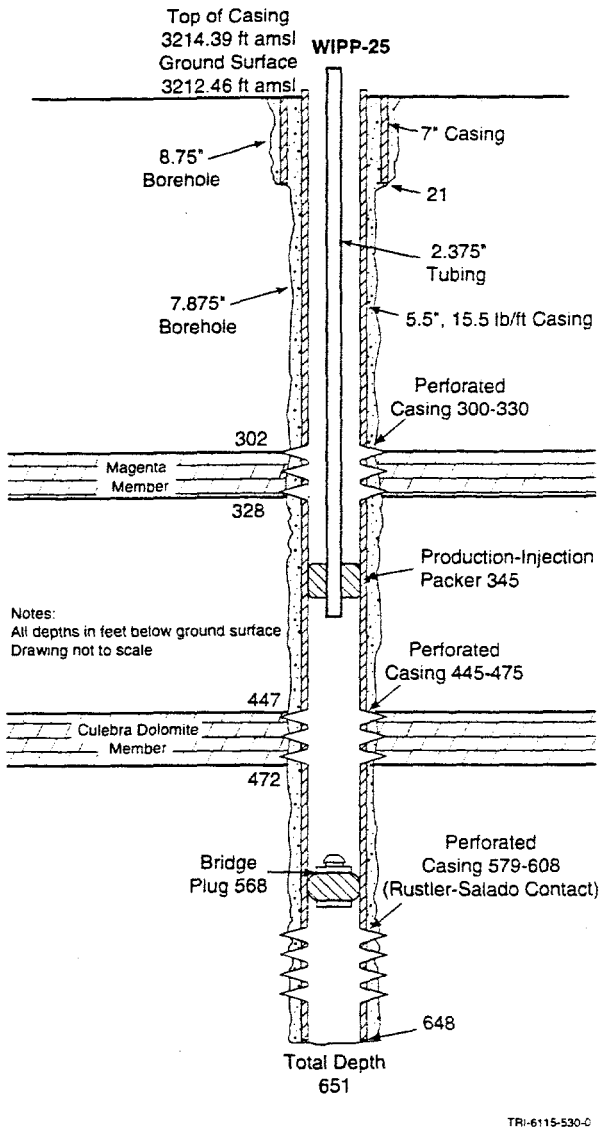

Figure 3-21. Configuration of WIPP-25 during the P-14 pumping test.

3.9 Wells WIPP-27 and WIPP-28

Well WIPP-27 is located approximately 6.3 miles (10.2 km) northwest of the northwest corner of the WIPP site, in the northwest quarter of Section 21, Township 21 south, Range 30 east. Well WIPP-28 is approximately 6.1 miles (9.8 km) north of the northern boundary of the WIPP site, in the northeast quarter of Section 18, Township 21 south, Range 31 east. The wells were drilled in August, September, and October 1978. Both wells were cased with 5.5-inch (14.0-cm) casing, WIPP-27 to a depth of 588 ft (179.2 m) BGS and WIPP-28 to a depth of 800 ft (243.8 m) BGS. Basic data for these wells are presented in Sandia National Laboratories and U.S. Geological Survey (1979b, 1979c).

During 1980, a testing program was conducted for each well in which the casing was successively perforated through the Rustler-Salado contact zone, the Culebra, and the Magenta so that the units could be successively subjected to bailing and slug tests. In WIPP-27, the interval from 290 to 320 ft (88.4 to 97.5 m) BGS was perforated with four holes/ft (Seward, 1982), encompassing the Culebra which lies from 292 to 318 ft (89.0 to 96.9 m) BGS. A bridge plug was set at 395.4 ft (120.5 m) BGS to isolate the Culebra from the Rustler-Salado contact zone for the testing of the Culebra. In WIPP-28, the Culebra interval from 420 to 446 ft (128.0 to 135.9 m) BGS was perforated with four holes/ft (Seward, 1982). A bridge plug was set at 521.7 ft (159.0 m) BGS to isolate the Culebra from the Rustler-Salado contact zone and a PIP on 2.375-inch (6.0-cm) tubing was set at 292.7 ft (89.2 m) BGS for a shut-in test and the first of the Culebra slug tests, after which it was removed. The configurations of WIPP-27 and WIPP-28 at the times of Culebra testing are shown in Figures 3-22 and 3-23, respectively.

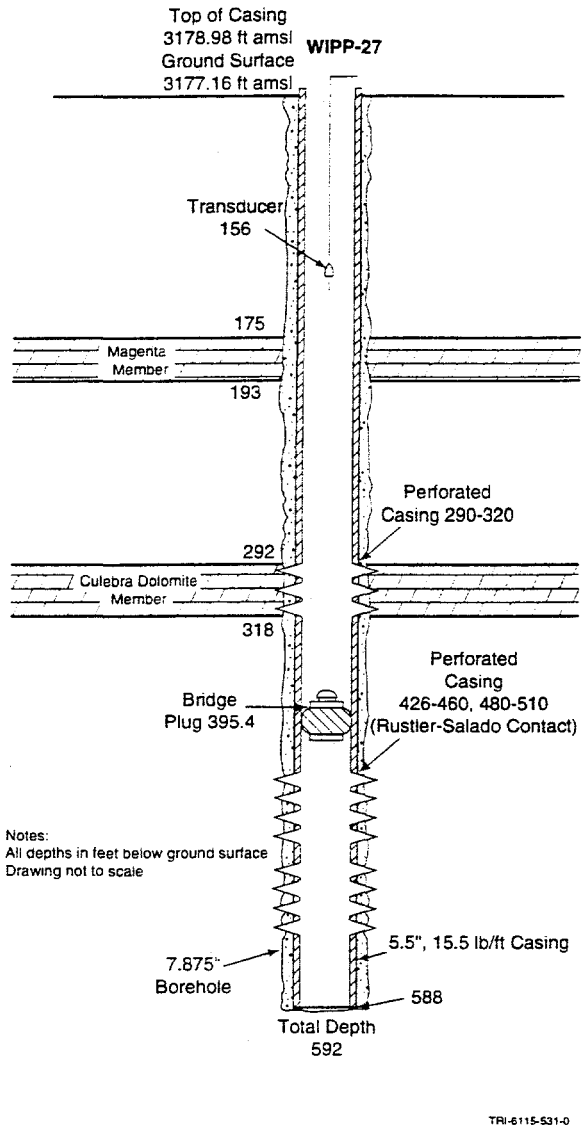

Figure 3-22. Configuration of WIPP-27 during the 1980 slug tests.

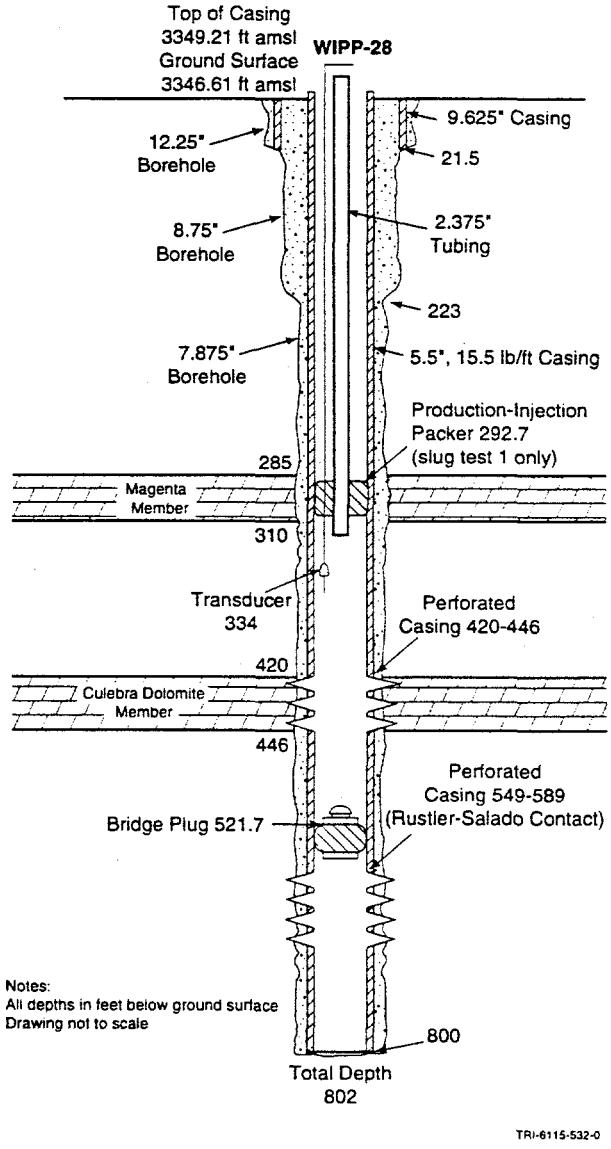

Figure 3-23. Configuration of WIPP-28 during the 1980 slug tests.

3.10 WQSP Wells

Seven WQSP wells were drilled on the WIPP site for Westinghouse Electric Corporation, the WIPP Management and Operating Contractor (MOC), between September and November 1994. Basic data for these wells are presented in WIPP MOC (1995). The construction techniques used were the same for all seven wells. The boreholes were drilled, cored, and reamed to a 9.875-inch (25.1-cm) diameter to total depth. Five-inch (12.7-cm) fiberglass well casing, including 10 inches (25.4 cm) of tailpipe below 25 ft (7.6 m) of slotted 5-inch (12.7-cm) screen, was set to total depth in each well. The screened intervals were gravel-packed, and the gravel was overlain by 3 to 11 ft (0.9 to 3.4 m) of sand, which was in turn overlain by 7 to 90 ft (2.1 to 27.4 m) of bentonite. The remainder of the casing was cemented in place. WQSP-1 through 6 are screened across the Culebra. Well-construction diagrams for WQSP-1, 2, 4, 5, and 6 are shown in Figures 3-24 through 3-28, respectively. No tests have been performed in WQSP-3.

While drilling WQSP-6 on 26 September 1994, water was encountered in the Dewey Lake Redbeds. The water was first noted at a depth of approximately 182 ft (55.5 m) BGS, although the water level was later measured at approximately 164 ft (50 m) BGS. The bottom of the producing zone was believed to lie at approximately 208 ft (63.4 m) BGS. WQSP-6A was sited 71 ft (21.6 m) from WQSP-6 and was drilled and reamed to a depth of 225 ft (68.6 m) BGS between 28 October and 1 November 1994. A video log of the borehole showed open fractures from approximately 184 to 208 ft (56.1 to 63.4 m) BGS. Below 208 ft (63.4 m), fractures are filled with gypsum. WQSP-6A is screened from 199.2 to 224.2 ft (60.7 to 68.3 m) BGS, packed with gravel from 175 to 225 ft (53.3 to 68.6 m) BGS, and packed with sand from 172 to 175 ft (52.4 to 53.3 m) BGS (Figure 3-29). A bentonite seal was placed from 152 to 172 ft (46.3 to 52.4 m) BGS and the remainder of the annulus between the casing and hole was filled with cement.

During the WQSP-1 pumping test, pressure responses were monitored in wells H-18 and WIPP-13. The locations of these wells with respect to WQSP-1 are shown in Figure 3-30. Completions of these wells are shown in Figures 3-31 and 3-32, respectively.

During the WQSP-2 pumping test, pressure responses were monitored in wells DOE-2, H-18, WIPP-12, WIPP-13, WIPP-18, WIPP-19, WQSP-1, and WQSP-3. The locations of these wells with respect to WQSP-2 are shown in Figure 3-33. Well-completion diagrams for DOE-2, H-18, WIPP-12, WIPP-13, and WQSP-1, the wells at which interpretable responses were observed, are shown in Figures 3-34, 3-31, 3-35, 3-32, and 3-24, respectively. Basic well-construction data for DOE-2, H-18, WIPP-12, and WIPP-13 are presented in Mercer et al. (1987), Mercer and Snyder (1990), Black (1982), and Sandia National Laboratories and D'Appolonia Consulting Engineers (1982), respectively.

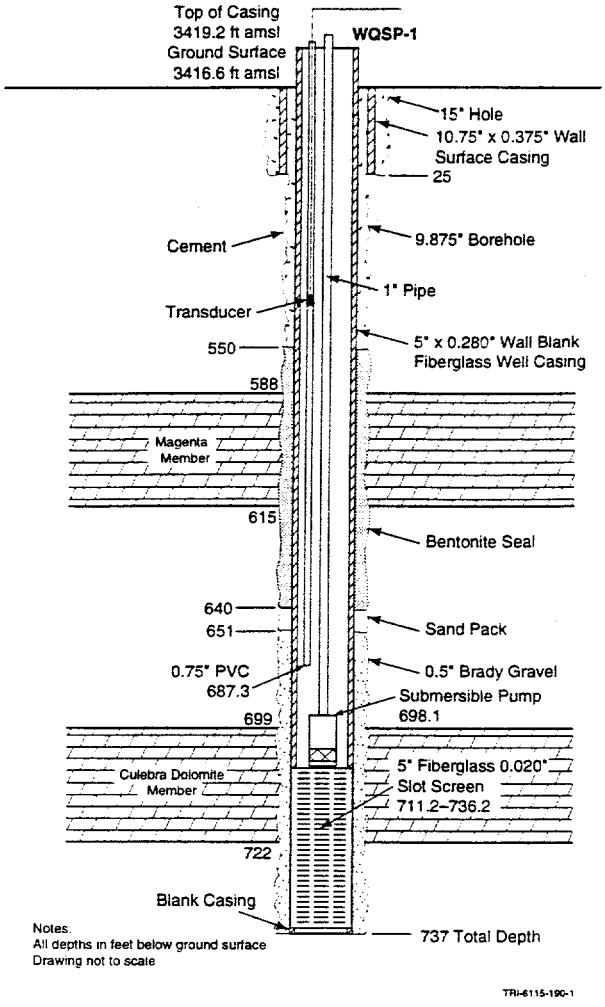

Figure 3-24. Configuration of WQSP-1 during the 1996 pumping test.

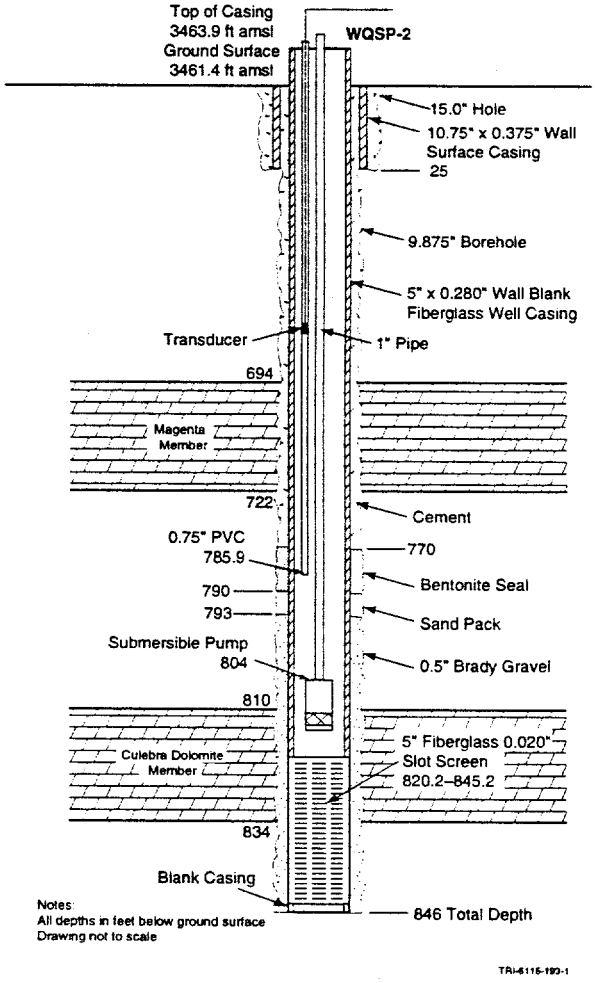

Figure 3-25. Configuration of WQSP-2 during the 1996 pumping test.

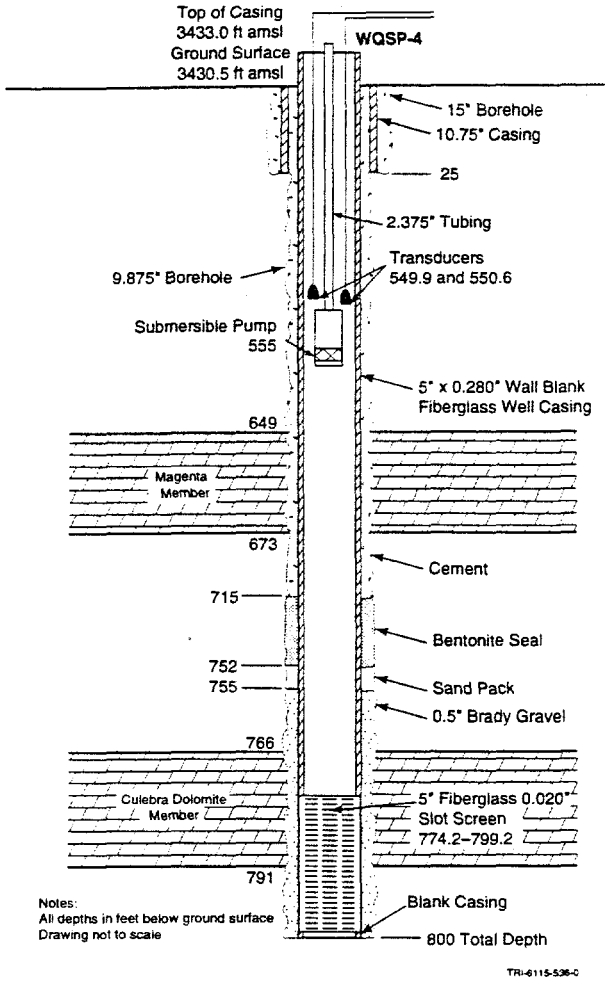

Figure 3-26. Configuration of WQSP-4 during the 1995 pumping test.

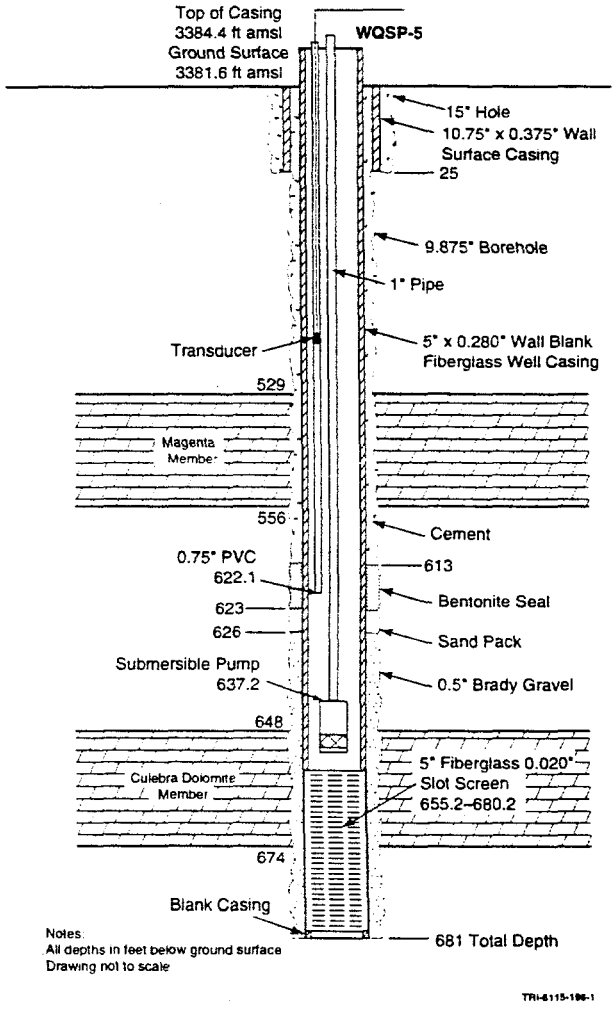

Figure 3-27. Configuration of WQSP-5 during the 1995 pumping test.

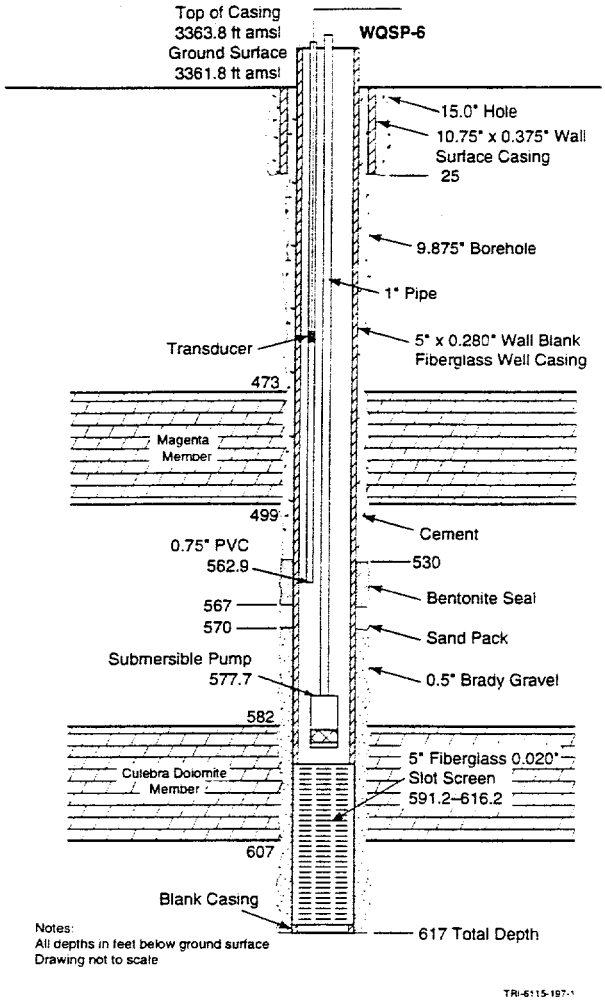

Figure 3-28. Configuration of WQSP-6 during the 1995 pumping test.

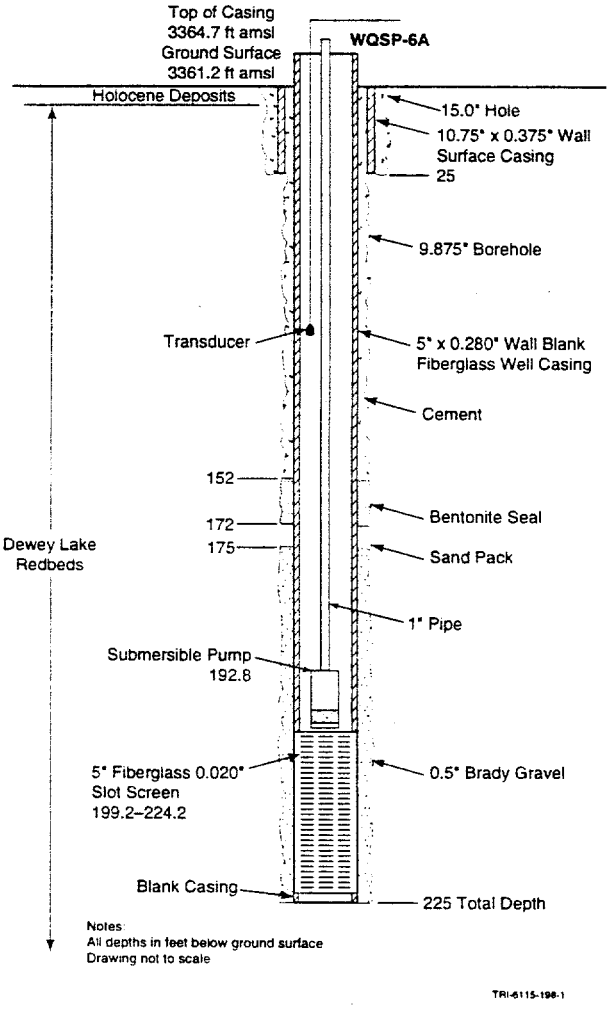

Figure 3-29. Configuration of WQSP-6A during the 1996 pumping test.

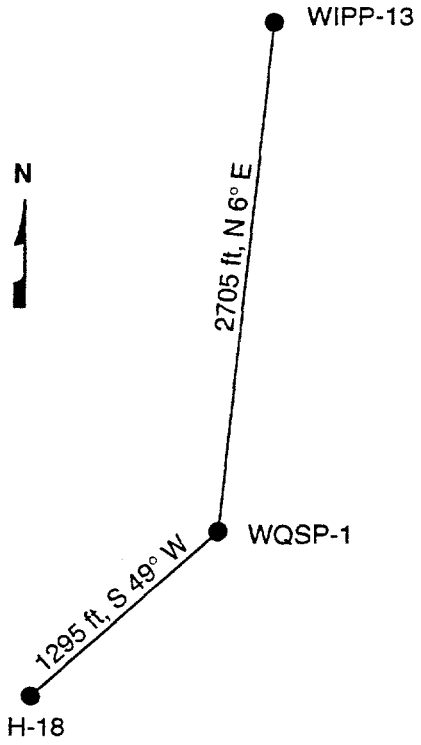

Figure 3-30. Relative locations of wells monitored during the WQSP-1 pumping test.

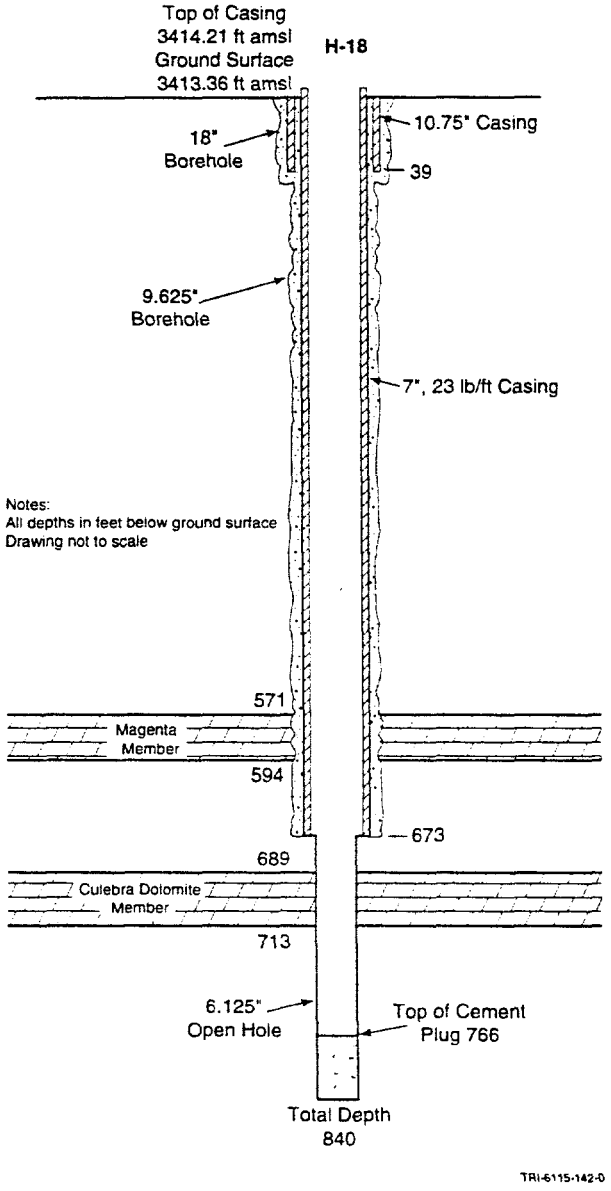

Figure 3-31. Configuration of H-18 during the WQSP-1 and WQSP-2 pumping tests.

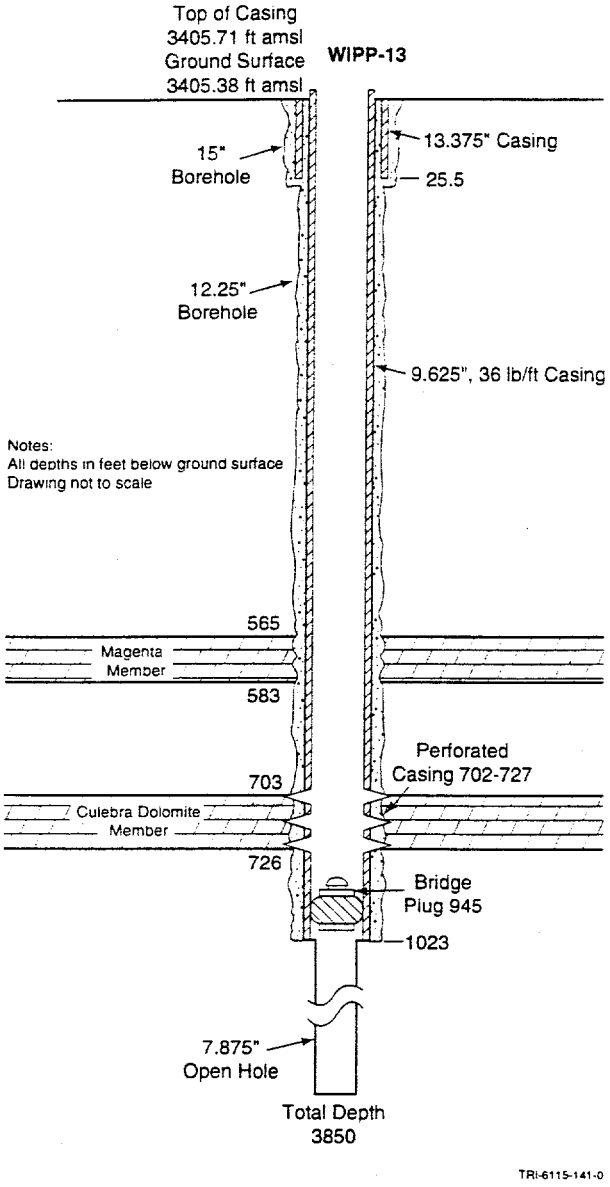

Figure 3-32. Configuration of WIPP-13 during the WQSP-1 and WQSP-2 pumping tests.

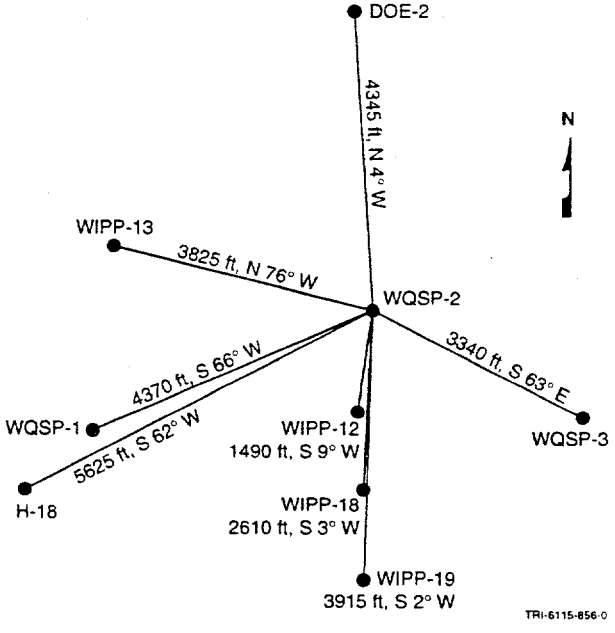

Figure 3-33. Relative locations of wells monitored during the WQSP-2 pumping test.

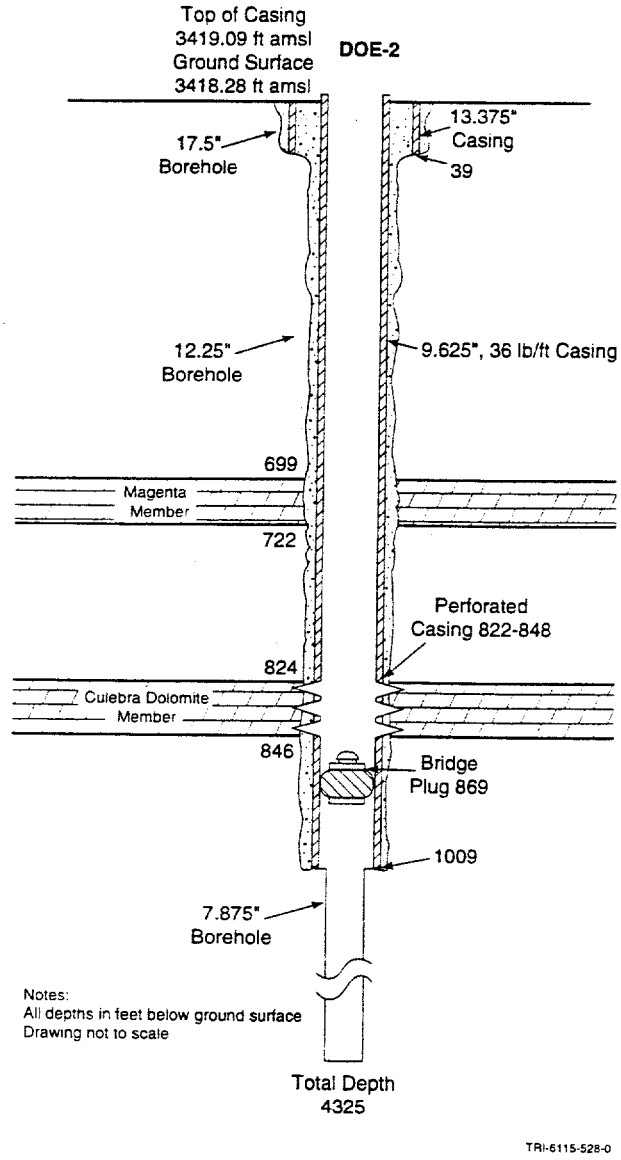

Figure 3-34. Configuration of DOE-2 during the WQSP-2 pumping test.

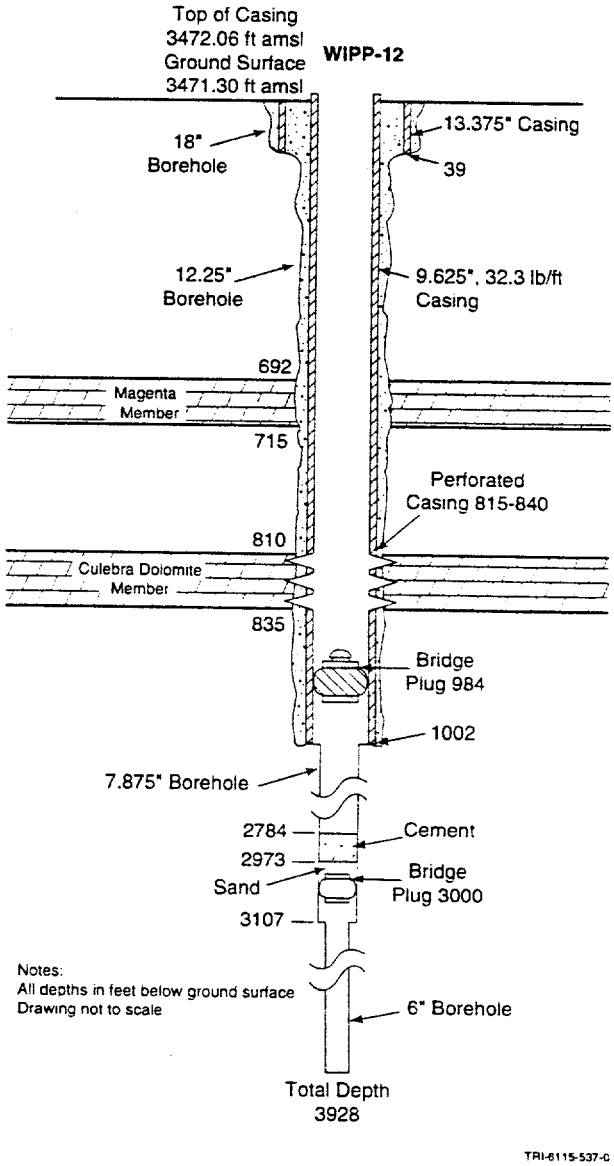

Figure 3-35. Configuration of WIPP-12 during the WQSP-2 pumping test.

4. TEST INSTRUMENTATION

Equipment used to perform the hydraulic tests consisted of pressure transducers in the test and observation wells; a data logger or data-acquisition system (DAS) to collect, process, and store data; packers, with feedthrough assemblies where needed, to isolate the Culebra test interval or to reduce the effects of wellbore storage; and, in the case of pumping tests, a pump to withdraw water and induce a pressure change in the Culebra and a discharge-measurement and flow-regulation system. In addition, water-level and barometric-pressure measurements were obtained during some tests. The equipment used for each test is described below.

NOTE: The use of brand names in this report is for identification purposes only and does not imply endorsement of specific products by Sandia National Laboratories.

4.1 H-2 Pumping Test

A single-acting piston pump driven by a 90-VDC motor on a Jensen jack assembly was installed in well H-2c for the 1981 pumping test on the H-2 hydropad. The pump drew water through 1.25-inch (3.2-cm) galvanized pipe connected to a PIP set from 612.5 to 618.0 ft (186.7 to 188.4 m) BGS (see Figure 3-2). The pump barrel and standing valve extended below the PIP to a depth of 633.0 ft (192.9 m) BGS. Discharge rates were measured with a 1000-mL graduated cylinder and a stopwatch. Transducers connected to a Fluke 2240B Datalogger were used to measure drawdowns in H-2c and H-2b, the only wells on the hydropad completed to the Culebra at the time of the test. Excitation power for the transducers was provided by Tektronix PS-503A dual power supplies, which are dual 0-20 VDC constant-voltage, current-limited, floating power supply units. Transducer output signals were processed by a Tektronix digital volt meter (DVM). Transducer calibrations were verified during the test by comparing the calculated drawdowns to drawdowns measured with a steel tape. Data were recorded on a Tektronix 4923 tape recorder and a Texas Instruments Silent 700 terminal was used to print data from tape. No additional information on either equipment or equipment configurations is available.

4.2 H-6 Pumping Tests

A submersible pump was set on 1.5-inch (3.8-cm) galvanized pipe at about 475 ft (144.8 m) below top of casing (BTC) in well H-6b for the first pumping test on the H-6 hydropad, and at about 538 ft (164.0 m) BTC in well H-6c for the second and third tests. A totalizing flow meter was used to calculate flow rates during all tests. Bell & Howell CEC and Celesco strain-gauge transducers, calibrated by the SNL Standards Laboratory, were used to monitor responses to the pumping. A Celesco 0-500 psi (0-3.4 MPa) transducer was set in the open tubing in H-6a to monitor Culebra responses during all tests (see Figure 3-4). Single Bell & Howell CEC 0-100 psi (0-0.7 MPa) transducers were set in the open casing of H-6b and H-6c during all tests, augmented by an additional Bell & Howell CEC 0-250 psi (0-1.7 MPa) transducer in whichever well served as the pumping well for a test. Transducers were set at 400 ft (121.9 m) BTC in observation wells and at 500 ft (152.4 m) BTC in pumping wells. In all tests, an additional transducer in the H-6a casing monitored the Magenta.

Excitation power for the transducers was provided by Tektronix PS-503A dual power supplies. Transducer output signals were processed by an HP-3495A digital volt meter (DVM). System control and data processing

were performed by an HP-9845B desktop computer, and data were stored by an HP-9885M disk drive on 8-inch (20.3-cm) floppy disks. The data-acquisition software was written in such a way that the user would input a measured depth to water in each well and the corresponding transducer millivolt signal at the moment of program initialization was assumed to correspond to that measured depth. Changes in the transducer signal after that time were converted to changes in water level, assuming a specific gravity of 1.0, and the program stored depths to water and/or deviations from the initial water level rather than pressures (or the raw millivolt signals). Additional information about the instrumentation used for the H-6 pumping tests is provided in Hydro Geo Chem, Inc. (1985).

4.3 H-7 Pumping Test

A 10-horsepower (h.p.) Simmons SS-6, four-stage submersible pump with a capacity of 150 gpm (9.5 L/s) was set at a depth of approximately 223 ft (68 m) BGS in well H-7b1 for the pumping test at the H-7 hydropad. To reduce the influence of wellbore storage on fluid-pressure responses, Baski 5.625-inch (14.3-cm) diameter sliding-end packers on 2.375-inch (6.0-cm) tubing were used as PIPs in all three wells involved in the test. Druck PDCR 10 0-100 psi (0-0.7 MPa) transducers were set 209.8, 201.4, and 221.6 ft (63.9, 61.4, and 67.5 m) BGS in wells H-7b1, H-7b2, and H-7c, respectively. The transducers were calibrated before the test, then recalibrated at the end of the test. Data collection was performed with an HP-9845B-controlled DAS similar to that described in Section 4.2, except that the software was written to calculate and store pressures rather than water levels. Water levels in the H-7b1 annulus above the packer were measured using a Solinst electric water-level sounder. Downhole equipment configurations are shown in Figure 3-6.

The pumping rate during the test was measured with a 1.5-inch (3.8-cm) Hays in-line totalizing flow meter, a 250-gpm (15.8-L/s) 2-inch (5.1-cm) cutthroat flume, and a 55-gallon (208-L) drum (used as a back-up system). Barometric pressure was measured approximately hourly during the H-7 pumping test with a Weathertronics Model 7105-A analog-output barometer located at the H-3 hydropad. The barometer has a linear response over a 10.15 to 15.95 psi (70.0 to 110.0 kPa) range, is temperature compensated, and produces a voltage signal that is read by the DAS. The barometer was in continuous operation during the pretest, pumping, and recovery periods of the H-7 pumping test. Additional information about the instrumentation used for the H-7 pumping test is provided in INTERA Technologies, Inc. (1986a).

4.4 H-9 Pumping Tests

A 5-h.p. Red Jacket submersible pump was installed in well H-9c on 1.5-inch (3.8-cm) galvanized pipe with its intake at a depth of 642.2 ft (195.7 m) BTC for the first pumping test at the H-9 hydropad and at a depth of 643 ft (196.0 m) BTC for the third test. For the second test, the pump was set in H-9b with its intake at a depth of 643.9 ft (196.3 m) BTC. Discharge rates were calculated from the readings of a Precision totalizing flow meter. Single transducers rated from 0-500 psi (0-3.4 MPa) during tests 1 and 2 and rated from 0-100 psi (0-0.7 MPa) during test 3 were installed in the tubing in well H-9a at 500 ft (152.4 m) BTC to monitor Culebra responses during all tests and, during the first test only, another transducer was installed in the casing at a depth of 340 ft (103.6 m) BTC to monitor the Magenta (see Figure 3-8). Two transducers were installed in the H-9b casing during all tests, 0-100 and 0-250 psi (0-0.7 and 0-1.7 MPa) gauges at 500 ft (152.4 m) BTC during tests 1 and 3 and two

0-250 psi (0-1.7 MPa) gauges at 636 ft (193.9 m) BTC during test 2. Two 0-250 psi (0-1.7 MPa) transducers were installed in the H-9c casing at 634.0 and 634.6 ft (193.2 and 193.4 m) BTC during test 1, a 0-100 psi (0-0.7 MPa) transducer and a 0-250 psi (0-1.7 MPa) transducer were both set at 500 ft (152.4 m) BTC during test 2, and one 0-250 psi (0-1.7 MPa) transducer was installed at a depth of 635 ft (193.5 m) BTC for test 3. The DAS, including software, used for the H-9 pumping tests was the same as that used for the H-6 pumping tests described in Section 4.2. Additional information about the instrumentation used for the H-9 pumping tests is provided in INTERA Technologies, Inc. and Hydro Geo Chem, Inc. (1985).

4.5 H-10b, WIPP-27, and WIPP-28 Slug Tests

Slug tests of the Culebra in wells H-10b, WIPP-27, and WIPP-28 were performed by the USGS using Bell and Howell CEC 1000 transducers, a Validyne CD19 carrier demodulator amplifier to provide AC excitation and a variable high-level output, and a Soltec VP-6723S strip-chart recorder and an Esterline Angus PD2064 digital data logger to record pressure data. Feedthrough tubes allowed transducers installed above the PIPs in H-10b and WIPP-28 to measure the pressures below the PIPs. Transducers were installed at depths of 156 and 334 ft (47.5 and 101.8 m) BGS in WIPP-27 and WIPP-28, respectively, for slug tests in the well casing (Figures 3-22 and 3-23). Those slug tests were initiated by either lowering a displacement barrel into the water or raising the barrel out of the water. Additional information about the instrumentation used by the USGS is provided by Basler (1983). Information specific to H-10b is presented in Richey (1986) and additional information specific to WIPP-27 and WIPP-28 is presented in Richey (1987).

4.6 H-11 Tracer/Pumping Test

A Griffin Progressing Cavity Pump was installed in well H-11b1 for the H-11 tracer/pumping test. A Baldor Series 15H Inverter Control was used to control the pump speed and maintain a constant flow rate. An Endress & Hauser Promag 30A digital flow meter was used to measure flow. Discharge was also measured using a Precision totalizing flow meter and by the timed filling of a volumetrically calibrated standpipe. The primary purposes of the pumping were to recover tracers previously injected into H-11b1 and to create a converging flow field for a tracer test involving tracer injections into H-11b2 and H-11b3 (Beauheim et al., 1995). Tracer-injection assemblies were installed within the Culebra intervals of H-11b1, H-11b2, and H-11b3 below packers (Figure 3-12). A PIP was used to isolate the Culebra in H-11b4. Druck PTX 161/D 0-300 psig (0-2.1 MPa) pressure transmitters were used to monitor pressures in the Culebra test zones of the four H-11 wells as well as in the casing above the packers.

The DAS for the H-11 pumping test consisted of a Gateway 2000 486/33 computer for system control, an HP-3497A data acquisition/control unit, an HP-3456A DVM, an Electronic Development Corporation (EDC) 501J programmable voltage standard, and Kepco PCX21-1MAT 0-40 VDC power supplies. The DAS software used for the test was PERM5 version 1.01 (WPO#20443).

4.7 H-19 Hydraulic Tests

Each of the H-19 hydraulic tests involved different equipment, described below.

4.7.1 H-19b1 Drillstem and Slug Tests of the Magenta

A 3.5-inch (8.9-cm) Baker Surface-Controlled Inflation (SCI) PIP was set from 621.8 to

626.0 ft (189.5 to 190.8 m) BGS on 2.375-inch (6.0-cm) tubing in the open H-19b1 borehole for drillstem and slug tests of the Magenta. A Baker Reciprocating Shut-In Tool situated above the PIP was used to open and close the connection between the tubing and the Magenta. Two Druck PTX 161/D 0-300 psig (0-2.1 MPa) pressure transmitters were set 607.6 and 609.3 ft (185.2 and 185.7 m) BGS with feedthrough lines passing through the PIP to monitor the Magenta pressure during testing. The data from the shallower transmitter were used for analysis because the line to the deeper transmitter got plugged during installation. A third transmitter was set at a depth of 604.8 ft (184.3 m) BGS to monitor the water level in the hole above the packer. The downhole equipment configuration in H-19b1 is shown in Figure 3-14. A 1.5-inch (3.8-cm) bailer was used to remove water from the tubing for the drillstem and slug tests. The DAS and software for the H-19b1 tests was the same as that used for the H-11 pumping test described in Section 4.6, except that a Gateway 2000 P5-90 computer was used.

4.7.2 H-19b2 Well-Development Pumping Test

For the well-development pumping test of H-19b2, a 4-inch (10.2-cm) Goulds submersible pump was set on 2.375-inch (6.0-cm) tubing in the open well casing with its intake at a depth of 730.8 ft (222.7 m) BGS (Figure 3-15). Two Druck PTX 161/D 0-300 psig (0-2.1 MPa) pressure transmitters were set 727.4 and 728.9 ft (221.7 and 222.2 m) BGS to monitor the Culebra pressure during testing, and provided essentially identical data. An Endress & Hauser Promag 30A digital flow meter was used to measure flow. Discharge was also measured using a Carlon totalizing flow meter. The DAS and BASys 1.A0 software used for the H-19b2 test were provided by Baker Oil Tools.

4.7.3 H-19 Tracer/Pumping Test

The equipment located at the surface for the H-19 tracer/pumping test included an Endress & Hauser Promag 30A digital flow meter to measure the flow rate, a Honeywell Electro-Pneumatic Valve Positioner to open or close a valve to achieve the desired flow rate, a Bailey, Fischer & Porter Process Control Station to process the flow meter output and send the appropriate signal to the valve positioner, and other data-acquisition equipment supplied by Baker Oil Tools. Baker also supplied the BASys 1.A0 software used for data acquisition. A Druck PTX 620 0-17 psia (0-117 kPa) pressure transmitter was used to monitor barometric pressure during the test.

Because the primary purpose of the experiment was to perform a tracer test, each of the seven wells on the H-19 hydropad contained tracer-injection equipment. H-19b0, the pumping well, was instrumented with a tool string that included three Baker packers. The upper and lower packers isolated the Culebra from the well casing and unnamed lower member, respectively, while the middle packer divided the Culebra into upper and lower parts. A tracer-injection tool was installed in the lower portion of the Culebra along with perforated pup joints of 2.625-inch (6.7-cm) tubing. A 1.5-h.p. Goulds pump was installed in a pump shroud located above the top packer and drew water through the perforations in the 2.625-inch (6.7-cm) tubing. Five Druck PTX 161/D 0-300 psig (0-2.1 MPa) pressure transmitters were installed in the well, two to measure the pressure in the lower Culebra, two for the upper Culebra, and one for the casing above the packers. The configuration of the equipment in H-19b0 is shown in Figure 3-16.

H-19b3, H-19b5, and H-19b7 each were instrumented with tool strings containing three TAM packers. The packers isolated upper

and lower Culebra intervals similar to those isolated in H-19b0. Tracer-injection tools were installed in each of the isolated intervals, allowing tracers to be injected independently into the upper and lower Culebra. Three Druck PTX 161/D 0-300 psig (0-2.1 MPa) pressure transmitters were installed in each well to measure pressures in the lower Culebra, upper Culebra, and well casing above the packers. The configurations of the equipment in H-19b3, H-19b5, and H-19b7 are shown in Figure 3-16.

H-19b2, H-19b4, and H-19b6 each were instrumented with tool strings containing two TAM packers. The packers isolated the entire Culebra from the unnamed lower member below and well casing above. Tracer-injection tools were installed in the isolated Culebra intervals. Two Druck PTX 161/D 0-300 psig (0-2.1 MPa) pressure transmitters were installed in each well to measure pressures in the Culebra and well casing above the packers. The configurations of the equipment in H-19b2, H-19b4, and H-19b6 are shown in Figure 3-17.

4.8 P-14 Pumping Test

The air-lift assembly used for the pumping test at P-14 consisted of an air compressor with valve and gage, an air line, and a discharge tee attached to the well casing. The air compressor was an Ingersoll-Rand XP-825-WCU Fast Track, which produced 825 cubic feet per minute (0.4 m^3/s) of compressed air at 125 psi (0.9 MPa). The air line was 1-inch (2.5-cm) galvanized pipe with a 2-ft (0.6-m) perforated section above a 5-ft (1.5-m) tail pipe (Figure 3-19). When the compressor was turned on, air entered the air line, displacing the water contained therein, and exited through the perforations into the well casing. As the volume of air increased, the water column between the casing and pipe was aerated, lifted, and discharged at the surface through the discharge tee mounted on the wellhead casing. The air-lift system was designed to pump up to 80 gpm (5 L/s) from depths in excess of 350 ft (107 m) BGS.

The discharge-measurement system used during the P-14 pumping test consisted of a batch tank, an orifice weir, and a discharge pit. Fluid and air were discharged from the well through the discharge tee into a 5 x 7 x 14-ft (1.5 x 2.1 x 4.3-m) batch tank. Water exited from the base of the tank through a 6-ft (1.8-m) long, 3-inch (7.6-cm) O.D. approach pipe and through a 2-inch (5.1-cm) orifice plate into a 20 x 20 x 5-ft (6.1 x 6.1 x 1.5-m) discharge pit. A manometer tube was attached to a 1/8-inch (0.3-cm) hole in the center of the approach pipe 3.5 ft (1.1 m) from the discharge end of the pipe.

The DAS used during the air-lift pumping test at P-14 was controlled by a Hewlett Packard Series 9000 Model 310 microcomputer with HP-UX multi-tasking software. The system consisted of Druck pressure transducers, a Weathertronics Model 7105-A analog-output barometer, Tektronix PS-503A power supplies, an HP-3455A DVM, an HP-3495A scanner, HP-9133L and HP-9127A disk drives, and plotters and printers. Two different models of Druck PDCR transducers were attached to the tail pipe of the air line in P-14 for the test, a PDCR 10/D, rated 0 to 250 psi (0 to 1.7 MPa), and a PDCR 830, rated 0 to 300 psi (0 to 2.1 MPa). Both transducers were calibrated before and after use. The barometer was factory-calibrated before the start of the test and observed to be within specifications.

Water-level measurements were performed at observation wells with a Solinst electric water-level sounder. Additional information about the instrumentation used for the P-14

pumping test is provided in Stensrud et al. (1990).

4.9 WQSP Pumping Tests

The pumps used for the pumping tests in wells WQSP-1, WQSP-2, WQSP-5, and WQSP-6 were installed by Westinghouse Electric Corporation. The pumps in wells WQSP-1 and WQSP-2 were 34-stage Grundfos pumps with 5-h.p. Franklin 3-phase motors. The pumps in wells WQSP-5 and WQSP-6 were 26-stage Grundfos pumps with 3-h.p. Franklin 3-phase motors. A 3-h.p. Goulds 10EJ pump was used in WQSP-6A. These pumps were suspended on 1-inch (2.5-cm) I.D. 304 stainless steel discharge pipe. For the test in WQSP-4, a Red Jacket 32BC pump was installed on 2.375-inch (6.0-cm) tubing. The pump and other equipment configurations in the WQSP wells are shown in Figures 3-24 through 3-29. For all tests except for that in WQSP-4, an Endress & Hauser Promag 30A digital flow meter and a Honeywell Electro-Pneumatic Valve Positioner Model 870020 were used to control and measure flow. Discharge from WQSP-4 was measured using a Carlon totalizing flow meter as well as by the timed filling of a volumetrically calibrated standpipe. A Precision totalizing flow meter and the calibrated standpipe were also used for all of the other WQSP well tests.

Druck PDCR 35/D 0-100 psig (0-0.7 MPa) transducers were used to monitor pressures in the well casing during testing of WQSP-1, WQSP-5, and WQSP-6. Druck PTX 161/D 0-300 psig (0-2.1 MPa) pressure transmitters were used for the WQSP-2, WQSP-4, and WQSP-6A tests. Barometric pressures were measured during all tests using a Druck PTX 620 0-17 psia (0-117 kPa) pressure transmitter (barometer). The barometer was located at the WQSP-4 pad for the WQSP-4 test and at H-19 for the remaining tests. Pressures in nearby wells were monitored during some of the WQSP pumping tests using Troll Model SP4000 gauges manufactured by In-Situ Inc. Trolls are battery-powered programmable gauges that record pressure at specified time and/or pressure intervals. Data from Trolls can be downloaded to a laptop computer whenever desired. Water levels in other wells were measured with Solinst electric water-level sounders.

The DAS for the WQSP pumping tests consisted of a Gateway 2000 P5-90 computer for system control, an HP-3497A data acquisition/control unit, an HP-3456A DVM, an EDC 501J programmable voltage standard, and Kepco PCX21-1MAT 0-40 VDC power supplies. The DAS software used for the tests was PERM5 version 1.01 (WPO#20443).

5. TEST DATA

Data collected during the various hydraulic tests are presented in this chapter. Data-reduction procedures are discussed along with measures taken to compensate data for pre-test trends and barometric effects. The maximum barometric-pressure fluctuation observed during any of the hydraulic tests was approximately 0.5 psi (3.5 kPa). The only data that needed barometric compensations were from wells at which the total test-induced pressure response was on the order of 2 psi (14 kPa) or less. Effects of earth tides, as reported by Robinson (1939), were typically evident in the responses of these same wells if monitored using transducers, but were not sufficiently significant to warrant compensation. Electrical-conductivity, temperature, and/or specific-gravity measurements were made during many of the pumping tests, but are not presented herein because they have little or no bearing on the interpretation of the tests. Those data can be found in the primary data references cited below.

5.1 H-2 Pumping Test

The pumping and recovery test at the H-2 hydropad analyzed herein was conducted between 29 April 1981 and 15 May 1981. Pumping of well H-2c began at 1200 hours, 29 April 1981, and continued for 71 hr until 1100 hours, 2 May 1981. During this time, the pumping rate averaged 0.25 gpm (0.016 L/s). Recovery was monitored for approximately 13 days, until 1200 hours, 15 May 1981.

Transducers connected to a datalogger were used to measure drawdown (in feet of fresh water) in the pumping well, H-2c, and observation well H-2b during the test. The datalogger records have been lost, but periodic measurements were recorded manually in field notes. The depth of the transducers is not known. An arbitrary pressure datum of 200 psig was used in converting the manually recorded transducer readings to pressures. A plot of the calculated-pressure data is shown in Figure 5-1.

5.2 H-6 Pumping Tests

Three pumping tests were conducted at the H-6 hydropad during May and June 1981 under a Field Operations Plan by Gonzalez (1981). H-6b was the pumping well for the first test and H-6c was the pumping well for the second and third tests. Totalizing flow meter readings were typically recorded once a day, leaving flow-rate fluctuations poorly documented. Each pumping well was equipped with two Culebra transducers and each observation well was equipped with one Culebra transducer. An additional transducer was installed in the casing of well H-6a to measure water levels in the Magenta, but this transducer failed before the first test began. The data obtained from these tests are listed in Hydro Geo Chem, Inc. (1985).

The DAS software was written in such a way that the signals from the transducers were stored as depth to water and drawdown (in feet of fresh water) from an initialized value. The stored water-level data were converted to equivalent pressures at the center of the Culebra by first calculating the pressure change represented by the "drawdown" and then subtracting that value from the initial pressure calculated as the pressure exerted at the center of the Culebra (615.5 ft [187.6 m] BGS) by the column of water in the well at the start of the test given a fluid specific gravity of 1.04 (Uhland and Randall, 1986). When data were available from two transducers monitoring the same zone, the data set subjectively determined to contain

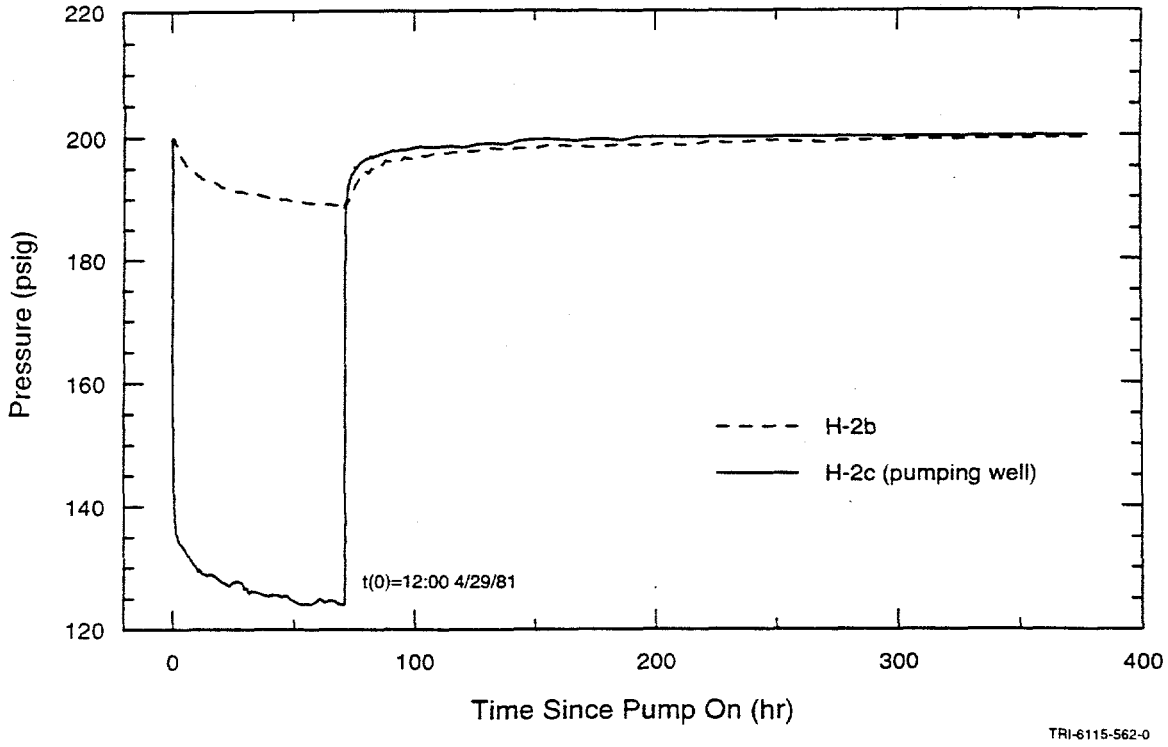

Figure 5-1. Pressures in H-2c and H-2b during the H-2 pumping test.

the least noise was selected for analysis. The data from H-6b were erratic between approximately 224 and 242 hr after the start of pumping for the third test, and were offset by approximately 2.4 psi (16.5 kPa) from the previous trend thereafter. The erratic data were deleted from the data file and the offset was removed before the data were analyzed. No other adjustments were made to any of the pressure data.

The first pumping test began at 1020 hours, 1 May 1981, and continued for 48 hr. Well H-6b was pumped at an average rate of 23.0 gpm (1.45 L/s), producing approximately 66,150 gallons (250,380 L) of water. The pumping rate decreased slightly during the test, dropping from 25.4 gpm (1.60 L/s) during the first few minutes of pumping to 23.2 gpm (1.46 L/s) over the first 25 hr of pumping to 22.7 gpm (1.43 L/s) over the last 23 hr of pumping. Recovery data were obtained until 1130 hours, 7 May 1981, a period of over 97 hr. Pressure data from H-6a, H-6b, and H-6c are shown in Figure 5-2.

The second test started at 1605 hours, 12 May 1981, and continued for over 33 hr until 0110 hours, 14 May 1981. About 37,430 gallons (141,670 L) of water were produced at an average rate of 18.9 gpm (1.19 L/s). The pumping rate increased from approximately 17.5 gpm (1.10 L/s) to slightly less than 19.0 gpm (1.20 L/s) after approximately 145 minutes of pumping. Recovery data were collected for almost 151 hr, ending at 0800 hours on 20 May 1981. The water level in the pumping well, H-6c, dropped below the transducer after a few minutes of pumping. Thus, no interpretable data were obtained from H-6c during the second test. Pressure data from H-6a and H-6b are shown in Figure 5-3.

Pumping for the last test began at 1045 hours on 21 May 1981 and continued for over 148

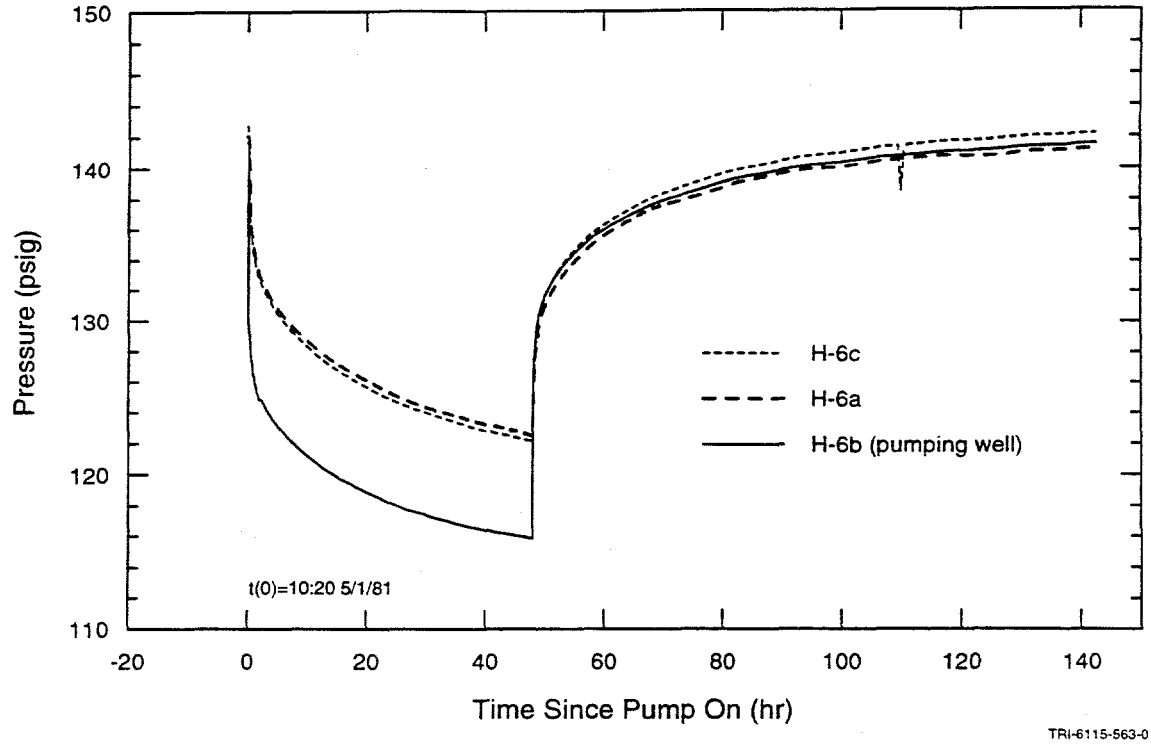

Figure 5-2. Pressures during H-6 pumping test #1.

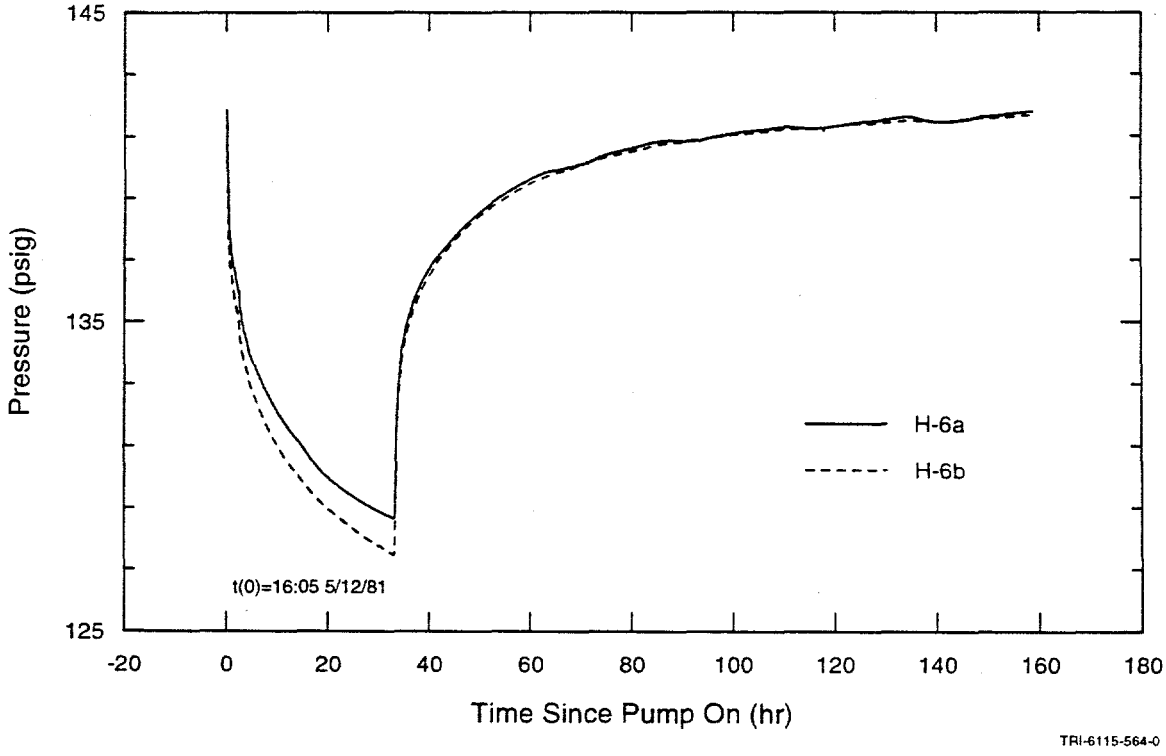

Figure 5-3. Pressures in H-6a and H-6b during H-6 pumping test #2.

hr until 1512 hours on 27 May 1981. The test produced nearly 147,000 gallons (556,400 L) of water at an average withdrawal rate of approximately 16.5 gpm (1.04 L/s). The pumping rate was erratic during the first few days of the test while decreasing from 19.4 to 16.4 gpm (1.22 to 1.03 L/s). The recovery period lasted for almost 192 hr, ending at 1500 hours, 4 June 1981. Pressure data from all three H-6 wells are shown in Figure 5-4.

5.3 H-7 Pumping Test

The H-7 pumping test was performed under the Field Operations Plan by INTERA Technologies, Inc. (1986b). The H-7 pumping period began at 1000 hours on 18 February 1986. The flow from H-7b1 maintained a stable rate of approximately 81.5 gpm (5.14 L/s) throughout most of the 3-day test (Figure 5-5). Pumping ended at 1000 hours on 21 February 1986. During the test, 352,874 gallons (1,335,630 L) of water were produced from the Culebra and discharged onto the land surface. Recovery was monitored until 0749 hours on 24 February 1986. Pressure data are shown in Figure 5-6. The stabilized pressures shown on the figure for the three H-7 wells differ because the transducers were installed at different depths in the wells, as discussed in Section 4.3.

The record of annulus water-level measurements in H-7b1 indicates that no leakage across the packer occurred during either the pumping or recovery periods. The slight (0.07 ft [0.02 m]) rise in the annulus water level noted during the test (INTERA Technologies, Inc., 1986a) represents a volume of approximately 0.1 gal (0.4 L) and may have been due to some small leakage from the discharge line.

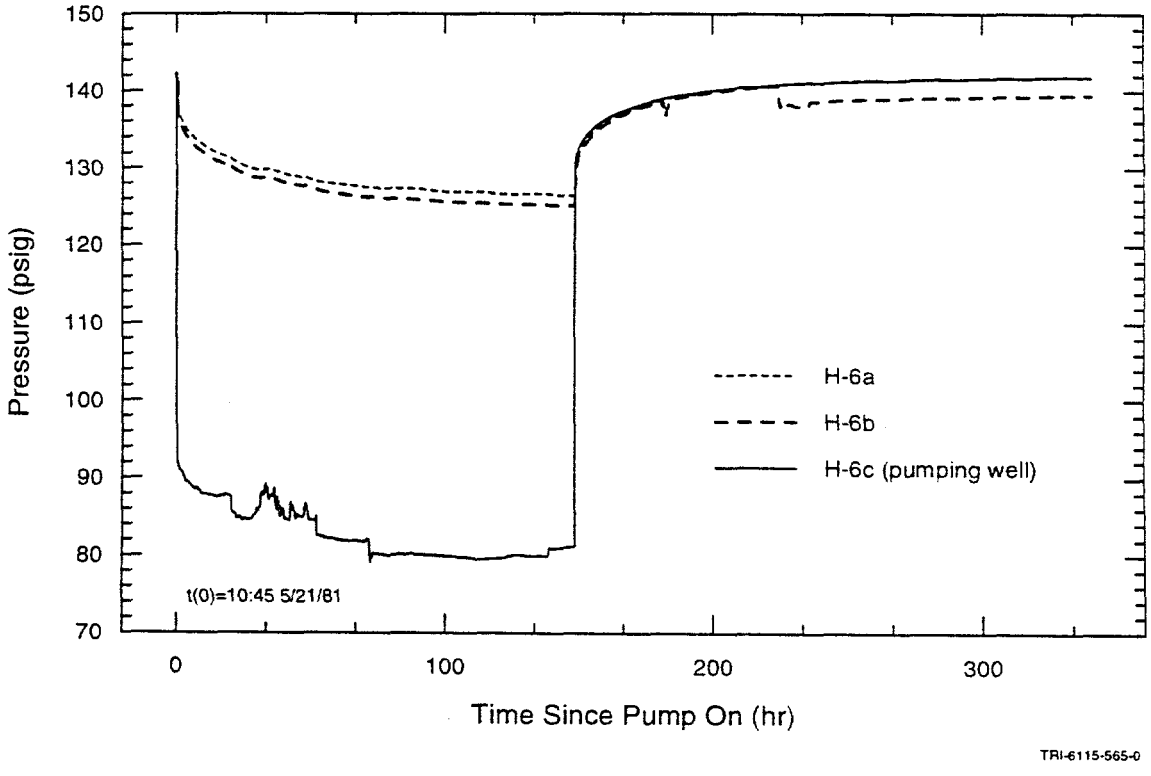

Figure 5-4. Pressures during H-6 pumping test #3.

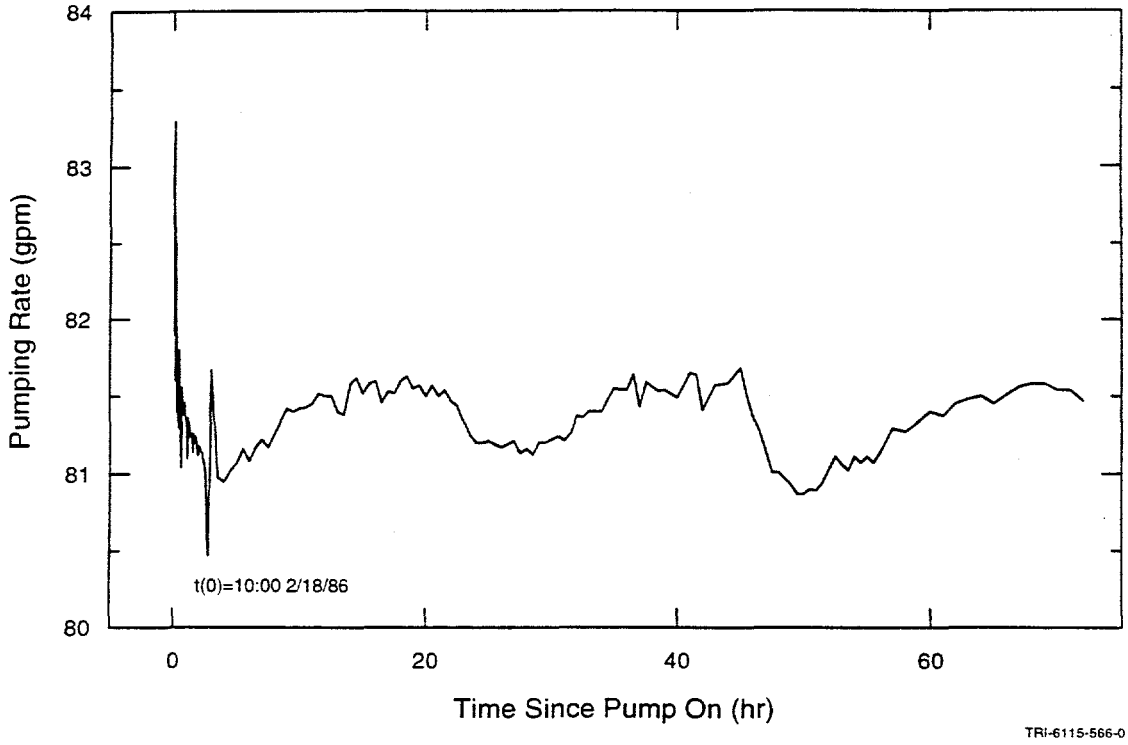

Figure 5-5. Pumping rate during the H-7 pumping test.

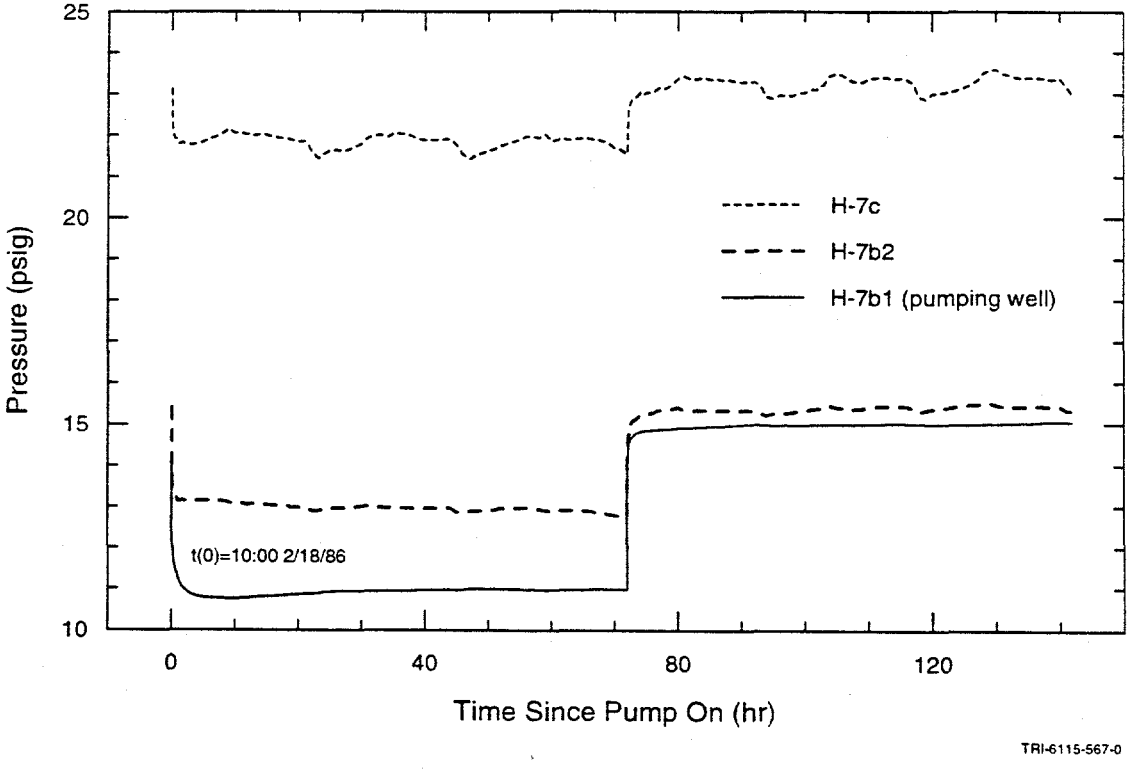

Figure 5-6. Pressures during the H-7 pumping test.

Diurnal fluctuations believed to be related to earth tides were evident in the pressure measurements from the H-7 wells, particularly H-7c (Figure 5-6). No barometric effects were apparent in the data collected during the H-7 test, perhaps because barometric pressure varied by less than 0.2 psi (1.4 kPa) during the testing period.

5.4 H-9 Pumping Tests

Three pumping tests were conducted at the H-9 hydropad from August to December 1983. Well H-9c was pumped during the first and third tests and well H-9b was pumped during the second test. Totalizing flow meter readings were typically recorded several times a day, but during daylight hours only, leaving flow-rate fluctuations poorly documented. Culebra responses were monitored by single transducers in H-9a during all tests and in H-9c during test 3. Two Culebra transducers were used in H-9b during all tests and in H-9c during tests 1 and 2. An additional transducer was installed in the casing of well H-9a to monitor the Magenta during test 1. Water levels were measured in the Engle well, a stock well completed to the Culebra located approximately 4,115 ft (1,255 m) southeast of H-9c (Figure 1-3), during test 3. The data obtained from these tests are listed in INTERA Technologies, Inc. and Hydro Geo Chem, Inc. (1985). No barometric data were collected during the H-9 tests.

The DAS software was written in such a way that the signals from the transducers were stored as depth to water and drawdown (in feet of fresh water) from an initialized value. The stored water-level data were converted to equivalent pressures at the center of the Culebra by first calculating the pressure change represented by the "drawdown" and then subtracting that value from the initial pressure calculated as the pressure exerted at the center of the Culebra (662 ft [201.8 m] BGS) by the column of water in the well at the start of the test given a fluid specific gravity of 1.00 (Uhland and Randall, 1986). When data were available from two transducers monitoring the same zone, the data set subjectively determined to contain the least noise was selected for analysis. No other adjustments were made to the data.

The pumping of well H-9c for the first test began at 1445 hours, 11 August 1983, and continued for 22.5 hr until 1315 hours, 12 August 1983. Recovery data were collected for nearly 65 hr, ending at 0605 hours, 15 August 1983. During the test, the discharge rate ranged from 10.0 to 10.4 gpm (0.63 to 0.66 L/s) and averaged 10.2 gpm (0.64 L/s). The total volume of water produced from well H-9c was about 13,800 gallons (52,200 L). Pressure data are shown in Figure 5-7.

Between the first and second pumping tests, well H-9a was sounded. Fill was encountered in the well at a depth of 651.7 ft (198.6 m) BGS, within the Culebra (see Figure 3-8). This fill remained in the well throughout the second and third pumping tests.

The second pumping test, using H-9b for the production well, began at 1000 hours, 20 September 1983. The pumping portion of the test lasted for 212 hr, terminating at 0600 hours, 29 September 1983. After that, recovery data were obtained for over 197 hr, through 1117 hours, 7 October 1983. The pumping rate was erratic during the first 28 hr of the test, ranging from 8.0 to 11.9 gpm (0.50 to 0.75 L/s). After that time, the pumping rate ranged between 9.6 and 10.2 gpm (0.61 and 0.64 L/s), and averaged 10.0 gpm (0.63 L/s) over the entire test. Total water production during the test was nearly 127,000 gallons (480,700 L). Pressure data are shown in Figure 5-8.

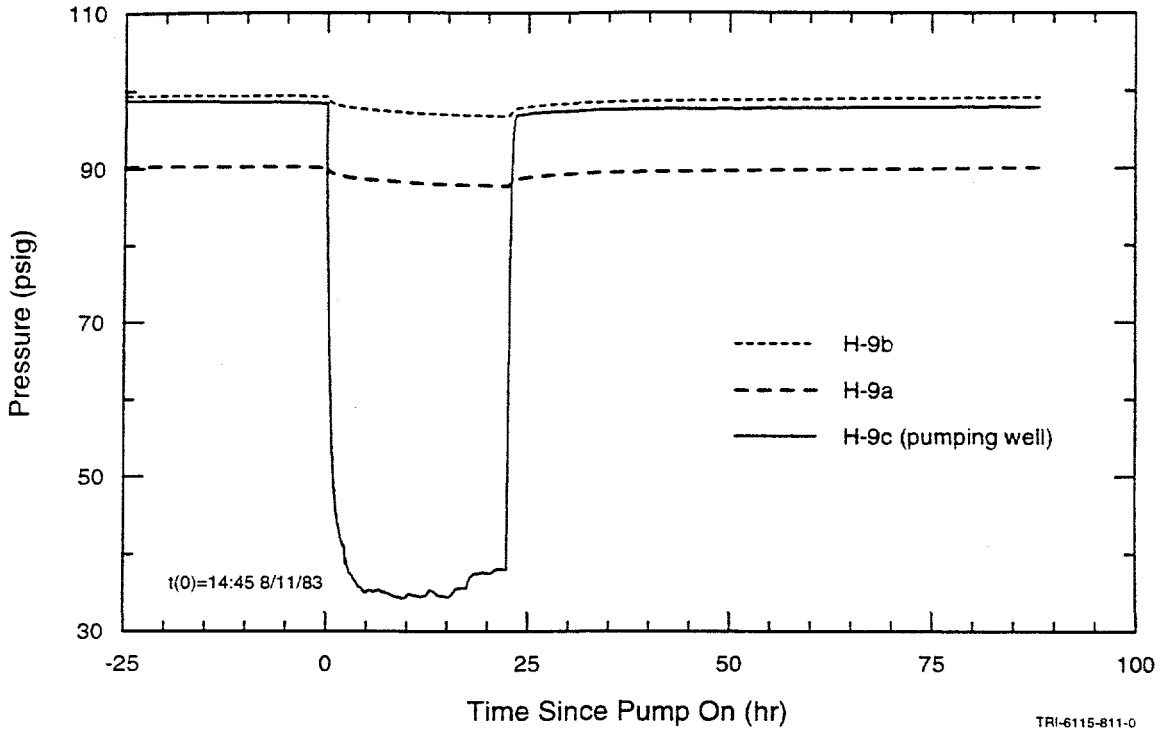

Figure 5-7. Pressures during H-9 pumping test #1.

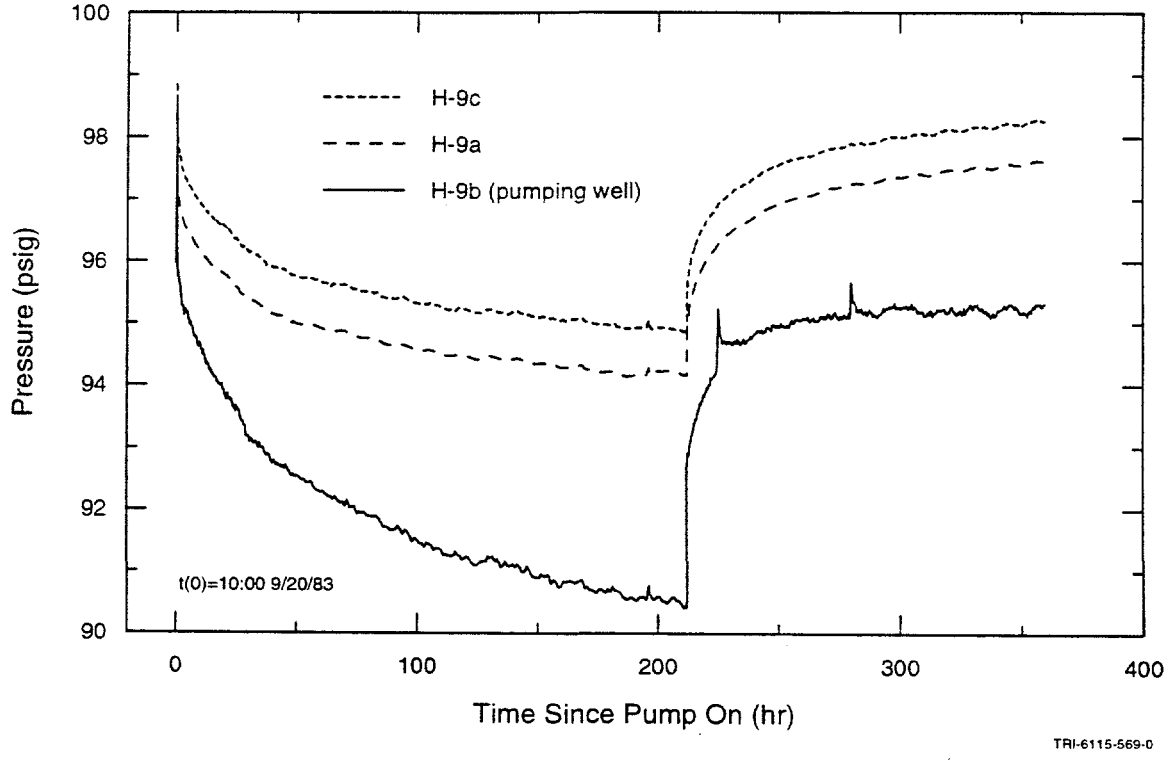

Figure 5-8. Pressures during H-9 pumping test #2.

The final pumping test at H-9 began at 1100 hours, 2 December 1983, using well H-9c as the production well. The withdrawal portion of the test continued through 1300 hours, 13 December 1983, for a duration of 266 hr. Measurement of recovery continued until 0910 hours on 21 December 1983, totaling over 188 hr. Well H-9c produced nearly 160,000 gallons (605,600 L) of water during the test at an average discharge rate of 10.0 gpm (0.63 L/s). The pumping rate is estimated to have been greater than 20 gpm (1.26 L/s) during the first five minutes of the test, and ranged between 9.5 and 10.3 gpm (0.60 and 0.65 L/s) thereafter. Pressure and pumping-rate data are shown in Figure 5-9. The water levels measured in the Engle well were converted to pressures at the midpoint of the Culebra assuming a fluid specific gravity of 1.002 (Randall et al., 1988). The calculated pressure data are shown in Figure 5-10.

5.5 H-10b Slug Tests

After bailing well H-10b on 26 February 1980, the USGS installed a PIP on open 2.375-inch (6.0-cm) tubing and allowed the well to recover. Two slug-injection tests were performed from 27-29 February 1980. Test descriptions and data are provided by Richey (1986). The first slug test was judged to have the best-quality data and was selected for analysis. The complete test data are shown in Figure 5-11.

5.6 H-11 Tracer/Pumping Test

The H-11 pumping test was performed in conjunction with single-well and convergent-flow tracer tests under the Test Plan by Beauheim et al. (1995). Tracers were injected into H-11b1 on 6 February 1996 and, after an overnight pause, pumping began on 7 February 1996. The pumping had two

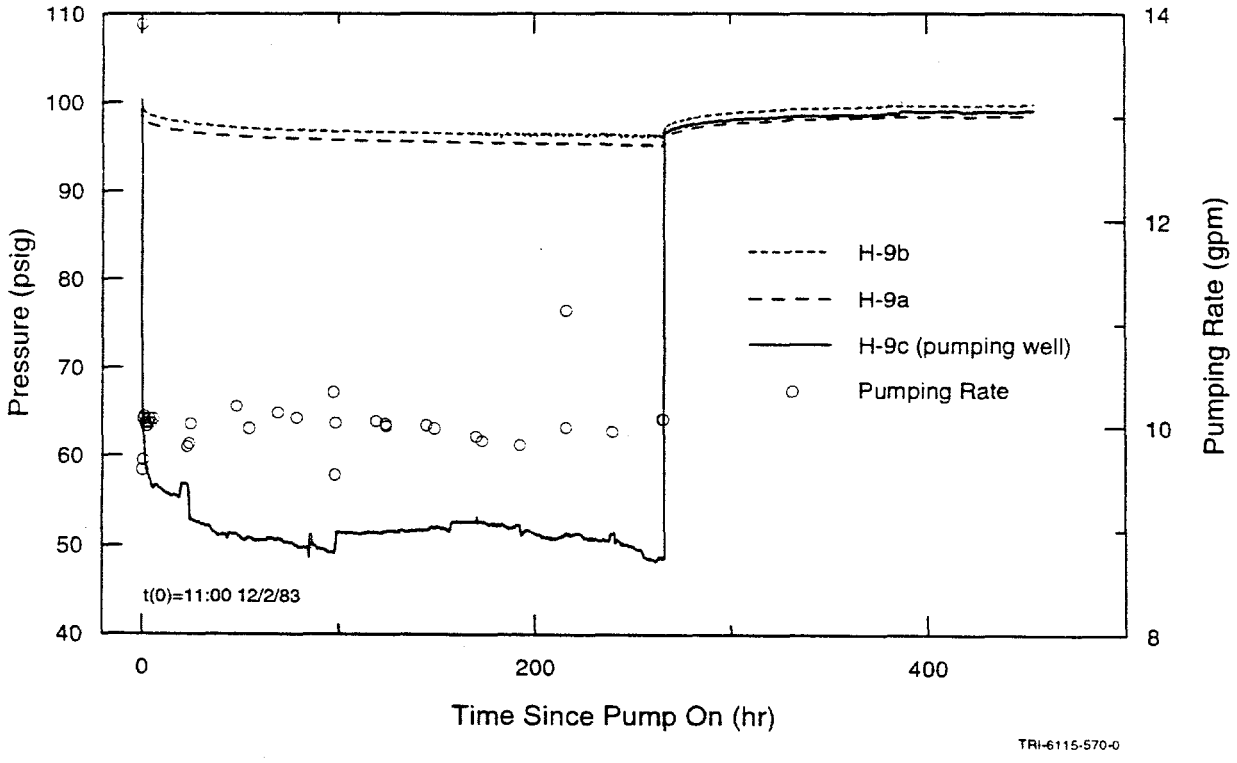

Figure 5-9. Pumping rate and pressures during H-9 pumping test #3.

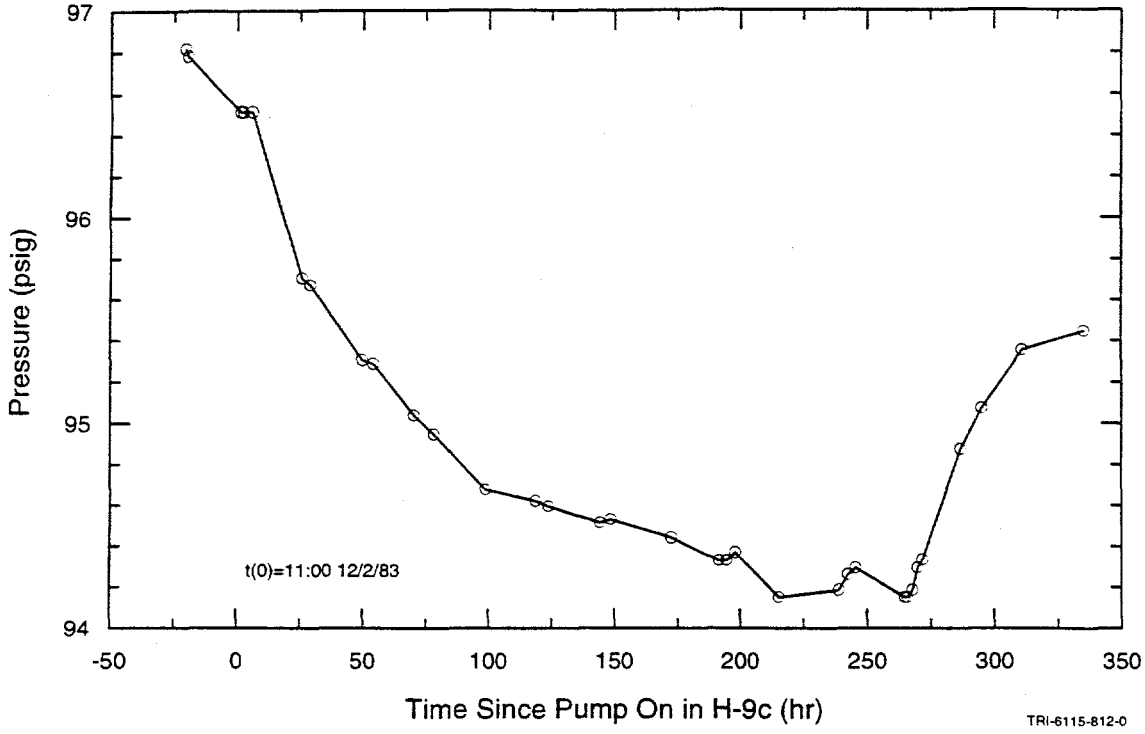

Figure 5-10. Pressure in the Engle well during H-9 pumping test #3.

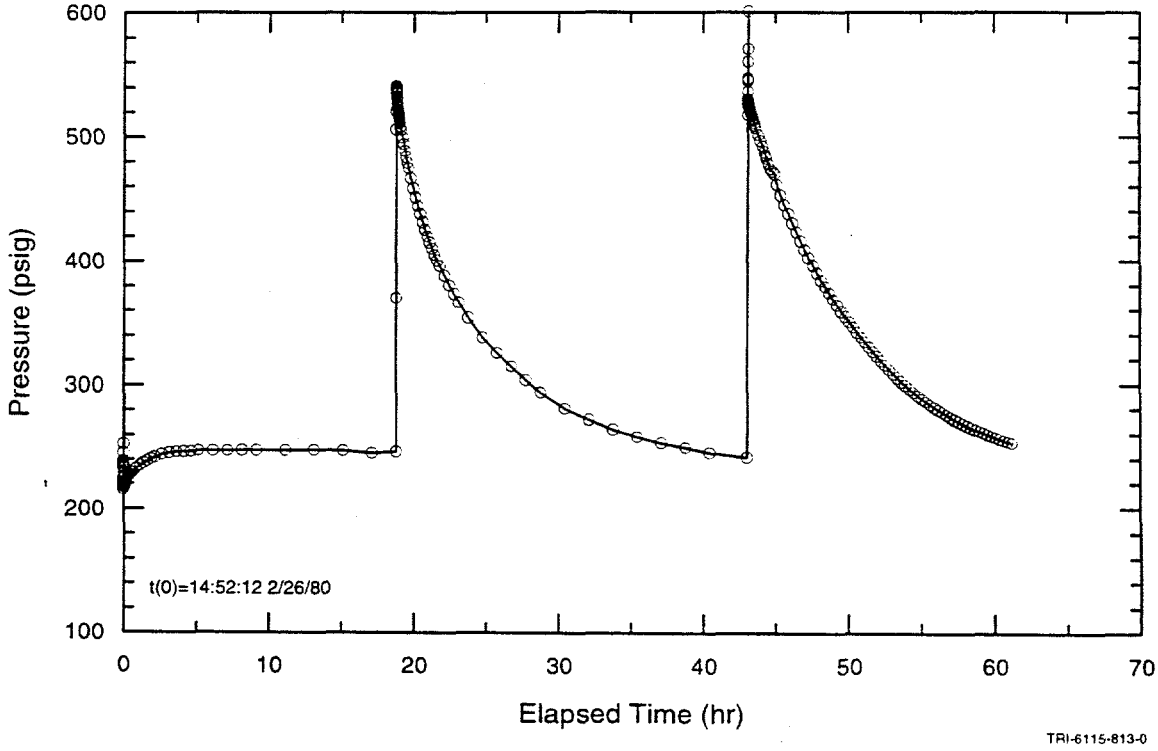

Figure 5-11. H-10b slug-test data.

primary purposes: to recover the tracers previously injected into H-11b1 and to create a converging flow field on the H-11 hydropad in preparation for a multiwell tracer test involving tracer injections into H-11b2 and H-11b3. The hydraulic data analyzed in this report were collected between 0939 hours on 6 February 1996, when tracer injection began into H-11b1, and 1729 hours on 12 February 1996, just before the packer in H-11b3 was deflated so that the injection tool could be lowered 1.6 ft (0.5 m).

A total of 775.4 gallons (2,935 L) of tracer and chaser solution was injected into H-11b1 over a period of 395 minutes between 0939 and 1614 hours on 6 February 1996. The average injection rate, therefore, was approximately 1.96 gpm (0.12 L/s). Pumping from H-11b1 began at 1000 hours on 7 February 1996 and was terminated at 0825 hours on 28 March 1996. The DAS records show that the Endress & Hauser flow meter had an average reading of -0.123 gpm (-0.0078 L/s) when no flow was occurring. Consequently, all readings during pumping were increased by that value to compensate for the offset. The average pumping rate during the first 127.5 hr was 3.61 gpm (0.23 L/s) (Figure 5-12).

Pressures were measured in the casing and packer-isolated Culebra intervals of all four wells on the hydropad. Three pressure transmitters were installed in H-11b1: two monitoring the Culebra and one monitoring the water level in the casing (see Figure 3-12). The data from the shallower of the Culebra transmitters and the casing transmitter are shown in Figure 5-12. The Culebra pressure data during the last approximately 60 hr shown contain electronic noise of unknown origin; the fluctuations cannot be explained by the pumping-rate fluctuations. The pressure in the casing was steady throughout the period of interest, but became noisy after the pump was turned on. Pairs of pressure transmitters were installed in H-11b2, H-11b3,

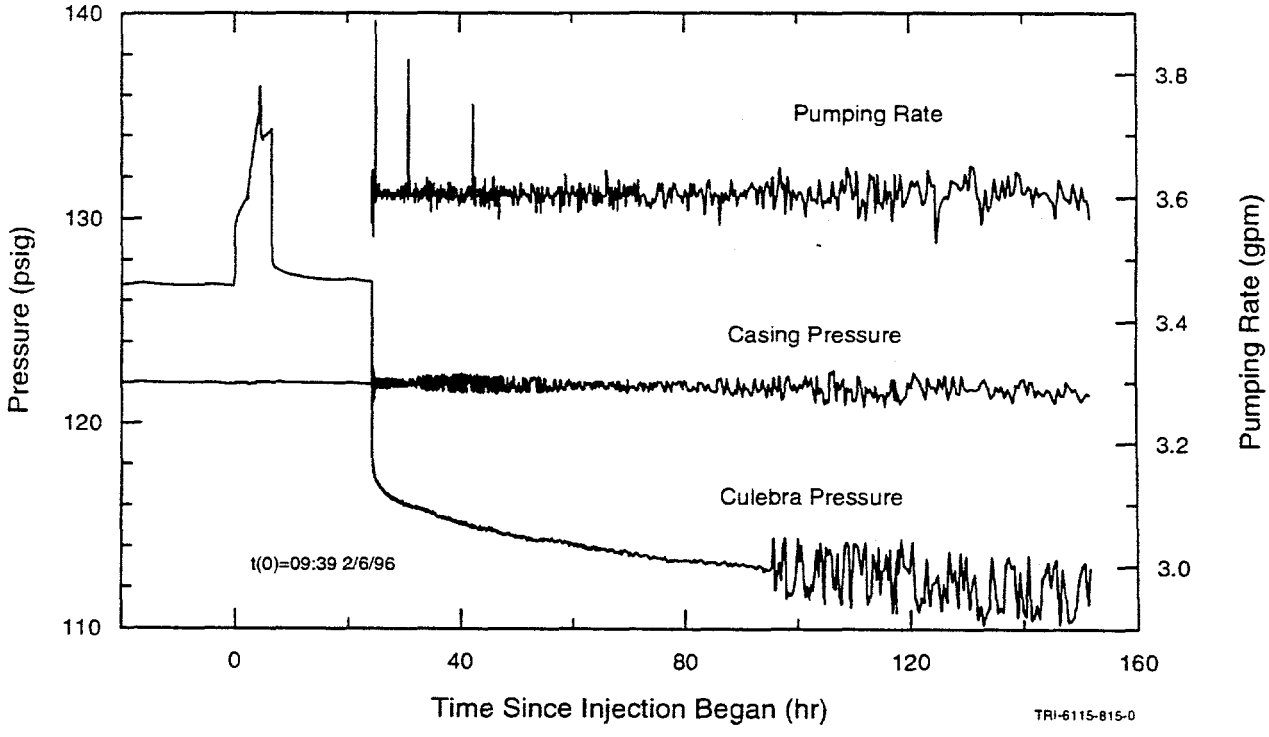

Figure 5-12. Pumping rate and pressures in H-11b1 during the H-11 tracer/pumping test.

and H-11b4 to monitor the Culebra and water levels in casing. The data from these transmitters are shown in Figure 5-13. None of the Culebra transmitters show the noise seen in the data from H-11b1 (Figure 5-12). The pressure in the H-11b2 casing held steady while the pressure in the H-11b4 casing declined by a few tenths of a psi (a few kPa) over the seven-day period shown. The casing transmitter in H-11b3 failed during the test.

5.7 H-19 Hydraulic Tests

The H-19 hydraulic tests included drillstem and slug tests of the Magenta in H-19b1, a well-development pumping test of the Culebra in H-19b2, and the H-19 tracer/pumping test of the Culebra. Data from these tests are summarized below. The tests in H-19b1 and H-19b2 were performed under the Field Operations Plan by Saulnier and Beauheim (1995). The H-19 tracer/pumping test was performed under the Test Plan by Beauheim et al. (1995).

5.7.1 H-19b1 Drillstem and Slug Tests of the Magenta

Hydraulic tests of the Magenta were conducted in H-19b1 from 2-4 March 1995. The drillstem testing (DST) sequence consisted of a 2.25-hr flow period followed by a 22.5-hr recovery period, a second flow period lasting 1.1 hr, and a second recovery period lasting 7.4 hr. A subsequent slug-withdrawal test lasted approximately 14.4 hr. The specific gravity of the Magenta fluid bailed from the well tubing was 1.01. The pressure data recorded during this test are shown in Figure 5-14.

The pressure data from the annulus between the tubing string and the borehole wall above the packer show a steady decline during the testing period. This decline probably reflects seepage of water from the hole into the open Dewey Lake and/or Forty-niner claystone. It could not reflect leakage past the packer into the Magenta interval because the Magenta pressure was higher most of the time.

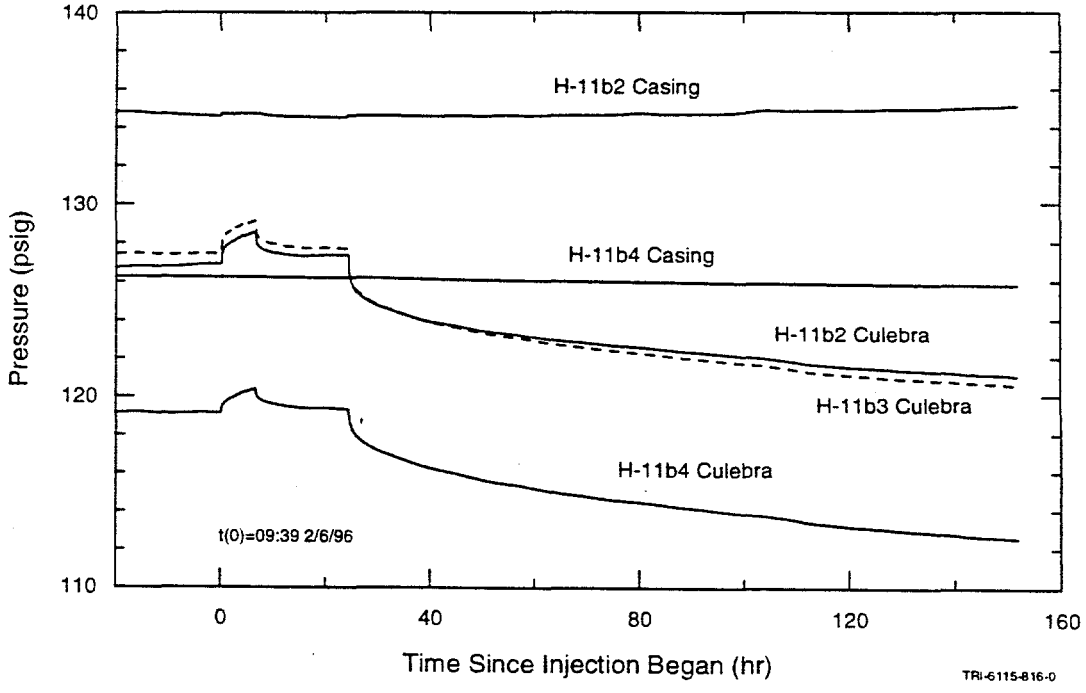

Figure 5-13. Pressures in H-11b2, H-11b3, and H-11b4 during the H-11 tracer/pumping test.

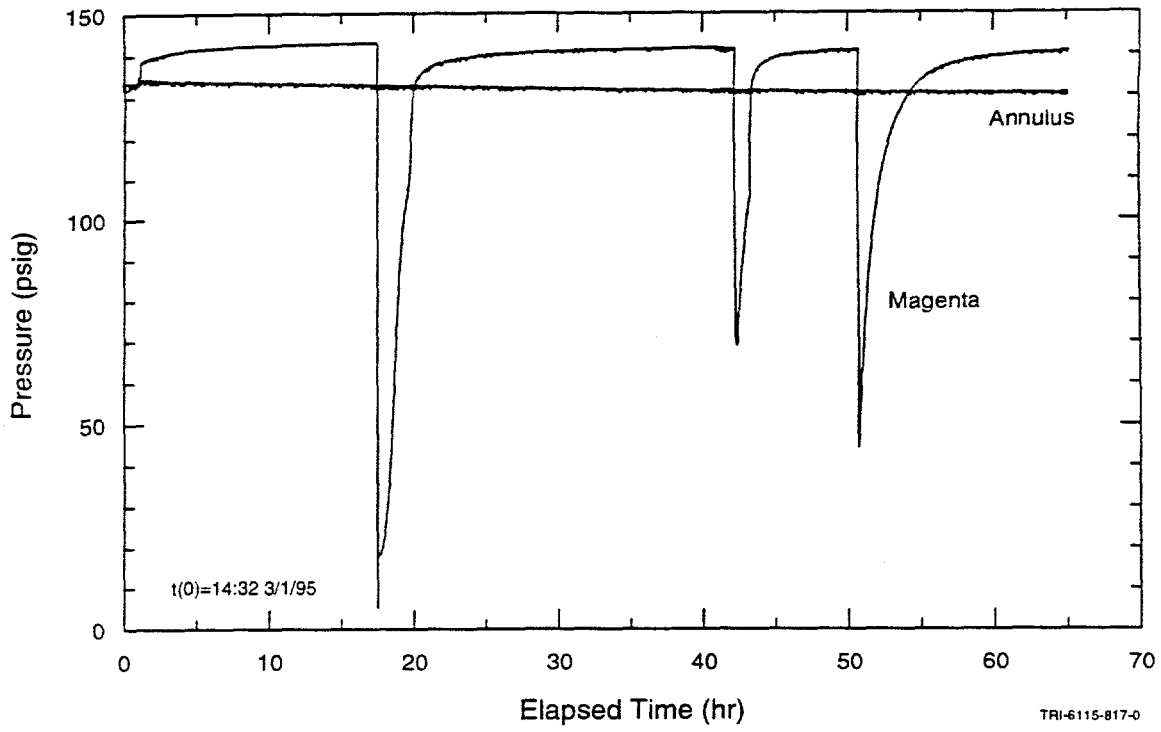

Figure 5-14. H-19b1 drillstem and slug-test data.

5.7.2 H-19b2 Well-Development Pumping Test

The well-development pumping test of the Culebra in well H-19b2 was conducted between 23 and 27 May 1995. The well was pumped at an average rate of approximately 1.9 gpm (0.12 L/s) for 6.1 hr, followed by 25.7 hr of pumping at approximately 3.8 gpm (0.24 L/s). A failure of a ground-fault interrupt (GFI) then led to 1.7 hr of pumping at a high, uncontrolled rate followed by 0.1 hr at a lower rate. Pressure recovery was monitored for approximately 50 hr. The DAS records show that the Endress & Hauser flow meter had an average reading of 0.014 gpm (0.0088 L/s) when no flow was occurring. Consequently, all readings during pumping were decreased by that value to compensate for the offset. The corrected pumping-rate data are shown in Figure 5-15. The data from the shallower of the two pressure transmitters in H-19b2 are also shown in Figure 5-15.

5.7.3 H-19 Tracer/Pumping Test

The H-19 pumping test was performed in conjunction with single-well and convergent-flow tracer tests. Tracers were injected into the lower portion of the Culebra in H-19b0 on 14 December 1995 and, after an overnight pause, pumping began on 15 December 1995. The pumping had two primary purposes: to recover the tracers previously injected into H-19b0 and to create a converging flow field on the H-19 hydropad in preparation for a multiwell tracer test involving tracer injections into wells H-19b2 through H-19b7. The hydraulic data analyzed in this report were collected between 1130 hours on 15 December 1995, when pumping of H-19b0 began, and 0806 hours on 20 December 1995, shortly before tracer injection into H-19b5 began. Pumping from H-19b0 for the tracer test continued until 11 April 1996.

For the tracer injection into H-19b0, a packer was inflated to divide the Culebra into upper

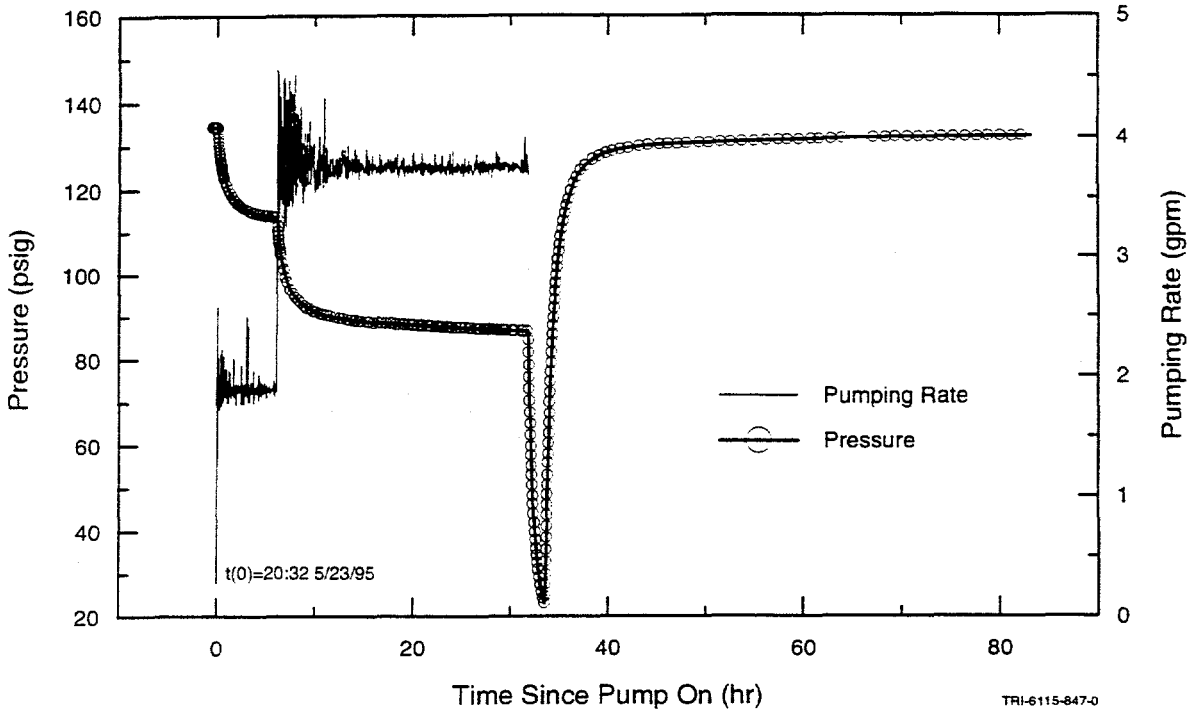

Figure 5-15. Pumping rate and pressures in H-19b2 during the well-development pumping test.

and lower portions. Deflation of this packer began approximately five minutes after the start of pumping and was complete six minutes later. The middle packers dividing the Culebra in H-19b3, H-19b5, and H-19b7 were inflated throughout the five-day period of concern.

The pumping rate during this period averaged approximately 4.4 gpm (0.28 L/s). The DAS records show that the Endress & Hauser flow meter had an average reading of 0.031 gpm (0.002 L/s) when no flow was occurring. Consequently, all readings during pumping were decreased by that value to compensate for the offset. The corrected pumping-rate data are shown in Figure 5-16. Throughout the test, the valve positioner had difficulty maintaining a constant flow rate, more so at some times than at others. For instance, the flow-meter readings continually fluctuated by as much as 0.1 gpm (0.006 L/s) and at times (e.g., 63-73, 80-92, and 106-117 hr on Figure 5-16) fluctuated by as much as 0.9 gpm (0.057 L/s). Pressure readings, particularly in the pumping well, reflected these fluctuations in the pumping rate.

Five pressure transmitters were installed in H-19b0 during the test: two monitoring the lower Culebra, two monitoring the upper Culebra, and one monitoring the water level in the casing above the packers. After the middle packer in the well was deflated, all four Culebra transmitters indicated essentially identical pressures. The data from one of the "lower Culebra" transmitters (DAS designation H190P2) and the casing transmitter are also shown in Figure 5-16. The pressure in the casing held steady throughout the five-day pumping period.

Pairs of pressure transmitters were installed in H-19b2, H-19b4, and H-19b6: one monitoring the Culebra and one monitoring the water level in the casing. The data from these transmitters are shown in Figure 5-17. The pressure in the H-19b2 casing held steady

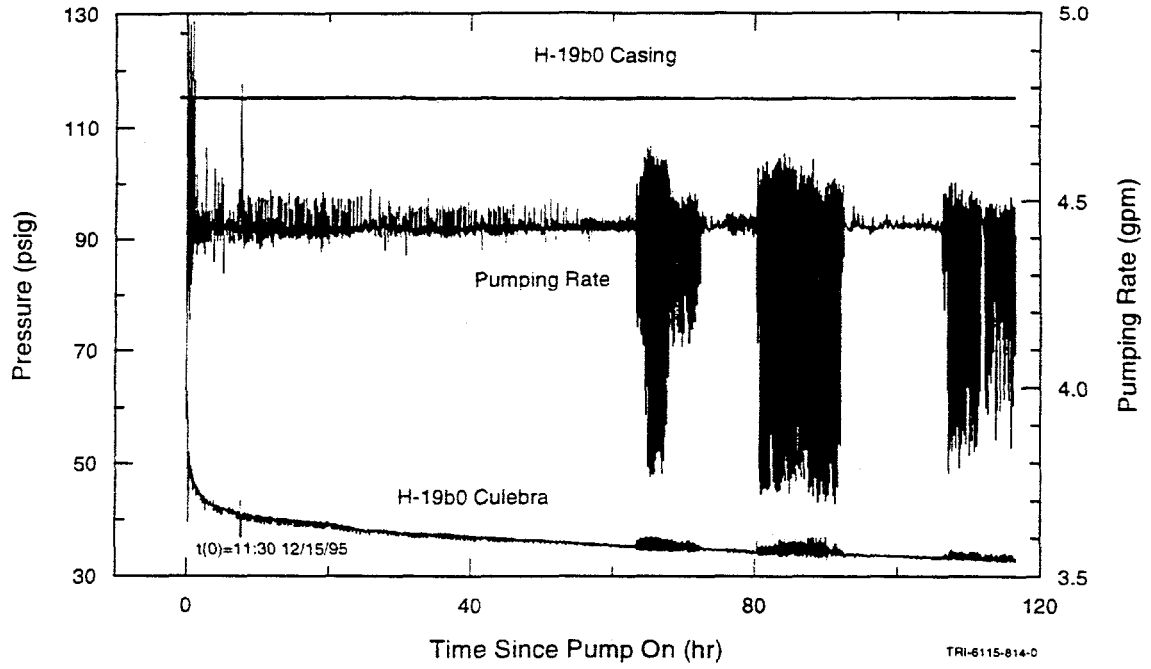

Figure 5-16. Pumping rate and pressures in H-19b0 during the H-19 tracer/pumping test.

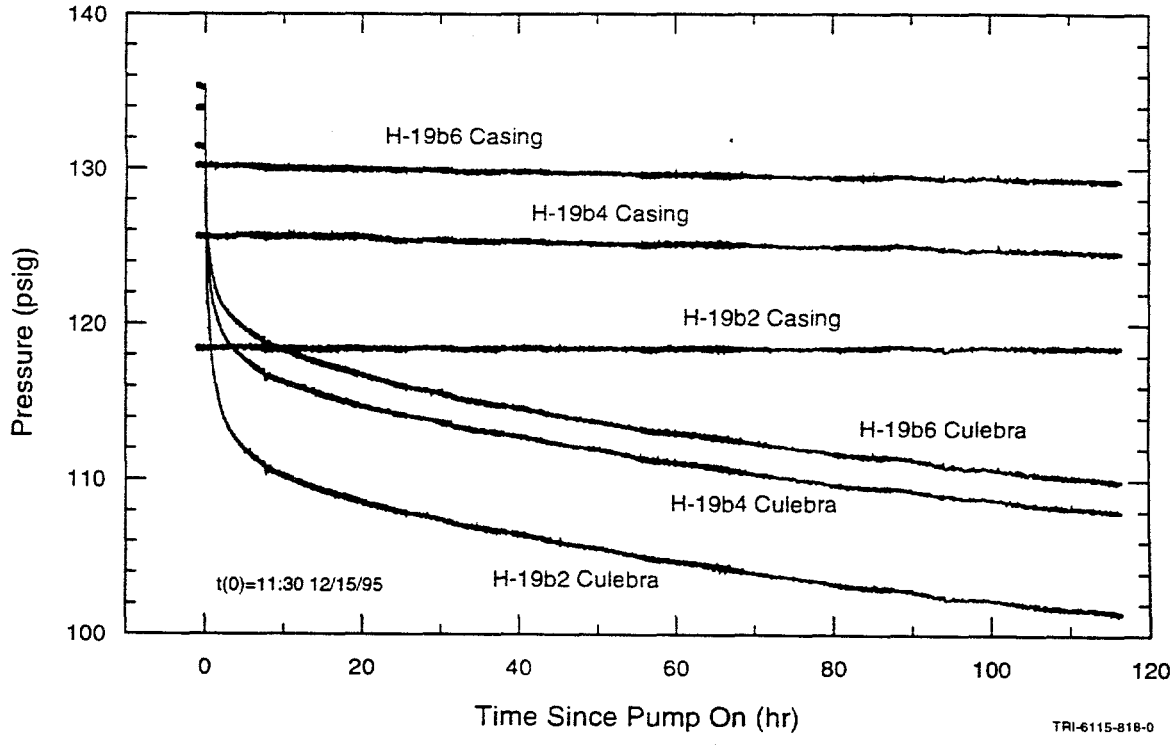

Figure 5-17. Pressures in H-19b2, H-19b4, and H-19b6 during the H-19 tracer/pumping test.

while the pressures in the H-19b4 and H-19b6 casing declined by approximately one psi (7 kPa) over the five-day period.

Three pressure transmitters were installed in each of H-19b3, H-19b5, and H-19b7: one monitoring the lower Culebra, one monitoring the upper Culebra, and one monitoring the water level in the casing. The data from H-19b3, H-19b5, and H-19b7 are shown in Figures 5-18, 5-19, and 5-20, respectively. Drawdowns in the upper and lower Culebra in both H-19b3 and H-19b7 tracked each other within a few tenths of a psi (a few kPa) throughout the test, while the drawdown in the upper Culebra in H-19b5 was 1-2 psi (7-14 kPa) lower than that in the lower Culebra. Pressures in the H-19b3 and H-19b7 casing held steady, but the pressure in the H-19b5 casing declined by approximately five psi (35 kPa) over the five-day period. Presumably, water in the H-19b5 casing was leaking past the upper packer into the upper-Culebra interval, causing the drawdown there to be less than it would otherwise have been.

5.8 P-14 Air-Lift Pumping Test

The airlift pumping test at well P-14 was performed under a Field Operations Plan by INTERA Technologies, Inc. (1986c). Details of the test have been reported in Stensrud et al. (1990). Summary information is as follows. Prior testing of P-14 indicated possible casing or perforation damage and poor formation-to-well communication. In February 1989, the P-14 casing was reperforated across the Culebra interval from 573 to 601 ft (174.7 to 183.2 m) BGS, after which the well was acid treated. After reperforation, acid treatment, and development, the pumping rate had increased from a previous low of 4.6 gpm (0.29 L/s) to as high as 80.4 gpm (5.07 L/s).

The pumping test was started at 0901 hours on 14 February 1989. The air compressor was shut off from 0950 to 1200 hours on 14 February 1989 because of a silting problem. The compressor was then operated until 1200 hours on 17 February 1989, and recovery

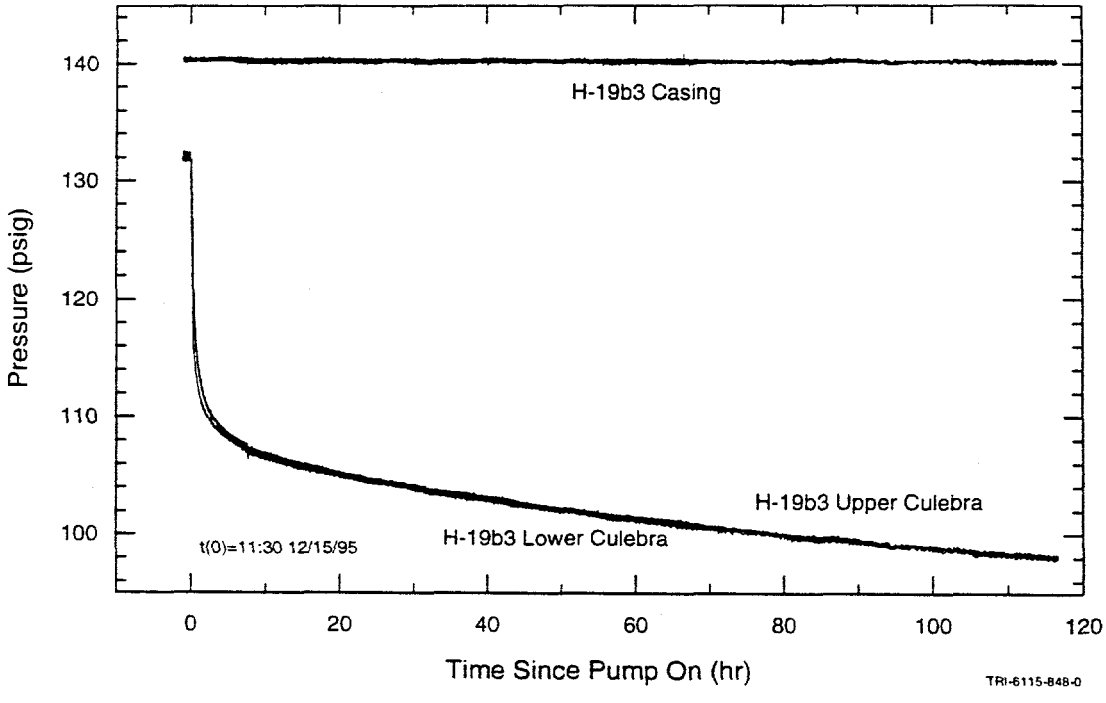

Figure 5-18. Pressures in H-19b3 during the H-19 tracer/pumping test.

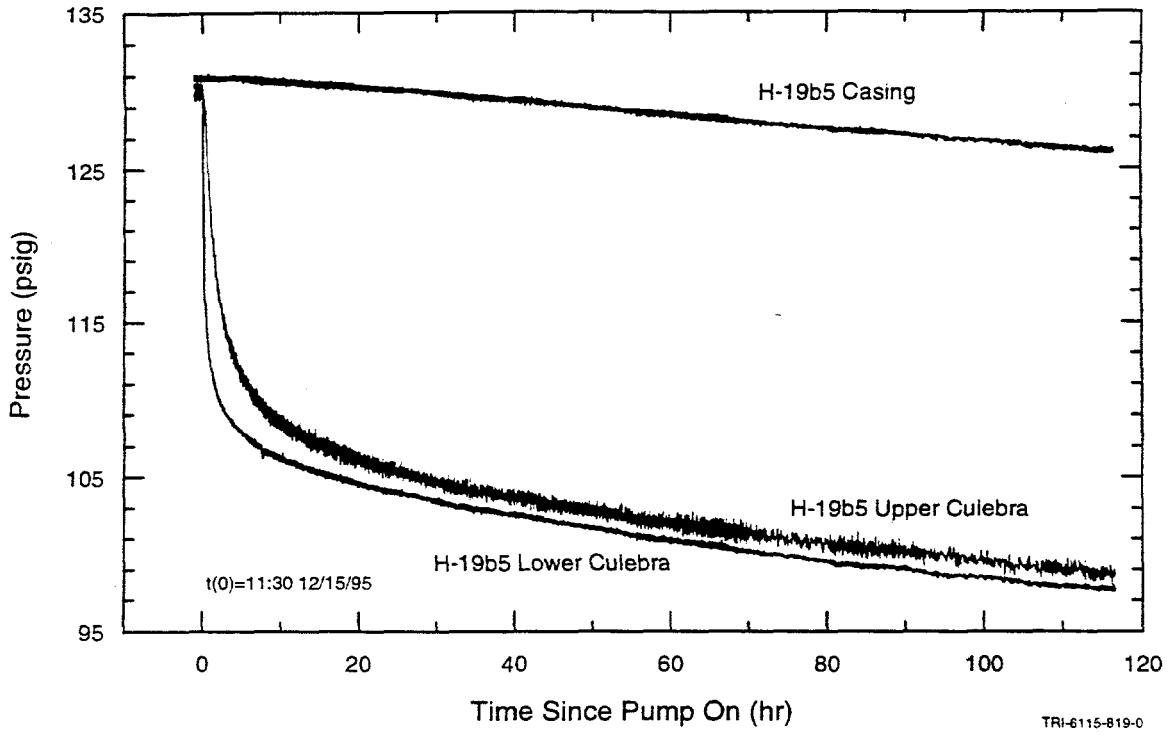

Figure 5-19. Pressures in H-19b5 during the H-19 tracer/pumping test

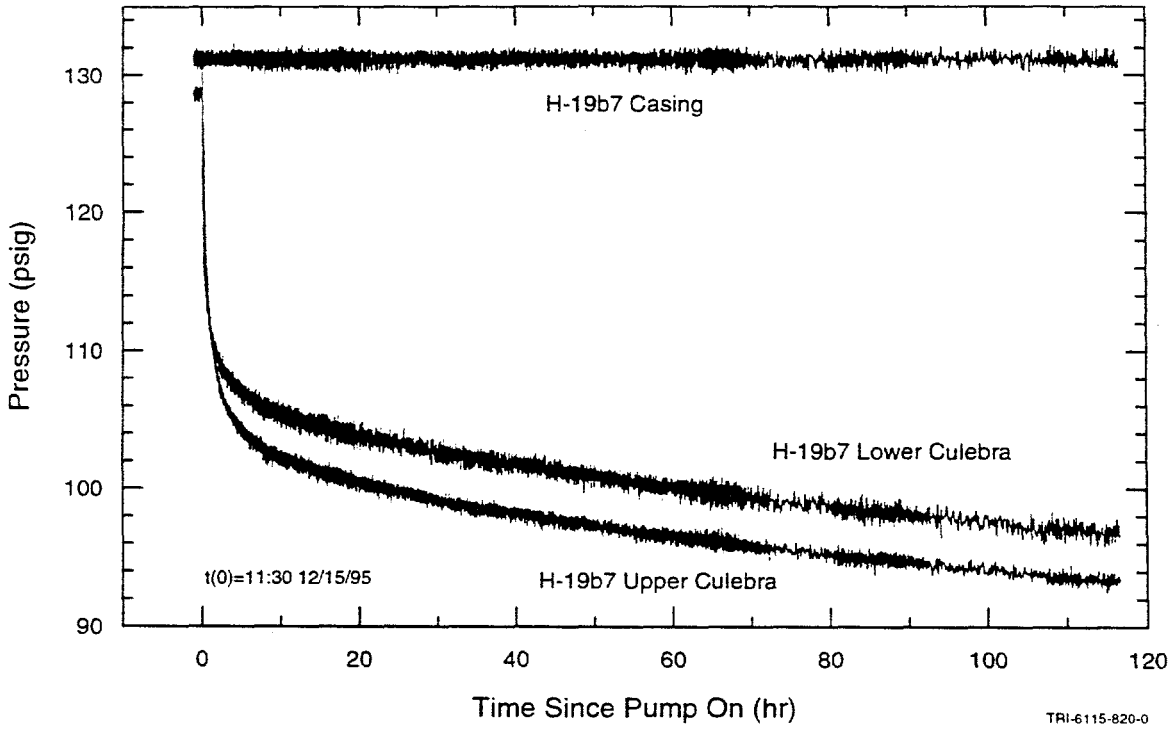

Figure 5-20. Pressures in H-19b7 during the H-19 tracer/pumping test

was monitored until 8 March 1989. The DAS was used only on well P-14; all other wells were gauged manually with water-level probes (Stensrud et al., 1990). The total volume of fluid pumped during the pumping test was approximately 252,000 gallons (953,800 L) at an average pumping rate of approximately 58 gpm (3.66 L/s). Figure 5-21 is a plot of the pumping rate versus time and Figure 5-22 shows pressures in well P-14. Figure 5-23 is a plot of barometric pressure versus time during the P-14 pumping test. Data were collected and recorded by the DAS for the period from 26 January through 8 March 1989.

Water levels were measured at observation wells D-268, DOE-2, H-2b2, H-6b, H-18, WIPP-13, WIPP-25, and WIPP-26 during the P-14 pumping test. Only the responses at the three closest wells, D-268, H-6b, and WIPP-25, shown in Figures 5-24 through 5-26, were adequately defined for analysis. D-268, H-6b, and WIPP-25 are 10,250 ft (3,125 m), 11,090 ft (3,380 m), and 11,125 ft (3,390 m), respectively, from P-14. The observation-well data show distinct influences from barometric fluctuations. Barometric effects were removed from the data by first converting the depth-to-water measurements to estimated pressures at the middle of the Culebra, calculating the barometric efficiency of each well, and applying an appropriate compensation. Depth-to-water measurements were converted to middle-of-Culebra pressures by calculating the pressure exerted by the column of water in the well, given the specific gravity of the water and the height of the column.

The barometric efficiency (BE) is defined by Domenico and Schwartz (1990, p. 128) as:

$$BE = \gamma_w \, (dh/dP_a)$$

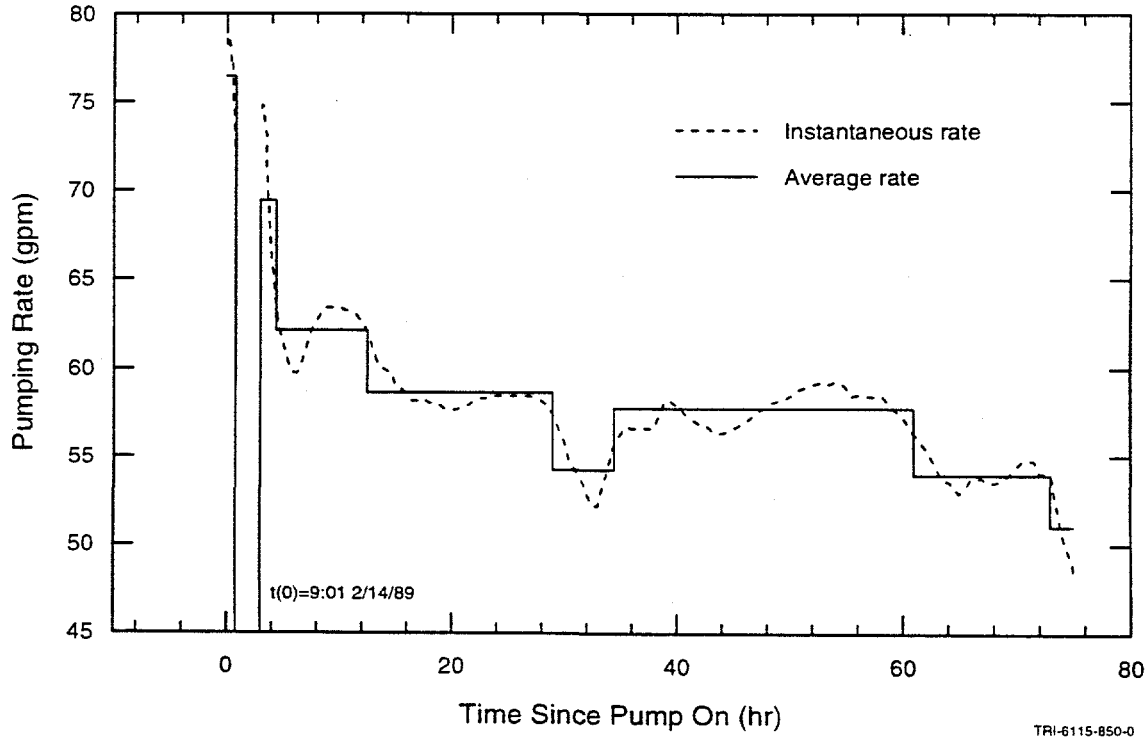

Figure 5-21. Pumping rate during the P-14 pumping test.

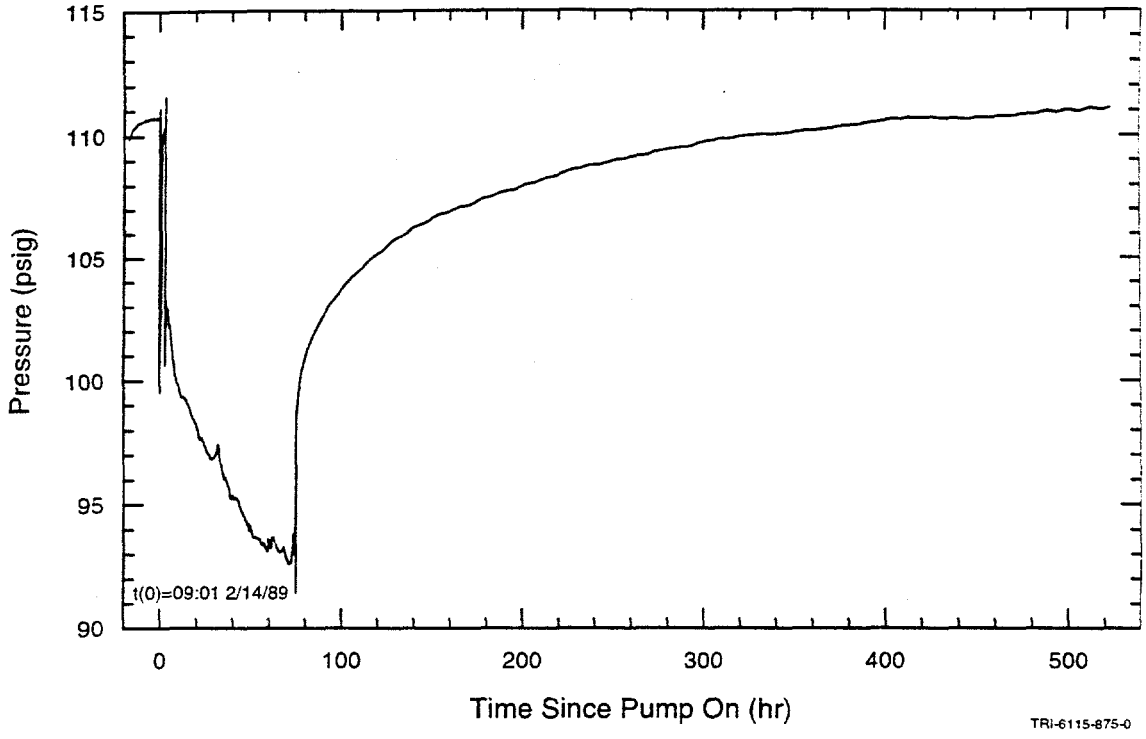

Figure 5-22. Pressure in P-14 during the P-14 pumping test.

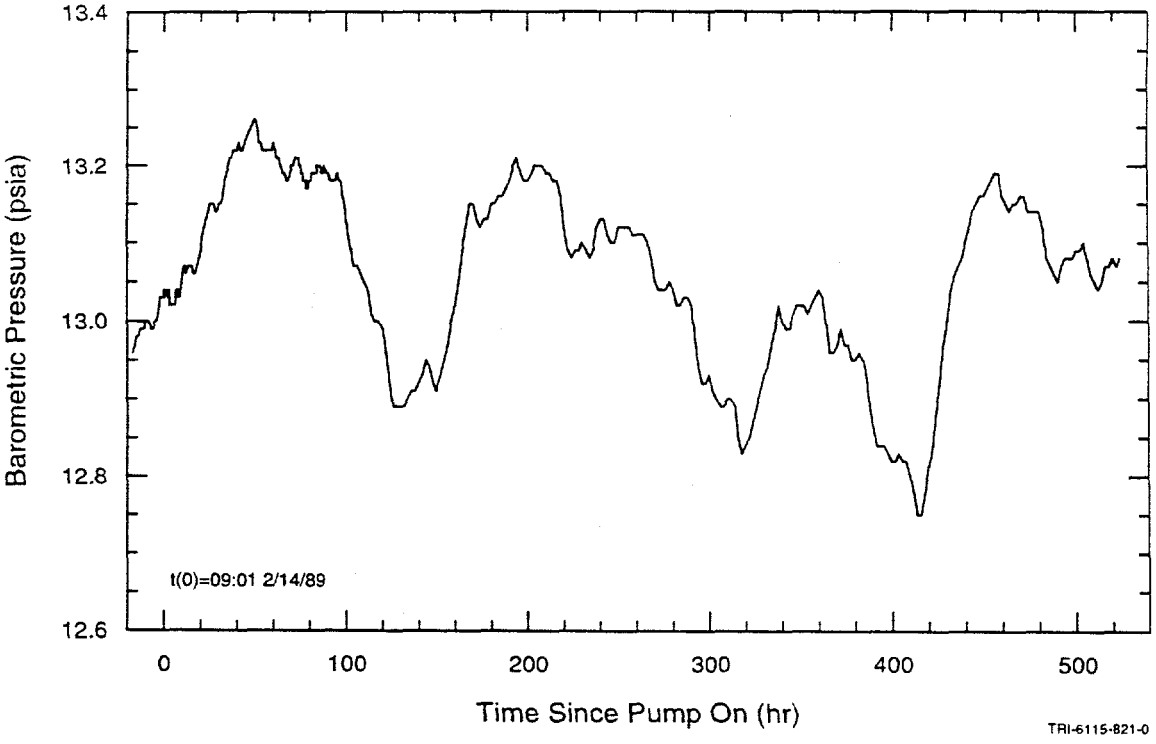

Figure 5-23. Barometric pressure during the P-14 pumping test.

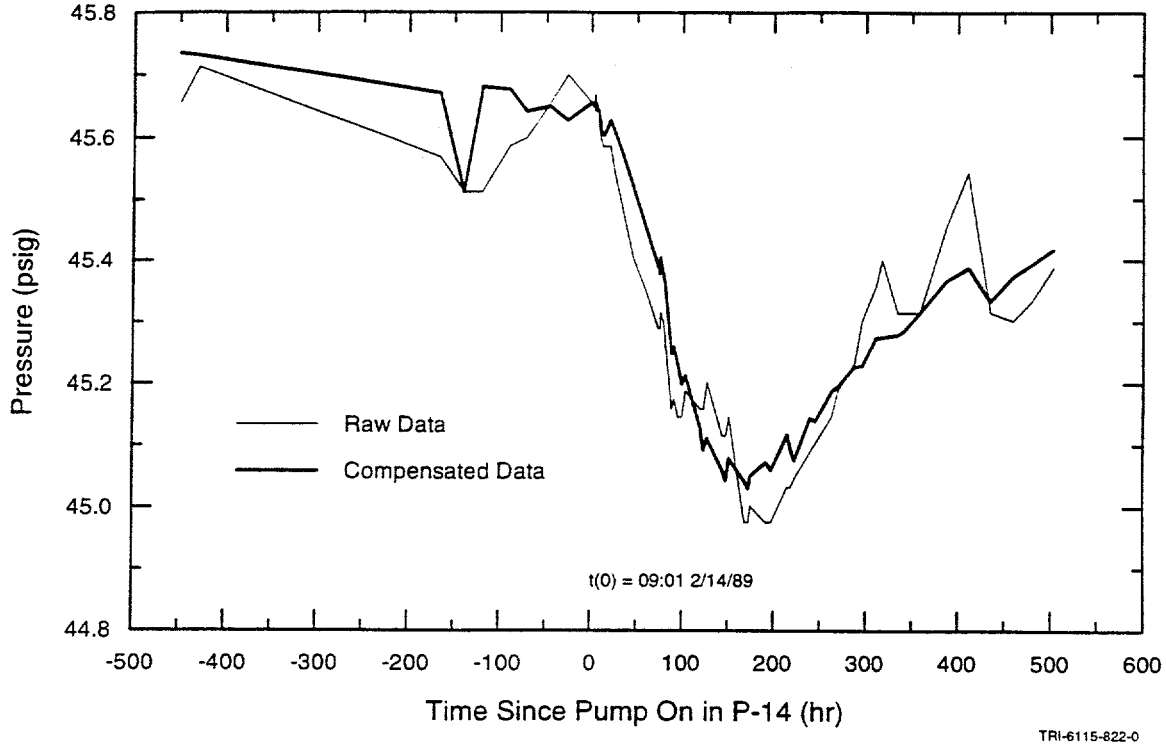

Figure 5-24. Pressure in D-268 during the P-14 pumping test.

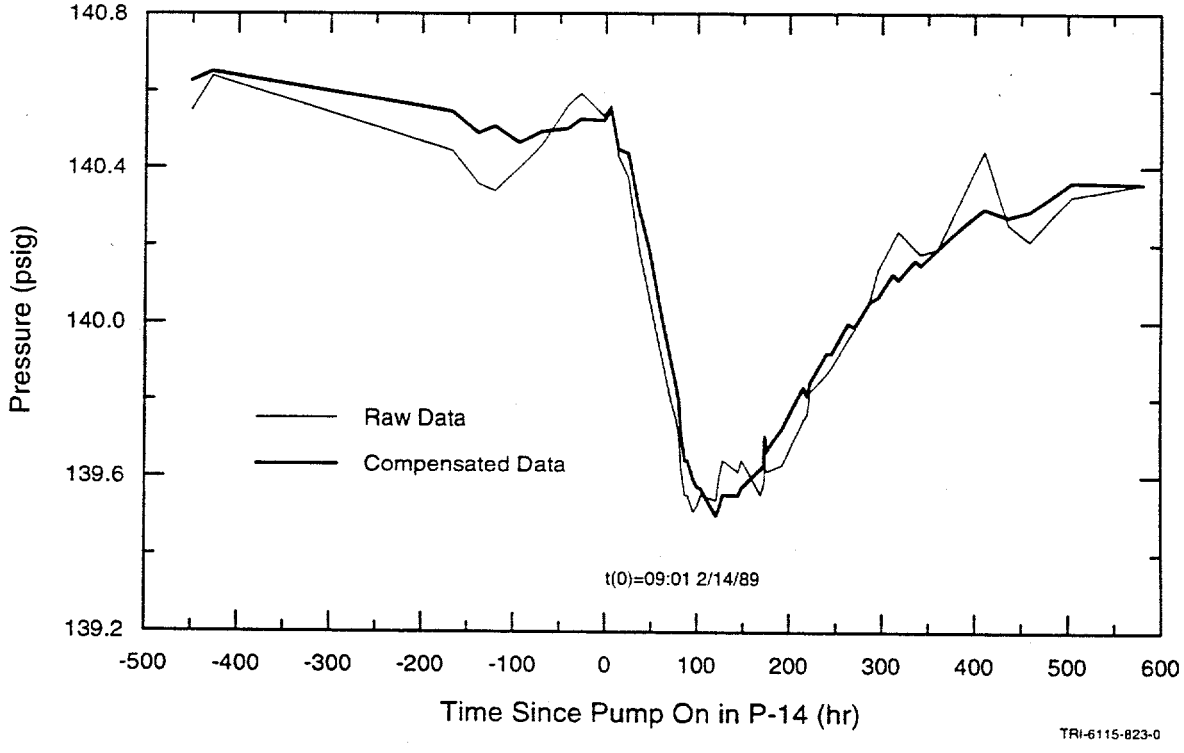

Figure 5-25. Pressure in H-6b during the P-14 pumping test.

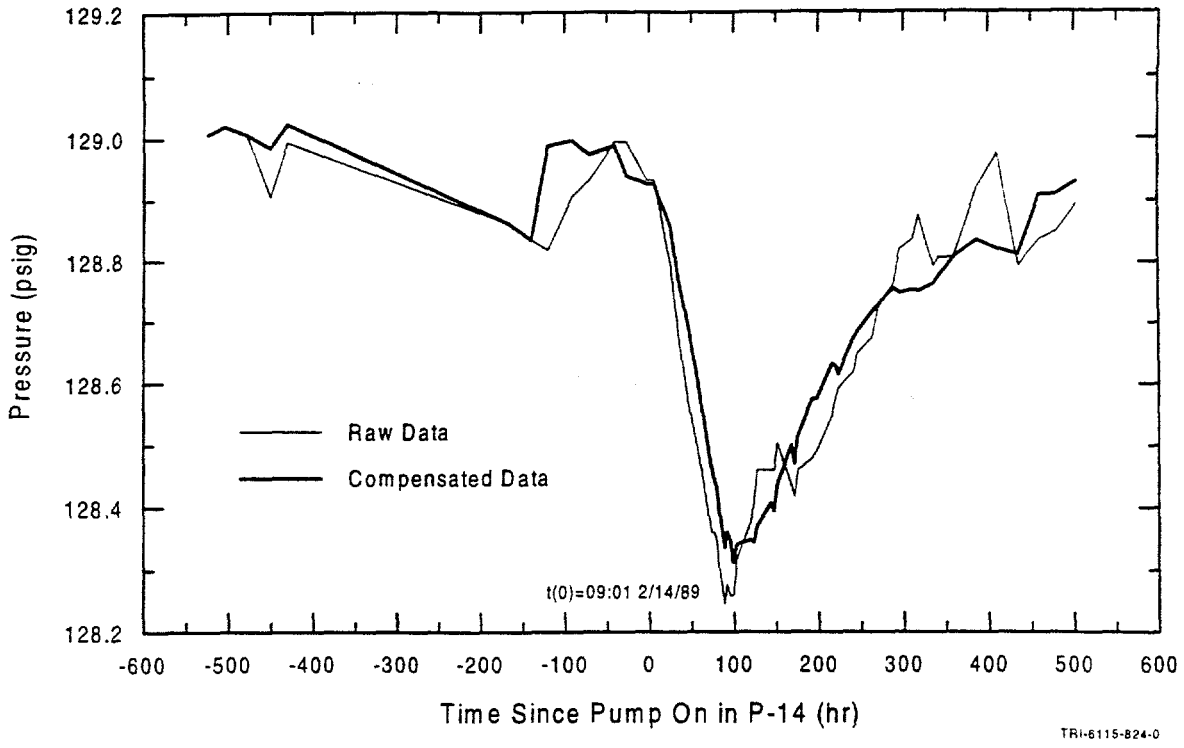

Figure 5-26. Pressure in WIPP-25 during the P-14 pumping test.

where:

γ_w = specific gravity of the fluid,
dh = change in hydraulic head, and
dP_a = change in atmospheric (barometric) pressure.

Barometric efficiencies were determined for each well by applying compensations for values of 0.3, 0.4, 0.5, 0.6, 0.7, and 0.8, graphing the data, and determining visually which compensation provided the smoothest data curve. In all cases, a value of 0.6 yielded the best compensation. The compensations were performed using the following equation:

$$CP(t) = P(t) + BE\ (BP(t) - 13.04\ psia)$$

where:

$CP(t)$ = pressure compensated for barometric effects (psig),
$P(t)$ = uncompensated pressure (psig),
BE = barometric efficiency (-),
$BP(t)$ = barometric pressure (psia), and
$13.04\ psia$ = barometric pressure at the start of the test.

The effects of compensating pressure for barometric effects can be seen in Figures 5-24 to 5-26, and consist of damping of the oscillations from barometric-pressure changes while preserving the overall trends.

5.9 WIPP-27 Slug Tests

A series of six slug tests was conducted by the USGS in WIPP-27 between 1000 hours and 1108 hours, 23 August 1980 under a Field Operation Plan by Statler (1980). A displacement barrel (Basler, 1983) was used to create the pressure differential within the well. In the first, third, and fifth tests, the barrel was lowered into the water and decay of the resultant pressure buildup was monitored. In the second, fourth, and sixth tests, the displacement barrel (which had been sub-

merged to initiate the first, third, and fifth tests) was raised out of the water and pressure recovery was observed. The fourth test was aborted due to an instrument malfunction. Test descriptions and data are provided by Richey (1987). The two successful slug-withdrawal tests, #2 and #6, were judged to have the best-quality data and were selected for analysis. The complete test data are shown in Figure 5-27.

5.10 WIPP-28 Slug Tests

Five slug tests were performed by the USGS in WIPP-28 under a Field Operation Plan by Statler (1980). A slug-injection test was performed between 1330 hours and 1400 hours, 21 August 1980, with a PIP installed in the well on 2.375-inch (6.0-cm) tubing. After removal of the PIP, four slug-displacement tests were run between 1000 hours and 1340 hours, 25 August 1980. In tests #2 and #4, a displacement barrel was lowered into the water, while in tests #3 and #5, the displacement barrel was raised. Test descriptions and data are provided by Richey (1987). The first slug-withdrawal test, #3, was judged to have the best-quality data and was selected for analysis. The data from the four slug-displacement tests are shown in Figure 5-28.

5.11 WQSP-1 Pumping Test

The WQSP-1 pumping test was conducted in January and February 1996 under the Test Plan by Stensrud (1995). WQSP-1 was pumped from 1318 hours on 25 January 1996 until 0741 hours on 28 January 1996 at an average rate of 6.8 gpm (0.43 L/s). The flow line was not completely full when the test was started, preventing the flow controller from maintaining a constant rate initially. As a result, the pumping rate fluctuated between 4.4 gpm (0.28 L/s) and an unknown upper value during the first five minutes of the test. For the balance of the test, the flow rate did not go below 6.3 gpm (0.40 L/s) and averaged 6.8 gpm (0.43 L/s). The DAS records show

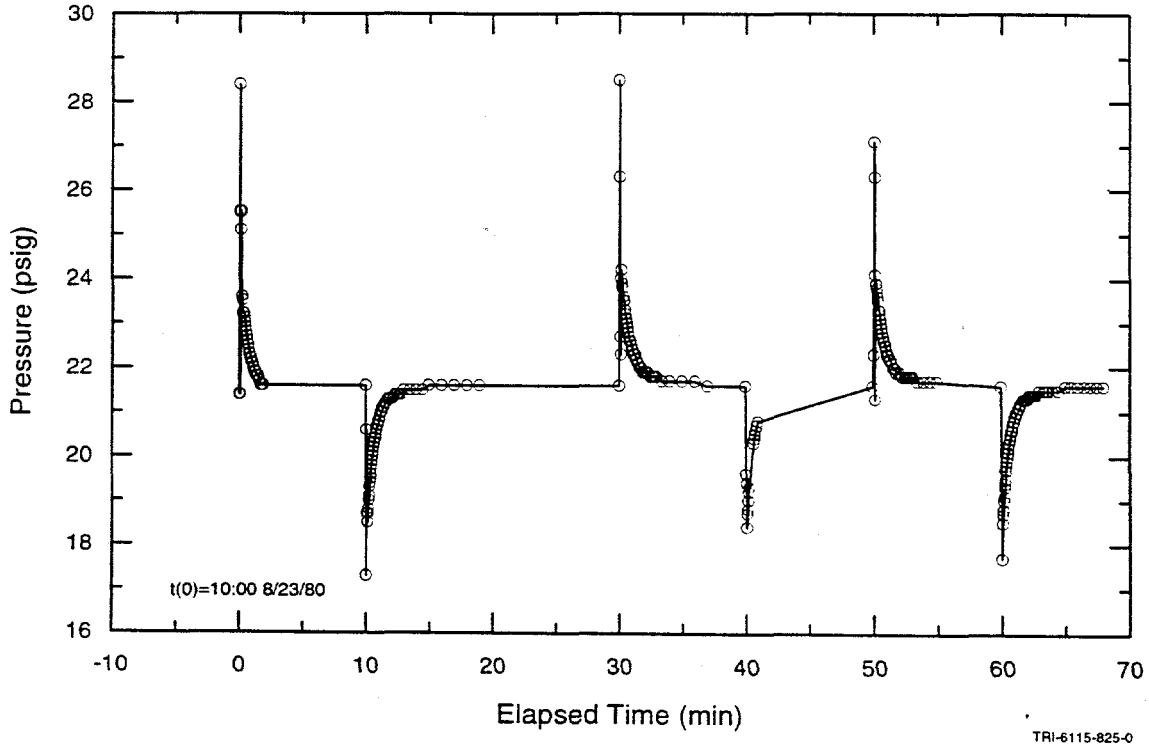

Figure 5-27. WIPP-27 slug-test data.

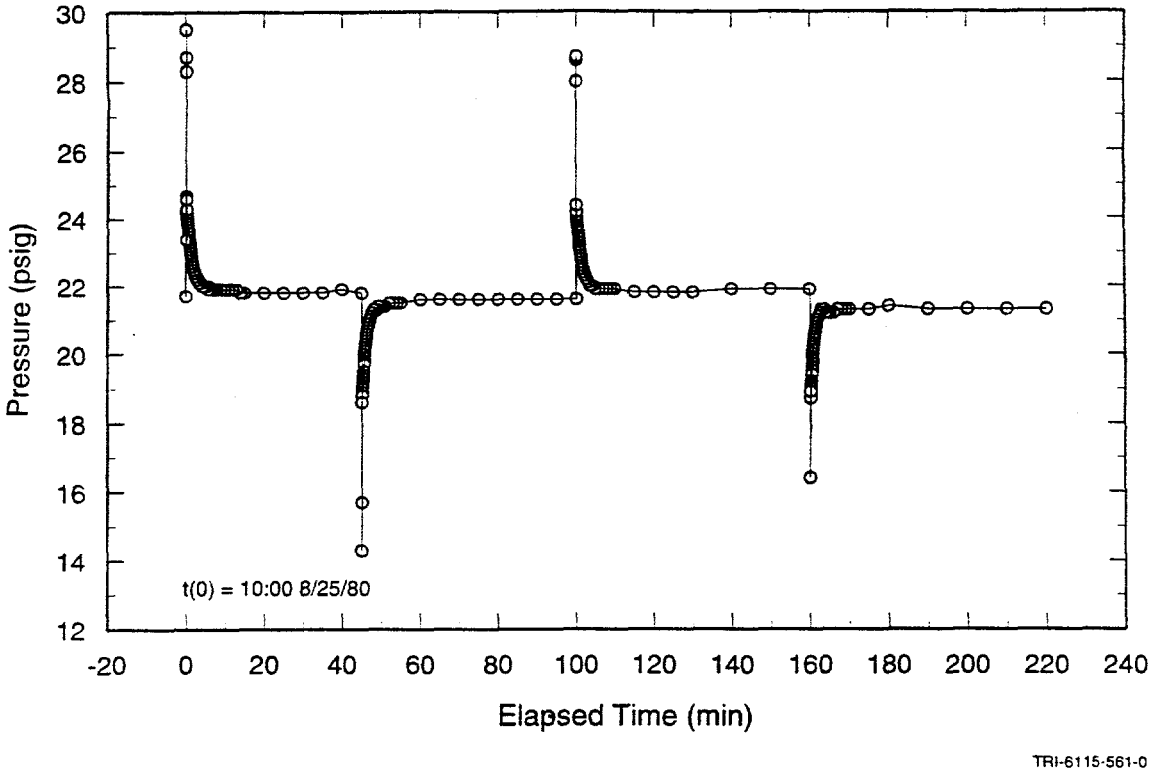

Figure 5-28. WIPP-28 slug-displacement test data.

that the Endress & Hauser flow meter had an average reading of -0.054 gpm (-0.0034 L/s) when no flow was occurring. Consequently, all readings during pumping were increased by 0.054 gpm (0.0034 L/s) to compensate for this offset. The corrected pumping-rate data are shown in Figure 5-29.

One of the transducers in WQSP-1 failed on 29 January 1996. The pressure data from the other transducer in WQSP-1 are shown in Figure 5-30. The pressure increased for an unknown reason on 4 February 1996 for approximately nine hours (244-253 hr on Figure 5-30) before returning to its previous level. The check valve in the flow line in WQSP-1 leaked when the pump was turned off, allowing backflow into the well. The recovery data were, therefore, uninterpretable and recovery monitoring at WQSP-1 was terminated at 1138 hours on 6 February 1996.

Troll memory gauges (see Section 4.8) were used to monitor pressures in wells H-18 and WIPP-13 during the WQSP-1 pumping test. The responses in these two wells were not affected by the leaking check valve in WQSP-1, allowing recovery data to be collected until the start of the WQSP-2 pumping test at 1130 hours on 20 February 1996. Data from H-18 and WIPP-13 are shown in Figures 5-31 and 5-32, respectively. The data from H-18 and WIPP-13 were clearly affected by fluctuations in barometric pressure. The record of barometric pressures measured at the H-19 hydropad during the period of the WQSP-1 pumping test is shown in Figure 5-33. No barometric data were available over the intervals from approximately 114 to 144 and 144 to 186 hr after pumping began. The barometric data were used to determine barometric efficiencies of H-18 and WIPP-13 and compensate the observed pressure data using the procedure

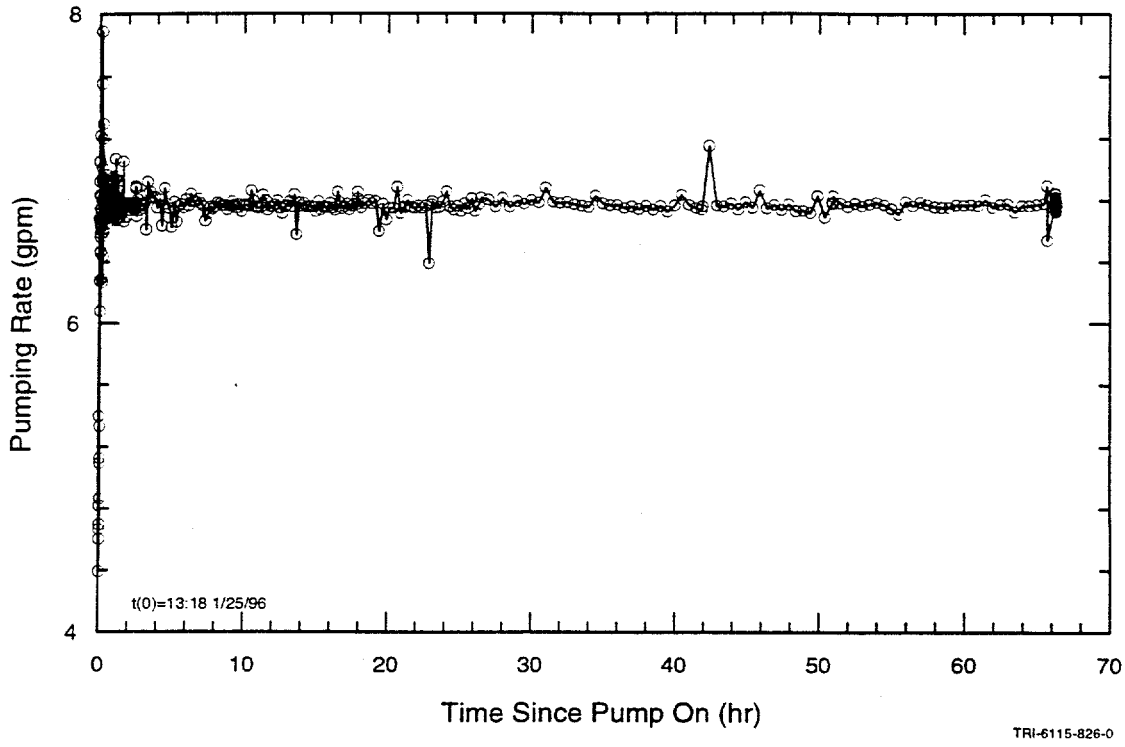

Figure 5-29. Pumping rate during the WQSP-1 pumping test.

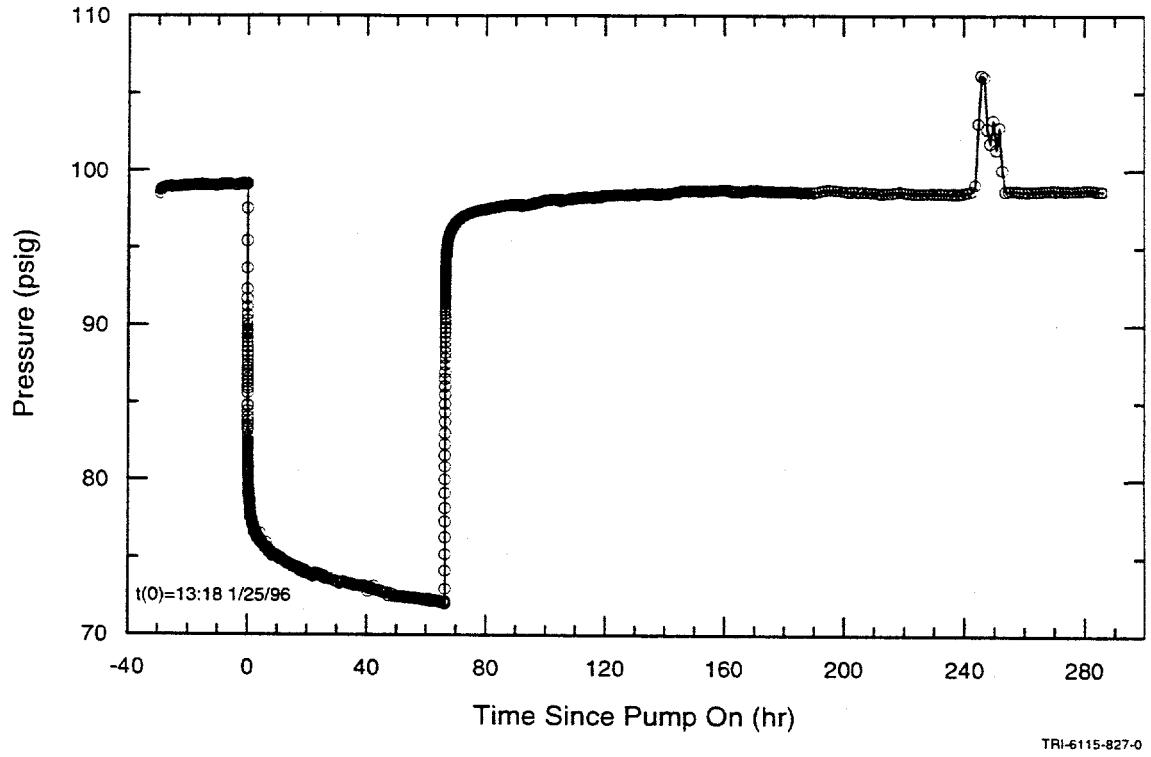

Figure 5-30. Pressure in WQSP-1 during the WQSP-1 pumping test.

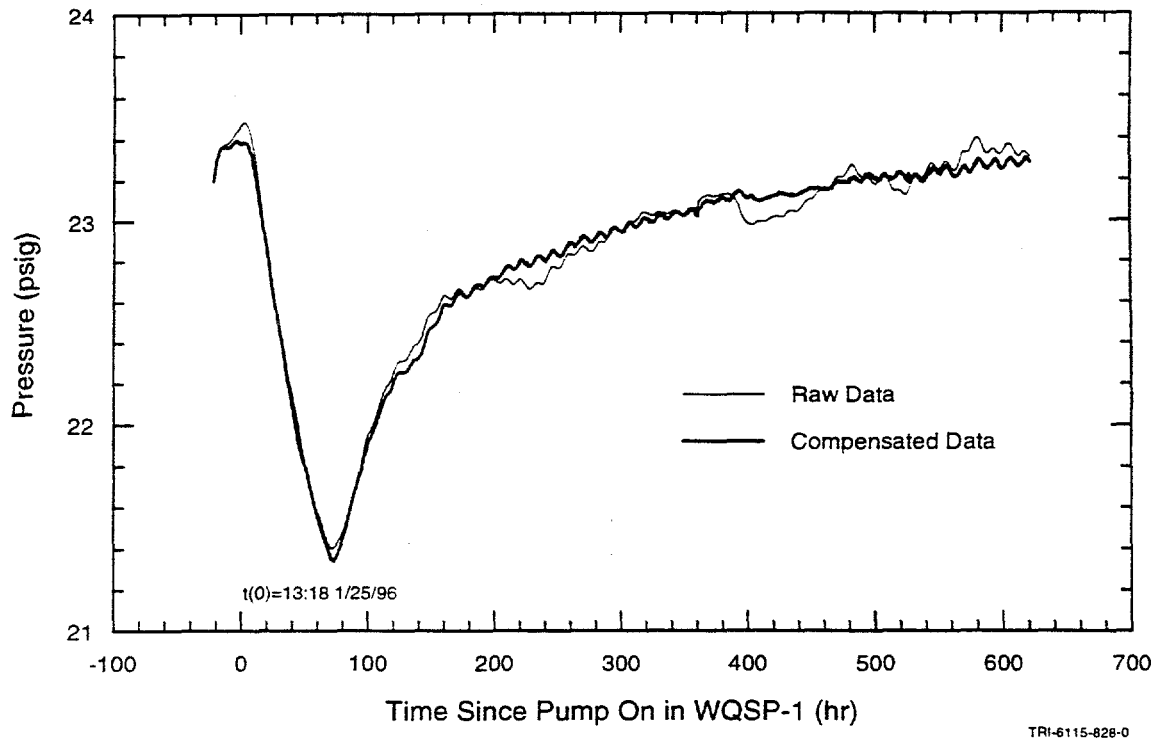

Figure 5-31. Pressure in H-18 during the WQSP-1 pumping test.

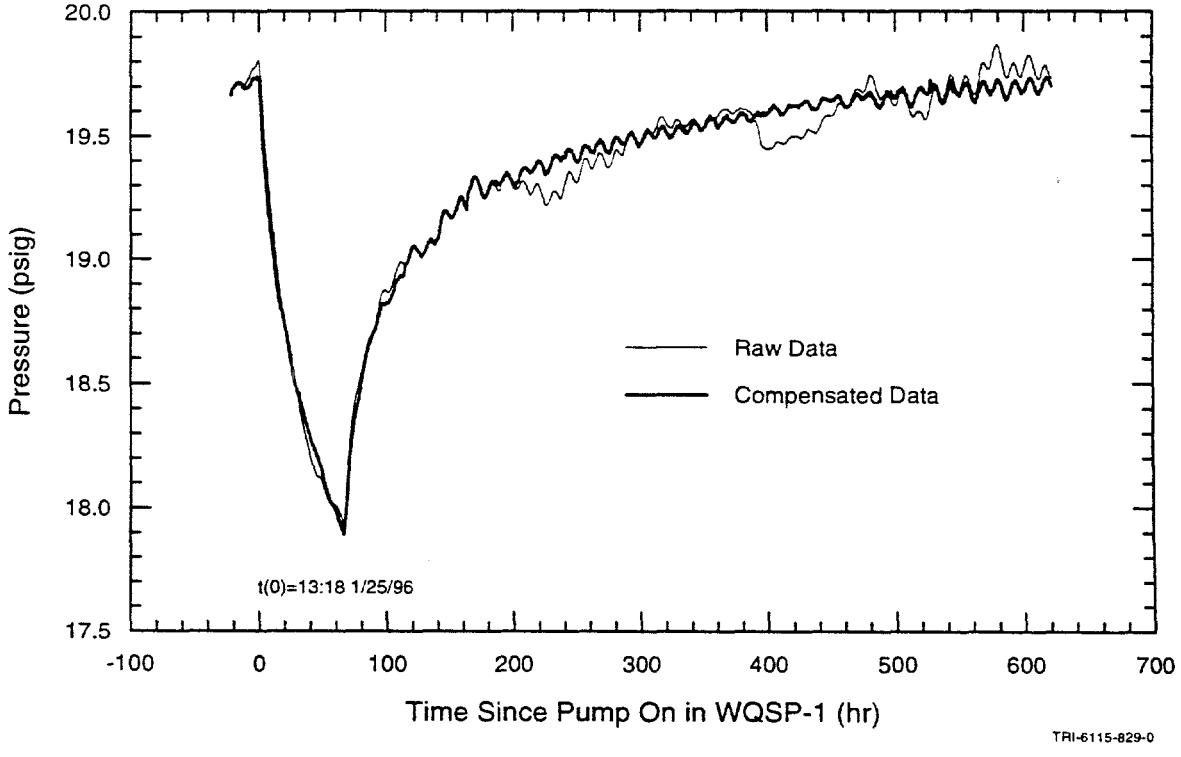

Figure 5-32. Pressure in WIPP-13 during the WQSP-1 pumping test.

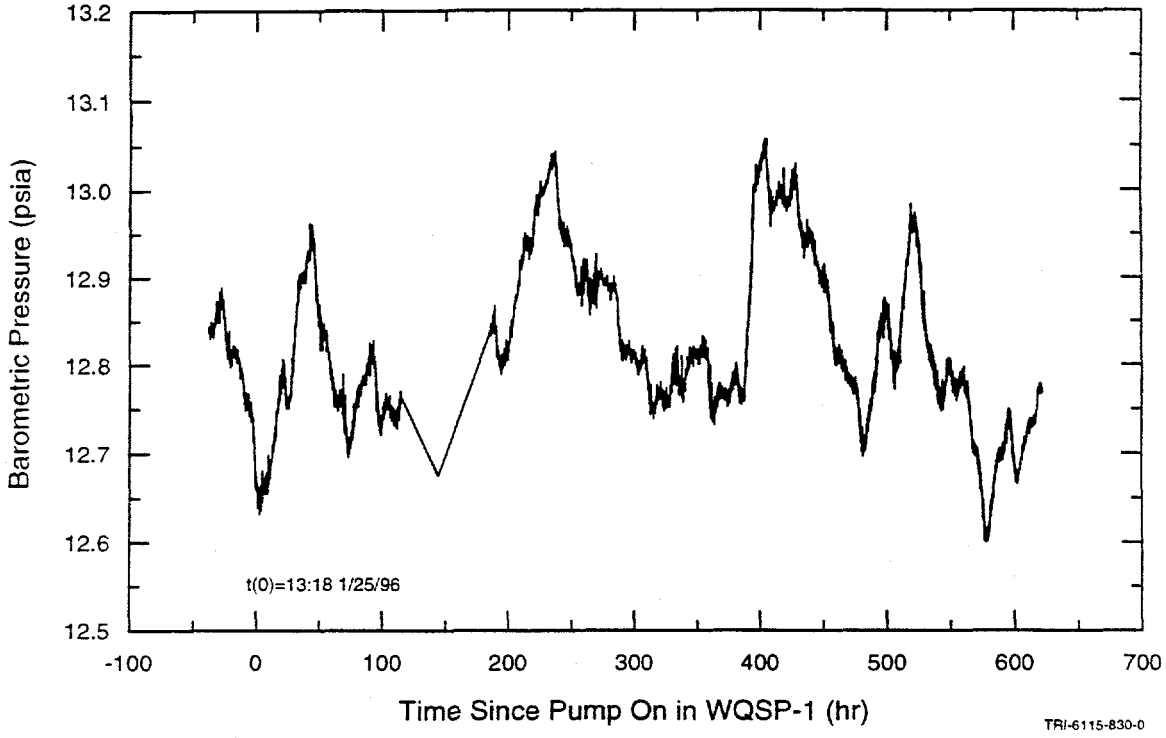

Figure 5-33. Barometric pressure during the WQSP-1 pumping test.

outlined in Section 5.7. The barometric efficiency of H-18 was determined to be 0.6 and that of WIPP-13 was determined to be 0.7. The barometric-compensated pressure data for H-18 and WIPP-13 are shown in Figures 5-31 and 5-32, respectively. Diurnal fluctuations caused by earth tides are clearly evident in the compensated data from both wells.

5.12 WQSP-2 Pumping Test

The WQSP-2 pumping test was conducted in February and March 1996 under the Test Plan by Stensrud (1995). WQSP-2 was pumped for exactly four days beginning at 1130 hours on 20 February 1996 at an average rate of 7.1 gpm (0.45 L/s). The pumping rate fluctuated between 4.2 and at least 11.2 gpm (0.26 and 0.71 L/s) during the first five minutes of the test, but was stable at approximately 7.1 gpm (0.45 L/s) for the remainder of the test. The DAS records show that the Endress & Hauser flow meter had an average reading of -0.029 gpm (-0.0018 L/s) when no flow was occurring. Consequently, all readings during pumping were increased by 0.029 gpm (0.0018 L/s) to compensate for this offset. The corrected pumping-rate data are shown in Figure 5-34.

The pressure data from the transducer in WQSP-2 are shown in Figure 5-35. The check valve in the flow line in WQSP-2 leaked when the pump was turned off, allowing backflow into the well. The recovery data were, therefore, uninterpretable and recovery monitoring at WQSP-2 was terminated at 1356 hours on 1 March 1996.

Troll memory gauges (see Section 4.8) were used to monitor pressures in wells DOE-2, H-18, WIPP-12, WIPP-13, WIPP-18, and WIPP-19 during the WQSP-2 pumping test. Water levels were monitored in wells WQSP-1 and WQSP-3 during the test. Responses that appeared interpretable were observed in wells DOE-2, H-18, WIPP-12,

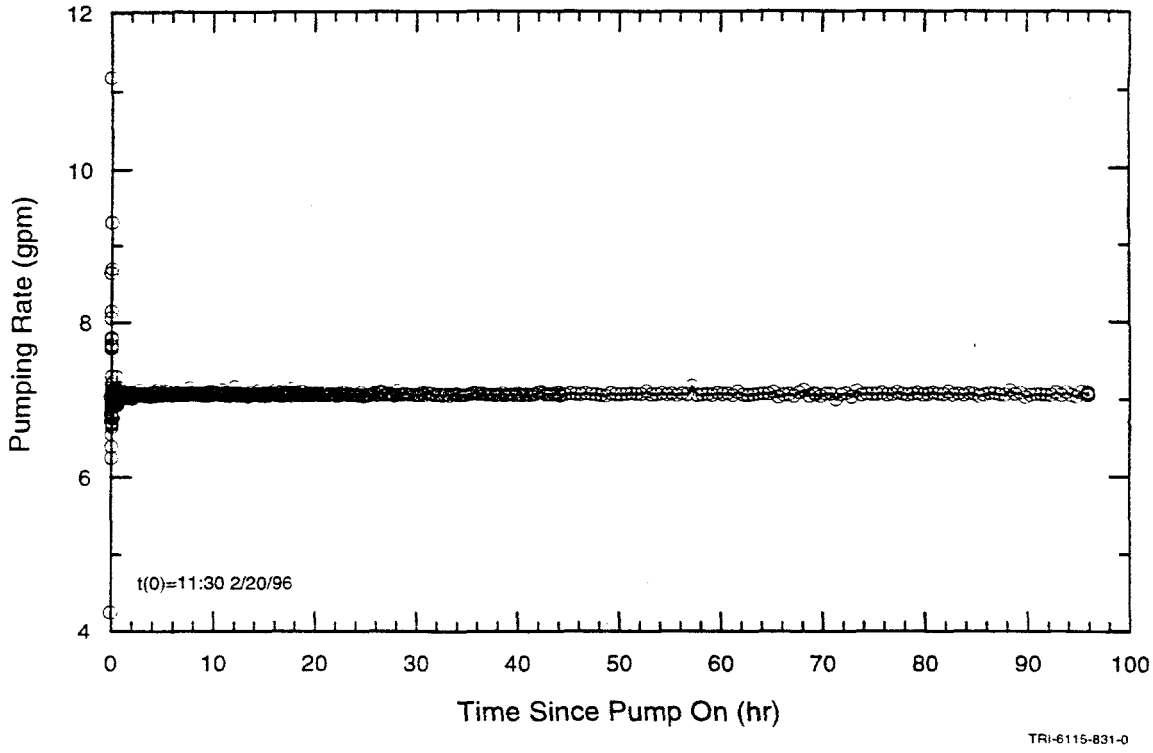

Figure 5-34. Pumping rate during the WQSP-2 pumping test.

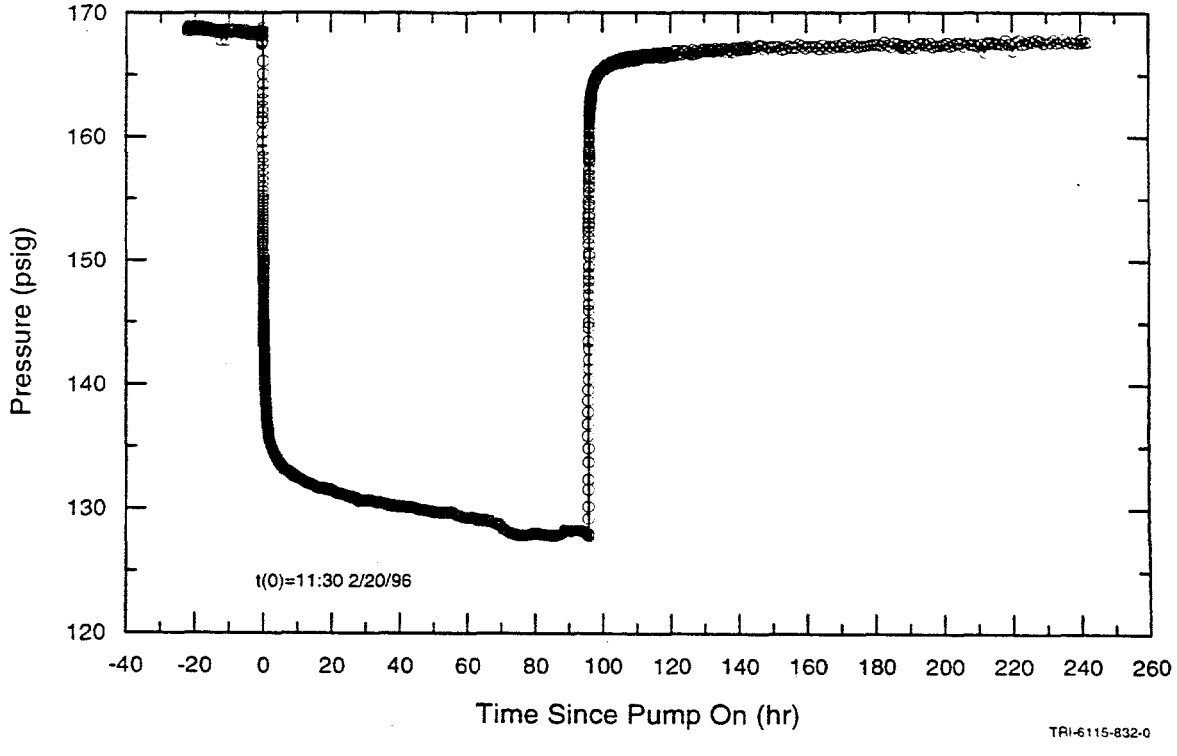

Figure 5-35. Pressure in WQSP-2 during the WQSP-2 pumping test.

WIPP-13, and WQSP-1. Recovery data were collected until 24 March 1996 in WQSP-1, until 28 March 1996 in DOE-2, H-18, and WIPP-13, and until 25 April 1996 in WIPP-12. The WQSP-1 water-level data were converted to pressures by calculating the pressure exerted at the center of the Culebra (713.1 ft [217.4 m] BTC) by the column of water in the well given a fluid specific gravity of 1.05 (Westinghouse, 1996). Offsets were evident in the data records from both WIPP-12 and WIPP-13 caused by repositioning the Trolls. These offsets were removed from the data for analysis. The raw data (corrected for offsets) from DOE-2, H-18, WIPP-12, WIPP-13, and WQSP-1 are shown in Figures 5-36 through 5-40, respectively. Pressures dropped slightly in WIPP-12 during the last several weeks of recovery monitoring for an unknown reason.

The data from all observation wells except WIPP-12 were clearly affected by fluctuations in barometric pressure. The record of barometric pressures measured at the H-19 hydropad during the period of the WQSP-2 pumping test is shown in Figure 5-41. These data were used to determine barometric efficiencies and compensate the observed pressure data using the procedure outlined in Section 5.7. The barometric efficiencies of DOE-2 and WIPP-13 were determined to be 0.7, that of H-18 was determined to be 0.6, and that of WQSP-1 was determined to be 0.8. No barometric compensation was required for the data from WIPP-12.

The data from DOE-2, H-18, WIPP-13, and WQSP-1 also exhibited trends of increasing pressure related to continuing recovery from the WQSP-1 pumping test. These trends were removed from the data using what we term a Horner compensation. A Horner compensation is based on the finding of Horner (1951) that late-time recovery data fall on a straight line on a plot of the logarithm of

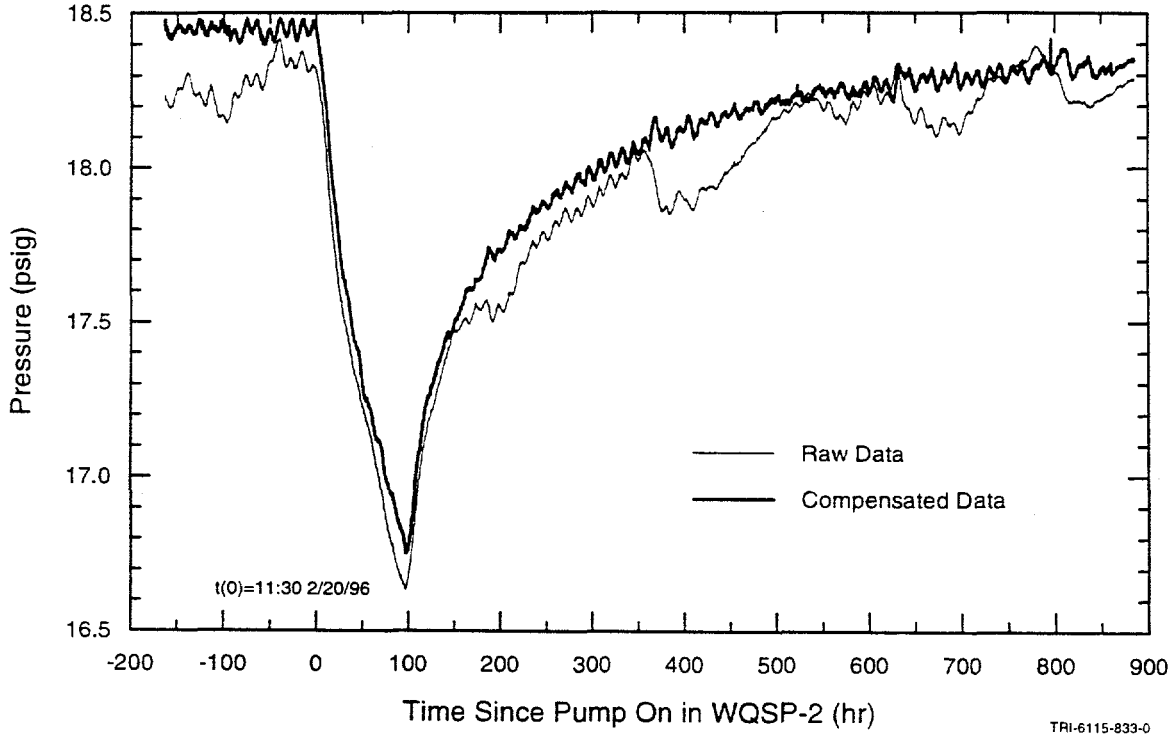

Figure 5-36. Pressure in DOE-2 during the WQSP-2 pumping test.

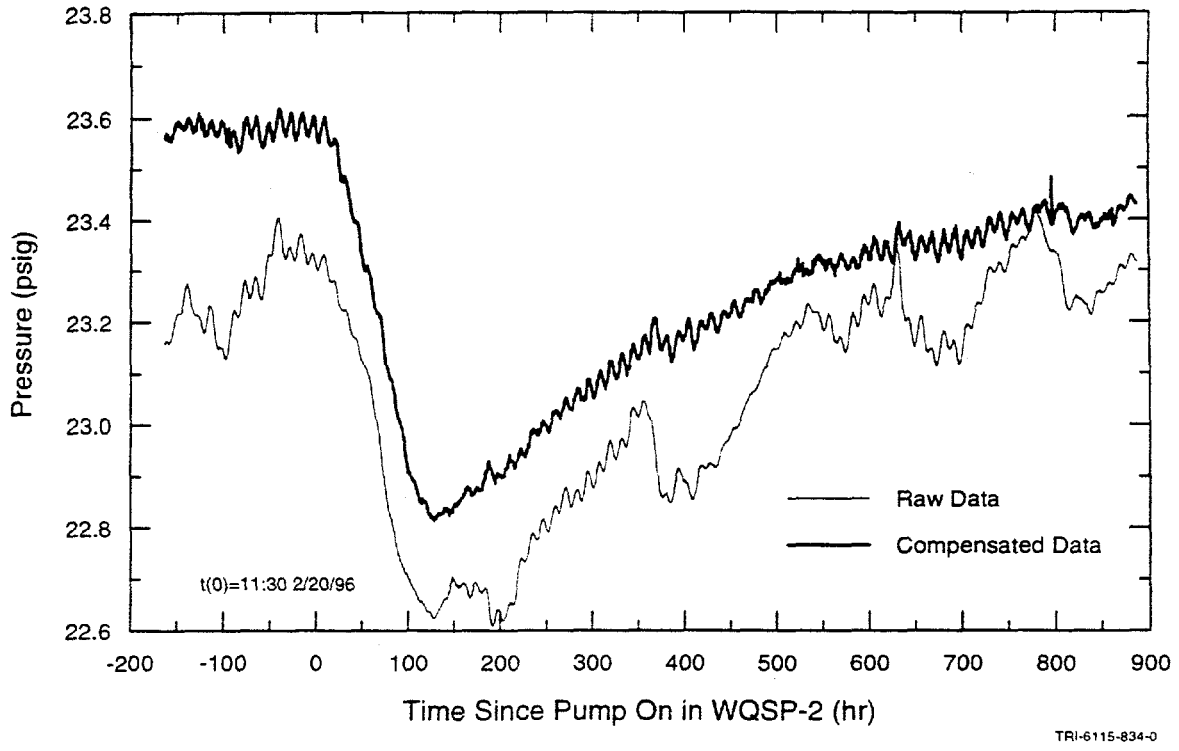

Figure 5-37. Pressure in H-18 during the WQSP-2 pumping test.

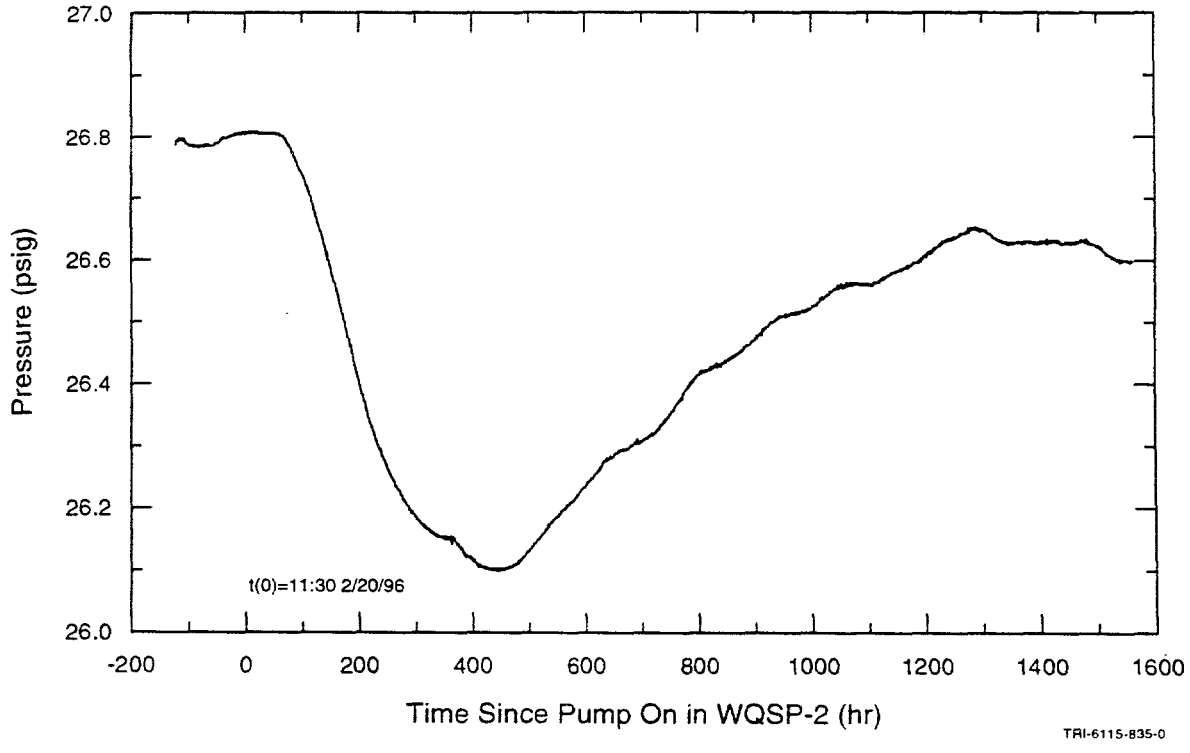

Figure 5-38. Pressure in WIPP-12 during the WQSP-2 pumping test.

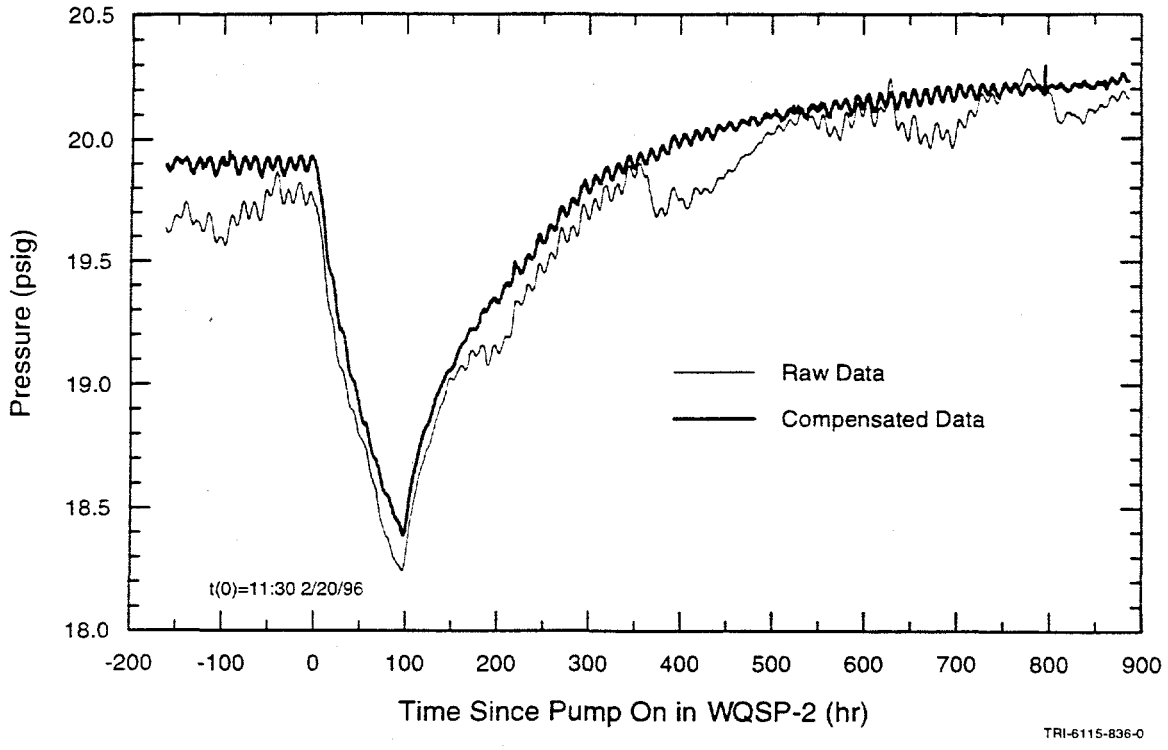

Figure 5-39. Pressure in WIPP-13 during the WQSP-2 pumping test.

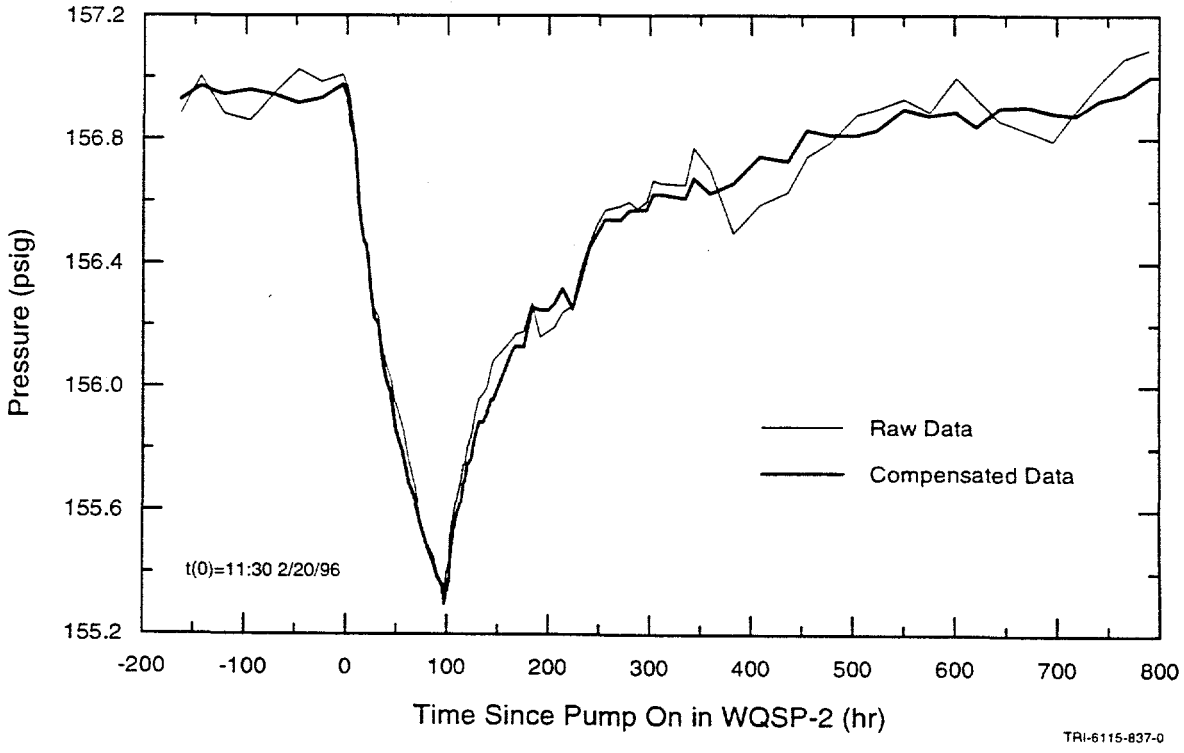

Figure 5-40. Pressure in WQSP-1 during the WQSP-2 pumping test.

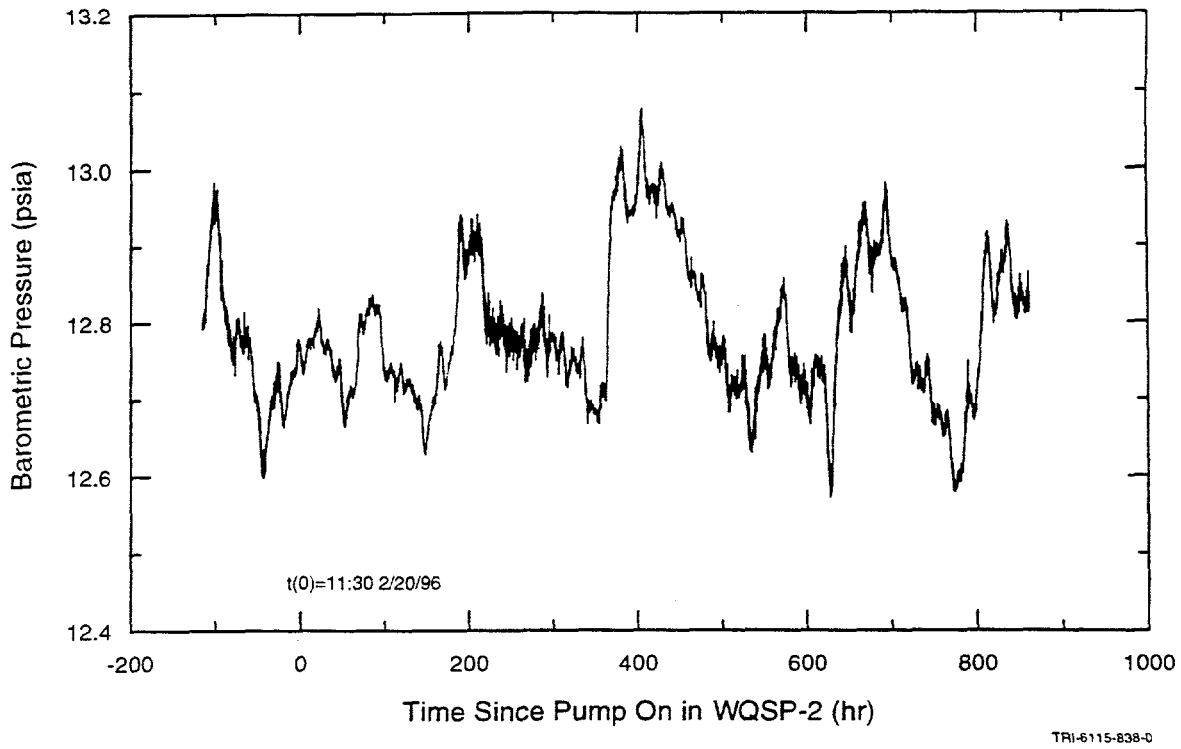

Figure 5-41. Barometric pressure during the WQSP-2 pumping test.

(pumping time plus recovery time)/(recovery time) versus pressure. We assumed that the trends were entirely due to recovery from pumping at WQSP-1 and that the recovery was sufficiently advanced that the data could be represented by a Horner straight line. Horner plots of the data were prepared, straight lines were fit through the data preceding the start of pumping in WQSP-2, the slopes of the lines were calculated, and the pressure data were compensated by adding the product of the negative of the calculated slope and the logarithm of the time function.

The pressure data from DOE-2, H-18, WIPP-12, WIPP-13, and WQSP-1 compensated for barometric effects and/or pretest trends are shown in Figures 5-36 through 5-40, respectively. Diurnal fluctuations caused by earth tides are evident in the compensated data from DOE-2, H-18, and WIPP-13 (Figures 5-36, 5-37, and 5-39, respectively). The WIPP-13 response shown in Figure 5-39 is peculiar in that the recovery from the WQSP-2 pumping test exceeds the stabilized pressure that existed before the test started.

5.13 WQSP-4 Pumping Test

The WQSP-4 pumping test was conducted in February and March 1995. WQSP-4 was pumped at an average rate of 4.2 gpm (0.26 L/s) from 1001 hours on 15 February 1995 until 1506 hours on 17 February 1995, at which time the rate was reduced to 2.2 gpm (0.14 L/s). Pumping continued at the reduced rate until 1545 hours on 19 February 1995. Pressure recovery was monitored until 0744 hours on 27 February 1995. Pumping rates were calculated from periodic readings of a totalizing flow meter. The calculated pumping rates are shown in Figure 5-42. Fluid pressures in WQSP-4 were monitored by two transducers during the test (Figure 3-26), which provided essentially identical data. The pressure data from the lower transducer are shown in Figure 5-43. The DAS failed from

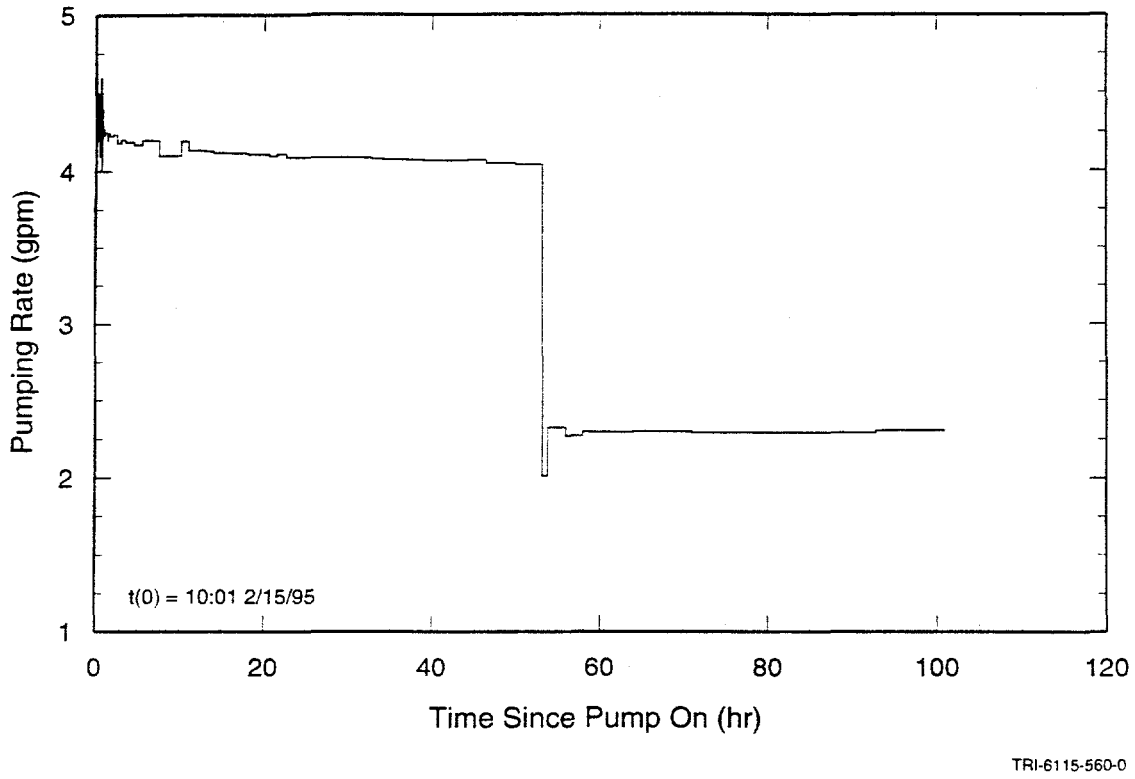

Figure 5-42. Pumping rate during the WQSP-4 pumping test.

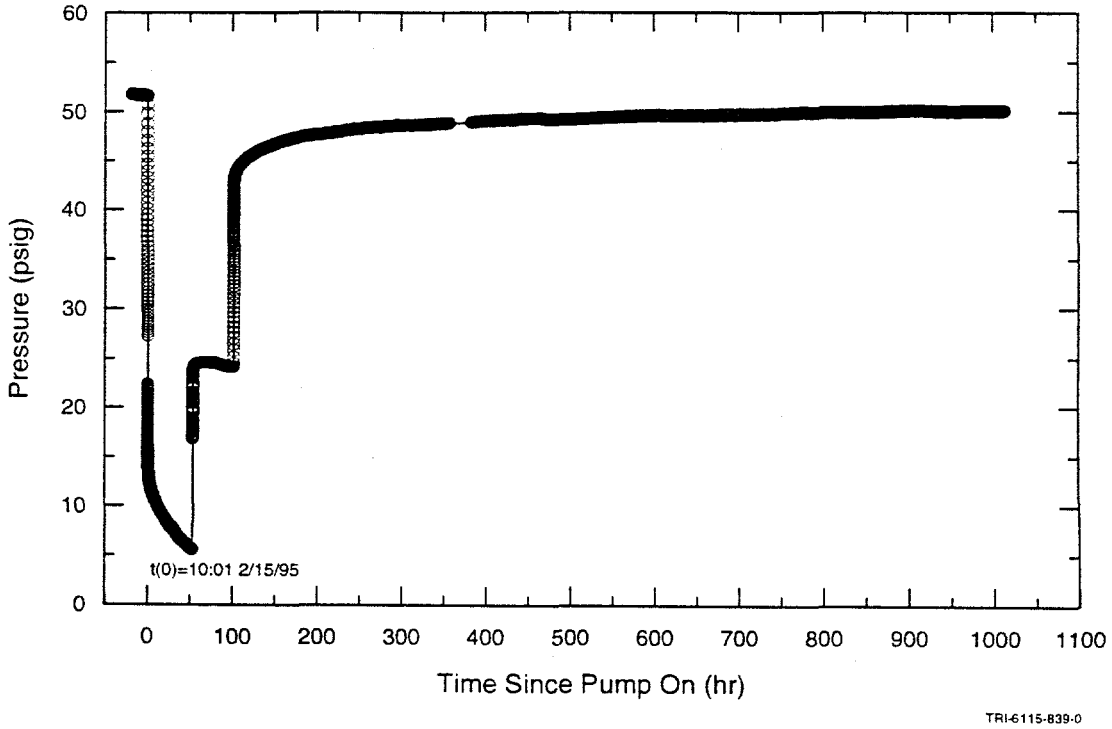

Figure 5-43. Pressure in WQSP-4 during the WQSP-4 pumping test.

approximately 1500 to 1515 hours on 17 February 1995, when the pumping rate was being adjusted. Thus, no early-time data are available for the second pumping period.

5.14 WQSP-5 Pumping Test

The WQSP-5 pumping test was conducted in November and December 1995 under the Test Plan by Stensrud (1995). WQSP-5 was pumped from 1827 hours on 29 November 1995 until 0746 hours on 1 December 1995. Pressure recovery was monitored until 0831 hours on 5 December 1995. The pump was turned off and on at least four times during the first hour of the test while attempting to get the Endress & Hauser flow meter to function properly. Continuous pumping began at 1928 hours on 29 November 1995. An average rate of 1.55 gpm (0.10 L/s) was maintained until 2245 hours on 29 November 1995, at which time the rate was reduced to avoid dewatering the well. A reduced average rate of 0.80 gpm (0.05 L/s) was maintained until the end of the pumping period. Pumping-rate data were not obtained during the first hour of the test when the pump was turned off and on. The pumping-rate data from the continuous-pumping portion of the test are shown in Figure 5-44. Fluid pressures in WQSP-5 were monitored by two transducers during the test (Figure 3-27), which provided essentially identical data. The pressure data from transducer #754612 are shown in Figure 5-45.

5.15 WQSP-6 Pumping Test

The WQSP-6 pumping test was conducted in December 1995 under the Test Plan by Stensrud (1995). WQSP-6 was first pumped from 1357 hours to 1948 hours on 8 December 1995 at an average rate of 0.56 gpm (0.035 L/s). When the pressure drop showed that the well could not sustain that high a

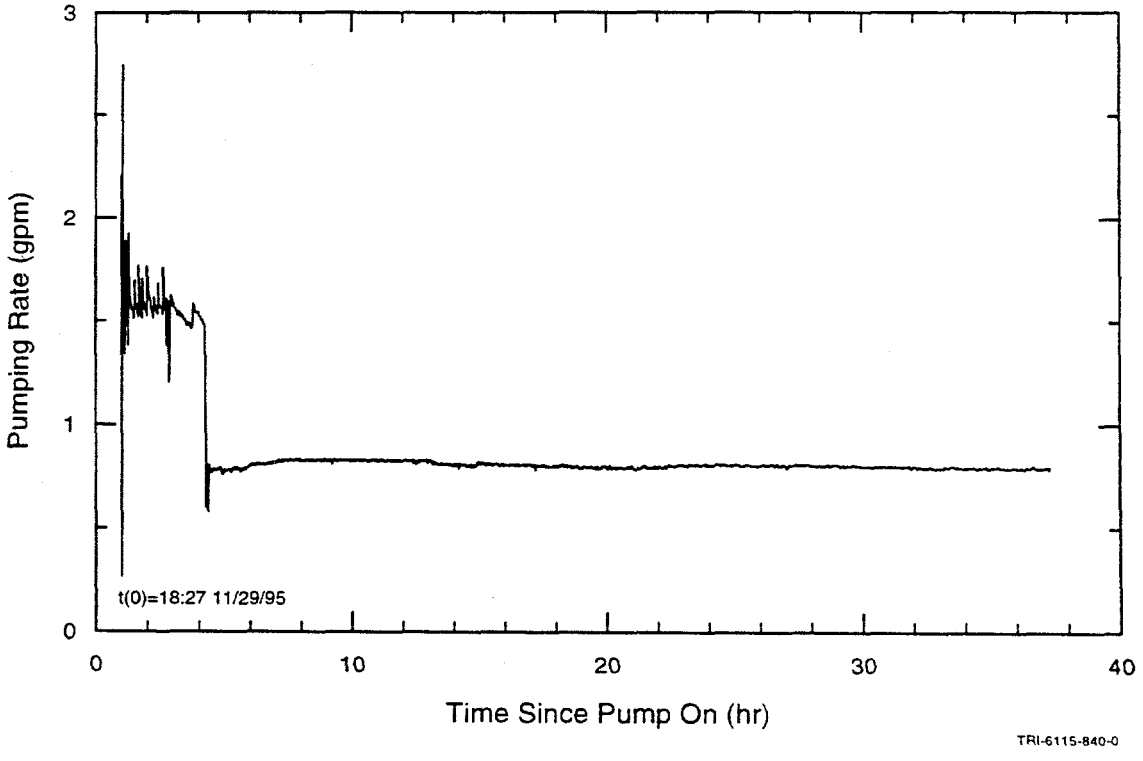

Figure 5-44. Pumping rate during the WQSP-5 pumping test.

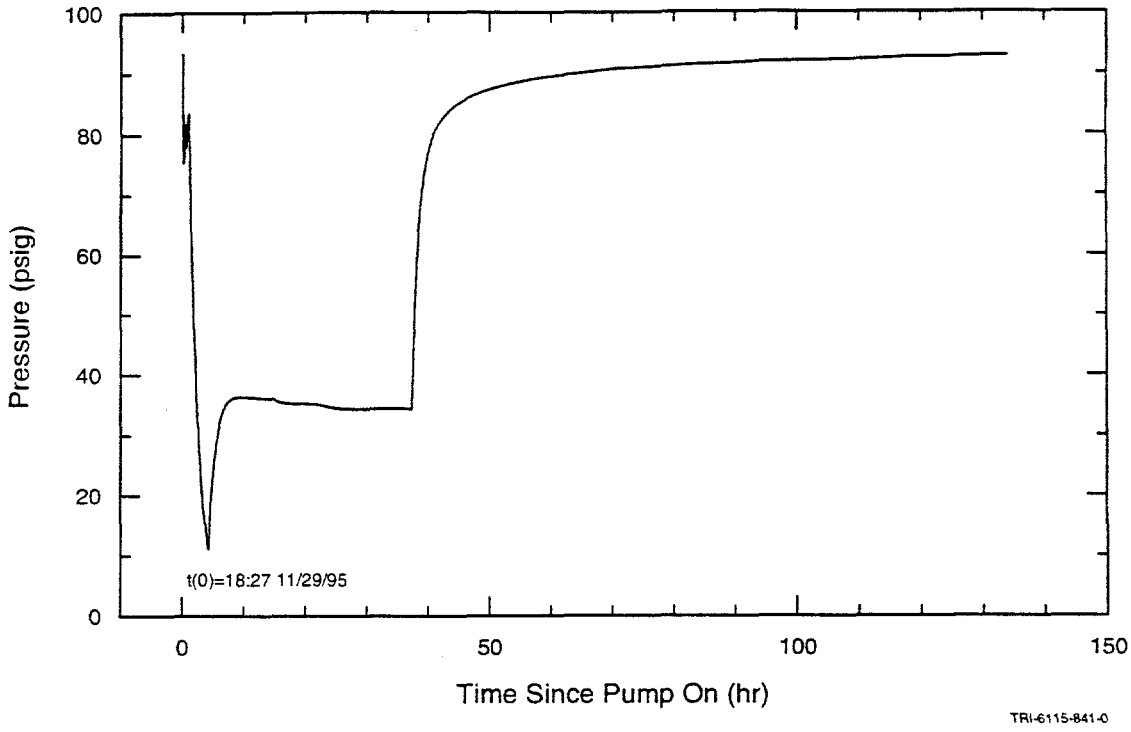

Figure 5-45. Pressure in WQSP-5 during the WQSP-5 pumping test.

pumping rate, pumping was suspended while a recirculation system was set up. Pumping resumed at 0952 hours on 18 December 1995 at a rate of approximately 3.5 gpm (0.22 L/s) with all water being recirculated back down into the well. The pressure transient caused by the time lag between turning on the pump and recirculated flow returning to the well was allowed to dissipate until 0739 hours on 20 December 1995, at which time approximately 10% of the flow was diverted out of the recirculation loop. An average of 0.34 gpm (0.021 L/s) was diverted until 0532 hours on 21 December 1995, when the pump was shut off. The recirculation line continued to drain for approximately one minute after the pump was turned off. The pumping-rate data are shown in Figure 5-46. Fluid pressures in WQSP-6 were monitored until 1631 hours on 3 January 1996 by two transducers (Figure 3-28), which provided essentially identical data. The pressure data from the upper transducer (#754612) are shown in Figure 5-47.

5.16 WQSP-6A Pumping Test of the Dewey Lake

The WQSP-6A pumping test of the Dewey Lake Redbeds was conducted in March and April 1996 under the Test Plan by Stensrud (1995). WQSP-6A was pumped at an average rate of 12.0 gpm (0.76 L/s) from 0802 hours on 25 March 1996 until 1233 hours on 28 March 1996. Pressure recovery was monitored until 0650 hours on 9 April 1996. However, a water-level measurement in the discharge line on 2 April 1996 showed that the in-line check valves had failed, invalidating the recovery data. The DAS records show that the Endress & Hauser flow meter had an average reading of -0.027 gpm (-0.0017 L/s) when no flow was occurring. Consequently, all readings during pumping

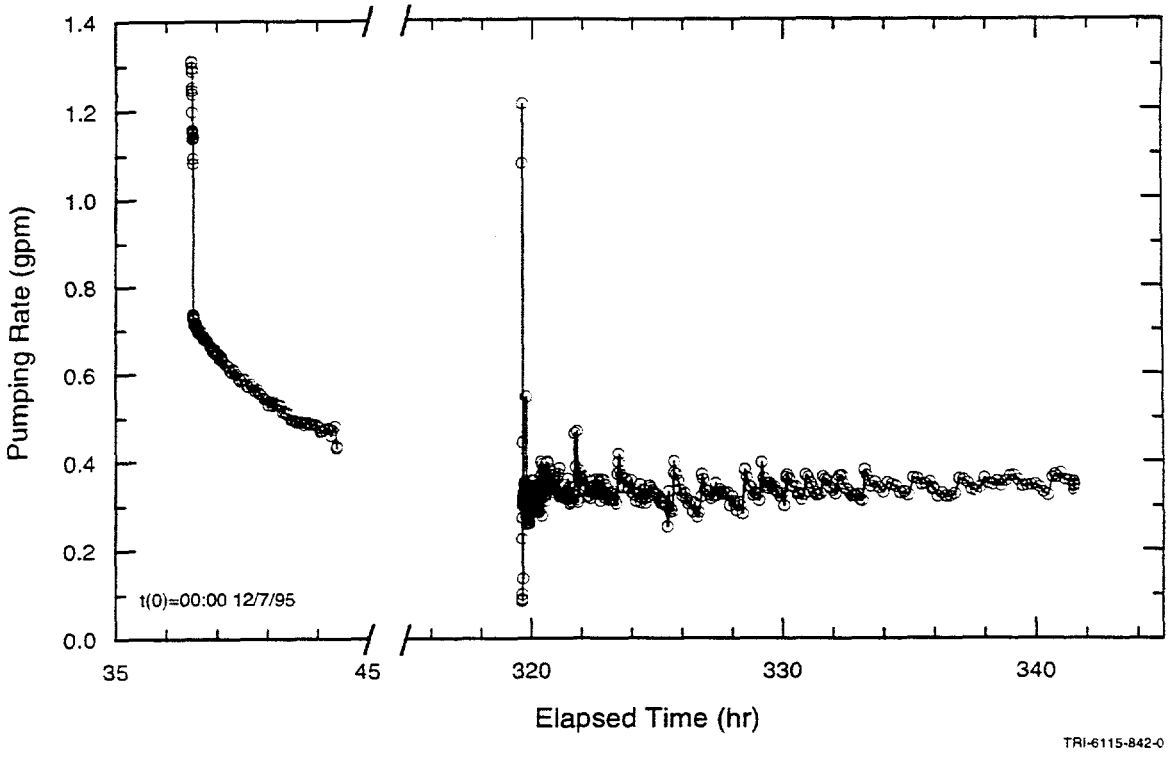

Figure 5-46. Pumping rates during the WQSP-6 pumping test.

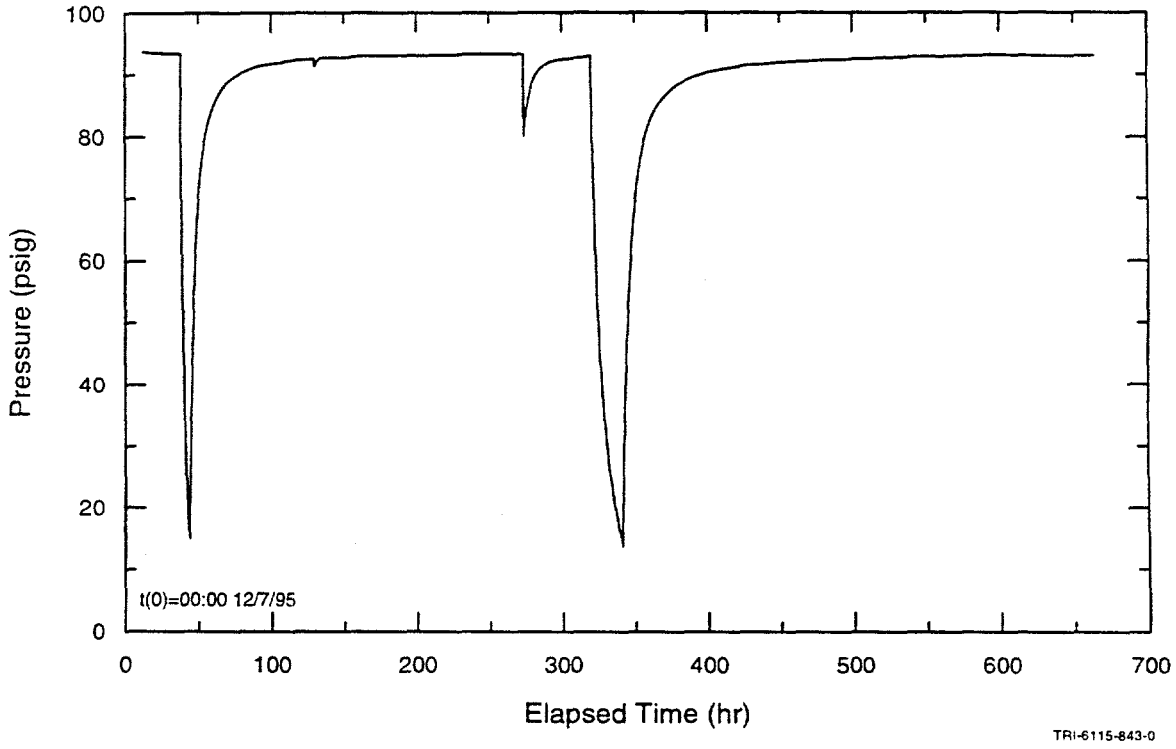

Figure 5-47. Pressure in WQSP-6 during the WQSP-6 pumping test.

were increased by 0.027 gpm (0.0017 L/s) to compensate for this offset. The corrected pumping-rate data are shown in Figure 5-48.

Fluid pressures in WQSP-6A were monitored by a single transducer during the test (Figure 3-29), the data from which are shown in Figure 5-49. The pressure was declining over the three days leading up to the test, but the post-test data show that the pressure at the start of pumping was within a few tenths of a psi (a few kPa) of the stabilized pressure. The pressure readings during pumping are erratic, reflecting electrical noise caused by the valve positioner. An offset of less than 0.5 psi (3.4 kPa) is evident in the pressure record approximately 191 hr after the pump was turned on, which corresponds to the time when the water-level measurement was made in the discharge line. The transducer cable may have been moved at that time by accident.

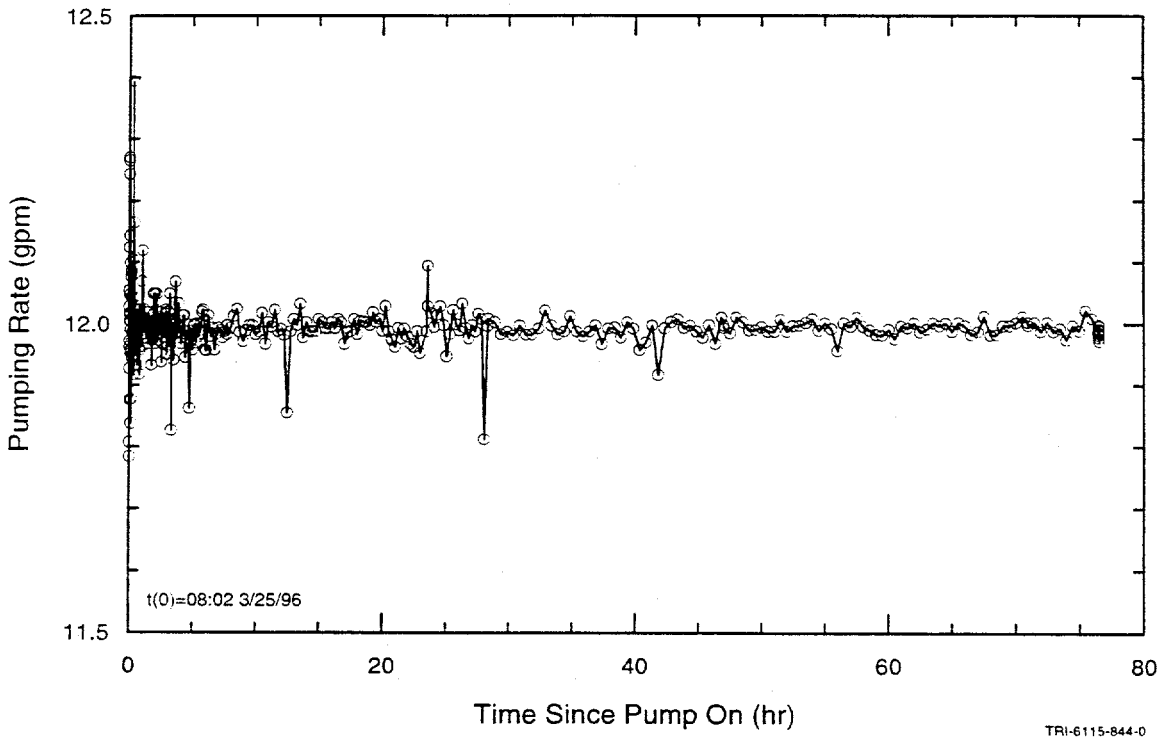

Figure 5-48. Pumping rate during the WQSP-6A pumping test.

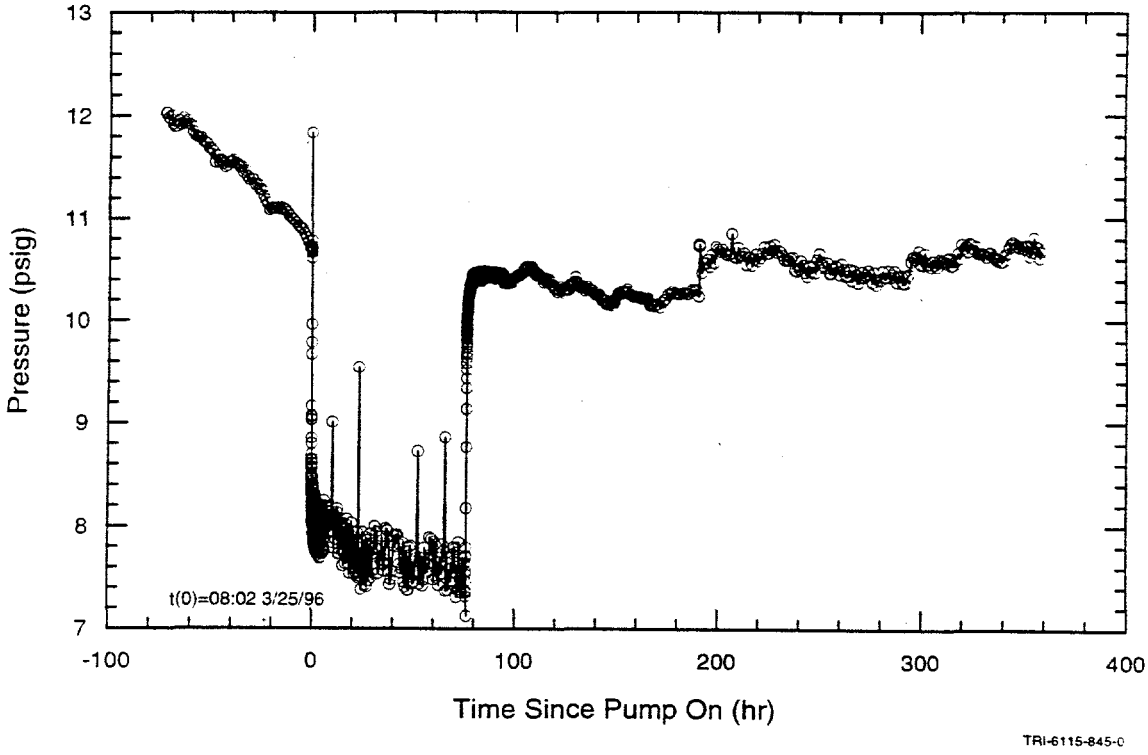

Figure 5-49. Pressure in WQSP-6A during the WQSP-6A pumping test.

6. TEST INTERPRETATION AND RESULTS

The drawdown and recovery data from the pumping tests were interpreted using techniques based on analytical solutions derived for different conceptual representations of aquifer response to pumping. All pumping-test analyses were performed with the Interpret/2 version 1.7 well-test interpretation code developed by A.C. Gringarten and Scientific Software-Intercomp. Slug-test analyses were performed using the code GTFM 6.0 (Pickens et al., 1987). The theoretical basis and use of these codes are discussed in Beauheim (1989) and Beauheim et al. (1991). The analysis of anisotropy is based upon theory and techniques presented in Grimestad (1995). Familiarity on the part of the reader with the material in those references is assumed in the following discussion.

The Interpret/2 software uses analytical solutions to generate simulations of the pressure response to pumping in the pumping and/or observation well(s) based on well geometry and characteristics, a conceptual model of the aquifer, boundary conditions, and specific values of parameters. Interpret/2 generates plots of the measured pressure data and superimposes the calculated responses over the data. Three plots typically used in diagnosing and verifying an interpretation model are the log-log plot of elapsed time versus pressure change and pressure derivative (displayed together), the semilog plot of pressure versus the Horner (1951) superposition time function, and the linear-linear sequence plot of measured pressure versus elapsed time, onto which are superimposed the simulated responses with the fitted parameters. Use of these plots in identifying the correct conceptual model for interpretation has been discussed by numerous authors, including Gringarten (1984, 1987), Ehlig-Economides (1988), and Bourdet et al. (1989). Once the appropriate model has been selected, Interpret/2 has a nonlinear parameter-estimation procedure to fit simulations to the data.

Interpret/2 incorporates models for single-porosity, double-porosity, multilayer, double-permeability, and radial-composite aquifers. Based on geologic descriptions of the Culebra such as that of Holt (1997), single-porosity, double-porosity, and multilayer conditions were considered most likely to occur at various locations. Tracer tests conducted in the Culebra at the WIPP site have also been interpreted using models based on single-porosity (H-2; Hydro Geo Chem, 1986), double-porosity (H-3, H-6, H-11, and H-19; Jones et al., 1992, and Meigs et al., 1997), and multilayer (H-4; Kelley and Pickens, 1986) conditions. Therefore, initial selection of a model for test interpretation was made from this short list based on the characteristics of the pressure derivative on the log-log diagnostic plot. If a satisfactory match could not be obtained with the initial model selected, alternative models were investigated.

The analytical techniques used to interpret the pumping-test data were developed for tests in homogeneous, porous media. These techniques readily and rigorously accommodate such factors as double-porosity and discrete boundaries. Large-scale heterogeneities, however, such as regional gradational changes in transmissivity and storativity with distance and direction, are not treated rigorously using these analytical techniques. In a heterogeneous system, the most information that can be obtained is a qualitative understanding of the nature of the heterogeneities and non-unique quantitative evaluations of average hydraulic properties over the distances of the observations.

For example, in a homogeneous, isotropic aquifer, water is contributed to the pumping well equally from all directions. In a heterogeneous aquifer, less permeable regions will contribute less water and more permeable regions will contribute more water. In a heterogeneous aquifer with smoothly and monotonically varying properties, this will cause more drawdown in the more permeable regions than would result from pumping at the same rate in a homogeneous system, and less drawdown in the less permeable regions. As a result, estimates of the transmissivity between the pumping well and an observation well in a more permeable region will be too low, and estimates of the transmissivity between the pumping well and an observation well in a less permeable region will be too high. In a more complex heterogeneous aquifer with an irregular distribution of properties, responses are more difficult to predict and could result in estimated hydraulic properties that are either too high or too low. Thus, the hydraulic properties inferred from the response of an observation well in a heterogeneous aquifer are best viewed qualitatively in the context of other information about the geology and local hydraulic properties of the aquifer. They should especially not be interpreted as the "true" or average properties that would be determined from a test at any scale conducted at that well.

Double-porosity media have two porosity sets that differ in permeability and specific storage. Typically, the two porosity sets are (1) a fracture network with higher permeability and lower specific storage and (2) the primary porosity of the rock matrix with lower permeability and higher specific storage. The diagnostic characteristic of a double-porosity medium on a log-log plot of pumping-test data is a minimum in the pressure derivative. This minimum occurs because of the interaction between fractures and matrix during pumping. When pumping first begins, most of the water produced comes from fractures, creating pressure disequilibrium between the fractures and matrix. With time, water flows from the matrix to the fractures, causing the rate of pressure change in the fractures to decrease temporarily until pressure equilibrium is reestablished. This transition from fracture-only to fracture+matrix flow is characterized by two parameters: the storativity ratio, ω, and the interporosity flow coefficient, λ (Warren and Root, 1963). The storativity ratio indicates the percentage of the total storativity of the medium that is due to the response of fractures. The interporosity flow coefficient controls the time at which pressure equilibrium between fractures and matrix occurs, and includes the ratio of matrix permeability to fracture permeability and a shape factor related to the geometry of the fracture network and inversely proportional to the square of fracture spacing. Hence, higher values of λ imply that equilibration occurs sooner because of a lesser contrast between matrix and fracture permeability and/or smaller matrix blocks between fractures.

The interpreted values of these parameters, however, are of little quantitative utility. Interpret/2 includes two types of models (actually analytical solutions) for double-porosity flow: one for restricted interporosity flow and one for unrestricted interporosity flow. (Restricted interporosity flow arises when clay or mineralization on fracture surfaces impedes flow between fractures and matrix.) Both of the models assume uniform fracture geometry and properties. Holt (1997) observed that both matrix composition and fracture geometry are heterogeneous in the Culebra, likely leading to multiple rates of diffusion between fractures and matrix. Meigs et al. (1997) found that tracer-test data from the H-11 and H-19 hydropads could not be matched using a double-porosity model with a single rate of

diffusion, but could using multiple rates of diffusion. Johns and Jalali-Yazdi (1991) showed that different distributions of matrix block sizes (i.e., non-uniform fracture geometry) combined with unrestricted interporosity flow cause the pressure derivative during the transition period to assume shapes intermediate between those produced by the restricted and unrestricted interporosity flow, uniform-geometry models contained in Interpret/2. Many of the observed responses discussed below cannot be exactly matched with either of the double-porosity models included in Interpret/2, probably reflecting the non-uniform properties noted by Holt (1997). The ω and λ values interpreted from the best matches obtained, therefore, are of questionable validity. (Transmissivity and storativity estimates are not affected by these differences between models.) Furthermore, differences between estimated values of λ for different testing locations are difficult to interpret because of uncertainty as to whether they reflect differences in the fracture/matrix permeability ratio, the shape factor, or both.

A final cautionary note is appropriate with regard to the hydraulic boundaries (image wells) used in the analyses presented below. Interpret/2 uses image wells at specific distances from the pumping well to simulate the effects of hydraulic boundaries. In defining the distances to the boundaries, an assumption is made that the aquifer is homogeneous. If these boundaries were in fact discrete hydrogeologic features such as faults or rivers intersecting the aquifer, and if the aquifer were homogeneous, the uncertainty in the distances presented would be, at best, about ±10 percent. In the case of the Culebra, the boundaries are believed to represent a heterogeneous distribution of transmissivity, and the significance of the distances provided by the analyses is unclear. Furthermore, in simulating the response from an observation well, Interpret/2 combines the distance from the pumping well to the boundary with the angle between the boundary and the observation well with respect to the pumping well. This combination is non-unique; that is, different pairs of distances and angles produce the same responses. Consequently, the boundary information provided by Interpret/2 should not be viewed quantitatively, but should be regarded as an indication of the type(s) of transmissivity change(s) occurring at some distance from a well.

GTFM 6.0 uses graph theory (Savage and Kesavan, 1979) to solve the flow equation numerically for n-dimensional flow that is symmetric about a borehole. For the slug tests discussed in this report, the formation was discretized radially with 500 to 5000 nodes and the external boundary was assigned a fixed pressure equal to the measured or estimated static formation pressure. The distance to the boundary was chosen (and verified) to be sufficiently large so that the boundary would have no effect on the calculated response in the borehole. Simulating the slug tests required selecting values for hydraulic conductivity, specific storage, and, in some instances, static formation pressure. The nonlinear optimization routines in GTFM 6.0 were used to define the values of these parameters that provided the best fit between the normalized pressure and pressure-derivative data and the simulations. Although specific storage is an important model parameter in matching slug-test data, the values used in the simulations are not considered representative of formation properties and, therefore, are not reported herein. In the analytical expressions describing slug-test responses, specific storage is always combined with the square of the effective well radius (Cooper et al., 1967), which is dependent on skin properties. Because specific storage and skin properties cannot be sepa-

rated on the basis of single-well test data alone, no skin zones were used in the slug-test simulations presented in this report and the specific-storage parameter was used in GTFM to represent their joint effects.

Subject to these limitations, interpretation of the data from each test had the following objectives:

- Determine the most appropriate conceptualization of the nature of the flow system in the vicinity of the tested well;
- Quantify the hydraulic properties of the tested unit in the vicinity of the tested well;
- Estimate the nature of the heterogeneities in the tested unit within the area influenced by the test; and
- When multiwell interference data are available from Culebra tests, estimate anisotropy.

Because of the large number of tests analyzed, only the plots of recovery data are shown below for most pumping tests. Plots of the drawdown interpretations are presented in Appendix A. The results presented in this chapter represent the simulations that were determined to provide both the best visual matches to the observed data when plotted in different formats and the most consistent parameter estimates for all of the wells and/or tests at a testing location. The entire process of trying and comparing different models and parameter values before arriving at the final results presented herein is documented in the Culebra Hydraulic Tests Analysis Package (WPO#38487) and in the Culebra H-19 Hydraulic Test Analyses Package (WPO #38401). The analyses were performed under the Analysis Plan by Ruskauff (1996).

6.1 H-2 Pumping Test

As discussed in Section 5.1, the H-2 pumping test involved pumping in well H-2c with well H-2b serving as an observation well. Interpretations of the pumping-well and observation-well responses are presented below.

6.1.1 H-2c

Figures 6-1 and 6-2 show the log-log and Horner plots, respectively, of the drawdown data from H-2c along with the best-fit Interpret/2 simulations. The derivative data on Figure 6-1 show the effects of pumping-rate fluctuations and, therefore, provide a poor basis for fitting. Consequently, fitting simulations to the data was done primarily by matching the pressure data on Figure 6-1 and the late-time slope on the Horner plot in Figure 6-2. The test response was simulated using a model for a well with wellbore storage and skin in an infinite, homogeneous, single-porosity medium having a transmissivity of 0.55 ft^2/d (5.9×10^{-7} m^2/s). The wellbore skin was modeled with a value of 4.6 (Table 6-1), indicating a poor connection between the well and the formation. Figure 6-3 is a linear-linear plot of the match between this model and the combined drawdown and recovery data. Simulations of the recovery data indicated higher transmissivity (by approximately 50%) and also much higher skin (12.2). These values are not considered representative of actual conditions because the recovery data showed 100% pressure recovery after only five days, which is not realistic. We suspect that a check valve or some other component of the discharge string leaked after the pump was turned off, allowing water to drain back to the Culebra.

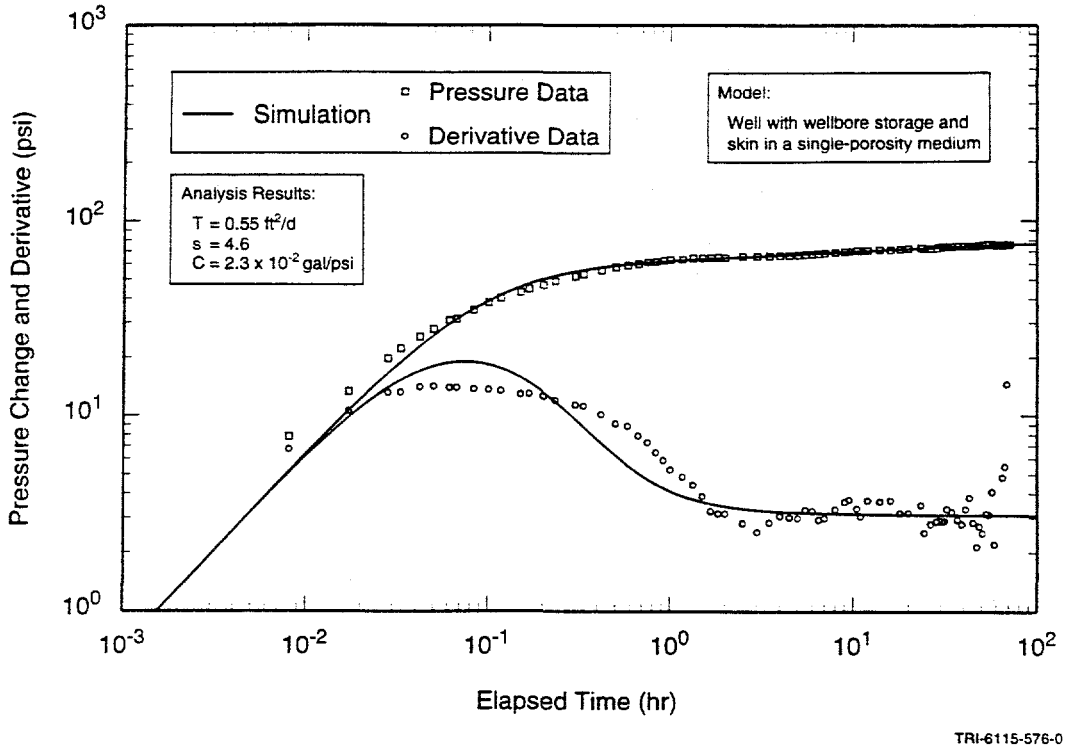

Figure 6-1. Log-log plot of H-2c drawdown data with Interpret/2 simulation.

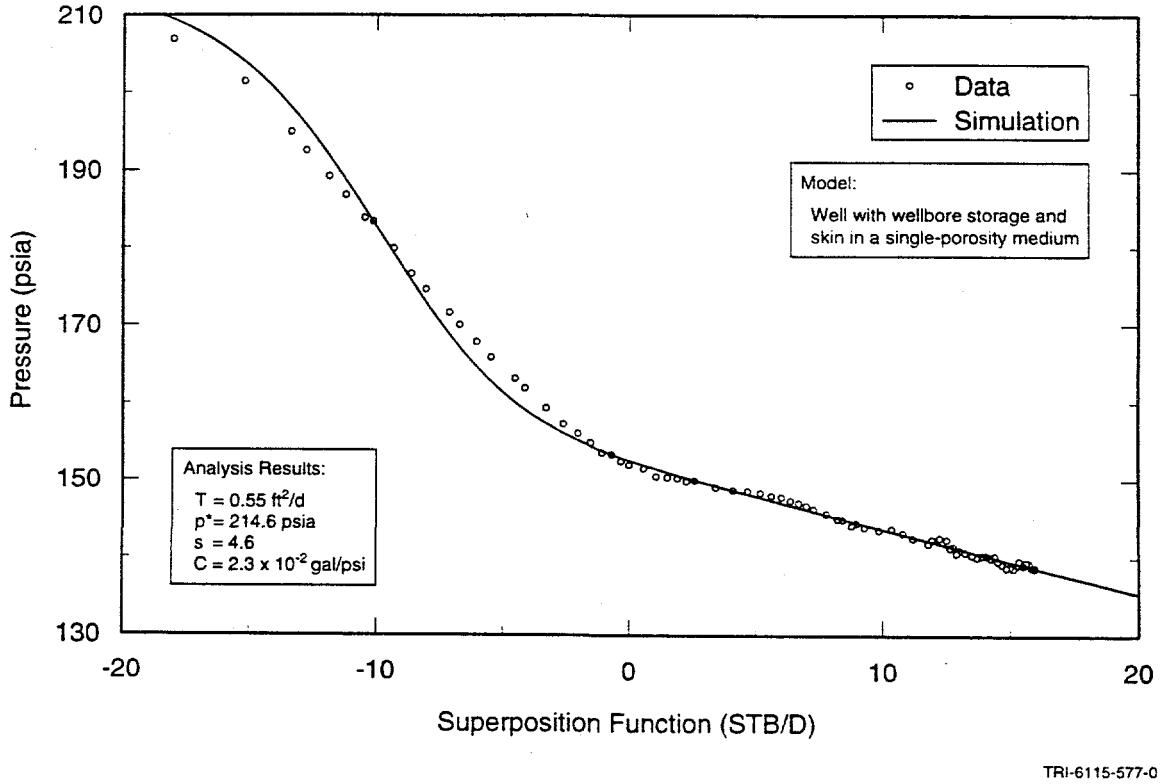

Figure 6-2. Horner plot of H-2c drawdown data with Interpret/2 simulation.

Table 6-1. Summary of Interpretation Results

Test Well	Observation Well	Test Type	Transmissivity $(ft^2/d)/(m^2/s)$ (T)	Storativity (S)	Skin (s)	Storativity ratio (ω)	Interporosity flow coefficient (λ)	Boundaries*
H-2c		Drawdown	$0.55/5.9 \times 10^{-7}$	NA	4.6	NA	NA	none
	H-2b	Drawdown	$0.55/5.9 \times 10^{-7}$	1.6×10^{-5}	NA	NA	NA	none
	H-2b	Recovery	$0.57/6.1 \times 10^{-7}$	1.4×10^{-5}	NA	NA	NA	none
H-6b (Test 1)		Drawdown	$45/4.9 \times 10^{-5}$	NA	-5.1	2.8×10^{-6}	7.7×10^{-7}	CP at 1200 ft
		Recovery	$38/4.0 \times 10^{-5}$	NA	-5.5	2.5×10^{-6}	9.1×10^{-7}	CP at 1140 ft
	H-6a	Drawdown	$38/4.1 \times 10^{-5}$	1.8×10^{-4}	NA	0.27	6.6×10^{-7}	CP
	H-6a	Recovery	$37/4.0 \times 10^{-5}$	1.9×10^{-4}	NA	0.066	1.5×10^{-6}	CP
	H-6c	Drawdown	$39/4.2 \times 10^{-5}$	1.3×10^{-4}	NA	0.12	7.5×10^{-7}	CP
	H-6c	Recovery	$36/3.8 \times 10^{-5}$	1.7×10^{-4}	NA	0.15	1.1×10^{-6}	CP
H-6c (Test 2)	H-6a	Recovery	$37/4.0 \times 10^{-5}$	2.6×10^{-4}	NA	0.12	1.5×10^{-6}	CP
	H-6b	Recovery	$37/4.0 \times 10^{-5}$	1.9×10^{-4}	NA	0.097	1.2×10^{-6}	CP
H-6c (Test 3)		Recovery	$38/4.1 \times 10^{-5}$	NA	1.2	0.031	7.2×10^{-7}	CP at 950 ft
	H-6a	Drawdown	$36/3.9 \times 10^{-5}$	2.1×10^{-4}	NA	0.18	1.1×10^{-6}	CP
	H-6a	Recovery	$36/3.9 \times 10^{-5}$	2.1×10^{-4}	NA	0.26	1.2×10^{-6}	CP
	H-6b	Drawdown	$39/4.2 \times 10^{-5}$	1.2×10^{-4}	NA	0.21	7.6×10^{-7}	CP
	H-6b	Recovery	$35/3.8 \times 10^{-5}$	1.6×10^{-4}	NA	0.24	9.0×10^{-7}	CP
H-7b1		Recovery	$1400/1.5 \times 10^{-3}$	NA	-5.1	0.016	1.3×10^{-7}	none
	H-7b2	Drawdown	$970/1.0 \times 10^{-3}$	1.2×10^{-2}	NA	0.004	1.8×10^{-7}	none
	H-7b2	Recovery	$970/1.0 \times 10^{-3}$	6.0×10^{-3}	NA	0.010	1.0×10^{-7}	none
	H-7c	Recovery	$1400/1.5 \times 10^{-3}$	6.9×10^{-3}	NA	0.020	3.0×10^{-7}	none
H-9c (Test 1)	H-9a	Drawdown	$105/1.1 \times 10^{-4}$	4.9×10^{-4}	NA	0.19	2.7×10^{-6}	none
	H-9a	Recovery	$98/1.1 \times 10^{-4}$	6.0×10^{-4}	NA	0.48	8.9×10^{-7}	none
	H-9b	Drawdown	$109/1.2 \times 10^{-4}$	4.1×10^{-4}	NA	0.13	4.4×10^{-6}	none
	H-9b	Recovery	$98/1.1 \times 10^{-4}$	5.9×10^{-4}	NA	0.41	1.4×10^{-6}	none
H-9b (Test 2)	H-9a	Drawdown	$97/1.0 \times 10^{-4}$	5.7×10^{-4}	NA	0.023	1.4×10^{-6}	none
	H-9a	Recovery	$101/1.1 \times 10^{-4}$	4.5×10^{-4}	NA	0.057	1.9×10^{-6}	none
	H-9c	Drawdown	$98/1.1 \times 10^{-4}$	5.2×10^{-4}	NA	0.058	5.0×10^{-6}	none
	H-9c	Recovery	$98/1.1 \times 10^{-4}$	5.5×10^{-4}	NA	0.087	4.2×10^{-6}	none

* CP=constant pressure; NF=no flow

Table 6-1. Summary of Interpretation Results (continued)

Test Well	Observation Well	Test Type	Transmissivity (ft^2/d)/(m^2/s) (T)	Storativity (S)	Skin (s)	Storativity ratio (ω)	Interporosity flow coefficient (λ)	Boundaries*
H-9c (Test 3)	H-9a	Drawdown	105/1.1 x 10^{-4}	6.0 x 10^{-4}	NA	0.045	2.4 x 10^{-6}	none
	H-9a	Recovery	93/1.0 x 10^{-4}	8.7 x 10^{-4}	NA	0.15	2.1 x 10^{-6}	none
	H-9b	Drawdown	107/1.2 x 10^{-4}	4.7 x 10^{-4}	NA	0.053	2.8 x 10^{-6}	none
	H-9b	Recovery	91/9.8 x 10^{-5}	7.3 x 10^{-4}	NA	0.16	2.4 x 10^{-6}	none
	Engle	Drawdown	96/1.0 x 10^{-4}	4.7 x 10^{-6}	NA	NA	NA	none
H-10b		Slug #1	0.041/4.4 x 10^{-8}	NA	?	NA	NA	none
H-11b1		Drawdown	45/4.8 x 10^{-5}	NA	0.57	5.9 x 10^{-4}	2.4 x 10^{-7}	2 NF at 280 and 1410 ft
	H-11b2	Drawdown	44/4.7 x 10^{-5}	6.7 x 10^{-5}	NA	0.080	2.5 x 10^{-6}	2 NF
	H-11b3	Drawdown	44/4.7 x 10^{-5}	4.2 x 10^{-5}	NA	0.16	2.9 x 10^{-6}	2 NF
	H-11b4	Drawdown	45/4.8 x 10^{-5}	3.3 x 10^{-5}	NA	0.22	1.4 x 10^{-6}	2 NF
H-19b1 (Magenta)		Slug	0.38/4.1 x 10^{-7}	NA	?	NA	NA	none
H-19b2		Drawdown 2	5.9/6.4 x 10^{-6}	NA	-2.5	0.16	1.9 x 10^{-7}	none
		Recovery	5.9/6.4 x 10^{-6}	NA	-2.5	0.12	3.5 x 10^{-7}	none
H-19b0		Drawdown	6.4/6.8 x 10^{-6}	NA	-1.5	0.12	5.1 x 10^{-7}	none
	H-19b2	Drawdown	5.6/6.0 x 10^{-6}	4.1 x 10^{-5}	NA	0.14	2.9 x 10^{-7}	none
	H-19b3 lower	Drawdown	6.4/6.8 x 10^{-6}	4.7 x 10^{-5}	NA	0.14	3.9 x 10^{-7}	none
	H-19b3 upper	Drawdown	6.4/6.9 x 10^{-6}	5.4 x 10^{-5}	NA	0.19	3.9 x 10^{-7}	none
	H-19b4	Drawdown	6.8/7.3 x 10^{-6}	5.0 x 10^{-5}	NA	0.14	4.3 x 10^{-7}	NF
	H-19b5 lower	Drawdown	6.0/6.5 x 10^{-6}	5.6 x 10^{-5}	NA	0.13	4.2 x 10^{-7}	none
	H-19b5 upper	Drawdown	6.0/6.5 x 10^{-6}	8.0 x 10^{-5}	NA	0.42	2.9 x 10^{-7}	none
	H-19b6	Drawdown	7.9/8.5 x 10^{-6}	3.7 x 10^{-5}	NA	0.18	3.8 x 10^{-7}	NF
	H-19b7 lower	Drawdown	5.7/6.1 x 10^{-6}	6.9 x 10^{-5}	NA	0.12	5.8 x 10^{-7}	none
	H-19b7 upper	Drawdown	5.6/6.0 x 10^{-6}	6.6 x 10^{-5}	NA	0.19	4.0 x 10^{-7}	none

* CP=constant pressure; NF=no flow

Table 6-1. Summary of Interpretation Results (continued)

Test Well	Observation Well	Test Type	Transmissivity (ft^2/d)/(m^2/s) (T)	Storativity (S)	Skin (s)	Storativity ratio (ω)	Interporosity flow coefficient (λ)	Boundaries*
P-14	(2ϕ) (1ϕ)	Recovery	$290/3.1 \times 10^{-4}$ $500/5.4 \times 10^{-4}$	NA NA	-6.0 -3.7	0.0093 NA	1.3×10^{-8} NA	2 NF at 1760/ 1560 and 2130/1600 ft
	D-268	Recovery	$160/1.7 \times 10^{-4}$	2.5×10^{-5}	NA	NA	NA	none
	H-6b	Recovery	$130/1.4 \times 10^{-4}$	1.1×10^{-5}	NA	NA	NA	none
	WIPP-25	Recovery	$240/2.5 \times 10^{-4}$	1.5×10^{-5}	NA	NA	NA	none
WIPP-27		Slug #2	$530/5.7 \times 10^{-4}$	NA	?	NA	NA	none
		Slug #6	$420/4.5 \times 10^{-4}$	NA	?	NA	NA	none
WIPP-28		Slug #3	$260/2.8 \times 10^{-4}$	NA	?	NA	NA	none
WQSP-1		Drawdown	$28/3.0 \times 10^{-5}$	NA	-1.7	0.19	5.7×10^{-8}	none
	H-18	Recovery	$21/2.3 \times 10^{-5}$	3.5×10^{-5}	NA	0.20	2.6×10^{-6}	NF
	WIPP-13	Recovery	$29/3.1 \times 10^{-5}$	1.0×10^{-5}	NA	0.069	4.5×10^{-8}	none
WQSP-2		Drawdown	$19/2.0 \times 10^{-5}$	NA	-2.0	0.23	2.5×10^{-8}	none
	DOE-2	Recovery	$31/3.3 \times 10^{-5}$	6.6×10^{-6}	NA	0.32	1.5×10^{-8}	none
	H-18	Recovery	$23/2.5 \times 10^{-5}$	9.8×10^{-6}	NA	0.24	3.7×10^{-8}	none
	WIPP-13**	Recovery	$23/2.4 \times 10^{-5}$	7.2×10^{-6}	NA	0.15	5.4×10^{-8}	none
	WQSP-1	Recovery	$29/3.2 \times 10^{-5}$	6.2×10^{-6}	NA	0.26	6.4×10^{-9}	none
WQSP-4		Drawdown 1	$13/1.4 \times 10^{-5}$	NA	0.47	0.11	1.6×10^{-7}	2 NF at 1230 and 1400 ft
		Recovery	$13/1.4 \times 10^{-5}$	NA	0.32	0.081	2.2×10^{-7}	2 NF at 1040 and 1190 ft
WQSP-5		Recovery	$1.2/1.3 \times 10^{-6}$	NA	-0.75	NA	NA	none
WQSP-6		Recovery	$0.25/2.7 \times 10^{-7}$	NA	-1.9	NA	NA	none
WQSP-6A (Dewey Lake)		Specific Capacity	$360/3.9 \times 10^{-4}$	NA	?	NA	NA	none

* CP=constant pressure; NF=no flow

** Data questionable.

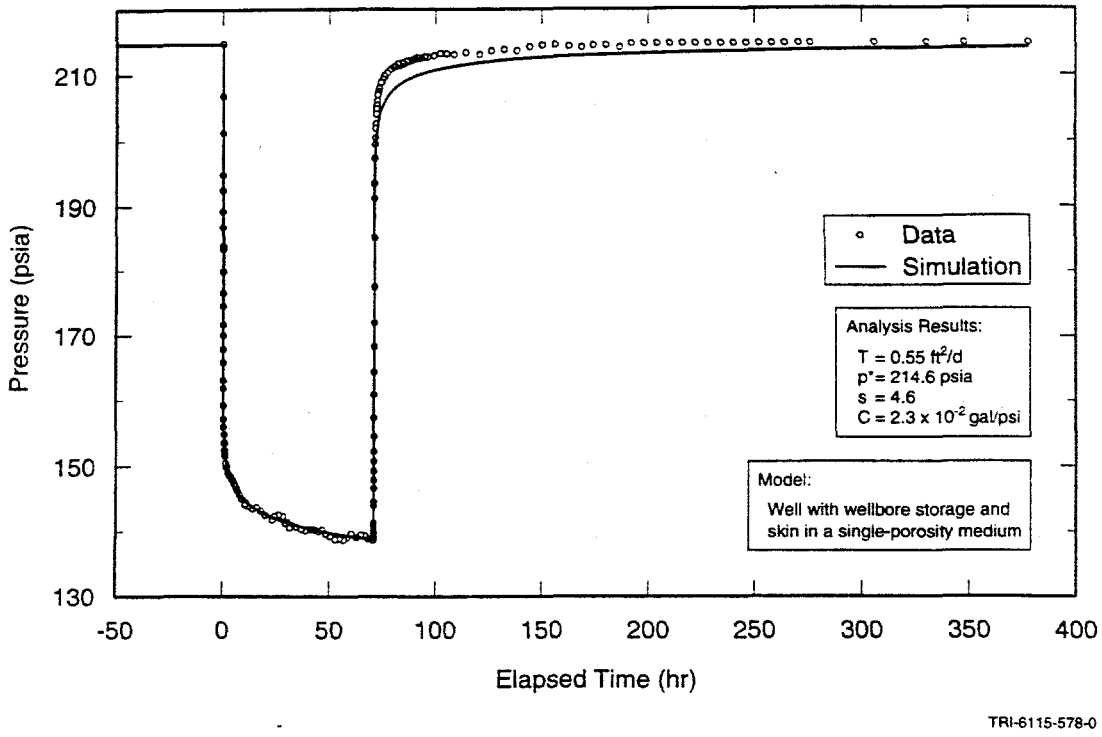

Figure 6-3. Linear-linear plot of H-2c data with Interpret/2 simulation derived from drawdown analysis.

6.1.2 H-2b

Figures 6-4 and 6-5 show the log-log and Horner plots, respectively, of the recovery data from H-2b along with the best-fit Interpret/2 simulations. The data were analyzed using a model for an infinite, homogeneous, single-porosity medium having a transmissivity of 0.57 ft^2/d (6.1 x 10^{-7} m^2/s) and a storativity of 1.4 x 10^{-5} (Table 6-1). Figure 6-6 is a linear-linear plot of the match between this model and the combined drawdown and recovery data. Log-log, Horner, and linear-linear plots of the drawdown data and best-fit simulations are presented in Appendix A (Figures A-1 through A-3). The transmissivity and storativity values interpreted from the drawdown data are 0.55 ft^2/d (5.9 x 10^{-7} m^2/s) and 1.6 x 10^{-5}, respectively (Table 6-1). The data and the simulations are in good agreement in all cases.

6.1.3 Summary of Results from the H-2 Pumping Test

The Culebra at the H-2 hydropad appears to behave hydraulically as a single-porosity medium with a transmissivity of approximately 0.55 ft^2/d (5.9 x 10^{-7} m^2/s) and a storativity of approximately 1.5 x 10^{-5}. No determination of anisotropy can be made with only one observation well.

6.2 H-6 Pumping Tests

Three pumping tests were performed at the H-6 hydropad. H-6b was the pumping well for the first test, and H-6c was the pumping well for the last two tests.

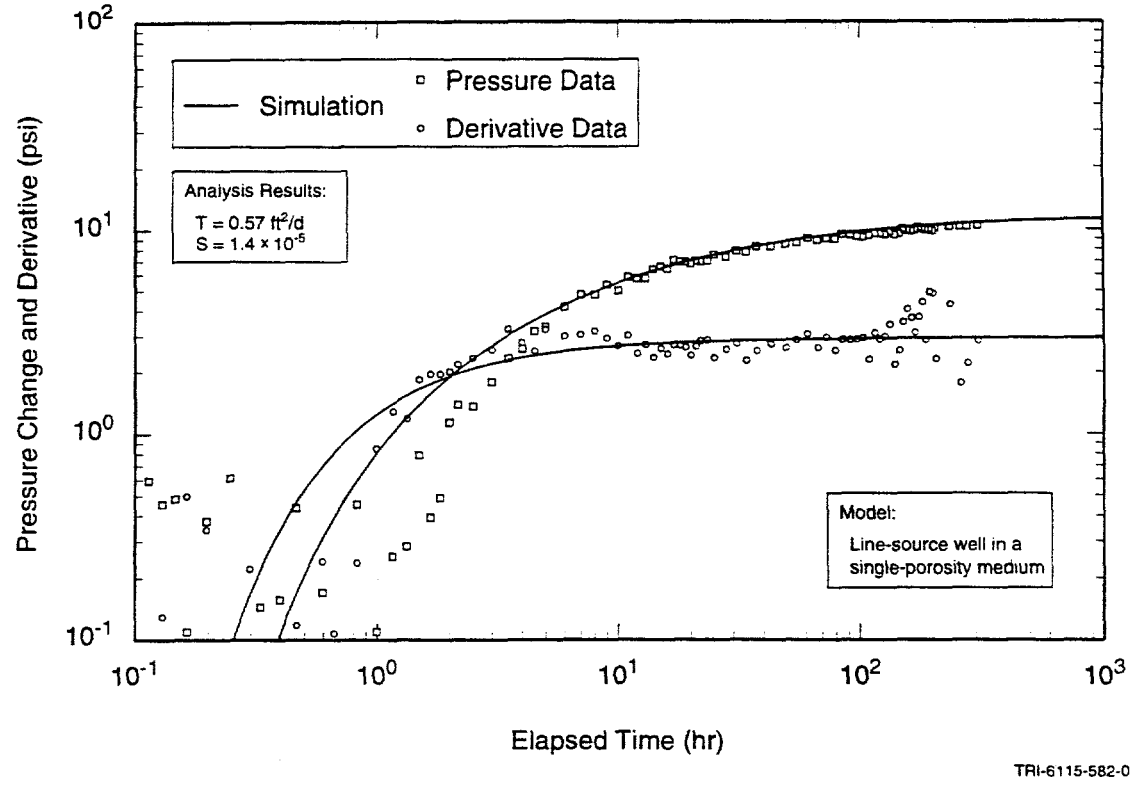

Figure 6-4. Log-log plot of H-2b recovery data with Interpret/2 simulation.

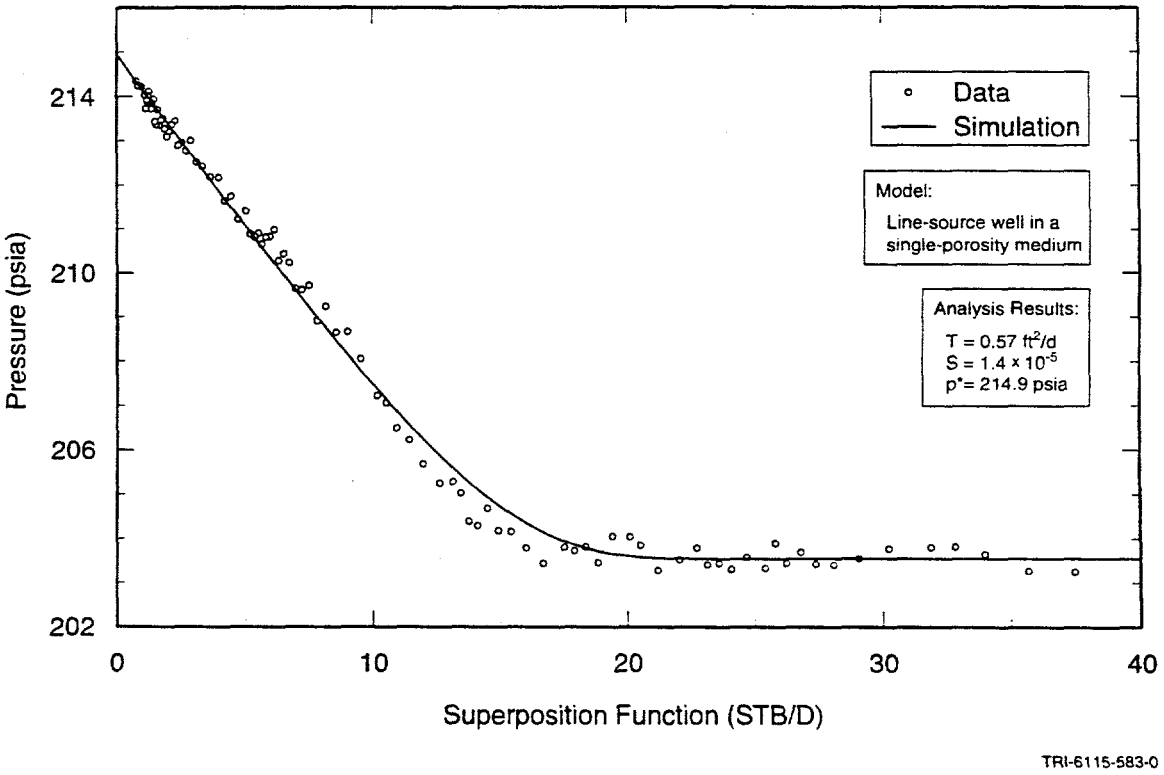

Figure 6-5. Horner plot of H-2b recovery data with Interpret/2 simulation.

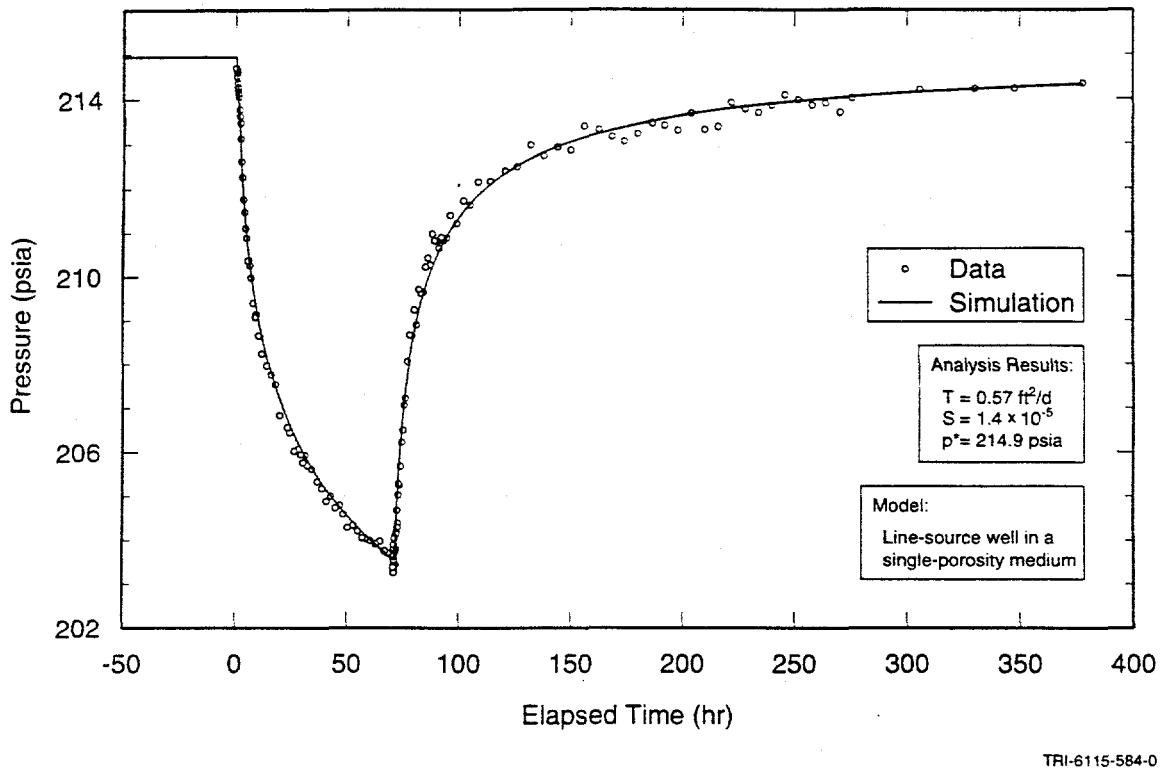

Figure 6-6. Linear-linear plot of H-2b data with Interpret/2 simulation derived from recovery analysis.

6.2.1 Test #1

As discussed in Section 5.2, the first pumping test at H-6 involved pumping H-6b for two days at a rate of approximately 23 gpm (1.5 L/s) while monitoring responses in H-6a and H-6c. Pressure recovery was monitored for four days after pumping.

6.2.1.1 H-6b

Figures 6-7 and 6-8 show the log-log and Horner plots, respectively, of the recovery data from H-6b during test #1 along with the best-fit Interpret/2 simulations. The data were analyzed using a model for a well with wellbore storage and skin in a double-porosity medium with unrestricted interporosity flow, slab geometry, and a constant-pressure boundary. The medium has a transmissivity of 38 ft^2/d (4.0×10^{-5} m^2/s). The boundary was modeled as a discrete feature 1,140 ft (350 m) from H-6b, but more likely represents the increase in Culebra transmissivity known to occur to the west in Nash Draw and/or to the east towards wells DOE-2 and WIPP-13 (Beauheim, 1986, 1987b). The estimated skin factor is strongly negative (-5.5), indicating a stimulated well in direct connection with fractures (Gringarten, 1984). Other interpreted parameters are listed in Table 6-1. Figure 6-9 is a linear-linear plot of the match of this model and the combined recovery and drawdown data.

Log-log, Horner, and linear-linear plots of the drawdown data and best-fit simulations are presented in Appendix A (Figures A-4 through A-6). The data and the simulations are in reasonable agreement in all cases, and the interpreted parameters are similar to those obtained from the recovery analysis (Table 6-1).

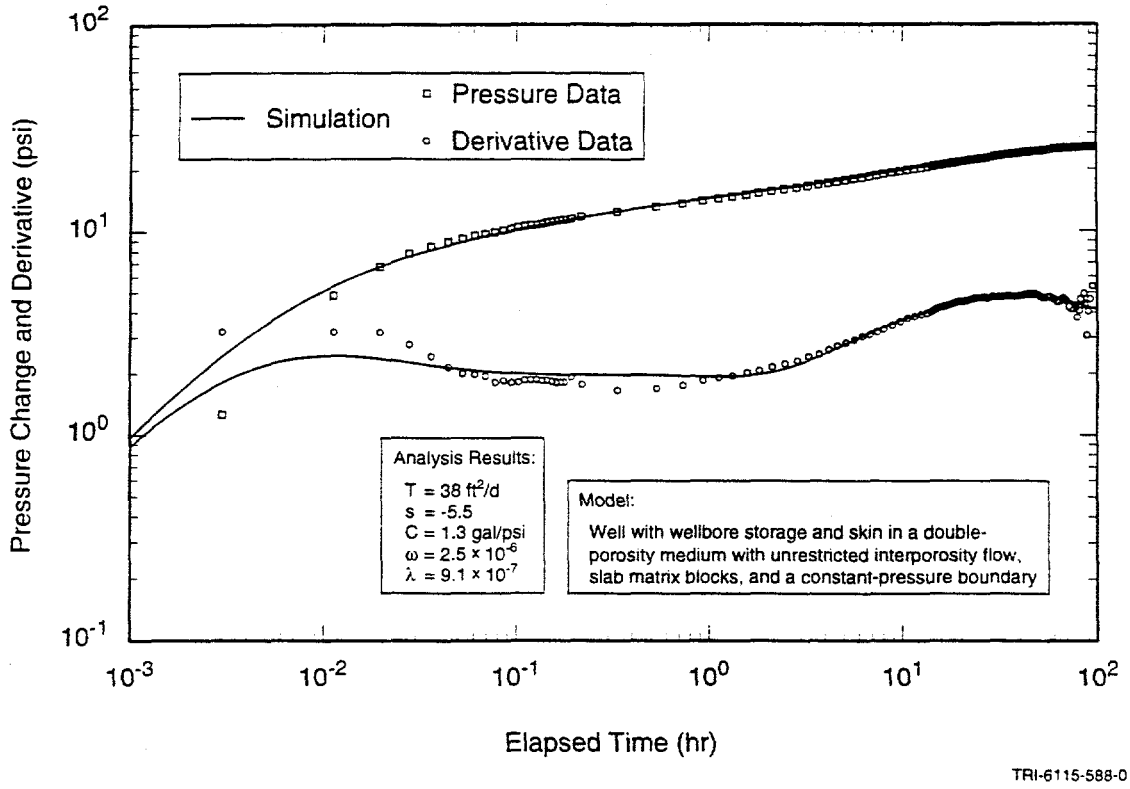

Figure 6-7. Log-log plot of H-6b recovery data from test #1 with Interpret/2 simulation.

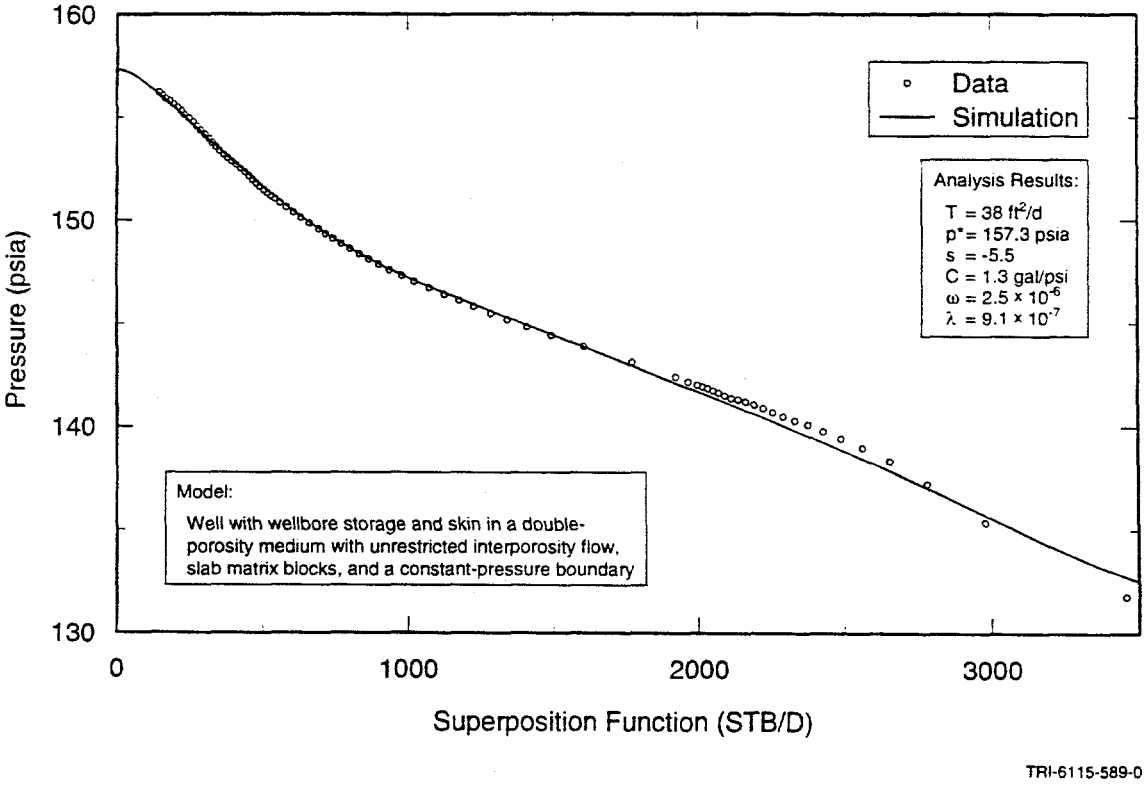

Figure 6-8. Horner plot of H-6b recovery data from test #1 with Interpret/2 simulation.

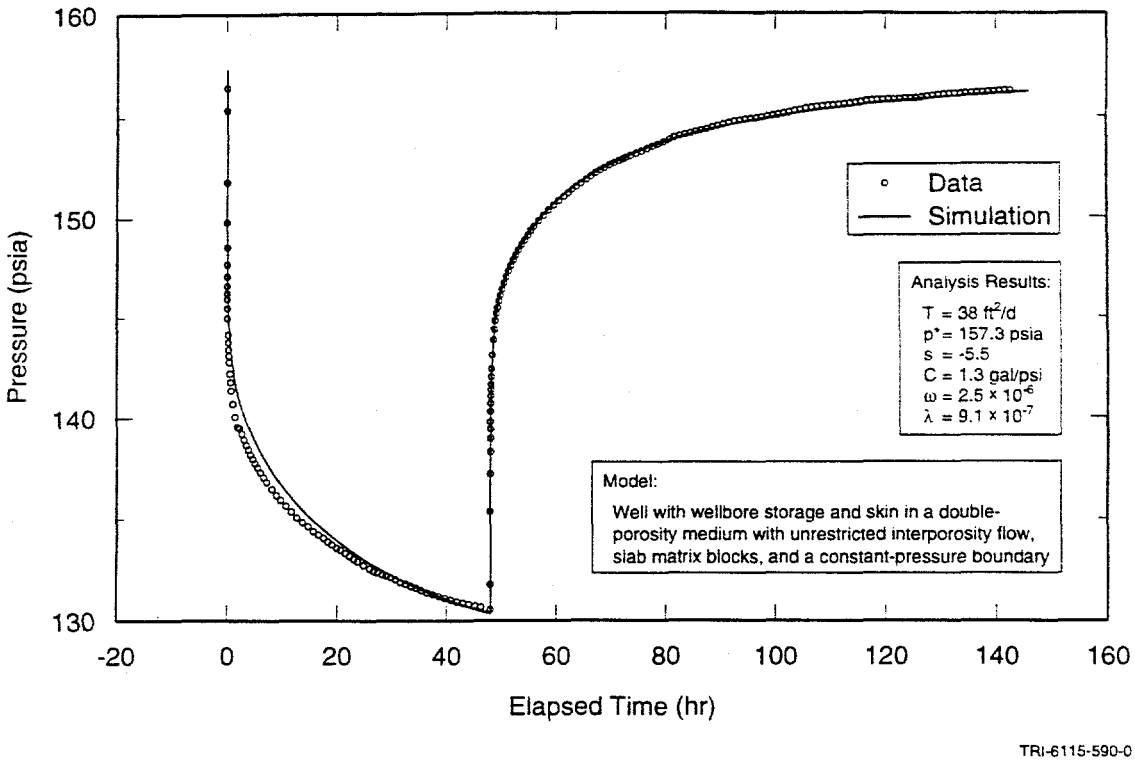

Figure 6-9. Linear-linear plot of H-6b data from test #1 with Interpret/2 simulation derived from recovery analysis.

6.2.1.2 OBSERVATION WELLS

Figures 6-10 through 6-12 and 6-13 through 6-15 show the log-log, Horner, and linear-linear plots of the recovery data from H-6a and H-6c, respectively, during test #1 along with the best-fit Interpret/2 simulations. The data were analyzed using models for line-source wells in a double-porosity medium having a constant-pressure boundary. The H-6a data were matched using a transmissivity of 37 ft^2/d (4.0×10^{-5} m^2/s) and a storativity of 1.9×10^{-4}, and the H-6c data were matched using a transmissivity of 36 ft^2/d (3.8×10^{-5} m^2/s) and a storativity of 1.7×10^{-4} (Table 6-1). The H-6a data were matched using a model with unrestricted interporosity flow and slab geometry while the H-6c data were matched using a model with restricted interporosity flow but, in both cases, the pressure-derivative data show behavior intermediate between those two extremes (i.e., a broader, less pronounced minimum than that provided by restricted interporosity flow but more pronounced than that provided by completely unrestricted interporosity flow). The interpreted double-porosity parameters are given in Table 6-1.

Log-log, Horner, and linear-linear plots of the drawdown data and best-fit simulations for H-6a and H-6c are presented in Appendix A (Figures A-7 through A-9 and A-10 through A-12, respectively). The data and the simulations are in reasonable agreement in all cases. The parameters interpreted from the drawdown analyses are listed in Table 6-1.

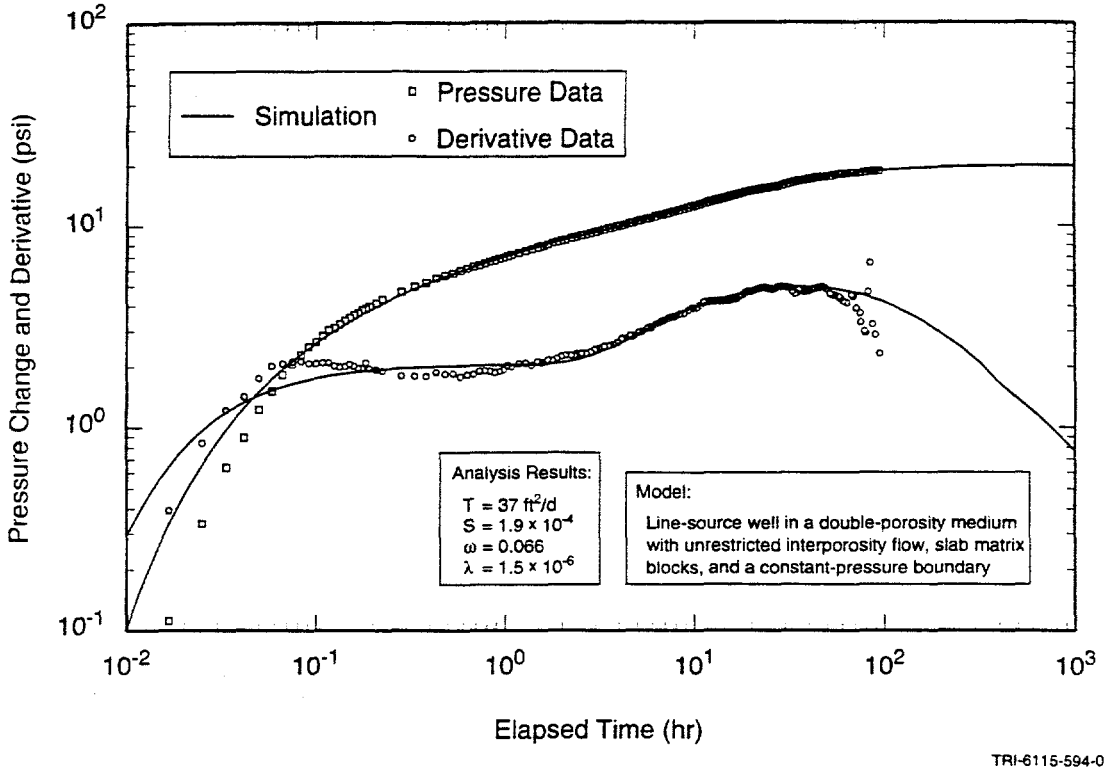

Figure 6-10. Log-log plot of H-6a recovery data from test #1 with Interpret/2 simulation.

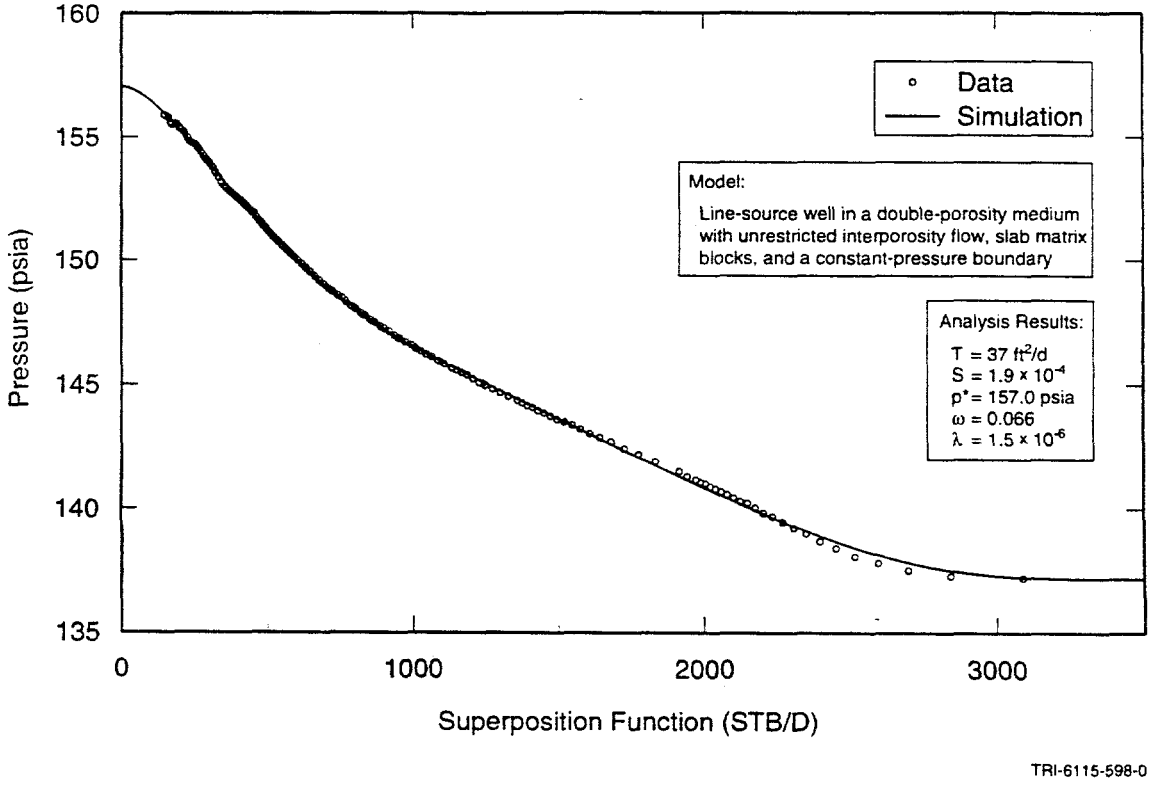

Figure 6-11. Horner plot of H-6a recovery data from test #1 with Interpret/2 simulation.

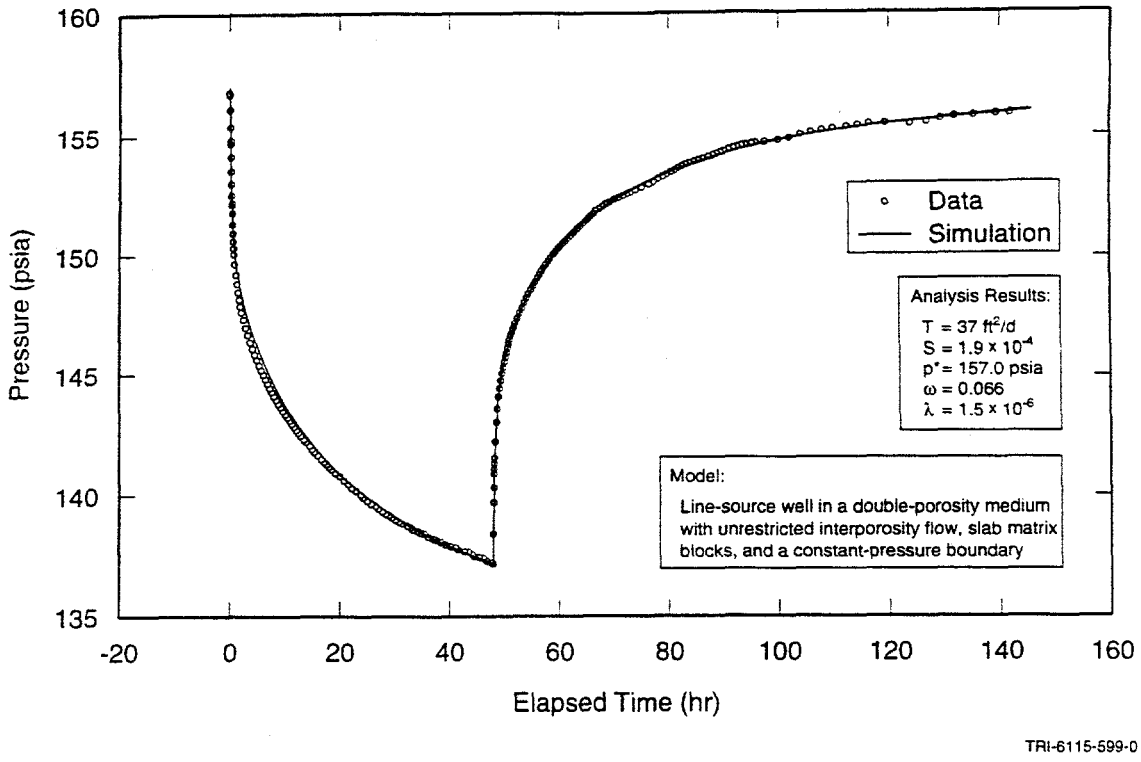

Figure 6-12. Linear-linear plot of H-6a data from test #1 with Interpret/2 simulation derived from recovery analysis.

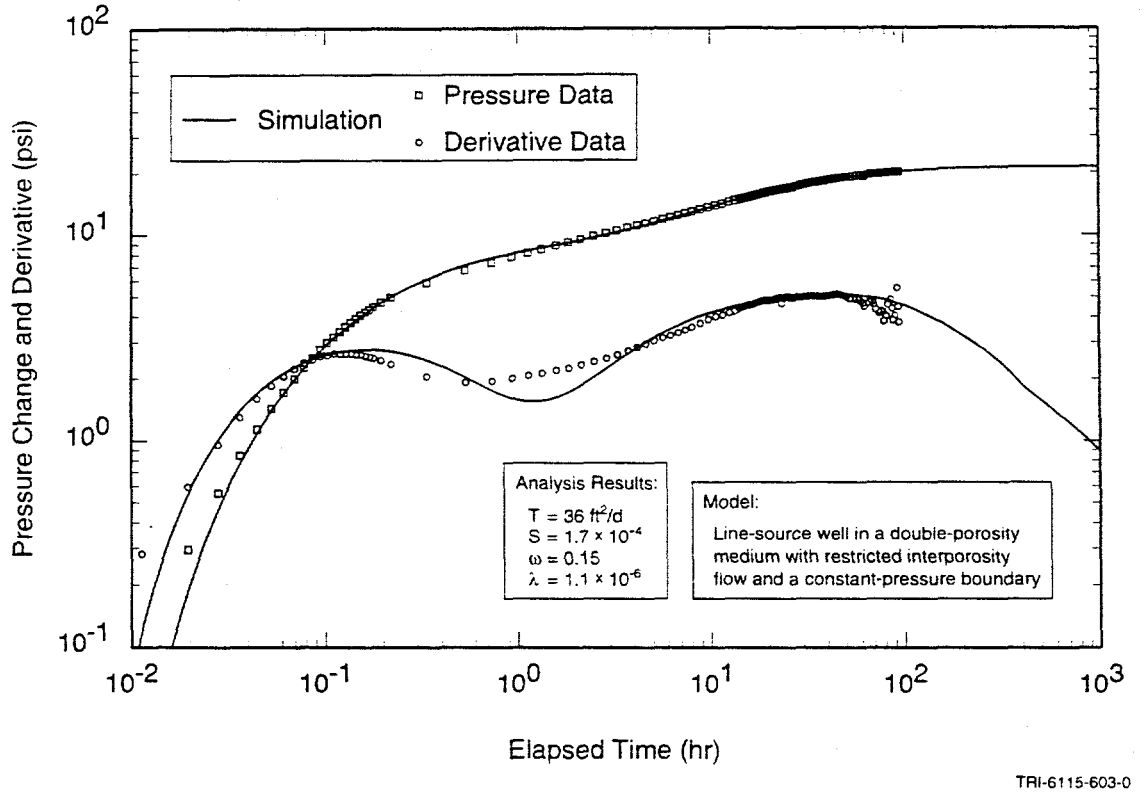

Figure 6-13. Log-log plot of H-6c recovery data from test #1 with Interpret/2 simulation.

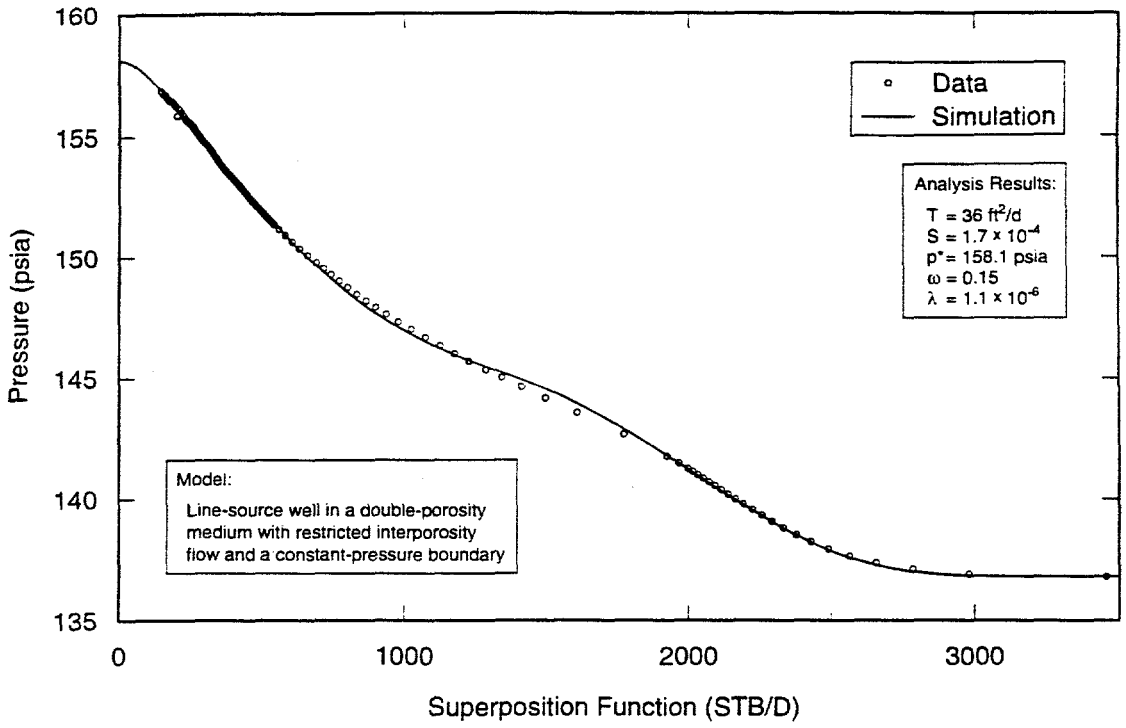

Figure 6-14. Horner plot of H-6c recovery data from test #1 with Interpret/2 simulation.

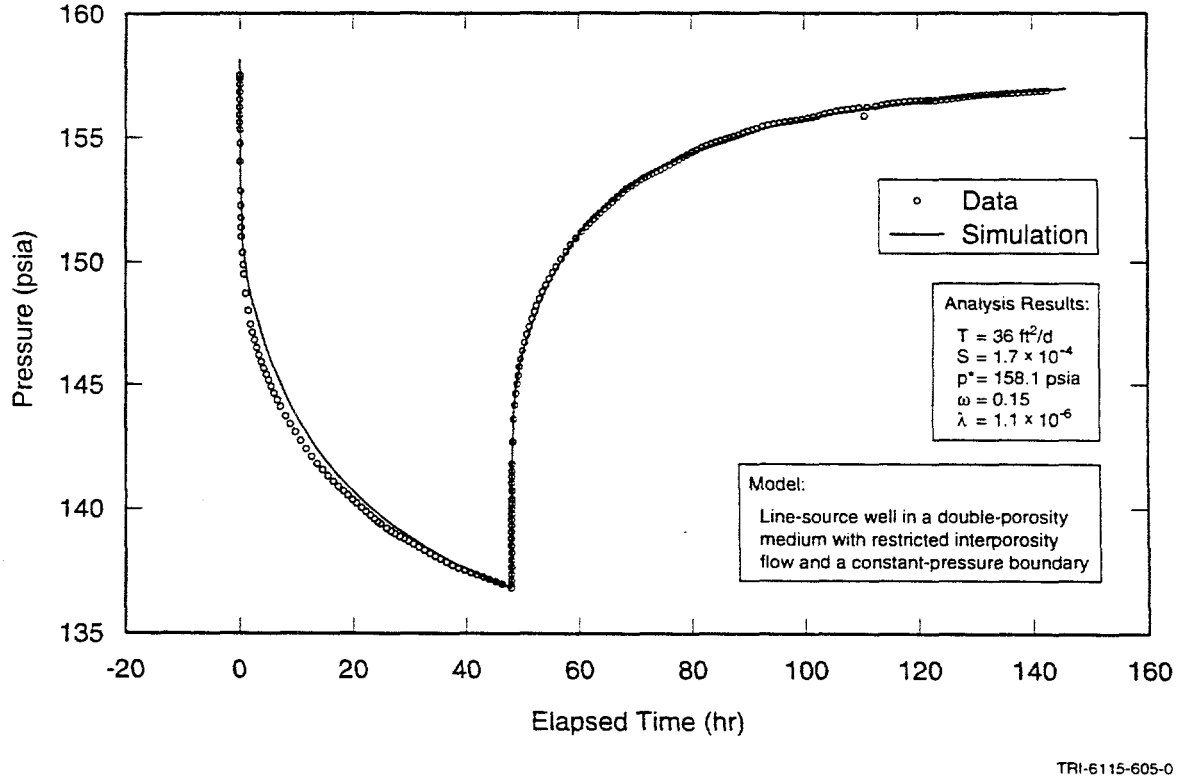

Figure 6-15 Linear-linear plot of H-6c data from test #1 with Interpret/2 simulation derived from recovery analysis.

6.2.2 Test #2

As discussed in Section 5.2, the second pumping test at H-6 involved pumping H-6c at approximately 18.9 gpm (1.19 L/s) for 1.38 days while monitoring responses in H-6a and H-6b. Pressure recovery was monitored for 6.28 days after pumping. Data from H-6c were not interpretable because the water level dropped below the transducer for much of the test. Undocumented flow-rate fluctuations made interpretation of the H-6a and H-6b drawdown data problematic, so only the recovery responses from those wells were analyzed.

Figures 6-16 through 6-18 and 6-19 through 6-21 show the log-log, Horner, and linear-linear plots of the recovery data from H-6a and H-6b, respectively, during test #2 along with the best-fit Interpret/2 simulations. The data were analyzed using a model for a line-source well in a double-porosity medium with unrestricted interporosity flow, slab geometry, and a constant-pressure boundary. Reasonable log-log and Horner matches are obtainable without a constant-pressure boundary, but the resulting linear-linear simulations cannot simultaneously match both the drawdown and recovery, a problem that disappears when a constant-pressure boundary is added. The H-6a data were matched using a transmissivity of 37 ft^2/d (4.0 x 10^{-5} m^2/s) and a storativity of 2.6 x 10^{-4}, and the H-6b data were matched using a transmissivity of 37 ft^2/d (4.0 x 10^{-5} m^2/s) and a storativity of 1.9 x 10^{-4}. Other interpreted parameters are given in Table 6-1.

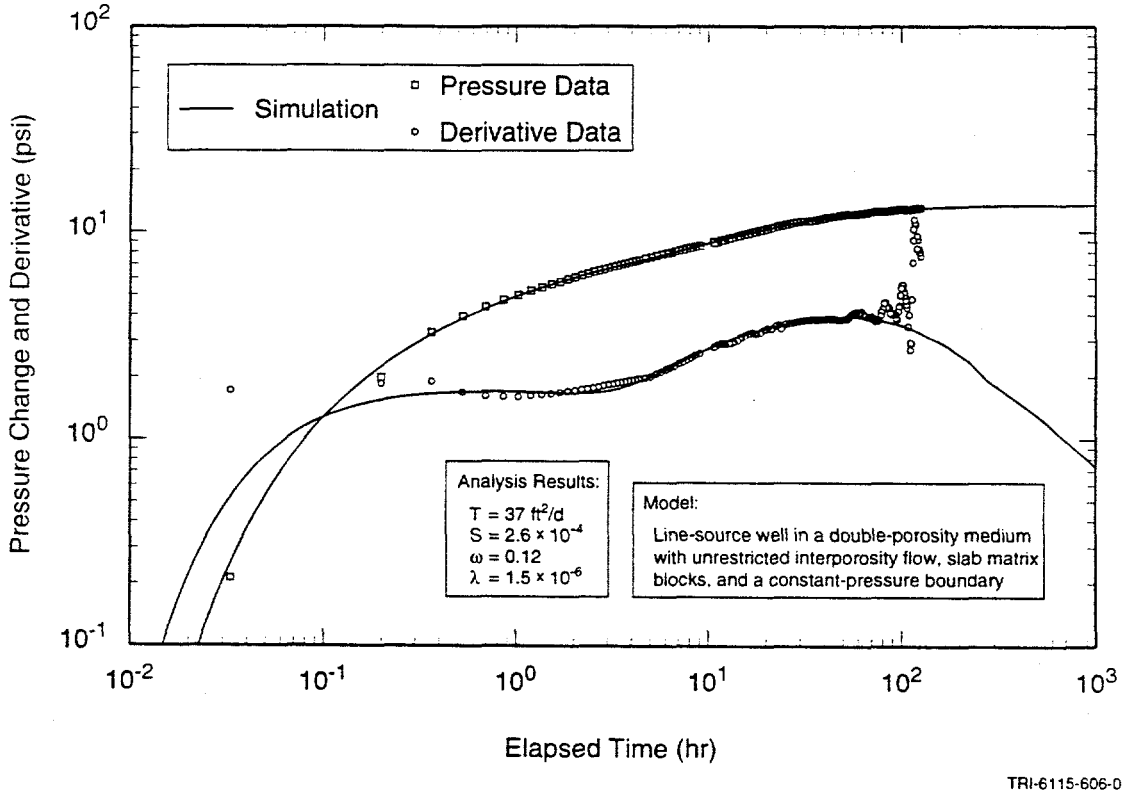

Figure 6-16. Log-log plot of H-6a recovery data from test #2 with Interpret/2 simulation.

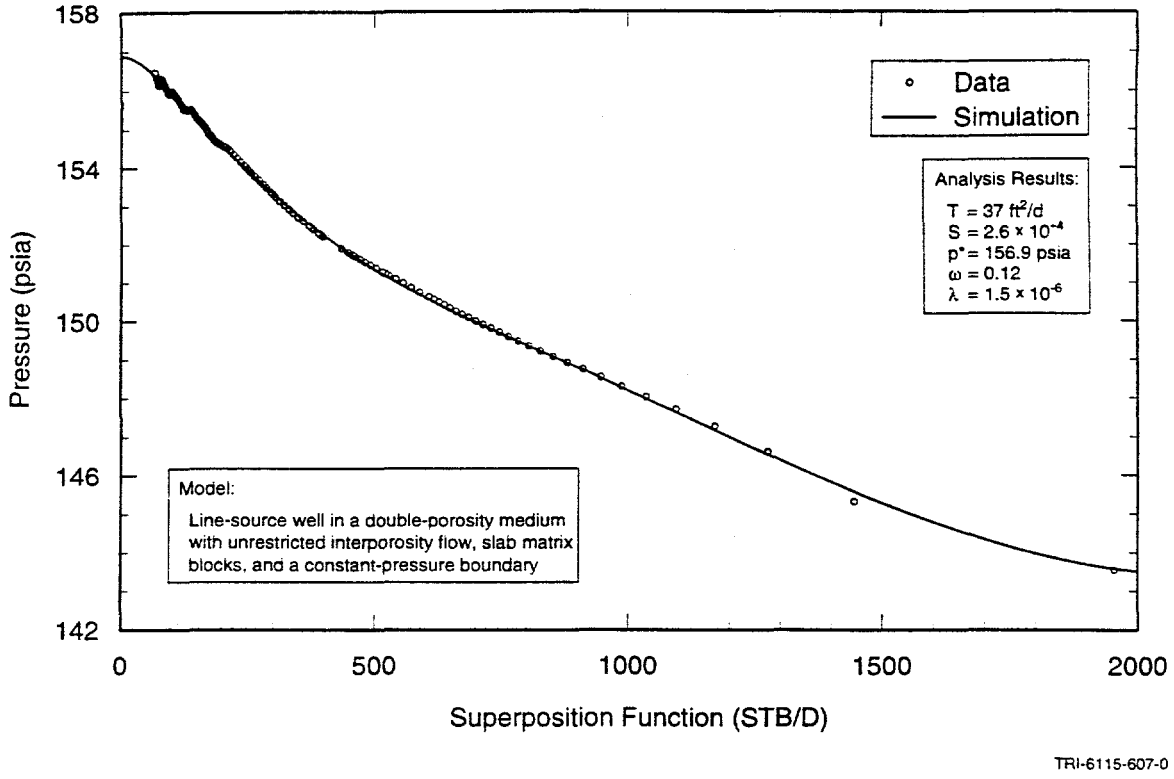

Figure 6-17. Horner plot of H-6a recovery data from test #2 with Interpret/2 simulation.

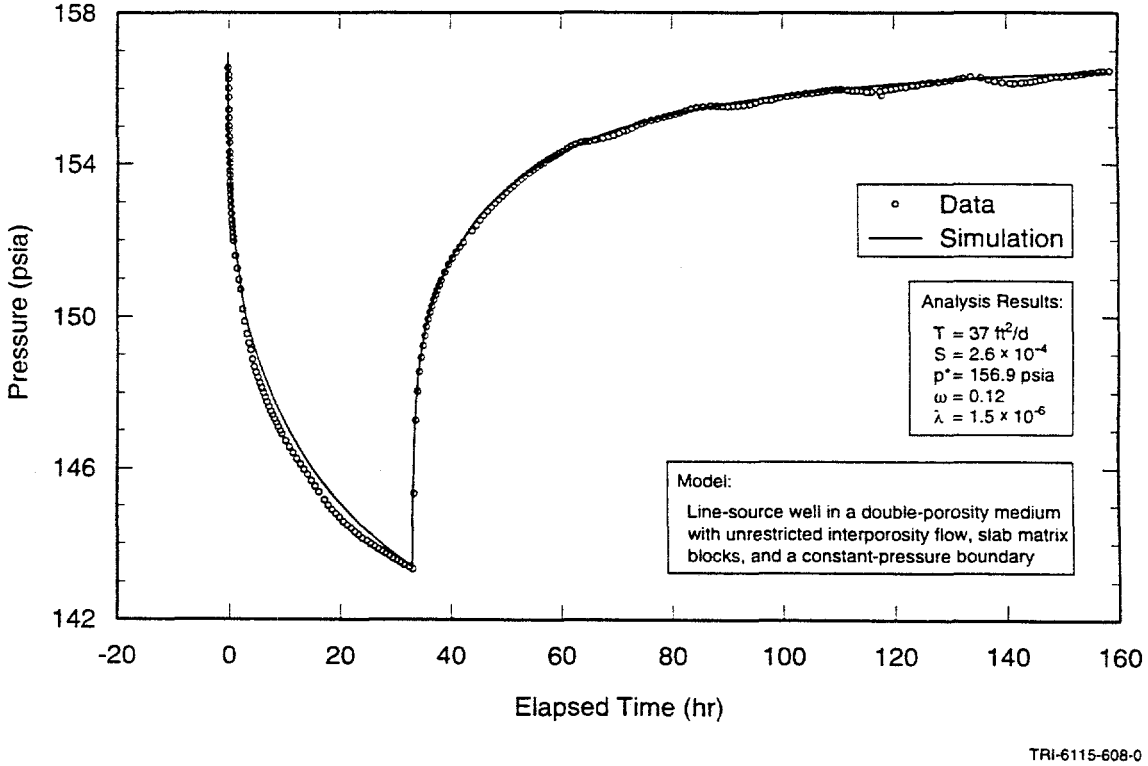

Figure 6-18. Linear-linear plot of H-6a data from test #2 with Interpret/2 simulation derived from recovery analysis.

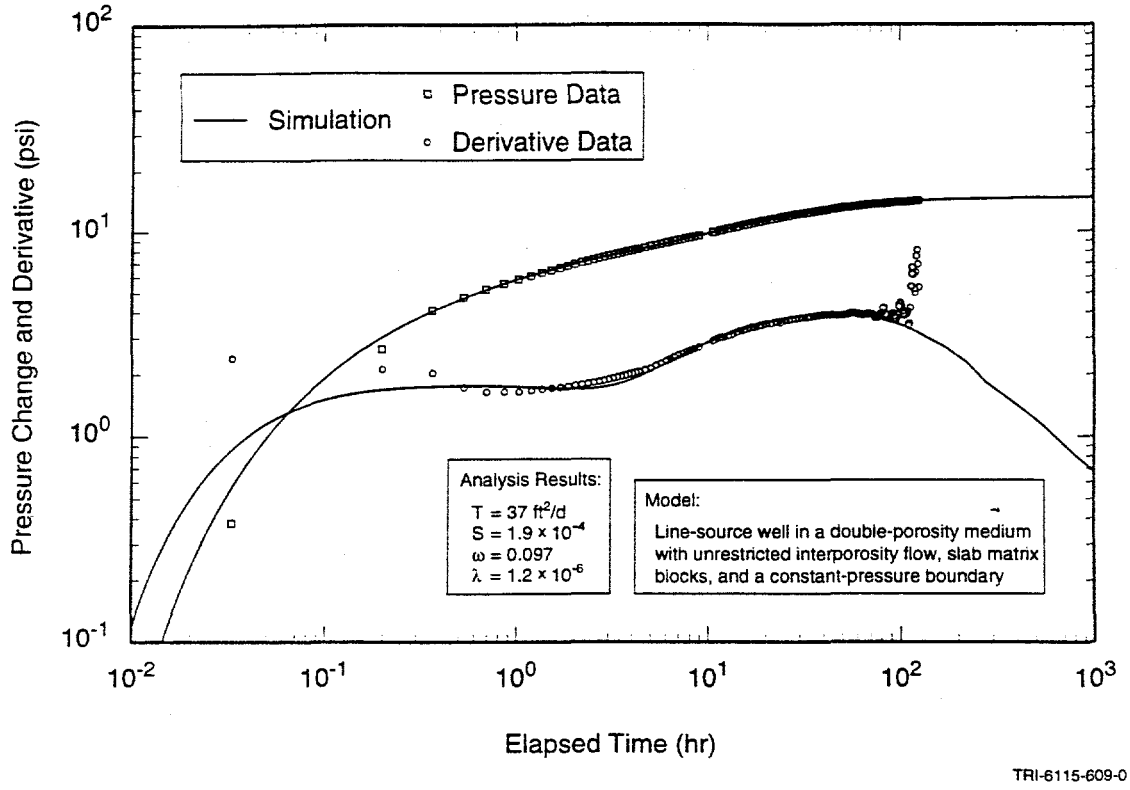

Figure 6-19. Log-log plot of H-6b recovery data from test #2 with Interpret/2 simulation.

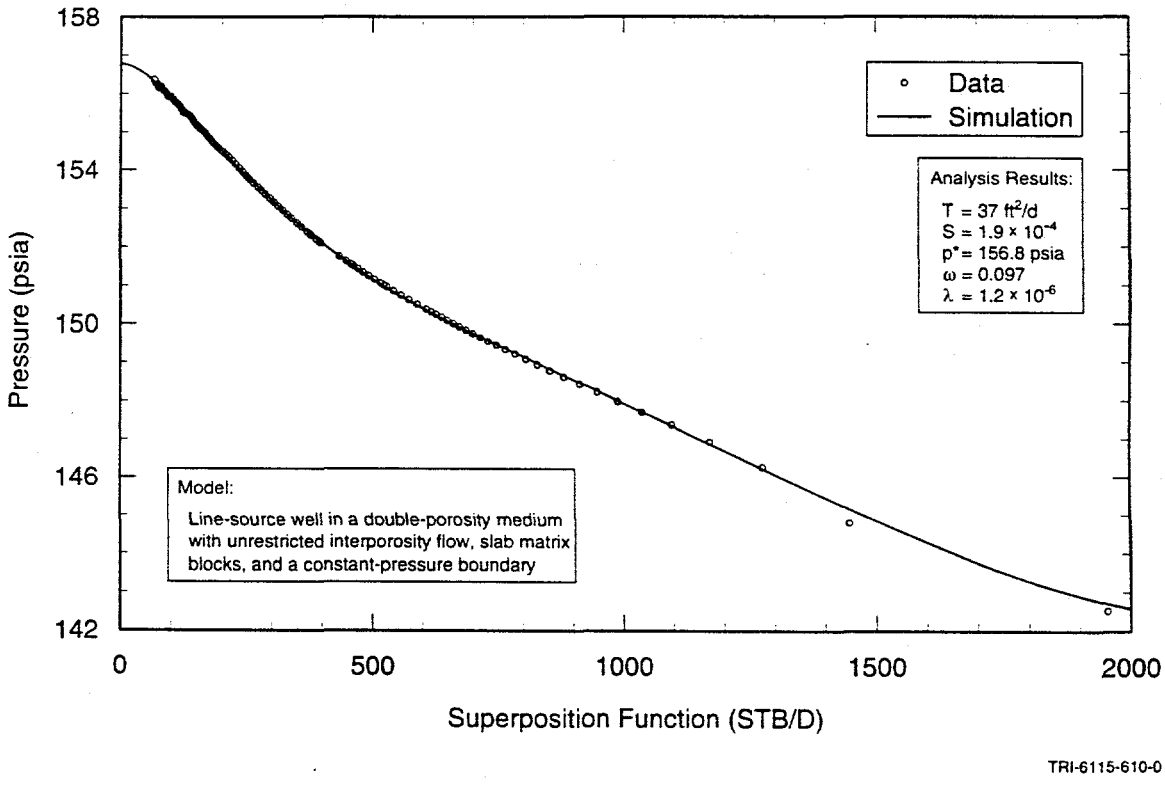

Figure 6-20. Horner plot of H-6b recovery data from test #2 with Interpret/2 simulation.

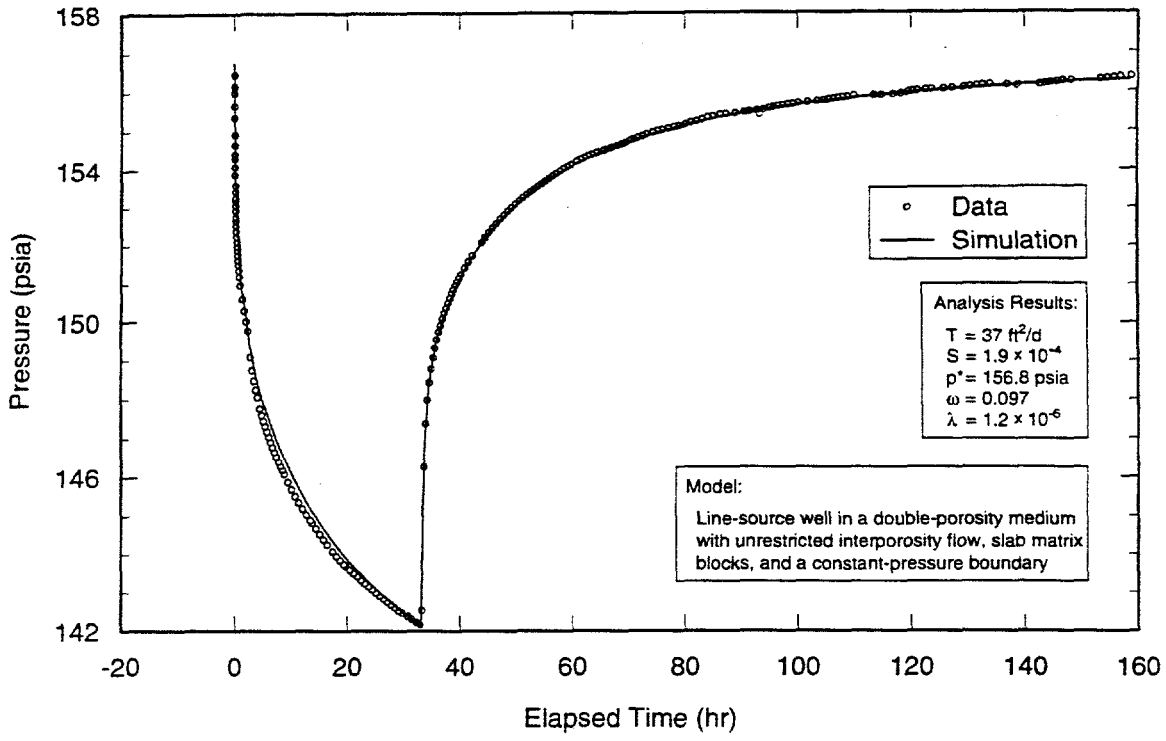

Figure 6-21. Linear-linear plot of H-6b data from test #2 with Interpret/2 simulation derived from recovery analysis.

6.2.3 Test #3

As discussed in Section 5.2, the third pumping test at the H-6 hydropad involved pumping H-6c at approximately 16.5 gpm (1.04 L/s) for 6.19 days while monitoring responses in H-6a and H-6b. Pressure recovery was monitored for eight days after pumping. The drawdown data from H-6c are considered uninterpretable because of undocumented flow-rate fluctuations.

6.2.3.1 H-6c

Figures 6-22 and 6-23 show the log-log and Horner plots, respectively, of the recovery data from H-6c during test #3 along with the best-fit Interpret/2 simulations. The data were analyzed using a model for a well with wellbore storage and skin in a double-porosity medium with restricted interporosity flow having a transmissivity of 38 ft^2/d (4.1 x 10^{-5} m^2/s) and a constant-pressure boundary at 950 ft (290 m). The estimated skin factor is 1.2, indicating a slightly degraded connection between the well and the Culebra. Other interpreted parameters are listed in Table 6-1. Figure 6-24 is a linear-linear plot of the match of this model and the combined recovery and drawdown data. The data and the simulation are in good agreement considering the flow-rate fluctuations that are not included in the model.

6.2.3.2 OBSERVATION WELLS

Figures 6-25 through 6-27 and 6-28 through 6-30 show the log-log, Horner, and linear-linear plots of the recovery data from H-6a and H-6b, respectively, during test #3 along with the best-fit Interpret/2 simulations. The data were analyzed using a model for a line-source well in a double-porosity medium with restricted interporosity flow and a constant-

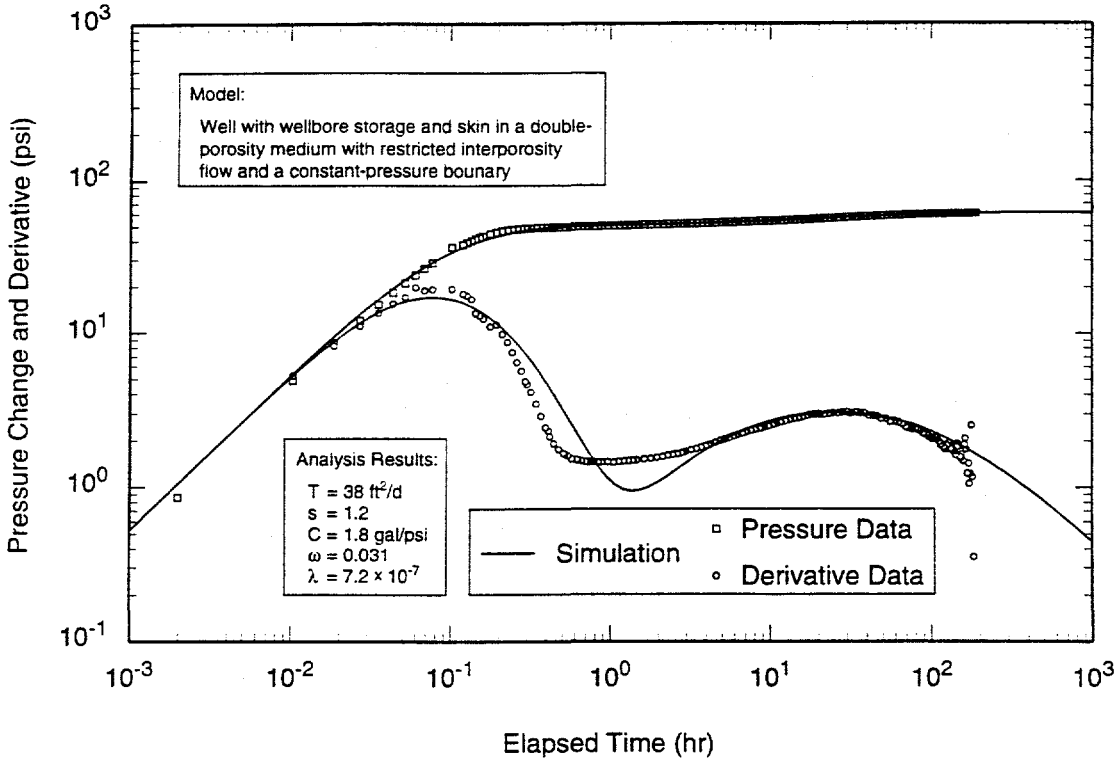

Figure 6-22. Log-log plot of H-6c recovery data from test #3 with Interpret/2 simulation.

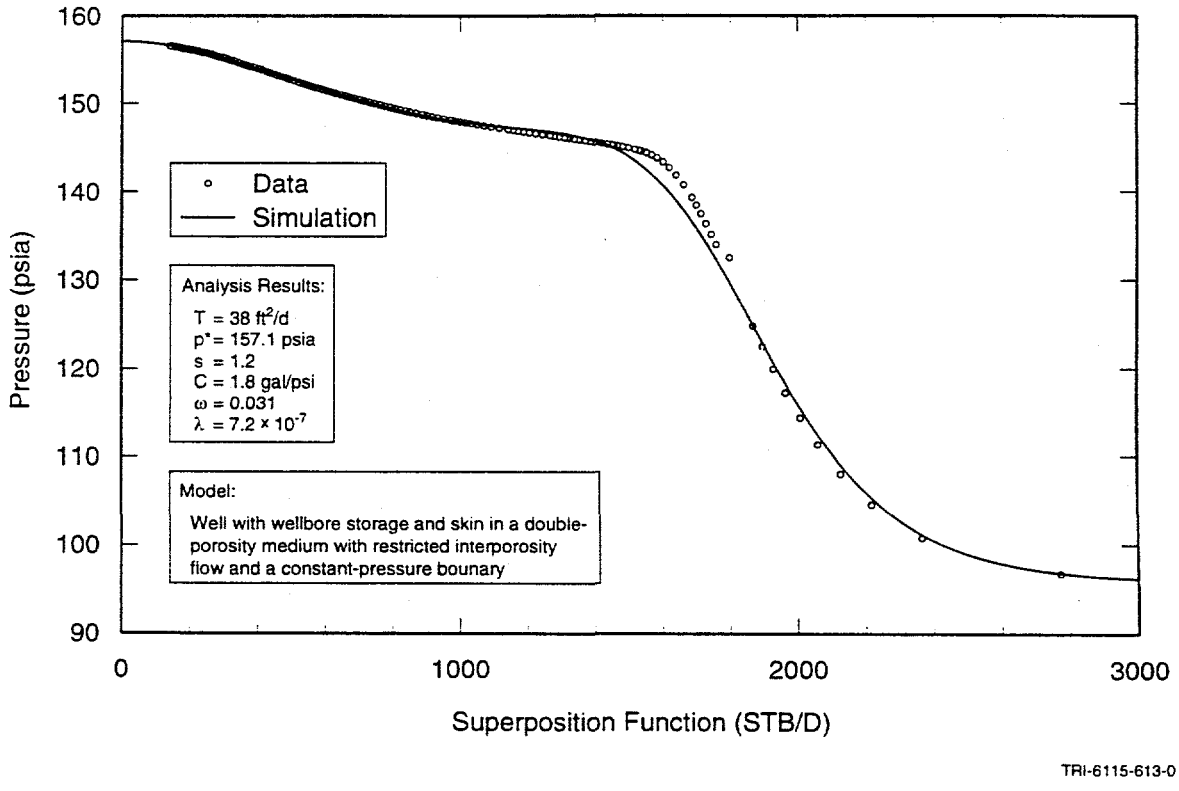

Figure 6-23. Horner plot of H-6c recovery data from test #3 with Interpret/2 simulation.

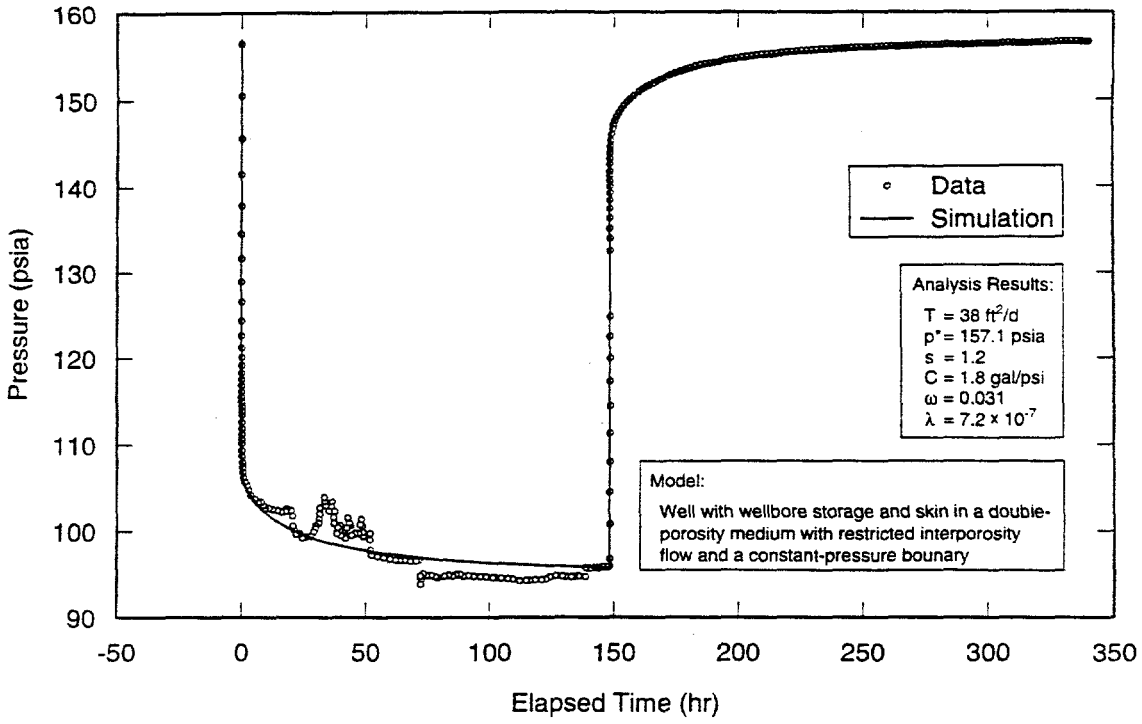

Figure 6-24. Linear-linear plot of H-6c data from test #3 with Interpret/2 simulation derived from recovery analysis.

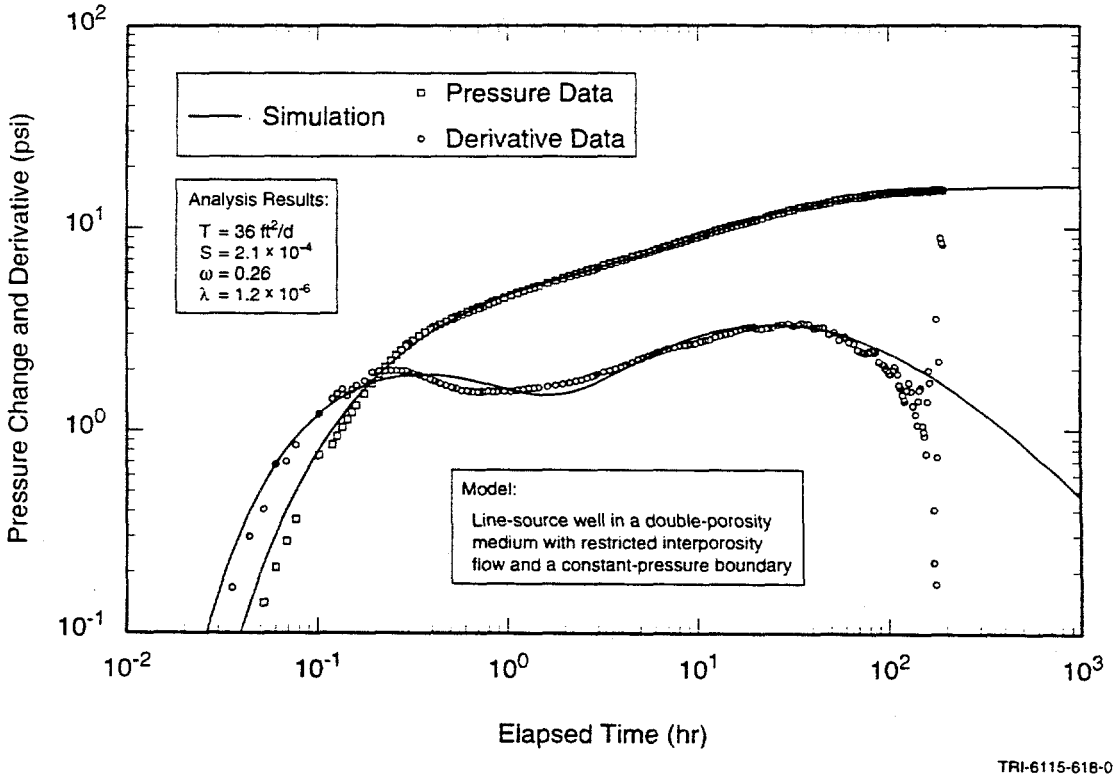

Figure 6-25. Log-log plot of H-6a recovery data from test #3 with Interpret/2 simulation.

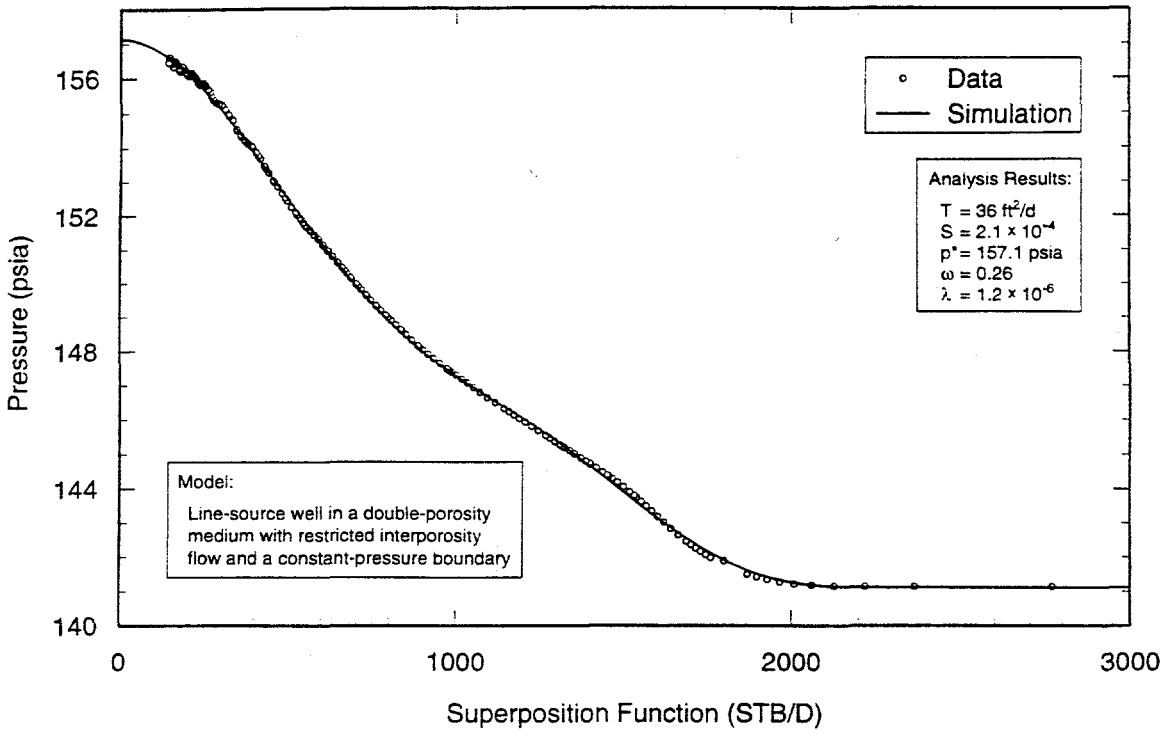

Figure 6-26. Horner plot of H-6a recovery data from test #3 with Interpret/2 simulation.

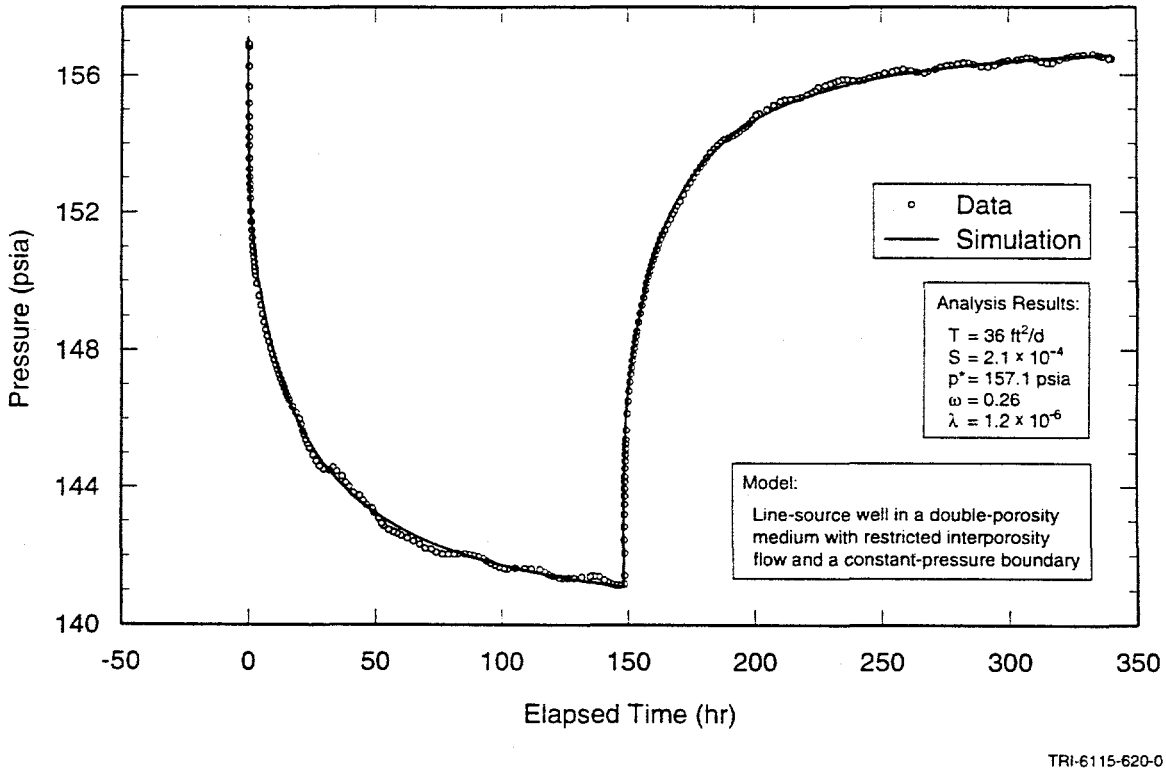

Figure 6-27. Linear-linear plot of H-6a data from test #3 with Interpret/2 simulation derived from recovery analysis.

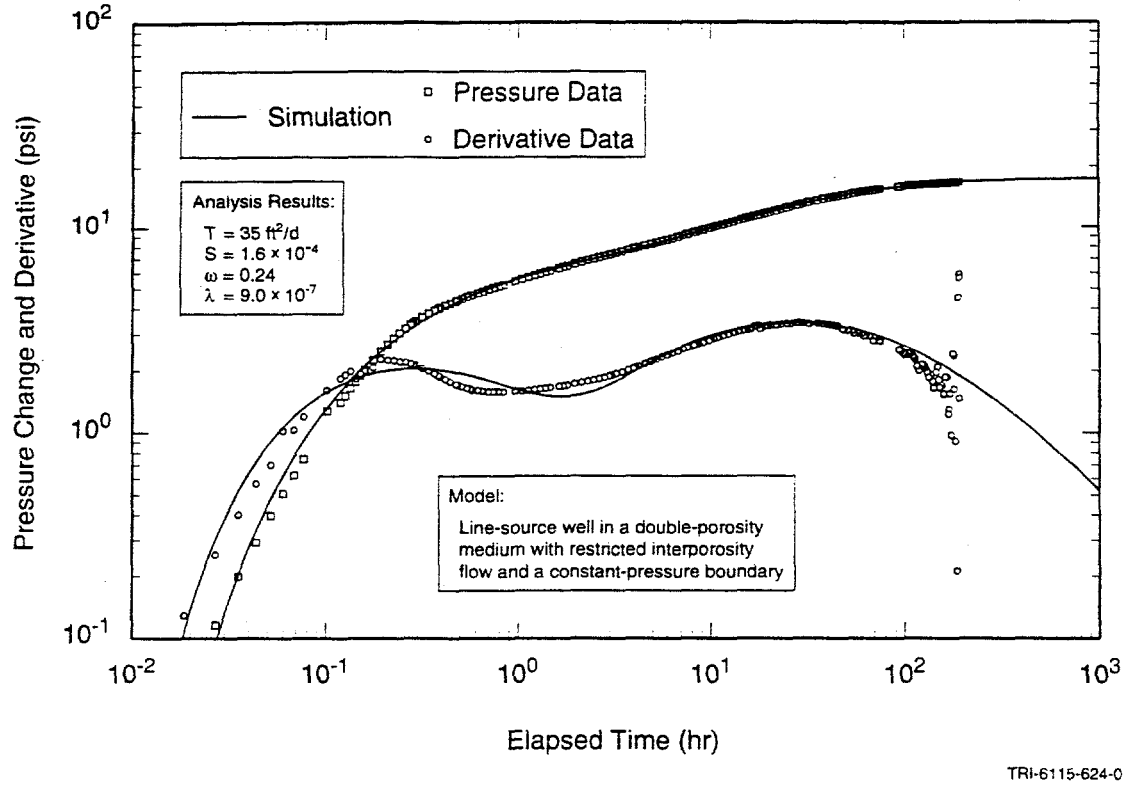

Figure 6-28. Log-log plot of H-6b recovery data from test #3 with Interpret/2 simulation.

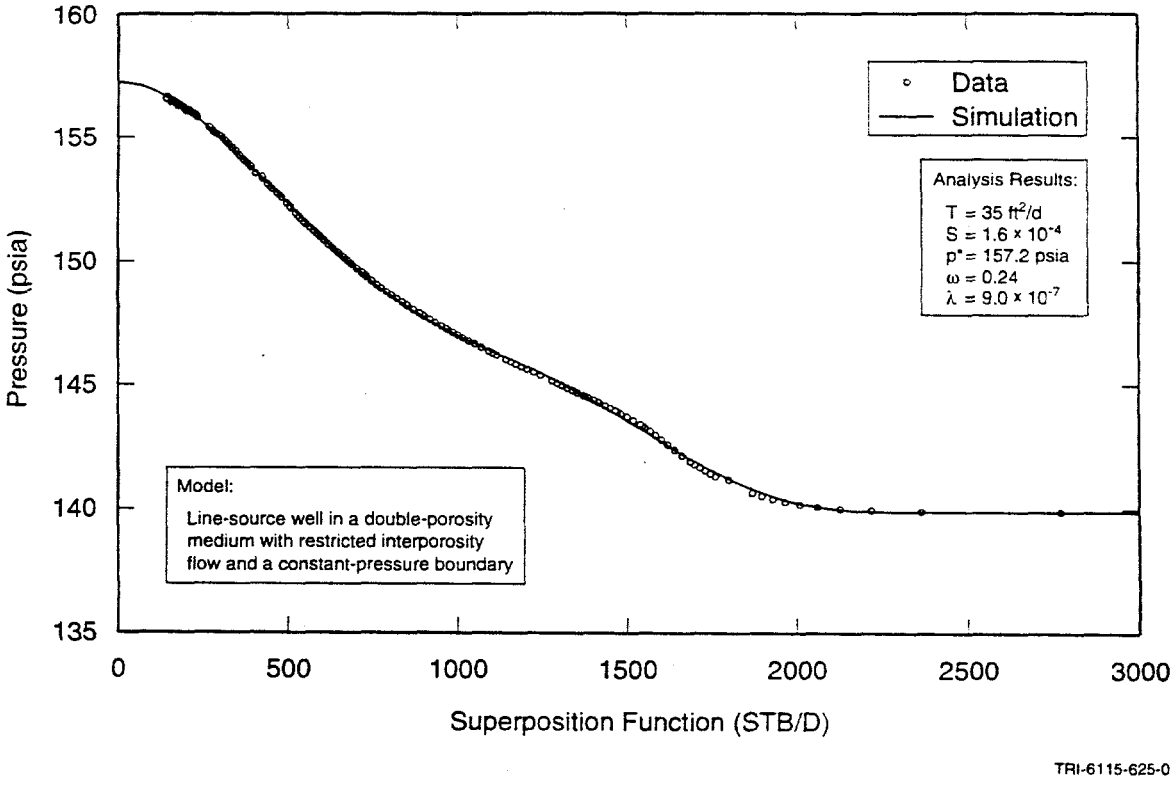

Figure 6-29. Horner plot of H-6b recovery data from test #3 with Interpret/2 simulation.

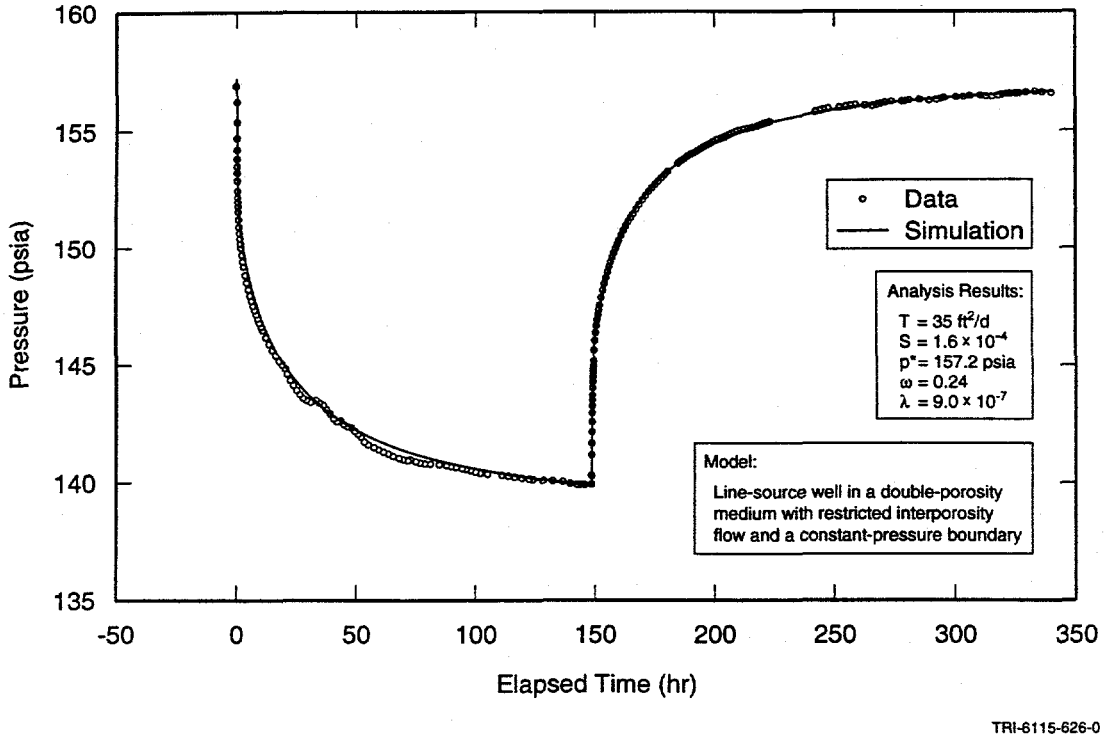

Figure 6-30. Linear-linear plot of H-6b data from test #3 with Interpret/2 simulation derived from recovery analysis.

pressure boundary. The H-6a data were matched using a transmissivity of 36 ft^2/d (3.9 x 10^{-5} m^2/s) and a storativity of 2.1 x 10^{-4}, and the H-6b data were matched using a transmissivity of 35 ft^2/d (3.8 x 10^{-5} m^2/s) and a storativity of 1.6 x 10^{-4}. Other interpreted parameters are given in Table 6-1.

Log-log, Horner, and linear-linear plots of the drawdown data and best-fit simulations for H-6a and H-6b are presented in Appendix A (Figures A-13 through A-15 and A-16 through A-18, respectively). The parameters interpreted from the drawdown analyses are listed in Table 6-1.

6.2.4 H-6 Anisotropy Analysis

Anisotropy at the H-6 hydropad has been previously evaluated by Neuman et al. (1984) and Grimestad (1995). Neuman et al. (1984) fit a single-porosity model to the early-time drawdown data from H-6a and H-6c from test #1 and from H-6a and H-6b from test #3 (which they designate Test 2) and determined transmissivities ranging from 67 to 70 ft^2/d (7.2 to 7.5 x 10^{-5} m^2/s). They calculated the ratio of maximum to minimum transmissivity to be 1.9, with the major axis of transmissivity having a magnitude of 95 ft^2/d (1.0 x 10^{-4} m^2/s) oriented N30°W and the minor axis having a magnitude of 50 ft^2/d (5.4 x 10^{-5} m^2/s) oriented N60°E. They estimated the effective transmissivity to be 69 ft^2/d (7.4 x 10^{-5} m^2/s) and storativity to be 1.9 x 10^{-5}.

Grimestad (1995) analyzed the same data as Neuman et al. (1984), but used a double-porosity model to fit all of the drawdown data except for that affected by a boundary at late time. He found the ratio of maximum to minimum transmissivity to be 1.6, with the major axis of transmissivity having a magnitude of 46 ft^2/d (5.0 x 10^{-5} m^2/s) oriented N20°W and the minor axis having a magnitude of 29 ft^2/d (3.1 x 10^{-5} m^2/s) oriented

N70°E. He estimated the effective transmissivity to be 37 ft^2/d (3.9 x 10^{-5} m^2/s) and storativity (the sum of his "aquifer" and "matrix" storativities) to be 1.3×10^{-4}.

We have used all of the H-6 observation-well transmissivity and storativity values presented in Table 6-1 to determine anisotropy using the method of Grimestad (1995). Our analysis results are similar to those of Grimestad (1995). We found that anisotropy is relatively weak at H-6, with the ratio of maximum to minimum transmissivity being only 1.6 (Table 6-2). The major axis of transmissivity has a magnitude of 47 ft^2/d (5.1 x 10^{-5} m^2/s) oriented N13°W. The minor axis of transmissivity has a magnitude of 29 ft^2/d (3.1 x 10^{-5} m^2/s) oriented N77°E. The fitted transmissivity ellipse is depicted graphically in Figure 6-31. The effective transmissivity is 37 ft^2/d (4.0 x 10^{-5} m^2/s) and the storativity is 1.8×10^{-4}.

Table 6-2. Anisotropy Results

Hydropad	$T_{maximum}$ $(ft^2/d)/(m^2/s)$	Orientation of $T_{maximum}$	$T_{minimum}$ $(ft^2/d)/(m^2/s)$	$T_{maximum}/T_{minimum}$	$T_{effective}$ $(ft^2/d)/(m^2/s)$	Storativity
H-6	$47/5.1 \times 10^{-5}$	N13°W	$29/3.1 \times 10^{-5}$	1.6	$37/4.0 \times 10^{-5}$	1.8×10^{-4}
H-19	$6.9/7.4 \times 10^{-6}$	N8°W	$5.9/6.3 \times 10^{-6}$	1.2	$6.4/6.8 \times 10^{-6}$	4.9×10^{-5}

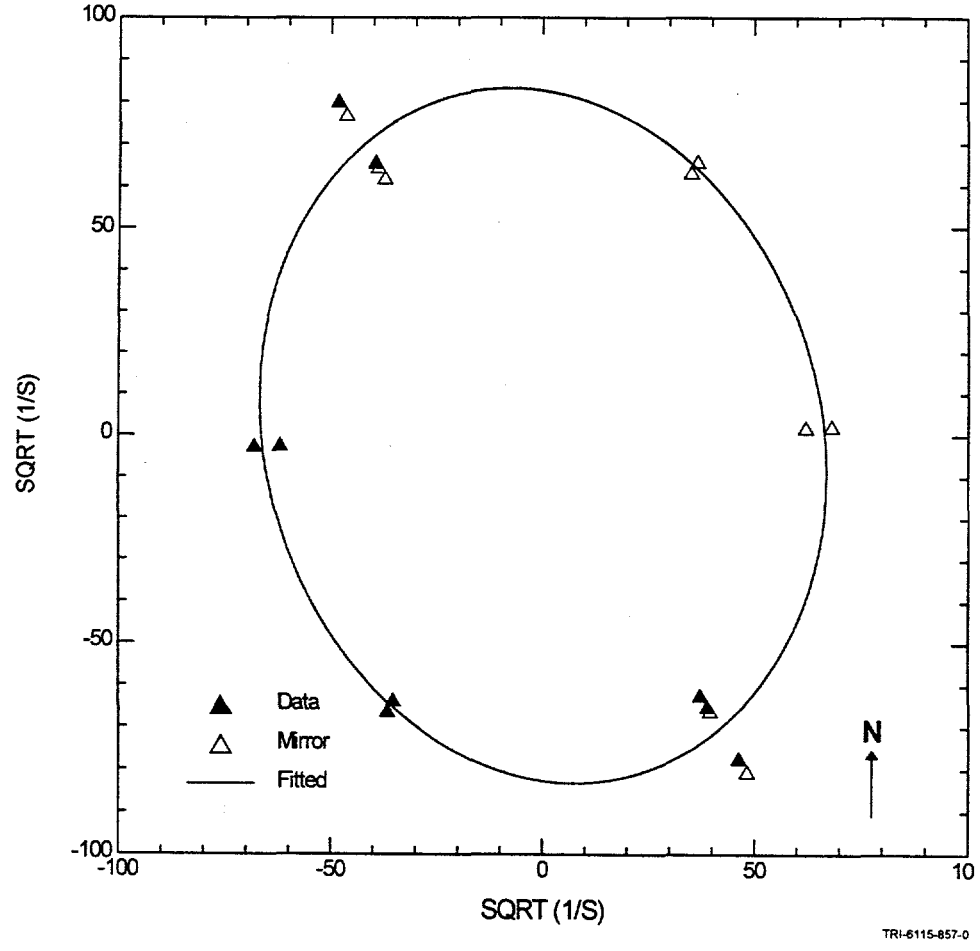

Figure 6-31. H-6 anisotropy ellipse.

6.2.5 Summary of Results from the H-6 Pumping Tests

Gonzalez (1983) gives the Culebra transmissivity at H-6 as 69 ft^2/d (7.4 x 10^{-5} m^2/s) and the storativity as 2 x 10^{-5}. The analysis he reported, however, was done on early-time data and neglected double-porosity effects. Mercer (1983) reported transmissivity at H-6b as 73 ft^2/d (7.8 x 10^{-5} m^2/s), again based on a single-porosity interpretation. Grimestad (1995) reanalyzed Gonzalez's data with a double-porosity model and reported an effective transmissivity of 37 ft^2/d (4.0 x 10^{-5} m^2/s) and storativity of 1.3 x 10^{-4}. The double-porosity analysis results presented here are similar to those of Grimestad, giving an effective transmissivity of 37 ft^2/d (4.0 x 10^{-5} m^2/s) and storativity of 1.8 x 10^{-4}. The ratio of maximum to minimum transmissivity is only 1.6, with the major axis of transmissivity oriented N13°W.

The double-porosity interpretations give lower values of transmissivity than the single-porosity interpretations because matrix blocks release significant volumes of fluid from storage and, consequently, fractures do not need to be as conductive as a single-porosity medium to provide the same amount of water at early time. Additional evidence that the Culebra is a double-porosity medium in the vicinity of the H-6 hydropad comes from video logs, core, and tracer-test interpretations. Video logs and core from the H-6 wells show the Culebra to be fractured, while tracer-breakthrough curves from H-6 can be simulated with a double-porosity model (involving flow through fractures and diffusion into and out of the rock matrix) but not with a single-porosity model (Jones et al., 1992). Thus, a firm basis exists for believing the Culebra to be a double-porosity medium at H-6.

Interpretations of the responses to pumping at H-6 consistently indicated the presence of a constant-pressure, or increased transmissivity, boundary within 1,200 ft (370 m) of the hydropad. This most likely represents increased transmissivity to the west in Nash Draw or to the east at wells DOE-2 and WIPP-13.

6.3 H-7 Pumping Test

As discussed in Section 5.3, the H-7 pumping test involved pumping in H-7b1 with wells H-7b2 and H-7c serving as observation wells. Interpretation of the pumping- and observation-well responses are described below.

6.3.1 H-7b1

As discussed in Section 5.3, earth-tidal effects are evident in the data from the H-7 wells. These effects introduce noise to the pressure-derivative data, making fitting to the derivative data impossible with Interpret/2. Figures 6-32 and 6-33 show the log-log and Horner plots, respectively, of the recovery data from H-7b1 along with the Interpret/2 simulations that best fit the pressure data. The simulations were obtained using a model for a well with wellbore storage and skin in an infinite double-porosity medium with restricted interporosity flow. The transmissivity used in the simulations is 1,400 ft^2/d (1.5 x 10^{-3} m^2/s). However, because of the low signal-to-noise ratio of the data, the simulations shown cannot be considered definitive. Other simulations using transmissivities between 1,000 and 2,000 ft^2/d (1 to 2 x 10^{-3} m^2/s) provide similarly good matches to the data. Therefore, we conclude only that the Culebra transmissivity at H-7b1 is on the order of 1,000 to 2,000 ft^2/d (1 to 2 x 10^{-3} m^2/s). The other parameter values used to produce the simulations shown in Figures 6-32 and 6-33 are listed in Table 6-1, but they should be considered to be as uncertain as the transmissivity estimate.

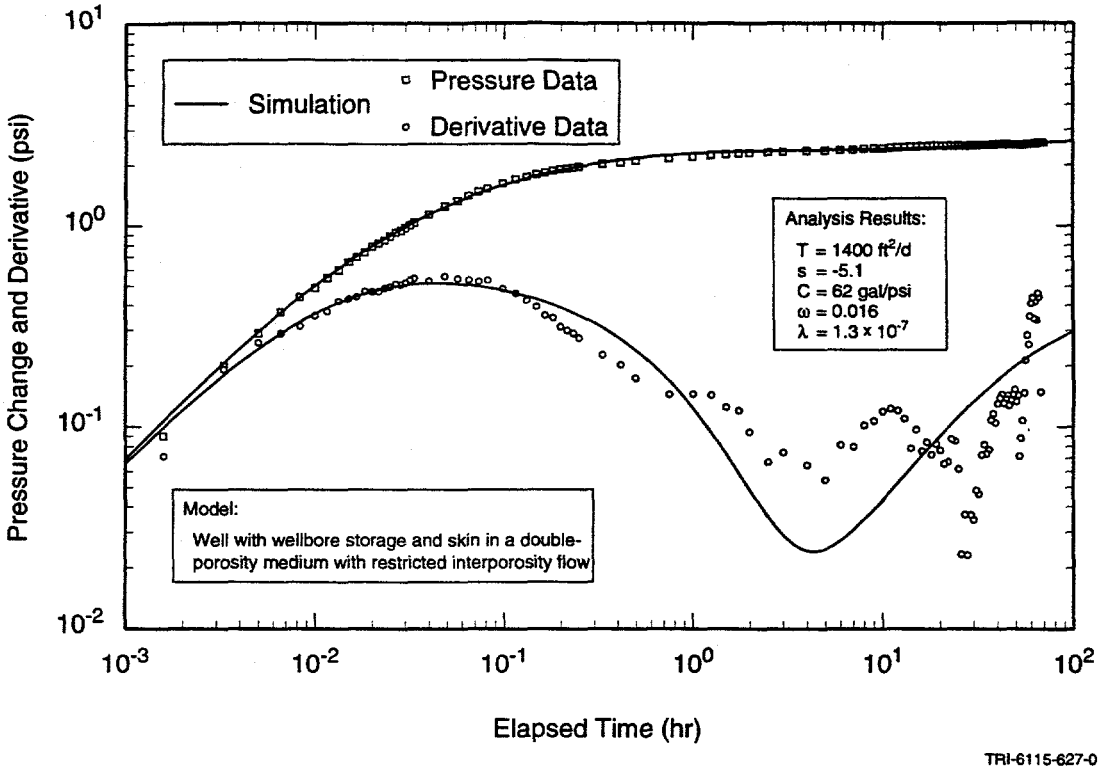

Figure 6-32. Log-log plot of H-7b1 recovery data with Interpret/2 simulation.

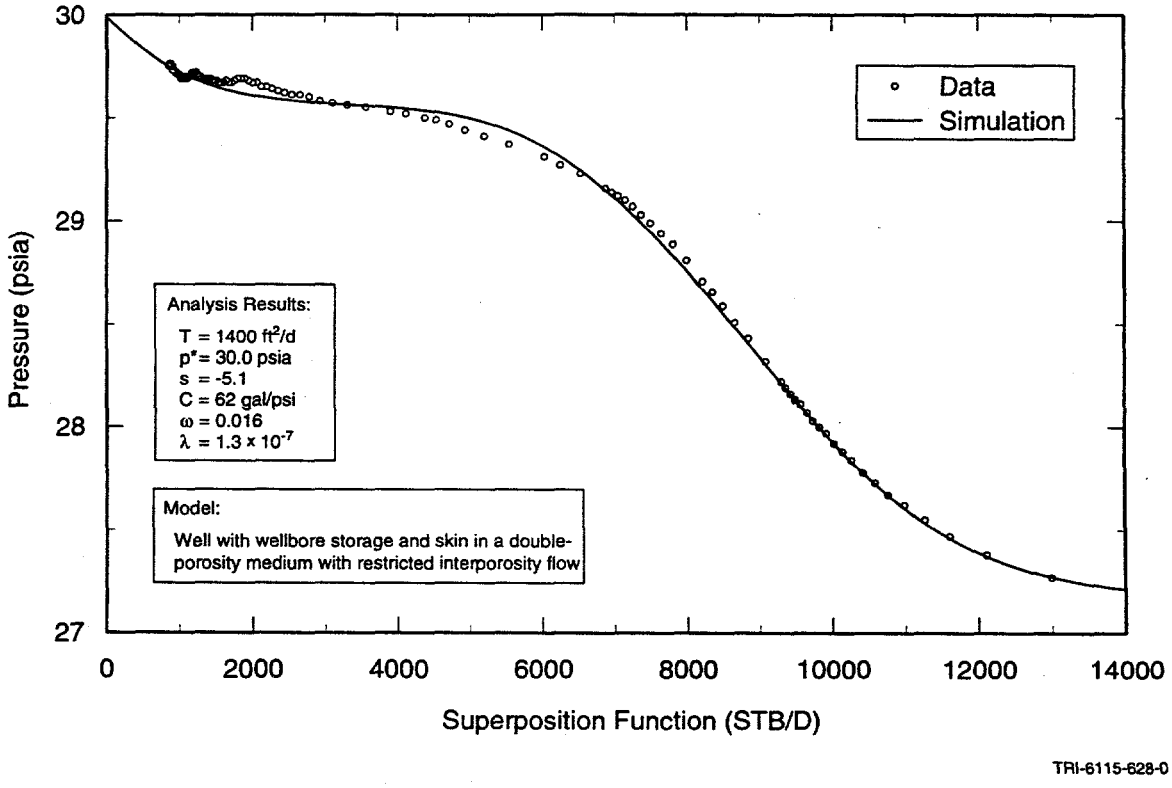

Figure 6-33. Horner plot of H-7b1 recovery data with Interpret/2 simulation.

Figure 6-34 shows a linear-linear plot of the match of the model described above and the combined drawdown and recovery data from H-7b1. The simulated drawdown is lower than that observed because well loss is not included in Interpret/2 simulations. Well loss, which is caused by pumping-induced turbulence in the wellbore, is estimated to have been responsible for approximately 1.5 psi (10 kPa) of the observed drawdown. The drawdown data were not analyzable because of well development that occurred during the first two days of pumping. Well development is shown by rising pressure while pumping at a constant rate (Figure 6-34).

6.3.2 H-7b2

Figures 6-35 and 6-36 show the log-log and Horner plots, respectively, of the recovery data from H-7b2 along with the best-fit Interpret/2 simulations. The deep trough in the derivative evident after about 1.0 hr suggests restricted double-porosity effects, although the data are fairly noisy. The data were analyzed using a model for a line-source well in an infinite double-porosity medium with restricted interporosity flow having a transmissivity of 970 ft^2/d (1.0 x 10^{-3} m^2/s) and storativity of 6.0 x 10^{-3}. Other interpreted parameters are given in Table 6-1. Figure 6-37 is a linear-linear plot of the match of this model and the combined recovery and drawdown data. The fitted model bisects the fluctuations from earth-tidal effects. Log-log, Horner, and linear-linear plots of the drawdown data and simulations are presented in Appendix A (Figures A-19 through A-21). The parameters interpreted from the drawdown simulations are listed in Table 6-1.

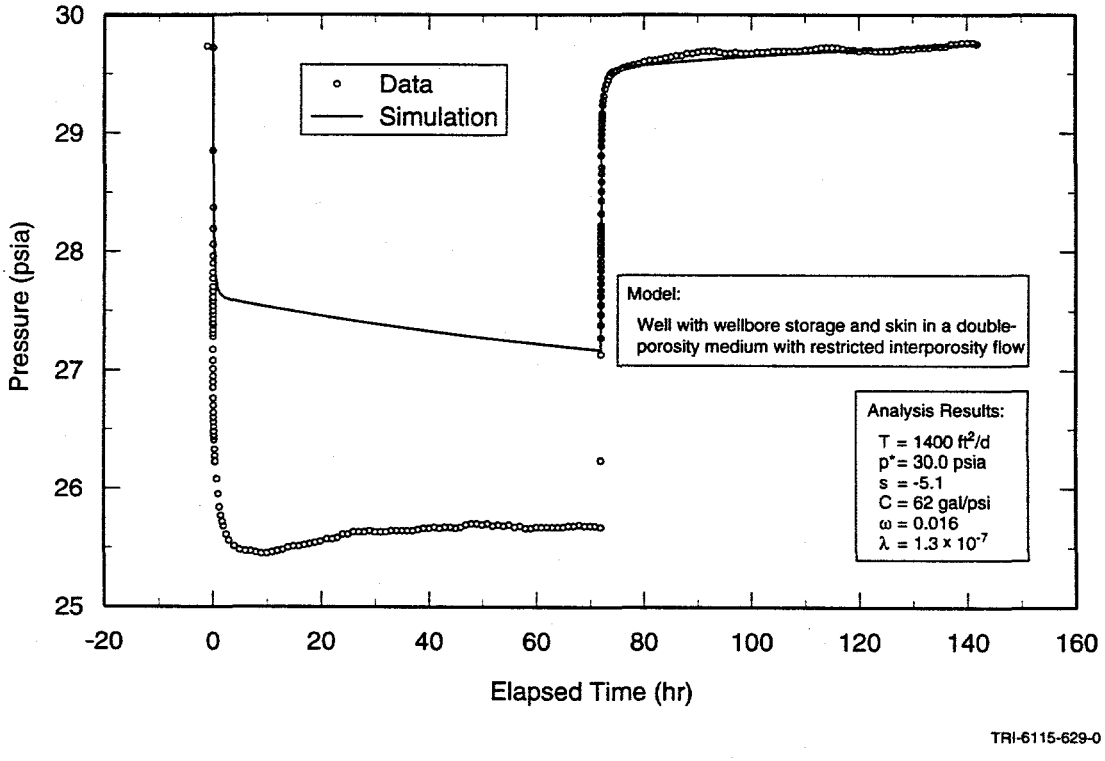

Figure 6-34. Linear-linear plot of H-7b1 data with Interpret/2 simulation derived from recovery analysis.

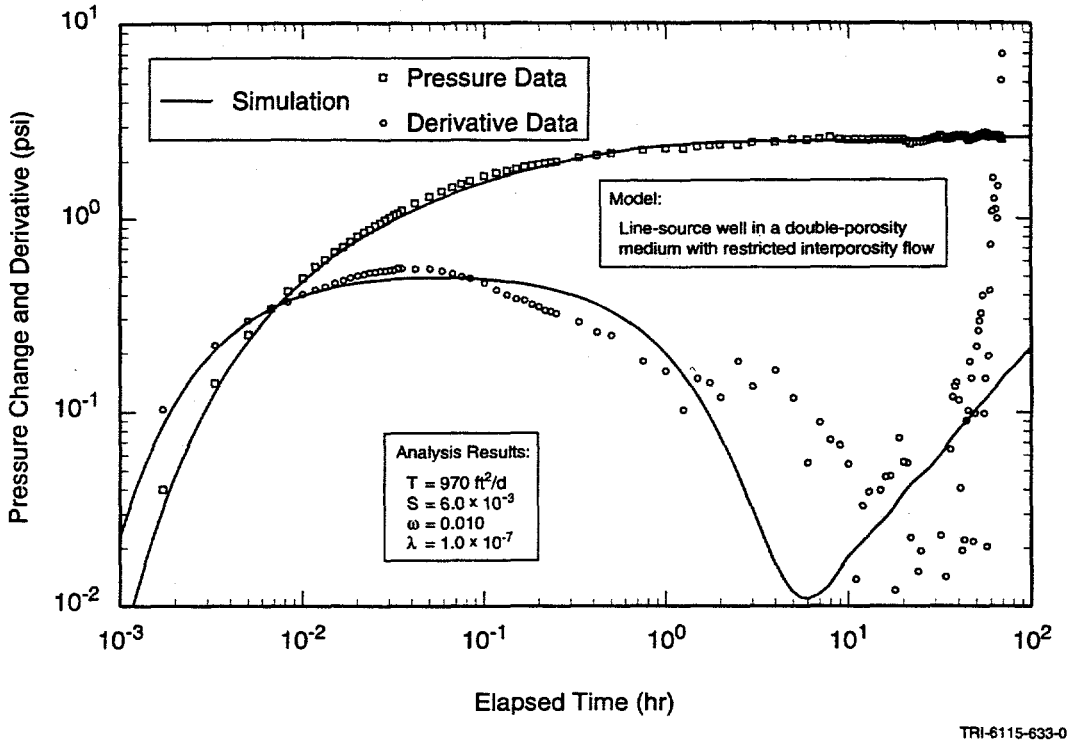

Figure 6-35. Log-log plot of H-7b2 recovery data with Interpret/2 simulation.

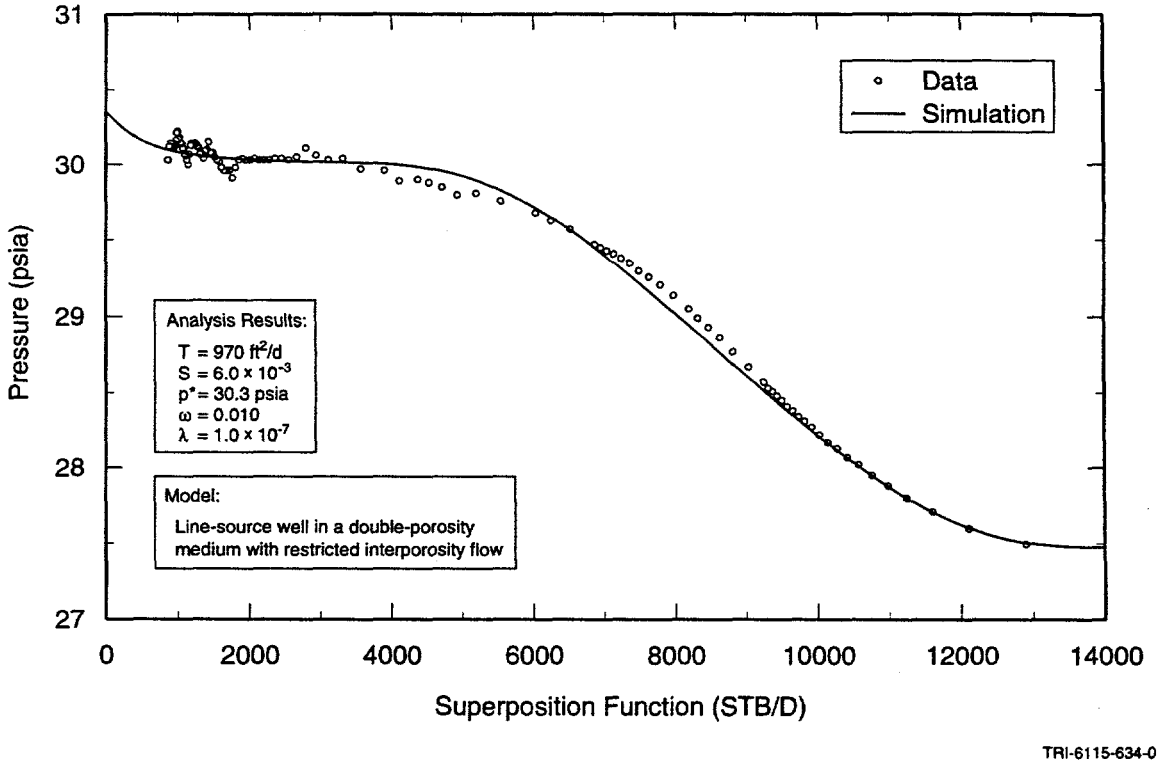

Figure 6-36. Horner plot of H-7b2 recovery data with Interpret/2 simulation.

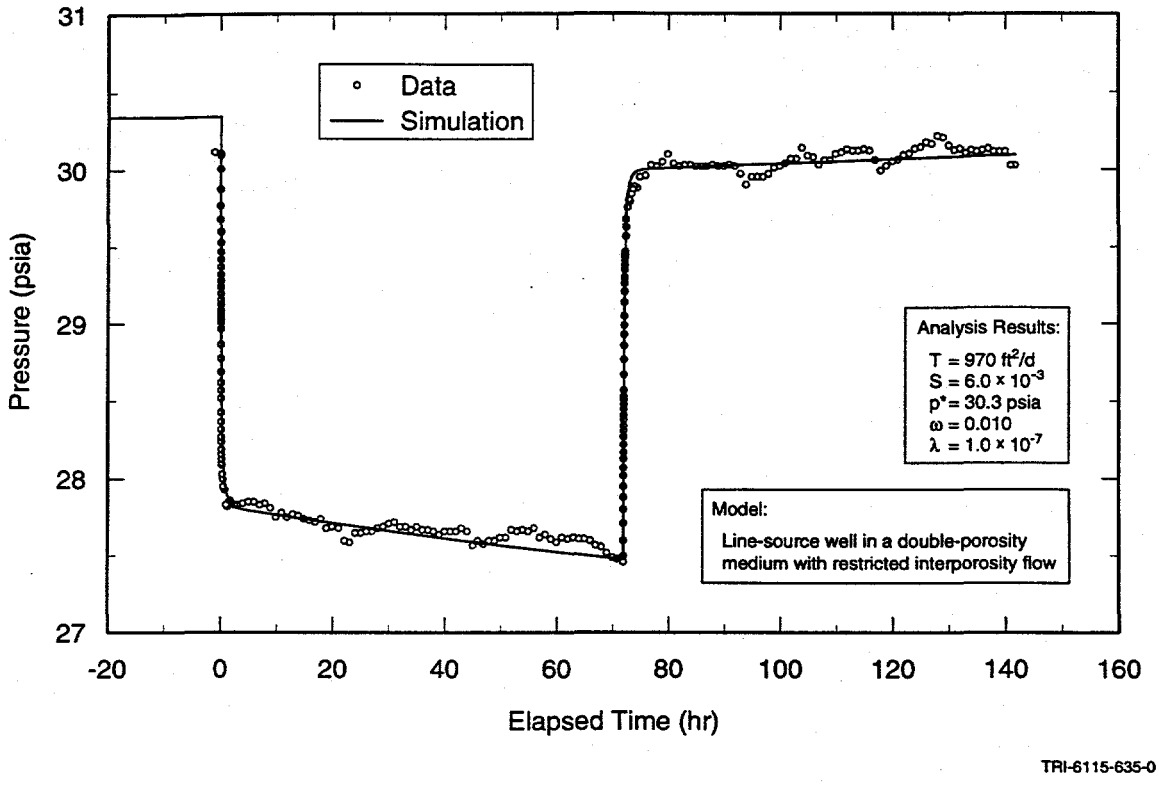

Figure 6-37. Linear-linear plot of H-7b2 data with Interpret/2 simulation derived from recovery analysis.

6.3.3 H-7c

Figures 6-38 and 6-39 show the log-log and Horner plots, respectively, of the recovery data from H-7c along with the best-fit Interpret/2 simulations. The trough in the derivative evident after about 0.1 hr suggests restricted double-porosity effects, although the data are fairly noisy. The data were analyzed using a model for a line-source well in an infinite double-porosity medium with restricted interporosity flow having a transmissivity of 1,400 ft^2/d (1.5 x 10^{-3} m^2/s) and storativity of 6.9 x 10^{-3}. Other interpreted parameters are given in Table 6-1. Figure 6-40 is a linear-linear plot of the match of this model and the combined recovery and drawdown data. The fitted model bisects the fluctuations from earth-tidal effects. No meaningful interpretation of the H-7c drawdown data could be performed because pressure changes caused by earth tides obscured the pressure response to the pumping of H-7b1 (see Figure 6-40).

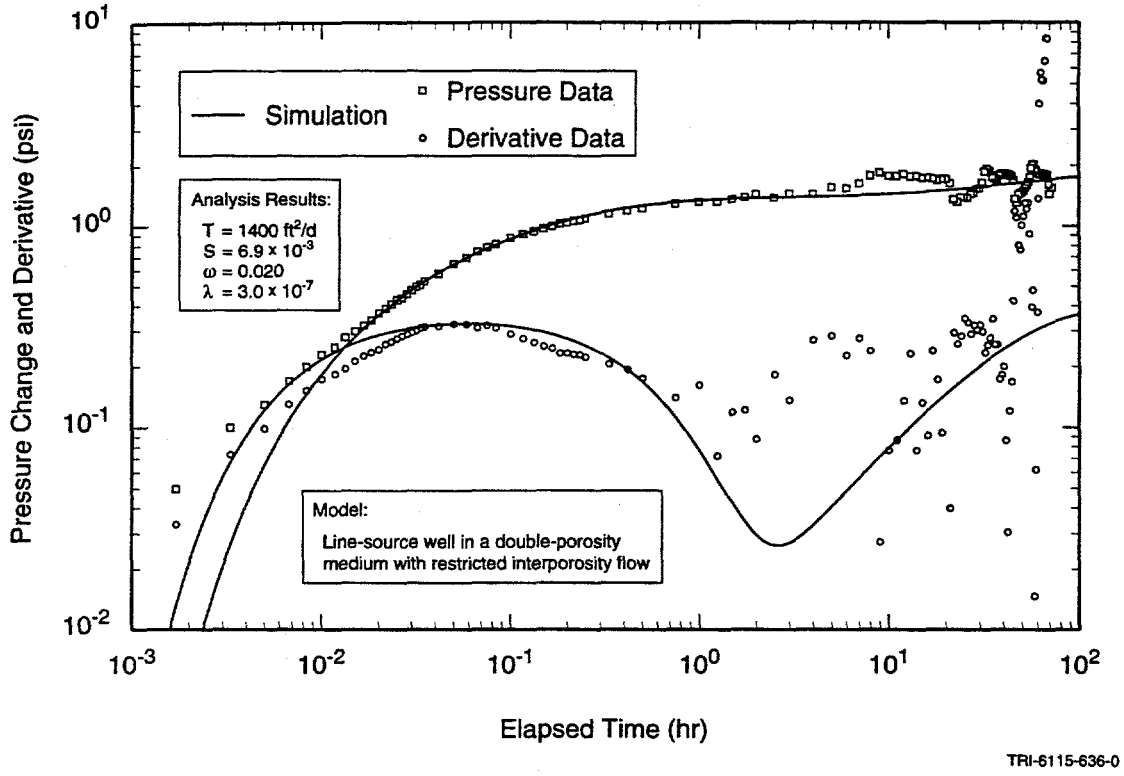

Figure 6-38. Log-log plot of H-7c recovery data with Interpret/2 simulation.

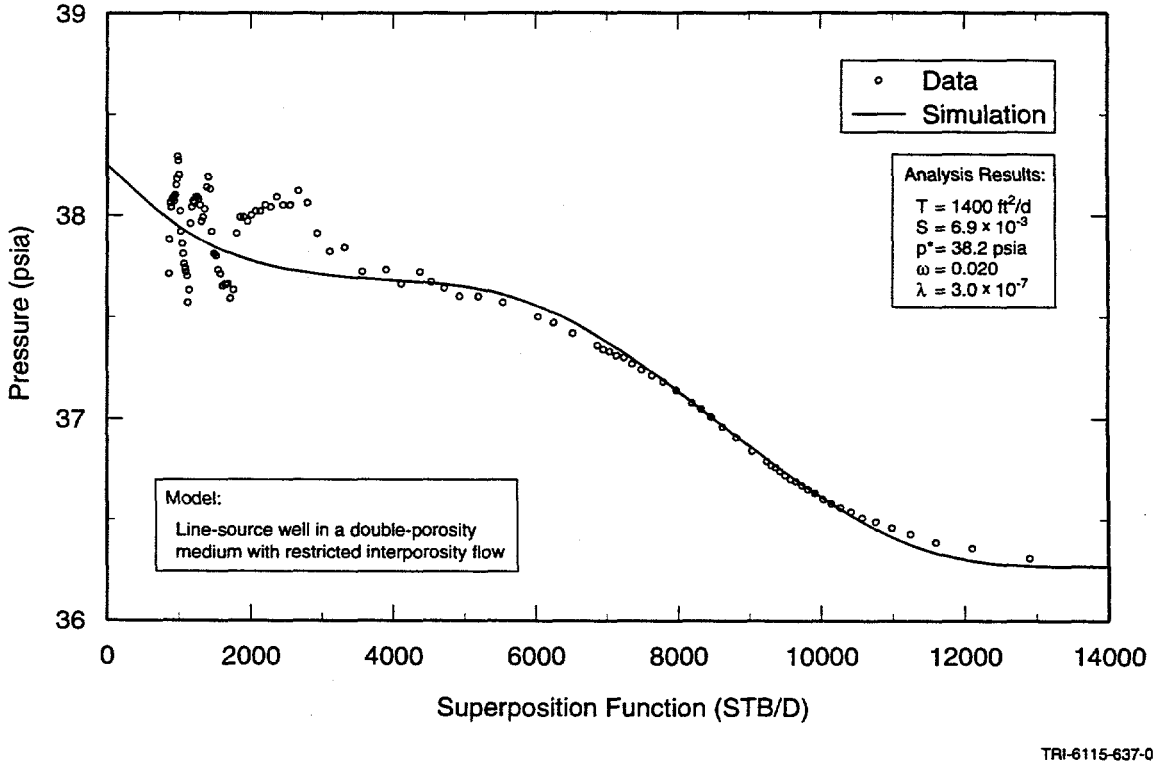

Figure 6-39. Horner plot of H-7c recovery data with Interpret/2 simulation.

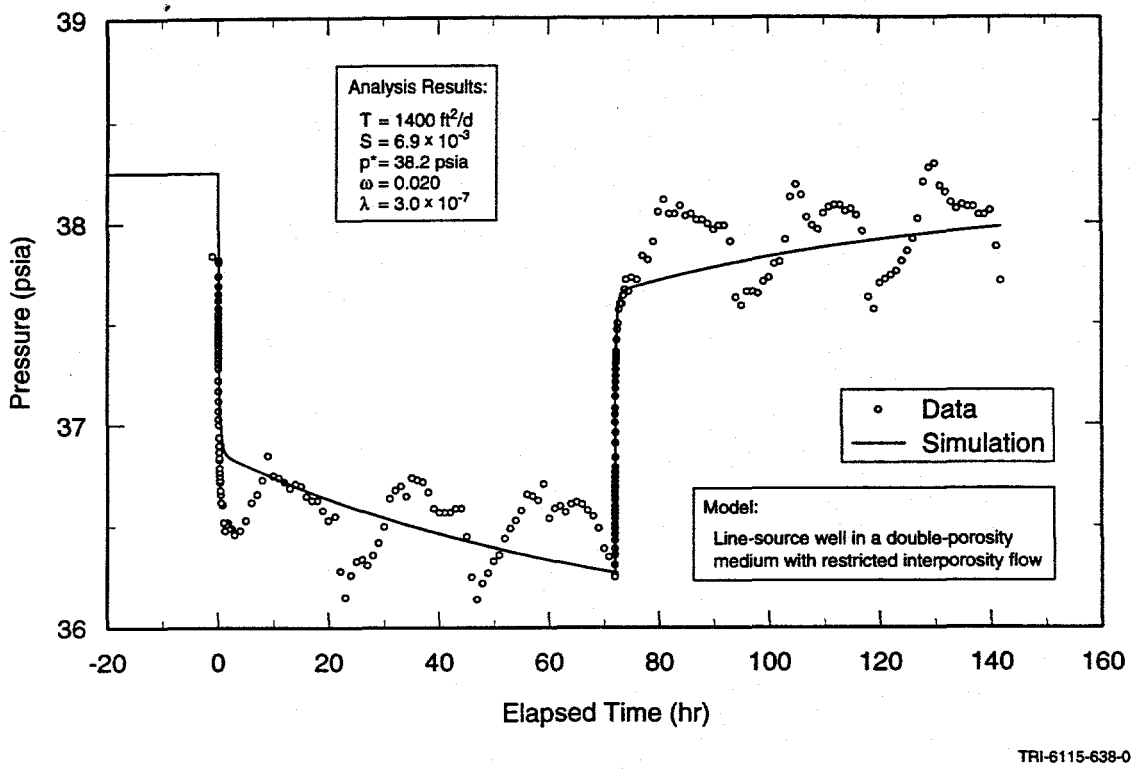

Figure 6-40. Linear-linear plot of H-7c data with Interpret/2 simulation derived from recovery analysis.

6.3.4 Summary of Results from the H-7 Pumping Test

Interpretation of the responses observed during the H-7 pumping test was hindered by well-development effects in the pumping well and by earth-tidal effects in the observation wells. Interpreted transmissivities range from 970 to 1,400 ft^2/d (1.0 to 1.5 x 10^{-3} m^2/s). Because of the noise in the data, however, the simulated fits must be considered non-unique and we conclude only that the transmissivity of the Culebra at the H-7 hydropad is between 1,000 and 2,000 ft^2/d (1 to 2 x 10^{-3} m^2/s). All of the well responses showed apparent double-porosity behavior. Fracturing would be expected in the Culebra at this location because of dissolution of the underlying Salado (Holt, 1997).

The Culebra is shallower at H-7 than at any other test location discussed in this report. Drellack and Wells (1982a) noted that selenite fracture fillings typically found in the Dewey Lake Redbeds over the WIPP site are absent at H-7. They attributed this absence to dissolution. They also found the Magenta to be fractured and the Rustler rocks to be generally "more altered, fractured, and porous than those within the WIPP site boundary." Mercer (1983) and Richey (1986) report that the Magenta at H-7 is unsaturated. Water levels reported for the Culebra at H-7 (e.g., Stensrud et al., 1990) are typically approximately 168 ft (51 m) BGS, below the elevation of the Magenta in the upper Tamarisk (see Figure 3-6). Culebra water at H-7 is much fresher than is typically found at the WIPP site, with total dissolved solids averaging approximately 3,000 mg/L (Westinghouse, 1991). The high storativities interpreted from the H-7b2 and H-7c responses, 6.0 x 10^{-3} and 6.9 x 10^{-3}, are much more typical of aquifers under unconfined (water-table) conditions than under confined conditions.

These observations all suggest that the Culebra may be unconfined at H-7. If this is true, the "double-porosity" responses interpreted above may actually reflect delayed yield (gravity drainage; Neuman, 1975). The calculations of transmissivity would not be affected by use of a delayed-yield, rather than double-porosity, model.

6.4 H-9 Pumping Tests

Three pumping tests were performed at the H-9 hydropad. H-9c was the pumping well for the first and third tests, and H-9b was the pumping well for the second test.

6.4.1 Test #1

As discussed in Section 5.4, the first pumping test at H-9 involved pumping at H-9c with H-9a and H-9b serving as observation wells.

6.4.1.1 H-9c

The drawdown data from H-9c were uninterpretable because of fluctuations in the pumping rate. A log-log plot of the recovery data (Figure 6-41) shows a long initial period when the data follow a unit-slope line, after which the pressure data flatten while the pressure-derivative data drop quickly before shifting to a slowly increasing trend. The final late-time drop in the derivative was caused by a slight decrease in the pressure and is not significant. The earlier data, however, show that the well possesses a high positive skin, meaning that it is poorly connected to the formation. No unique simulation of the data could be obtained because numerous combinations of skin and transmissivity values produce similar results.

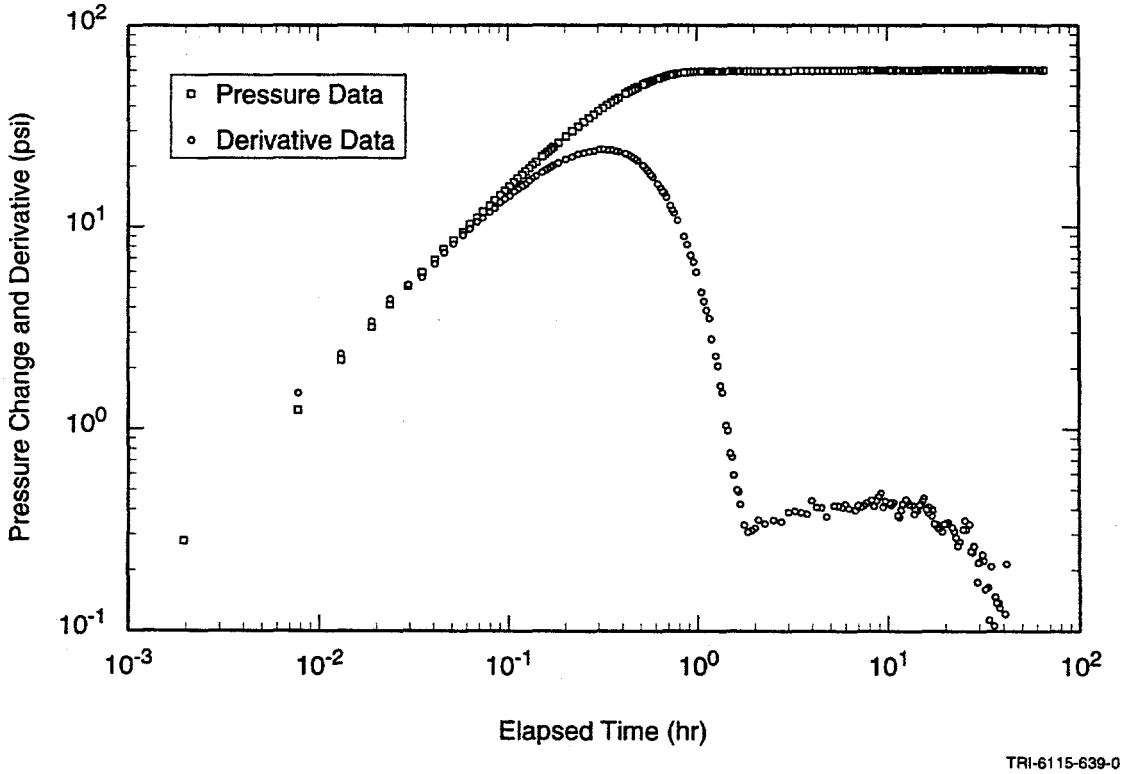

Figure 6-41. Log-log diagnostic plot of H-9c recovery data from test #1.

6.4.1.2 OBSERVATION WELLS

Figures 6-42 through 6-44 and 6-45 through 6-47 show the log-log, Horner, and linear-linear plots of the recovery data from H-9a and H-9b, respectively, during test #1 along with the best-fit Interpret/2 simulations. The data were analyzed using a model for a line-source well in an infinite double-porosity medium with restricted interporosity flow and a transmissivity of 98 ft^2/d (1.1 x 10^{-4} m^2/s). The H-9a data were matched using a storativity of 6.0 x 10^{-4} and the H-9b data were matched using a storativity of 5.9 x 10^{-4}. Other interpreted parameters are given in Table 6-1.

Log-log, Horner, and linear-linear plots of the drawdown data and best-fit simulations for H-9a and H-9b are presented in Appendix A (Figures A-22 through A-24 and A-25 through A-27, respectively). The parameters interpreted from the drawdown analyses are listed in Table 6-1.

6.4.2 Test #2

As discussed in Section 5.4, the second pumping test at H-9 involved pumping at H-9b with H-9a and H-9c serving as observation wells. No interpretation was made of the H-9b response to pumping because the data from the transducers used in that well are not considered reliable. The two transducers used in H-9b showed different drawdowns of 8.4 and 6.6 psi (58 and 46 kPa) at the end of the pumping period, whereas water-level measurements made with a steel tape indicated the drawdown was approximately 5.5 psi (38 kPa). Furthermore, both transducers showed pressure stabilizing at the end of the recovery period several psi (10-20 kPa) lower than the pre-pumping pressure,

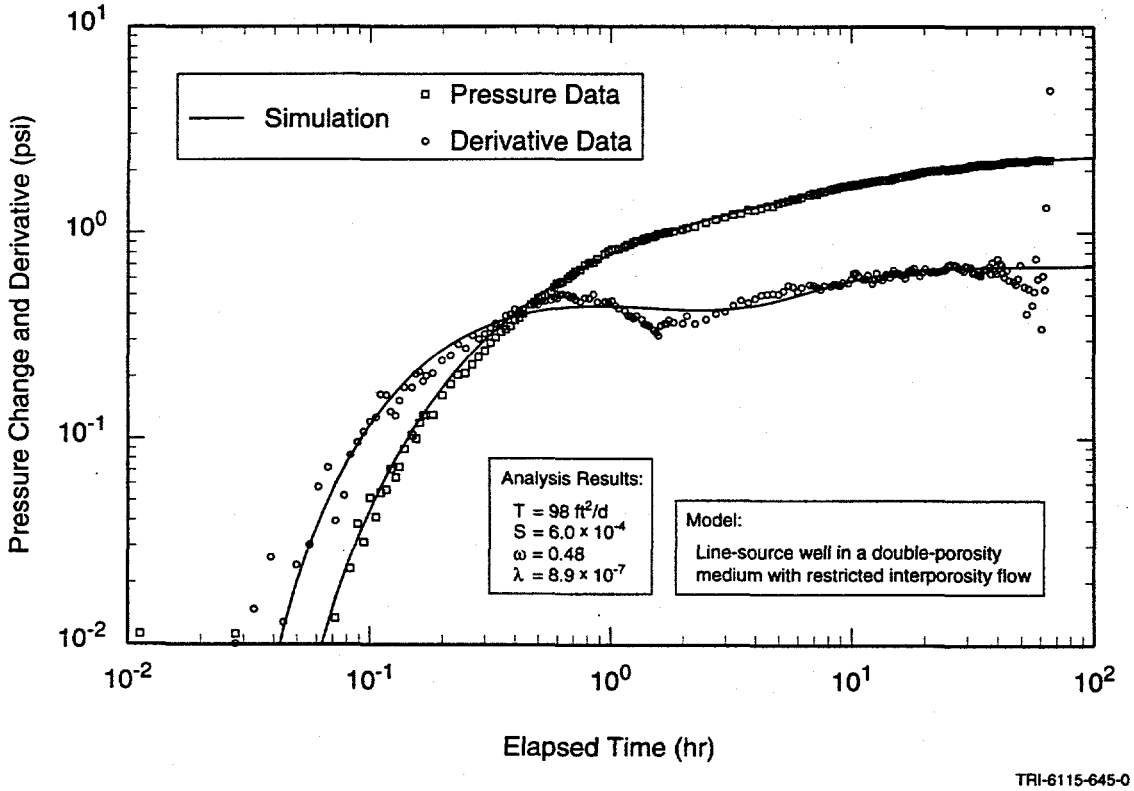

Figure 6-42. Log-log plot of H-9a recovery data from test #1 with Interpret/2 simulation.

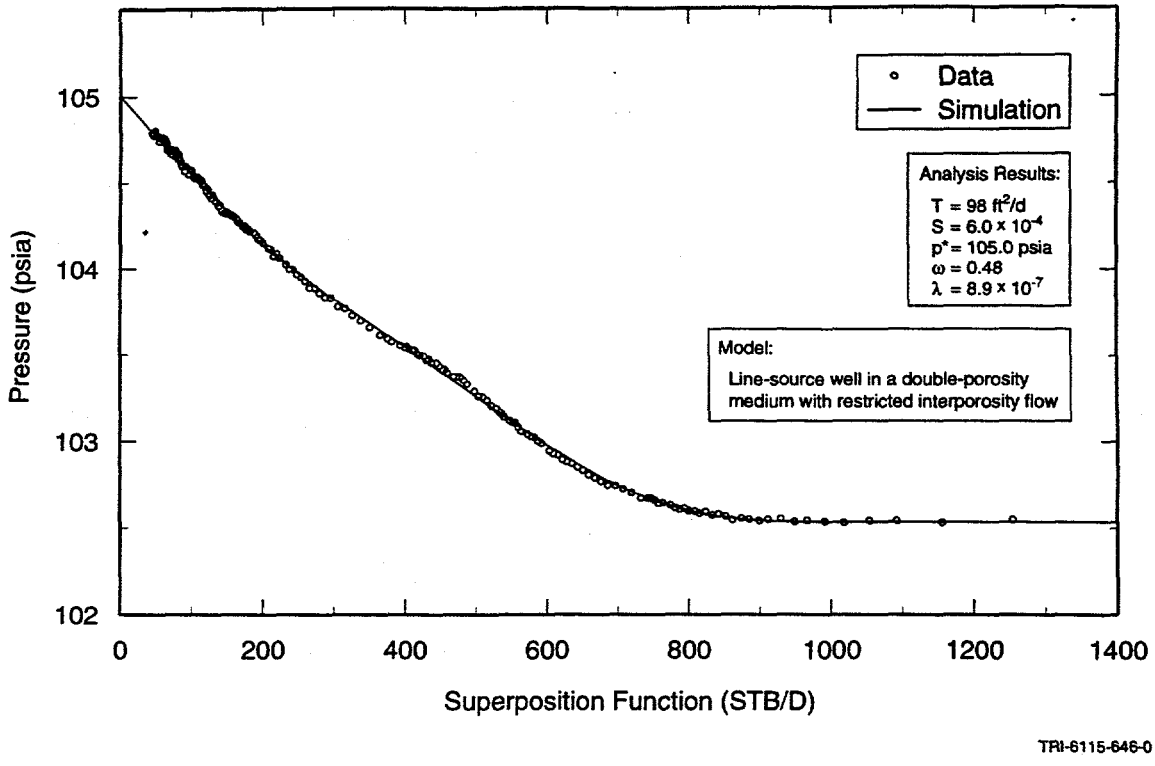

Figure 6-43. Horner plot of H-9a recovery data from test #1 with Interpret/2 simulation.

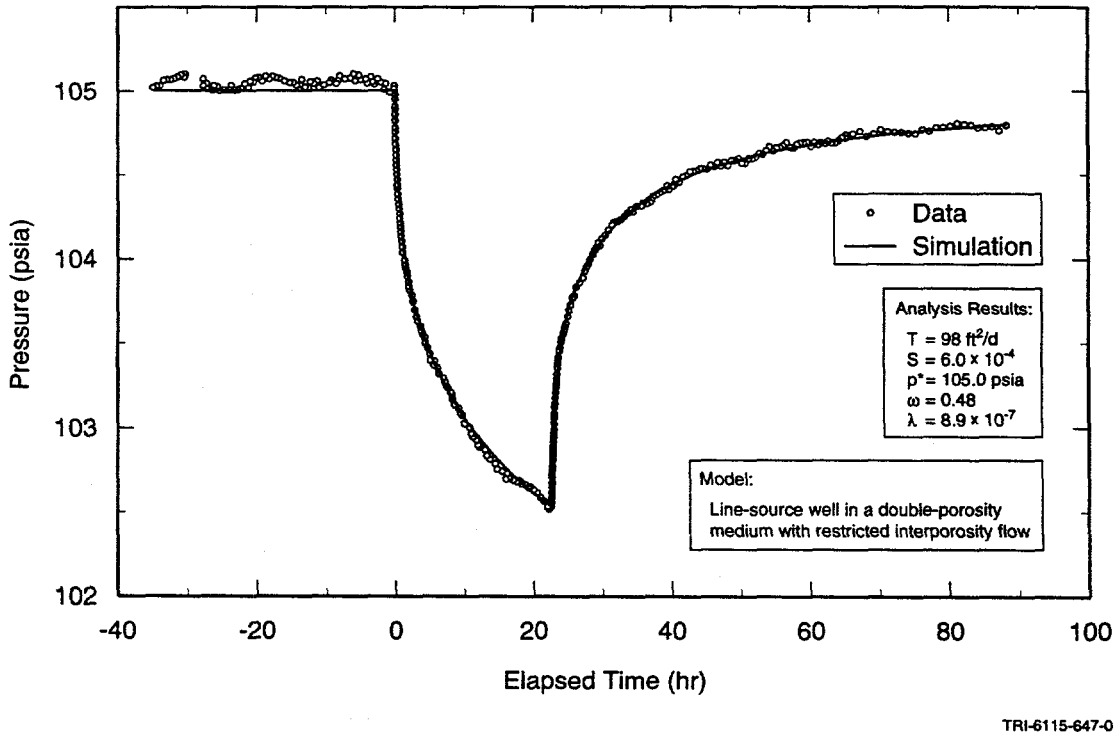

Figure 6-44. Linear-linear plot of H-9a data from test #1 with Interpret/2 simulation derived from recovery analysis.

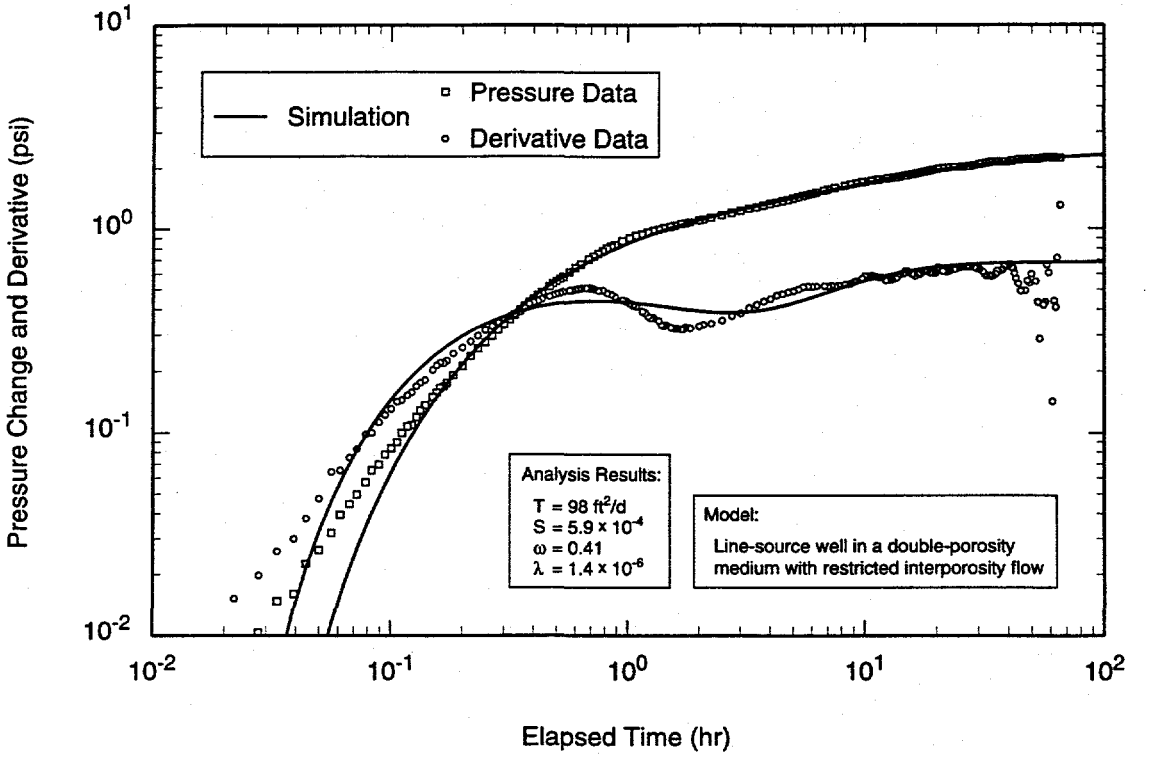

Figure 6-45. Log-log plot of H-9b recovery data from test #1 with Interpret/2 simulation.

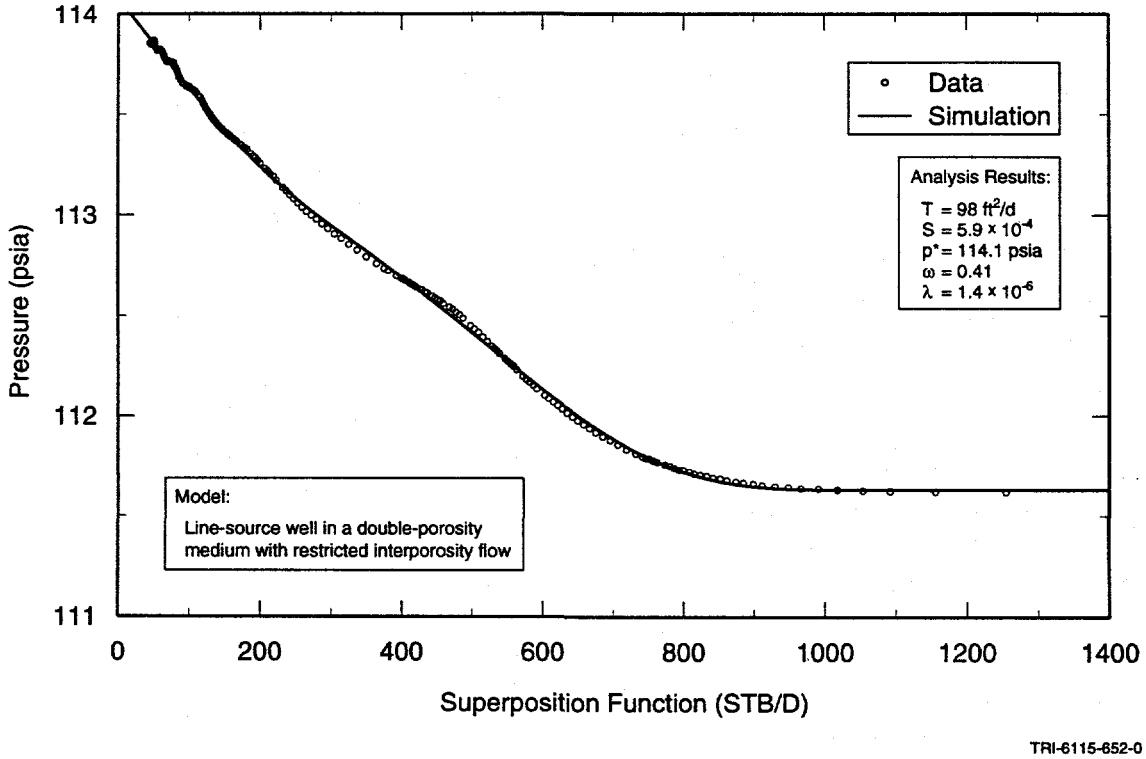

Figure 6-46. Horner plot of H-9b recovery data from test #1 with Interpret/2 simulation.

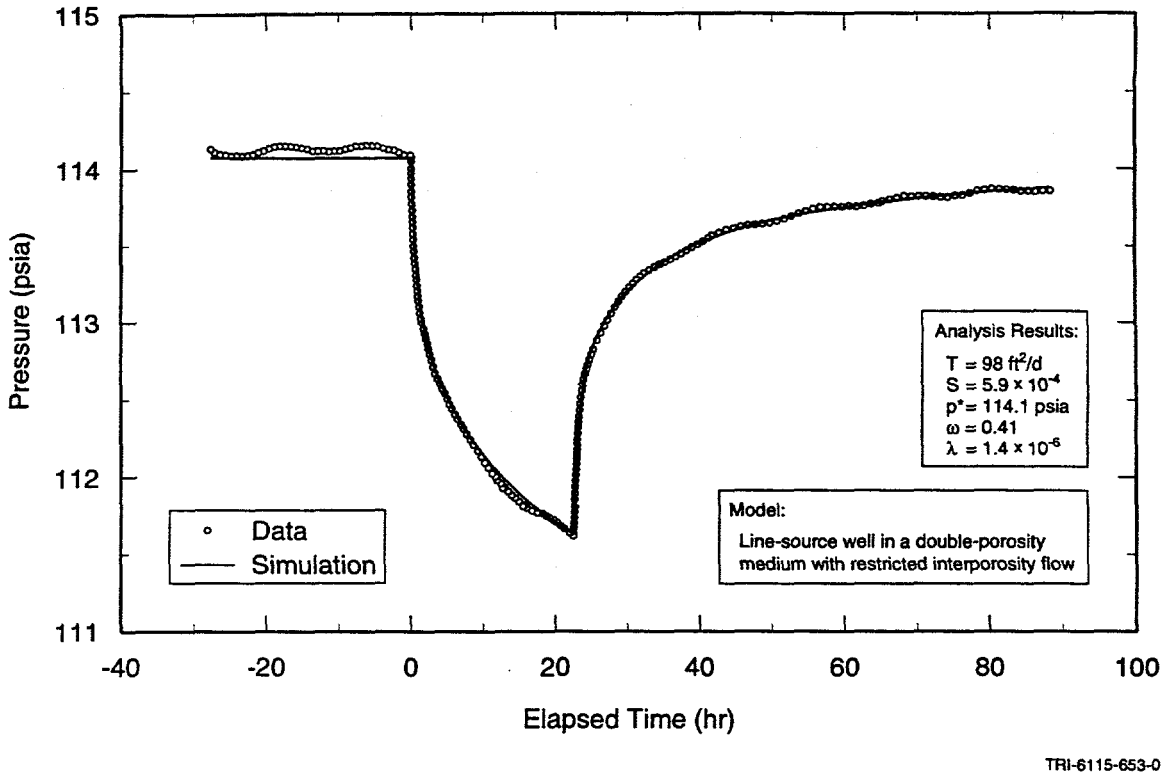

Figure 6-47. Linear-linear plot of H-9b data from test #1 with Interpret/2 simulation derived from recovery analysis.

whereas water levels measured before and after the test were nearly the same. Consequently, only the data from the observation wells were analyzed.

Figures 6-48 through 6-50 and 6-51 through 6-53 show the log-log, Horner, and linear-linear plots of the recovery data from H-9a and H-9c, respectively, during test #2 along with the best-fit Interpret/2 simulations. The data were analyzed using a model for a line-source well in an infinite double-porosity medium with restricted interporosity flow. The H-9a data were matched using a transmissivity of 101 ft^2/d (1.1 x 10^{-4} m^2/s) and a storativity of 4.5 x 10^{-4} and the H-9c data were matched using a transmissivity of 98 ft^2/d (1.1 x 10^{-4} m^2/s) and a storativity of 5.5 x 10^{-4}. Other interpreted parameters are given in Table 6-1.

Log-log, Horner, and linear-linear plots of the drawdown data and best-fit simulations for H-9a and H-9c are presented in Appendix A (Figures A-28 through A-30 and A-31 through A-33, respectively). The parameters interpreted from the drawdown analyses are listed in Table 6-1.

6.4.3 Test #3

As discussed in Section 5.4, the third pumping test at H-9 involved pumping at H-9c with H-9a, H-9b, and the Engle well serving as observation wells. The data from H-9c were uninterpretable for the same reasons as for test #1: pumping-rate fluctuations and excessive wellbore skin. Consequently, only the data from the observation wells were analyzed.

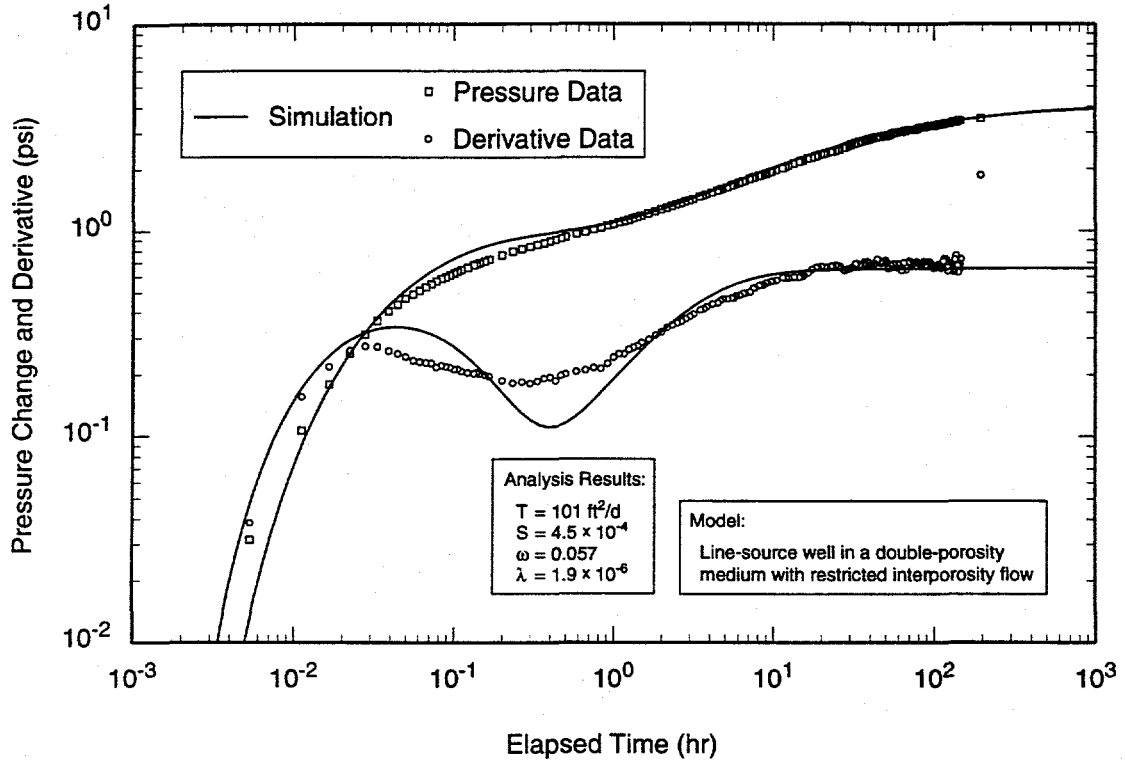

Figure 6-48. Log-log plot of H-9a recovery data from test #2 with Interpret/2 simulation.

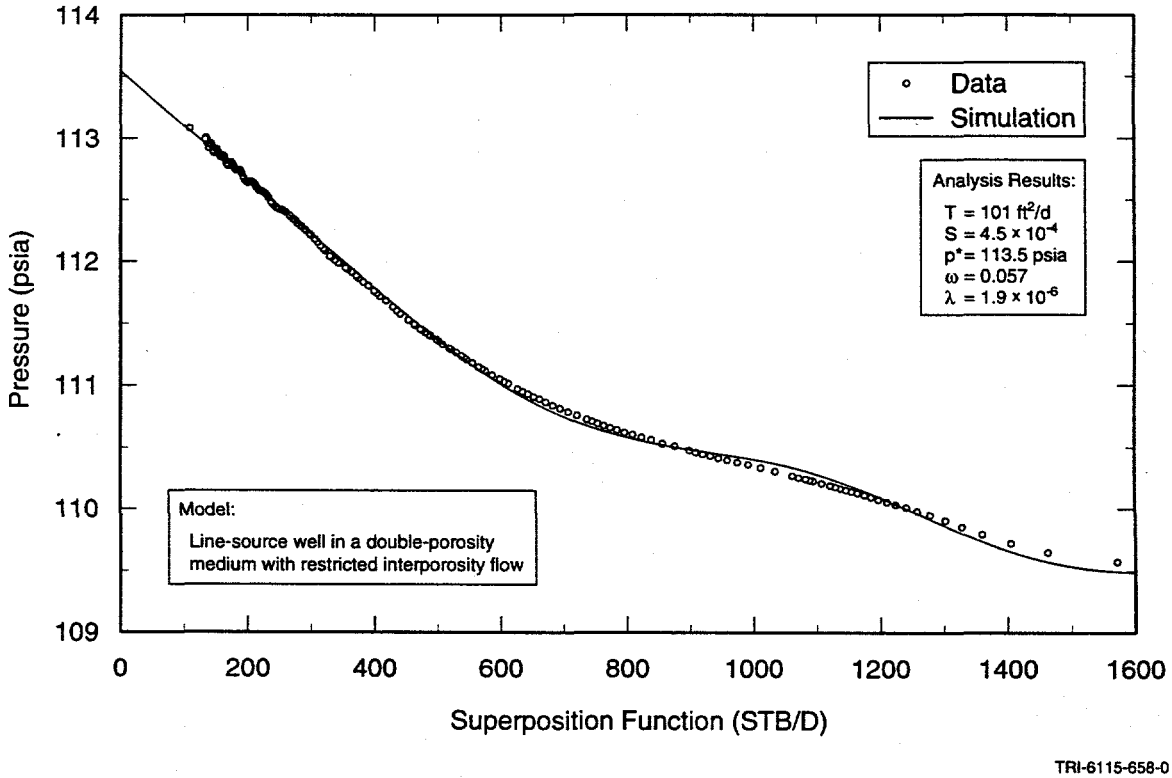

Figure 6-49. Horner plot of H-9a recovery data from test #2 with Interpret/2 simulation.

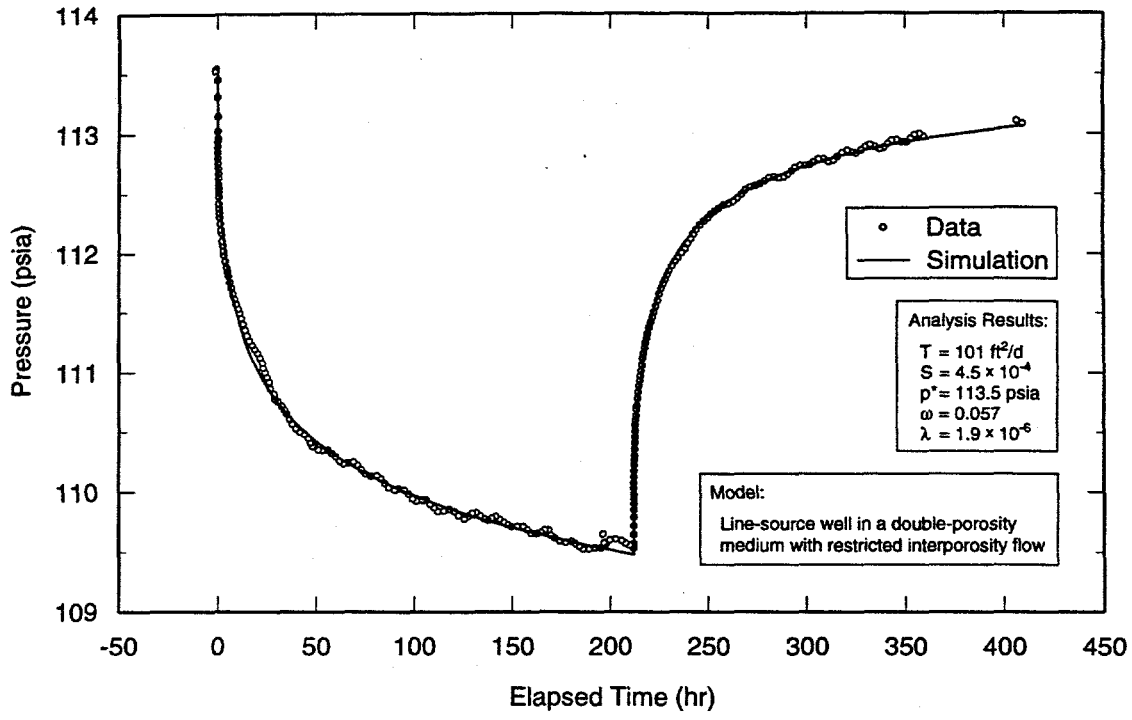

Figure 6-50. Linear-linear plot of H-9a data from test #2 with Interpret/2 simulation derived from recovery analysis.

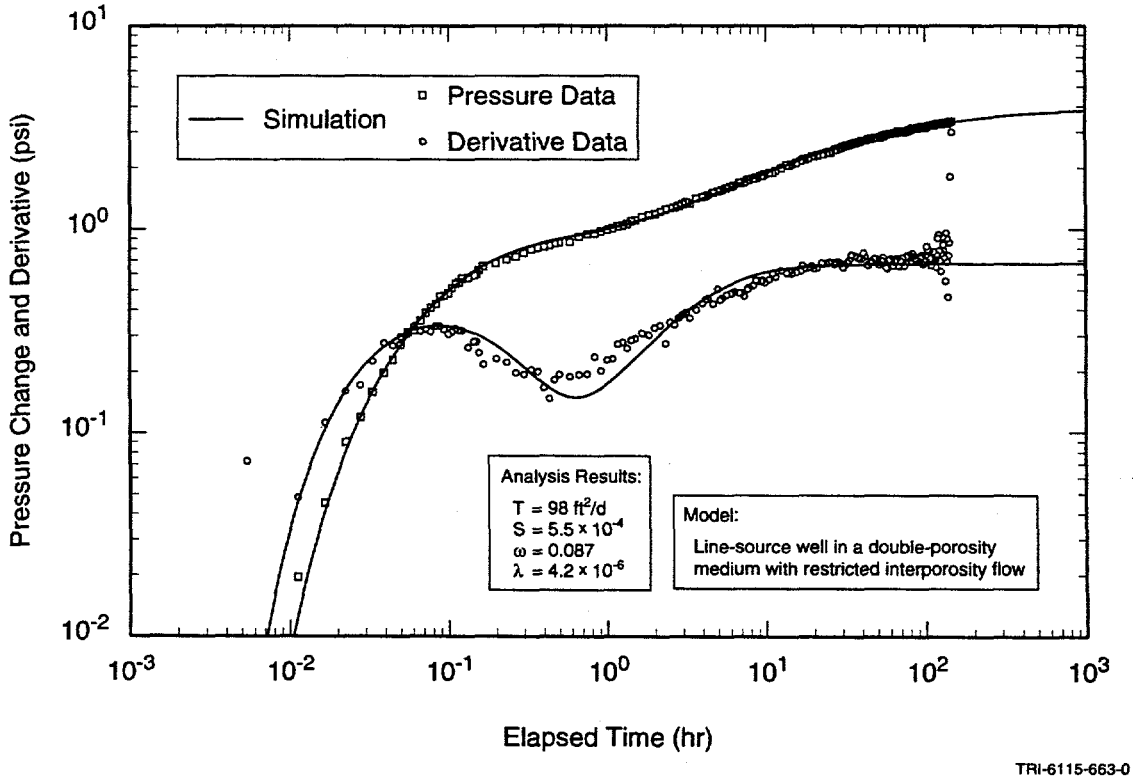

Figure 6-51. Log-log plot of H-9c recovery data from test #2 with Interpret/2 simulation.

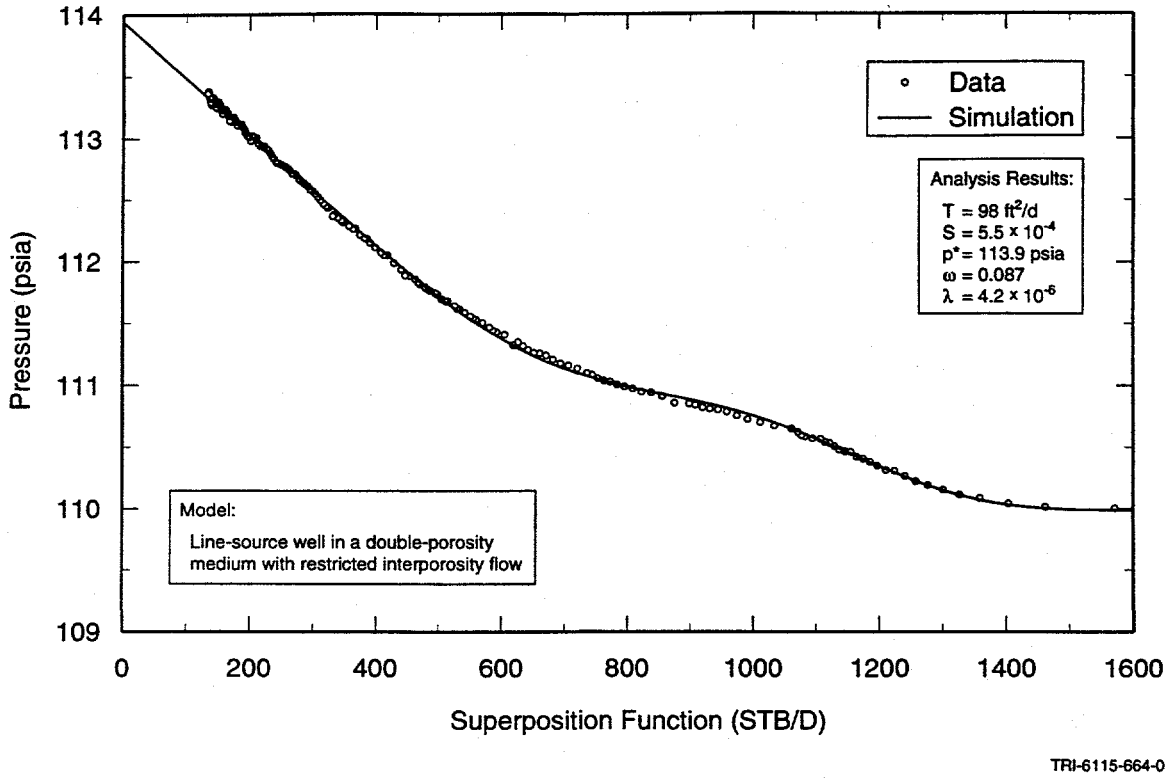

Figure 6-52. Horner plot of H-9c recovery data from test #2 with Interpret/2 simulation.

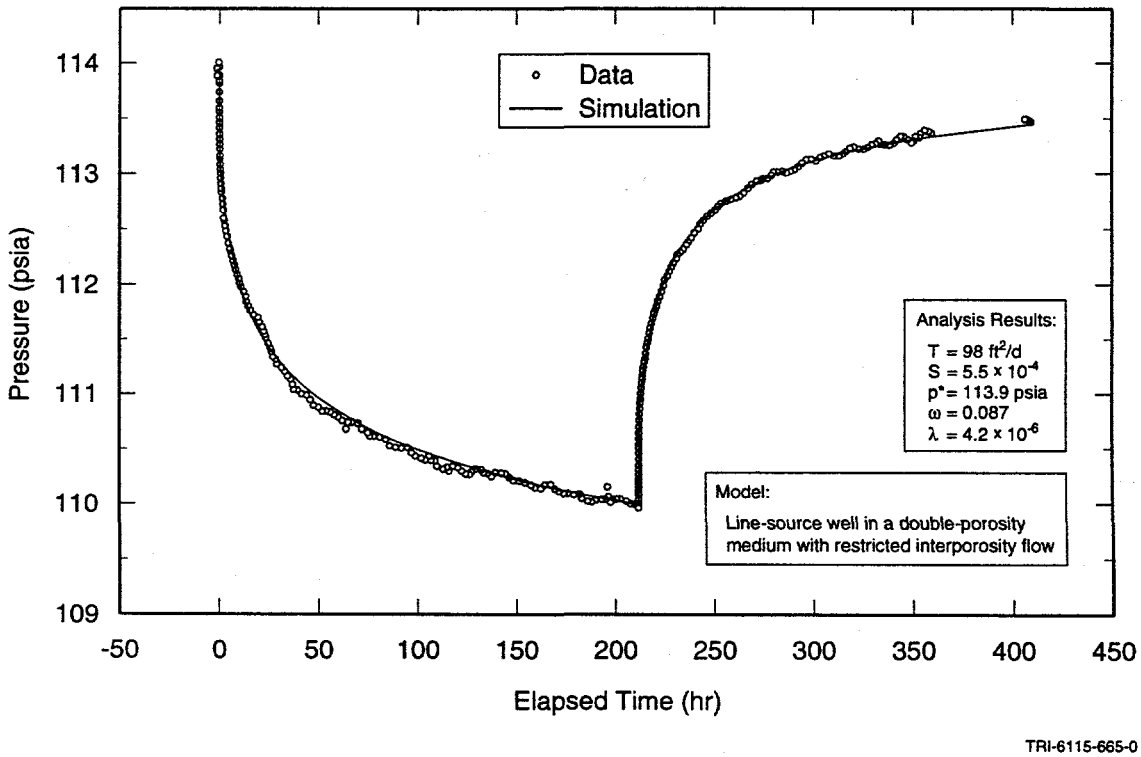

Figure 6-53. Linear-linear plot of H-9c data from test #2 with Interpret/2 simulation derived from recovery analysis.

Figures 6-54 through 6-56 and 6-57 through 6-59 show the log-log, Horner, and linear-linear plots of the recovery data from H-9a and H-9b, respectively, during test #3 along with the best-fit Interpret/2 simulations. The data were analyzed using a model for a line-source well in an infinite double-porosity medium with unrestricted interporosity flow and slab matrix blocks. The H-9a data were matched using a transmissivity of 93 ft^2/d (1.0×10^{-4} m^2/s) and a storativity of 8.7×10^{-4} and the H-9b data were matched using a transmissivity of 91 ft^2/d (9.8×10^{-5} m^2/s) and a storativity of 7.3×10^{-4}. Other interpreted parameters are given in Table 6-1.

Log-log, Horner, and linear-linear plots of the drawdown data and best-fit simulations for H-9a and H-9b are presented in Appendix A (Figures A-34 through A-36 and A-37 through A-39, respectively). The parameters interpreted from the drawdown analyses are listed in Table 6-1.

Figures 6-60 and 6-61 show log-log and Horner plots, respectively, of the drawdown data from the Engle well during test #3 along with the best-fit Interpret/2 simulations. The simulations were generated using a model for a line-source well in an infinite single-porosity medium with a transmissivity of 96 ft^2/d (1.0×10^{-4} m^2/s) and a storativity of 4.7×10^{-6}.

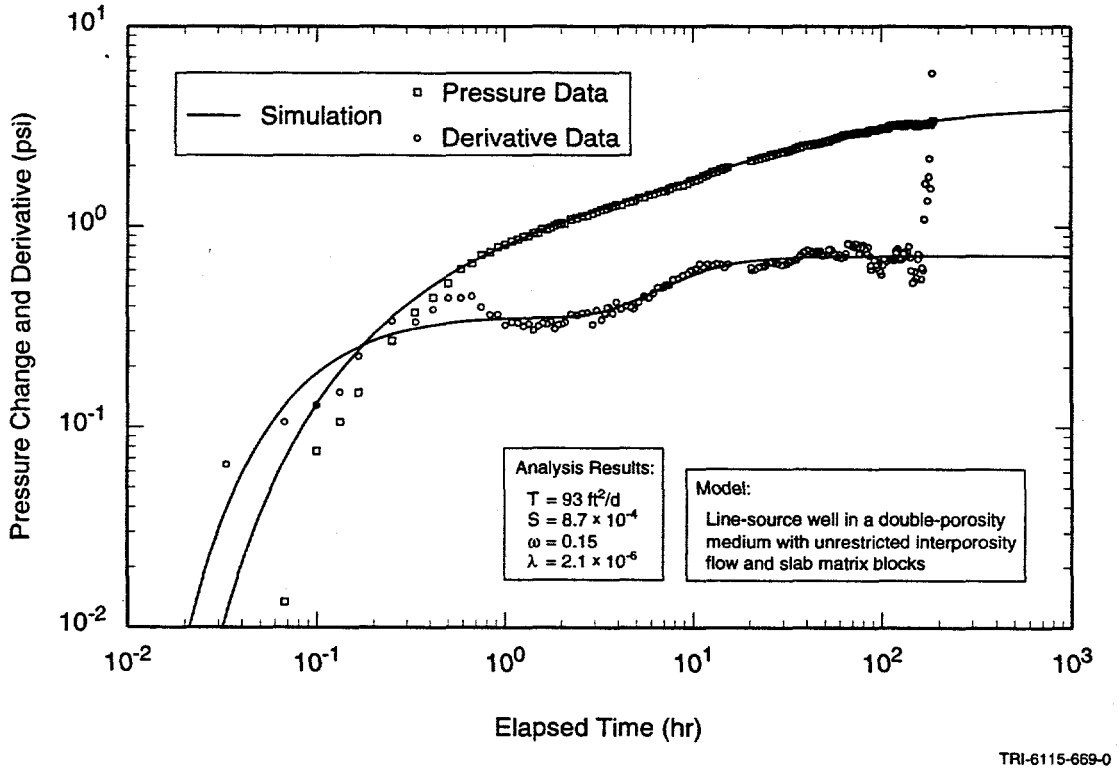

Figure 6-54. Log-log plot of H-9a recovery data from test #3 with Interpret/2 simulation.

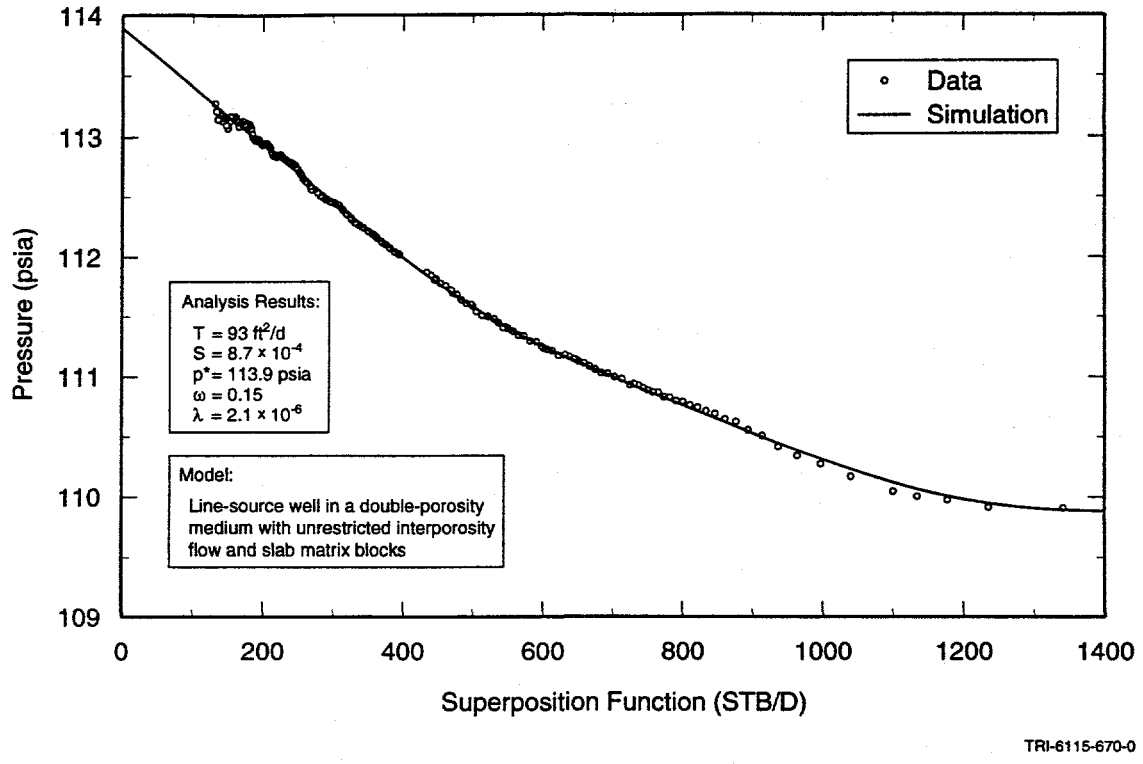

Figure 6-55. Horner plot of H-9a recovery data from test #3 with Interpret/2 simulation.

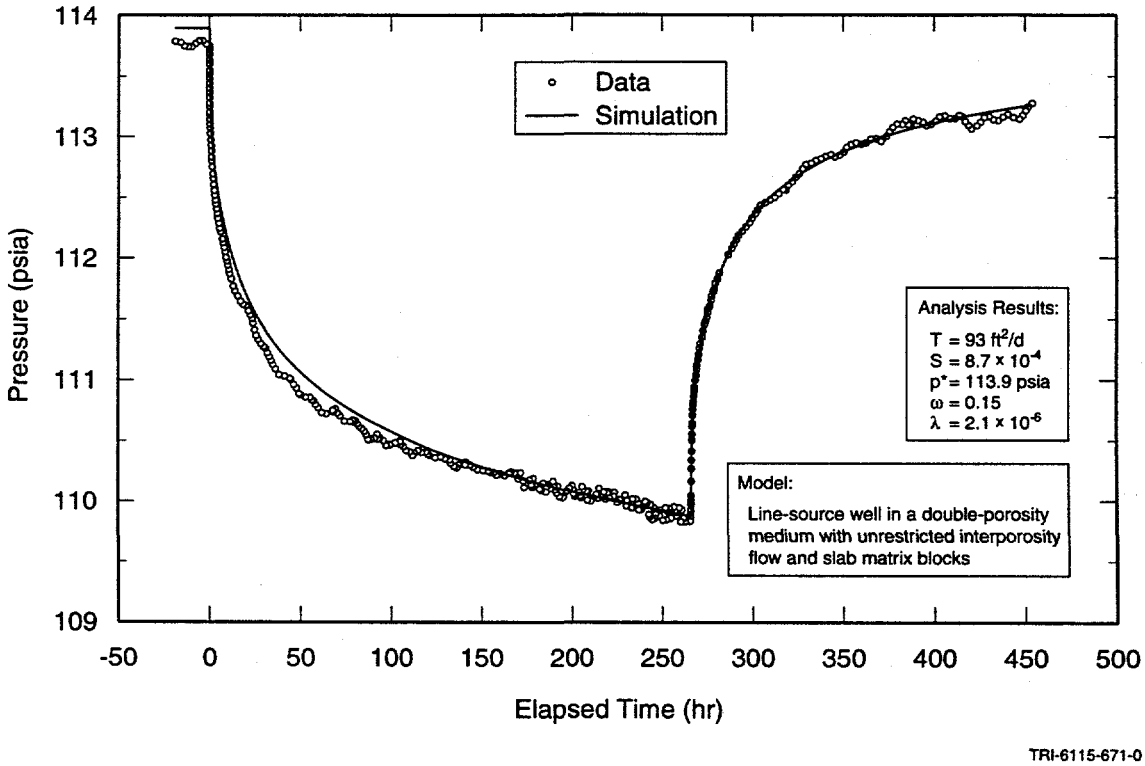

Figure 6-56. Linear-linear plot of H-9a data from test #3 with Interpret/2 simulation derived from recovery analysis.

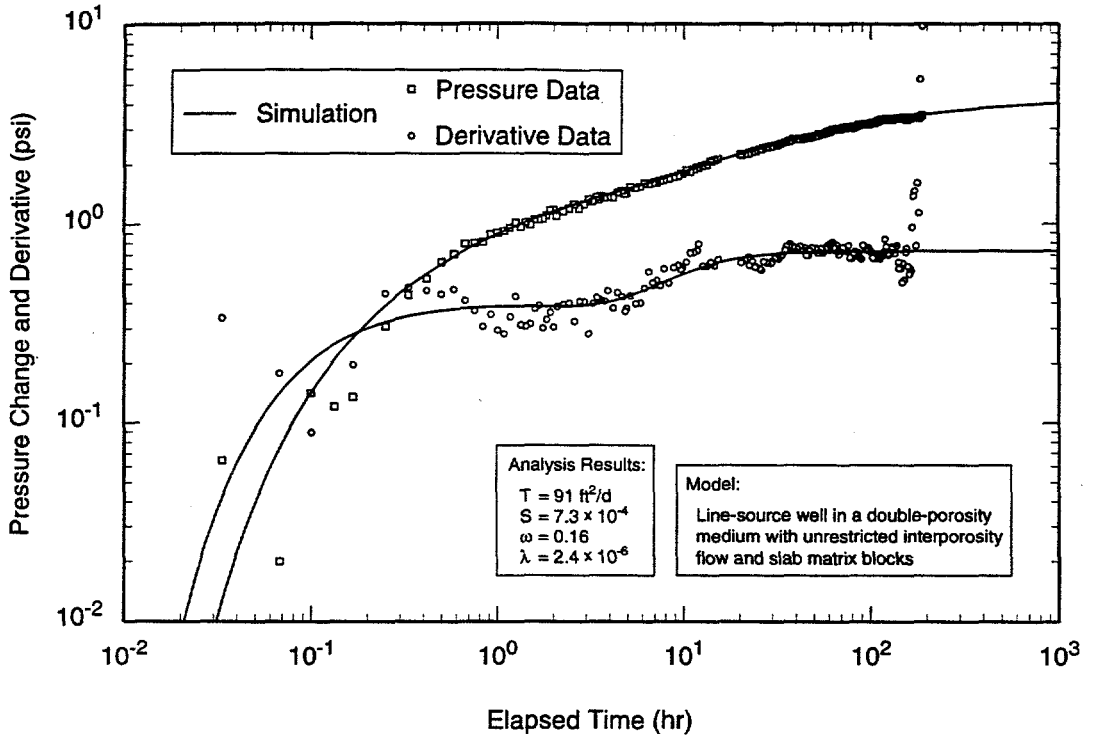

Figure 6-57. Log-log plot of H-9b recovery data from test #3 with Interpret/2 simulation.

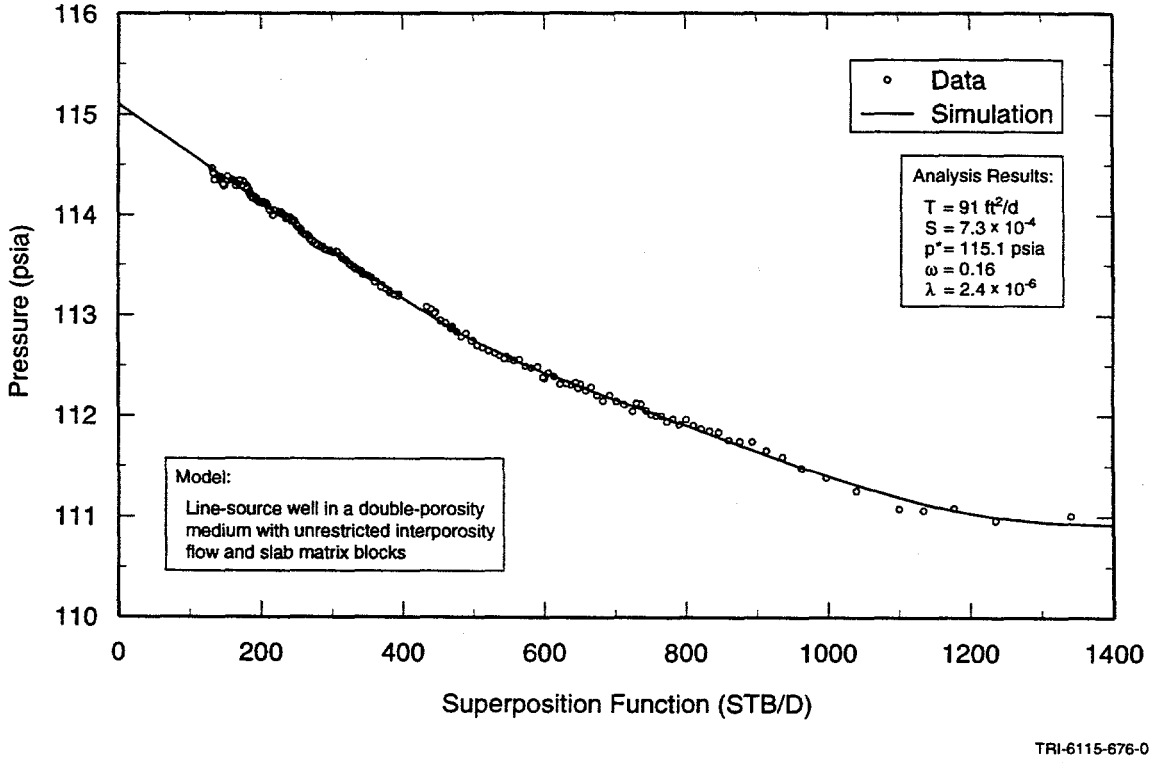

Figure 6-58. Horner plot of H-9b recovery data from test #3 with Interpret/2 simulation.

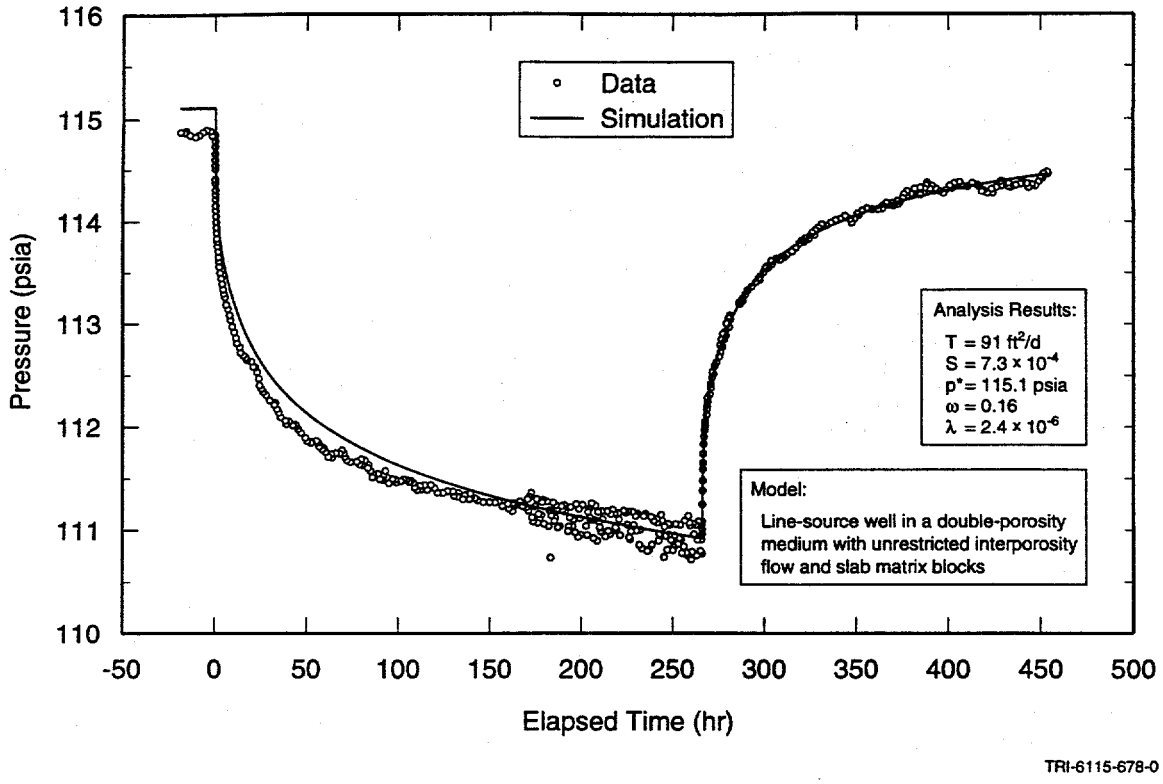

Figure 6-59. Linear-linear plot of H-9b data from test #3 with Interpret/2 simulation derived from recovery analysis.

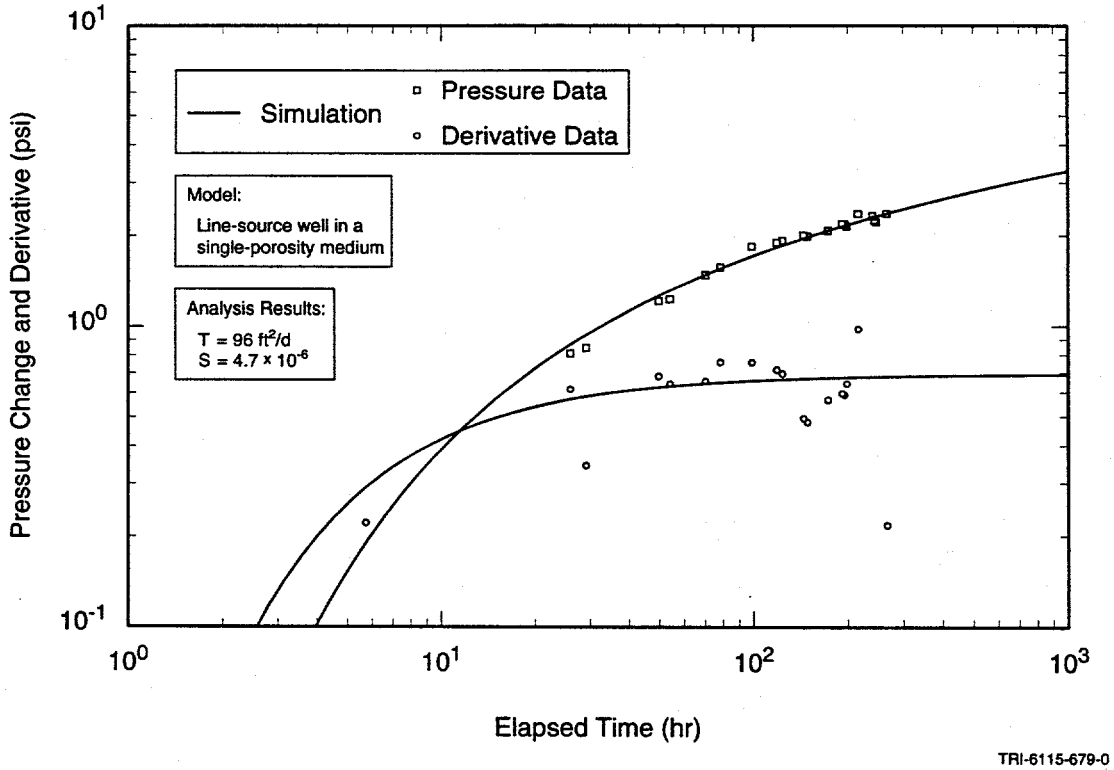

Figure 6-60. Log-log plot of Engle drawdown data from H-9 pumping test #3 with Interpret/2 simulation.

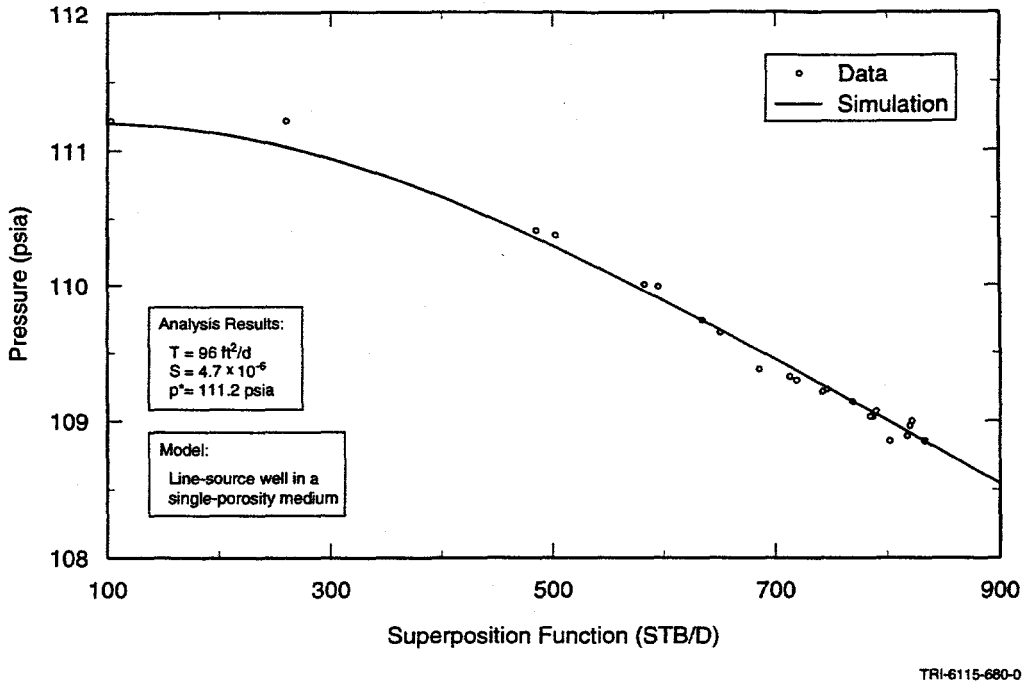

Figure 6-61. Horner plot of Engle drawdown data from H-9 pumping test #3 with Interpret/2 simulation.

Figure 6-62 shows a linear-linear plot of the match between this model and the combined drawdown and recovery data. Insufficient data were collected for an independent interpretation of the recovery response at the Engle well. The Engle well is too far from H-9c (4,115 ft [1,255 m]) and the data are too sparse for any determination of the presence or absence of double-porosity conditions.

6.4.4 H-9 Anisotropy Analysis

As discussed in Grimestad (1995), estimation of anisotropy is based on differences in the interpreted values of storativity along different directions. The three pumping tests on the H-9 hydropad provided 12 sets of data for interpretation of storativity: six sets for the H-9b to H-9c path, four sets for the H-9c to H-9a path, and two sets for the H-9b to H-9a path. Differences in interpreted storativities along the same path for different test phases, however, were as great or greater than the differences between paths, precluding definition of anisotropy. Figure 6-63 shows the storativity data along with a circle for reference. Regardless of the scatter in the data, anisotropy, if it exists at all at H-9, is clearly very weak.

6.4.5 Summary of Results from the H-9 Pumping Tests

The responses to pumping observed in the H-9 wells showed consistently clear evidence of double-porosity behavior. All data sets show a pronounced minimum in the pressure derivative followed by a well-defined stabilization. Transmissivities interpreted from the responses of the H-9 wells range from 91 to 109 ft^2/d (9.8×10^{-5} to 1.2×10^{-4} m^2/s), with a geometric mean of 100 ft^2/d (1.1×10^{-4} m^2/s). Interpreted storativities range from 4.1×10^{-4} to 8.7×10^{-4}, with a geometric mean of 5.6×10^{-4}. Anisotropy at the H-9 hydropad appears to be weak to non-existent. The infilling that partially obstructed the Culebra in H-9a (see Section 5.4) had no apparent effect on the hydraulic responses observed in that well.

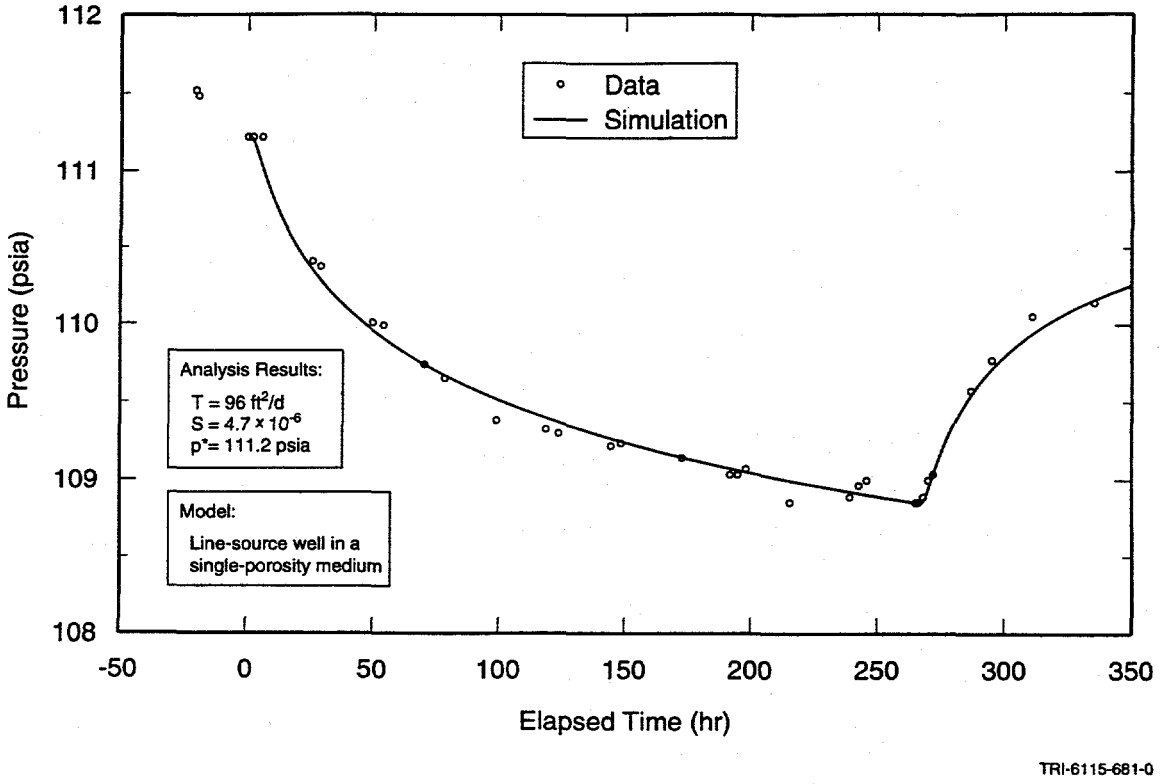

Figure 6-62. Linear-linear plot of Engle data from H-9 pumping test #3 with Interpret/2 simulation derived from drawdown analysis.

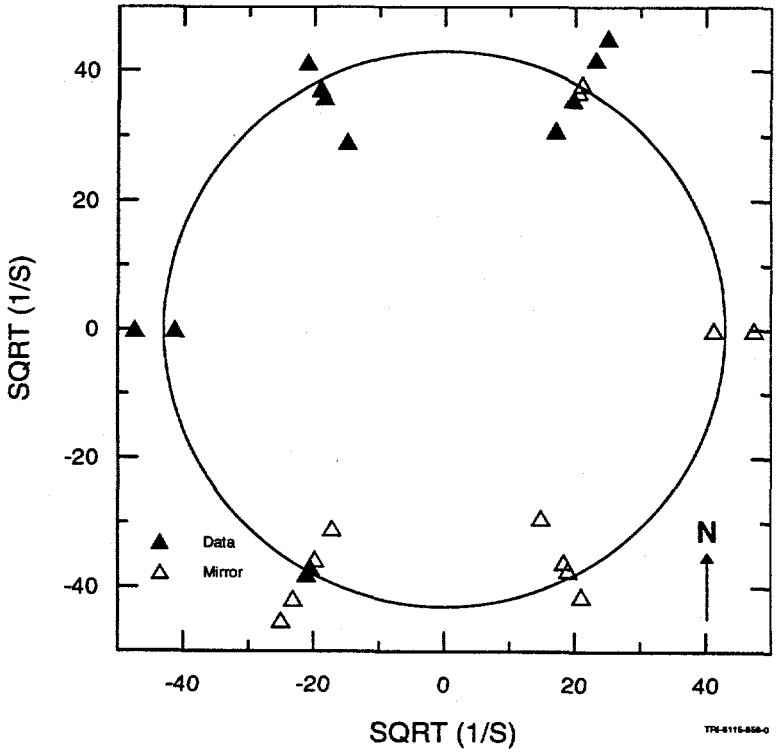

Figure 6-63. H-9 anisotropy data.

The transmissivity interpreted from the response of the Engle well during test #3, 96 ft^2/d (1.0 x 10^{-4} m^2/s), is consistent with the values from H-9. The storativity value interpreted from the Engle response, 4.7 x 10^{-6}, is two orders of magnitude lower than the values from H-9, which may indicate that the pressure transient was propagated primarily through fractures across the 4,115-ft (1,255-m) distance between H-9c and the Engle well.

6.5 H-10b Slug Test

Slug-test data reported by Richey (1986) for H-10b were analyzed using GTFM. Slug test #1 was the best of the tests reported, with a slug injection that raised the pressure in the well by approximately 300 psi (2.0 MPa) (Figure 5-11). The pressure decline was monitored for approximately one day. Figure 6-64 shows a semilog plot of the normalized pressure data and derivative with the best-fit GTFM simulation. The test was simulated using a model of a well in an infinite single-porosity domain with a transmissivity of 0.041 ft^2/d (4.4 x 10^{-8} m^2/s) (Table 6-1). The static formation pore pressure used in the simulation is 215 psig (1.5 MPa), indicating that the pressure was not fully stabilized at the start of the test.

6.6 H-11 Tracer/Pumping Test

As part of single-well and convergent-flow tracer tests, well H-11b1 was pumped for 50 days. The drawdown data collected from H-11b1 and from observation wells H-11b2, H-11b3, and H-11b4 during the first 5.3 days of this pumping, before tracers were injected into H-11b2 and H-11b3, are interpreted below. Effects of tracer injection into H-11b1 before pumping began are included in the

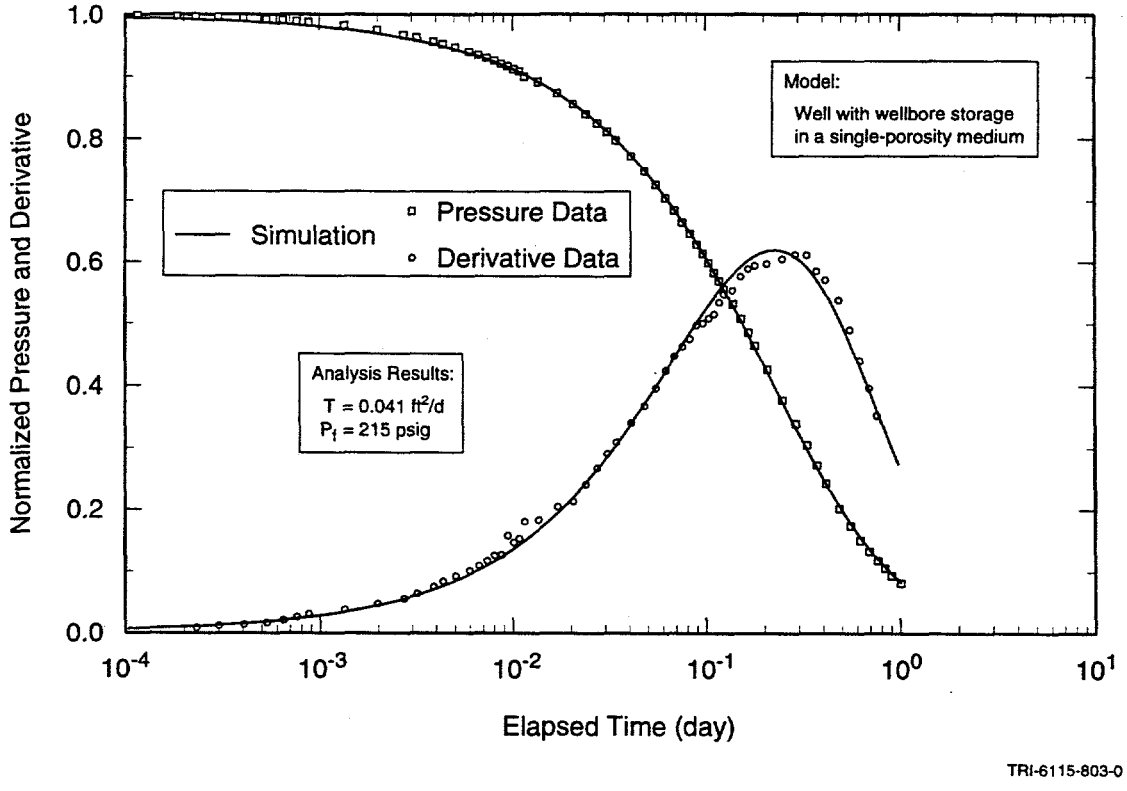

Figure 6-64. Semilog plot of normalized H-10b slug-test #1 data with GTFM simulation.

data and simulations. The tracer injection did not occur at a constant rate, but was simulated as if it did for the sake of simplicity, given that the only purpose of simulating the injection was to provide reasonable initial conditions for the drawdown period.

6.6.1 H-11b1

Figures 6-65, 6-66, and 6-67 show log-log, Horner, and linear-linear plots, respectively, of the drawdown data from H-11b1 along with the best-fit Interpret/2 simulations. The data-acquisition rate was not fast enough to capture the early-time well response. The data collected during the last approximately 60 hr shown were affected by electronic noise in the DAS. The simulations were generated using a model for a well with wellbore storage and skin in a double-porosity medium with unrestricted interporosity flow, slab matrix blocks, and channel (parallel) no-flow boundaries. The inclusion of channel boundaries was necessitated by the sustained late-time rise in the pressure derivative on the log-log plot (Figure 6-65). In reality, the rise in the pressure derivative is probably caused by decreasing transmissivity at some distance from the H-11 hydropad instead of by actual parallel boundaries. The simulations were generated using a transmissivity of 45 ft^2/d (4.8 x 10^{-5} m^2/s) and other parameters as listed in Table 6-1.

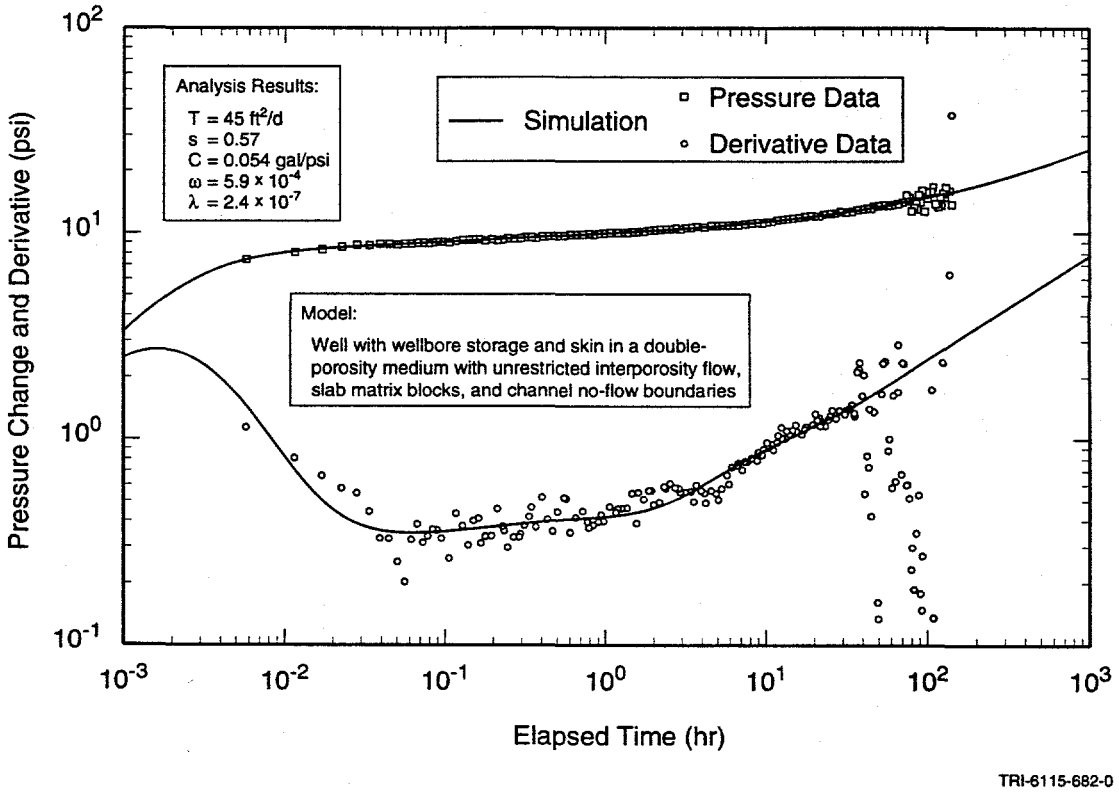

Figure 6-65. Log-log plot of H-11b1 drawdown data with Interpret/2 simulation.

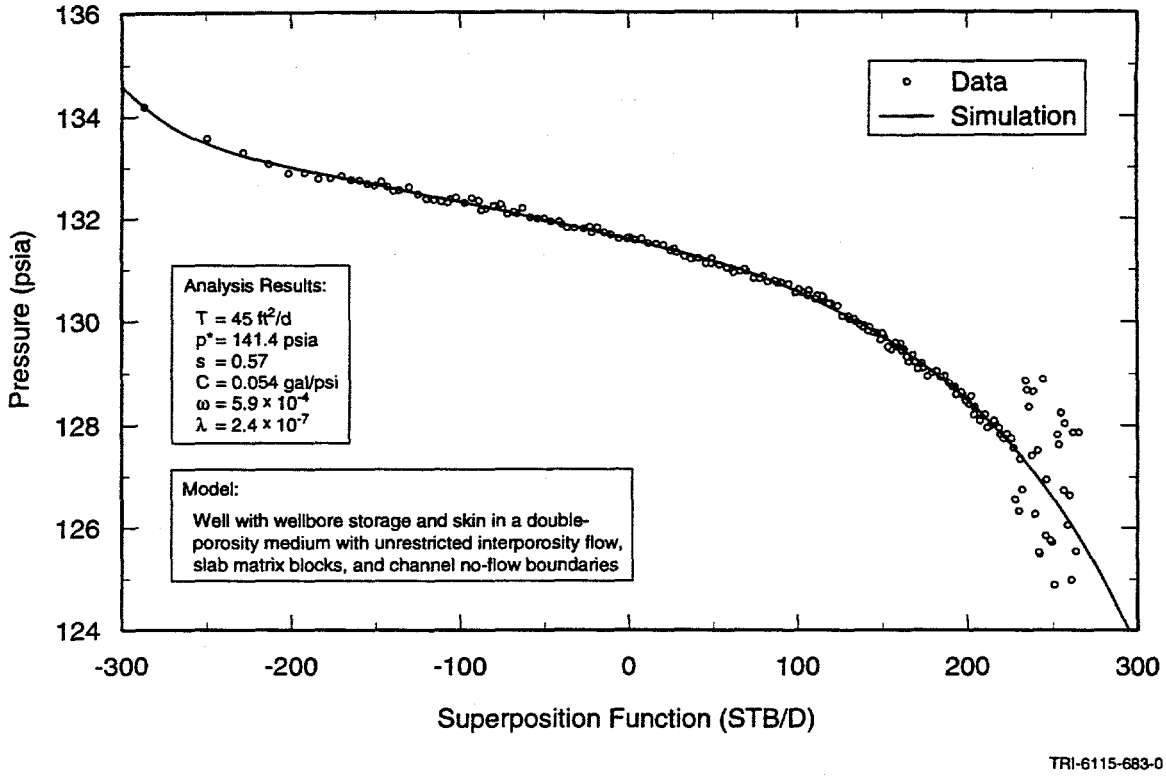

Figure 6-66. Horner plot of H-11b1 drawdown data with Interpret/2 simulation.

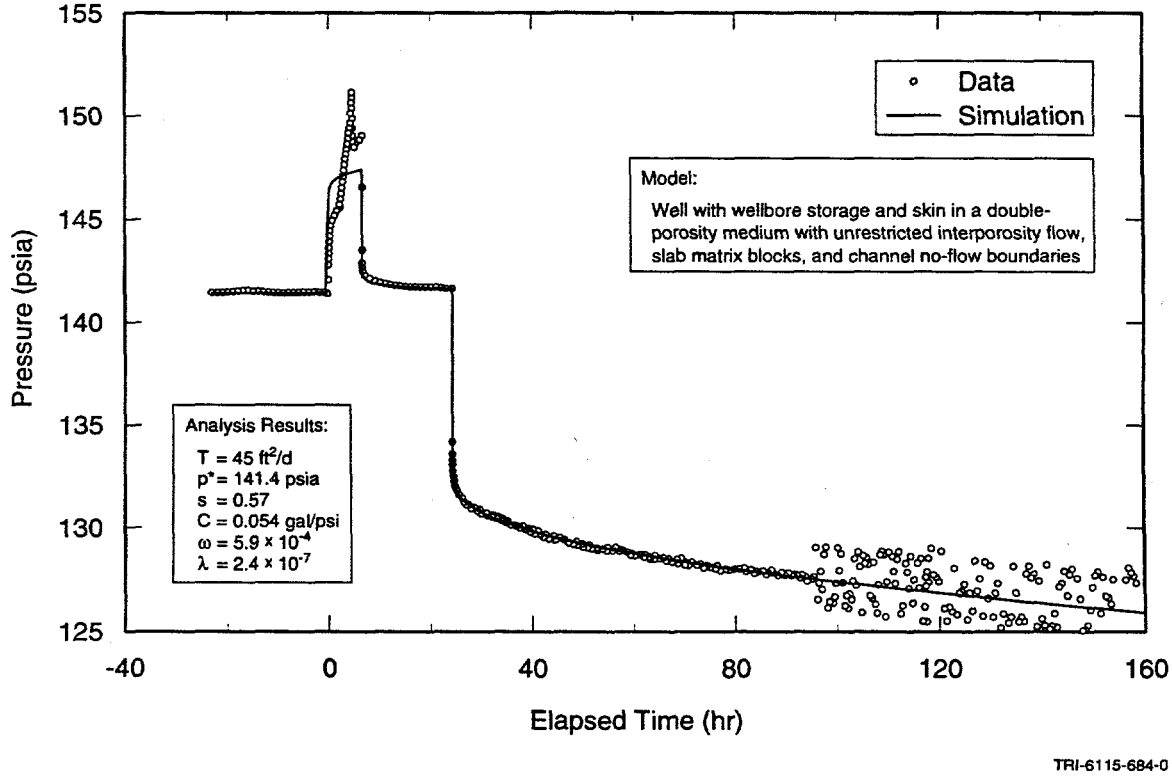

Figure 6-67. Linear-linear plot of H-11b1 data with Interpret/2 simulation derived from drawdown analysis.

6.6.2 Observation Wells

Figures 6-68 through 6-70, 6-71 through 6-73, and 6-74 through 6-76 show log-log, Horner, and linear-linear plots of the drawdown data from H-11b2, H-11b3, and H-11b4, respectively, along with the best-fit Interpret/2 simulations. In all cases, the data were simulated using a model for a line-source well in a double-porosity formation with unrestricted interporosity flow, slab matrix blocks, and channel no-flow boundaries. The interpreted transmissivities for H-11b2 and H-11b3 are 44 ft^2/d (4.7 x 10^{-5} m^2/s) and for H-11b4 is 45 ft^2/d (4.8 x 10^{-5} m^2/s). Interpreted storativities are 6.7 x 10^{-5}, 4.2 x 10^{-5}, and 3.3 x 10^{-5} for H-11b2, H-11b3, and H-11b4, respectively. Other interpreted parameters are listed in Table 6-1.

6.6.3 Summary of Results from the H-11 Tracer/Pumping Test

The data from all four H-11 wells could be analyzed using a model for a double-porosity medium with channel boundaries. However, the heterogeneity represented by the boundaries affected the well responses early enough in the test to affect the estimation of all parameters. Transmissivity changes of at least ±10% could be compensated by changes in storativity and distances to boundaries without significantly altering the model fits to the data. Because of these uncertainties, any calculation of anisotropy at the H-11 hydropad would not be meaningful. Similarly, the simulated distances to the boundaries are not considered sufficiently reliable for the differences between them to be considered significant. The geometric mean of the transmissivities interpreted for the four wells at the hydropad is 44 ft^2/d (4.7 x 10^{-5} m^2/s), similar to results from earlier tests reported by Beauheim (1989), and the geometric mean storativity is 4.5 x 10^{-5}, which falls within the range reported for the earlier tests.

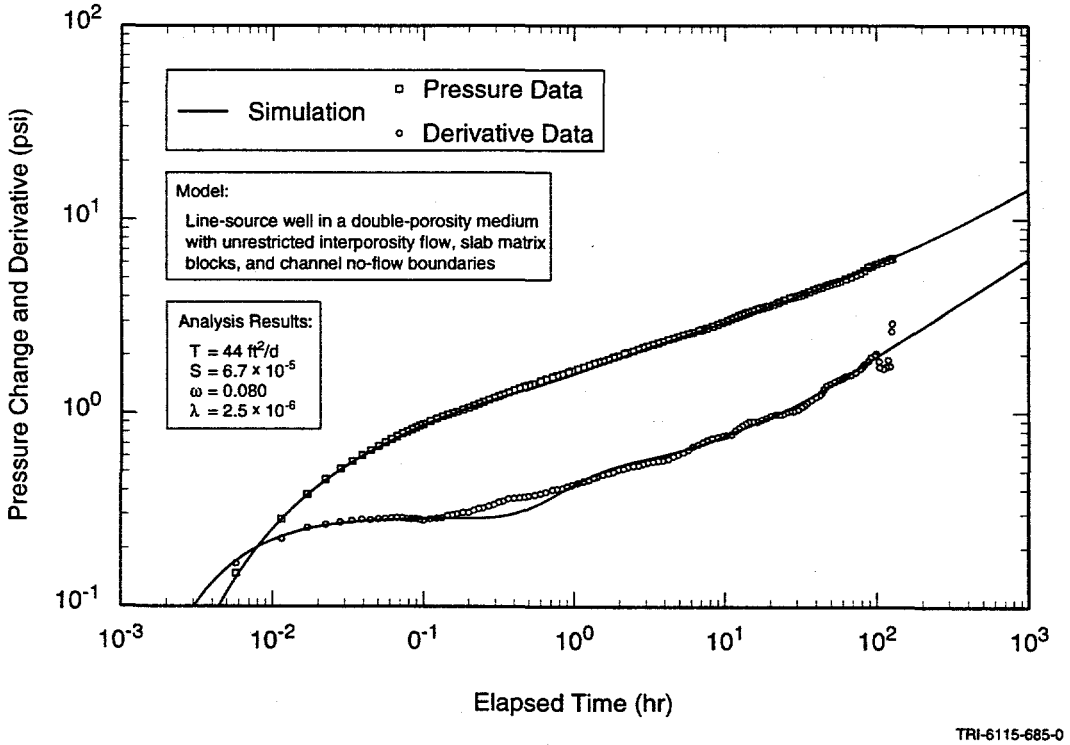

Figure 6-68. Log-log plot of H-11b2 drawdown data with Interpret/2 simulation.

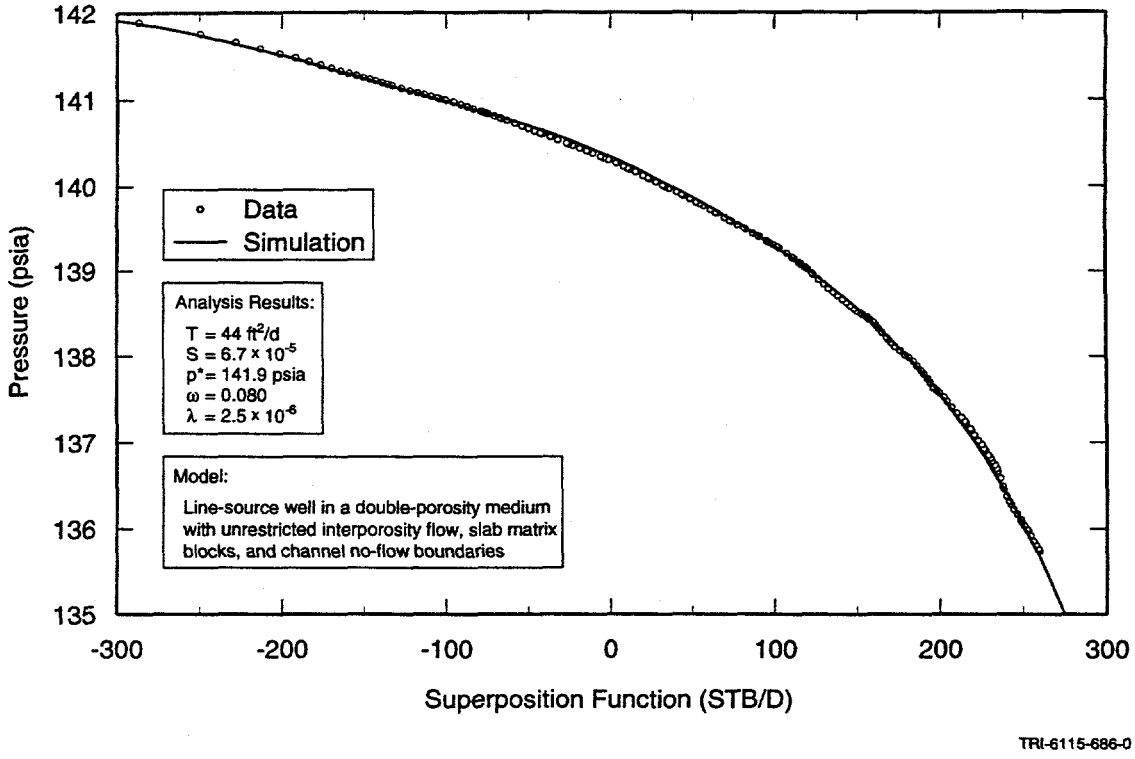

Figure 6-69. Horner plot of H-11b2 drawdown data with Interpret/2 simulation.

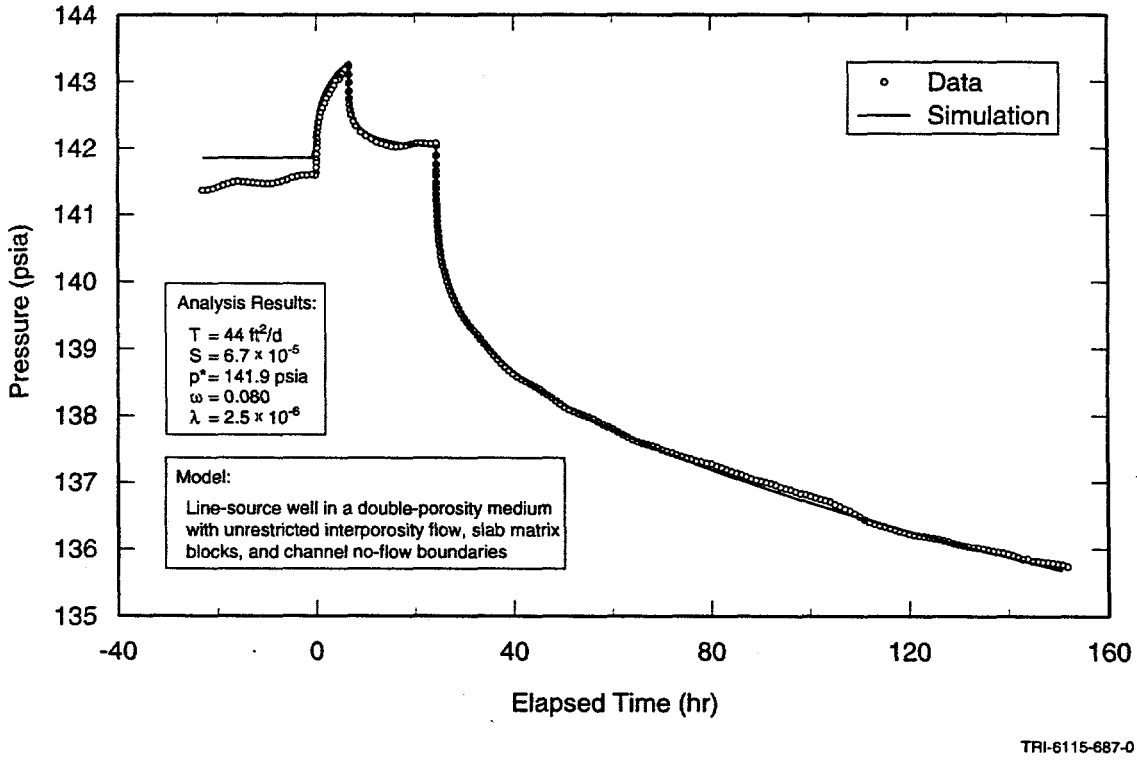

Figure 6-70. Linear-linear plot of H-11b2 data with Interpret/2 simulation derived from drawdown analysis.

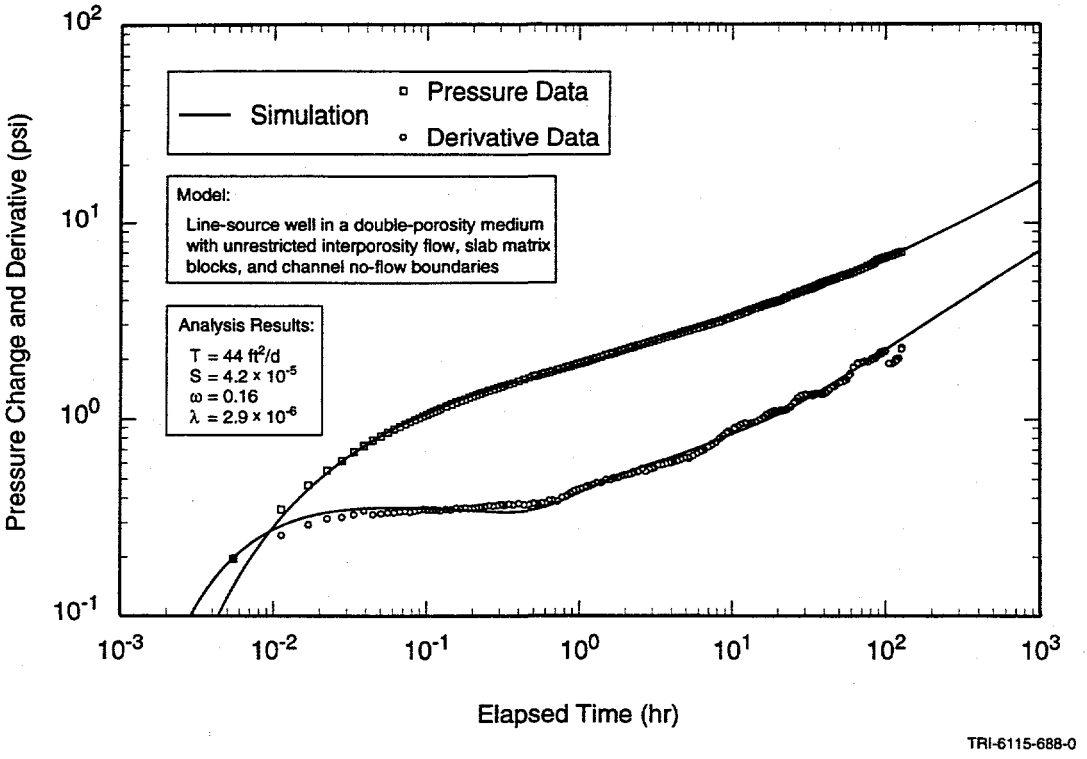

Figure 6-71. Log-log plot of H-11b3 drawdown data with Interpret/2 simulation.

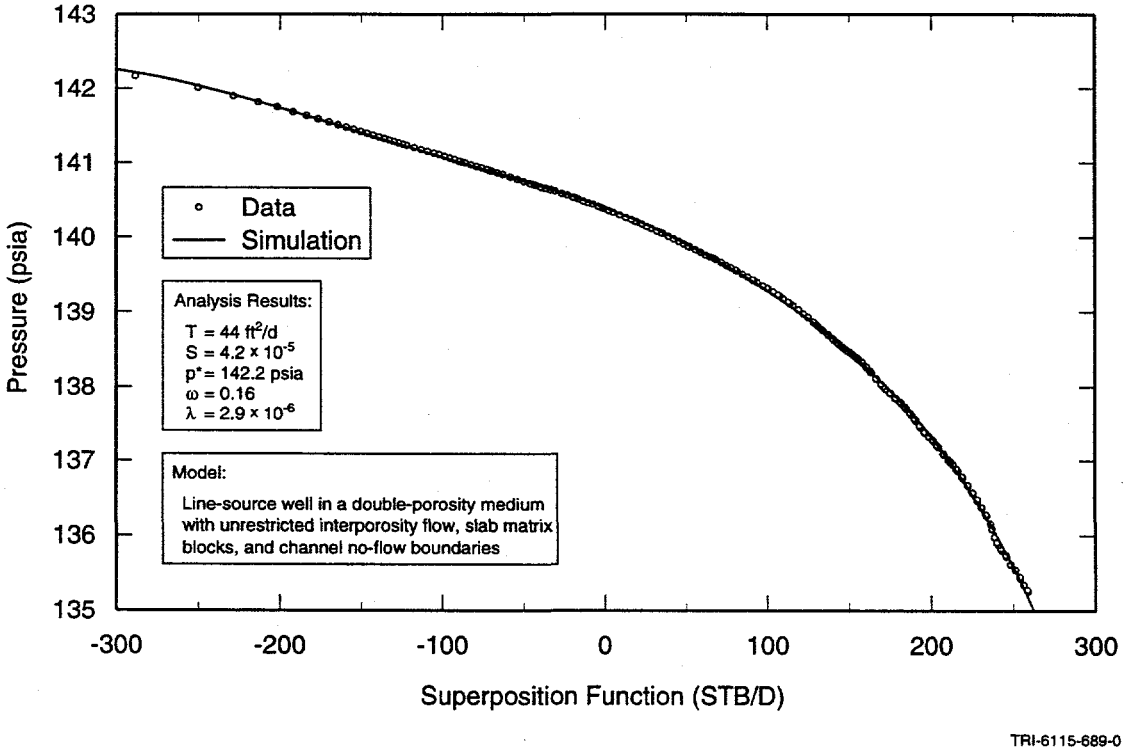

Figure 6-72. Horner plot of H-11b3 drawdown data with Interpret/2 simulation.

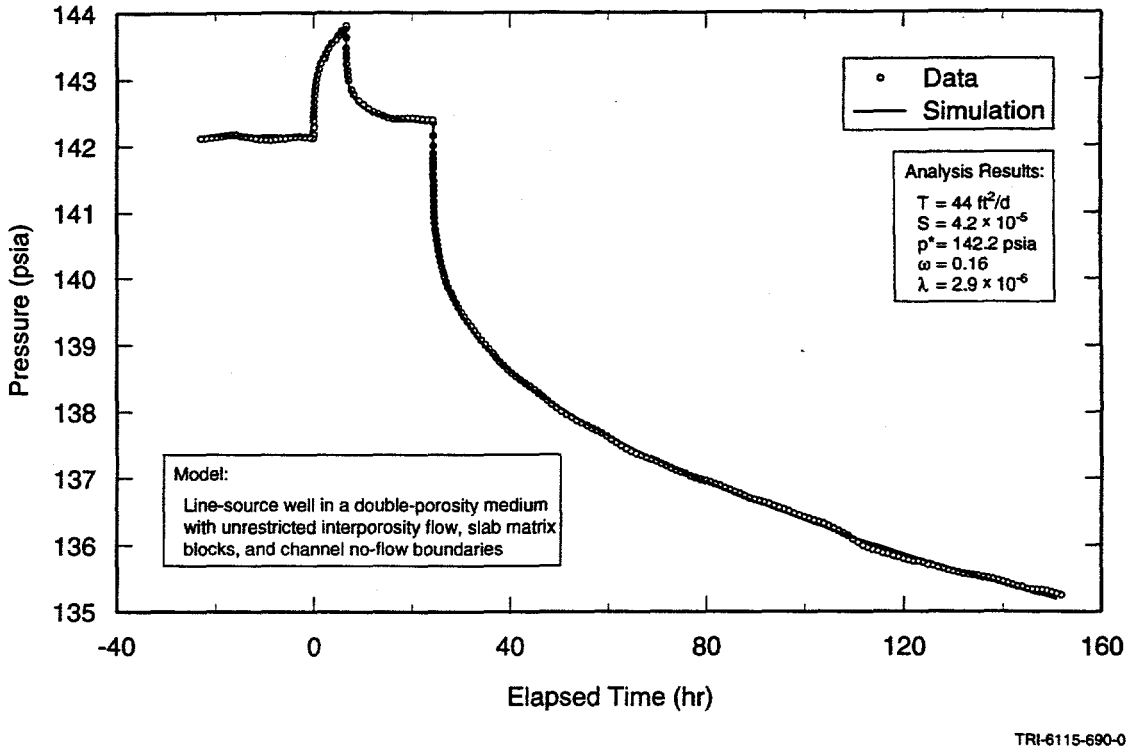

Figure 6-73. Linear-linear plot of H-11b3 data with Interpret/2 simulation derived from drawdown analysis.

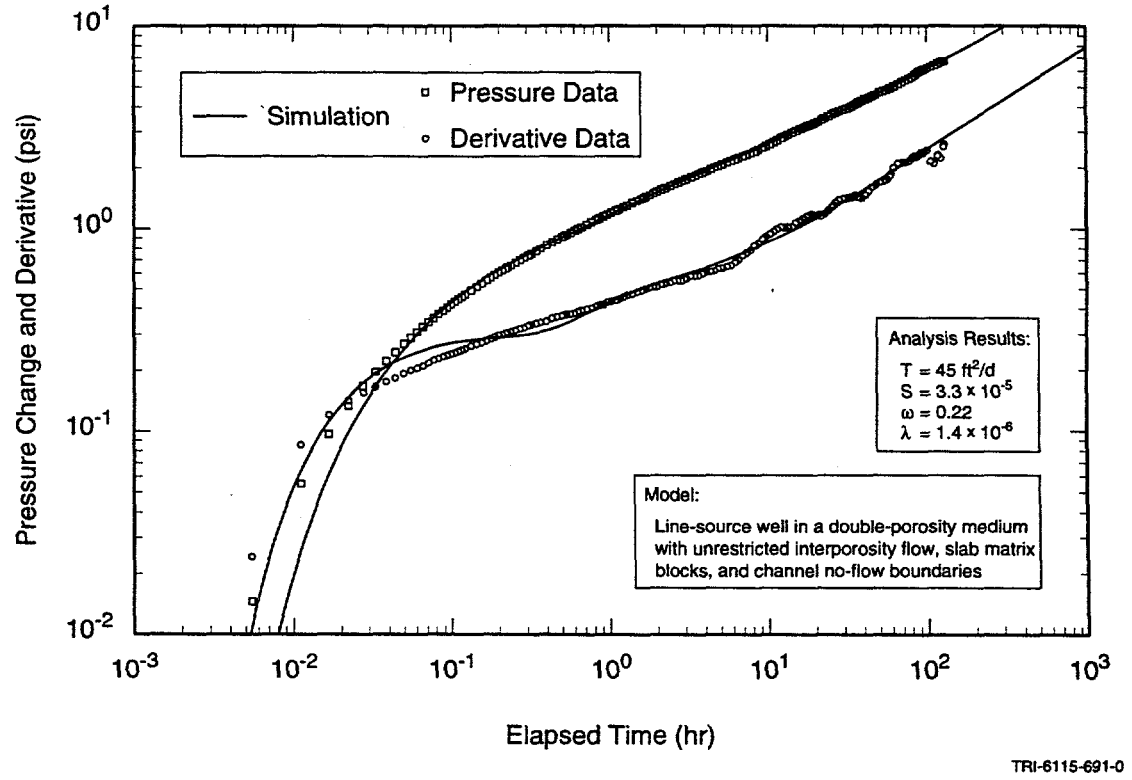

Figure 6-74. Log-log plot of H-11b4 drawdown data with Interpret/2 simulation.

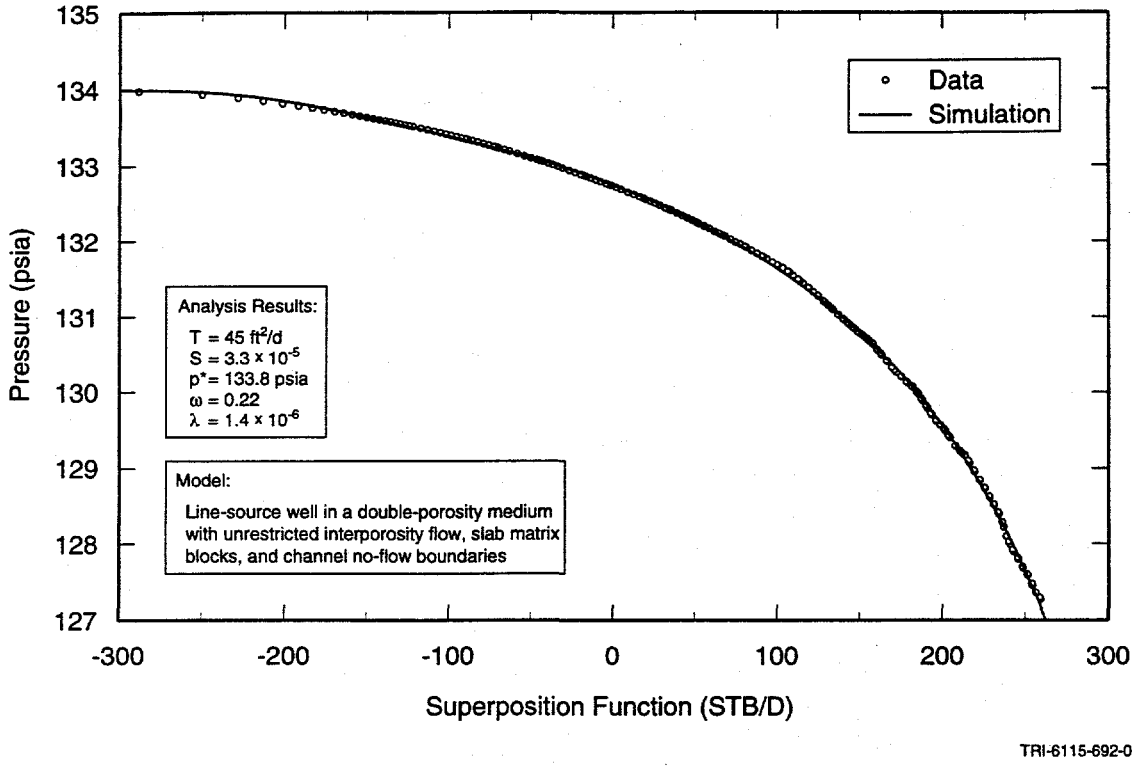

Figure 6-75. Horner plot of H-11b4 drawdown data with Interpret/2 simulation.

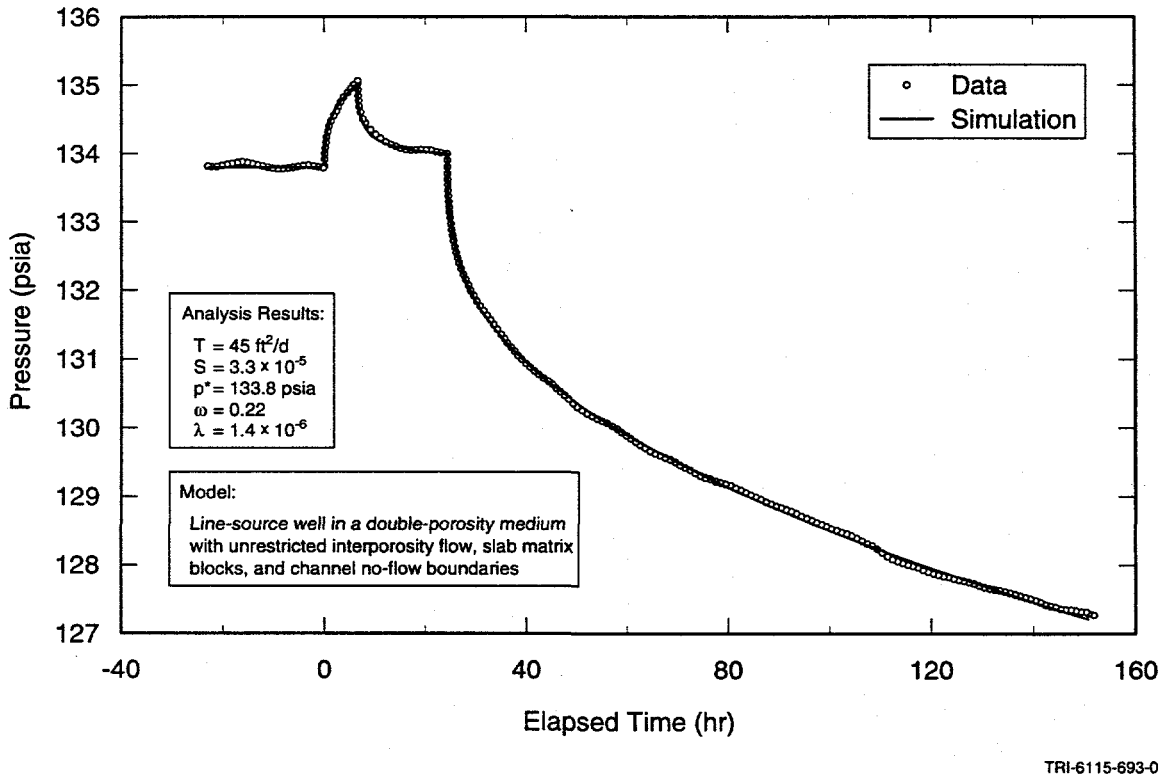

Figure 6-76. Linear-linear plot of H-11b4 data with Interpret/2 simulation derived from drawdown analysis.

Although the simulations presented above were generated using a model for a double-porosity system, simulations that look visually almost as good could be produced using a model for a single-porosity system with channel no-flow boundaries and higher transmissivity (80-90 ft^2/d; 8.6 to 9.7 x 10^{-5} m^2/s). This is because, at H-11, the distinctive double-porosity feature of transition from fracture-only to total-system behavior is not clearly separated in time from wellbore-storage and skin effects or from the effects of heterogeneity. The double-porosity model results are presented in this report because slug tests performed in H-11b4 showed a clear double-porosity signature (Beauheim, 1989) and because breakthrough curves from a convergent-flow tracer test at H-11 could be simulated using a double-porosity model but not using a single-porosity model (Jones et al., 1992).

6.7 H-19 Hydraulic Tests

The H-19 hydraulic tests consisted of drillstem and slug tests of the Magenta in H-19b1, a well-development pumping test in H-19b2, and the tracer/pumping test for which H-19b0 was the pumping well.

6.7.1 H-19b1 Drillstem and Slug Tests of the Magenta

The early-time data from the first DST flow period show a concave-upward curvature in Figure 5-14, which is different from the more typical concave-downward curvature shown by the data from the slug test. Concave-upward curvature reflects well development, which makes the data from that test phase difficult to analyze. Clay plugging the shut-in tool delayed the pressure response when the tool was opened to initiate the second flow period, and caused excessive "squeeze" when the tool was closed to start the second recovery period, rendering interpretation of data from both of those periods problematic. Consequently, interpretation of the H-19b1 Magenta tests focused on the slug test.

The data from the slug test were analyzed using GTFM. Figure 6-77 shows a semilog plot of the normalized pressure data and derivative with the best-fit GTFM simulation. The late-time derivative data exhibit significant noise, but the simulation captures the overall response very well. The simulation model is of a well in an infinite single-porosity domain with a transmissivity of 0.38 ft^2/d (4.1 x 10^{-7} m^2/s).

6.7.2 H-19b2 Well-Development Pumping Test

As discussed in Section 5.7.2, the H-19b2 well-development pumping test involved pumping at 1.9 gpm (0.12 L/s) for approximately 6.1 hr followed by pumping at 3.8 gpm (0.24 L/s) for approximately 25.7 hr. A GFI failure then led to 1.7 hr of pumping at an uncontrolled, higher rate followed by 0.1 hr at a lower rate. Through an iterative trial-and-error approach involving fitting the drawdowns observed during the first two known rates and then estimating the unknown rates until the corresponding drawdowns were matched, the two unknown rates were determined to be approximately 10.5 and 3.8 gpm (0.66 and 0.24 L/s). Using this rate history, the data from the second drawdown period and the recovery period were analyzed using Interpret/2.

Figures 6-78 and 6-79 show the log-log and Horner plots, respectively, of the recovery data from H-19b2 along with the best-fit Interpret/2 simulations. The data were analyzed using a model for a well with wellbore storage and skin in an infinite double-porosity medium with restricted interporosity flow. The medium has a transmissivity of 5.9 ft^2/d

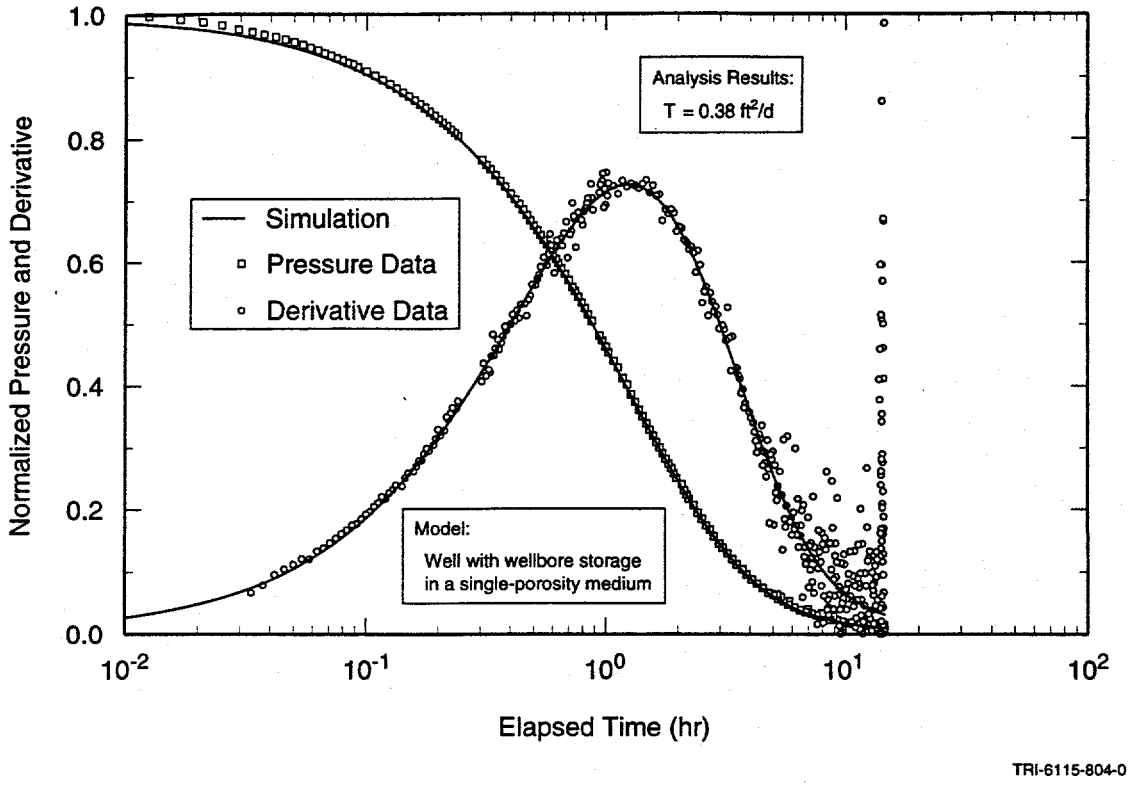

Figure 6-77. Semilog plot of normalized H-19b1 slug-test data with GTFM simulation.

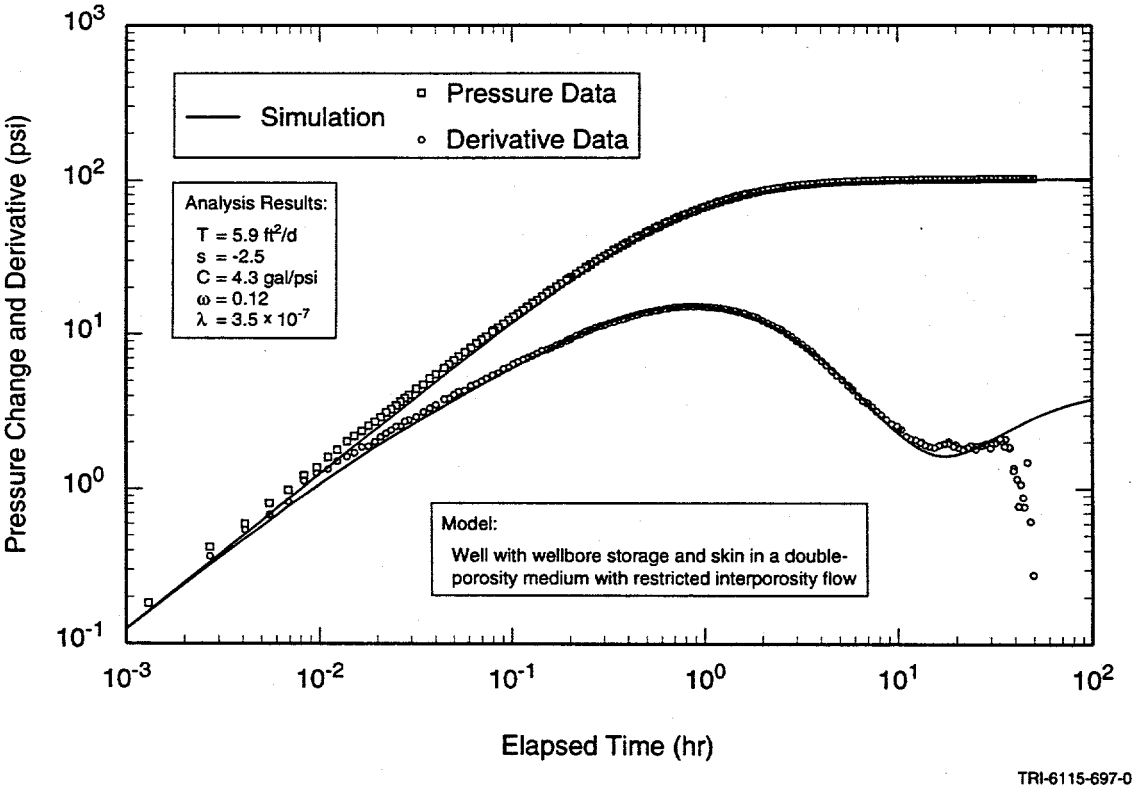

Figure 6-78. Log-log plot of H-19b2 recovery data with Interpret/2 simulation.

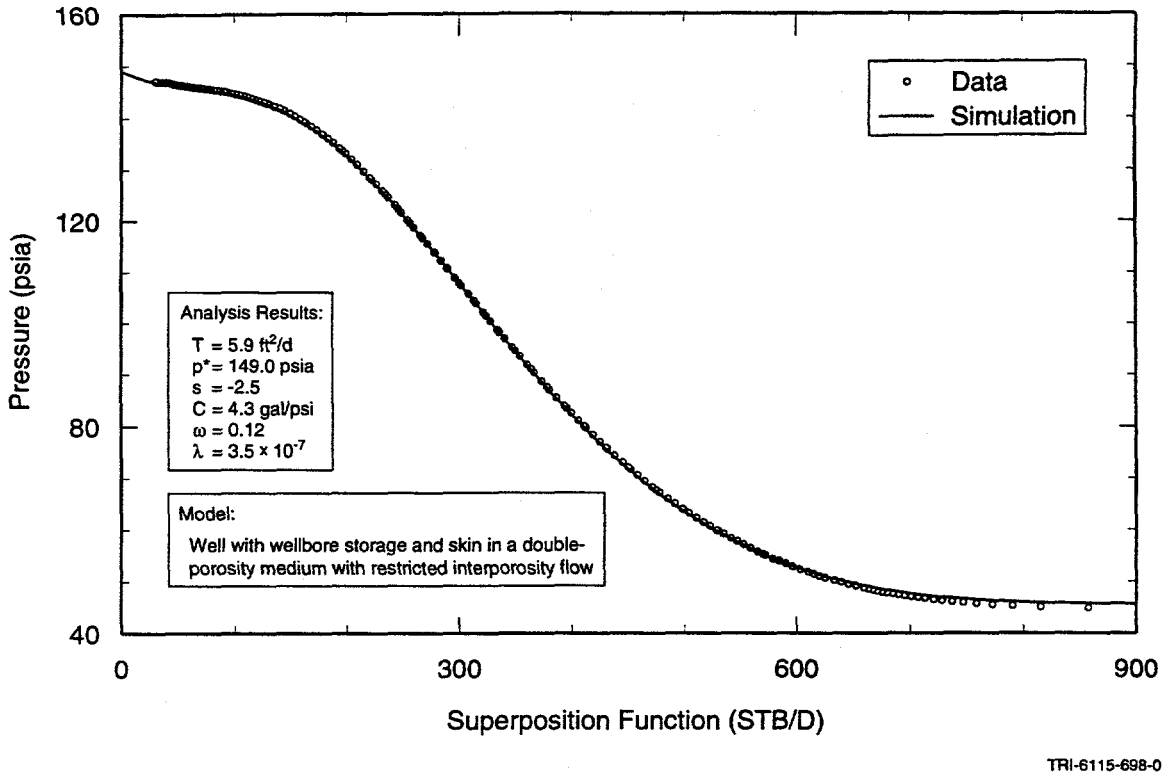

Figure 6-79. Horner plot of H-19b2 recovery data with Interpret/2 simulation.

(6.4×10^{-6} m^2/s) and the well appears to have a negative skin of -2.5. Other interpreted parameters are listed in Table 6-1. Figure 6-80 is a linear-linear plot of the match between this model and the combined drawdown and recovery data. The pumping periods are represented well by the simulation. Interpret/2 simulations of the data from the second pumping period are shown in Appendix A (Figures A-40 through A-42) and the interpreted parameters are listed in Table 6-1.

Evidence for double-porosity conditions in the Culebra at H-19b2 is not compelling based on the data from this test alone, because neither the drawdown nor recovery periods lasted long enough to provide fully stabilized derivative data. Double-porosity simulations are presented because single-porosity simulations do not match the derivative data quite as well and because of the unequivocal findings of double-porosity conditions during the H-19 tracer/pumping test (see Section 6.7.3).

6.7.3 H-19 Tracer/Pumping Test

As discussed in Section 5.7.3, the H-19 tracer/pumping test entailed pumping of H-19b0 while monitoring responses in the entire Culebra intervals of H-19b2, H-19b4, and H-19b6, and upper and lower Culebra intervals in H-19b3, H-19b5, and H-19b7. The data analyzed herein were collected during the first 117 hr of pumping, when the pumping rate averaged 4.4 gpm (0.28 L/s).

6.7.3.1 H-19b0

The DAS was set to scan all pressure transmitters every ten seconds at the start of the H-19 tracer/pumping test. The first scan made after the pump was turned on showed a 29-psi (200-kPa) drawdown in the lower Culebra zone of H-19b0 (the middle packer

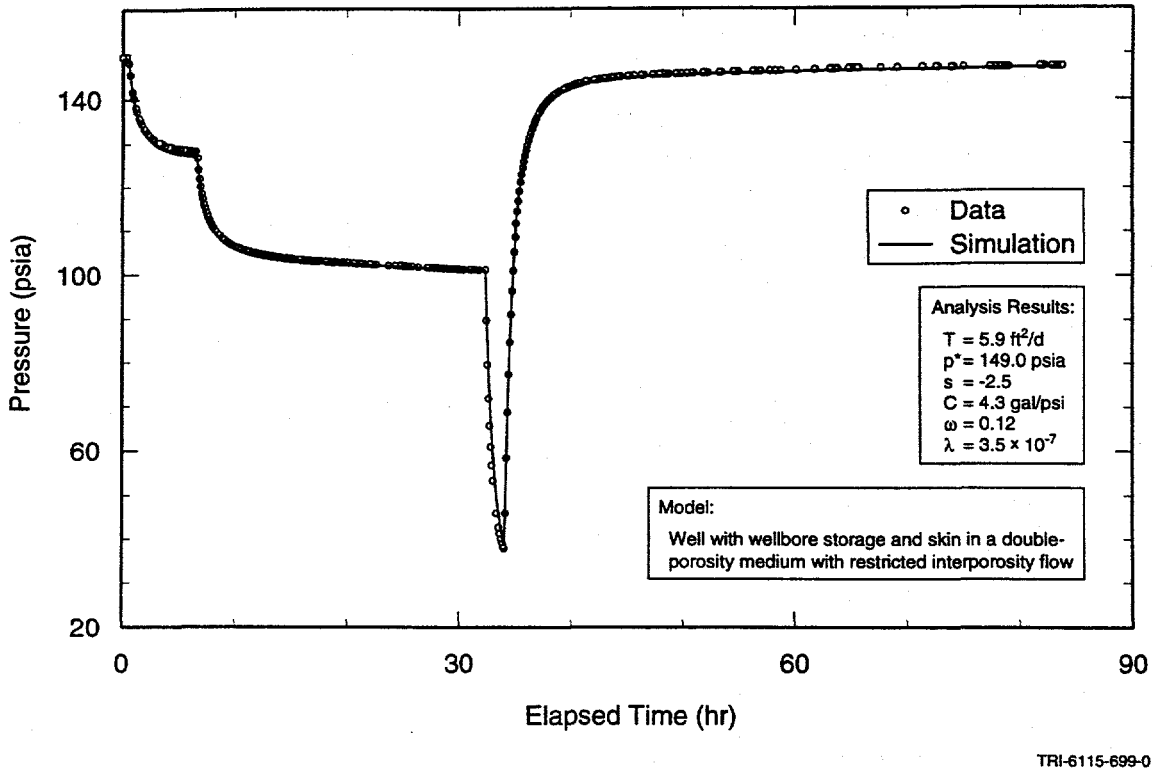

Figure 6-80. Linear-linear plot of H-19b2 data with Interpret/2 simulation derived from recovery analysis.

had not yet been deflated). The next several scans showed drawdowns of approximately 3 psi (21 kPa). The order-of-magnitude disparity between the initial and subsequent drawdowns leads us to believe that the initial drawdown was primarily caused by well loss and does not represent the response of the formation. Therefore, the pressure value reflecting the 29-psi (200-kPa) drop was taken to be the "true" initial pressure for all subsequent drawdowns in the analyses presented below.

Figures 6-81, 6-82, and 6-83 show the log-log, Horner, and linear-linear plots, respectively, of the drawdown data from H-19b0 along with the best-fit Interpret/2 simulations. The data were analyzed using a model for a well with wellbore storage and skin in an infinite double-porosity medium with restricted interporosity flow. The medium has a transmissivity of 6.4 ft^2/d (6.8 x 10^{-6} m^2/s) and the well appears to have a negative skin of -1.5. Other interpreted parameters are listed in Table 6-1.

6.7.3.2 H-19b2, H-19b4, AND H-19b6

Figures 6-84 through 6-86, 6-87 through 6-89, and 6-90 through 6-92 show log-log, Horner, and linear-linear plots of the drawdown data from H-19b2, H-19b4, and H-19b6, respectively, along with the best-fit Interpret/2 simulations. In all cases, the data were simulated using a model for a line-source well in a double-porosity formation with restricted interporosity flow. The H-19b4 and H-19b6 simulations include the influence of a no-flow boundary at late time. The interpreted transmissivities for H-19b2, H-19b4, and H-19b6 are 5.6, 6.8, and 7.9 ft^2/d (6.0 x 10^{-6}, 7.3 x 10^{-6}, and 8.5 x 10^{-6} m^2/s), respectively. Interpreted storativities are 4.1 x 10^{-5}, 5.0 x 10^{-5}, and 3.7 x 10^{-5} for H-19b2, H-19b4,

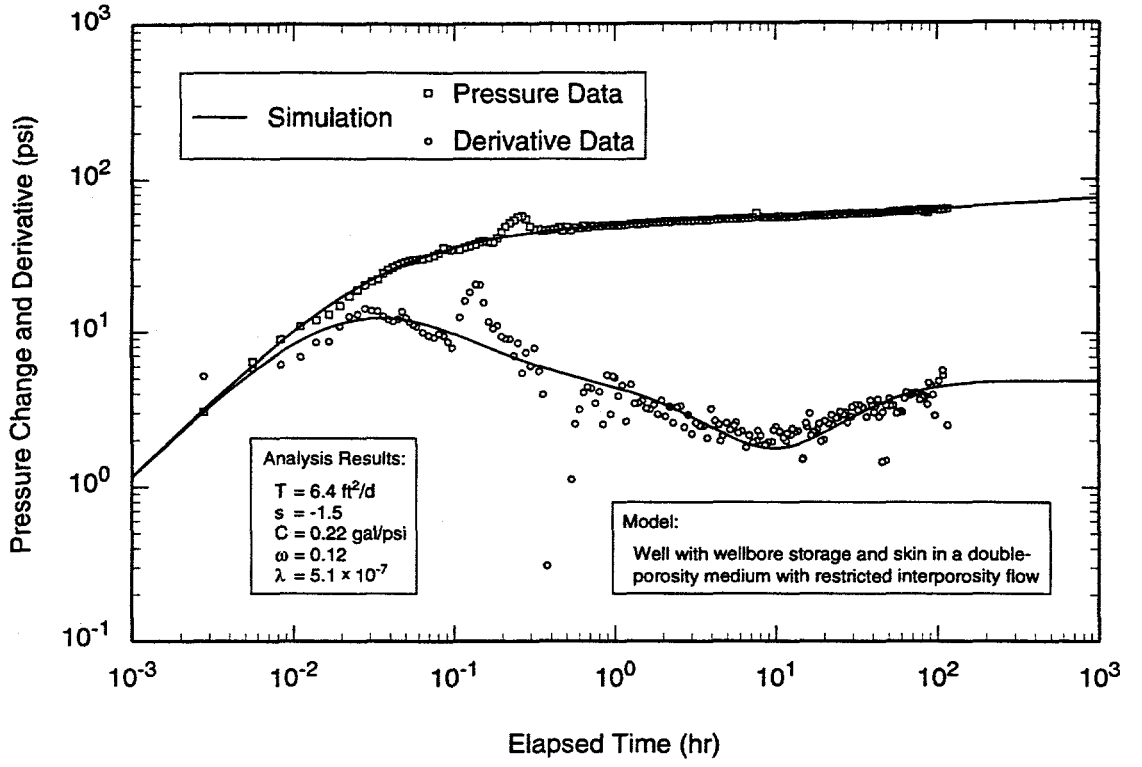

Figure 6-81. Log-log plot of H-19b0 drawdown data with Interpret/2 simulation.

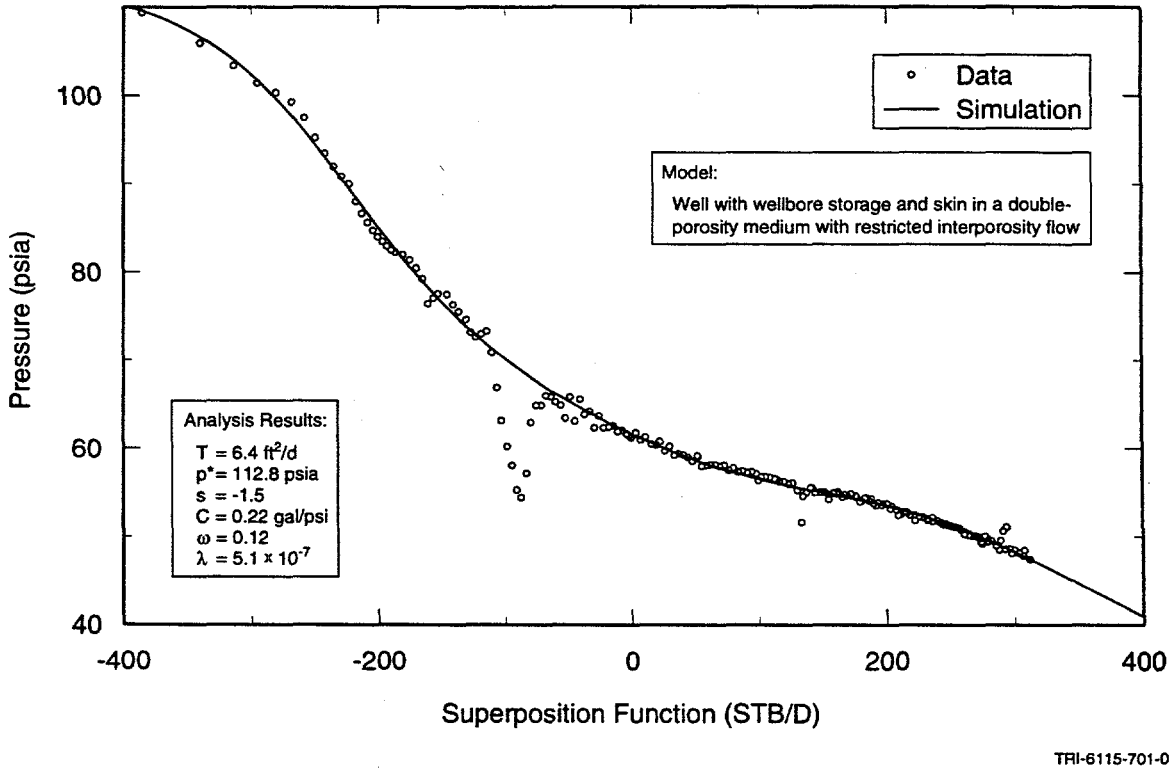

Figure 6-82. Horner plot of H-19b0 drawdown data with Interpret/2 simulation.

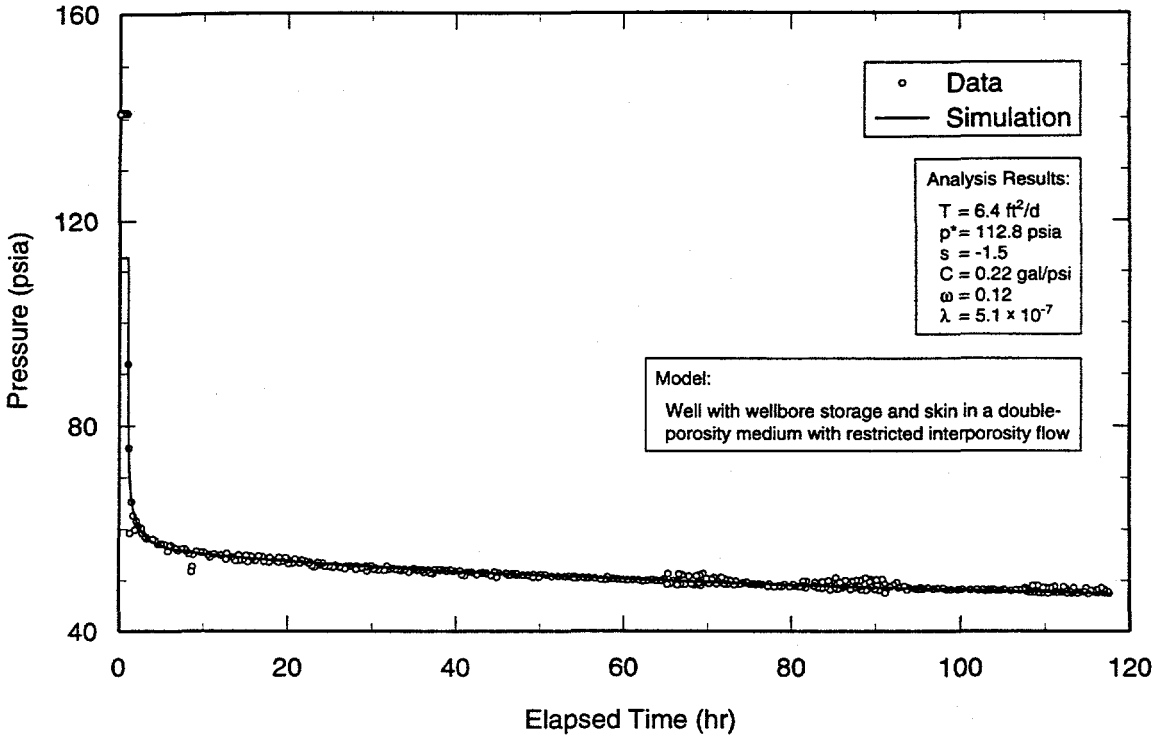

Figure 6-83. Linear-linear plot of H-19b0 drawdown data with Interpret/2 simulation.

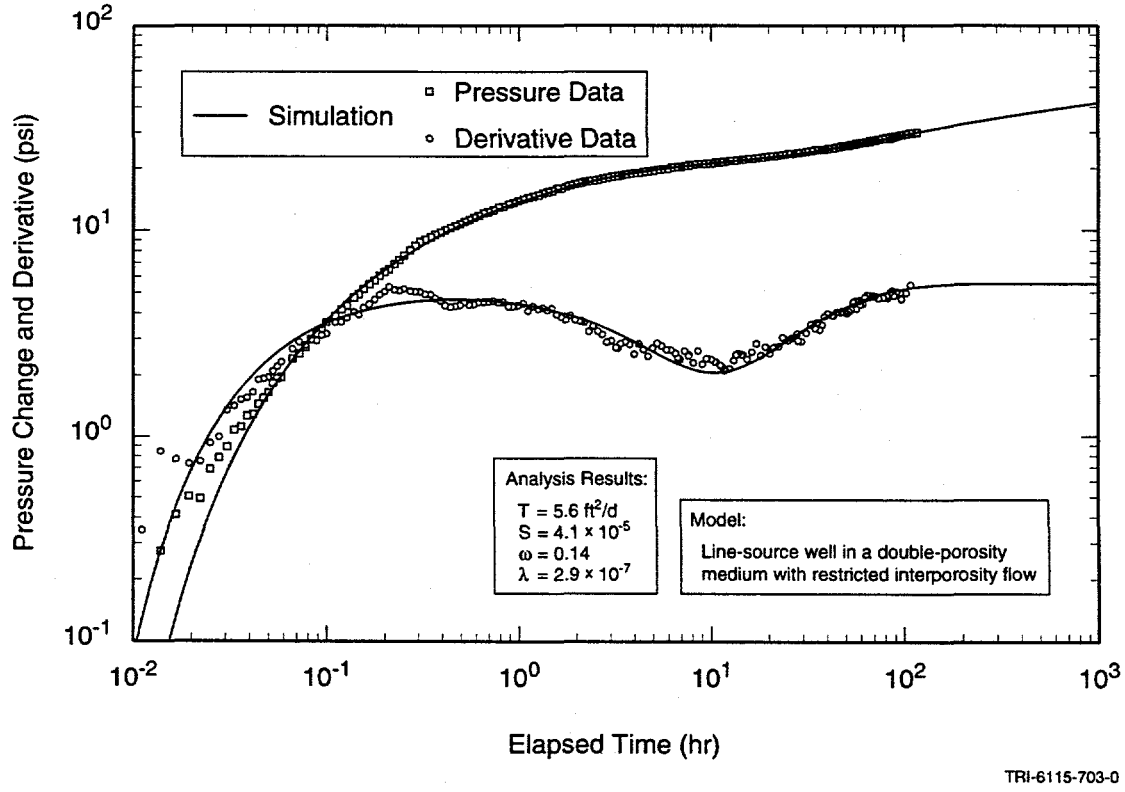

Figure 6-84. Log-log plot of H-19b2 drawdown data with Interpret/2 simulation.

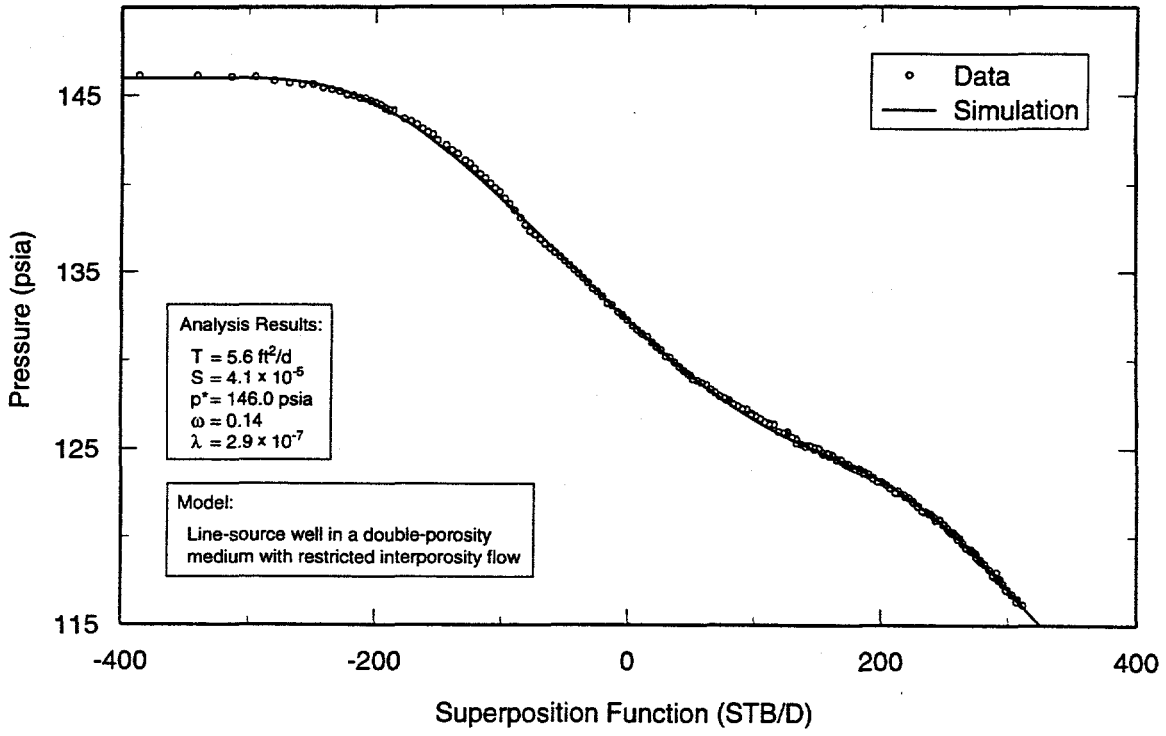

Figure 6-85. Horner plot of H-19b2 drawdown data with Interpret/2 simulation.

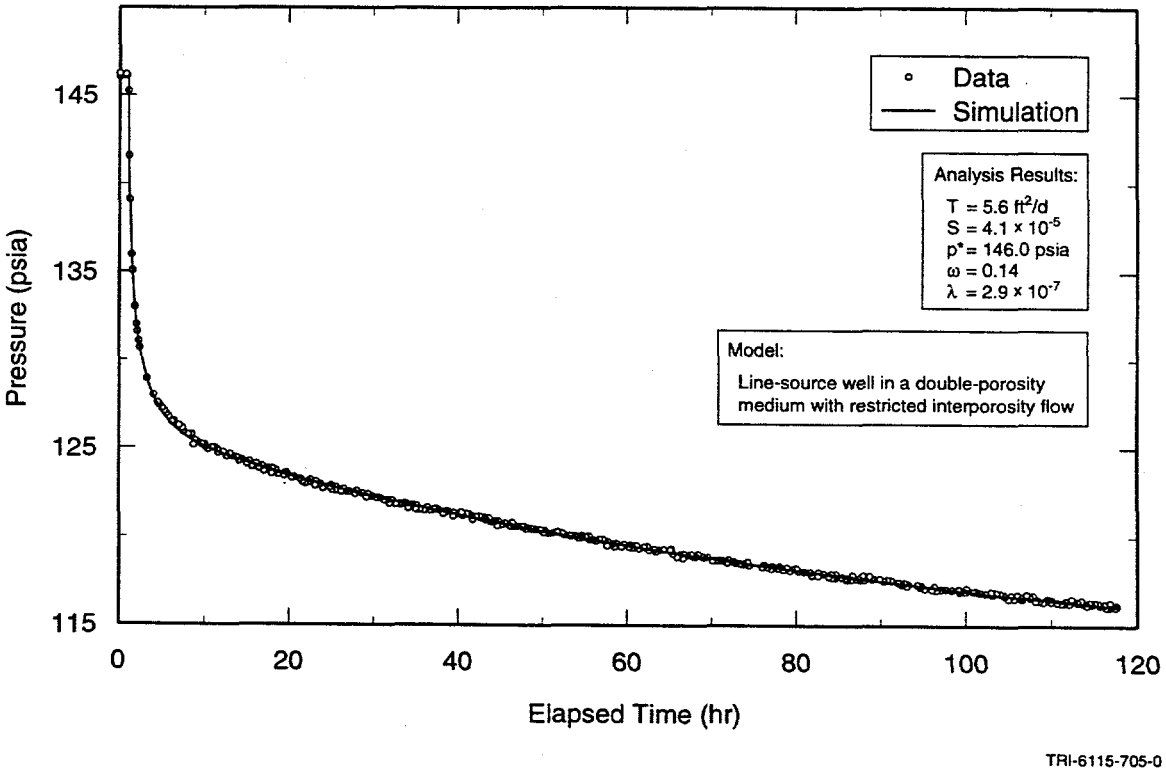

Figure 6-86. Linear-linear plot of H-19b2 drawdown data with Interpret/2 simulation.

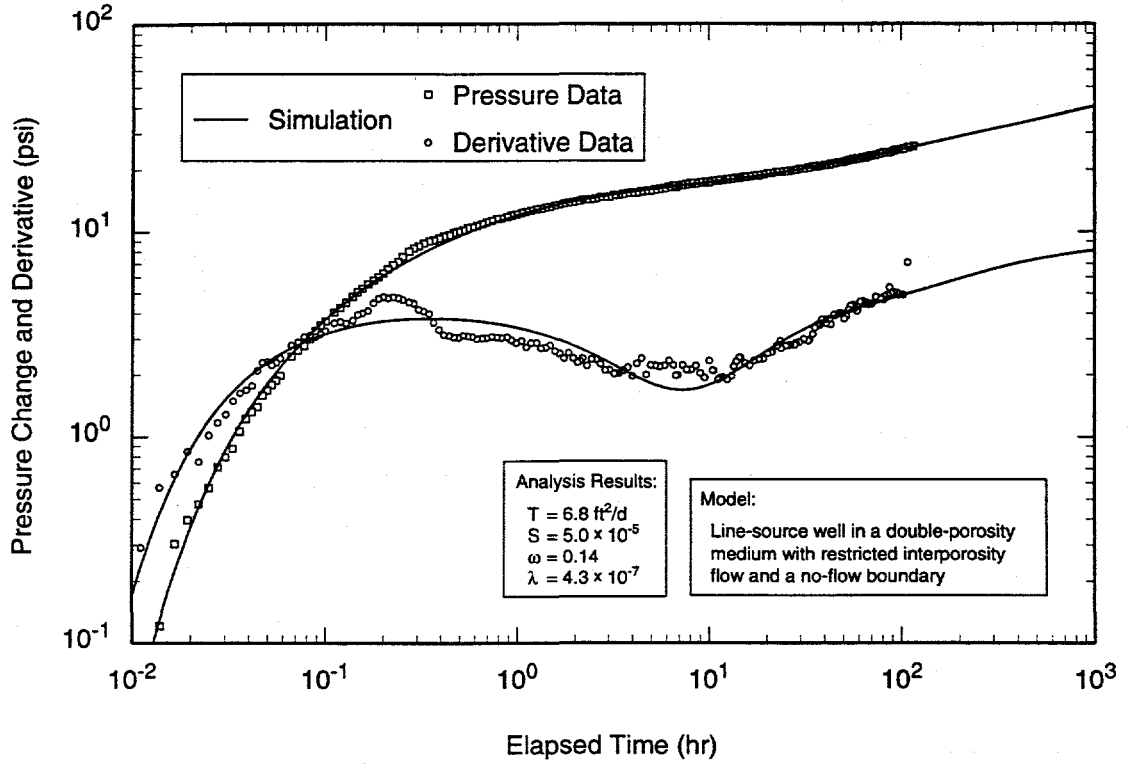

Figure 6-87. Log-log plot of H-19b4 drawdown data with Interpret/2 simulation.

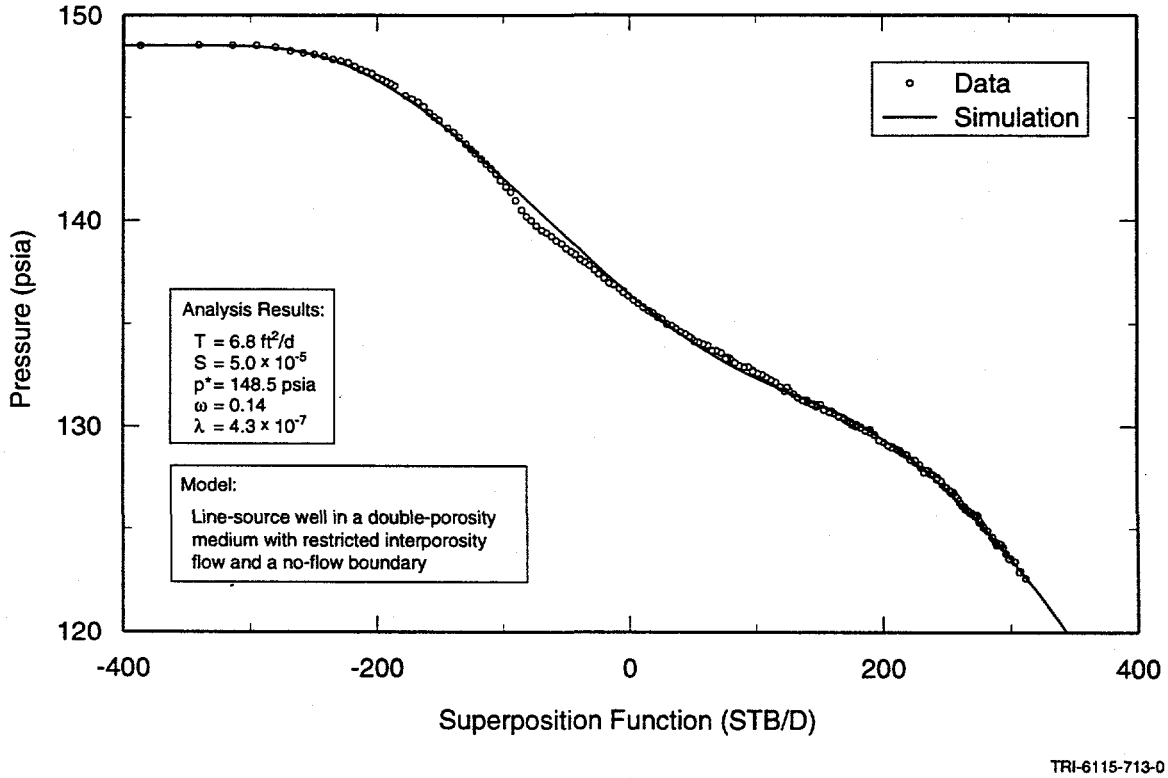

Figure 6-88. Horner plot of H-19b4 drawdown data with Interpret/2 simulation.

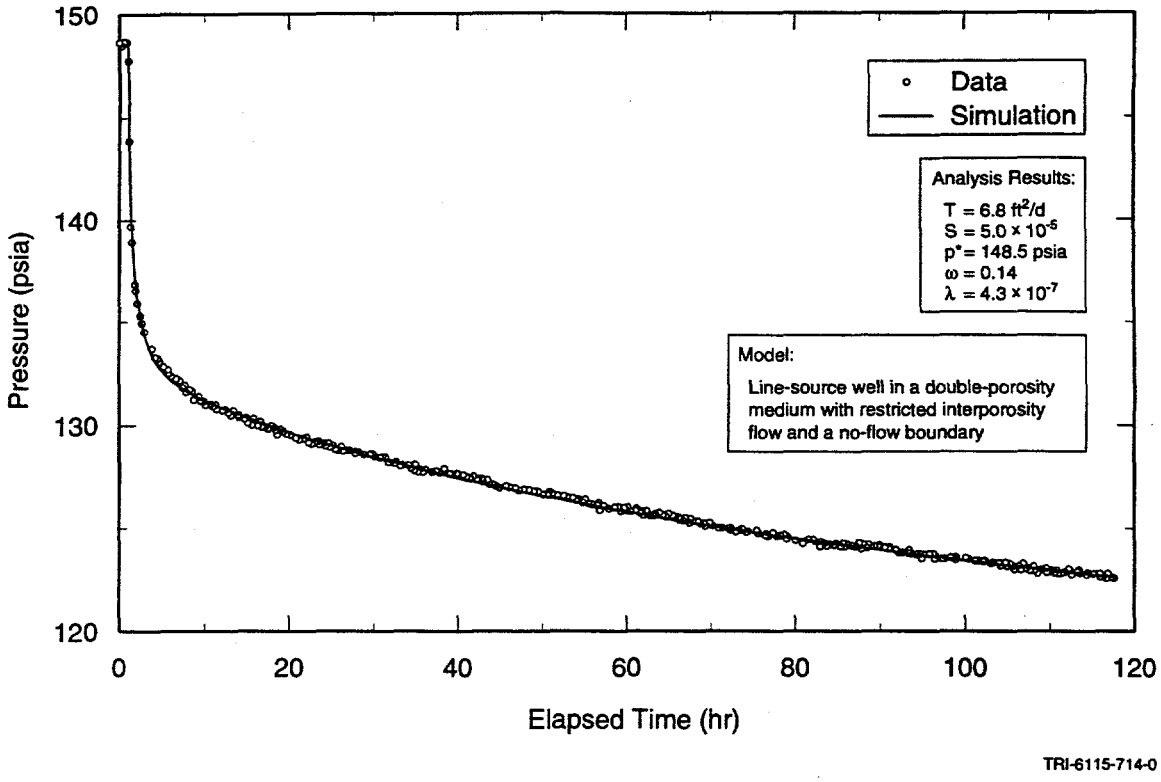

Figure 6-89. Linear-linear plot of H-19b4 drawdown data with Interpret/2 simulation.

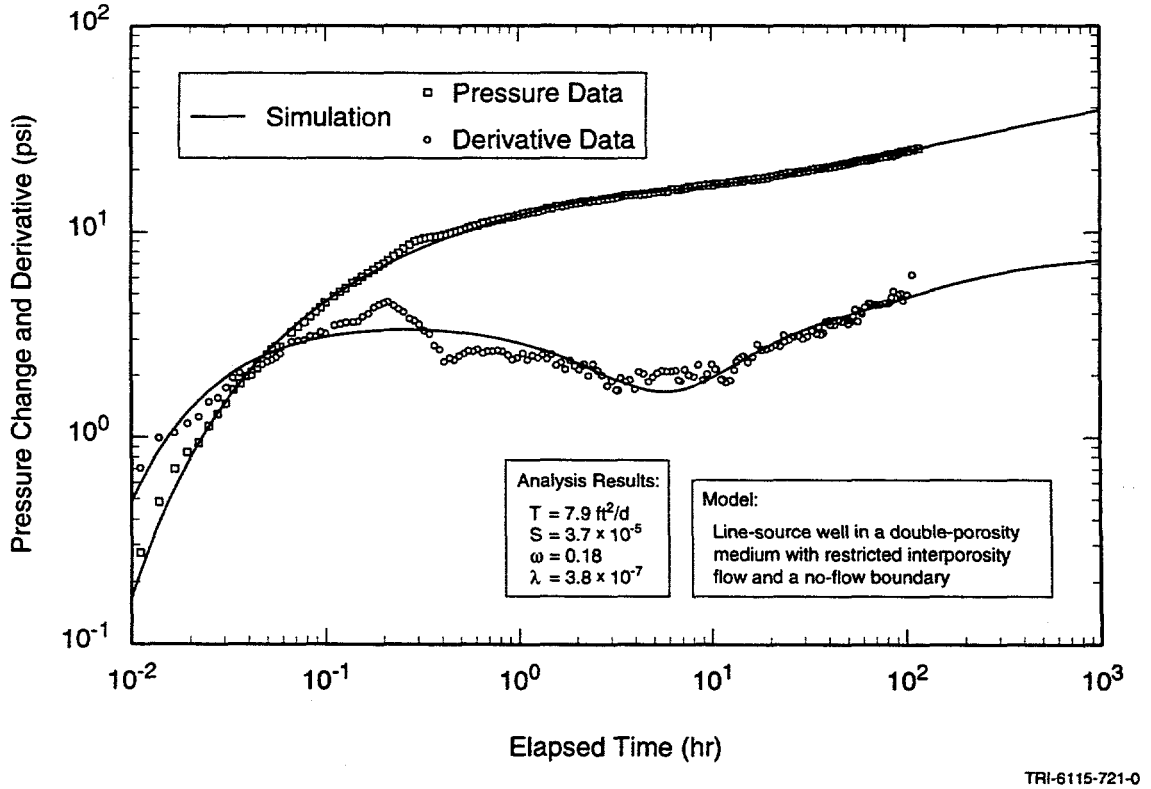

Figure 6-90. Log-log plot of H-19b6 drawdown data with Interpret/2 simulation.

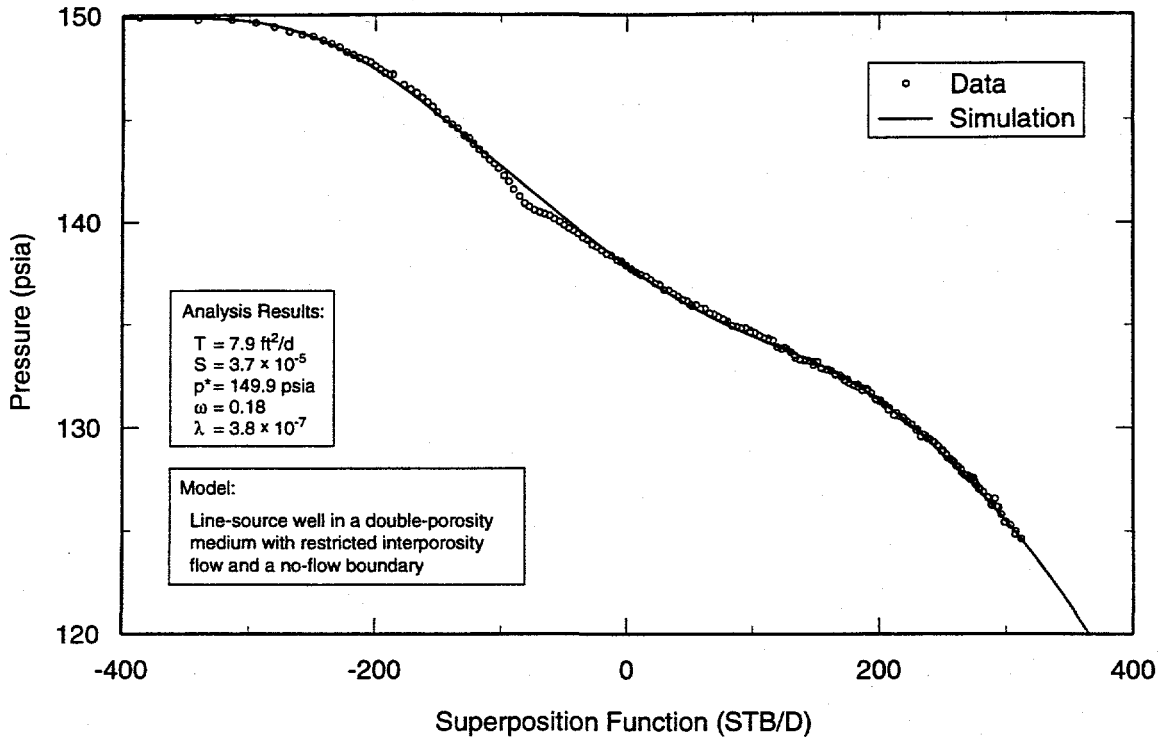

Figure 6-91. Horner plot of H-19b6 drawdown data with Interpret/2 simulation.

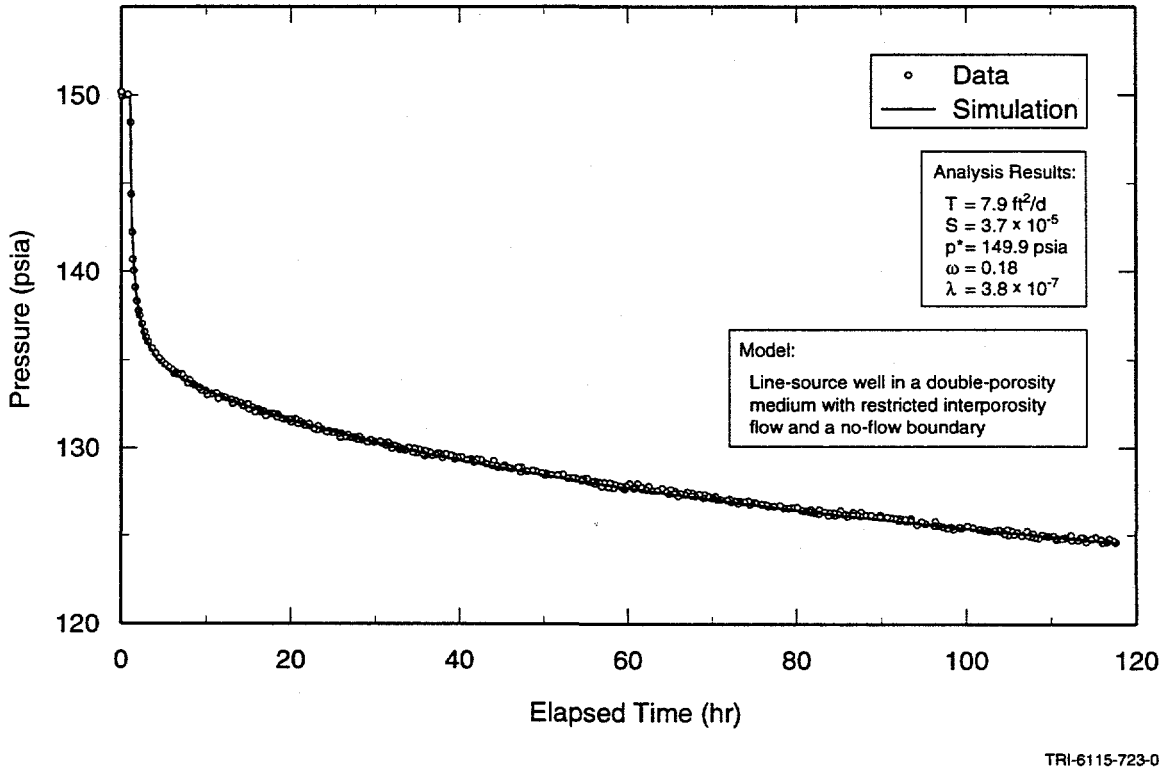

Figure 6-92. Linear-linear plot of H-19b6 drawdown data with Interpret/2 simulation.

and H-19b6, respectively. The simulated distances to the boundaries are 3,200 and 2,800 ft (975 and 855 m) from H-19b0 for H-19b4 and H-19b6, respectively. A no-flow boundary at a distance greater than 3,600 ft (1.1 km) could be added to the simulation of the H-19b2 response without affecting the match to the observed data. Other interpreted parameters are listed in Table 6-1.

6.7.3.3 H-19b3, H-19b5, AND H-19b7

The lower- and upper-zone responses in H-19b3, H-19b5, and H-19b7 were analyzed independently in an attempt to gain insight into how the hydraulic properties of the lower and upper Culebra might differ. Figures 6-93 through 6-95, 6-96 through 6-98, and 6-99 through 6-101 show log-log, Horner, and linear-linear plots of the drawdown data from the lower zones of H-19b3, H-19b5, and H-19b7, respectively, along with the best-fit Interpret/2 simulations. In all cases, the data were simulated using a model for a line-source well in an infinite double-porosity formation with restricted interporosity flow. The transmissivities interpreted from the lower-zone data from H-19b3, H-19b5, and H-19b7 are 6.4, 6.0, and 5.7 ft^2/d (6.8 x 10^{-6}, 6.5 x 10^{-6}, and 6.1 x 10^{-6} m^2/s), respectively. Interpreted storativities are 4.7 x 10^{-5}, 5.6 x 10^{-5}, and 6.9 x 10^{-5} for H-19b3, H-19b5, and H-19b7, respectively. Other interpreted parameters are listed in Table 6-1.

We initially attempted to match the entire data sets from the upper zones of H-19b3, H-19b5, and H-19b7 in the same way as the lower-zone data were matched, but found that any model that matched the early- to mid-time data well provided a poor match to the late-time data. Similarly, any model that matched the mid- to late-time data well provided a poor

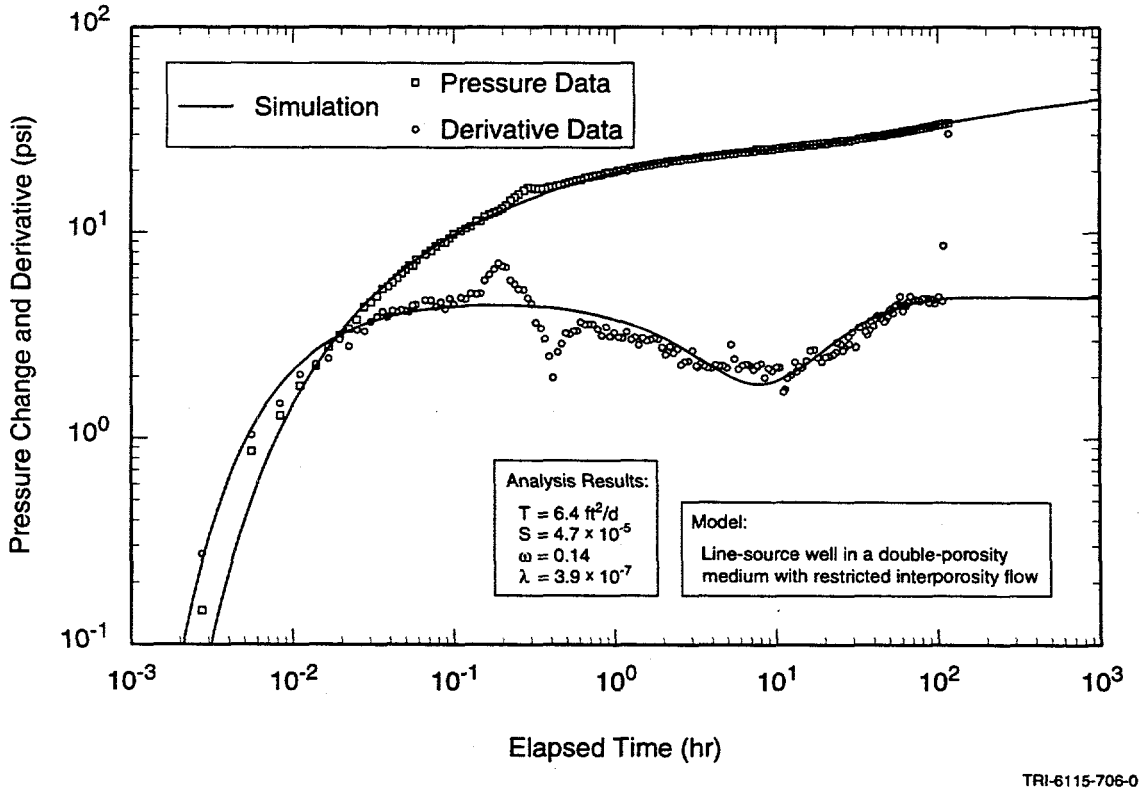

Figure 6-93. Log-log plot of H-19b3 lower-Culebra drawdown data with Interpret/2 simulation.

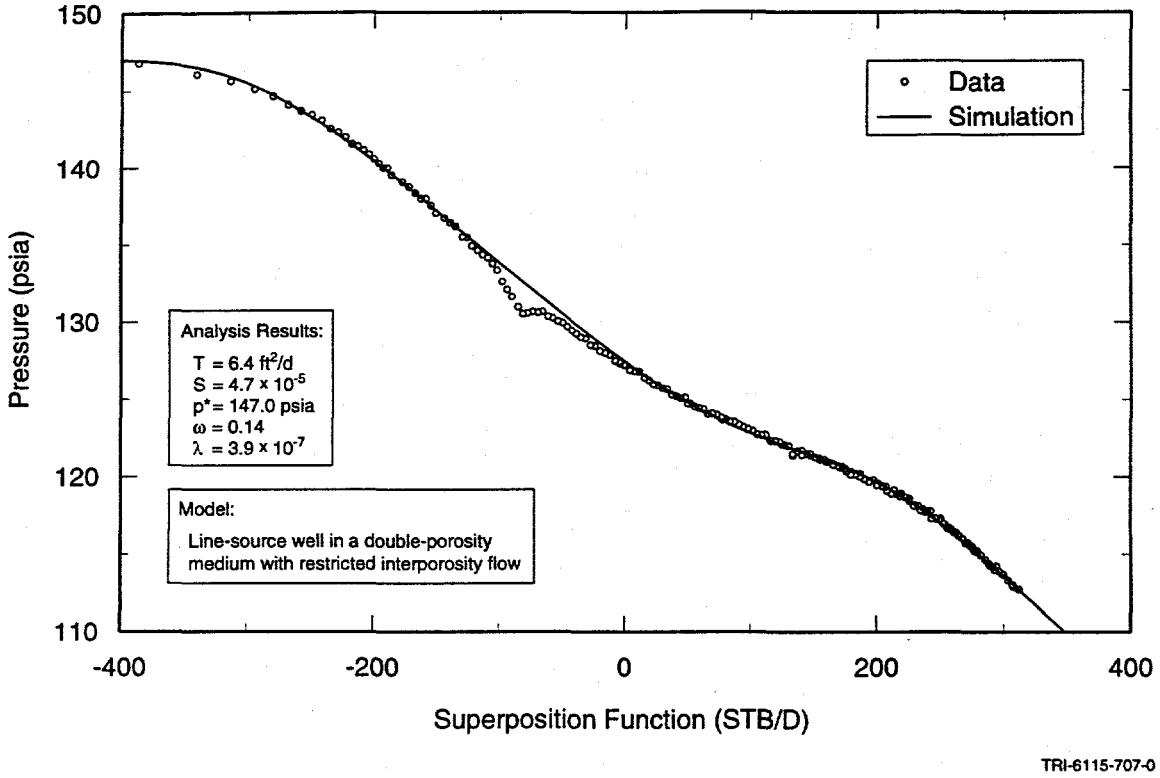

Figure 6-94. Horner plot of H-19b3 lower-Culebra drawdown data with Interpret/2 simulation.

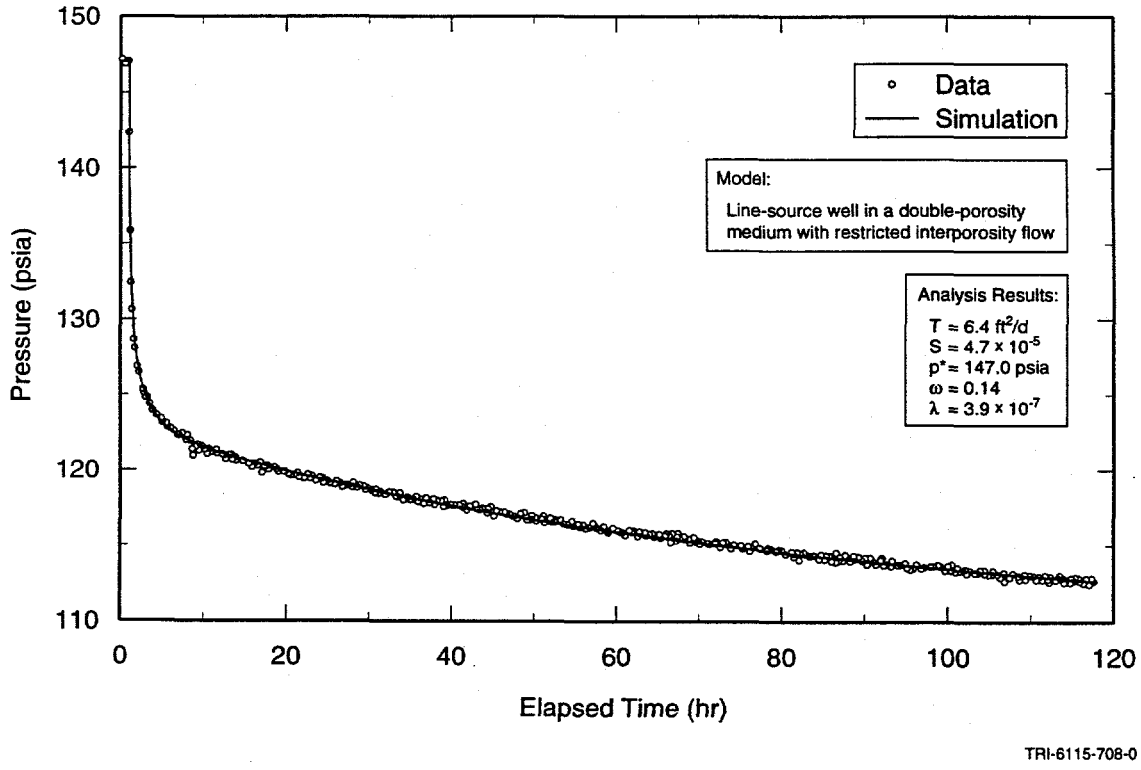

Figure 6-95. Linear-linear plot of H-19b3 lower-Culebra drawdown data with Interpret/2 simulation.

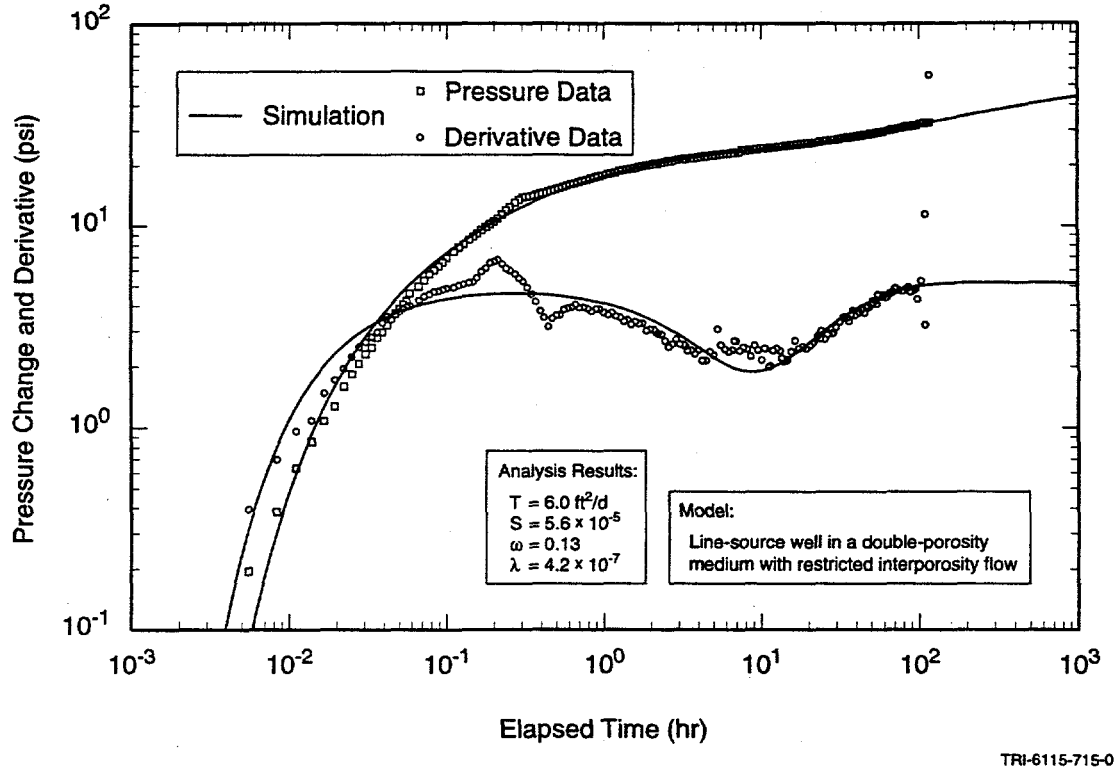

Figure 6-96. Log-log plot of H-19b5 lower-Culebra drawdown data with Interpret/2 simulation.

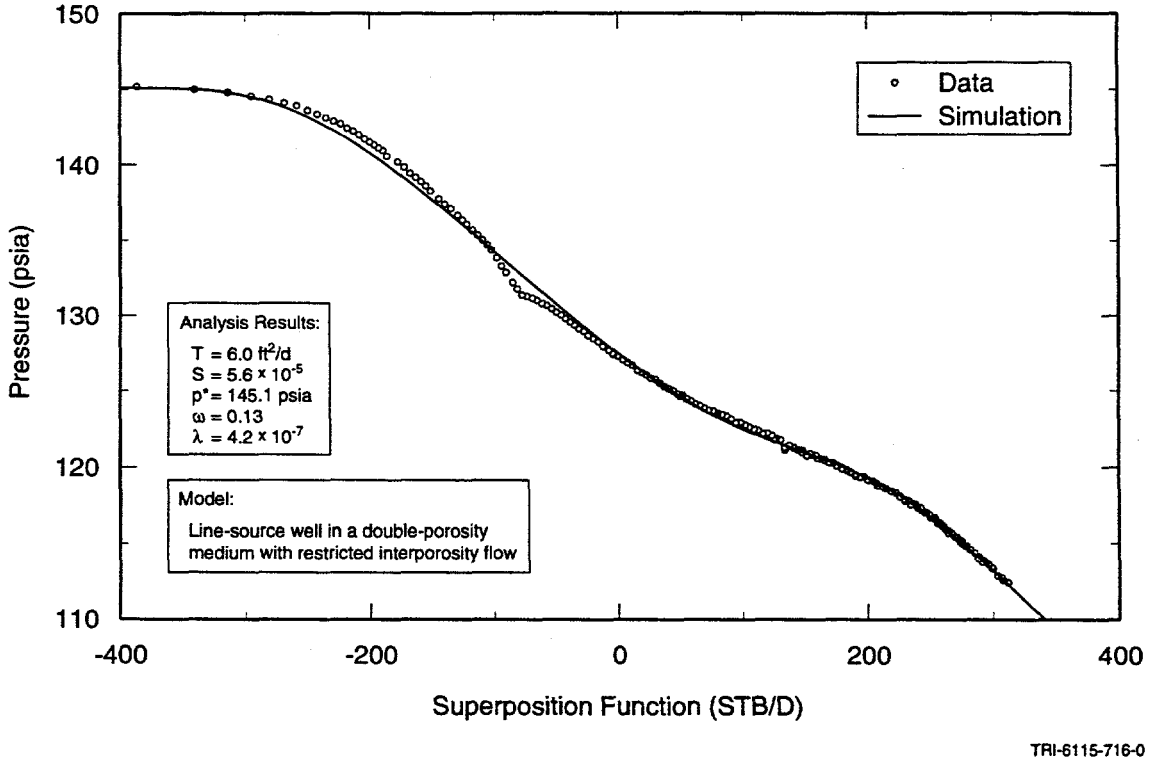

Figure 6-97. Horner plot of H-19b5 lower-Culebra drawdown data with Interpret/2 simulation.

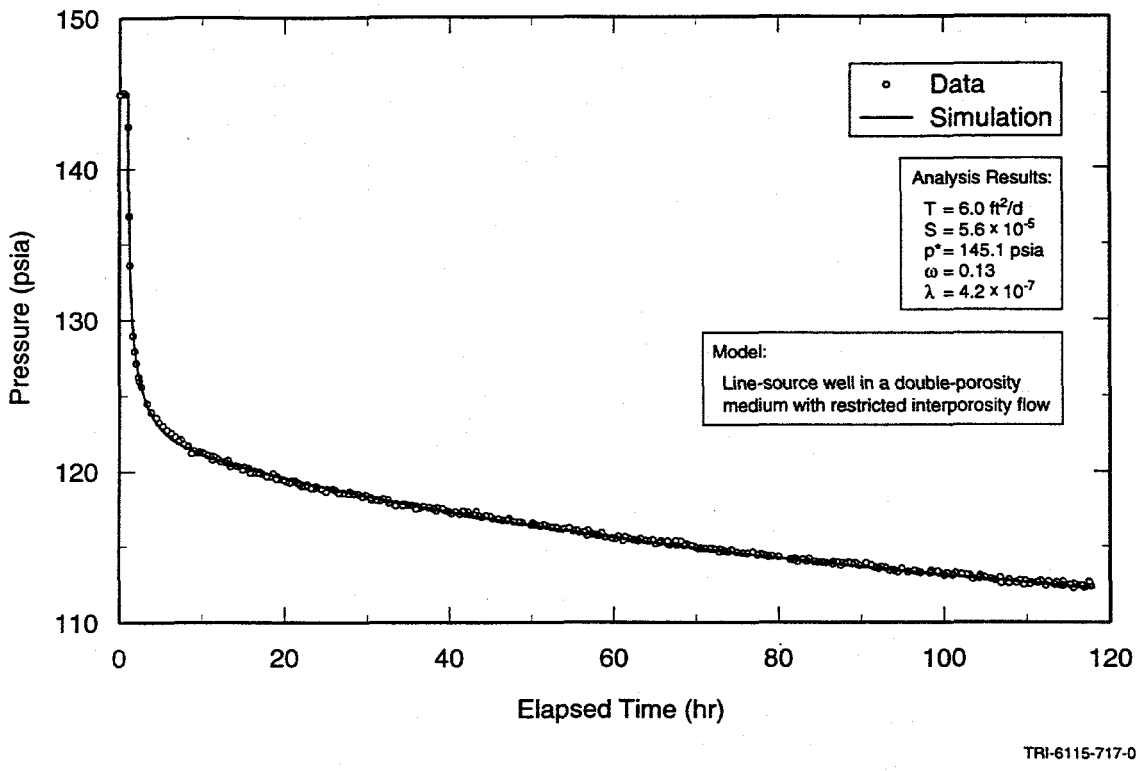

Figure 6-98. Linear-linear plot of H-19b5 lower-Culebra drawdown data with Interpret/2 simulation.

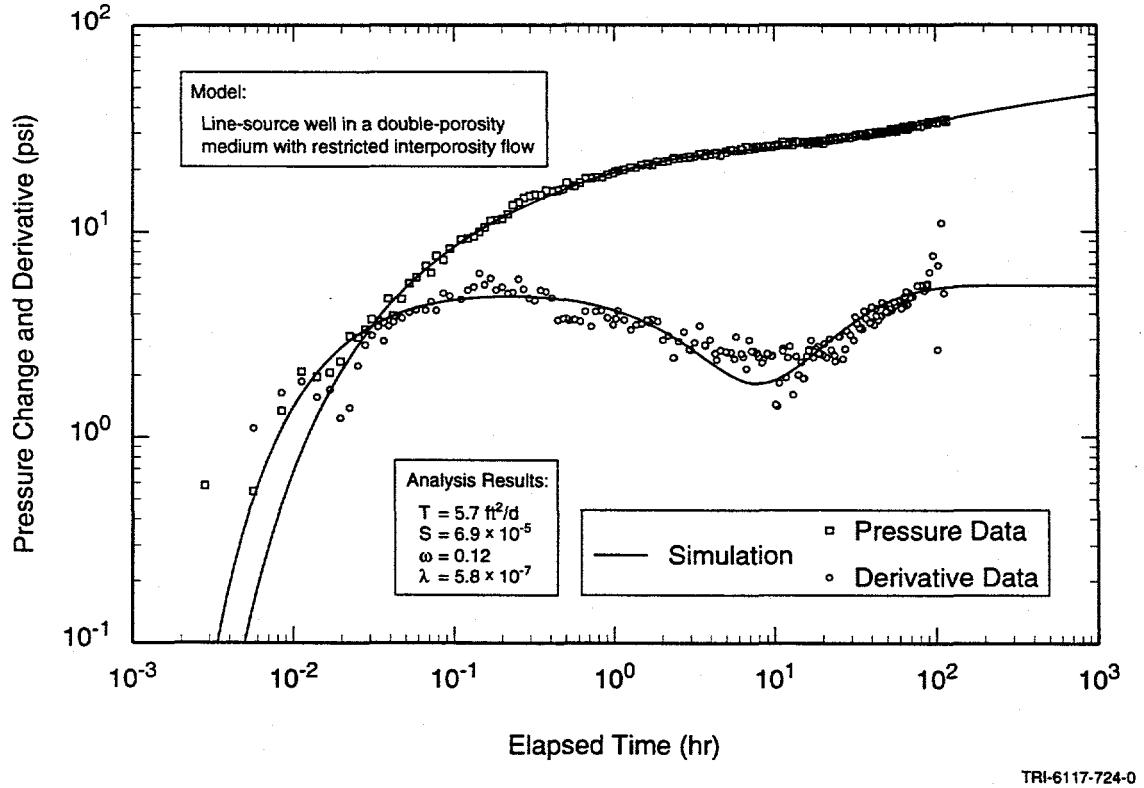

Figure 6-99. Log-log plot of H-19b7 lower-Culebra drawdown data with Interpret/2 simulation.

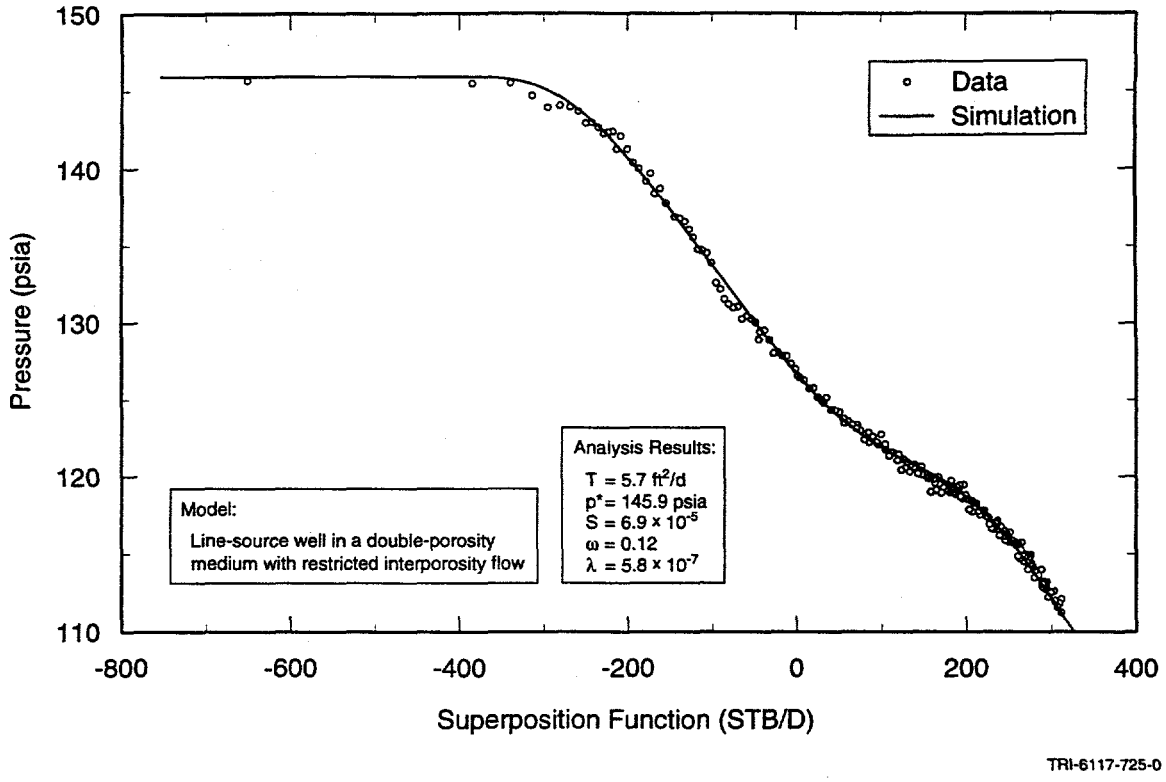

Figure 6-100. Horner plot of H-19b7 lower-Culebra drawdown data with Interpret/2 simulation.

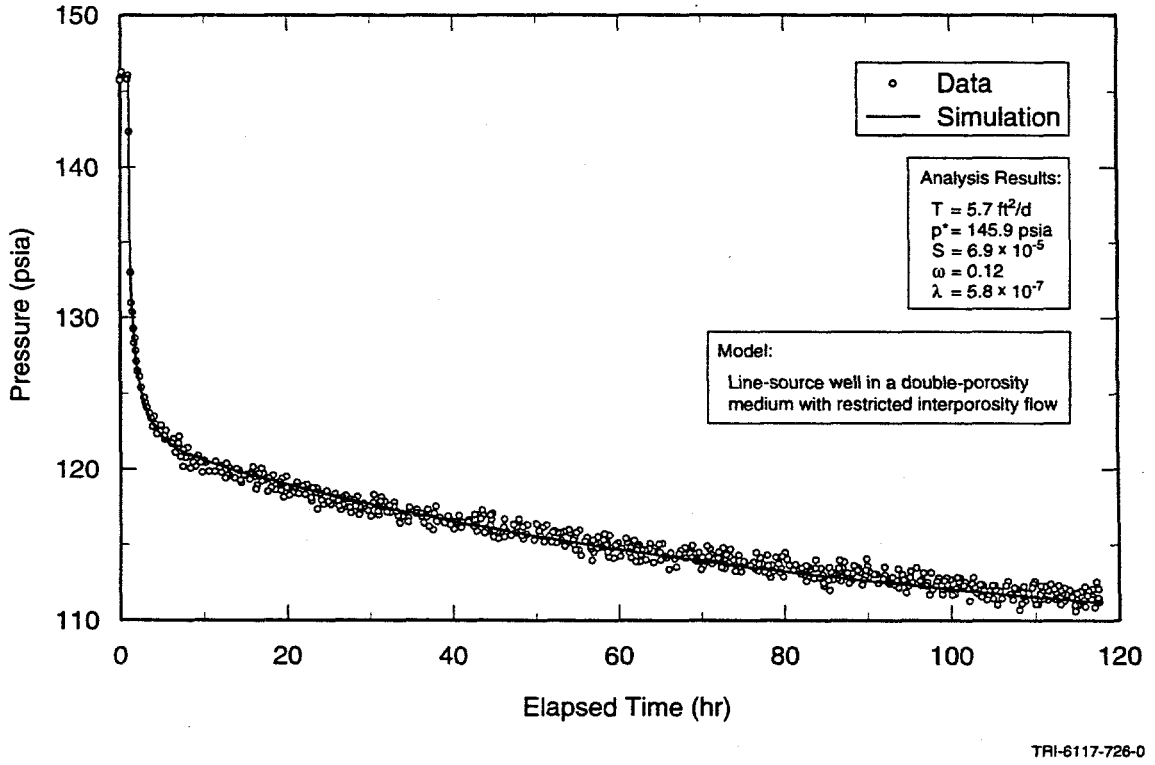

Figure 6-101. Linear-linear plot of H-19b7 lower-Culebra drawdown data with Interpret/2 simulation.

match to the early-time data. We surmise that the early- and late-time data reflect different behaviors for the following reasons. For the first five to eleven minutes of the test, the middle packer was inflated in H-19b0 and all water pumped came from the lower Culebra. The pressure responses in the upper Culebra in H-19b3, H-19b5, and H-19b7 during this period would, therefore, have been caused more by vertical flow than horizontal flow and would have lagged behind the responses in the lower Culebra. After the packer in H-19b0 was deflated, a portion of the water pumped came from the upper Culebra by horizontal flow, and pressure equilibrium between the upper and lower Culebra was reached. Consequently, the early-time data are not interpretable in terms of radial flow towards H-19b0 whereas the late-time data are. Estimates of storativity, however, could be in error because of the lack of early-time fitting.

Figures 6-102 through 6-104, 6-105 through 6-107, and 6-108 through 6-110 show log-log, Horner, and linear-linear plots of the drawdown data from the upper zones of H-19b3, H-19b5, and H-19b7, respectively, along with the best-fit Interpret/2 simulations of the mid- to late-time data. In all cases, the data were simulated using a model for a line-source well in an infinite double-porosity formation with restricted interporosity flow. The transmissivities interpreted from the upper-zone data from H-19b3, H-19b5, and H-19b7 are 6.4, 6.0, and 5.6 ft^2/d (6.9 x 10^{-6}, 6.5 x 10^{-6}, and 6.0 x 10^{-6} m^2/s), respectively, virtually identical (as expected) to the values interpreted from the lower-zone responses (Table 6-1). Interpreted storativities are 5.4 x 10^{-5}, 8.0 x 10^{-5}, and 6.6 x 10^{-5} for H-19b3, H-19b5, and H-19b7, respectively. Other interpreted parameters are listed in Table 6-1.

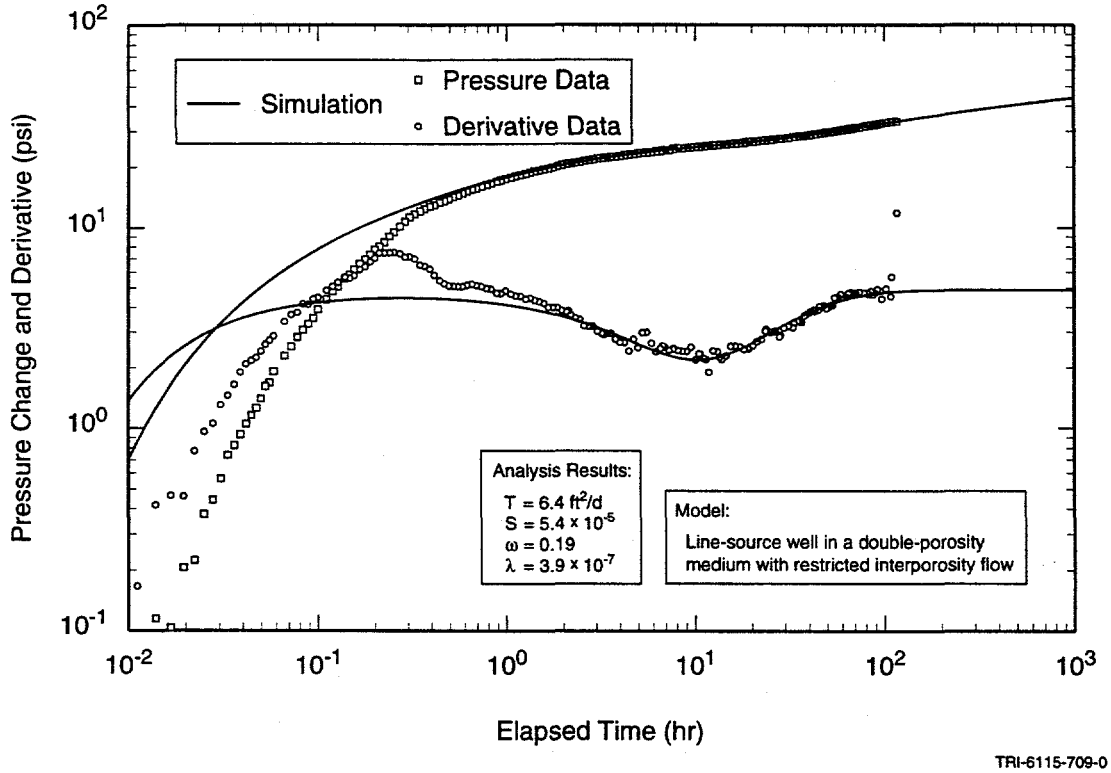

Figure 6-102. Log-log plot of H-19b3 upper-Culebra drawdown data with Interpret/2 simulation.

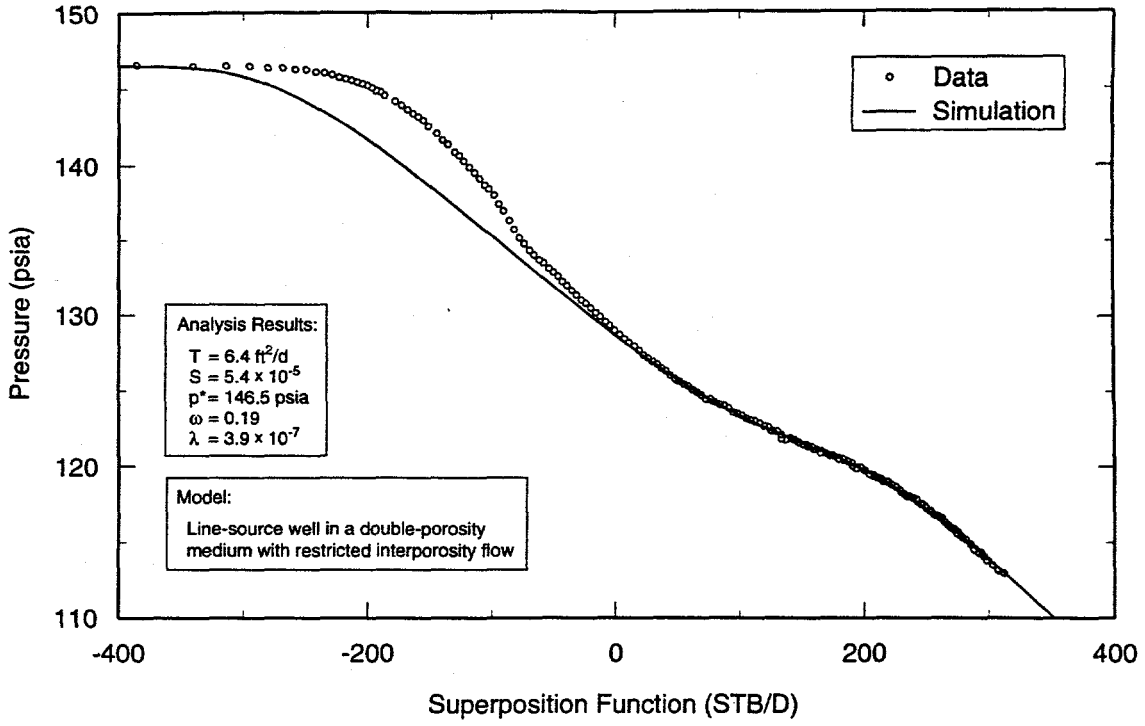

Figure 6-103. Horner plot of H-19b3 upper-Culebra drawdown data with Interpret/2 simulation.

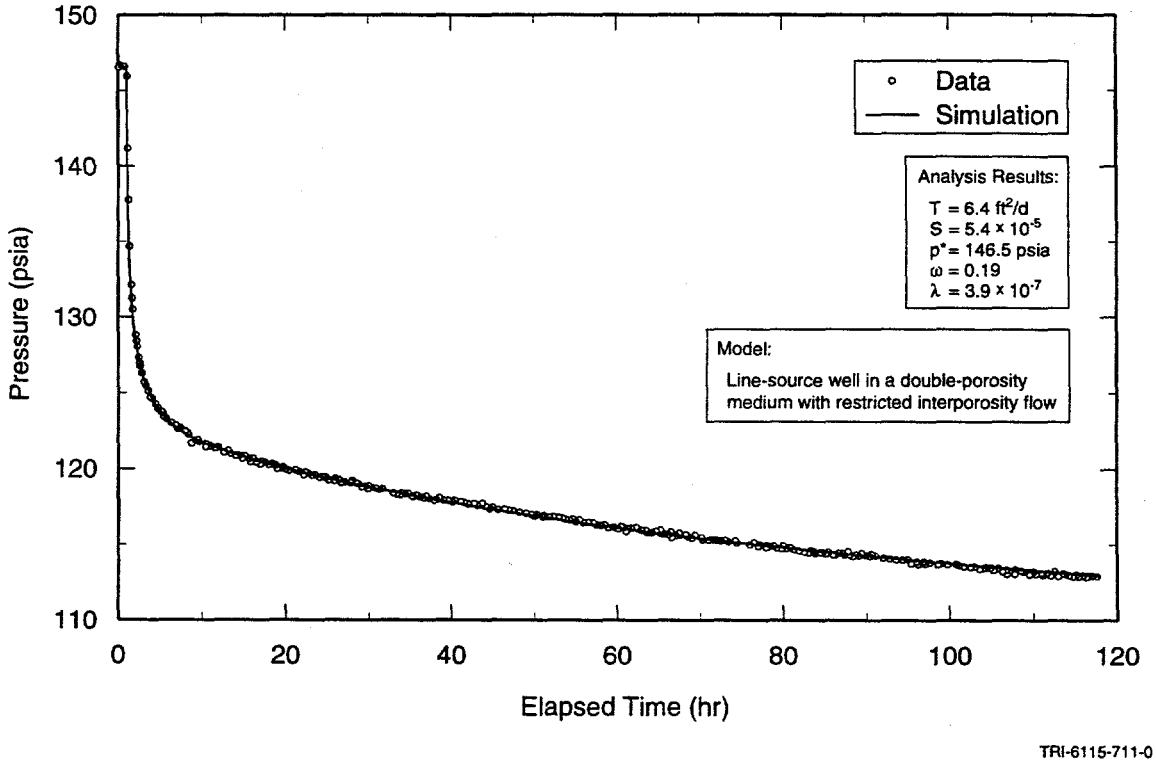

Figure 6-104. Linear-linear plot of H-19b3 upper-Culebra drawdown data with Interpret/2 simulation.

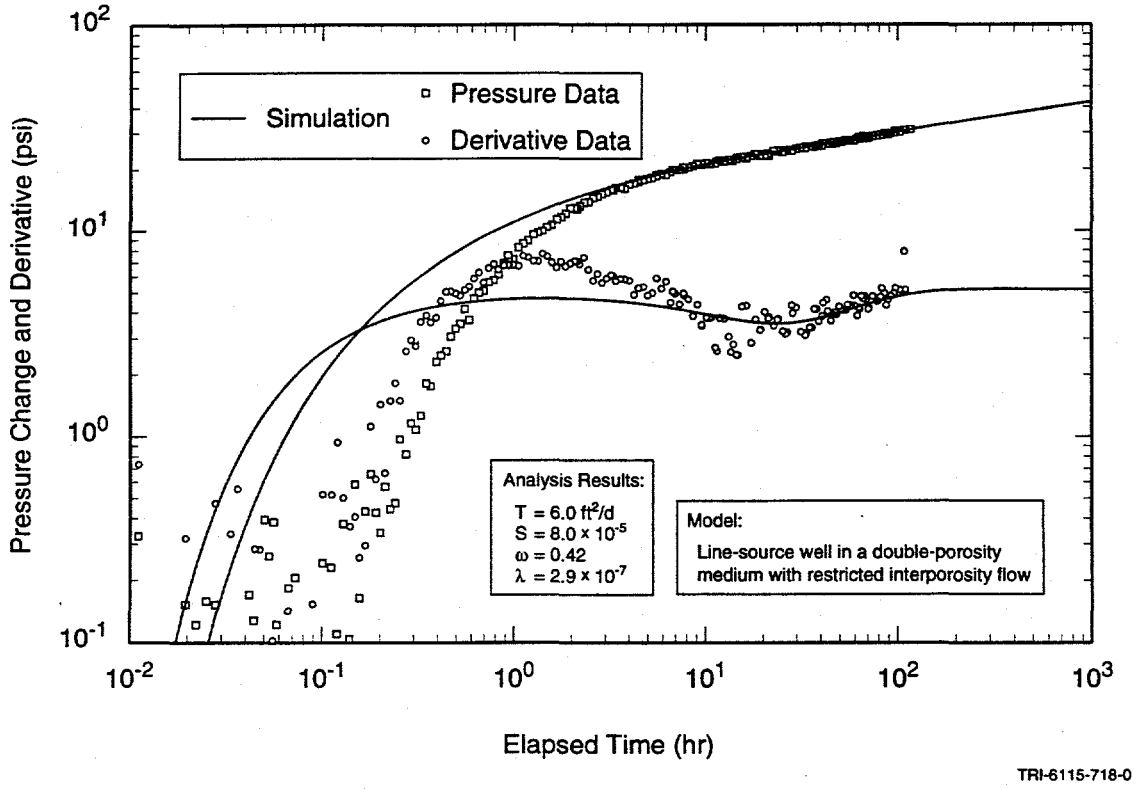

Figure 6-105. Log-log plot of H-19b5 upper-Culebra drawdown data with Interpret/2 simulation.

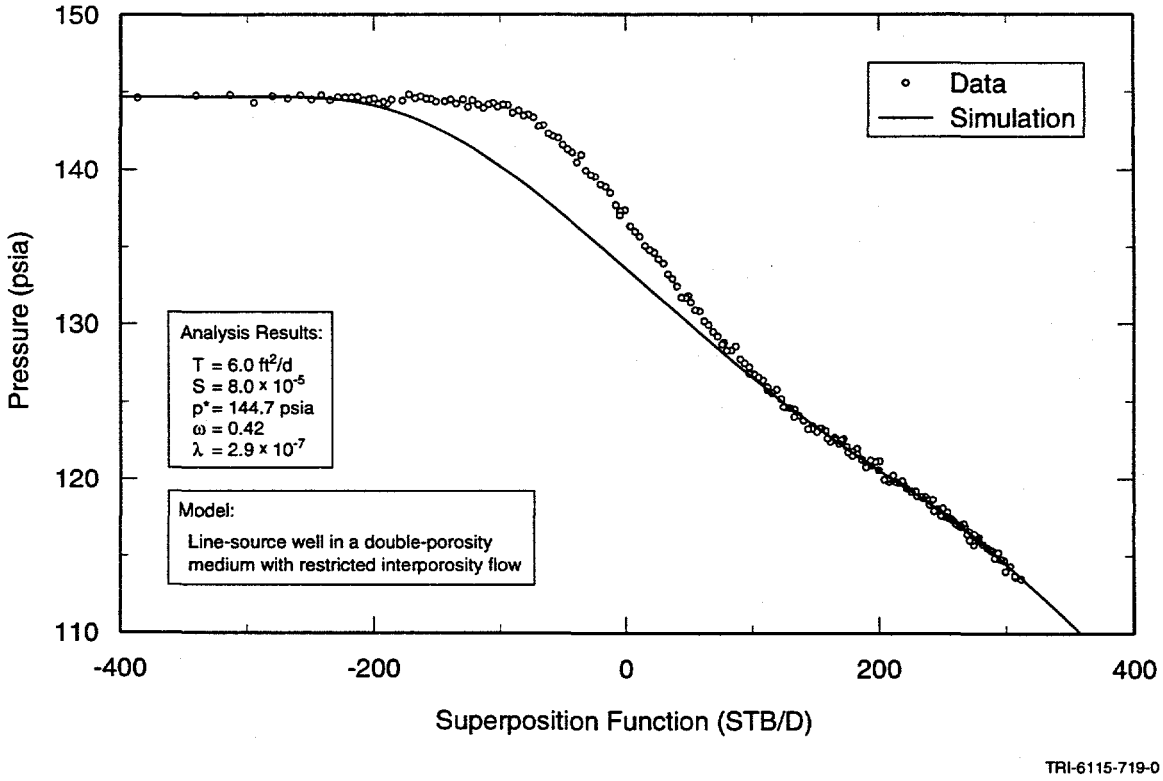

Figure 6-106. Horner plot of H-19b5 upper-Culebra drawdown data with Interpret/2 simulation.

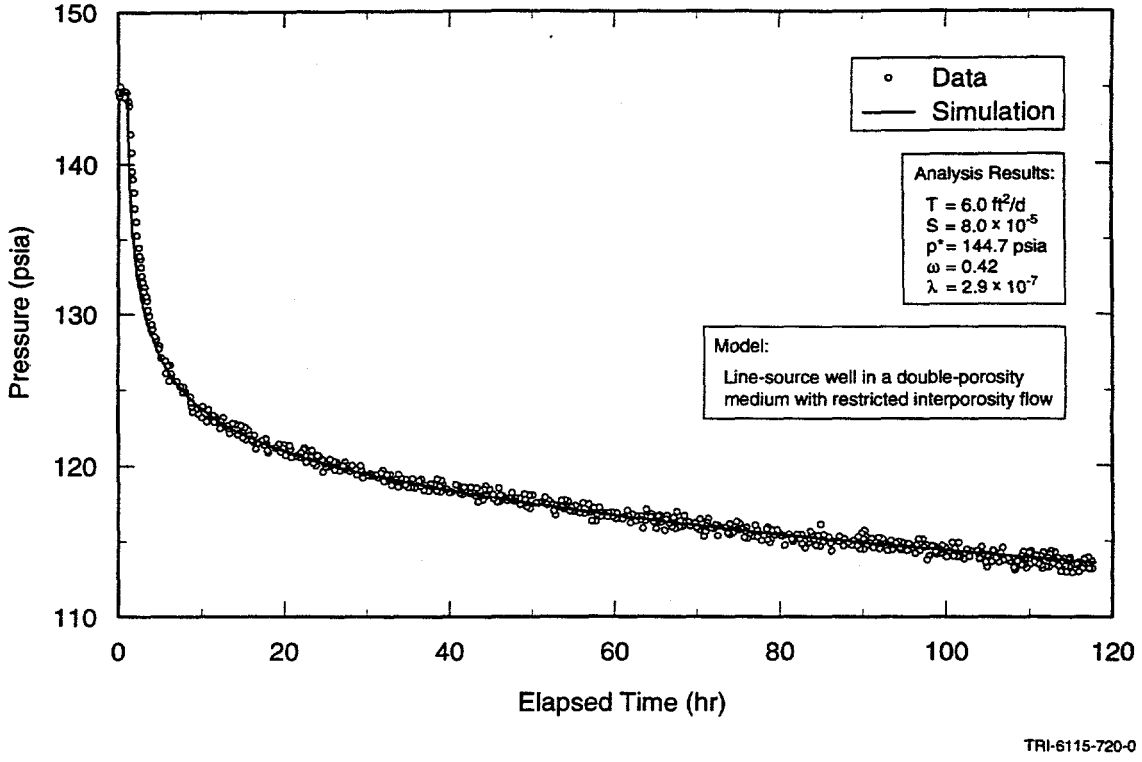

Figure 6-107. Linear-linear plot of H-19b5 upper-Culebra drawdown data with Interpret/2 simulation.

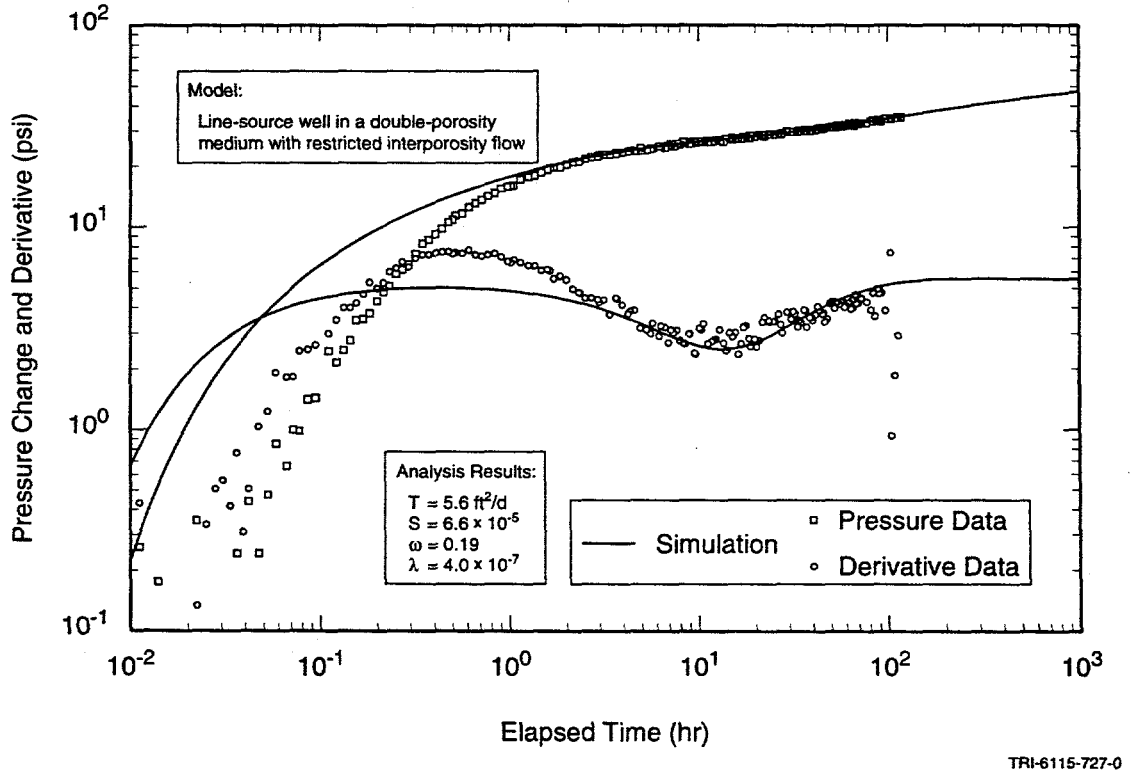

Figure 6-108. Log-log plot of H-19b7 upper-Culebra drawdown data with Interpret/2 simulation.

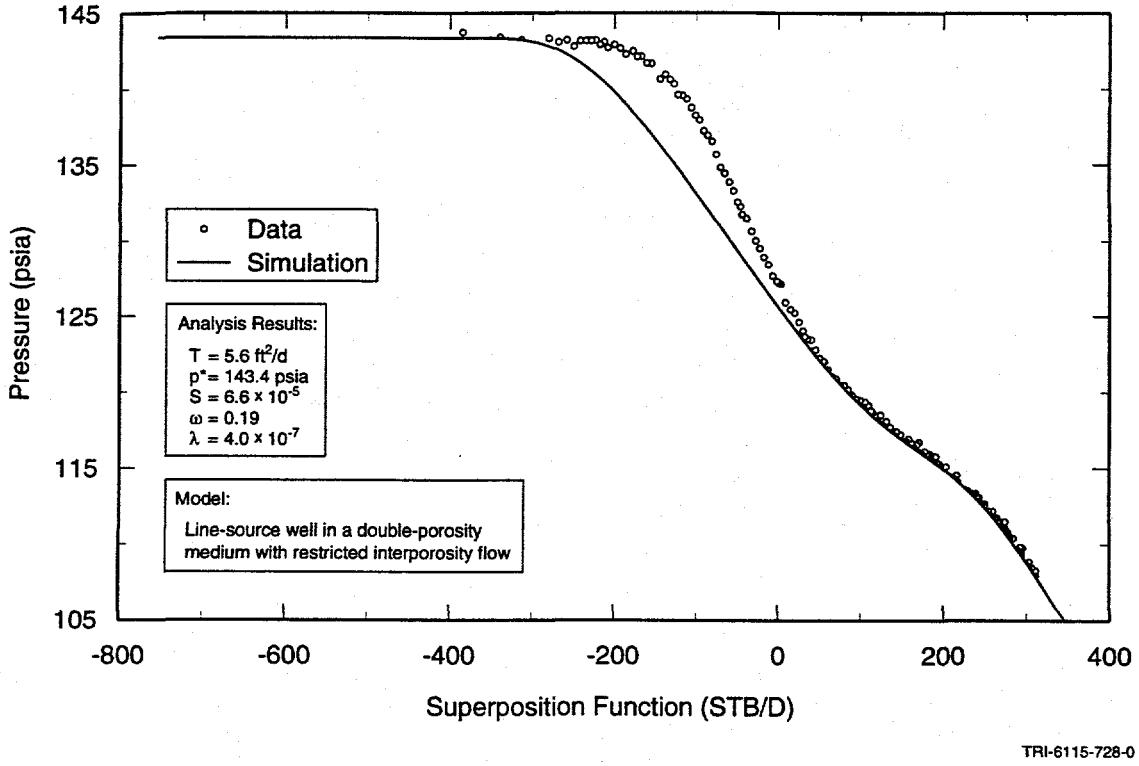

Figure 6-109. Horner plot of H-19b7 upper-Culebra drawdown data with Interpret/2 simulation.

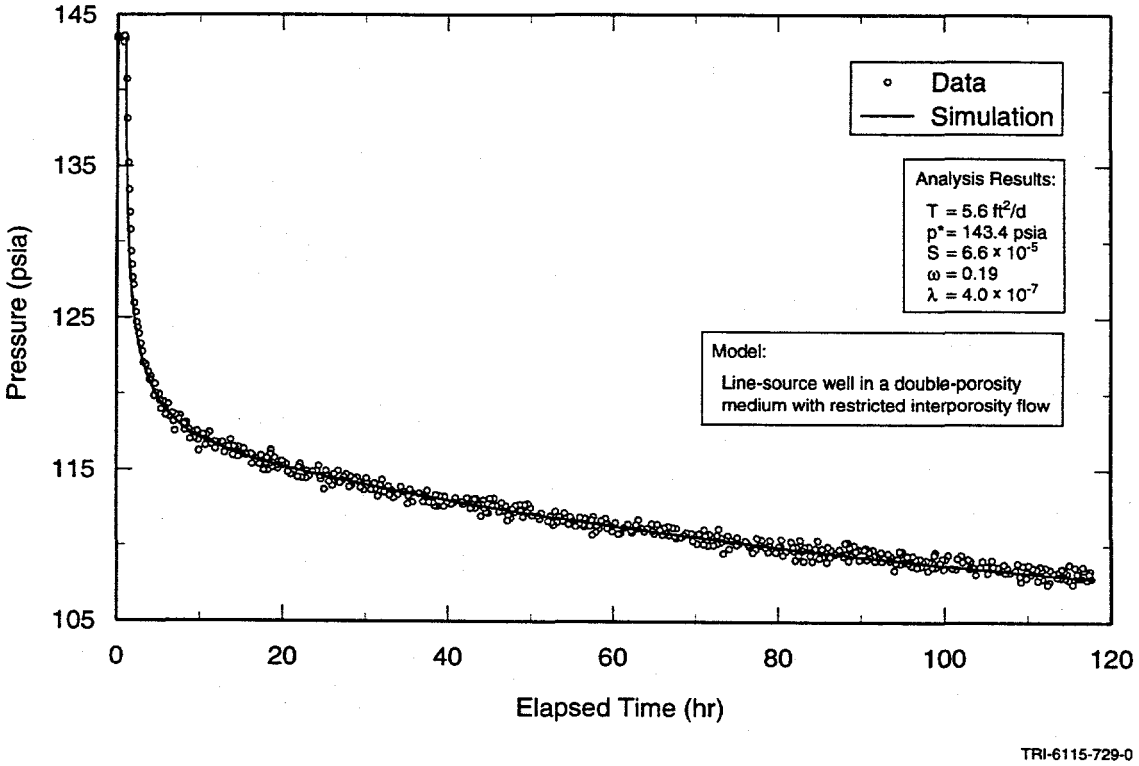

Figure 6-110. Linear-linear plot of H-19b7 upper-Culebra drawdown data with Interpret/2 simulation.

Two of the interpreted parameters from the upper-zone response in H-19b5 are notable: the storativity of 8.0 x 10^{-5} and the storativity ratio of 0.42. The storativity is high compared to the lower-zone value of 5.6 x 10^{-5}, and the storativity ratio is much higher than any other value interpreted from any of the H-19 well responses, which ranged only from 0.12 to 0.19. These values are probably high because of leakage past the upper packer in H-19b5, as discussed in Section 5.7.3. Leakage would have led to less drawdown being observed than would otherwise have occurred.

6.7.3.4 H-19 ANISOTROPY ANALYSIS

The values of transmissivity and storativity interpreted from the responses of H-19b2, H-19b4, H-19b6, and the lower zones of H-19b3, H-19b5, and H-19b7 were used to evaluate anisotropy at the H-19 hydropad. Most of the variation in the data comes from the three wells having the most similar azimuths: H-19b2, H-19b6, and H-19b7. Figure 6-111 shows the storativity data and the best-fit ellipse. The interpreted anisotropy is insignificant. The ratio of maximum to minimum transmissivity is only 1.2 (Table 6-2). The major axis of transmissivity has a magnitude of 6.9 ft^2/d (7.4 x 10^{-6} m^2/s) and is oriented N8°W, while the minor axis has a magnitude of 5.9 ft^2/d (6.3 x 10^{-6} m^2/s) and is oriented N82°E. The effective transmissivity is 6.4 ft^2/d (6.8 x 10^{-6} m^2/s) and the storativity is 4.9 x 10^{-5}.

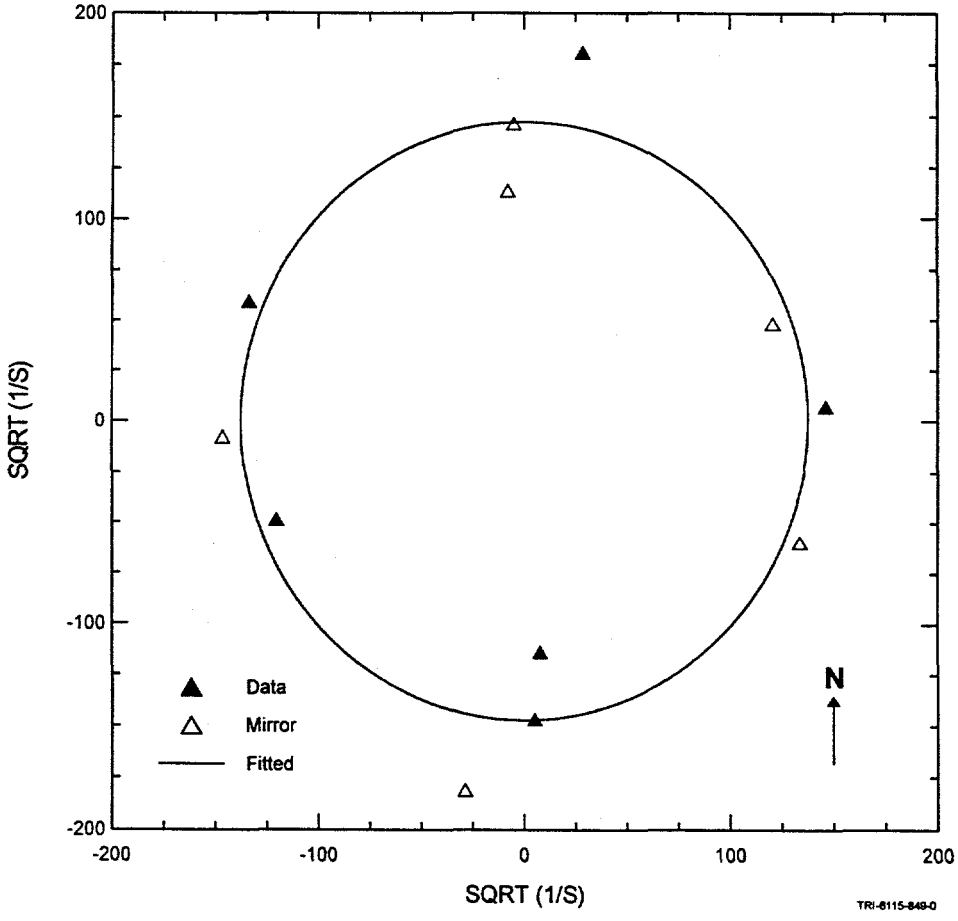

Figure 6-111. H-19 anisotropy ellipse.

6.7.3.5 SUMMARY OF RESULTS FROM THE H-19 TRACER/PUMPING TEST

The responses to pumping observed in the H-19 wells showed consistently clear evidence of double-porosity behavior. All data sets show a pronounced minimum in the pressure derivative and most showed indications of stabilization. The extreme late-time data from H-19b4 and H-19b6, the two wells farthest north and west, appeared to show evidence of no-flow (reduced transmissivity) boundaries. Additional evidence for boundaries (or heterogeneity) might have been apparent had the interval from the start of pumping to the start of tracer injection been longer. Anisotropy at the H-19 hydropad appears to be insignificant. The effective transmissivity is 6.4 ft^2/d (6.8 x 10^{-6} m^2/s) and the storativity is 4.9 x 10^{-5}.

6.8 P-14 Air-Lift Pumping Test

As discussed in Section 5.8, the pumping test at P-14 involved air-lift pumping at P-14 with D-268, H-6b, and WIPP-25 serving as observation wells. The flow rate decreased from approximately 79 to 48 gpm (5.0 to 3.0 L/s) during the test, with numerous fluctuations (Figure 5-21). For analysis purposes, the pumping history was represented by a sequence of nine pumping events with different constant rates. The periods and rates used for these events are shown graphically superimposed on the discrete flow-rate measurements in Figure 5-21. This simplified pumping history was used in the analysis of the recovery data from P-14 and the three observation wells.

6.8.1 P-14

The flow-rate fluctuations that occurred during the P-14 pumping period (Figure 5-21) rendered the drawdown data uninterpretable using Interpret/2. Figures 6-112, 6-113, and 6-114 show log-log, Horner, and linear-linear plots, respectively, of the recovery data from

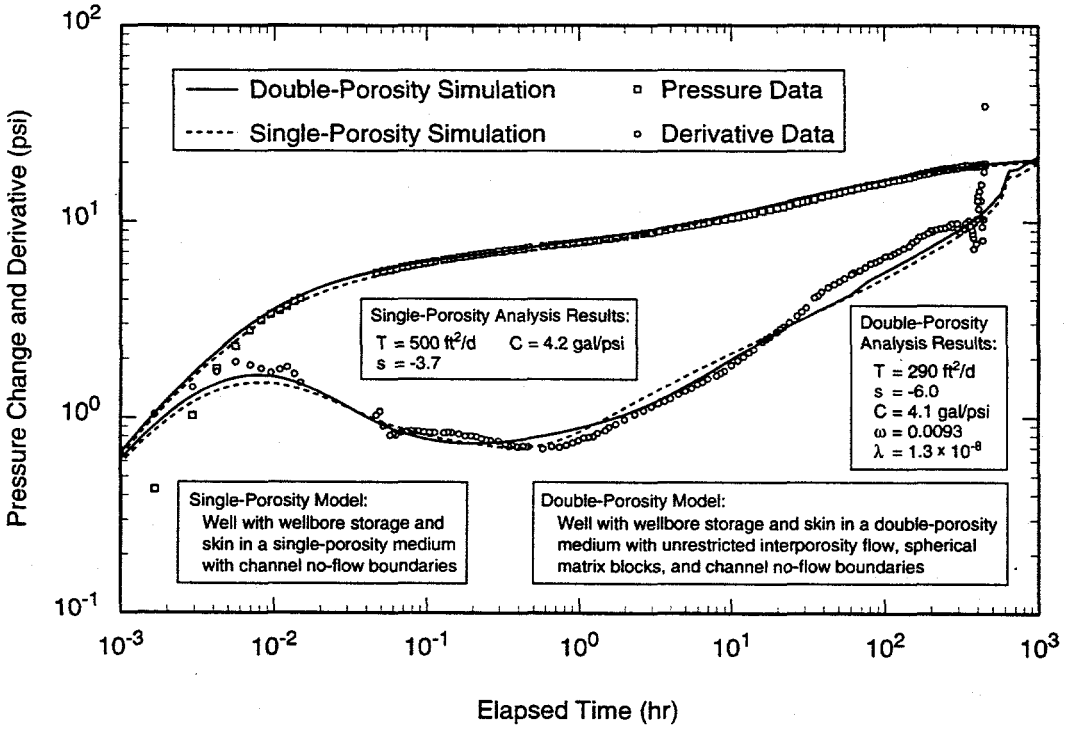

Figure 6-112. Log-log plot of P-14 recovery data with Interpret/2 simulations.

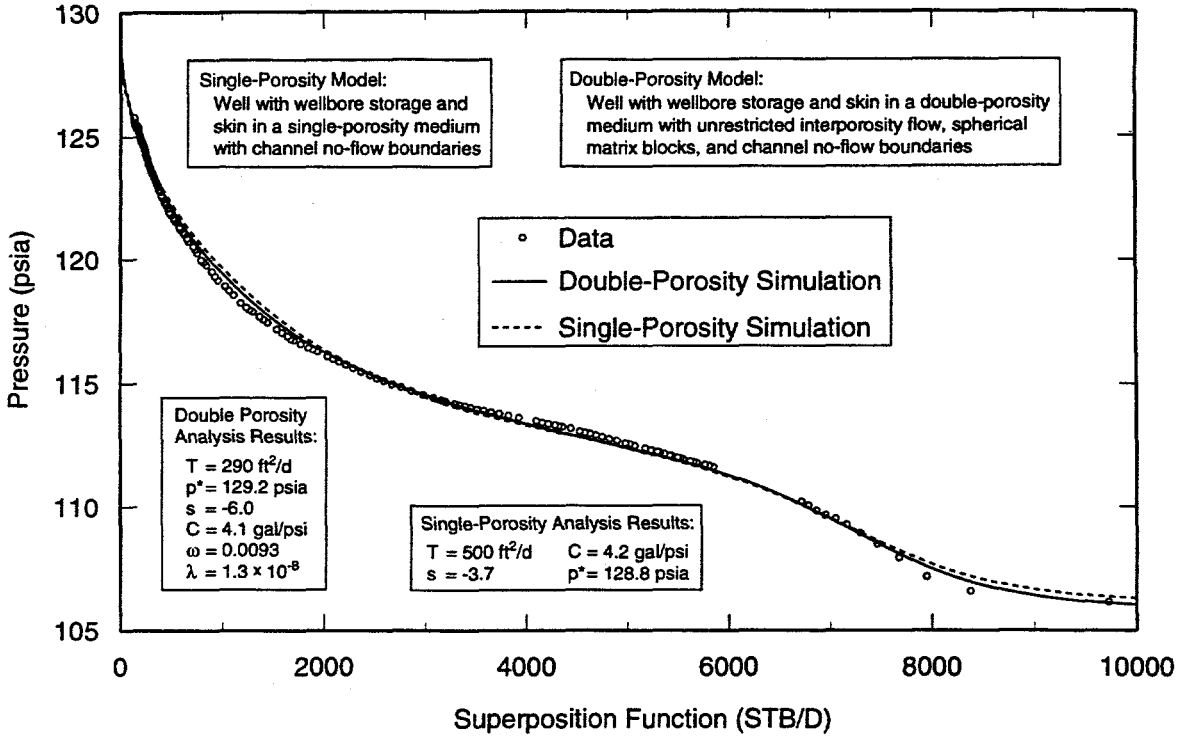

Figure 6-113. Horner plot of P-14 recovery data with Interpret/2 simulations.

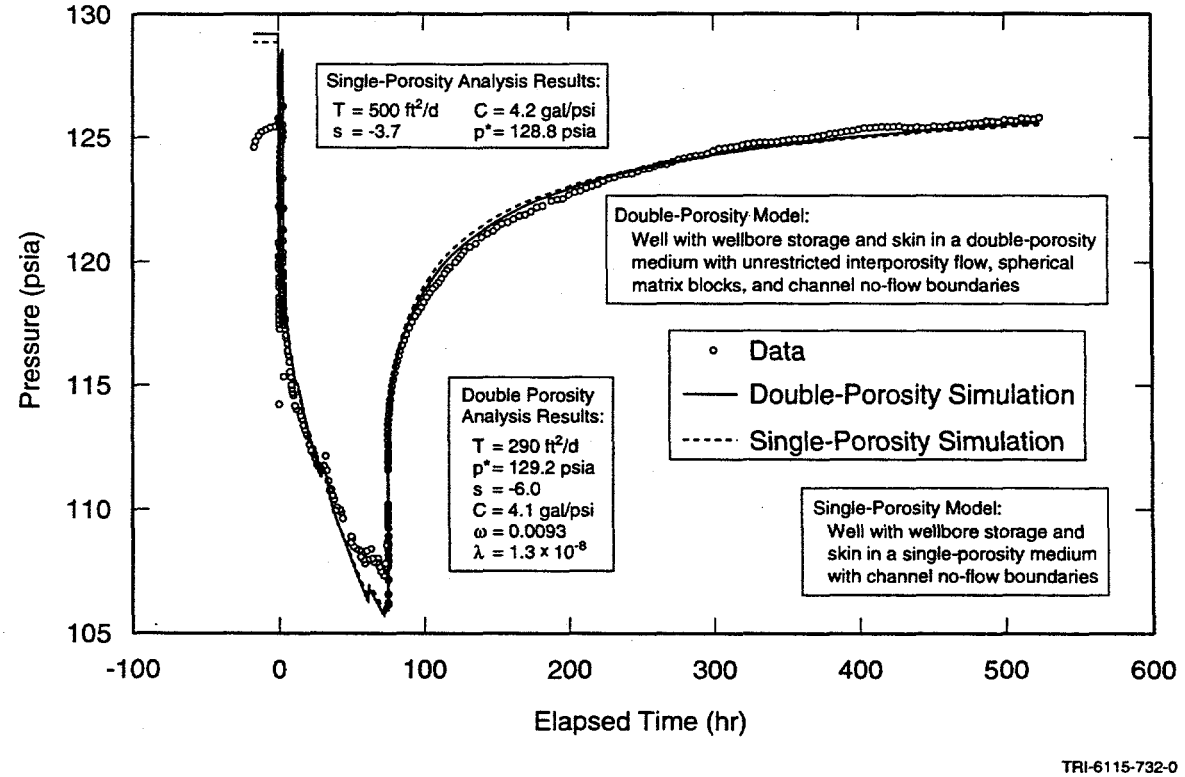

Figure 6-114. Linear-linear plot of P-14 data with Interpret/2 simulations derived from recovery analyses.

P-14 along with Interpret/2 simulations. Equally good fits to the data were obtained using single-porosity and double-porosity models with channel (parallel) no-flow boundaries. The single-porosity fits were obtained assuming that the derivative data between 0.1 and 1 hr on Figure 6-112 represent stabilization of the system before boundary effects became apparent. The double-porosity fits were obtained assuming that the same derivative data represent the minimum resulting from a medium with unrestricted interporosity flow and spherical matrix blocks. In both cases, the inclusion of channel boundaries was necessary to match the sustained late-time rise in the pressure derivative on the log-log plot (Figure 6-112). In reality, the rise in the pressure derivative is probably caused by the decrease in transmissivity known to occur to the east (e.g., H-2) and south (e.g., D-268) of P-14 instead of by actual parallel boundaries. The single-porosity simulations were generated using a wellbore skin of -3.7, a transmissivity of 500 ft^2/d (5.4×10^{-4} m^2/s), and distances to the boundaries of 1,560 and 1,600 ft (475 and 490 m) (Table 6-1). The double-porosity simulations were generated using a wellbore skin of -6.0, a transmissivity of 290 ft^2/d (3.1×10^{-4} m^2/s), distances to the boundaries of 1,760 and 2,130 ft (535 and 650 m), and other parameters as listed in Table 6-1. The highly negative skin indicated by both sets of simulations probably reflects the effects of the acid treatment that preceded the pumping test.

Ordinarily, the simplest model that can fit data is preferable, which in this case would be the single-porosity model. The double-porosity simulation results are also presented for two reasons. First, high Culebra transmissivities are typically associated with fracturing, which suggests that a double-porosity model is appropriate. Second, the equivalence of the single- and double-porosity fits shows that the data are inadequate to distinguish between the two models, so we wish to show what effect this uncertainty has on the interpreted hydraulic parameters. The transmissivities interpreted from the two models differ by less than a factor of two (500 vs. 290 ft^2/d; 3.1 to 5.4×10^{-4} m^2/s), and both fall within the uncertainty range for transmissivity at P-14 used in the WIPP Compliance Certification Application (1.9 to 7.8×10^{-4} m^2/s; US DOE, 1996).

6.8.2 Observation Wells

Figures 6-115 through 6-117, 6-118 through 6-120, and 6-121 through 6-123 show log-log, Horner, and linear-linear plots of the recovery data from D-268, H-6b, and WIPP-25, respectively, along with the best-fit Interpret/2 simulations. In all cases, the simulations used a model for a line-source well in an infinite single-porosity medium. Interpreted transmissivities are 160 ft^2/d (1.7×10^{-4} m^2/s), 130 ft^2/d (1.4×10^{-4} m^2/s), and 240 ft^2/d (2.5×10^{-4} m^2/s), and storativities are 2.5×10^{-5}, 1.1×10^{-5}, and 1.5×10^{-5} for D-268, H-6b, and WIPP-25, respectively (Table 6-1). Equivalent matches were obtained using double-porosity models with similar values of transmissivity and storativity, showing that double-porosity conditions could be present without providing distinctive hydraulic responses.

Despite the necessity for channel no-flow boundaries in the interpretation of the P-14 recovery data, no boundaries were used in the analyses of the observation-well responses. Because of the distances of the observation wells from P-14 and the short duration of the pumping period, the responses observed at those wells were not sufficiently advanced to distinguish clearly between infinite-acting and bounded behavior. The fact that the simulations of the entire testing

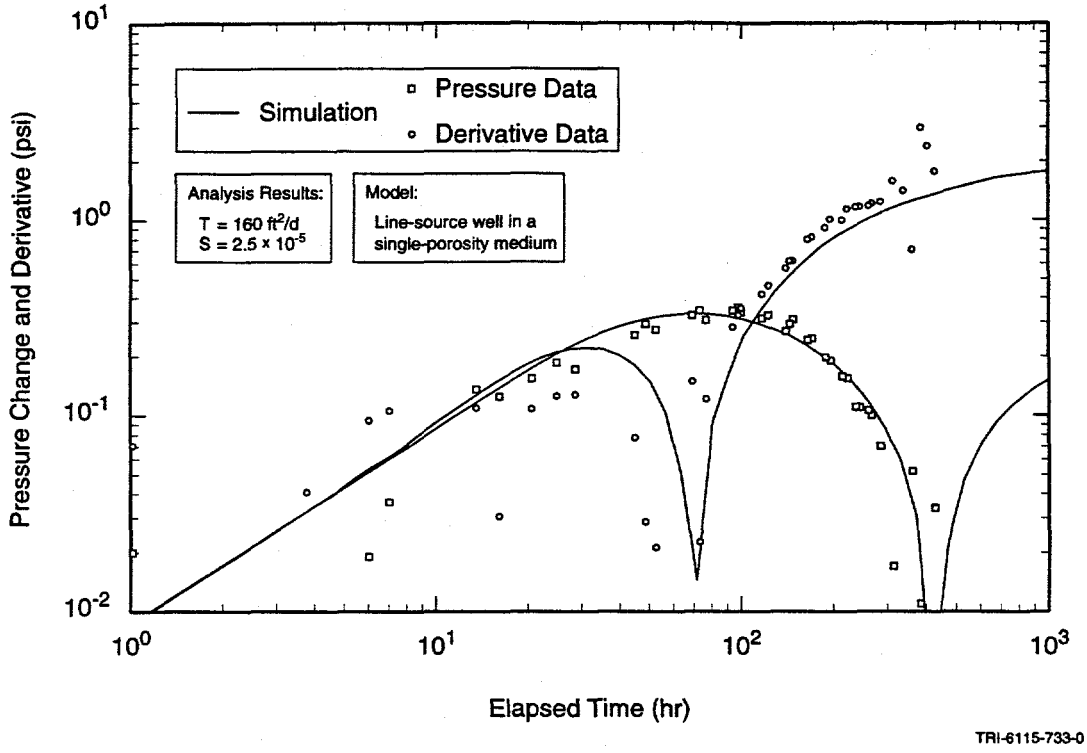

Figure 6-115. Log-log plot of D-268 recovery data from P-14 pumping test with Interpret/2 simulation.

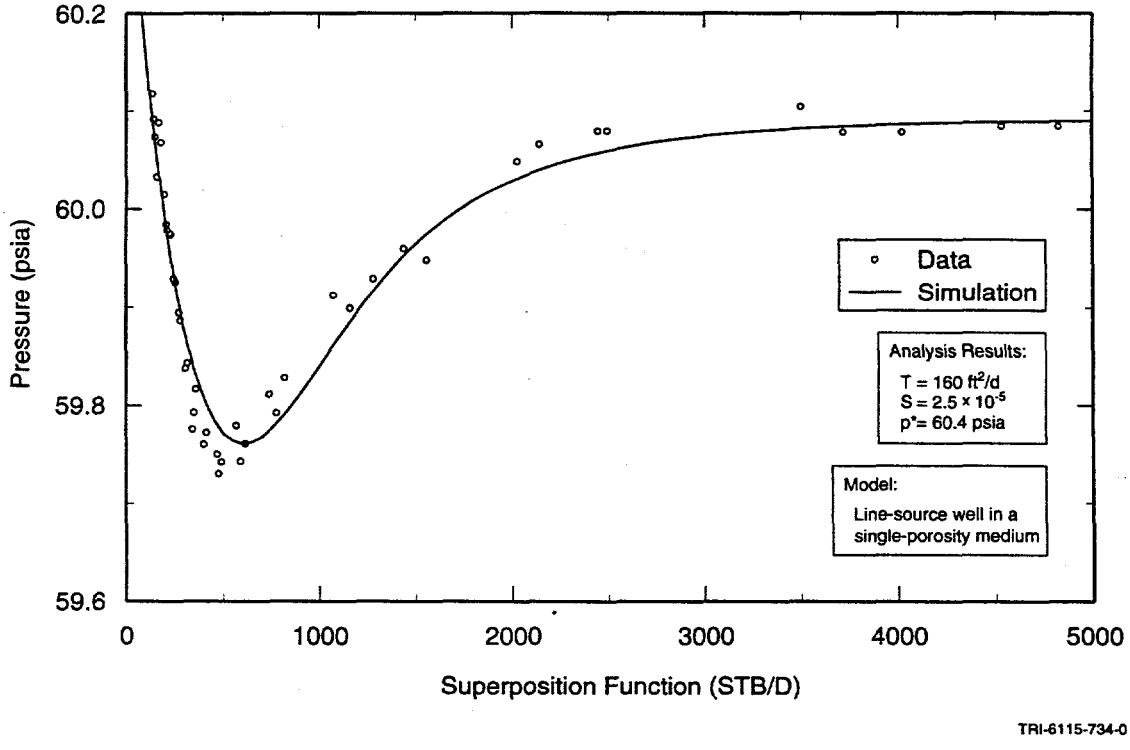

Figure 6-116. Horner plot of D-268 recovery data from P-14 pumping test with Interpret/2 simulation.

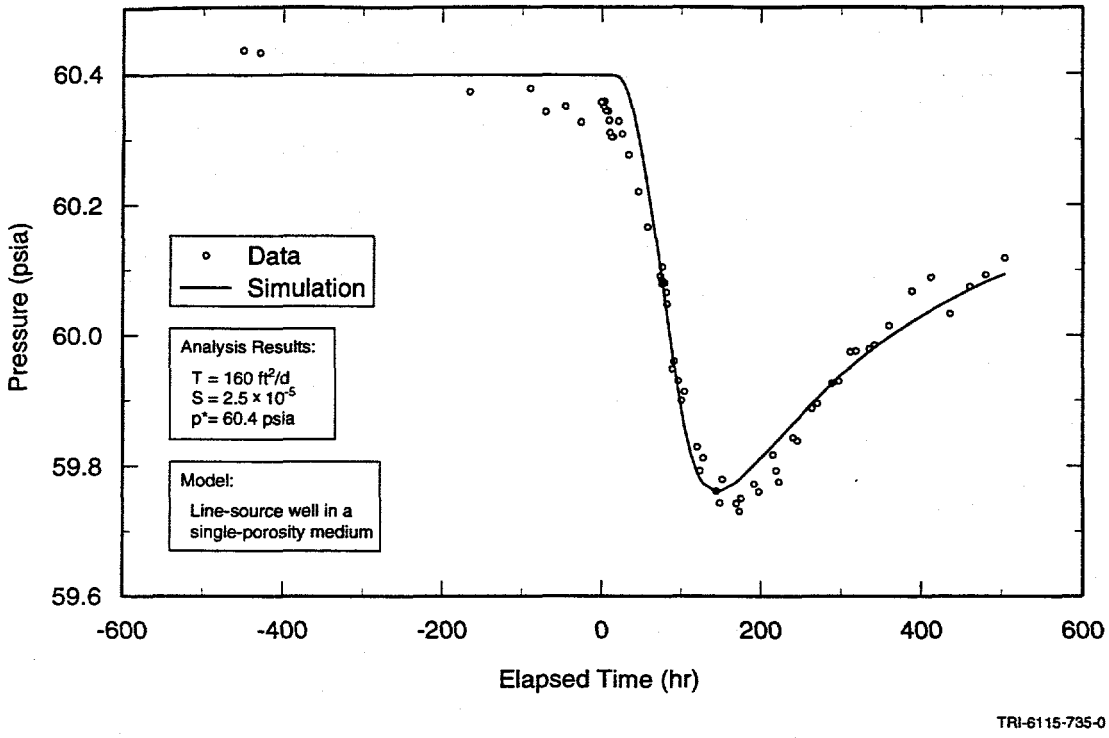

Figure 6-117. Linear-linear plot of D-268 data from P-14 pumping test with Interpret/2 simulation derived from recovery analysis.

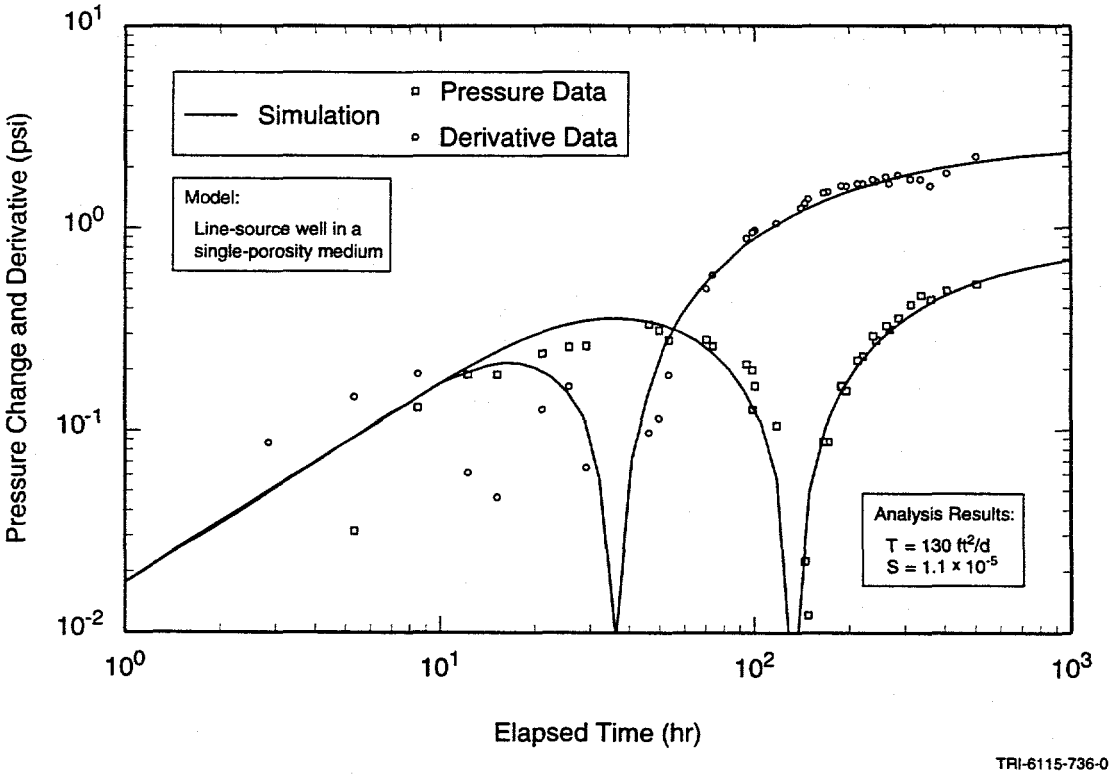

Figure 6-118. Log-log plot of H-6b recovery data from P-14 pumping test with Interpret/2 simulation.

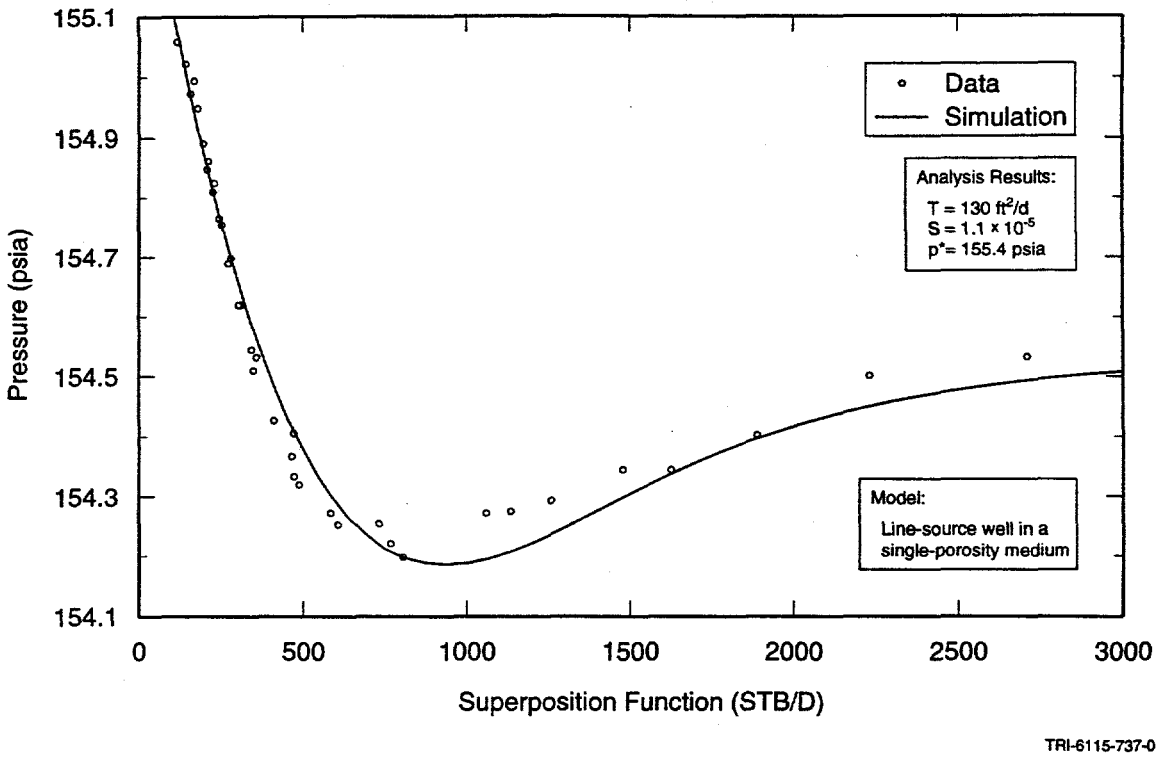

Figure 6-119. Horner plot of H-6b recovery data from P-14 pumping test with Interpret/2 simulation.

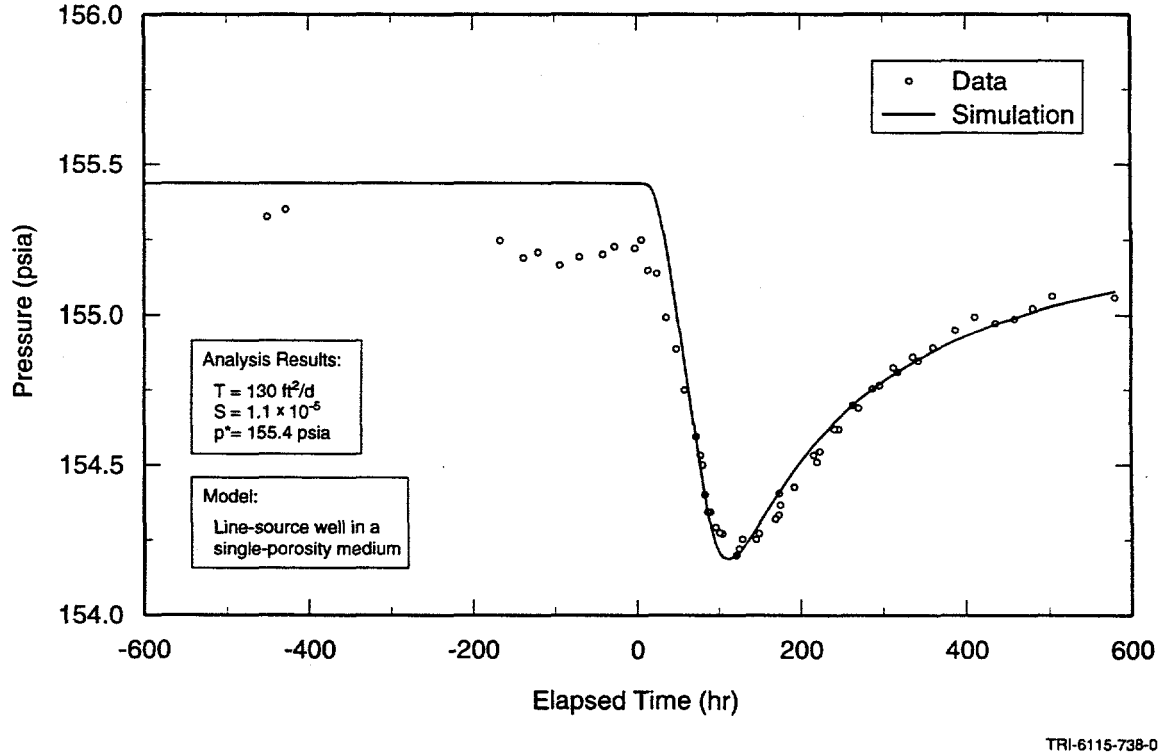

Figure 6-120. Linear-linear plot of H-6b data from P-14 pumping test with Interpret/2 simulation derived from recovery analysis.

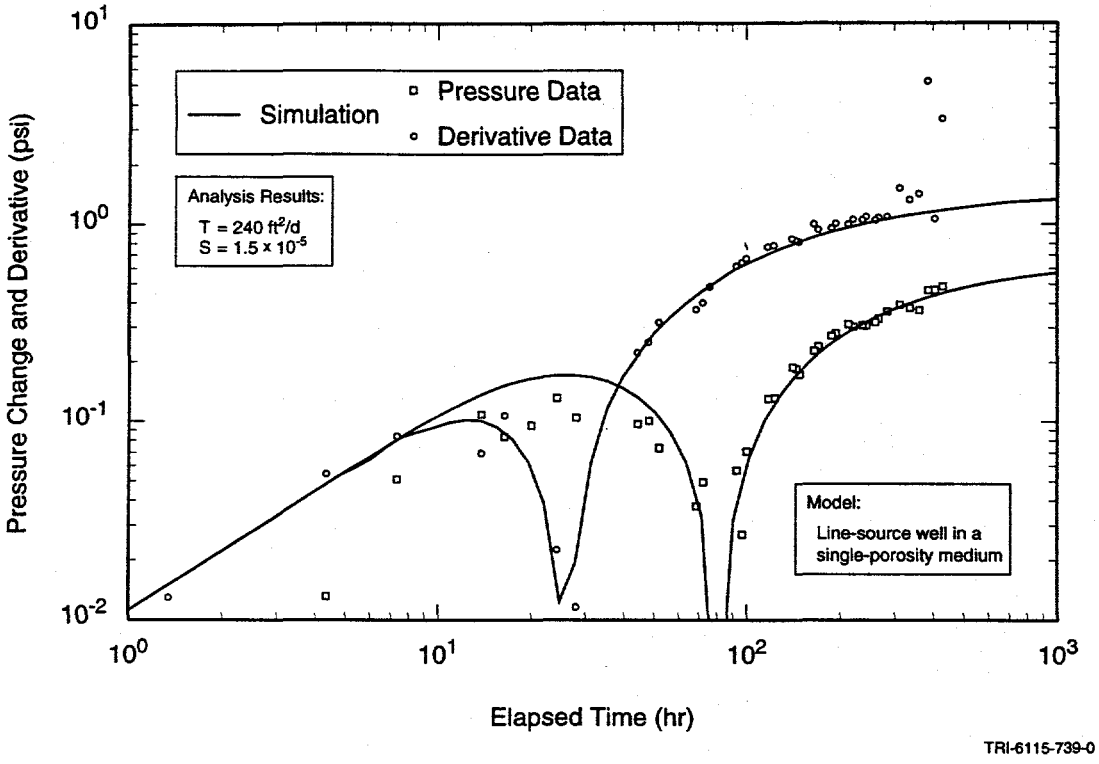

Figure 6-121. Log-log plot of WIPP-25 recovery data from P-14 pumping test with Interpret/2 simulation.

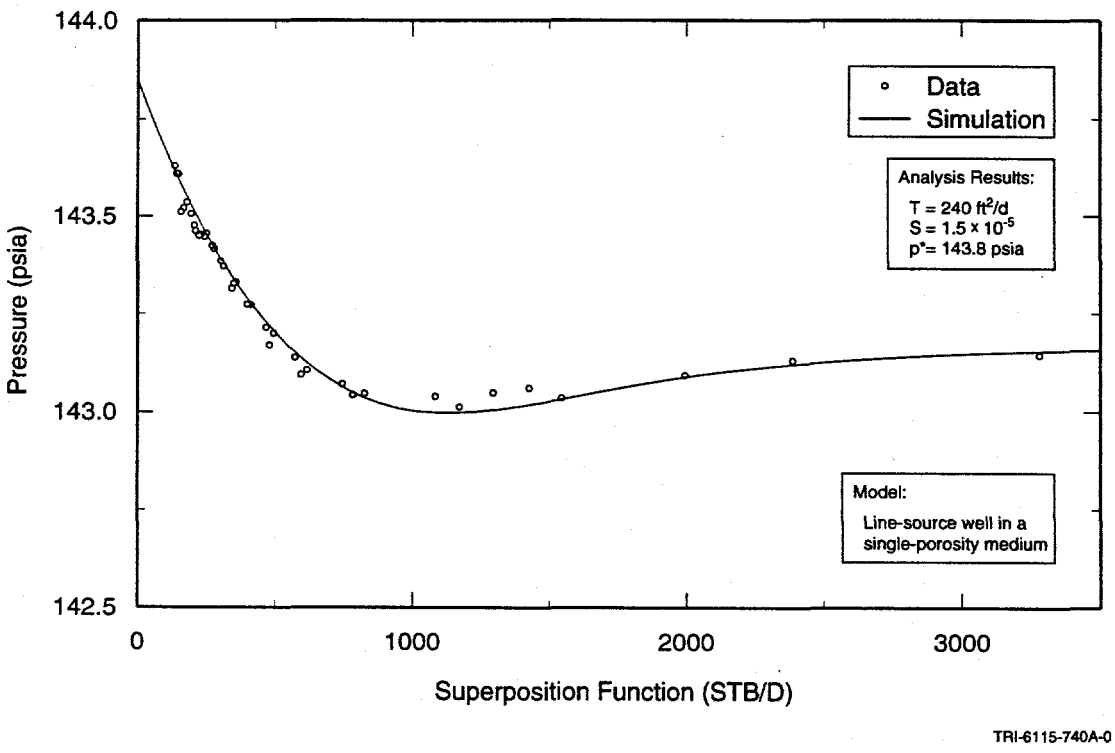

Figure 6-122. Horner plot of WIPP-25 recovery data from P-14 pumping test with Interpret/2 simulation.

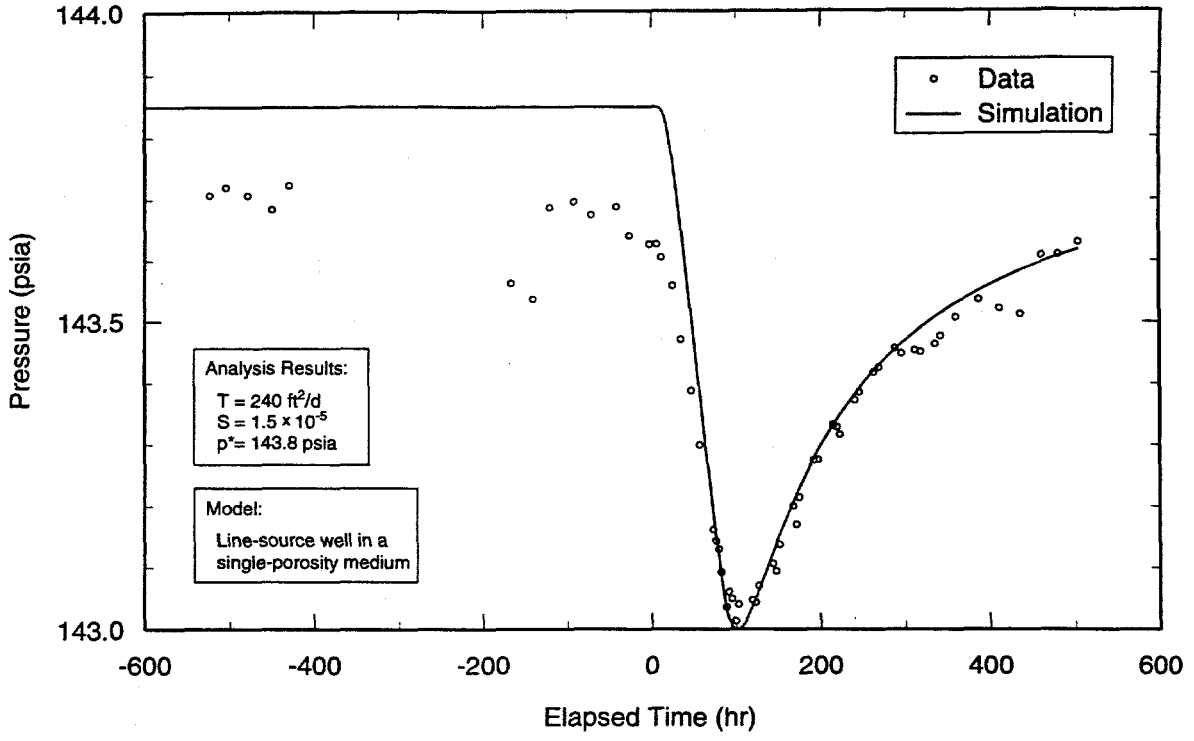

Figure 6-123. Linear-linear plot of WIPP-25 data from P-14 pumping test with Interpret/2 simulation derived from recovery analysis.

period indicate initial pressures slightly higher than were observed (Figures 6-117, 6-120, and 6-123) may reflect the effects of boundaries (heterogeneities) not included in the models.

6.8.3 Summary of Results from the P-14 Pumping Test

Analysis of the P-14 recovery response indicates that the local transmissivity of the Culebra is on the order of 290 to 500 ft^2/d (3.1 to 5.4 x 10^{-4} m^2/s). The data do not allow definitive determination of either single- or double-porosity hydraulic behavior at P-14. No-flow boundaries indicated by the analysis probably reflect decreased transmissivity to the east and south of P-14. The observation-well responses could also be interpreted equally well using either single- or double-porosity models. Transmissivities interpreted from the D-268, H-6b, and WIPP-25 responses are 160, 130, and 240 ft^2/d (1.7, 1.4, and 2.5 x 10^{-4} m^2/s), respectively. Transmissivities inferred from tests conducted at D-268 and H-6b are significantly lower, being 2 ft^2/d (2.2 x 10^{-6} m^2/s; Beauheim et al., 1991) and 37 ft^2/d (4.0 x 10^{-5} m^2/s; Section 6.2), respectively. As noted by Beauheim (1987a, 1989), transmissivities interpreted from observation-well responses in heterogeneous media tend to be intermediate between the local transmissivity values at the pumping well and at the observation wells, reflecting areal averaging. Storativities interpreted from the observation-well responses range from 1.1 to 2.5 x 10^{-5}, with a geometric mean of 1.6 x 10^{-5}.

6.9 WIPP-27 Slug Tests

Richey (1987) reported data from six slug tests performed in the Culebra at WIPP-27. Tests #2 and #6 were selected as having the

best quality data, and were analyzed using GTFM. Figure 6-124 shows a semilog plot of the best-fit GTFM simulation of the data from test #2. The test was simulated using a model of a well in an infinite single-porosity domain with a transmissivity of 530 ft^2/d (5.7×10^{-4} m^2/s). Figure 6-125 shows a semilog plot of the data and best-fit GTFM simulation for test #6. This simulation used a transmissivity of 420 ft^2/d (4.5×10^{-4} m^2/s). All plots show excellent agreement between data and simulations. While the best-fit values of transmissivity differ between the two tests, the data from both tests can be fit reasonably well with either value as well as with intermediate values. The different results simply reflect the difficulties inherent in accurately quantifying the hydraulic properties of highly transmissive media using slug tests.

At other locations where the Culebra has high transmissivities, such as H-7 and H-9, double-porosity hydraulic behavior is noted during pumping tests. The characteristic signature of a double-porosity system is a rapid initial response, reflecting only fracture transmissivity and storativity, followed by an equilibration period as water flows between the fractures and matrix, and ending with continued drawdown (or recovery) reflecting the combined properties of the fractures and matrix. No double-porosity behavior is evident in the WIPP-27 slug-test responses, but this may be because the tests were too short and stressed the Culebra too little for such behavior to be observed. Complete pressure recovery was obtained within five minutes during each of the slug tests. The interpreted parameters, therefore, are probably representative only of fractures.

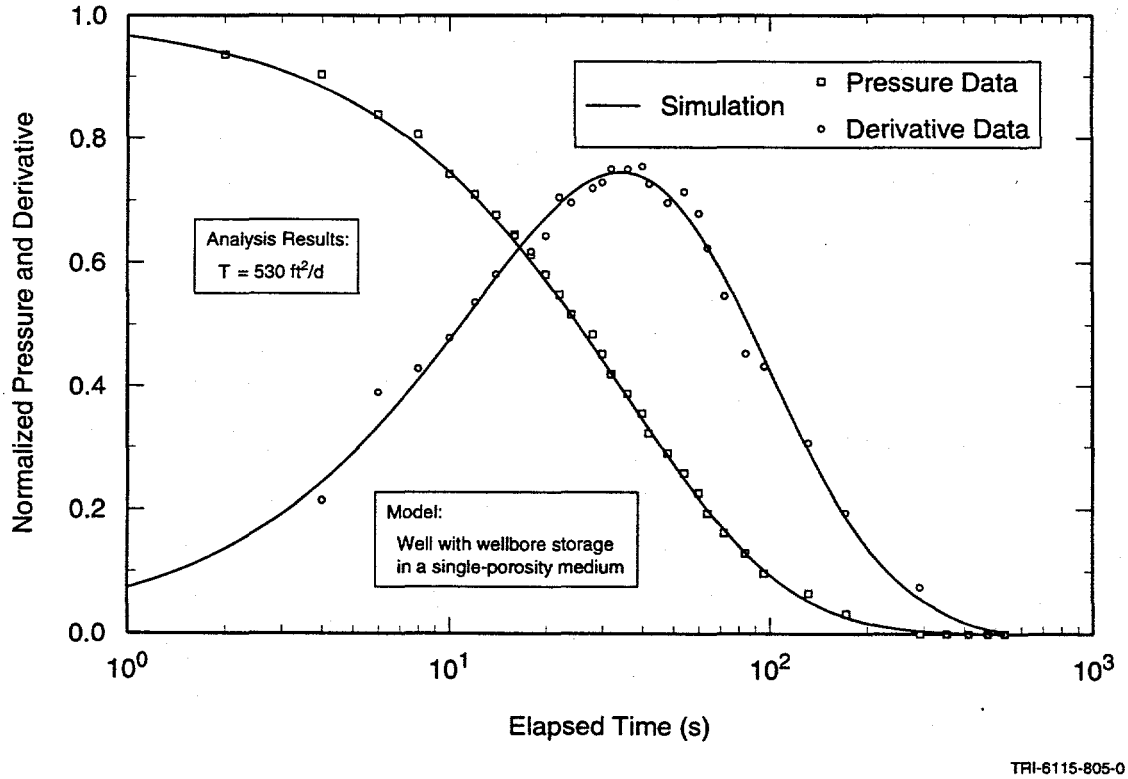

Figure 6-124. Semilog plot of normalized WIPP-27 slug-test #2 data with GTFM simulation.

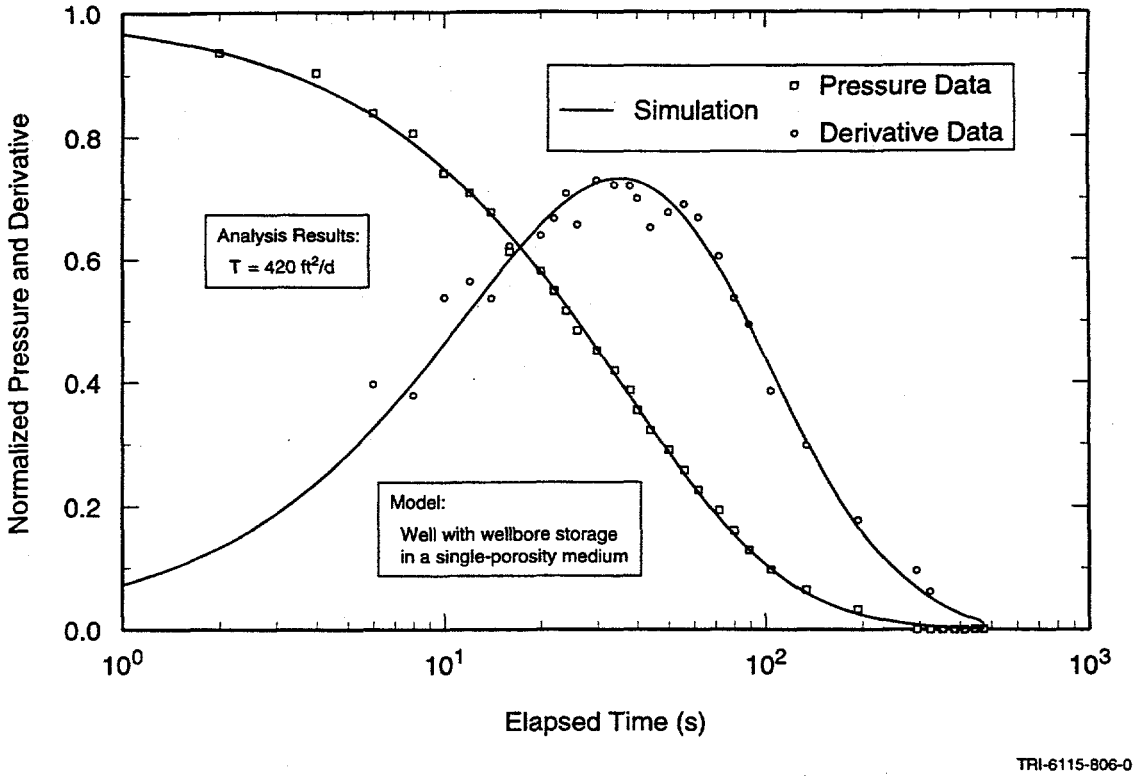

Figure 6-125. Semilog plot of normalized WIPP-27 slug-test #6 data with GTFM simulation.

6.10 WIPP-28 Slug Test

Of the five slug tests reported by Richey (1987) at WIPP-28, the data from test #3 were least perturbed by the slug-initiation technique and were selected for analysis using GTFM. Figure 6-126 shows a semilog plot of the data and best-fit GTFM simulation for test #3. The test was simulated using a model of a well in an infinite single-porosity domain with a transmissivity of 260 ft^2/d (2.8×10^{-4} m^2/s). As discussed above with respect to the tests at WIPP-27, double-porosity conditions might be expected to exist at WIPP-28, but could not be identified from a slug test lasting only 30 minutes. The interpreted transmissivity presented above is probably representative only of fractures.

6.11 WQSP-1 Pumping Test

The WQSP-1 pumping test involved pumping of WQSP-1 at an average rate of 6.8 gpm (0.43 L/s) for approximately 66.4 hr while monitoring responses in wells H-18 and WIPP-13.

6.11.1 WQSP-1

As described in Section 5.11, the pumping rate in WQSP-1 fluctuated during the first five minutes of the test, resulting in uninterpretable data. The data from the balance of the pumping period are interpretable using a simplified two-rate representation of the rates during the initial five minutes. The recovery data from WQSP-1 are invalid because the check valve in the discharge line failed, allowing water to drain back into the well. Therefore, analysis focused on the drawdown data from the period when the pumping rate was constant.

Figures 6-127 and 6-128 show the log-log and Horner plots, respectively, of the

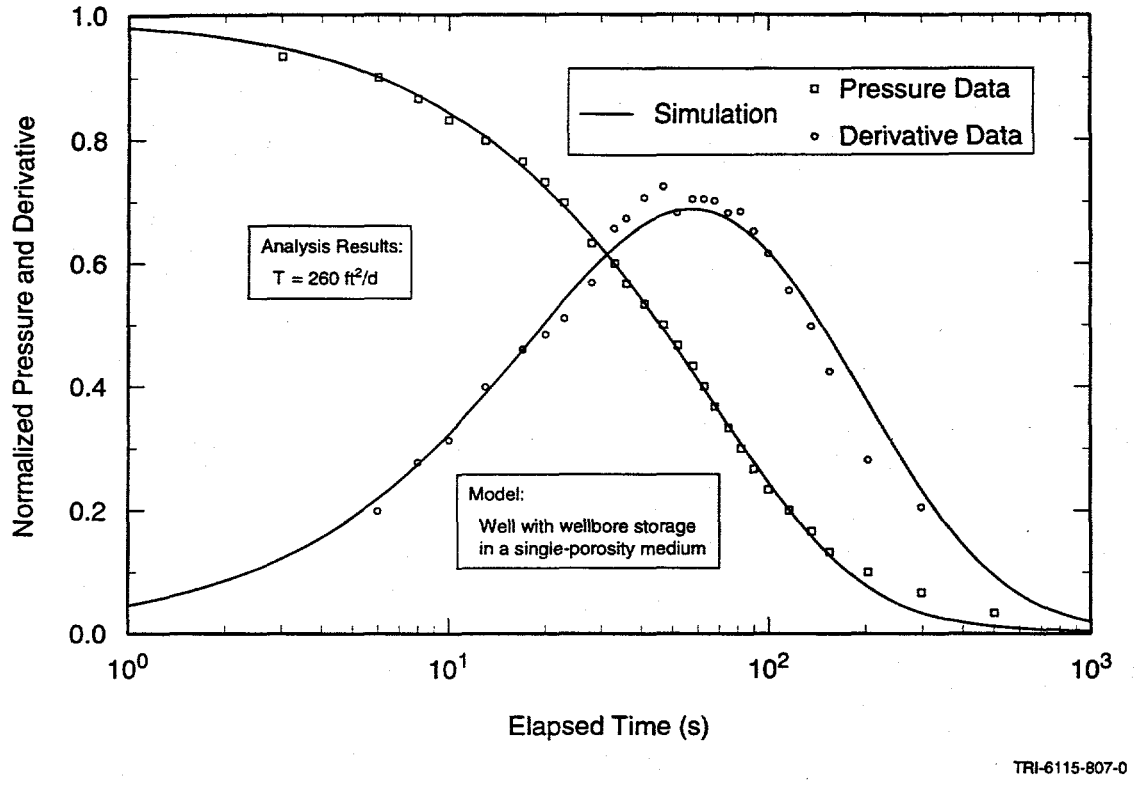

Figure 6-126. Semilog plot of normalized WIPP-28 slug-test #3 data with GTFM simulation.

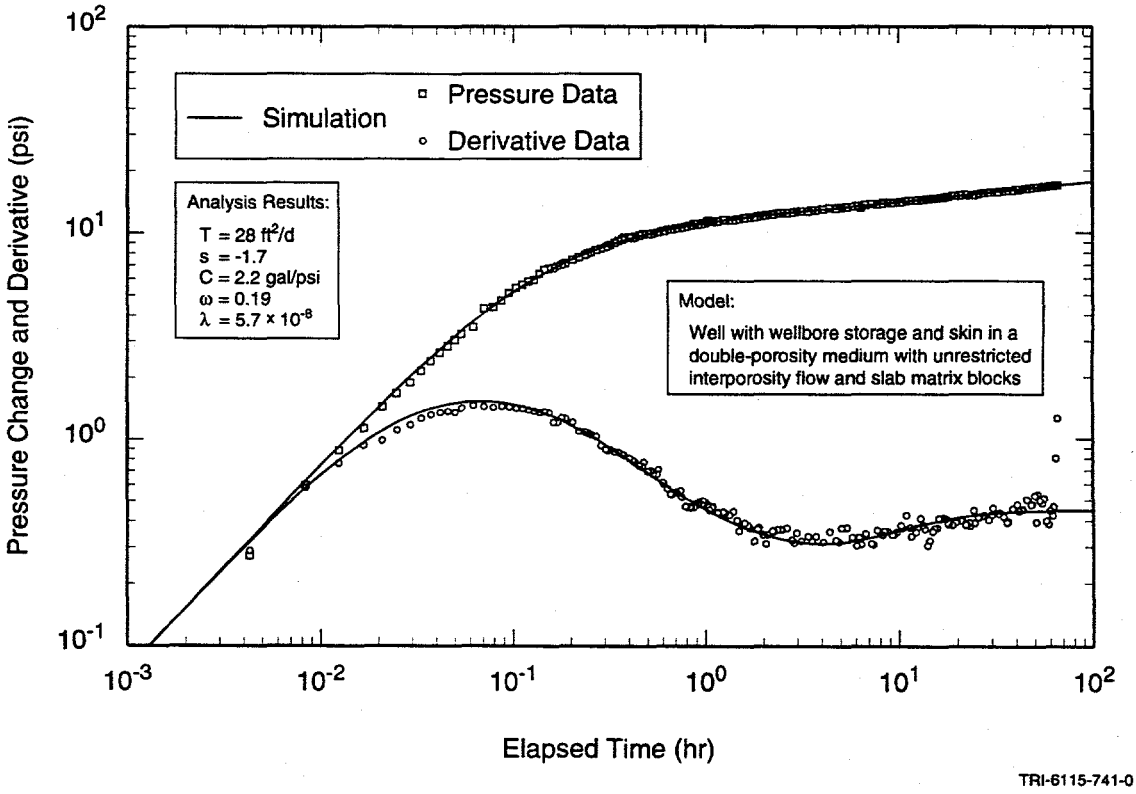

Figure 6-127. Log-log plot of WQSP-1 drawdown data with Interpret/2 simulation.

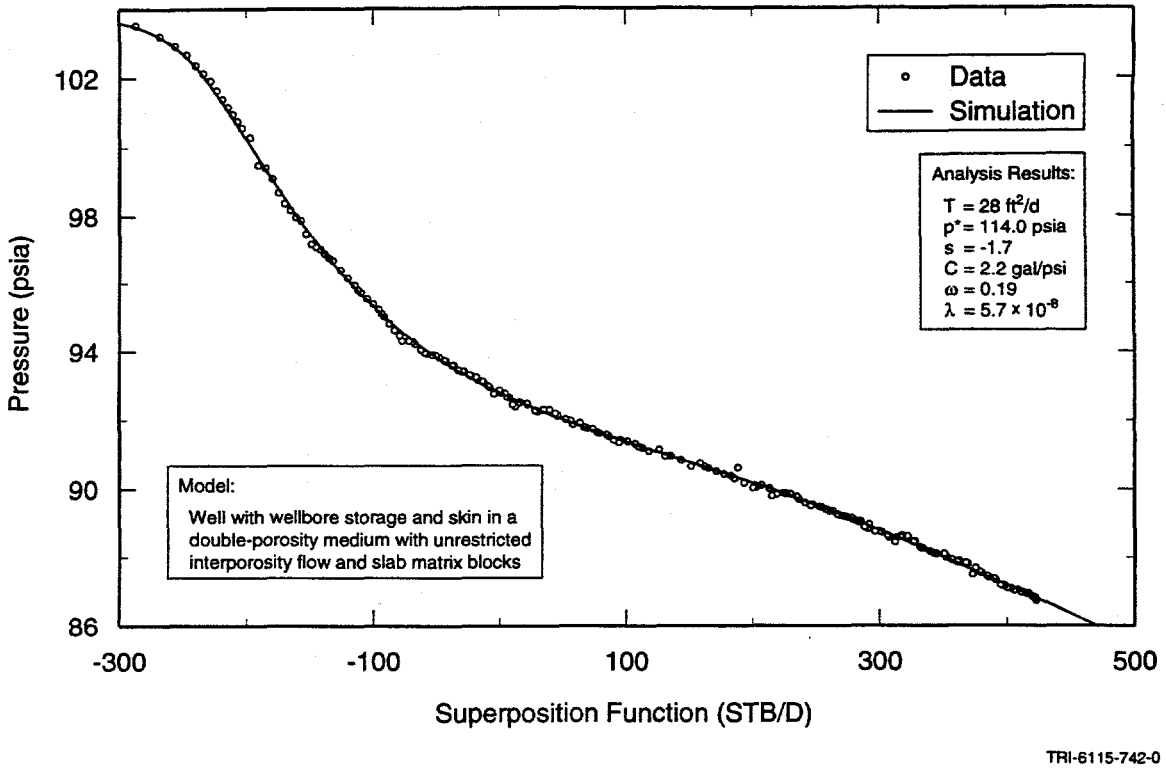

Figure 6-128. Horner plot of WQSP-1 drawdown data with Interpret/2 simulation.

drawdown data from WQSP-1 along with the best-fit Interpret/2 simulations. The data were analyzed using a model for a well with wellbore storage and skin in an infinite double-porosity medium with unrestricted interporosity flow and slab (horizontal) matrix blocks. The medium has a transmissivity of 28 ft^2/d (3.0 x 10^{-5} m^2/s) and the well appears to have a negative skin of -1.7. Other interpreted parameters are listed in Table 6-1. Figure 6-129 is a linear-linear plot of the match between this model and the combined drawdown and recovery data. The entire pumping period is represented well by the simulation, but actual recovery occurred faster than simulated because of the leaking check valve.

6.11.2 H-18

Well H-18 is far enough from WQSP-1 (1,295 ft [395 m]) that the early-time pumping-rate fluctuations and the failure of the check valve during recovery did not appear to affect the observed responses. Therefore, the entire data set is interpretable. Both the drawdown and recovery data can be matched using models for either single-porosity or double-porosity media with similar values for transmissivity and storativity. With either model, matching the late-time recovery data requires inclusion of a no-flow boundary. The effects of this boundary were not evident during the shorter drawdown period. Figures 6-130 and 6-131 show the log-log and Horner plots, respectively, of the recovery data from H-18 along with the best-fit Interpret/2 simulations using a model for a line-source well in a double-porosity medium with unrestricted interporosity flow, slab matrix blocks, and a no-flow boundary. The double-porosity simulations are presented because they provide a match to the early-time data that visually looks slightly better than that of the single-porosity simulations, and because of

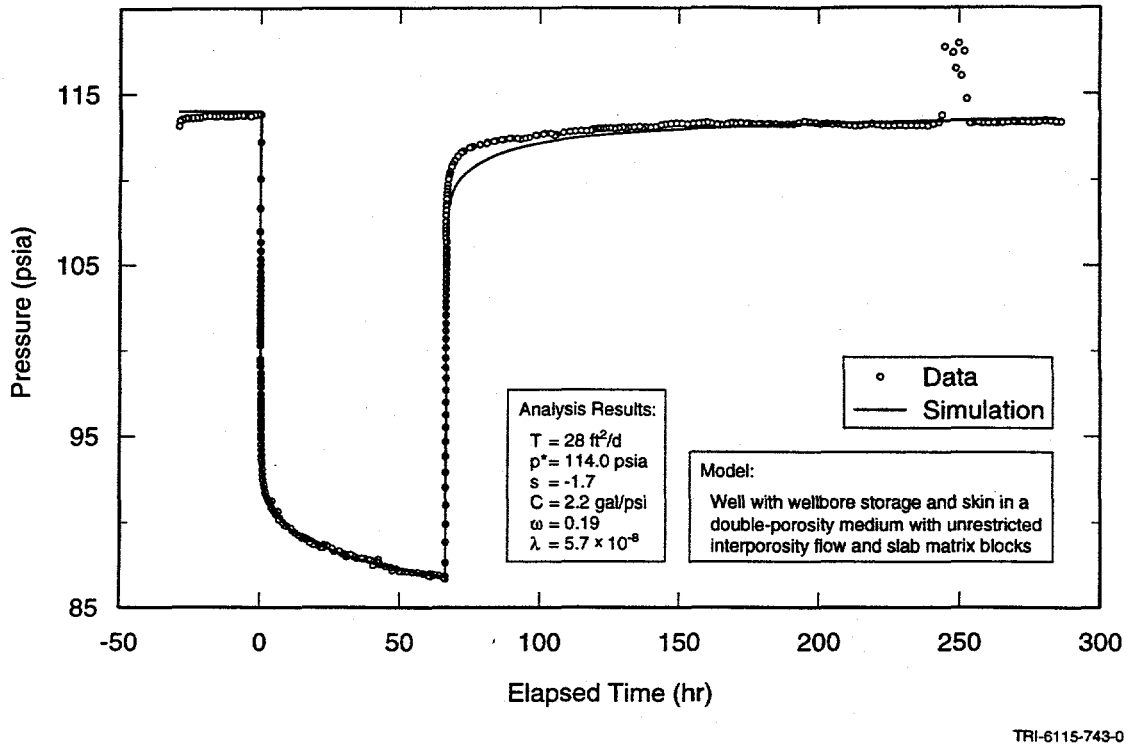

Figure 6-129. Linear-linear plot of WQSP-1 data with Interpret/2 simulation derived from drawdown analysis.

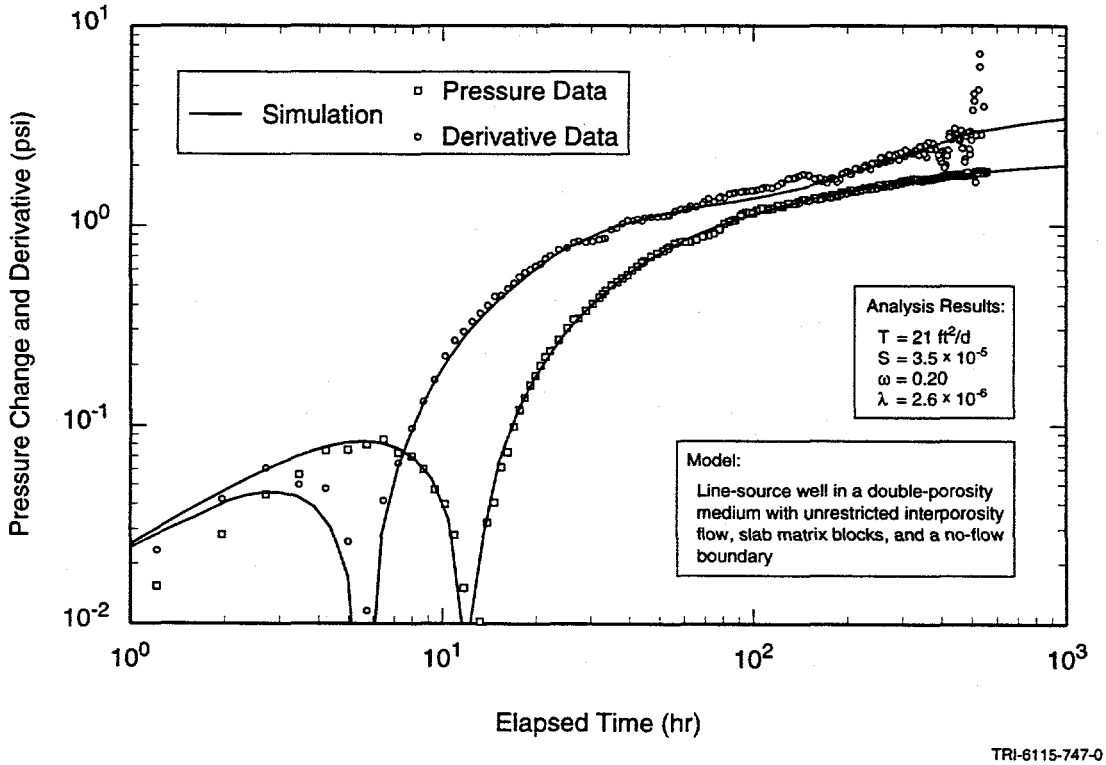

Figure 6-130. Log-log plot of H-18 recovery data from WQSP-1 pumping test with Interpret/2 simulation.

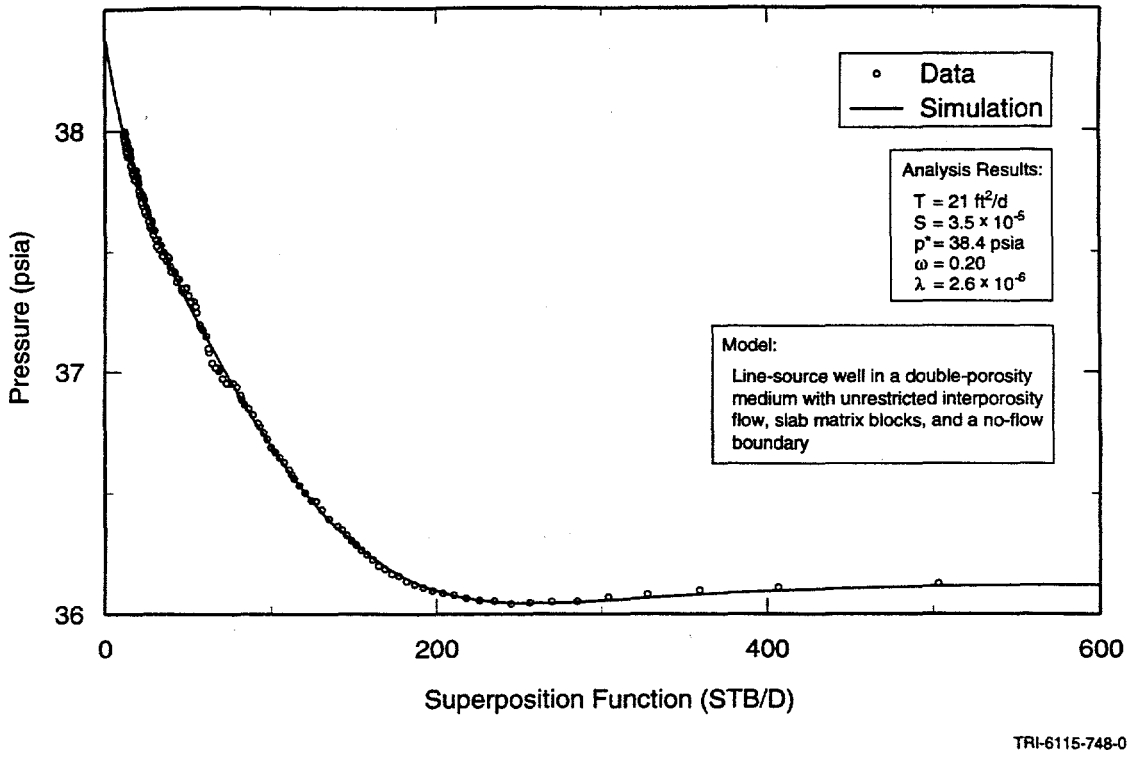

Figure 6-131. Horner plot of H-18 recovery data from WQSP-1 pumping test with Interpret/2 simulation.

the interpretation of double porosity at WQSP-1 (Section 6.11.1). The medium has a transmissivity of 21 ft^2/d (2.3 x 10^{-5} m^2/s), a storativity of 3.5 x 10^{-5}, and other parameter values as listed in Table 6-1. Figure 6-132 is a linear-linear plot of the match between this model and the combined drawdown and recovery data. The entire testing period is represented well by the simulation, although the simulated initial pressure is approximately 0.3 psi (2 kPa) higher than that observed. This discrepancy probably results from our inability to compensate for the slight rising trend evident in the pretest data.

6.11.3 WIPP-13

The responses observed at WIPP-13 during the WQSP-1 pumping test also appeared to be unaffected by the early-time flow-rate fluctuations and leaking check valve. The data from WIPP-13 can be matched equally well using either a model for a single-porosity medium with channel no-flow boundaries or a model for an infinite double-porosity medium, with the single-porosity interpretation providing a transmissivity estimate 4.2 times higher than that from the double-porosity interpretation. The results from the double-porosity model are presented herein because double-porosity hydraulic behavior is interpreted both at WQSP-1 (Section 6.11.1) and WIPP-13 (Beauheim, 1987b), and because the existence of channel no-flow boundaries is not supported by the response at WQSP-1. Figures 6-133 and 6-134 show the log-log and Horner plots, respectively, of the recovery data from WIPP-13 along with the best-fit double-porosity simulations. The medium has a transmissivity of 29 ft^2/d (3.1 x 10^{-5} m^2/s), a storativity of 1.0 x 10^{-5}, and other parameter values as listed in Table 6-1. Figure 6-135 is a linear-linear plot of the match between this model and the combined drawdown and recovery data. The entire

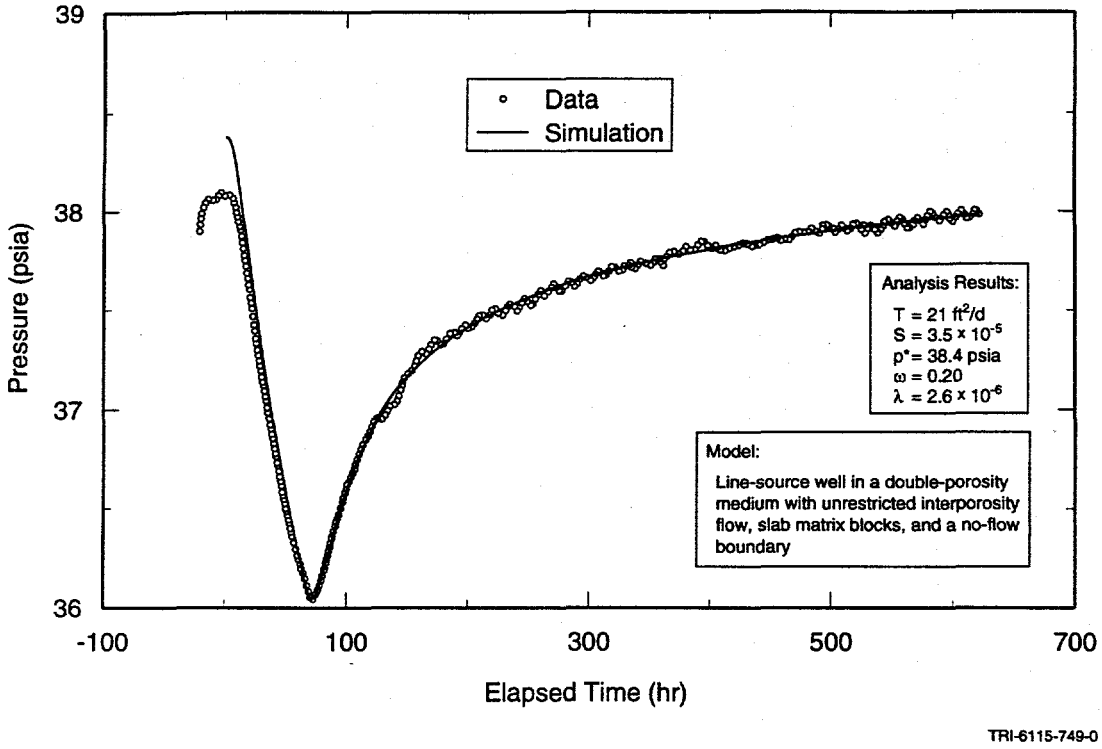

Figure 6-132. Linear-linear plot of H-18 data from WQSP-1 pumping test with Interpret/2 simulation derived from recovery analysis.

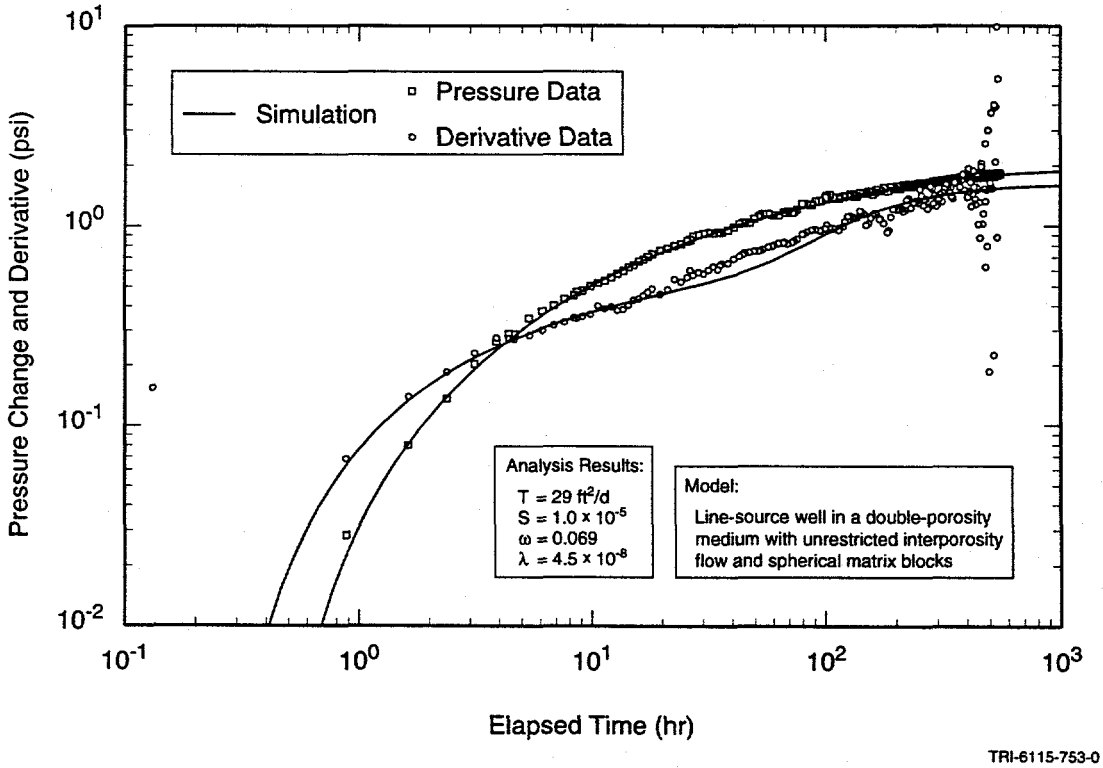

Figure 6-133. Log-log plot of WIPP-13 recovery data from WQSP-1 pumping test with Interpret/2 simulation.

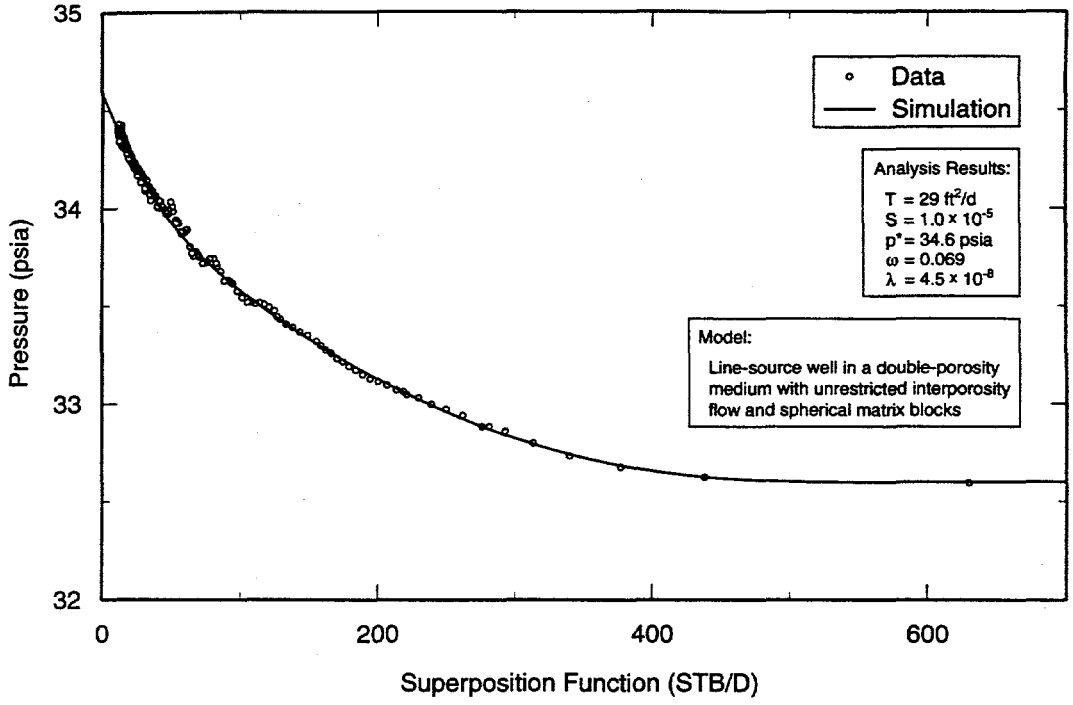

Figure 6-134. Horner plot of WIPP-13 recovery data from WQSP-1 pumping test with Interpret/2 simulation.

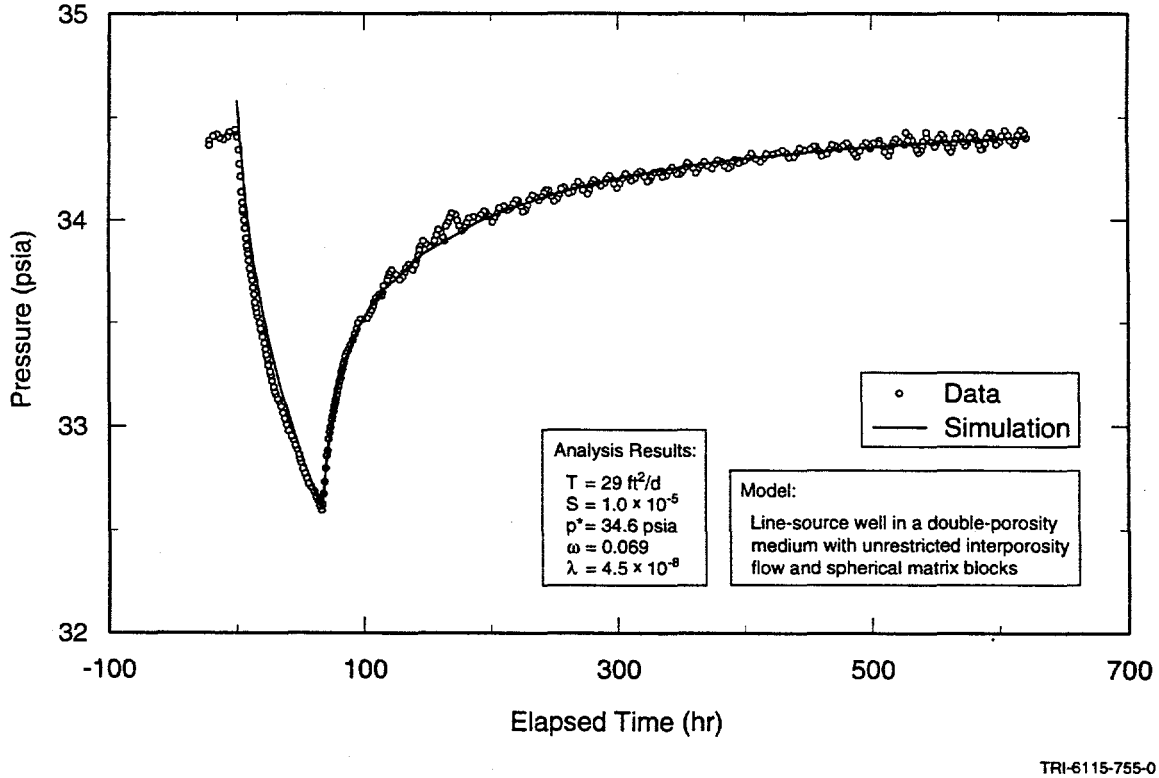

Figure 6-135. Linear-linear plot of WIPP-13 data from WQSP-1 pumping test with Interpret/2 simulation derived from recovery analysis.

testing period is represented well by the simulation, except that the simulated starting pressure for the test is almost 0.2 psi (1.4 kPa) higher than was observed.

6.11.4 Summary of Results from the WQSP-1 Pumping Test

Interpretation of the drawdown response in WQSP-1 indicates that the Culebra behaves hydraulically as a double-porosity medium with a transmissivity of 28 ft^2/d (3.0×10^{-5} m^2/s) within the region affected by the test. Both the H-18 and WIPP-13 recovery responses were interpreted using double-porosity models for the sake of consistency with other interpretations, although similar results could be obtained using single-porosity models. Interpreted transmissivities are 21 and 29 ft^2/d (2.3×10^{-5} and 3.1×10^{-5} m^2/s) and interpreted storativities are 3.5×10^{-5} and 1.0×10^{-5} for H-18 and WIPP-13, respectively. The slight differences between the estimated hydraulic properties probably reflect heterogeneity.

6.12 WQSP-2 Pumping Test

The WQSP-2 pumping test involved pumping of WQSP-2 at an average rate of 7.1 gpm (0.45 L/s) for four days while monitoring responses in wells DOE-2, H-18, WIPP-12, WIPP-13, and WQSP-1 (Section 5.12).

6.12.1 WQSP-2

As described in Section 5.12, the pumping rate in WQSP-2 fluctuated during the first five minutes of the test, resulting in uninterpretable data. The data from the balance of the pumping period are interpretable using a simplified three-rate representation of the rates during the initial five minutes. The recovery data from WQSP-2 are invalid because the check valve in the discharge line failed, allowing water to drain back into the well. Therefore, analysis focused on the drawdown data from the period when the pumping rate was constant.

Figures 6-136 and 6-137 show the log-log and Horner plots, respectively, of the drawdown data from WQSP-2 along with the best-fit Interpret/2 simulations. The data were analyzed using a model for a well with wellbore storage and skin in an infinite double-porosity medium with restricted interporosity flow. The medium has a transmissivity of 19 ft^2/d (2.0×10^{-5} m^2/s) and the well appears to have a negative skin of -2.0. Other interpreted parameters are listed in Table 6-1. Figure 6-138 is a linear-linear plot of the match between this model and the combined drawdown and recovery data. The entire pumping period is represented well by the simulation, but actual recovery occurred faster than simulated because of the leaking check valve.

6.12.2 Observation Wells

All of the observation wells are sufficiently far from WQSP-2 that the early-time pumping-rate fluctuations and the failure of the check valve in WQSP-2 during recovery did not appear to affect the observed responses. However, the pumping period was not long enough for definitive determination of hydraulic properties from the observation-well responses, so only the recovery data can be analyzed with confidence. Figures 6-139 through 6-141, 6-142 through 6-144, 6-145 through 6-147, and 6-148 through 6-150 show log-log, Horner, and linear-linear plots of the recovery data from DOE-2, H-18, WIPP-13, and WQSP-1, respectively, along with the best-fit Interpret/2 simulations. In all cases, the simulations used a model for a line-source well in an infinite double-porosity medium with unrestricted interporosity flow and slab matrix blocks. Interpreted transmissivities are 31 ft^2/d (3.3×10^{-5} m^2/s), 23 ft^2/d (2.5×10^{-5} m^2/s), 23 ft^2/d (2.4×10^{-5} m^2/s),

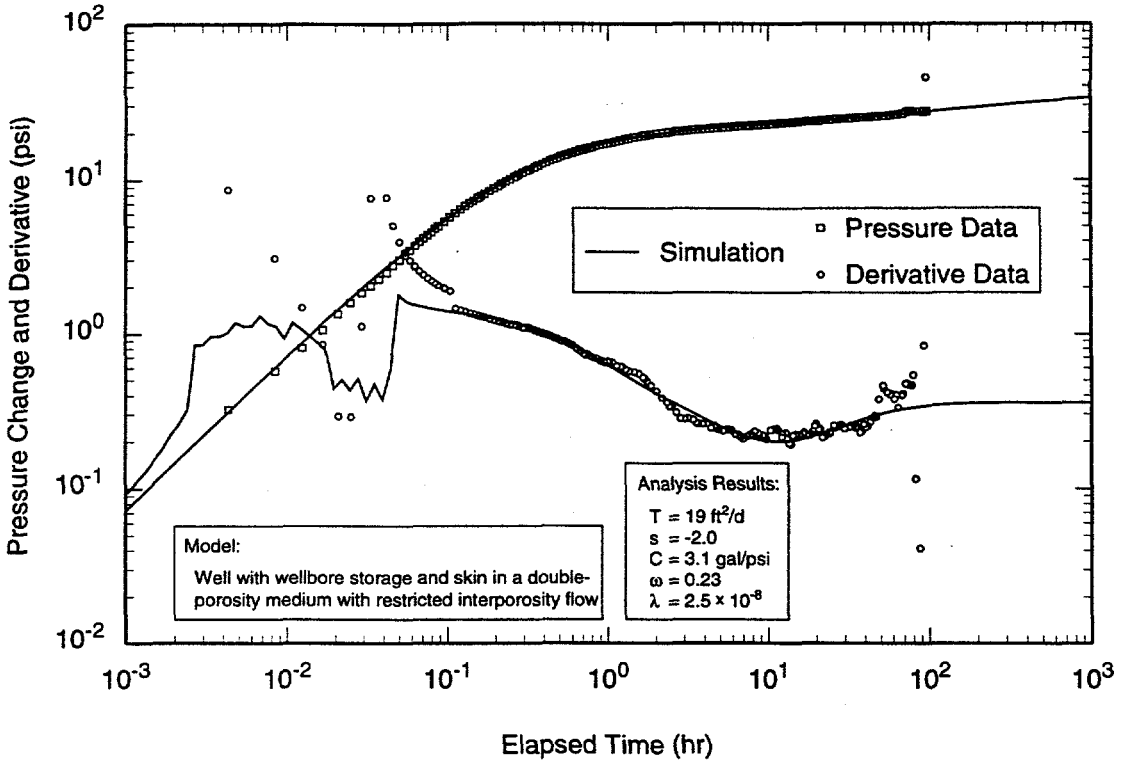

Figure 6-136. Log-log plot of WQSP-2 drawdown data with Interpret/2 simulation.

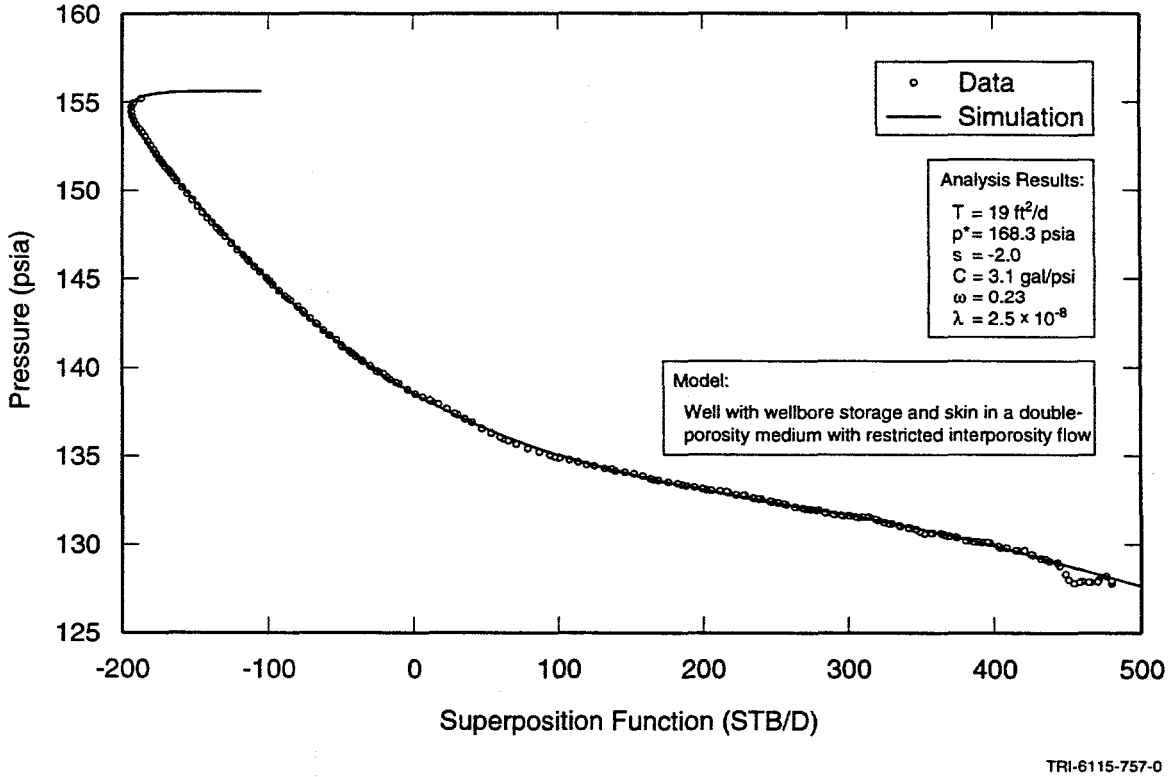

Figure 6-137. Horner plot of WQSP-2 drawdown data with Interpret/2 simulation.

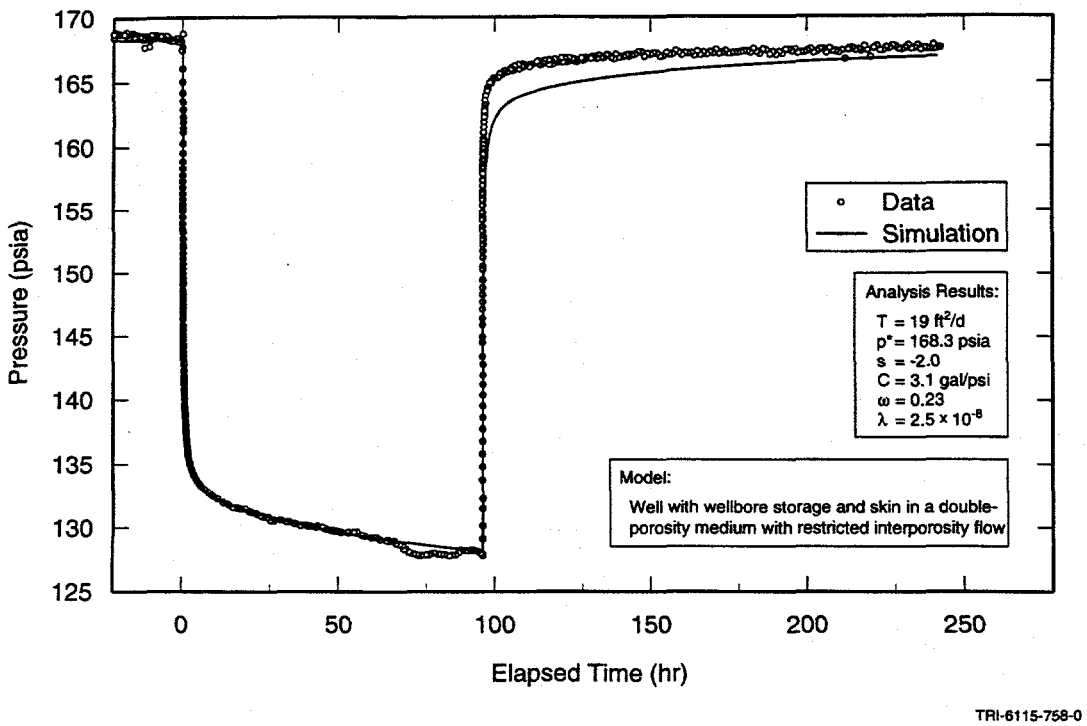

Figure 6-138. Linear-linear plot of WQSP-2 data with Interpret/2 simulation derived from drawdown analysis.

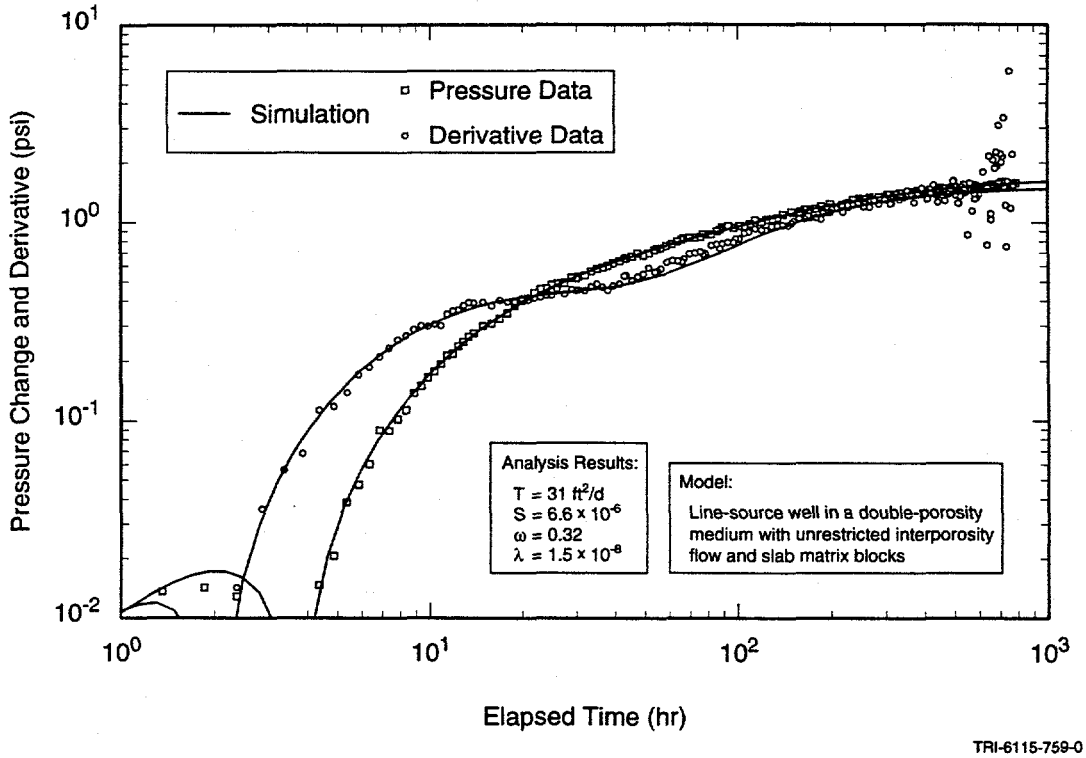

Figure 6-139. Log-log plot of DOE-2 recovery data from WQSP-2 pumping test with Interpret/2 simulation.

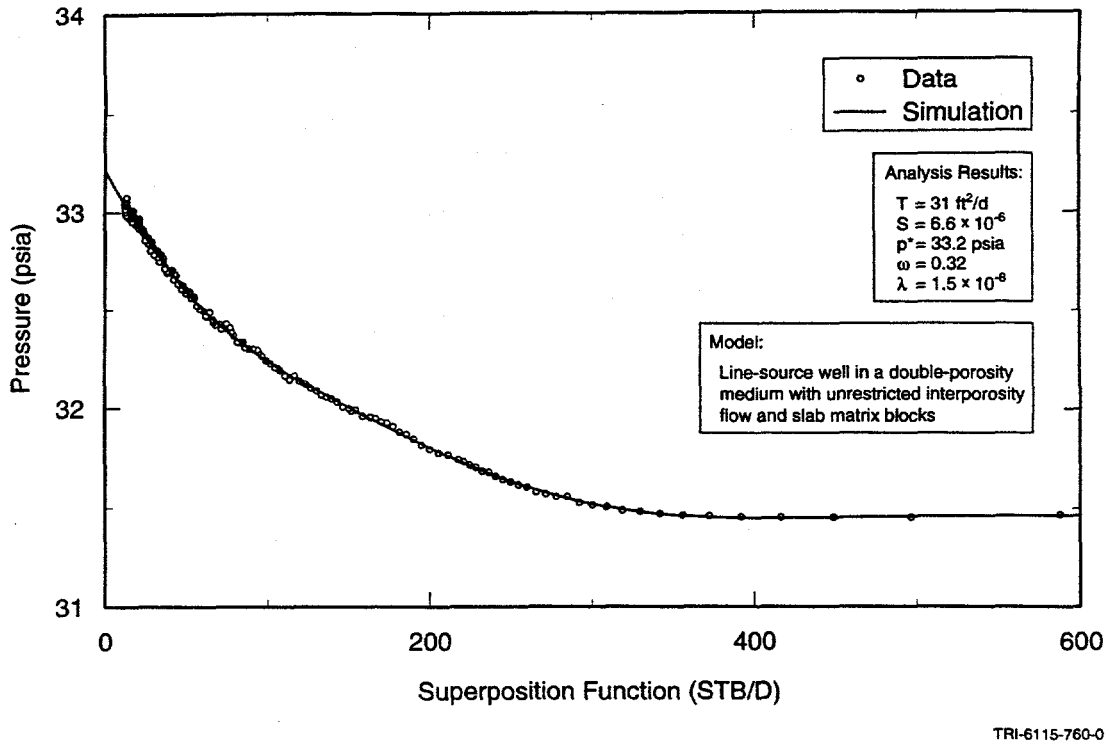

Figure 6-140. Horner plot of DOE-2 recovery data from WQSP-2 pumping test with Interpret/2 simulation.

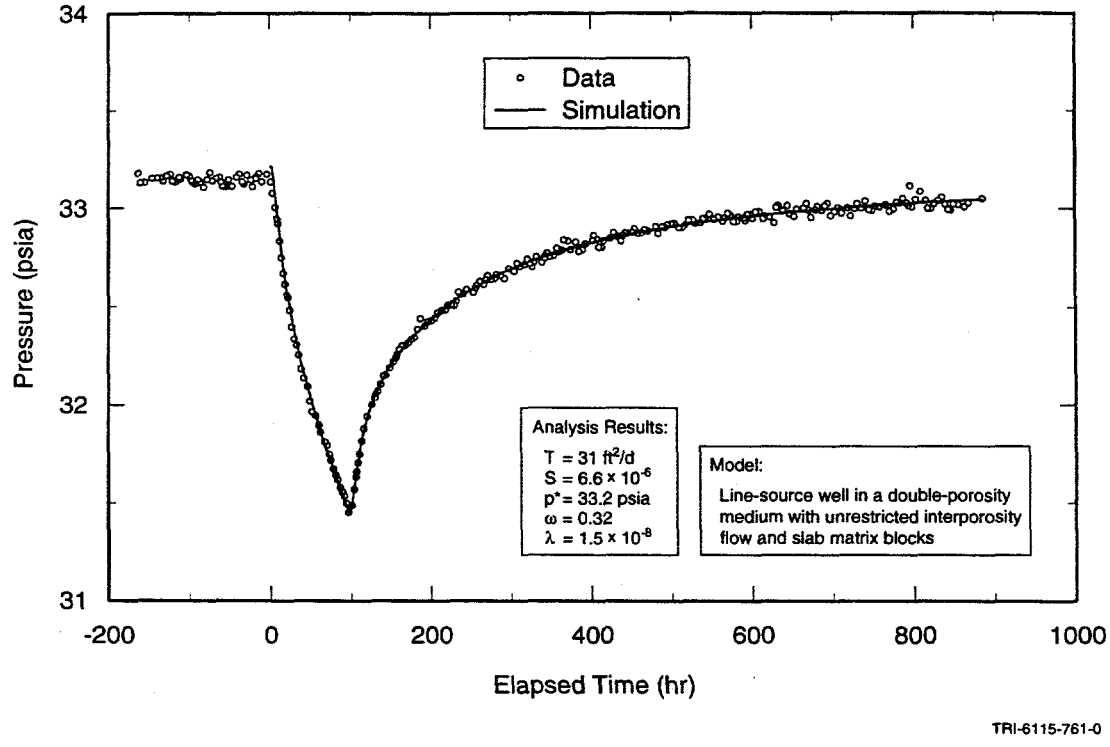

Figure 6-141. Linear-linear plot of DOE-2 data from WQSP-2 pumping test with Interpret/2 simulation derived from recovery analysis.

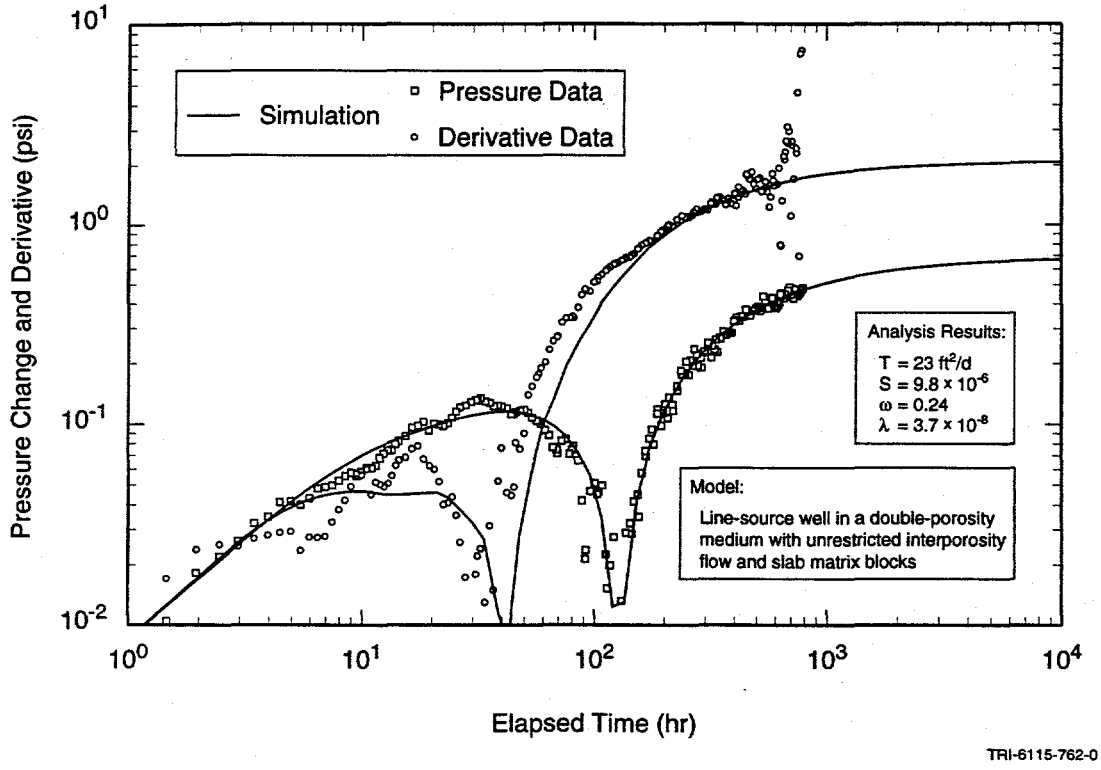

Figure 6-142. Log-log plot of H-18 recovery data from WQSP-2 pumping test with Interpret/2 simulation.

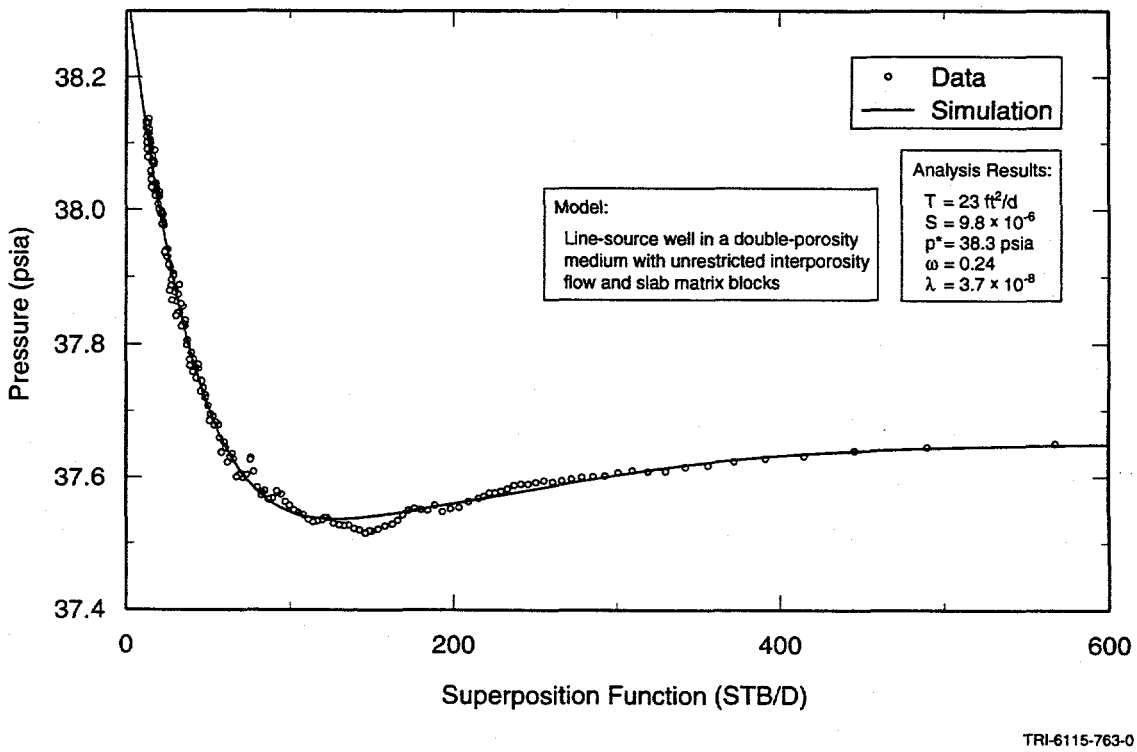

Figure 6-143. Horner plot of H-18 recovery data from WQSP-2 pumping test with Interpret/2 simulation.

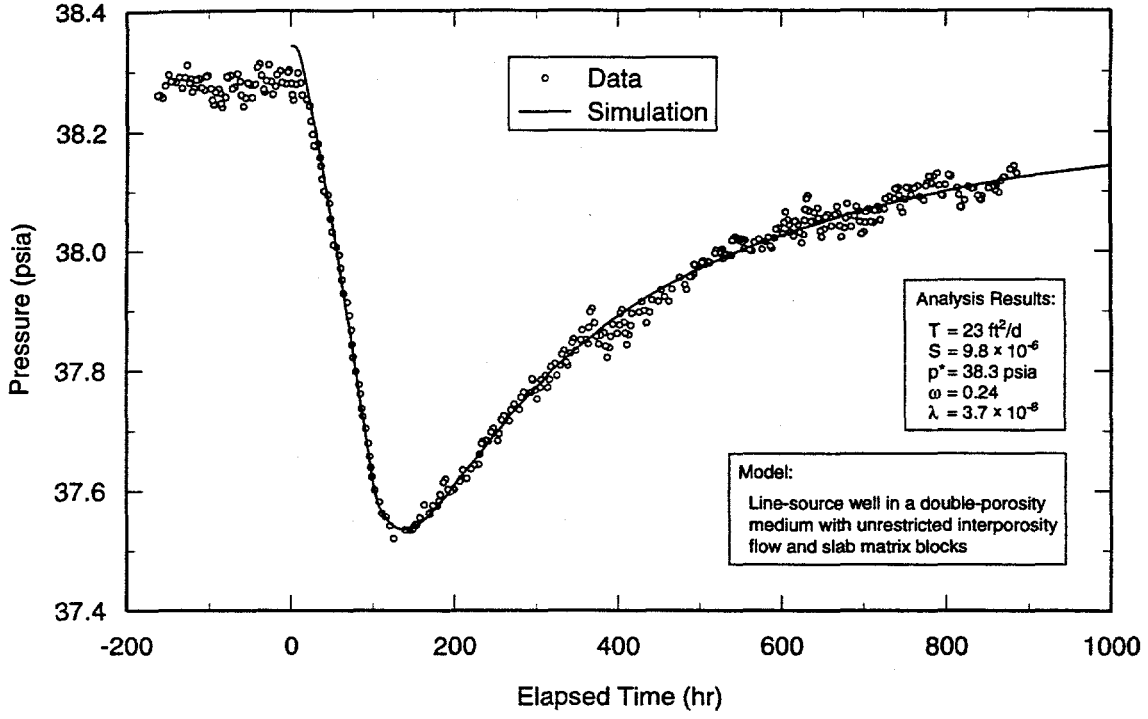

Figure 6-144. Linear-linear plot of H-18 data from WQSP-2 pumping test with Interpret/2 simulation derived from recovery analysis.

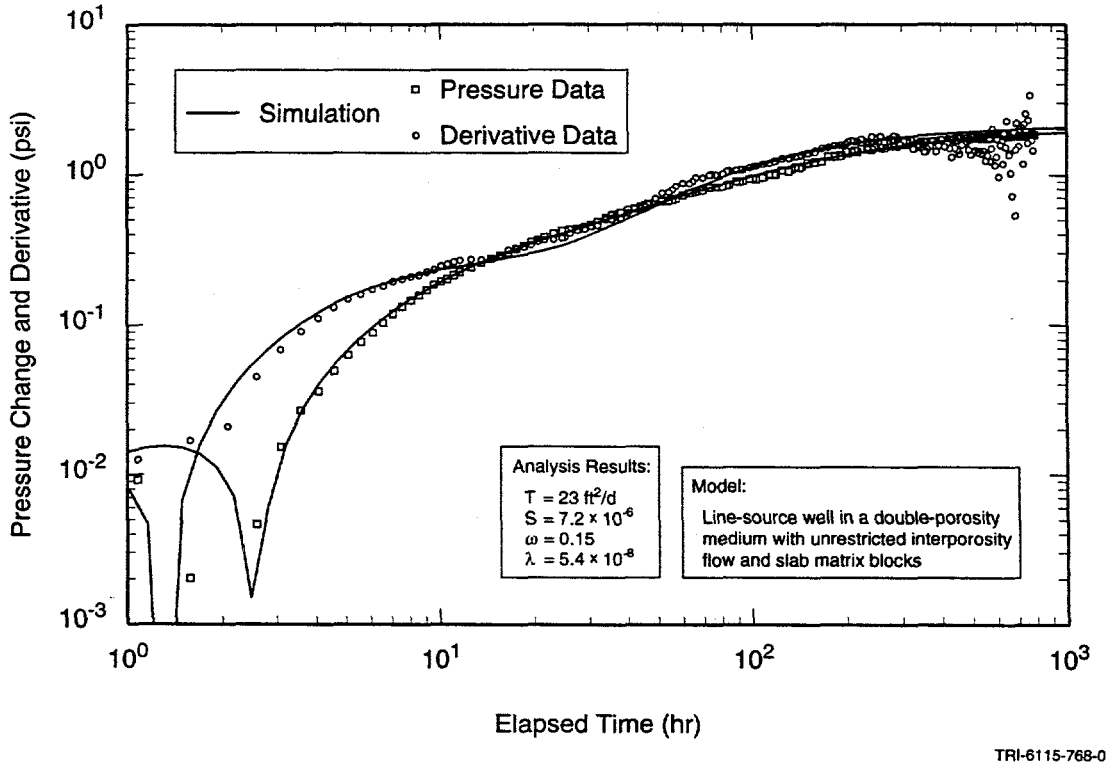

Figure 6-145. Log-log plot of WIPP-13 recovery data from WQSP-2 pumping test with Interpret/2 simulation.

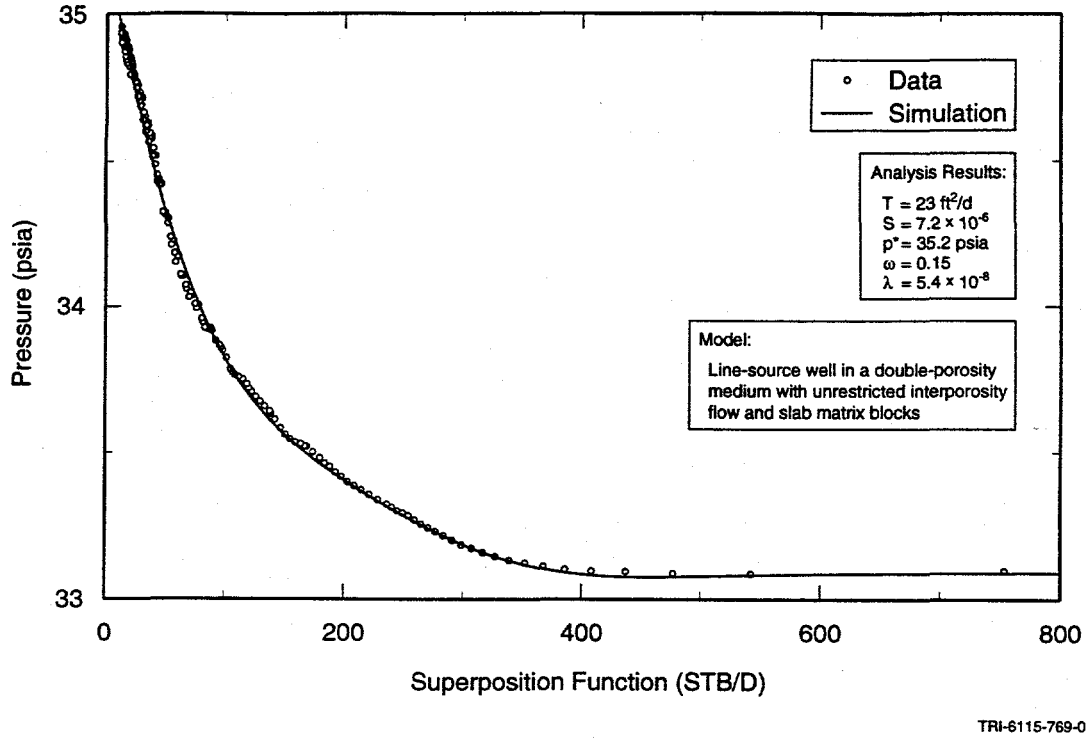

Figure 6-146. Horner plot of WIPP-13 recovery data from WQSP-2 pumping test with Interpret/2 simulation.

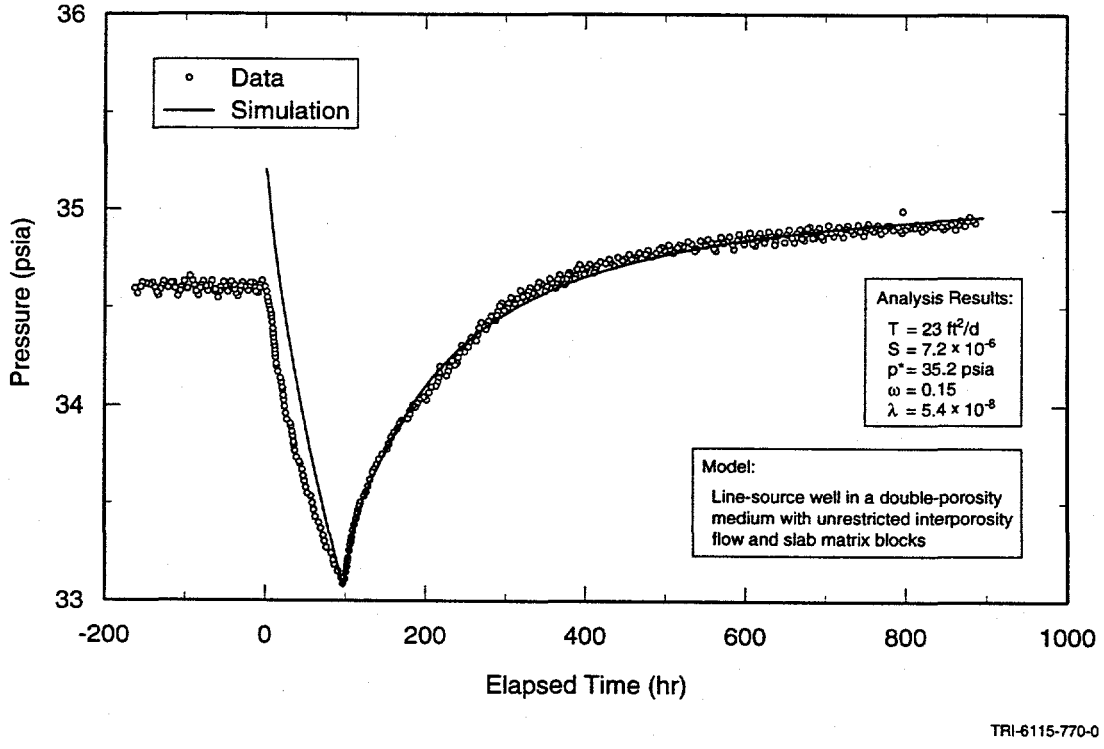

Figure 6-147. Linear-linear plot of WIPP-13 data from WQSP-2 pumping test with Interpret/2 simulation derived from recovery analysis.

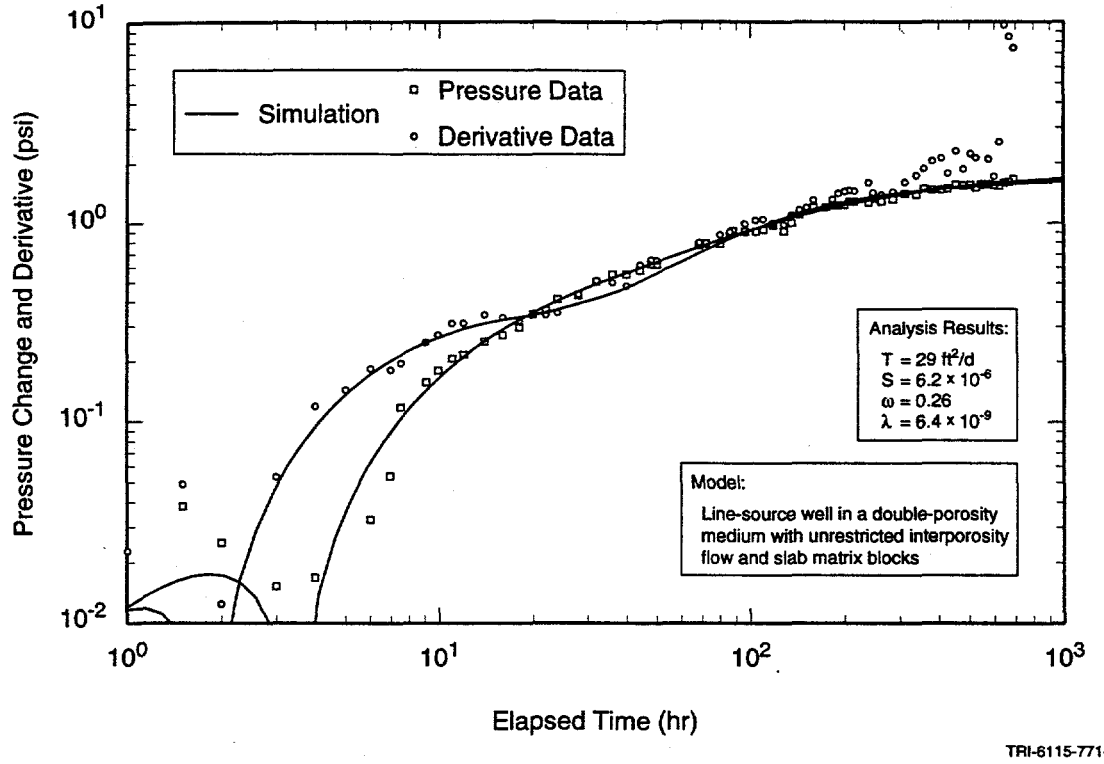

Figure 6-148. Log-log plot of WQSP-1 recovery data from WQSP-2 pumping test with Interpret/2 simulation.

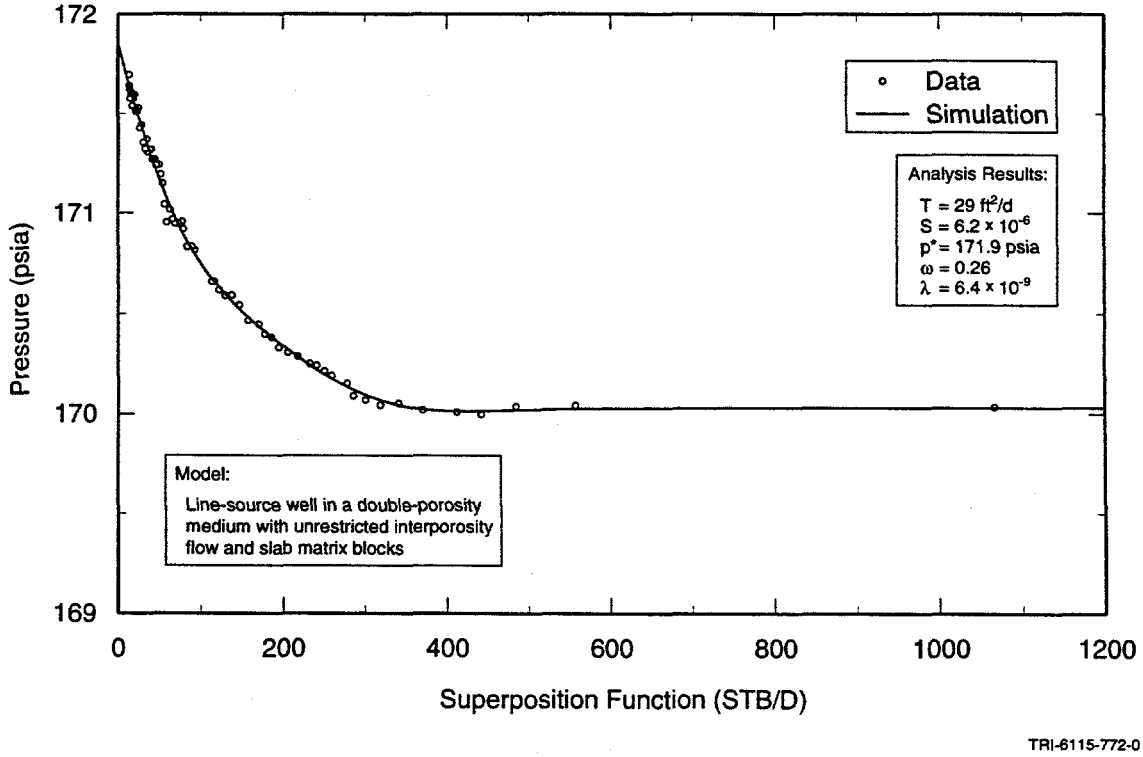

Figure 6-149. Horner plot of WQSP-1 recovery data from WQSP-2 pumping test with Interpret/2 simulation.

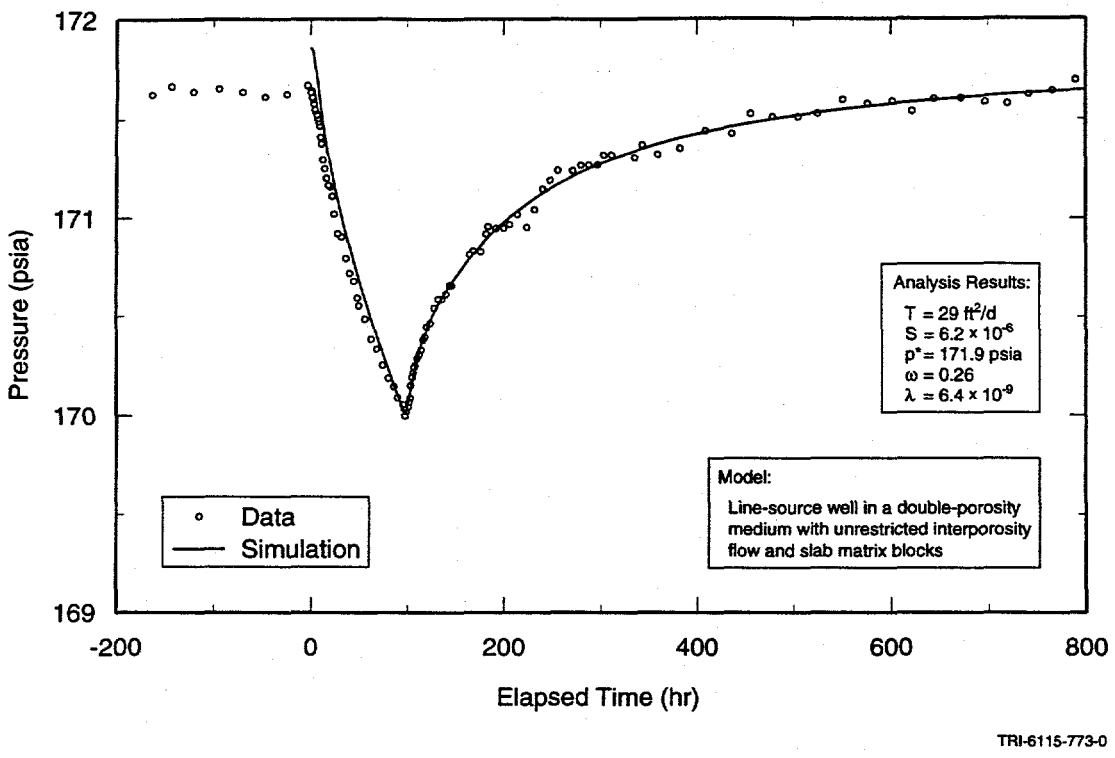

Figure 6-150. Linear-linear plot of WQSP-1 data from WQSP-2 pumping test with Interpret/2 simulation derived from recovery analysis.

and 29 ft^2/d (3.2 x 10^{-5} m^2/s), and storativities are 6.6 x 10^{-6}, 9.8 x 10^{-6}, 7.2 x 10^{-6}, and 6.2 x 10^{-6} for DOE-2, H-18, WIPP-13, and WQSP-1, respectively. Other parameters are given in Table 6-1. In the cases of DOE-2, H-18, and WQSP-1, the simulations of the entire testing period indicate initial pressures slightly higher than were observed, reflecting slight undercompensations for the pre-test trends discussed in Section 5.12. In the case of WIPP-13, the simulated initial pressure was approximately 0.5 psi (3 kPa) higher than observed (Figure 6-147) and recovery pressures exceeded the pre-test pressure, as discussed in Section 5.12. Because we do not understand the reason for this occurrence, we believe our analysis of the WIPP-13 recovery data should be viewed with some skepticism, even though the results are consistent with those obtained for the other observation wells.

The data from WIPP-12 could not be analyzed at all. Drawdown at WIPP-12 did not begin until the pump had been on in WQSP-2 for approximately 60 hr, and recovery did not begin until the pump had been off for more than 340 hr. Recovery stopped and pressures began to decline again for an unknown reason approximately 1200 hr after pumping ended. As a result, no stabilization of the pressure derivative (necessary for definitive determination of hydraulic properties) is evident in the log-log plot of the WIPP-12 recovery data (Figure 6-151).

6.12.3 Summary of Results from the WQSP-2 Pumping Test

Interpretation of the drawdown response in WQSP-2 indicates that the Culebra behaves hydraulically as a double-porosity medium with a transmissivity of 19 ft^2/d (2.0 x 10^{-5} m^2/s) within the region affected by the test.

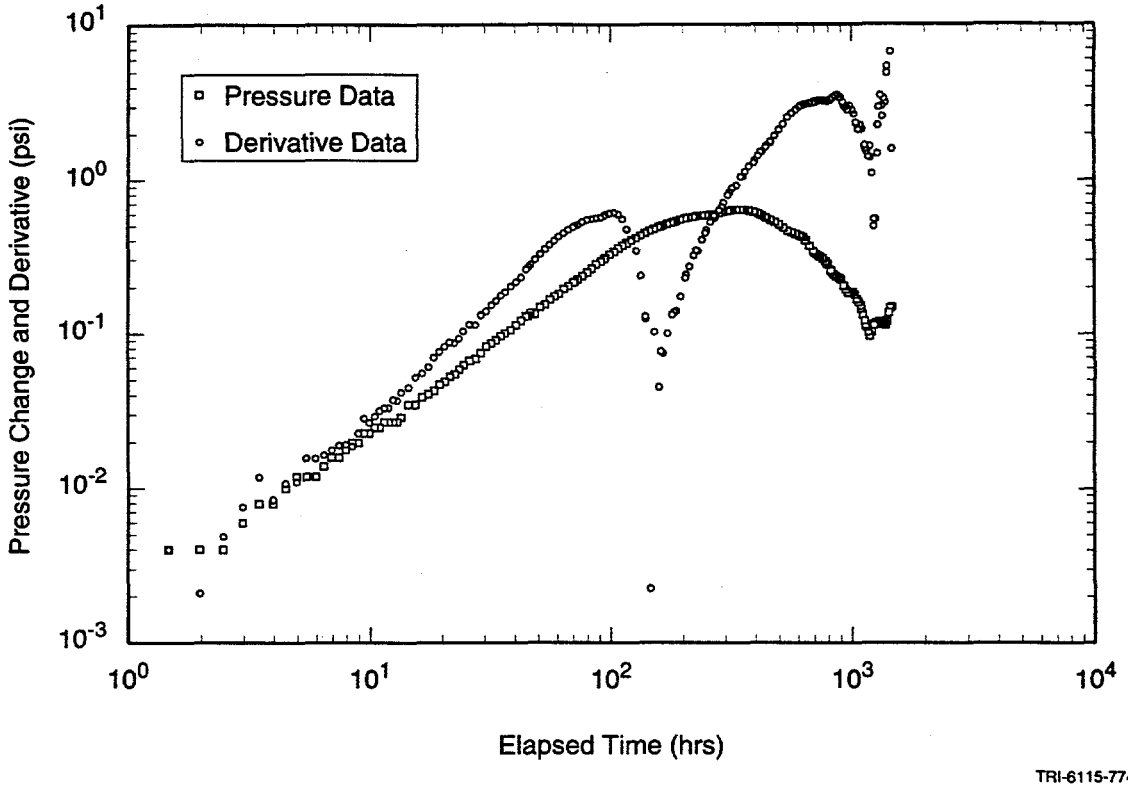

Figure 6-151. Log-log diagnostic plot of WIPP-12 recovery data from WQSP-2 pumping test.

Interpretations of the responses observed at DOE-2, H-18, WIPP-13, and WQSP-1 indicate double-porosity behavior, with transmissivities ranging from 23 to 31 ft^2/d (2.4 to 3.3 x 10^{-5} m^2/s) and storativities ranging from 6.2 x 10^{-6} to 9.8 x 10^{-6}.

6.13 WQSP-4 Pumping Test

As discussed in Section 5.13, the WQSP-4 pumping test involved pumping at 4.2 gpm (0.26 L/s) for approximately 53.1 hr followed by pumping at 2.2 gpm (0.14 L/s) for approximately 48.6 hr. Data from the first drawdown period and the recovery period are analyzable using Interpret/2. Data from the second drawdown period cannot be analyzed because of the DAS failure over the time period when the pumping rate was changed (Section 5.13). Figures 6-152 and 6-153 show the log-log and Horner plots, respectively, of the recovery data from WQSP-4 along with the best-fit Interpret/2 simulations.

The data were analyzed using a model for a well with wellbore storage and skin in a double-porosity medium with restricted interporosity flow and channel (parallel no-flow) boundaries. The medium has a transmissivity of 13 ft^2/d (1.4 x 10^{-5} m^2/s) and the well appears to have a slightly positive skin of 0.32. The channel boundaries are simulated at 1,040 and 1,190 ft (315 and 365 m) from WQSP-4. The simulated boundaries probably reflect gradual decreases in transmissivity to the east and west of WQSP-4 rather than discrete linear features. Other interpreted parameters are listed in Table 6-1. Figure 6-154 is a linear-linear plot of the match between this model and the combined drawdown and recovery data. The pumping periods are represented reasonably well by

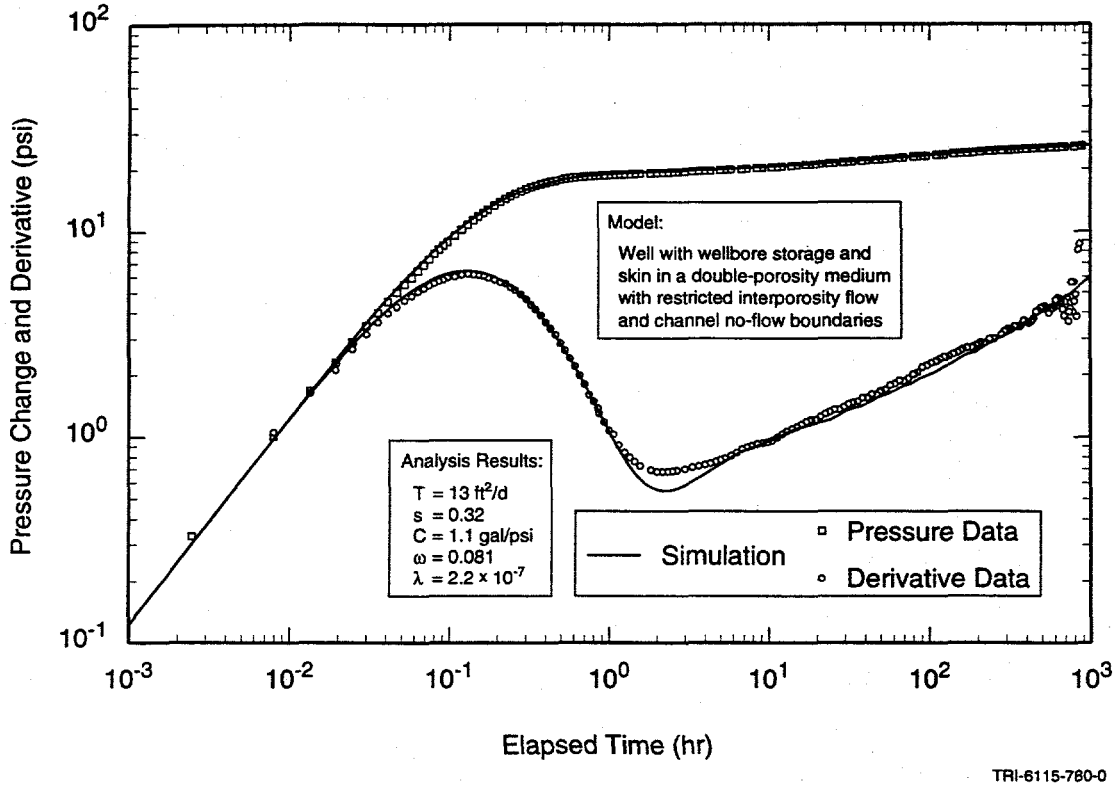

Figure 6-152. Log-log plot of WQSP-4 recovery data with Interpret/2 simulation.

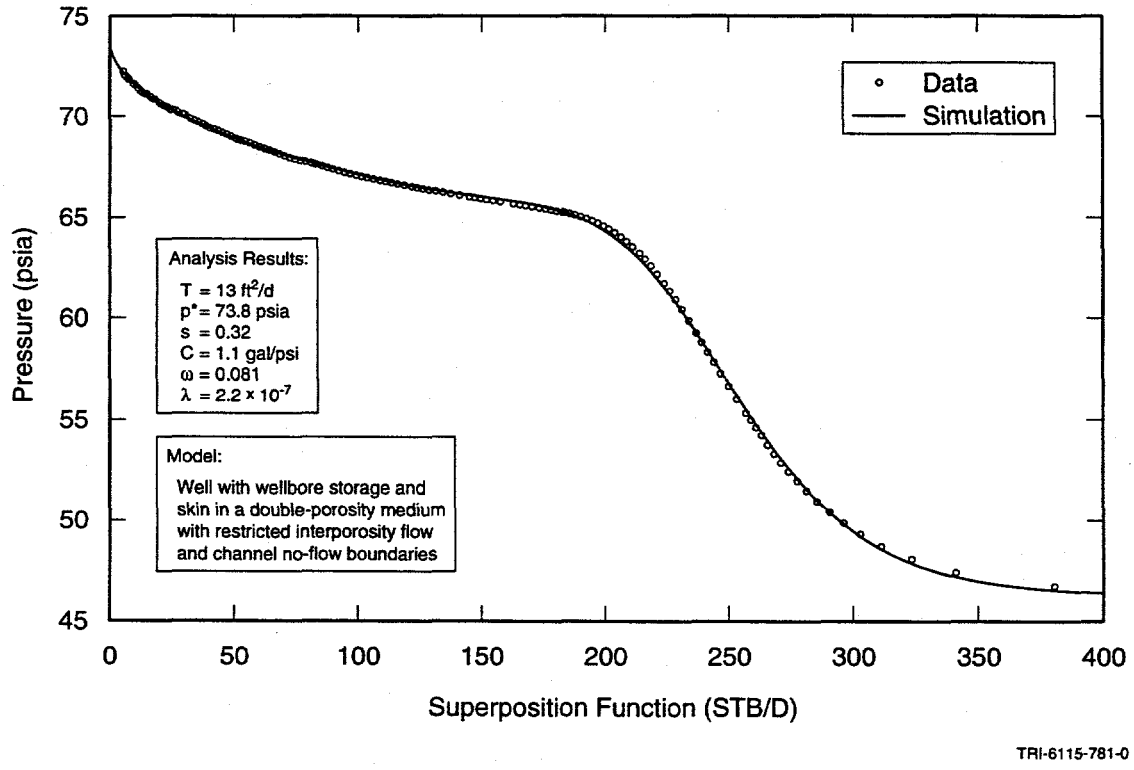

Figure 6-153. Horner plot of WQSP-4 recovery data with Interpret/2 simulation.

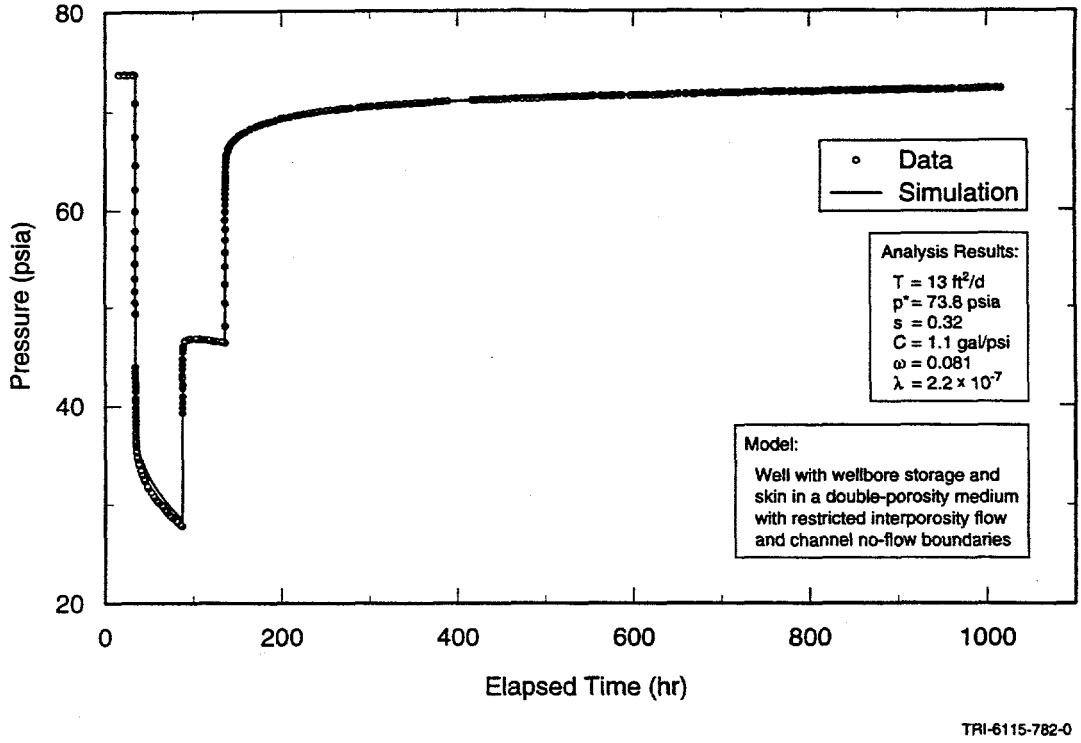

Figure 6-154. Linear-linear plot of WQSP-4 data with Interpret/2 simulation derived from recovery analysis.

the simulation. Interpret/2 simulations of the data from the first pumping period are shown in Appendix A (Figures A-43 through A-45).

6.14 WQSP-5 Pumping Test

The WQSP-5 pumping test involved several pumping episodes of a few minutes duration while adjusting the pump, followed by a 3.3-hr period of pumping at 1.55 gpm (0.10 L/s) and a 33-hr period of pumping at 0.80 gpm (0.05 L/s) (Section 5.14). Only the data from the recovery period after pumping are adequate for definitive determination of transmissivity. Figures 6-155 and 6-156 show the log-log and Horner plots, respectively, of the recovery data from WQSP-5 along with the best-fit Interpret/2 simulations. The data were analyzed using a model for a well with wellbore storage and skin in an infinite, homogeneous, single-porosity medium having a transmissivity of 1.2 ft^2/d (1.3 x 10^{-6} m^2/s). The well appears to have a slightly negative (-0.75) skin.

Even though the derivative stabilization level and, hence, transmissivity are well defined on Figure 6-155, the curvature of the pressure-derivative data could not be exactly matched using the single-porosity model. Because WQSP-5 is located between the two testing locations at which vertical heterogeneity in hydraulic properties has been observed, H-14 and H-19, we also attempted to match the data using a two-layer model. These efforts resulted in a similar estimate of transmissivity with no improvement in the derivative match. Therefore, the results from the simpler, single-porosity model are presented in this report. Figure 6-157 is a linear-linear plot of the match between this model and the combined drawdown and recovery data. The pumping periods are represented reasonably well by the simulation.

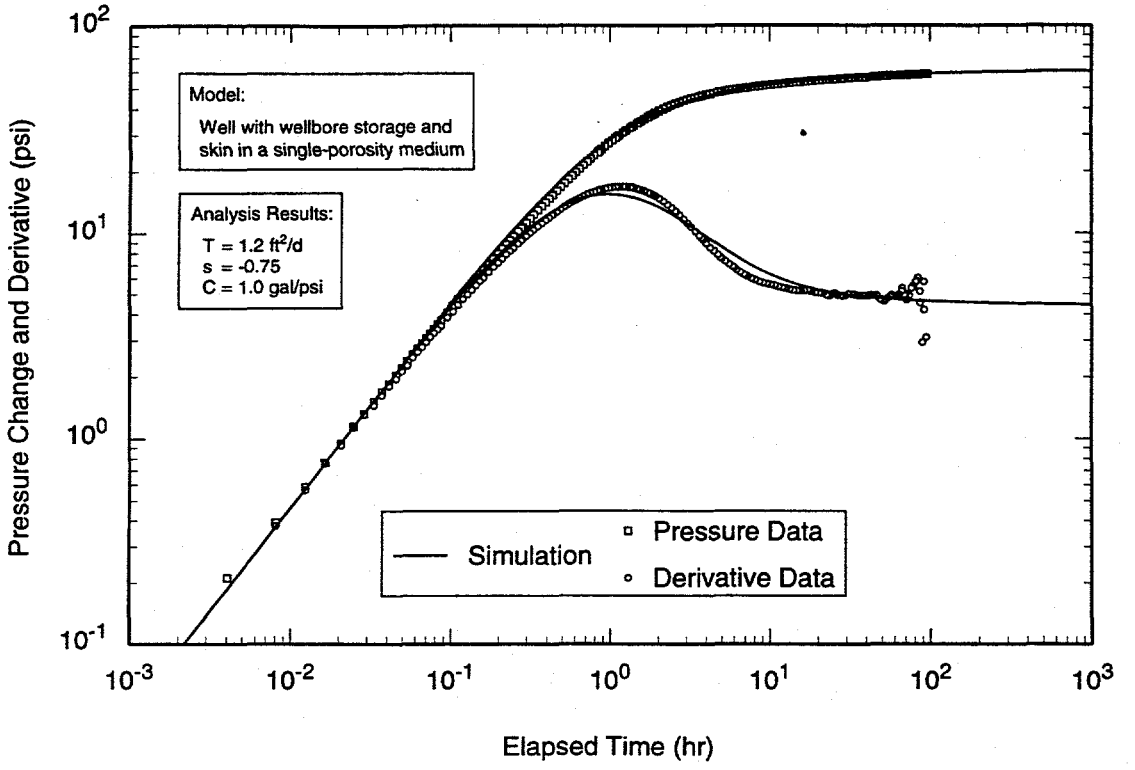

Figure 6-155. Log-log plot of WQSP-5 recovery data with Interpret/2 simulation.

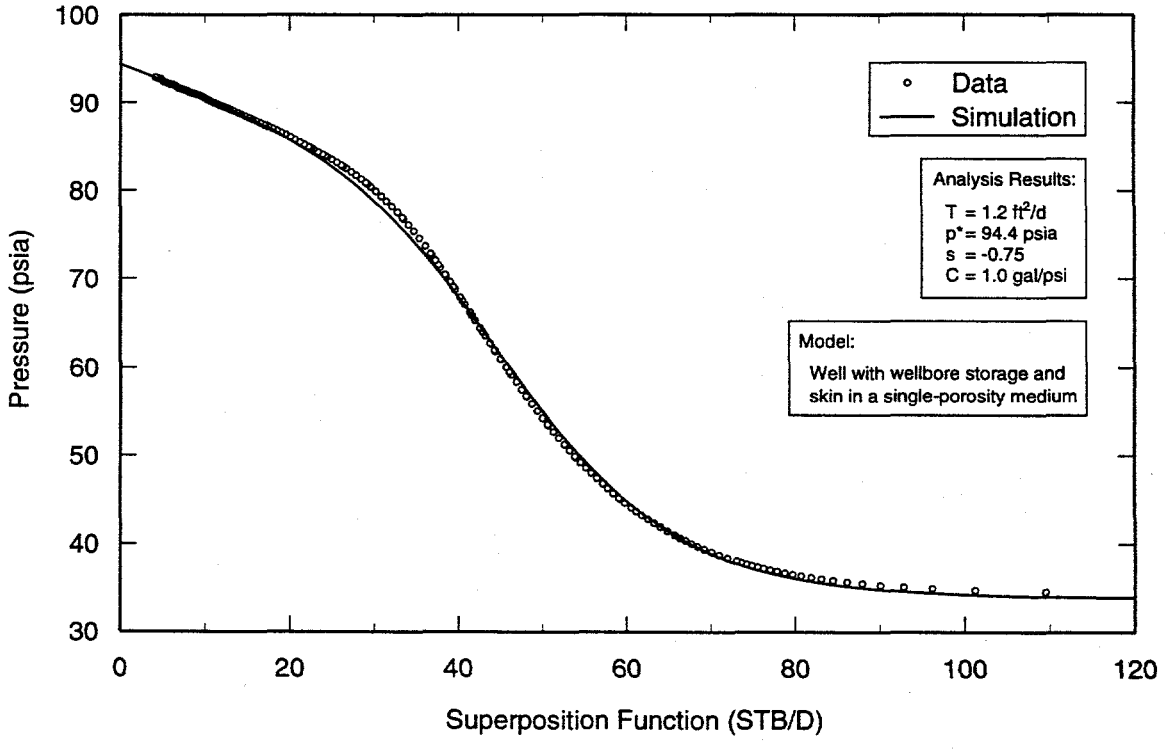

Figure 6-156. Horner plot of WQSP-5 recovery data with Interpret/2 simulation.

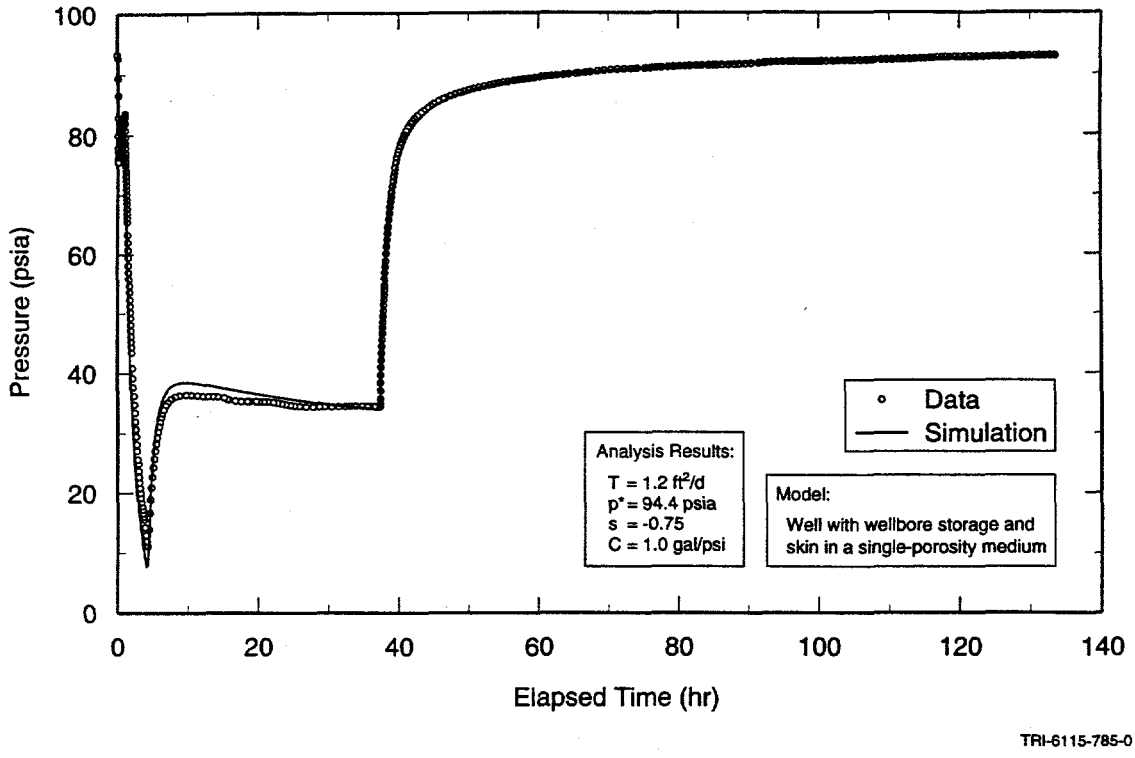

Figure 6-157. Linear-linear plot of WQSP-5 data with Interpret/2 simulation derived from recovery analysis.

6.15 WQSP-6 Pumping Test

As discussed in Section 5.15, the WQSP-6 pumping test involved an initial pumping period at a rate too high for the well to sustain. A recirculation loop was then set up in which water was pumped from the well at a rate that was possible for the pump and simply sent back down the well. After the pressure in the well approached equilibrium, a portion of the flow was diverted into a surface reservoir while the remainder was recirculated into the well. Even with only 0.34 gpm (0.021 L/s) being diverted at the surface, however, the well was nearly dewatered after approximately 22 hr. Consequently, the pumping period did not last long enough to provide data adequate for reliable estimation of transmissivity.

Figures 6-158 and 6-159 show the log-log and Horner plots, respectively, of the recovery data from WQSP-6 along with the best-fit Interpret/2 simulations. The data were analyzed using a model for a well with wellbore storage and skin in an infinite, homogeneous, single-porosity medium having a transmissivity of 0.25 ft^2/d (2.7 x 10^{-7} m^2/s). The well appears to have a negative skin of -1.9. Figure 6-160 is a linear-linear plot of the match between this model and the combined data from all pumping and recovery periods. All periods are represented reasonably well by the simulation.

6.16 WQSP-6A Pumping Test of the Dewey Lake Redbeds

The WQSP-6A pumping test was intended to provide data to estimate the transmissivity of the saturated portion of the Dewey Lake Redbeds open to the well. The electronic noise in the drawdown data from WQSP-6A (Figure 5-49) rendered the data uninterpretable using Interpret/2. The recovery data could not be analyzed because of the failure

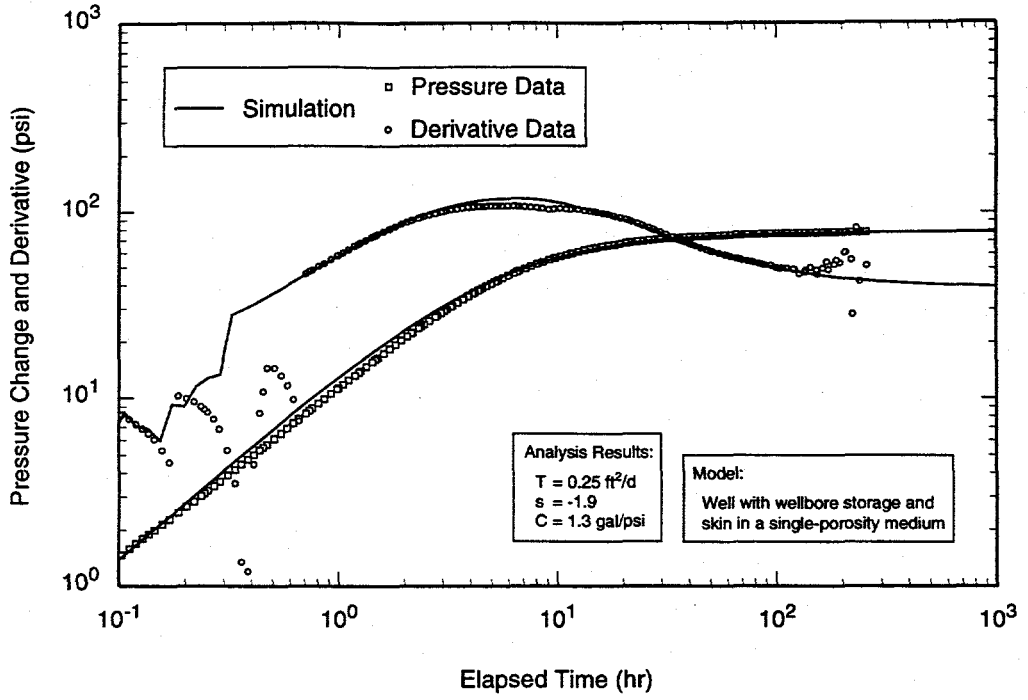

Figure 6-158. Log-log plot of WQSP-6 recovery data with Interpret/2 simulation.

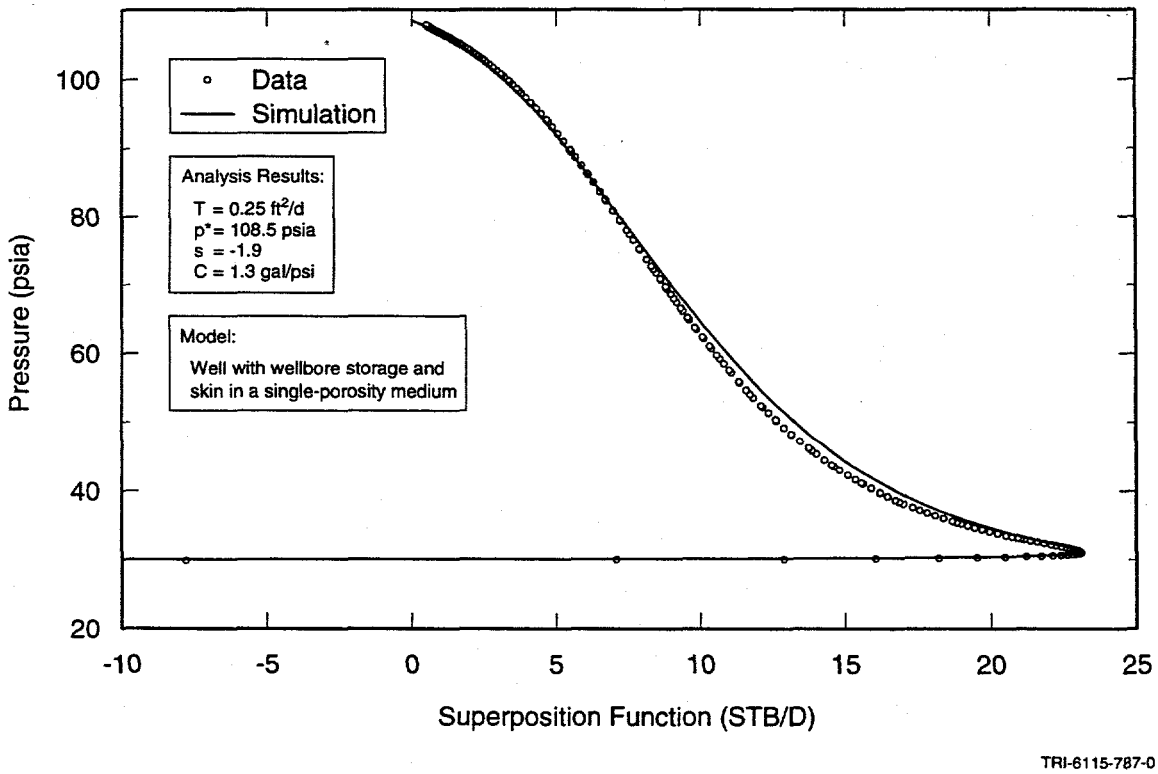

Figure 6-159. Horner plot of WQSP-6 recovery data with Interpret/2 simulation.

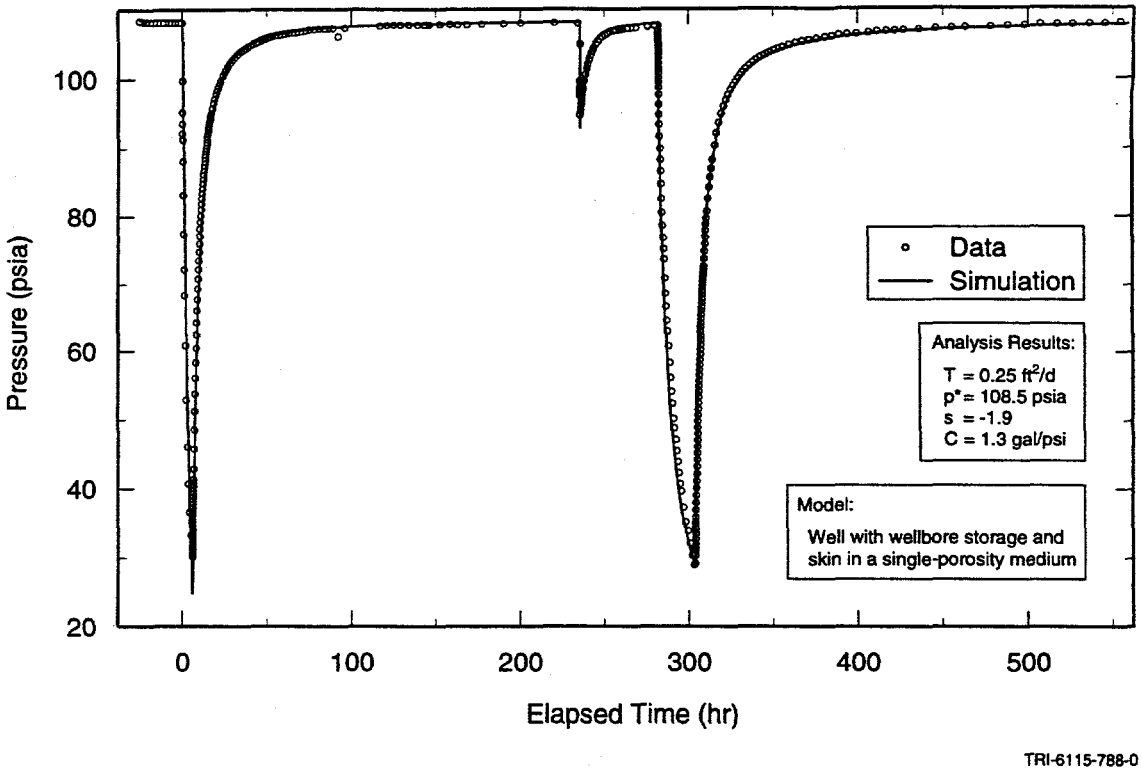

Figure 6-160. Linear-linear plot of WQSP-6 data with Interpret/2 simulation derived from recovery analysis.

of the check valves in the discharge line. Therefore, transmissivity was estimated from the specific capacity of the well. Driscoll (1986, p. 1021) relates the transmissivity of an unconfined aquifer to its specific capacity using the equation:

$$T = 1{,}500\ Q/s$$

where:

T = transmissivity (gpd/ft)
Q = pumping rate (gpm)
s = drawdown (ft)

The pumping rate during the WQSP-6A test was 12 gpm (0.76 L/s) and Figure 6-161 shows that the drawdown at the end of the pumping period was approximately 2.9 psi (20 kPa), which corresponds to approximately 6.7 ft (2.0 m) of fresh water. The transmissivity of the tested portion of the Dewey Lake, therefore, is approximately 2,700 gpd/ft, or 360 ft^2/d (3.9×10^{-4} m^2/s).

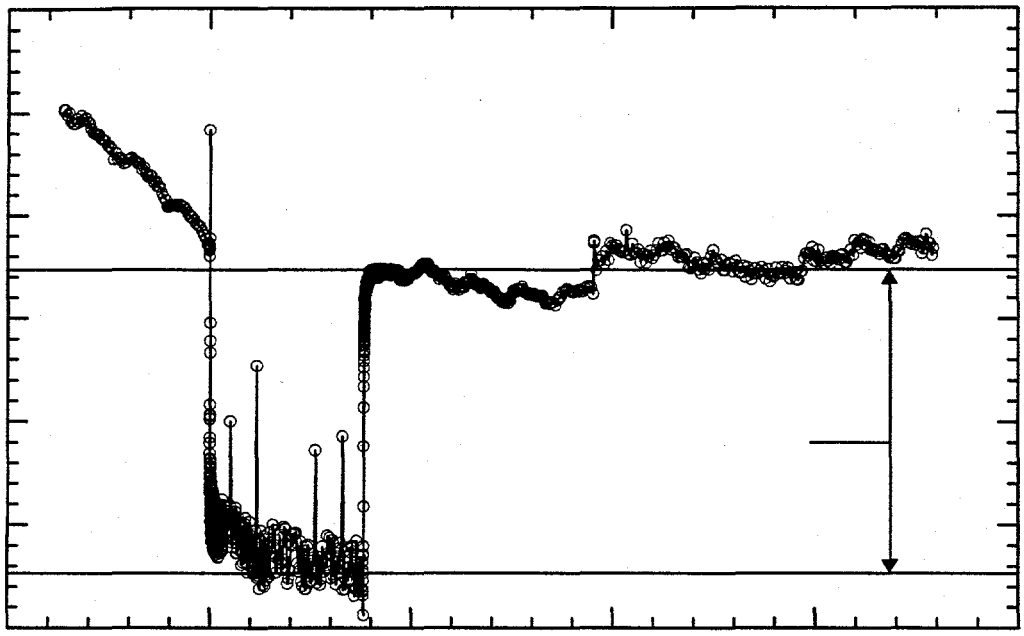

Figure 6-161. Linear-linear plot of WQSP-6A data showing drawdown used to estimate specific capacity.

This Page Intentionally Left Blank

7. SUMMARY AND CONCLUSIONS

This report presents interpretations/estimates of the hydraulic conditions and properties of the Culebra Dolomite Member of the Rustler Formation based on 21 tests conducted at 15 well locations. Hydraulic properties of the Magenta Member and Dewey Lake Redbeds have been estimated based on tests at single locations. These findings are discussed and summarized below in the context of the entire hydrogeologic database developed for these units at the WIPP site.

7.1 Culebra Dolomite Member

Spatial variations observed in Culebra hydraulic properties are discussed below in connection with geologic information and other modeling results.

7.1.1 Transmissivity

The transmissivity of the Culebra ranges from approximately 4×10^{-2} to 2×10^{3} ft^2/d (4×10^{-8} to 2×10^{-3} m^2/s) at the 15 test locations discussed in this report. The spatial distribution of these and previously reported transmissivity values is shown in Figure 7-1. Also shown on the figure are two lines: one representing the easternmost limit of dissolution of the upper Salado and one representing the western margin of halite in the unnamed lower member of the Rustler (Beauheim, 1987c). The five highest values of transmissivity are all associated with wells lying in the region where dissolution of the upper Salado has occurred: H-7, WIPP-27, USGS-1, P-14, and WIPP-28. Transmissivity is also relatively high at H-6, which lies very near the margin of upper Salado halite dissolution. Where dissolution of the upper Salado has occurred, the overlying rocks, including the Culebra, have collapsed and fractured. High Culebra transmissivities would, therefore, be expected in these locations. Transmissivity is also relatively high at H-9 and the Engle well, close to the Salado halite dissolution margin and west of the occurrence of halite in the unnamed lower member. According to the geologic model of Holt and Powers (1988), halite may originally have been deposited slightly beyond the present-day margin in the unnamed lower member and subsequently dissolved, causing collapse of the overlying Culebra.

Holt (1997) relates the remaining variation in Culebra transmissivity shown on Figure 7-1 to a variety of processes. He believes fracturing due to stress relief occurred in the Cenozoic as 1,150 to 2,130 ft (350 to 650 m) of overburden was eroded at the WIPP site. More fracturing occurred as the depth of burial of the Culebra decreased, imparting a general east-to-west (updip) trend of increasing fracturing and, hence, transmissivity, modified by processes discussed below. This fracturing tended to occur along bedding planes in the mechanically homogeneous upper Culebra (CU-1) and more randomly in the mechanically heterogeneous lower Culebra (Section 2). The pore waters that entered these fractures were saturated with gypsum, which precipitated and filled the fractures as they opened. Anhydrite nodules were also replaced with gypsum. Groundwater circulation is slow on the eastern side of the WIPP site and further east where the depth of the Culebra is greatest, and low-ionic-strength waters capable of dissolving gypsum have never reached some areas, leaving the Culebra with low transmissivity (e.g., at H-5, H-15, P-18, H-10). To the west of this zone, circulating groundwaters were undersaturated with respect to gypsum and fracture and pore fillings were dissolved, leading to additional small-scale fracturing as vugs (empty nodule spaces) collapsed (e.g., at DOE-1, DOE-2,

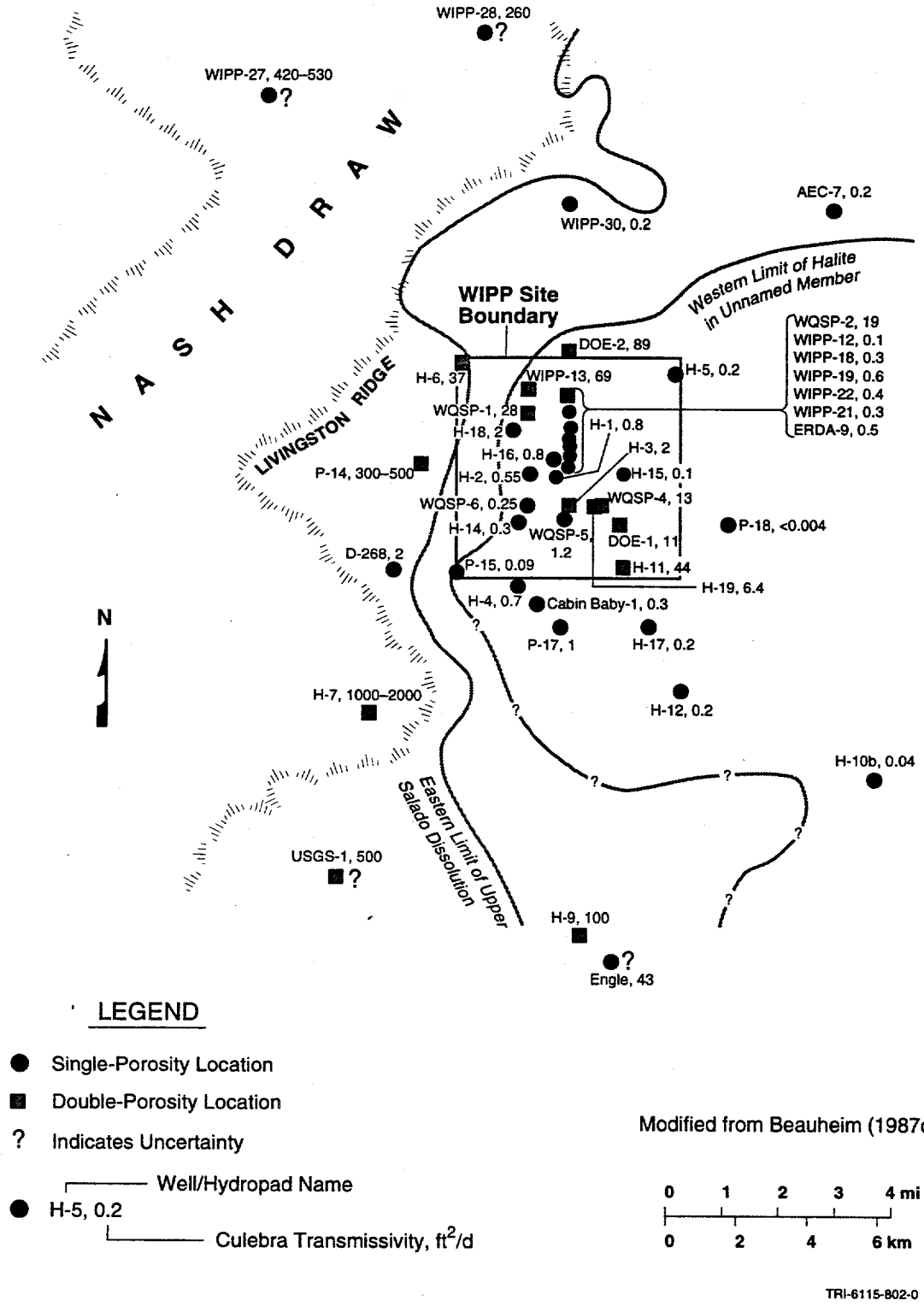

Figure 7-1. Distribution of Culebra transmissivity and halite margins around the WIPP site.

H-11, H-19, WIPP-13, WQSP-1, WQSP-2, WQSP-4). In parts of the western portion of the WIPP site, groundwater chemistry changed again and some fractures, pores, and vugs were filled once again with gypsum (e.g., at H-2, H-4, H-14, P-15, WQSP-6). Wells such as WQSP-5, D-268, and H-18 appear to lie in transitional areas in which most but not all fractures are filled with gypsum.

Double-porosity hydraulic behavior has been interpreted from tests conducted at 14 locations, indicated by square symbols in Figure 7-1. (Inclusion of USGS-1 is speculative; the actual test data are not available.) Tracer tests at the H-3, H-6, H-11, and H-19 hydropads have also been interpreted in terms of double-porosity, with most advective transport occurring through fractures while solutes diffuse between the fractures and matrix (Jones et al., 1992; Meigs et al., 1997). Transmissivities greater than approximately 2 ft^2/d (2 x 10^{-6} m^2/s) appear to be correlated with double-porosity conditions. Double-porosity hydraulic behavior reflects the dominance of open fractures in determining transmissivity. The slug tests conducted at WIPP-27 and WIPP-28 probably provided an inadequate determination of the presence or absence of double-porosity conditions, as discussed in Sections 6.9 and 6.10. The apparent single-porosity behavior observed at the Engle well may reflect inadequate well development (Beauheim, 1987c). Single-porosity hydraulic behavior is observed at the 26 wells indicated by circular symbols in Figure 7-1. At these locations, fractures are largely filled with gypsum.

7.1.2 Storativity

Storativity values were determined from hydropad-scale hydraulic responses at H-2, H-6, H-7, H-9, H-11, and H-19, and from responses over distances of up to 2.1 miles (3.4 km) when pumping H-9, P-14, WQSP-1, and WQSP-2 (Table 6-1). Of the hydropad-scale storativity values, those from H-2, H-11, and H-19 are the lowest: 1.5 x 10^{-5}, 4.5 x 10^{-5}, and 4.9 x 10^{-5}, respectively. The values from H-6 and H-9, where the Culebra may have been affected by dissolution of the unnamed lower member and/or upper Salado, are an order of magnitude higher: 1.8 x 10^{-4} and 5.6 x 10^{-4}, respectively. The value from H-7, where the Culebra has been affected by dissolution of the upper Salado and may be unconfined, is another order of magnitude higher: 6.4 x 10^{-3}.

The storativity values determined from responses over larger distances tend to be smaller. The response of the Engle well to pumping at H-9 indicates a storativity of 4.7 x 10^{-6}, two orders of magnitude lower than the hydropad-scale value from the same test. Geometric-mean storativity values from the P-14, WQSP-1, and WQSP-2 pumping tests are 1.6 x 10^{-5}, 1.9 x 10^{-5}, and 7.3 x 10^{-6}, respectively. These values probably reflect pressure-transient propagation through low-storage fractures over the distances involved.

7.1.3 Anisotropy

The data from testing at the H-6, H-9, and H-19 hydropads were analyzed to determine anisotropy at those locations. Anisotropy was found to be weak at all three locations, with the largest ratio of maximum to minimum transmissivity being 1.6 at H-6. The major axis of transmissivity is oriented N13°W at H-6. Within the uncertainty of the data, the Culebra appears to be isotropic at H-9. At H-19, the anisotropy ratio is approximately 1.2, with the major axis of transmissivity oriented N8°W.

Tracer-test data show that solute transport is more strongly directionally dependent than the interpretations of hydraulic anisotropy would indicate. Jones et al. (1992) inter-

preted convergent-flow tracer-test data from H-6 using a double-porosity model with a maximum-to-minimum transmissivity ratio of 7 and a major-axis orientation of N31°W. Tracer-test data from H-19 (Meigs et al., 1997) show that transport along flow paths with largely north-south orientations is more rapid than transport along flow paths with larger east-west components by a greater degree than would be predicted using an anisotropy ratio of only 1.2. At both hydropads, the direction of fastest transport can be predicted from the hydraulic anisotropy results, but the differences between flow paths would be underestimated. The hydraulic data used to interpret anisotropy reflect averaging of properties over an area much larger than an individual hydropad, whereas the tracer data are more representative of between-well properties. Also, tracer tests provide information that is inherently more sensitive to the orientation and value of extreme formation properties than the diffusive pressure-transmission process of a pumping test.

7.1.4 Heterogeneity (boundaries)

Interpretations of the tests at H-6, H-11, H-19, P-14, WQSP-1, WQSP-2, and WQSP-4 indicated that Culebra hydraulic properties are heterogeneous within the areas of influence of the tests. The H-6 test interpretations (Section 6.2) showed the effects of increased transmissivity within 1,200 ft (370 m) of the hydropad. Most likely, this represents increased transmissivity to the west (Figure 7-1), where dissolution of the upper Salado has led to collapse and fracturing of the Culebra, or to the east where higher transmissivities are found at DOE-2 and WIPP-13.

Heterogeneity was evident during the WQSP-2 pumping test (Section 6.12), as significant and rapid drawdowns were observed to the north and west of WQSP-2 at DOE-2, WIPP-13, WQSP-1, and H-18, while drawdowns in wells closer to WQSP-2 but to the south and east (WIPP-12, WIPP-18, WIPP-19, and WQSP-3) were of lower magnitude and slower (or nonexistent). These differences reflect the relatively high transmissivities to the north and west of WQSP-2 and the relatively low transmissivities to the south and east (Figure 7-1).

Interpretations of the H-18 recovery response from pumping at WQSP-1 indicated the presence of lower transmissivity within the region affected by the test, although this was not evident from either the WQSP-1 drawdown response or the WIPP-13 response (Section 6.11). This difference is probably due to H-18 lying close to, if not within, the area of low transmissivity south of WQSP-1. In addition, drawdowns at H-18 and WIPP-13 were of similar magnitude during the WQSP-1 test with the WIPP-13 response being "sharper" than the H-18 response, even though WIPP-13 is more than twice as far from WQSP-1 as is H-18 (Figure 3-30). This pattern of responses is also indicative of higher transmissivity to the north of WQSP-1 than to the south.

Interpretations of tests at H-11, WQSP-4, and P-14 indicated the presence of lower transmissivity on two sides of those wells (channel boundaries). For H-11 and WQSP-4, these boundaries probably reflect lower transmissivities to the east, as exemplified by P-18, and lower transmissivities to the west, as at WQSP-5. Because of the close proximity of WQSP-4 and H-19, similar boundary effects should be evident in test data from both locations. The extreme late-time data from H-19b4 and H-19b6 (Section 6.7.3.2) showed the effects of lower transmissivity which may have been manifested in the responses of the other H-19 wells at a later time. The apparent boundaries near P-14 probably represent lower transmissivity to the east and south.

These interpretations are all qualitatively consistent with the results of modeling of the Culebra flow system at the WIPP site. LaVenue et al. (1995) created 70 realizations of the spatial distribution of Culebra transmissivity by calibrating a flow model to estimated steady-state hydraulic heads and transient heads resulting from long-term pumping tests and leakage into WIPP shafts. The ensemble average of the 70 realizations shows transmissivity changes in the vicinities of the tested wells discussed above consistent with the interpreted hydraulic boundaries (Figure 7-2).

7.2 Magenta Member

The estimated transmissivity of the Magenta at H-19b1 is 0.38 ft^2/d (4.1 x 10^{-7} m^2/s). This value is slightly higher than the 0.3 ft^2/d (3 x 10^{-7} m^2/s) reported from H-6a (Dennehy, 1982), which had heretofore been the highest Magenta transmissivity reported on the WIPP site (Beauheim and Holt, 1990). We believe the relatively high transmissivity is related to the poorly consolidated nature of the middle and lower portions of the Magenta at H-19b1. Even so, the Magenta transmissivity at H-19 is much lower than that of the Culebra, just as has been observed at all other testing locations.

7.3 Dewey Lake Redbeds

A saturated portion of the upper Dewey Lake was tested in well WQSP-6A, which is located 0.44 mile (0.71 km) southwest of the WIPP disposal panels. Transmissivity is estimated to be approximately 360 ft^2/d (3.9 x 10^{-4} m^2/s) from specific-capacity data. A zone of open fractures, believed to be the most transmissive interval open to the well, was observed from approximately 184 to 208 ft (56.1 to 63.4 m) BGS (3153 to 3177 ft [961.0 to 968.3 m] amsl) in a video log. The stabilized water level in WQSP-6A is approximately 162 ft (49.4 m) BGS (3199 ft [975.1 m] amsl; Jones, 1997), 22 ft (6.7 m) above the point at which it was first observed during drilling. A water level higher than the level at which water is first observed flowing into a well could indicate confined conditions, but we believe that the permeability of unfractured Dewey Lake is too low to produce appreciable water and that the presence of water is simply not noticed until high-permeability fractures are encountered. Thus, we believe that the water observed in the Dewey Lake at WQSP-6A exists under water-table conditions.

This water table may continue to the south from WQSP-6A, as water was encountered in the Dewey Lake at similar elevations during the drilling of P-9 on the present-day H-11 hydropad (Jones, 1978) and of Cabin Baby-1 (Beauheim et al., 1983). Water was noted in P-9 when drilling reached a depth of 220 ft (67.1 m) BGS (3189 ft [972.0 m] amsl); no water level was measured. Water was first observed in Cabin Baby-1 when drilling reached a depth of 190 ft (57.9 m) BGS (3137 ft [956.2 m] amsl) and the water level was later measured to be 140 ft (42.7 m) BGS (3187 ft [971.4 m] amsl).

Observations made at H-1 and the H-2 and H-3 hydropads (Figure 1-3), however, show that the water table does not continue to the north and east over the WIPP disposal panels. H-1, H-2a, H-2b, H-2c, and H-3b1 were all drilled using compressed air as the circulation medium. Moisture was detected in the drill cuttings from all five wells at depths ranging from 175 to 185 ft (53.3 to 56.4 m) BGS, but no water collected in the holes during five- to nine-hr waiting periods (Mercer and Orr, 1979). While drilling well H-3d in April 1987, drilling-fluid circulation was lost at

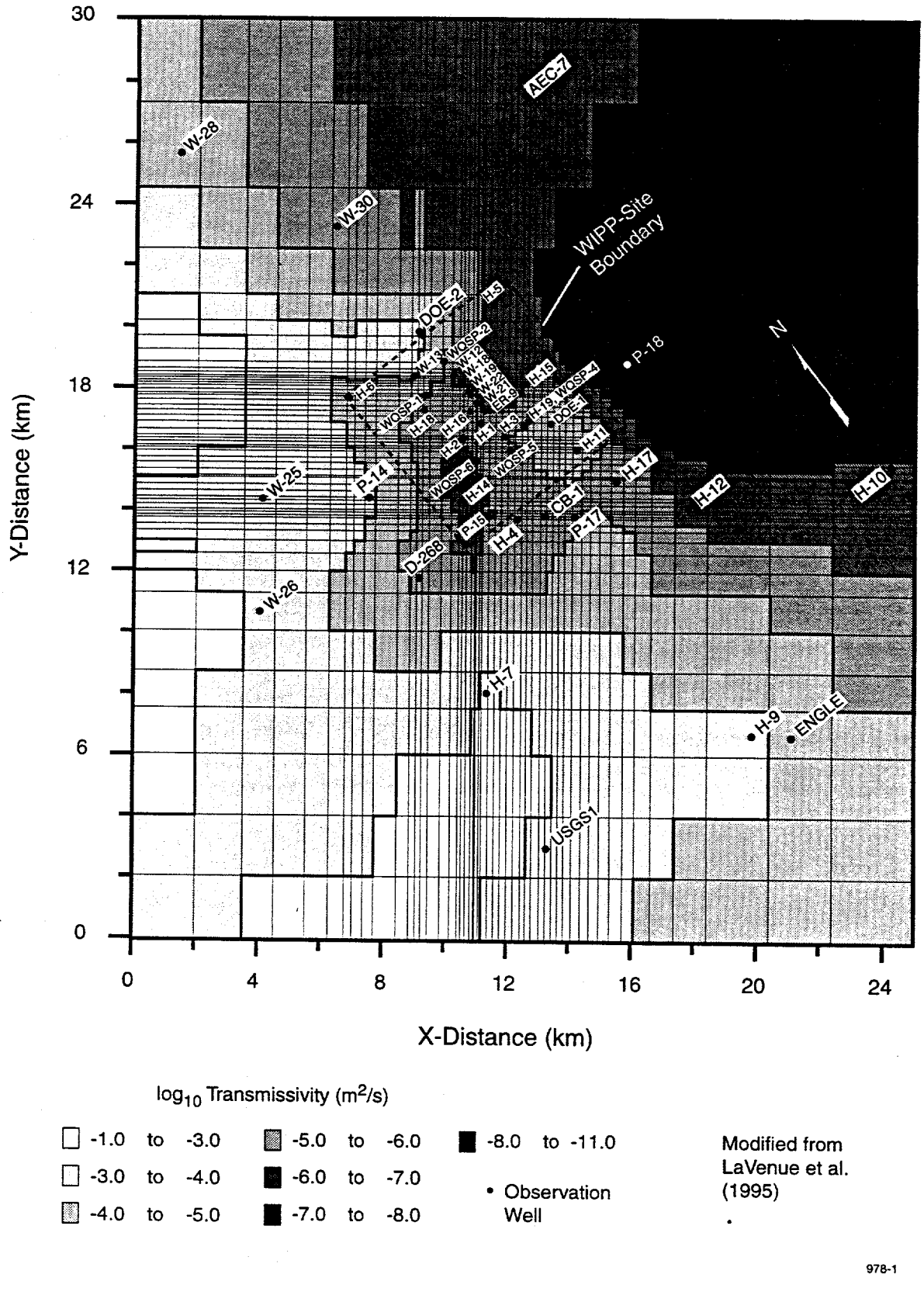

Figure 7-2. Ensemble average of calibrated Culebra transmissivity fields.

a depth of 169.5 ft (51.7 m) BGS (3219 ft [981.2 m] amsl). After the hole was completed in the Forty-niner Member of the Rustler Formation, fluid was evacuated from the hole with compressed air. Video logging then showed water draining into the hole from fractures at the depth where circulation was lost. The water level reached a peak of 285 ft (86.9 m) BGS, 115 ft (35.1 m) below the level of the fractures, in June 1987 (Stensrud et al., 1988) and has been declining ever since. Thus, we conclude that the water observed draining from the fractures was lost drilling fluid and that the fractures were originally, and are again, unsaturated. The slow decline in the water level observed over the past ten years probably reflects water seeping into the lower, tightly cemented portion of the Dewey Lake. If a water table exists in the lower Dewey Lake at H-3d, it must be deeper than 317 ft (96.6 m) BGS (3072 ft [936.3 m] amsl), the water level measured in August 1997 (Jones, 1997).

7.4 Conclusions

This report completes documentation of hydraulic-test interpretations used as input to the WIPP Compliance Certification Application (US DOE, 1996). Interpretations are presented for 21 tests of the Culebra Dolomite Member of the Rustler Formation conducted at 15 well locations near the WIPP site, one test of the Magenta Member, and one test of the Dewey Lake Redbeds. These tests were conducted between 1980 and 1996. Slug tests were performed at three of the Culebra sites (H-10, WIPP-27, and WIPP-28) and at the Magenta site (H-19b1). Five single-well pumping tests were performed, four at Culebra sites (H-19b2, WQSP-4, WQSP-5, and WQSP-6) and one at the Dewey Lake site (WQSP-6A). Multiwell pumping tests of the Culebra were conducted on the H-2, H-6, H-7, H-9, H-11, and H-19 hydropads, where well spacings vary between 36 and 141 ft (11 and 43 m). Interpretable responses to pumping tests at H-9, P-14, WQSP-1, and WQSP-2 were monitored at wells 1,295 to 11,125 ft (395 to 3,390 m) away.

The transmissivity of the Culebra ranges from approximately 4×10^{-2} to 2×10^{3} ft^2/d (4×10^{-8} to 2×10^{-3} m^2/s) at the tested locations. The Culebra behaves hydraulically as a double-porosity medium at nine of the locations, where open fractures are thought to dominate hydraulic responses. The slug-test data from WIPP-27 and WIPP-28 are inadequate for differentiation of single- from double-porosity behavior. At the four locations where the Culebra transmissivity is 1.2 ft^2/d (1.3×10^{-6} m^2/s) or lower, the Culebra responds as a single-porosity medium. Culebra storativity was found to range from 4.7×10^{-6} to 6.4×10^{-3}. The ratio of maximum to minimum Culebra transmissivity was found to be 1.6 or lower at three tested locations, reflecting little to no hydraulic anisotropy, although transport anisotropy determined from tracer tests is significant. Hydraulic boundaries or other evidence of heterogeneity in hydraulic properties were indicated by the responses observed during testing at seven of the high-transmissivity, double-porosity locations.

The transmissivity of the Magenta at H-19b1 is 0.38 ft^2/d (4.1×10^{-7} m^2/s), the highest value yet encountered on the WIPP site. However, as at all other locations where both the Culebra and Magenta have been tested, the transmissivity of the Magenta is much lower than that of the Culebra at H-19.

The transmissivity of a saturated fractured zone within the upper Dewey Lake Redbeds at WQSP-6A, 0.44 mile (0.71 km) southwest of the WIPP disposal panels, is estimated to be approximately 360 ft^2/d (3.9×10^{-4} m^2/s). This zone of saturation appears to extend south of WQSP-6A, but not to the northeast over the disposal panels.

This Page Intentionally Left Blank

8. REFERENCES

Basler, J.A. 1983. *Instrumentation Used for Hydraulic Testing of Potential Water-Bearing Formations at the Waste Isolation Pilot Plant Site in Southeastern New Mexico.* Open-File Report 83-144. Albuquerque, NM: USGS.

Beauheim, R.L. 1986. *Hydraulic-Test Interpretations for Well DOE-2 at the Waste Isolation Pilot Plant (WIPP) Site.* SAND86-1364. Albuquerque, NM: Sandia National Laboratories.

Beauheim, R.L. 1987a. *Analysis of Pumping Tests of the Culebra Dolomite Conducted at the H-3 Hydropad at the Waste Isolation Pilot Plant (WIPP) Site.* SAND86-2311. Albuquerque, NM: Sandia National Laboratories.

Beauheim, R.L. 1987b. *Interpretation of the WIPP-13 Multipad Pumping Test of the Culebra Dolomite at the Waste Isolation Pilot Plant (WIPP) Site.* SAND87-2456. Albuquerque, NM: Sandia National Laboratories.

Beauheim, R.L. 1987c. *Interpretations of Single-Well Hydraulic Tests Conducted At and Near the Waste Isolation Pilot Plant (WIPP) Site, 1983-1987.* SAND87-0039. Albuquerque, NM: Sandia National Laboratories.

Beauheim, R.L. 1989. *Interpretation of H-11b4 Hydraulic Tests and the H-11 Multipad Pumping Test of the Culebra Dolomite at the Waste Isolation Pilot Plant (WIPP) Site.* SAND89-0536. Albuquerque, NM: Sandia National Laboratories.

Beauheim, R.L., and R.M. Holt. 1990. "Hydrogeology of the WIPP Site," *Geological and Hydrological Studies of Evaporites in the Northern Delaware Basin for the Waste Isolation Pilot Plant (WIPP), New Mexico, GSA Field Trip #14 Guidebook.* Dallas, TX: Dallas Geological Society. 131-179.

Beauheim, R.L., B.W. Hassinger, and J.A. Klaiber. 1983. *Basic Data Report for Borehole Cabin Baby-1 Deepening and Hydrologic Testing.* WTSD-TME-020. Albuquerque, NM: US DOE Waste Isolation Pilot Plant. (Available from the NTIS as DE86004332/XAB.)

Beauheim, R.L., T.F. Dale, and J.F. Pickens. 1991. *Interpretations of Single-Well Hydraulic Tests of the Rustler Formation Conducted in the Vicinity of the Waste Isolation Pilot Plant Site, 1988-1989.* SAND89-0869. Albuquerque, NM: Sandia National Laboratories.

Beauheim, R.L., L.C. Meigs, G.J. Saulnier, Jr., and W.A. Stensrud. 1995. "Culebra Transport Program Test Plan: Tracer Testing of the Culebra Dolomite Member of the Rustler Formation at the H-19 and H-11 Hydropads on the WIPP Site." Albuquerque, NM: Sandia National Laboratories. (On file in the SWCF under WPO#30156.)

Black, S.R. 1982. *Basic Data Report Borehole WIPP-12 Deepening.* TME 3148. Albuquerque, NM: US DOE. (Available from the NTIS as DE86004343/XAB.)

Bourdet, D., J.A. Ayoub, and Y.M. Pirard. 1989. "Use of Pressure Derivative in Well-Test Interpretation," *SPE Formation Evaluation.* Vol. 4, no. 2, 293-302.

Cauffman, T.L., A.M. LaVenue, and J.P. McCord. 1990. *Ground-Water Flow Modeling of the Culebra Dolomite, Volume II: Data Base.* SAND89-7068/2. Albuquerque, NM: Sandia National Laboratories.

Cooper, H.H., Jr., J.D. Bredehoeft, and I.S. Papadopulos. 1967. "Response of a Finite-Diameter Well to an Instantaneous Charge of Water," *Water Resources Research.* Vol. 3, no. 1, 263-269.

Dennehy, K.F. 1982. *Results of Hydrologic Tests and Water-Chemistry Analyses, Wells H-6A, H-6B, and H-6C, at the Proposed Waste Isolation Pilot Plant Site, Southeastern New Mexico.* Water-Resources Investigations Report 82-8. Albuquerque, NM: USGS.

Domenico, P.A., and F.W. Schwartz. 1990. *Physical and Chemical Hydrogeology.* New York: John Wiley & Sons Inc.

Drellack, S.L., Jr., and J.G. Wells. 1982a. *Geologic and Well-Construction Data for the H-7 Borehole Complex Near the Proposed Waste Isolation Pilot Plant Site, Southeastern New Mexico.* Water-Resources Investigations Report 82-38. Albuquerque, NM: USGS.

Drellack, S.L., Jr., and J.G. Wells. 1982b. *Geologic and Well-Construction Data for the H-9 Borehole Complex Near the Proposed Waste Isolation Pilot Plant Site, Southeastern New Mexico.* Water-Resources Investigations Report 82-4111. Albuquerque, NM: USGS.

Driscoll, F.G. 1986. *Groundwater and Wells.* 2nd ed. St. Paul, MN: Johnson Division.

Ehlig-Economides, C. 1988. "Use of the Pressure Derivative for Diagnosing Pressure-Transient Behavior," *JPT, Journal of Petroleum Technology.* Vol. 40, no. 10, 1280-1282.

Gonzales, M.M. 1989. *Compilation and Comparison of Test-Hole Location Surveys in the Vicinity of the Waste Isolation Pilot Plant Site.* SAND88-1065. Albuquerque, NM: Sandia National Laboratories.

Gonzalez, D.D. 1981. "Field Operations Plan of Sandia Laboratories WIPP Site Investigations WIPP Tracer Program." Albuquerque, NM: Sandia National Laboratories. (On file in the SWCF under WPO#1871.)

Gonzalez, D.D. 1983. *Groundwater Flow in the Rustler Formation, Waste Isolation Pilot Plant (WIPP), Southeast New Mexico (SENM): Interim Report.* SAND82-1012. Albuquerque, NM: Sandia National Laboratories.

Grimestad, G. 1995. "Analysis of Data from Pumping Tests in Anisotropic Aquifers: Equations and Graphical Solutions," *Water Resources Research.* Vol. 31, no. 4, 933-941.

Gringarten, A.C. 1984. "Interpretation of Tests in Fissured and Multilayered Reservoirs With Double-Porosity Behavior: Theory and Practice," *JPT, Journal of Petroleum Technology.* Vol. 36, no. 4, 549-564.

Gringarten, A.C. 1987. "How To Recognize 'Double-Porosity' Systems From Well Tests," *JPT, Journal of Petroleum Technology.* Vol. 39, no. 6, 631-633.

Holt, R.M. 1997. *Conceptual Model for Transport Processes in the Culebra Dolomite Member, Rustler Formation.* SAND97-0194. Albuquerque, NM: Sandia National Laboratories.

Holt, R.M., and D.W. Powers. 1990. *Geologic Mapping of the Air Intake Shaft at the Waste Isolation Pilot Plant.* DOE/WIPP 90-051. Carlsbad, NM: Westinghouse Electric Corporation for the US DOE.

Horner, D.R. 1951. "Pressure Build-Up in Wells," *Proceedings of the Third World Petroleum Congress, The Hague, Netherlands, May 29, 1951.* Leiden, The Netherlands: E.J. Brill. Sec. II, 503-523. Reprinted 1967. *Pressure Analysis Methods.* SPE Reprint Series Vol. 9. New York, NY: American Institute of Mining, Metallurgical and Petroleum Engineers, Inc. 25-43.

Hydro Geo Chem, Inc. 1985. *WIPP Hydrology Program, Waste Isolation Pilot Plant, SENM, Hydrologic Data Report #1.* SAND85-7206. Albuquerque, NM: Sandia National Laboratories.

Hydro Geo Chem, Inc. 1986. *Two-Well Recirculation Tracer Tests at the H-2 Hydropad, Waste Isolation Pilot Plant (WIPP), Southeastern New Mexico.* SAND86-7092. Albuquerque, NM: Sandia National Laboratories.

INTERA Technologies, Inc. 1986a. *WIPP Hydrology Program, Waste Isolation Pilot Plant, Southeastern New Mexico, Hydrologic Data Report #3.* SAND86-7109. Albuquerque, NM: Sandia National Laboratories.

INTERA Technologies, Inc. 1986b. "Field Operations Plan for the H-7 Hydropad Pumping Test at the WIPP Site." Albuquerque, NM: Sandia National Laboratories. (On file in the SWCF under WPO#2747.)

INTERA Technologies, Inc. 1986c. "Field Operations Plan for Hydrologic Testing at P-14, P-15, P-17, H-14, H-15, ERDA-9, and Cabin Baby-1." Albuquerque, NM: Sandia National Laboratories. (On file in the SWCF under WPO#3188.)

INTERA Technologies, Inc. and Hydro Geo Chem, Inc. 1985. *WIPP Hydrology Program, Waste Isolation Pilot Plant, Southeastern New Mexico, Hydrologic Data Report #2.* SAND85-7263. Albuquerque, NM: Sandia National Laboratories.

Johns, R.T., and Y. Jalali-Yazdi. 1991. "Comparison of Pressure-Transient Response in Intensely and Sparsely Fractured Reservoirs," *SPE Formation Evaluation.* Vol. 6, no. 4, 513-518.

Jones, C.L. 1978. *Test Drilling for Potash Resources: Waste Isolation Pilot Plant Site, Eddy County, New Mexico.* Open-File Report 78-592, 2 vols. Denver, CO: USGS.

Jones, S.B. 1997. "Transmittal of the Groundwater Level Data for August 1997." Memo to Les Hill dated August 29, 1997. Carlsbad, NM: Westinghouse Electric Corporation, Waste Isolation Division. (Copy on file in the SWCF under WPO#48021.)

Jones, T.L., V.A. Kelley, J.F. Pickens, D.T. Upton, R.L. Beauheim, and P.B. Davies. 1992. *Integration of Interpretation Results of Tracer Tests Performed in the Culebra Dolomite at the Waste Isolation Pilot Plant Site.* SAND92-1579. Albuquerque, NM: Sandia National Laboratories.

Kelley, V.A., and J.F. Pickens. 1986. *Interpretation of the Convergent-Flow Tracer Tests Conducted in the Culebra Dolomite at the H-3 and H-4 Hydropads at the Waste Isolation Pilot Plant (WIPP) Site.* SAND86-7161. Albuquerque, NM: Sandia National Laboratories.

LaVenue, A.M., B.S. RamaRao, G. de Marsily, and M.G. Marietta. 1995. "Pilot Point Methodology for Automated Calibration of an Ensemble of Conditionally Simulated Transmissivity Fields, 2. Application," *Water Resources Research.* Vol. 31, no. 3, 495-516.

Meigs, L.C., R.L. Beauheim, J.T. McCord, Y.W. Tsang, and R. Haggerty. 1997. "Design, Modelling, and Current Interpretations of the H-19 and H-11 Tracer Tests at the WIPP Site," *Field Tracer Experiments: Role in the Prediction of Radionuclide Migration, Synthesis and Proceeding of an NEA/EC GEOTRAP Workshop, Cologne, Germany, 28-30 August 1996.* Paris, France: OECD NEA. 157-169.

Mercer, J.W. 1983. *Geohydrology of the Proposed Waste Isolation Pilot Plant Site, Los Medaños Area, Southeastern New Mexico.* Water-Resources Investigations Report 83-4016. Albuquerque, NM: USGS.

Mercer, J.W. 1990. *Basic Data Report for Drillholes at the H-11 Complex (Waste Isolation Pilot Plant - WIPP).* SAND89-0200. Albuquerque, NM: Sandia National Laboratories.

Mercer, J.W., and B.R. Orr. 1979. *Interim Data Report on the Geohydrology of the Proposed Waste Isolation Pilot Plant Site, Southeast New Mexico.* Water-Resources Investigations Report 79-98. Albuquerque, NM: USGS.

Mercer, J.W., and R.P. Snyder. 1990. *Basic Data Report for Drillholes H-17 and H-18 (Waste Isolation Pilot Plant - WIPP).* SAND89-0204. Albuquerque, NM: Sandia National Laboratories.

Mercer, J.W., R.L. Beauheim, R.P. Snyder, and G.M. Fairer. 1987. *Basic Data Report for Drilling and Hydrologic Testing of Drillhole DOE-2 at the Waste Isolation Pilot Plant (WIPP) Site.* SAND86-0611. Albuquerque, NM: Sandia National Laboratories.

Mercer, J.W., D.L. Cole, and R.M. Holt. 1998. *Basic Data Report for Drillholes on the H-19 Hydropad (Waste Isolation Pilot Plant - WIPP).* SAND98-0071. Albuquerque, NM: Sandia National Laboratories.

Neuman, S.P. 1975. "Analysis of Pumping Test Data From Anisotropic Unconfined Aquifers Considering Delayed Gravity Response," *Water Resources Research.* Vol. 11, no. 2, 329-342.

Neuman, S.P., G.R. Walter, H.W. Bentley, J.J. Ward, and D.D. Gonzalez. 1984. "Determination of Horizontal Aquifer Anisotropy with Three Wells," *Ground Water.* Vol. 22, no. 1, 66-72.

Pickens, J.F., G.E. Grisak, J.D. Avis, D.W. Belanger, and M. Thury. 1987. "Analysis and Interpretation of Borehole Hydraulic Tests in Deep Boreholes: Principles, Model Development, and Applications," *Water Resources Research.* Vol. 23, no. 7, 1341-1375.

Randall, W.S., M.E. Crawley, and M.L. Lyon. 1988. *Annual Water Quality Data Report for the Waste Isolation Pilot Plant, May 1988.* DOE/WIPP-88-006. Carlsbad, NM: Westinghouse Electric Corporation for the US DOE.

Richey, S.F. 1986. *Hydrologic-Test Data from Wells at Hydrologic-Test Pads H-7, H-8, H-9, and H-10 Near the Proposed Waste Isolation Pilot Plant Site, Southeastern New Mexico.* Open-File Report 86-413. Albuquerque, NM: USGS.

Richey, S.F. 1987. *Preliminary Hydrologic Data for Wells Tested in Nash Draw, Near the Proposed Waste Isolation Pilot Plant Site, Southeastern New Mexico.* Open-File Report 87-37. Albuquerque, NM: USGS.

Robinson, T.W. 1939. "Earth-Tides Shown by Fluctuations of Water-Levels in Wells in New Mexico and Iowa," *Transactions of 1939, American Geophysical Union.* Vol. 20, 656-666.

Ruskauff, G.J. 1996. "Sandia National Laboratories Waste Isolation Pilot Plant Analysis Plan 007: Analysis Plan for Hydraulic-Test Interpretation." Albuquerque, NM: Sandia National Laboratories. (On file in the SWCF under WPO#37260.)

Sandia National Laboratories and D'Appolonia Consulting Engineers. 1982. *Basic Data Report for Deepening of Drillhole WIPP 13 (Waste Isolation Pilot Plant - WIPP).* SAND82-1880. Albuquerque, NM: Sandia National Laboratories.

Sandia National Laboratories and U.S. Geological Survey. 1979a. *Basic Data Report for Drillhole WIPP 25 (Waste Isolation Pilot Plant - WIPP).* SAND79-0279. Albuquerque, NM: Sandia National Laboratories.

Sandia National Laboratories and U.S. Geological Survey. 1979b. *Basic Data Report for Drillhole WIPP 27 (Waste Isolation Pilot Plant - WIPP).* SAND79-0281. Albuquerque, NM: Sandia National Laboratories.

Sandia National Laboratories and U.S. Geological Survey. 1979c. *Basic Data Report for Drillhole WIPP 28 (Waste Isolation Pilot Plant - WIPP).* SAND79-0282. Albuquerque, NM: Sandia National Laboratories.

Saulnier, G.J., Jr., and R.L. Beauheim. 1995. "Culebra Transport Program Field Operations Plan: Well Construction and Preliminary Testing on the H-19 Hydropad at the WIPP Site." Albuquerque, NM: Sandia National Laboratories. (On file in the SWCF under WPO#20256.)

Savage, G.J., and H.K. Kesavan. 1979. "The Graph-Theoretic Field Model--1. Modelling and Formulations," *Journal of the Franklin Institute.* Vol. 307, no. 2, 107-147.

Seward, P.D., comp. 1982. *Abridged Borehole Histories for the Waste Isolation Pilot Plant (WIPP) Studies.* SAND82-0080. Albuquerque, NM: Sandia National Laboratories.

Statler, R.D. 1980. "Field Operation Plan for Hydrological Testing, Nash Draw Wells WIPP-25 through 30, June - August, 1980." Albuquerque, NM: Sandia National Laboratories. (On file in the SWCF under WPO#2731.)

Stensrud, W.A. 1995. "Culebra Transport Program Test Plan: Hydraulic Tests at Wells WQSP-1, WQSP-2, WQSP-3, WQSP-4, WQSP-5, WQSP-6, and WQSP-6A at the Waste Isolation Pilot Plant (WIPP) Site." Albuquerque, NM: Sandia National Laboratories. (On file in the SWCF under WPO#27664.)

Stensrud, W.A., M.A. Bame, K.D. Lantz, T.L. Cauffman, J.B. Palmer, and G.J. Saulnier, Jr. 1988. *WIPP Hydrology Program, Waste Isolation Pilot Plant, Southeastern New Mexico, Hydrologic Data Report #6.* SAND87-7166. Albuquerque, NM: Sandia National Laboratories.

Stensrud, W.A., M.A. Bame, K.D. Lantz, J.B. Palmer, and G.J. Saulnier, Jr. 1990. *WIPP Hydrology Program, Waste Isolation Pilot Plant, Southeastern New Mexico, Hydrologic Data Report #8.* SAND89-7056. Albuquerque, NM: Sandia National Laboratories.

Uhland, D.W., and W.S. Randall. 1986. *Annual Water Quality Data Report for the Waste Isolation Pilot Plant, September 1986.* DOE-WIPP 86-006. Carlsbad, NM: Westinghouse Electric Corporation for the US DOE.

US Department of Energy. 1996. *Title 40 CFR Part 191 Compliance Certification Application for the Waste Isolation Pilot Plant, Vol. XVIII, Appendix TFIELD.* DOE/CAO-1996-2184. Carlsbad, NM: US DOE Waste Isolation Pilot Plant, Carlsbad Area Office.

Warren, J.E., and P.J. Root. 1963. "The Behavior of Naturally Fractured Reservoirs," *Society of Petroleum Engineers Journal.* Vol. 3, no. 3, 245-255.

Waste Isolation Pilot Plant Management and Operating Contractor (WIPP MOC). 1995. *Basic Data Report for WQSP 1, WQSP 2, WQSP 3, WQSP 4, WQSP 5, WQSP 6, and WQSP 6a.* DOE/WIPP 95-2154. Carlsbad, NM: Westinghouse Electric Corporation for the US DOE.

Wells, J.G., and S.L. Drellack, Jr. 1983. *Geologic and Well-Construction Data for the H-10 Borehole Complex Near the Proposed Waste Isolation Pilot Plant Site, Southeastern New Mexico.* Water-Resources Investigations Report 83-4124. Albuquerque, NM: USGS.

Westinghouse Electric Corporation. 1991. *Annual Water Quality Data Report for the Waste Isolation Pilot Plant, 1990.* DOE/WIPP 91-025. Carlsbad, NM: Westinghouse Electric Corporation for the US DOE.

APPENDIX A

DRAWDOWN SIMULATIONS

CONTENTS

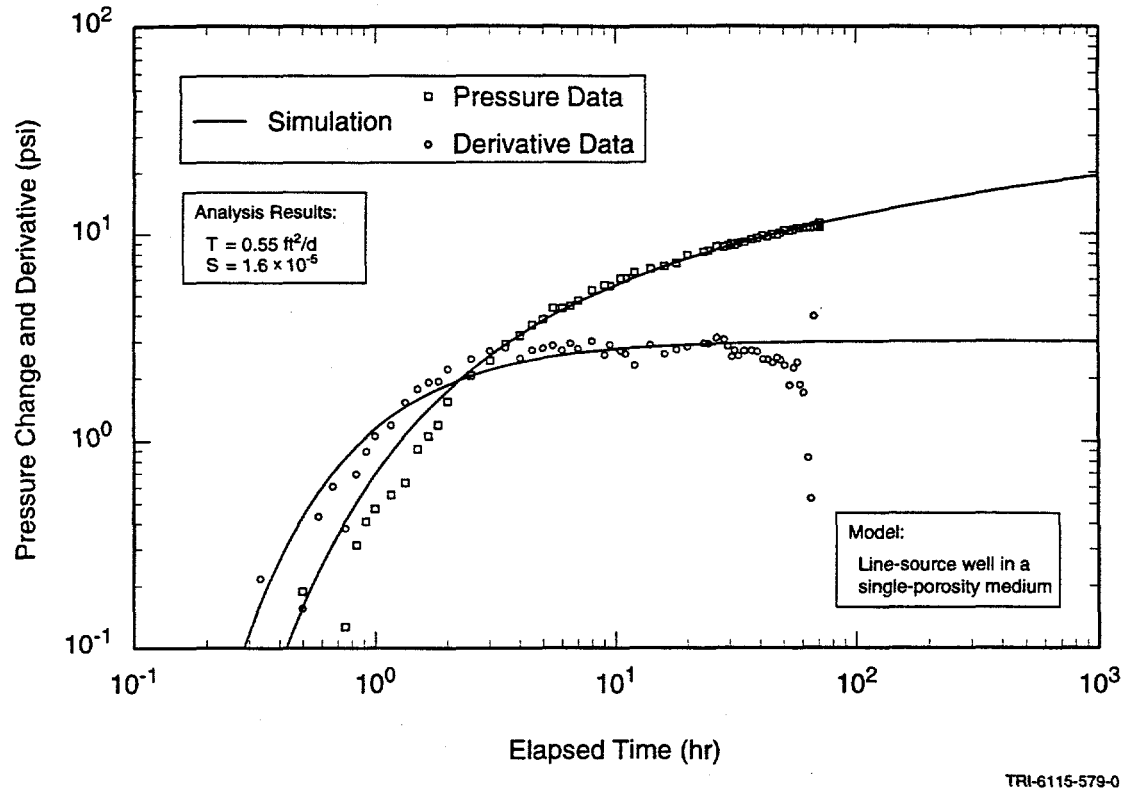

Figure A-1. Log-log plot of H-2b drawdown data with Interpret/2 simulation.

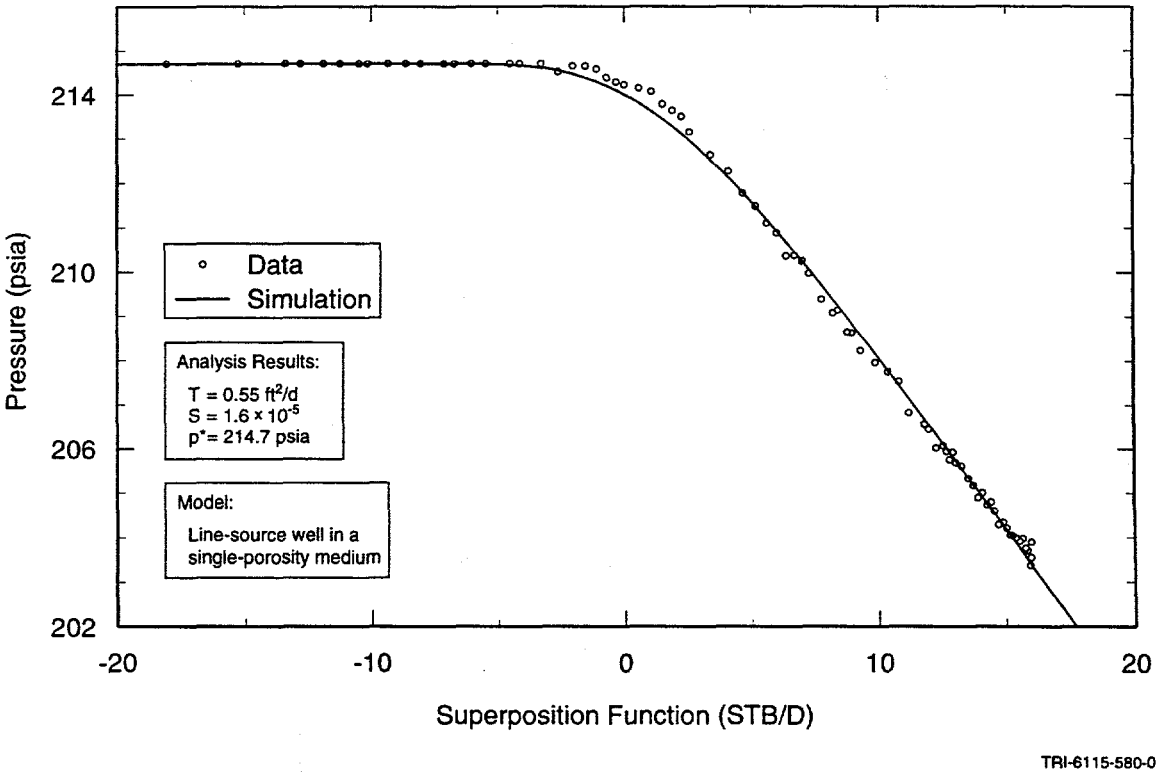

Figure A-2. Horner plot of H-2b drawdown data with Interpret/2 simulation.

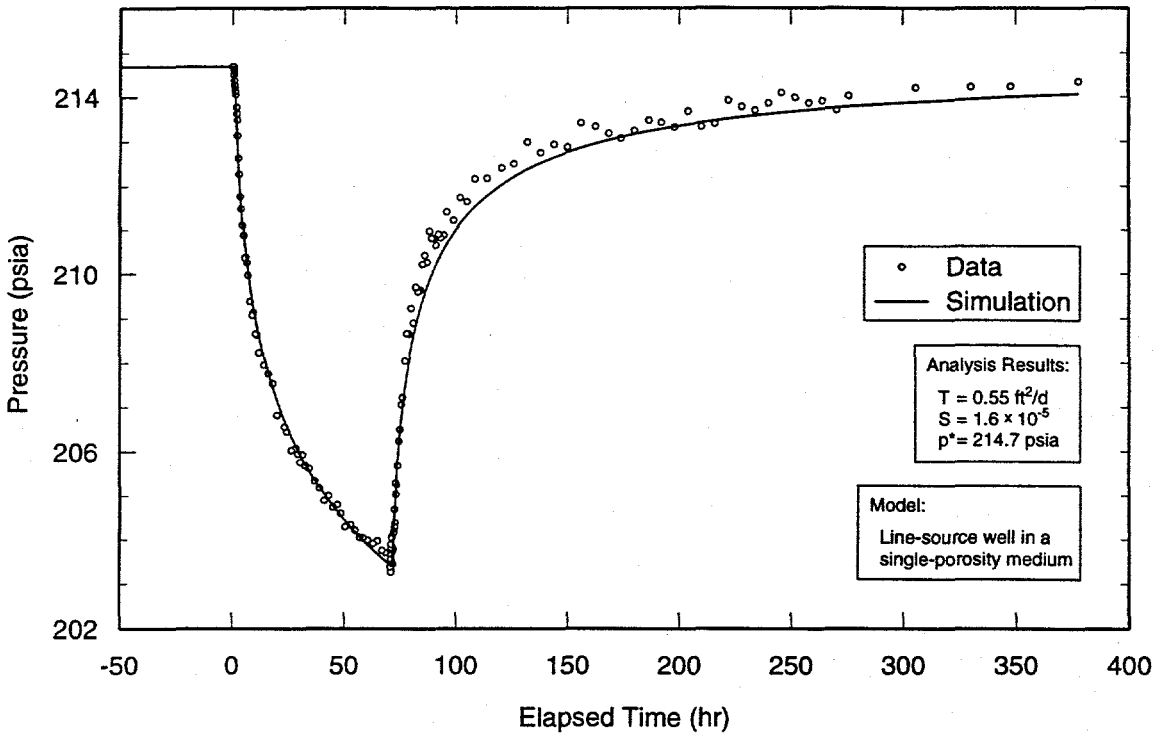

Figure A-3. Linear-linear plot of H-2b data with Interpret/2 simulation derived from drawdown analysis.

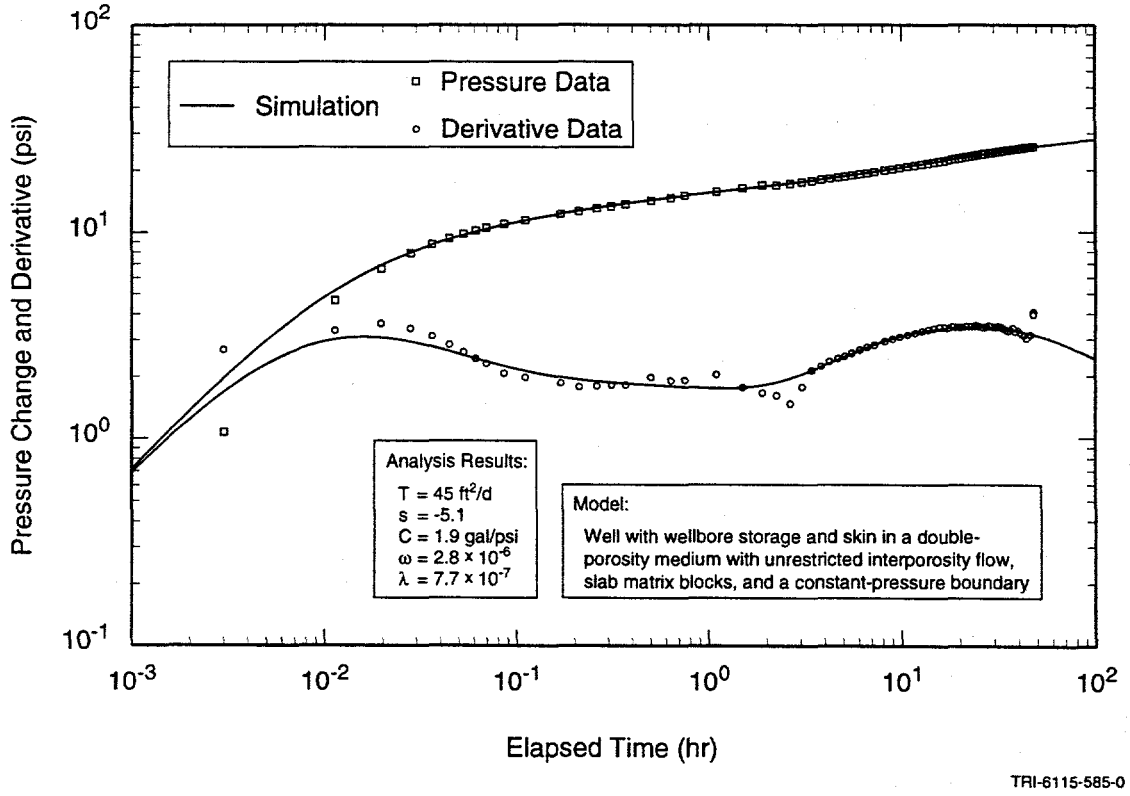

Figure A-4. Log-log plot of H-6b drawdown data from test #1 with Interpret/2 simulation.

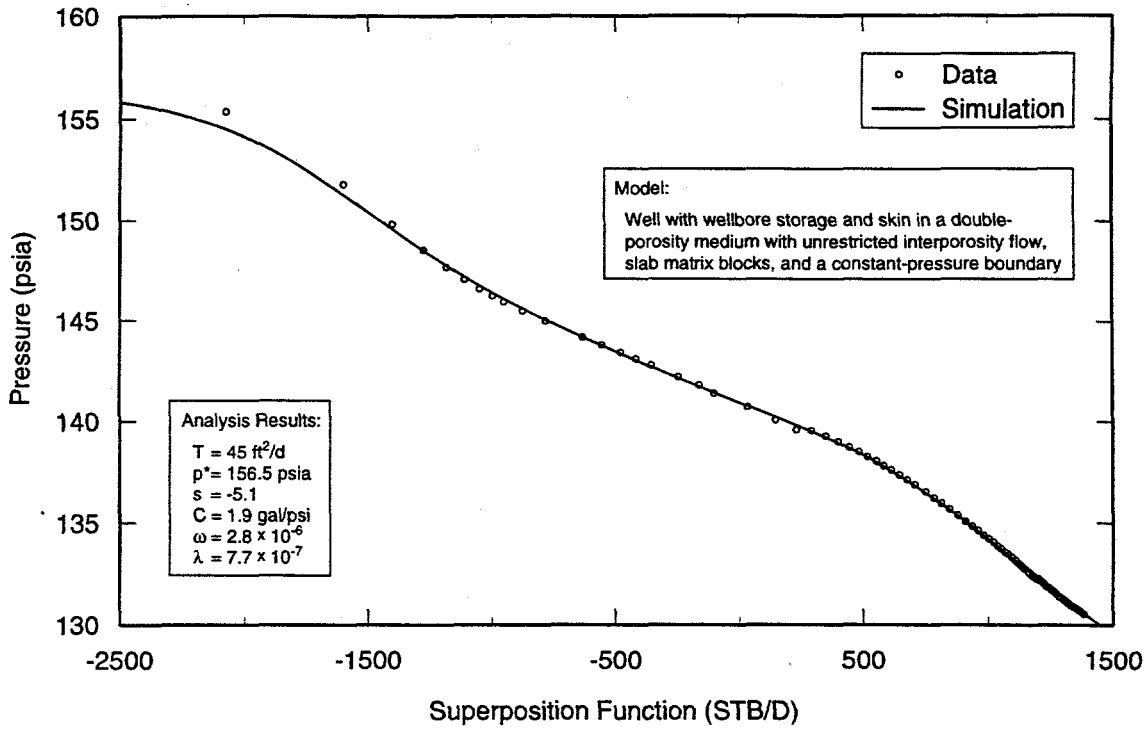

Figure A-5. Horner plot of H-6b drawdown data from test #1 with Interpret/2 simulation.

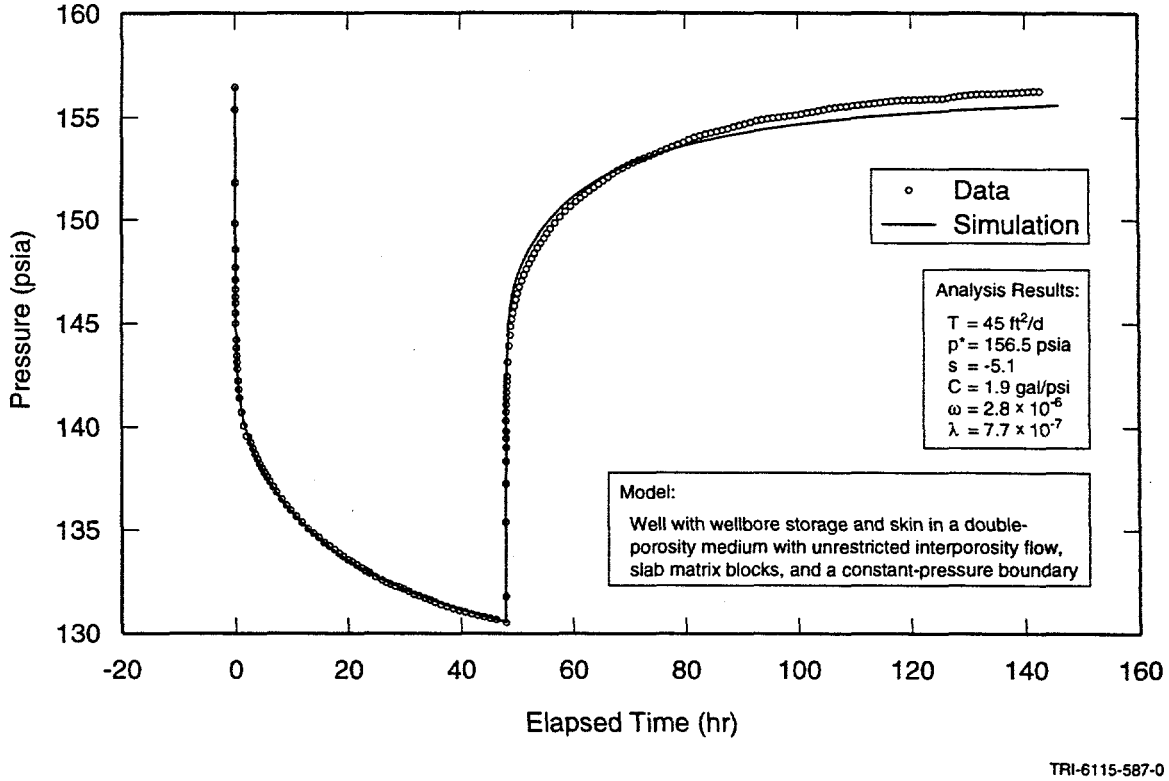

Figure A-6. Linear-linear plot of H-6b data from test #1 with Interpret/2 simulation derived from drawdown analysis.

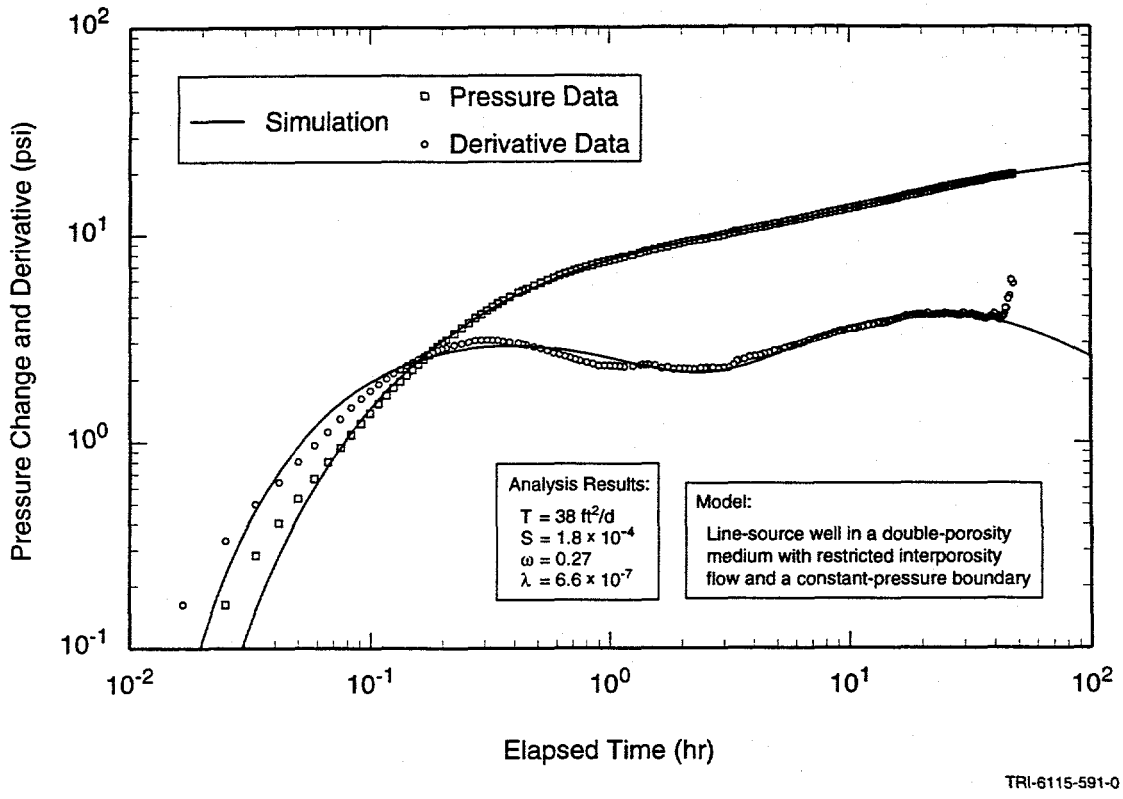

Figure A-7. Log-log plot of H-6a drawdown data from test #1 with Interpret/2 simulation.

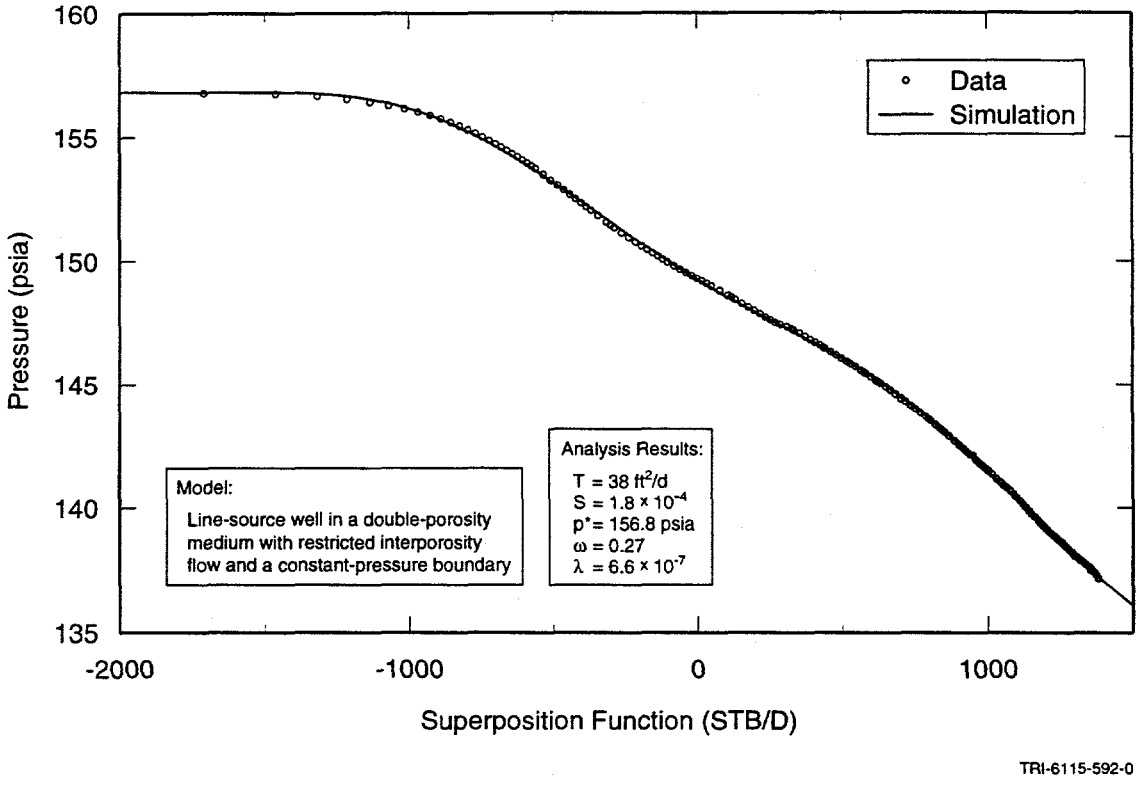

Figure A-8. Horner plot of H-6a drawdown data from test #1 with Interpret/2 simulation.

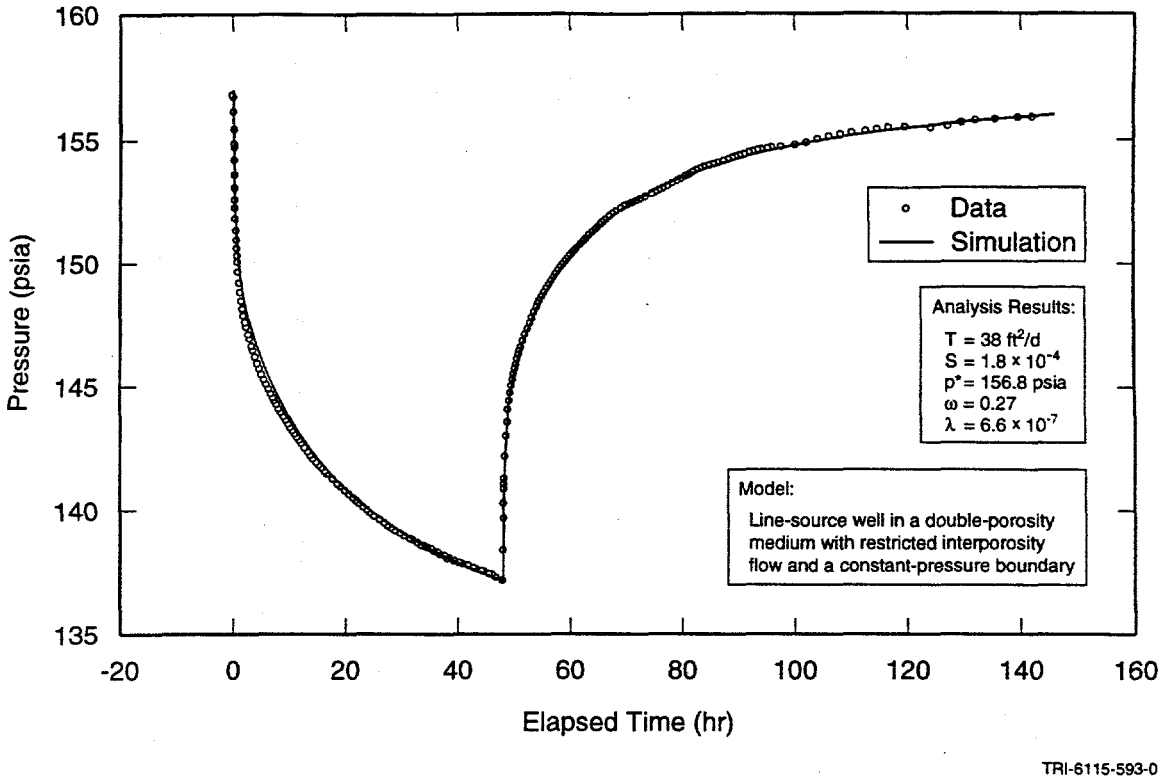

Figure A-9. Linear-linear plot of H-6a data from test #1 with Interpret/2 simulation derived from drawdown analysis.

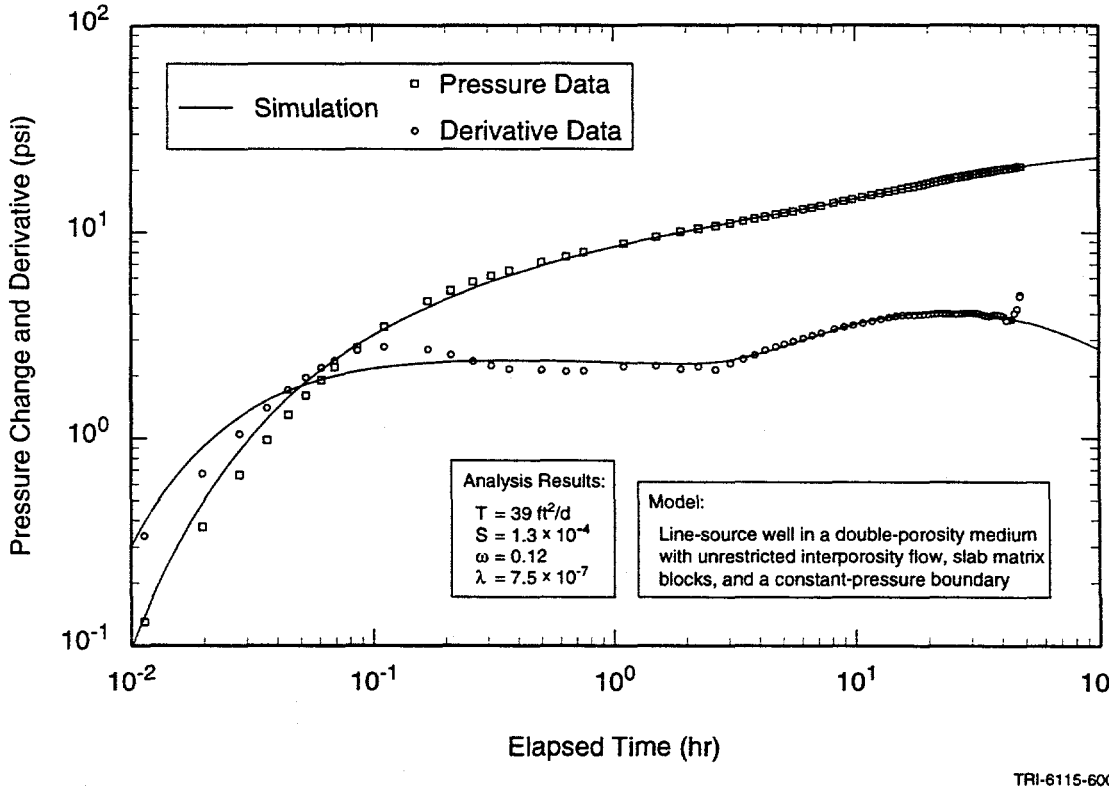

Figure A-10. Log-log plot of H-6c drawdown data from test #1 with Interpret/2 simulation.

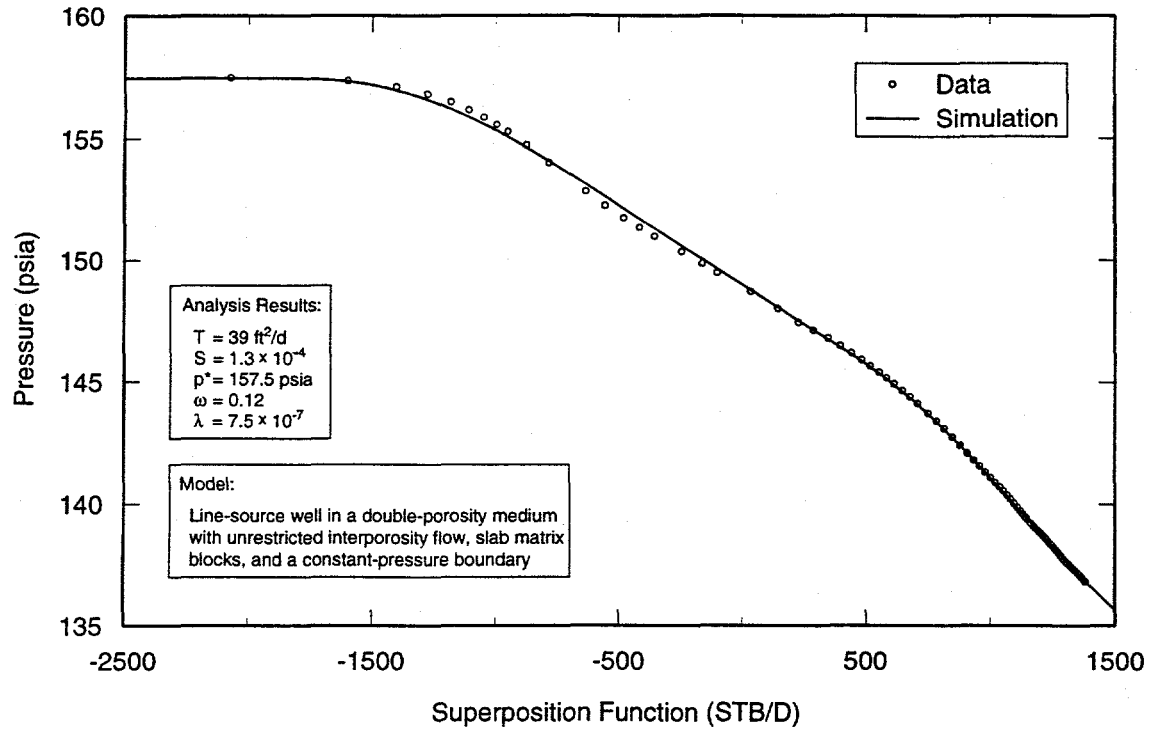

Figure A-11. Horner plot of H-6c drawdown data from test #1 with Interpret/2 simulation.

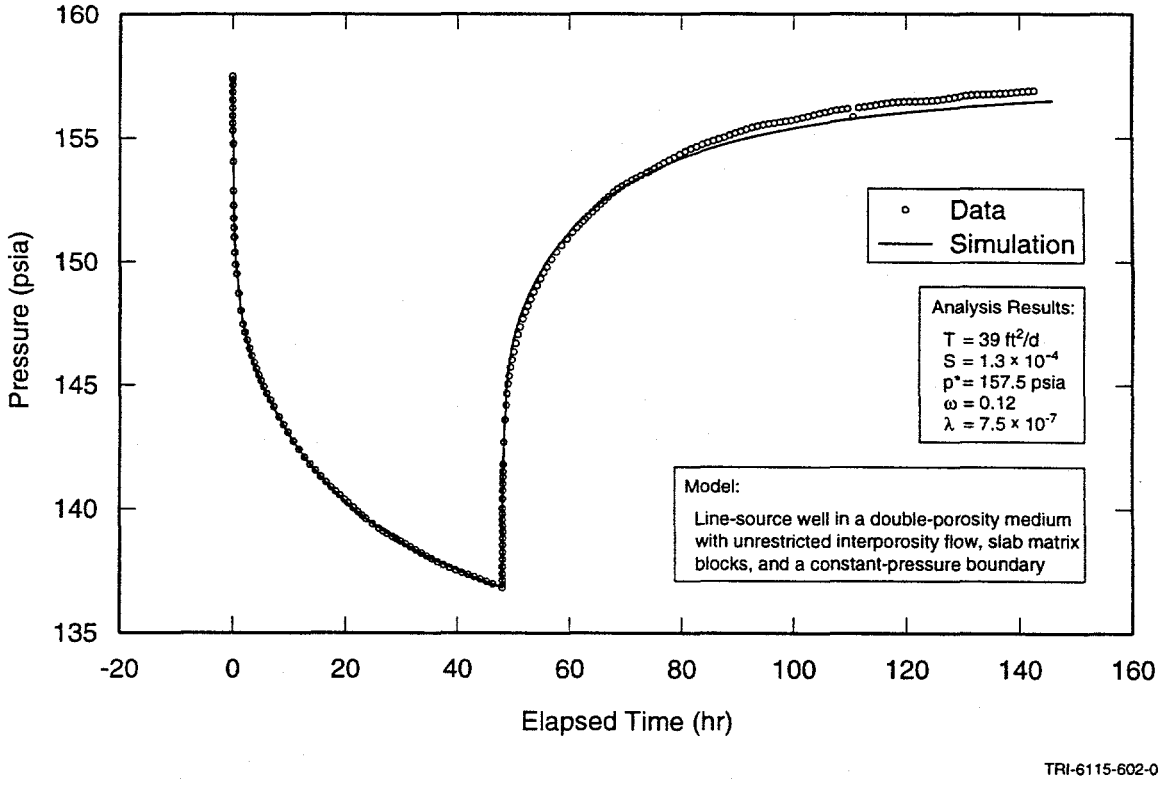

Figure A-12. Linear-linear plot of H-6c data from test #1 with Interpret/2 simulation derived from drawdown analysis.

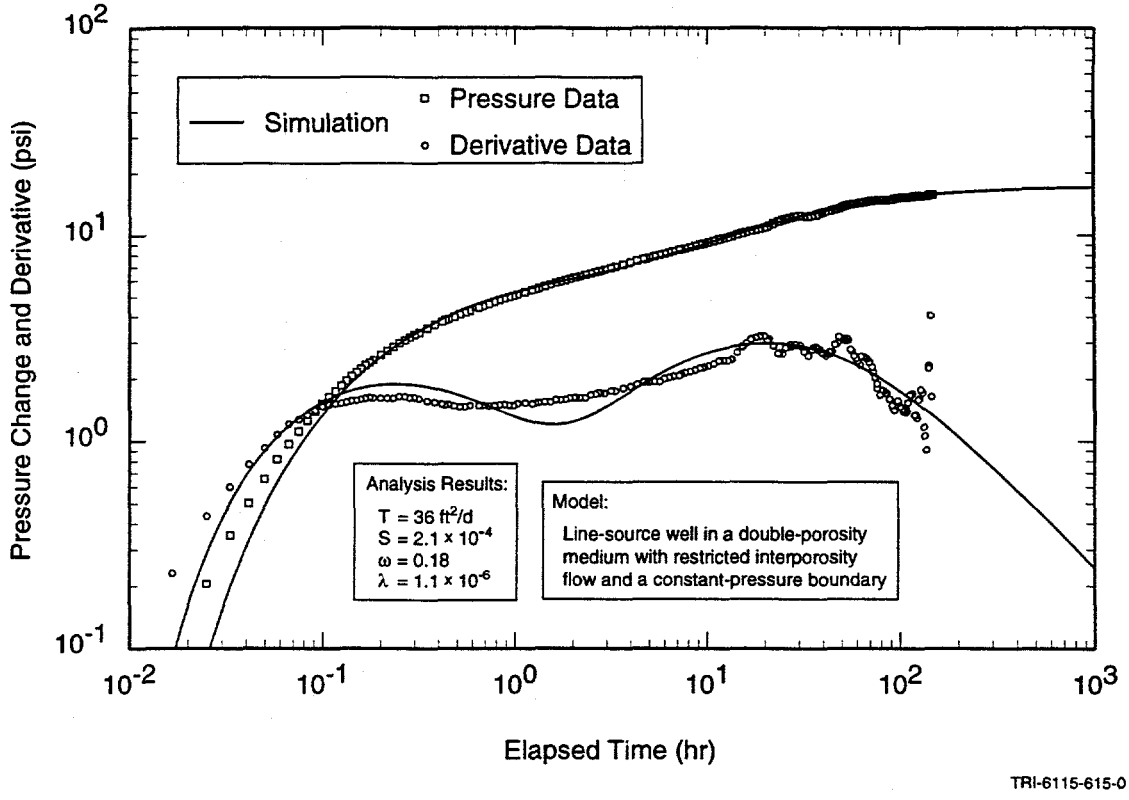

Figure A-13. Log-log plot of H-6a drawdown data from test #3 with Interpret/2 simulation.

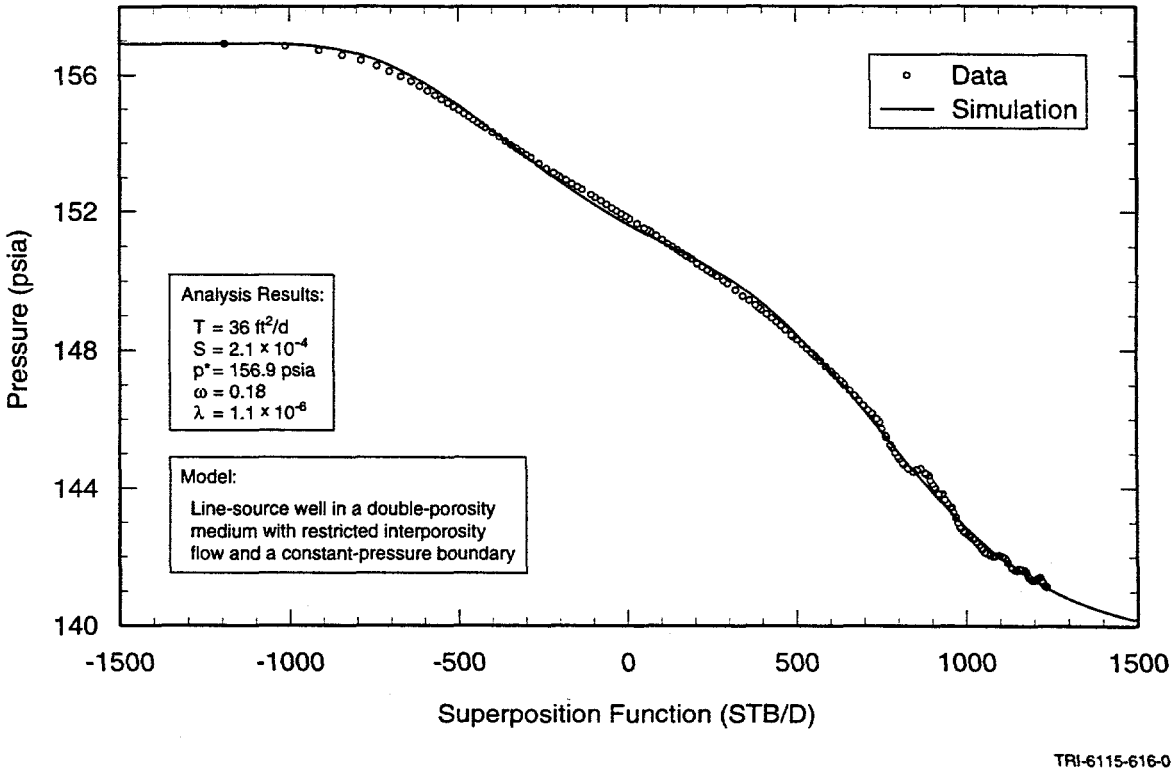

Figure A-14. Horner plot of H-6a drawdown data from test #3 with Interpret/2 simulation.

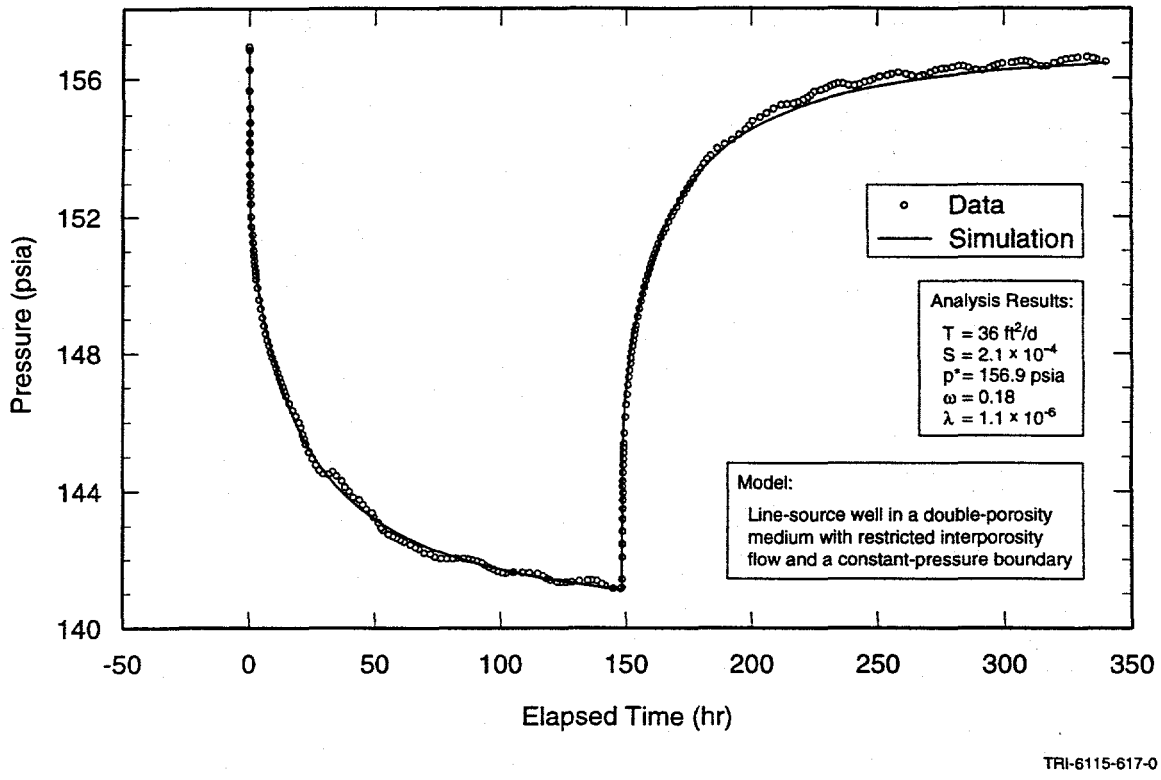

Figure A-15. Linear-linear plot of H-6a data from test #3 with Interpret/2 simulation derived from drawdown analysis.

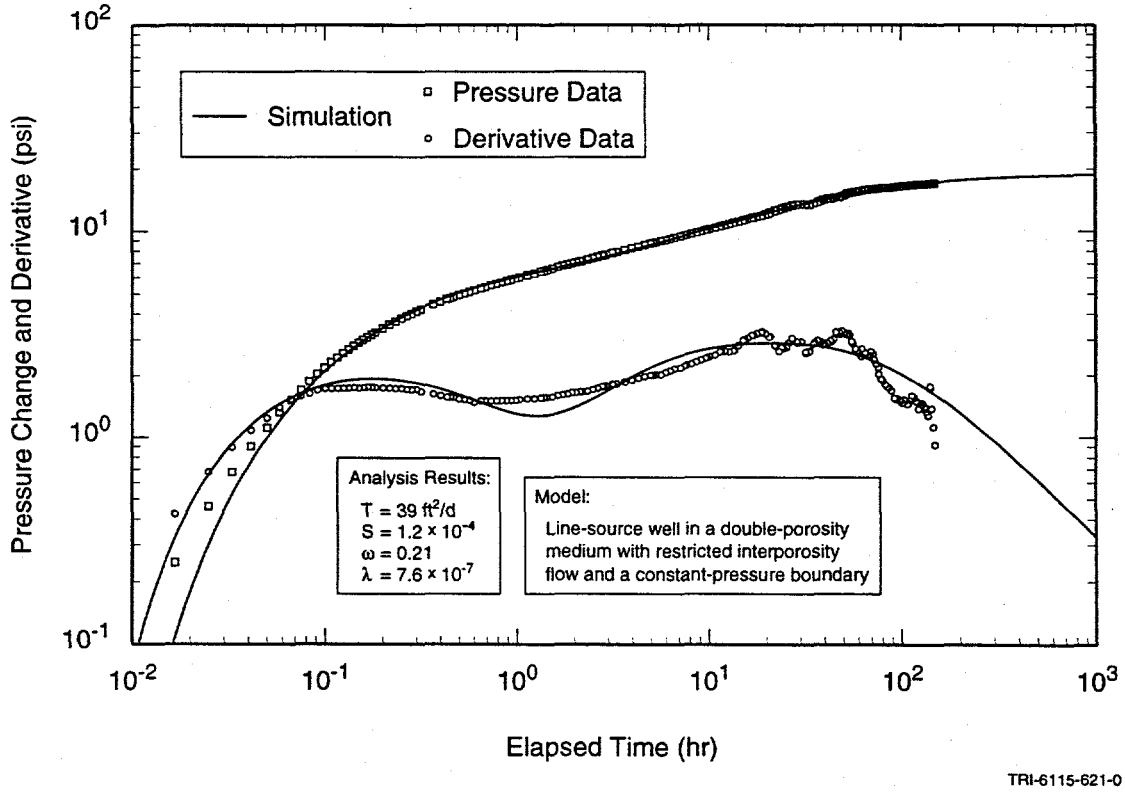

Figure A-16. Log-log plot of H-6b drawdown data from test #3 with Interpret/2 simulation.

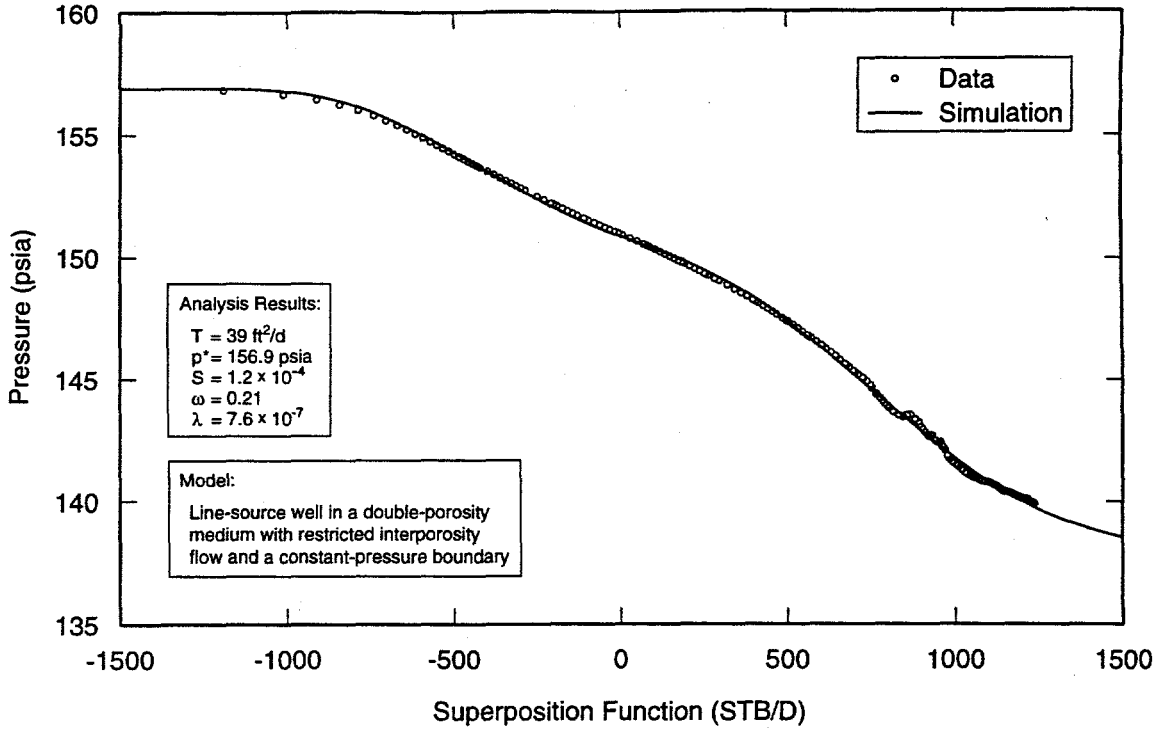

Figure A-17. Horner plot of H-6b drawdown data from test #3 with Interpret/2 simulation.

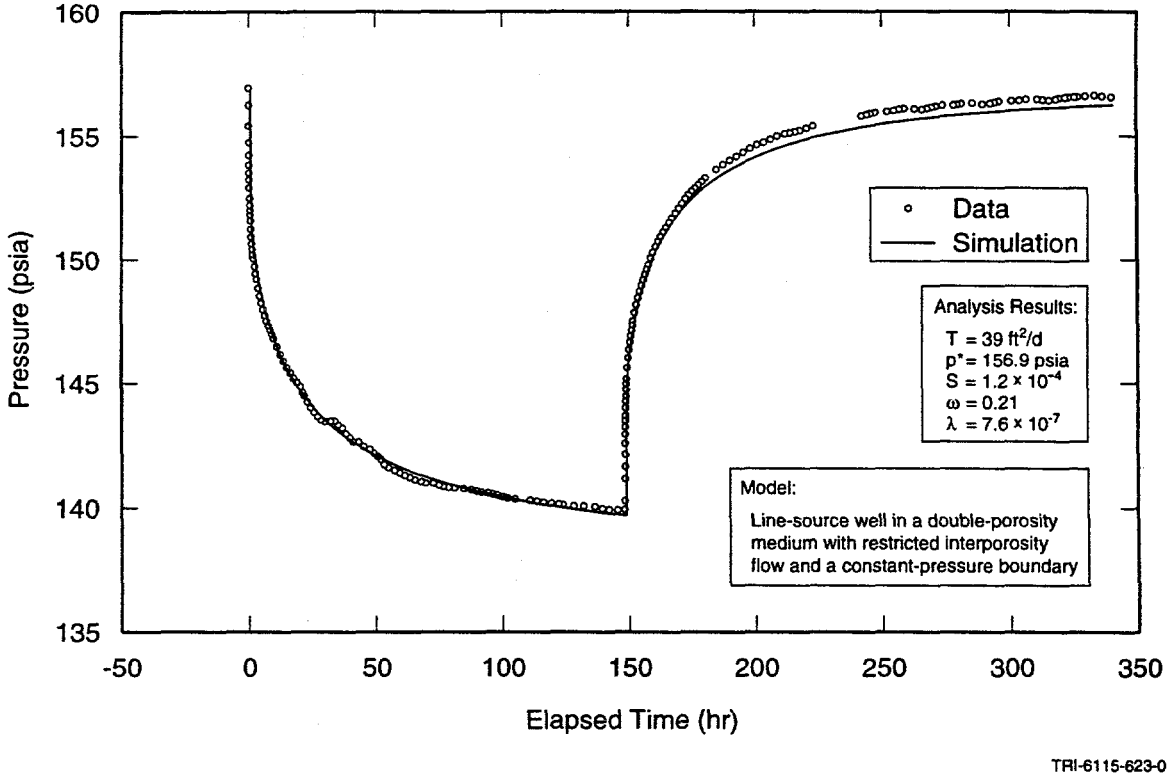

Figure A-18. Linear-linear plot of H-6b data from test #3 with Interpret/2 simulation derived from drawdown analysis.

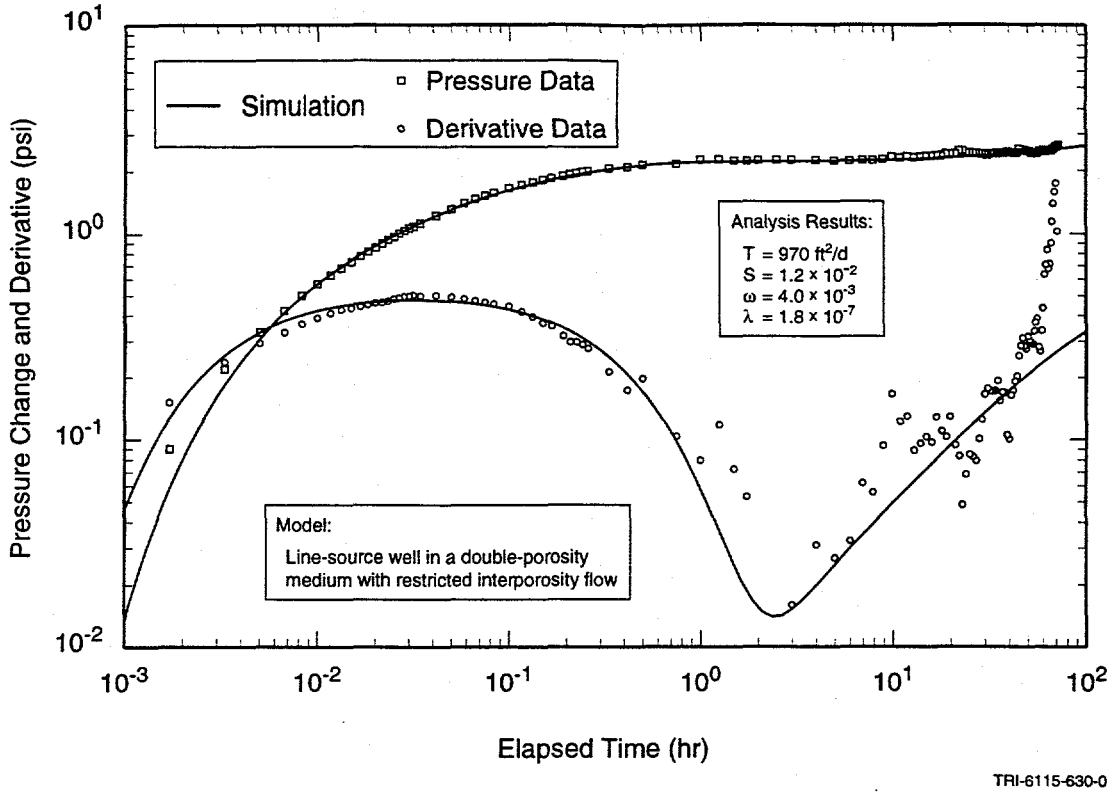

Figure A-19. Log-log plot of H-7b2 drawdown data with Interpret/2 simulation.

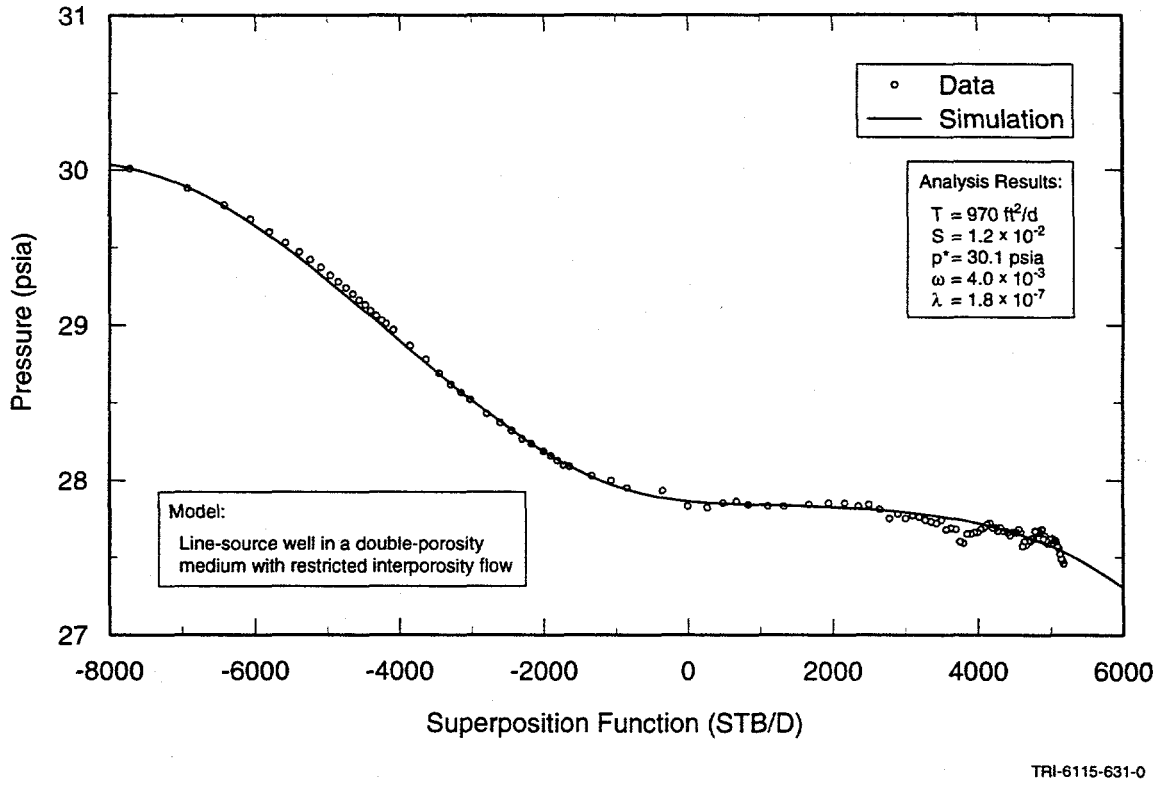

Figure A-20. Horner plot of H-7b2 drawdown data with Interpret/2 simulation.

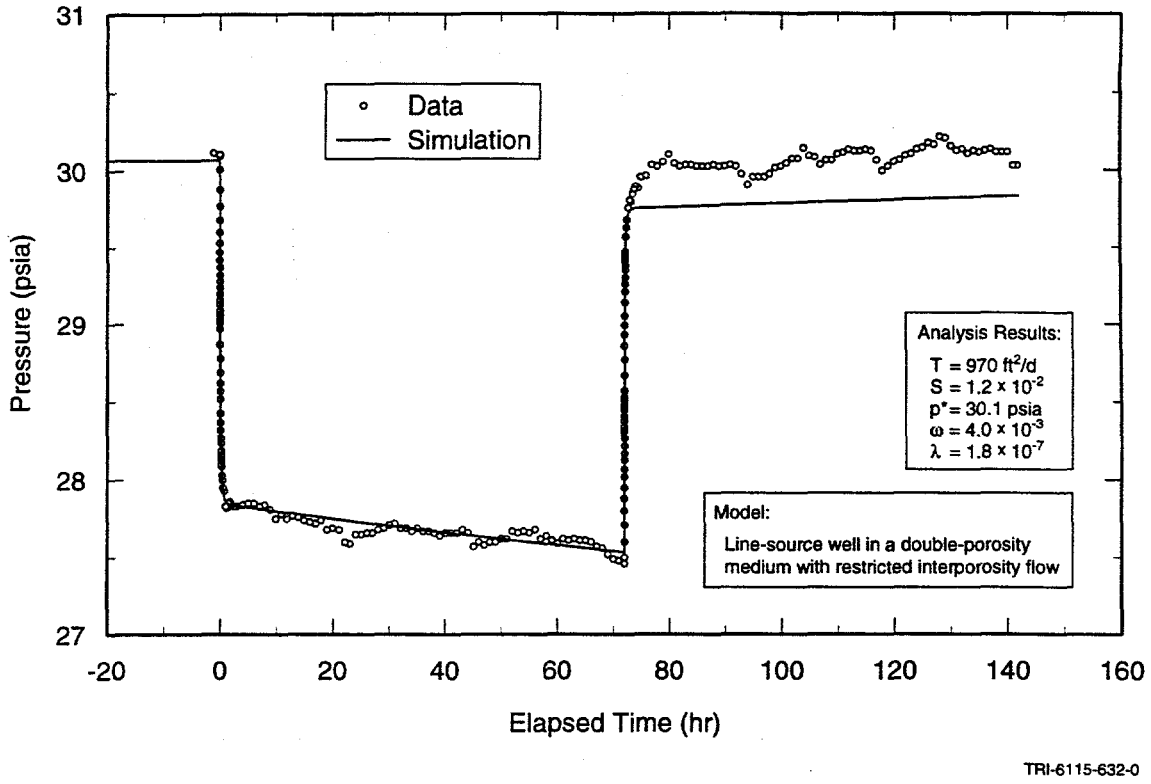

Figure A-21. Linear-linear plot of H-7b2 data with Interpret/2 simulation derived from drawdown analysis.

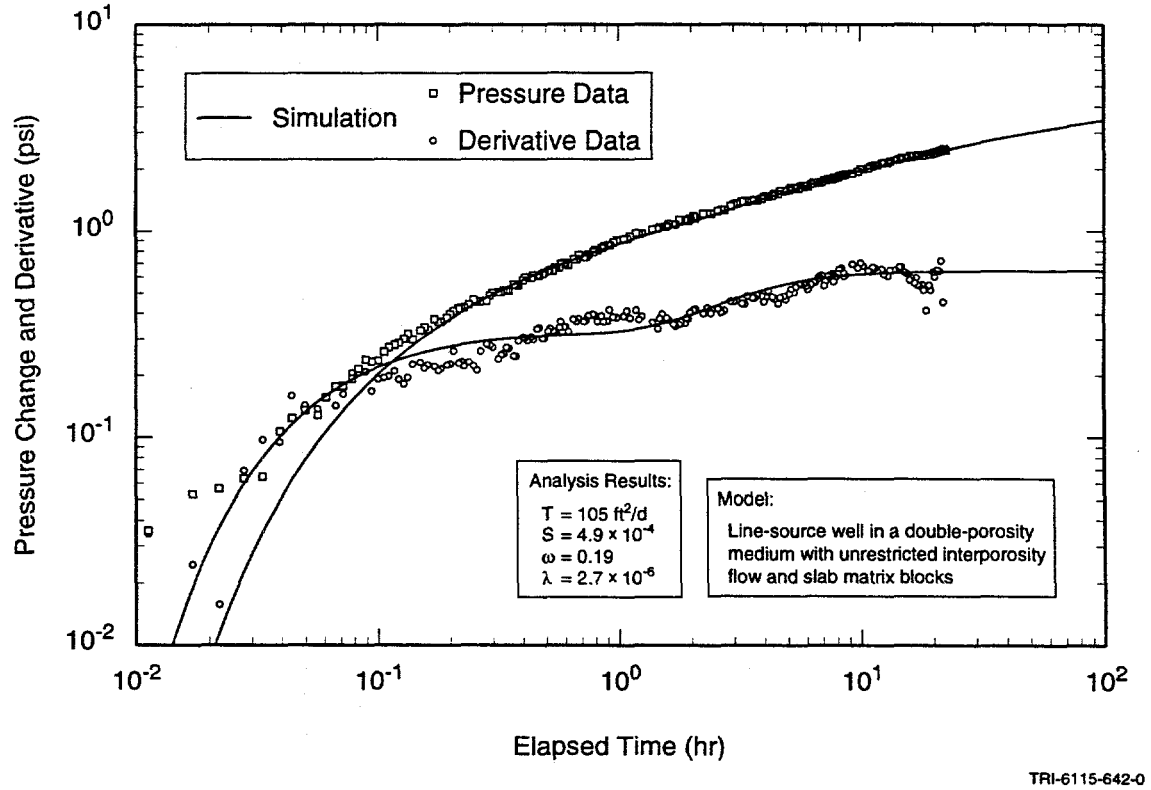

Figure A-22. Log-log plot of H-9a drawdown data from test #1 with Interpret/2 simulation.

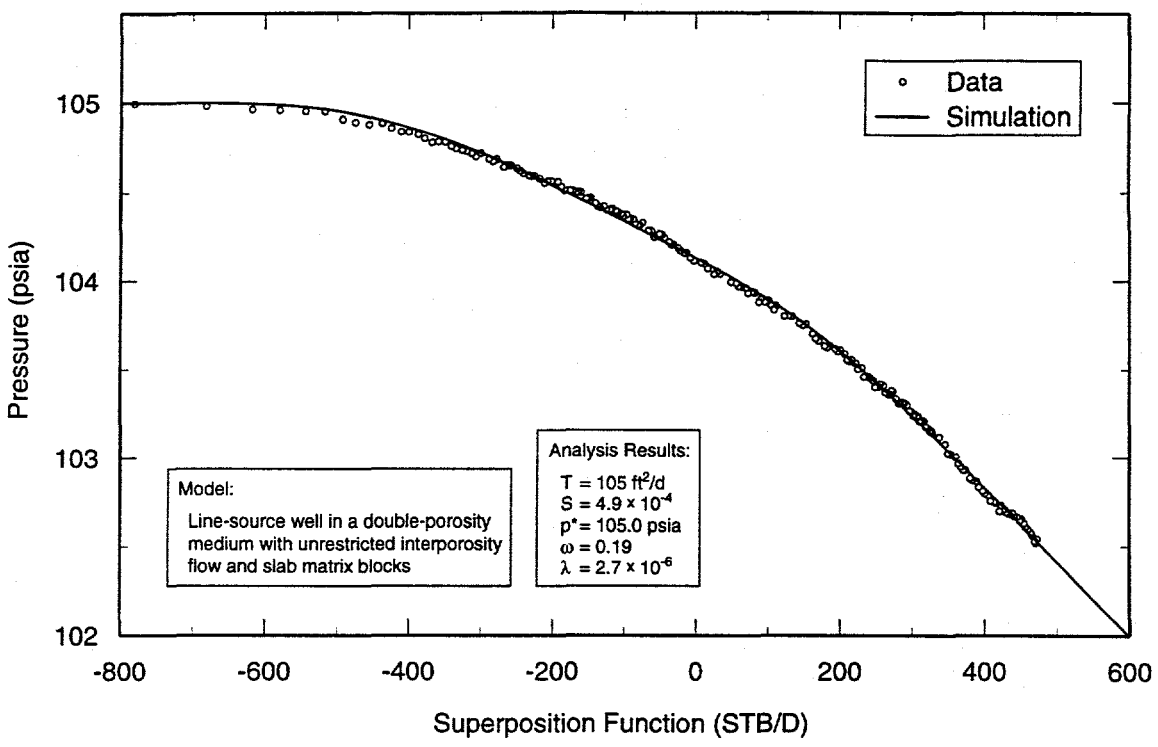

Figure A-23. Horner plot of H-9a drawdown data from test #1 with Interpret/2 simulation.

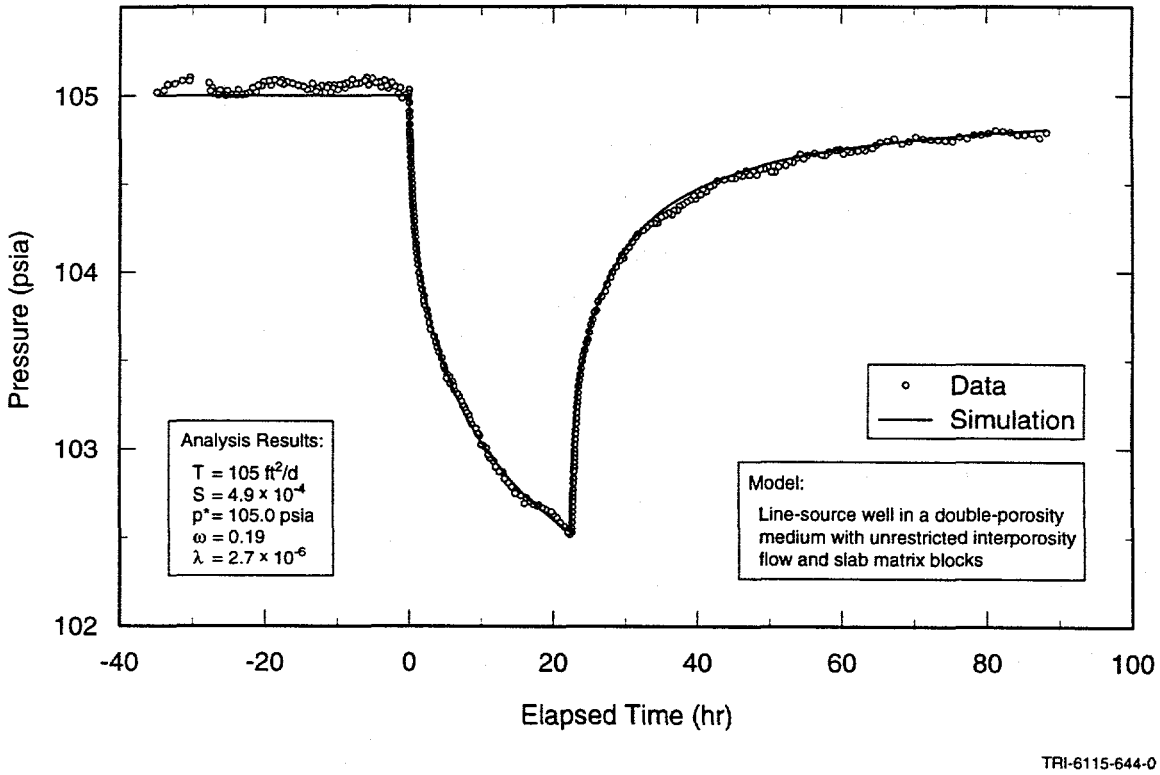

Figure A-24. Linear-linear plot of H-9a data from test #1 with Interpret/2 simulation derived from drawdown analysis.

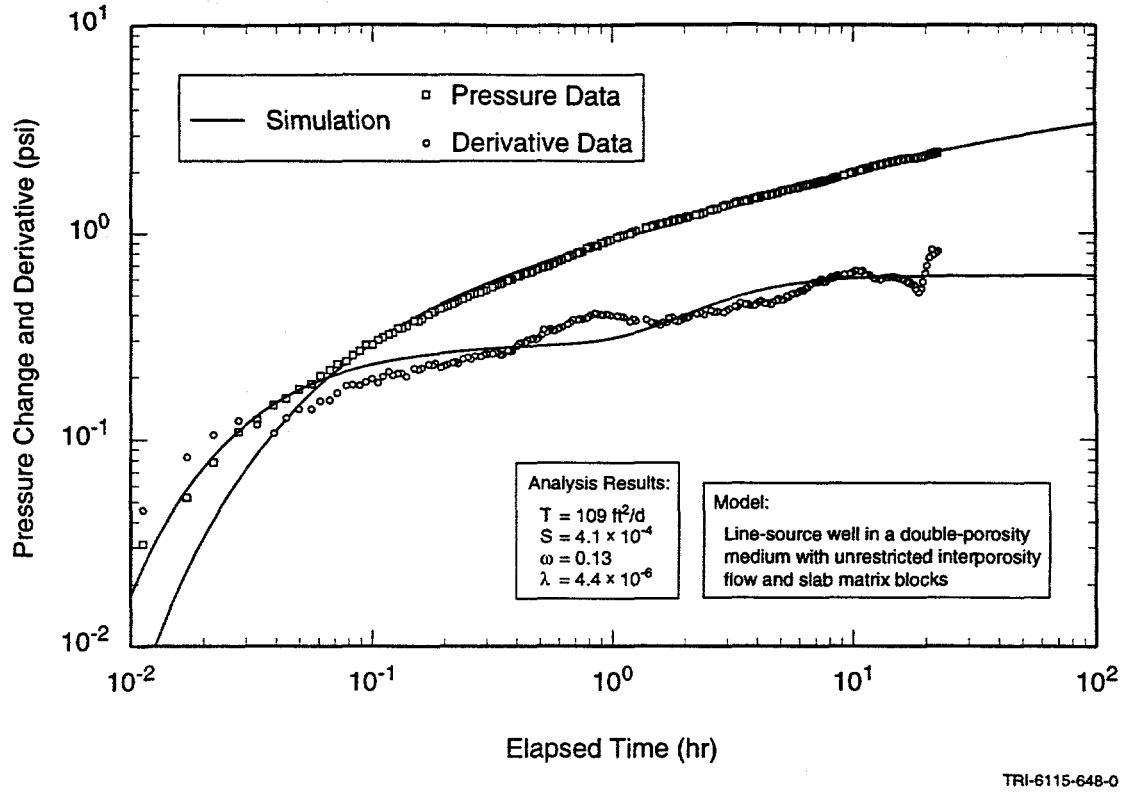

Figure A-25. Log-log plot of H-9b drawdown data from test #1 with Interpret/2 simulation.

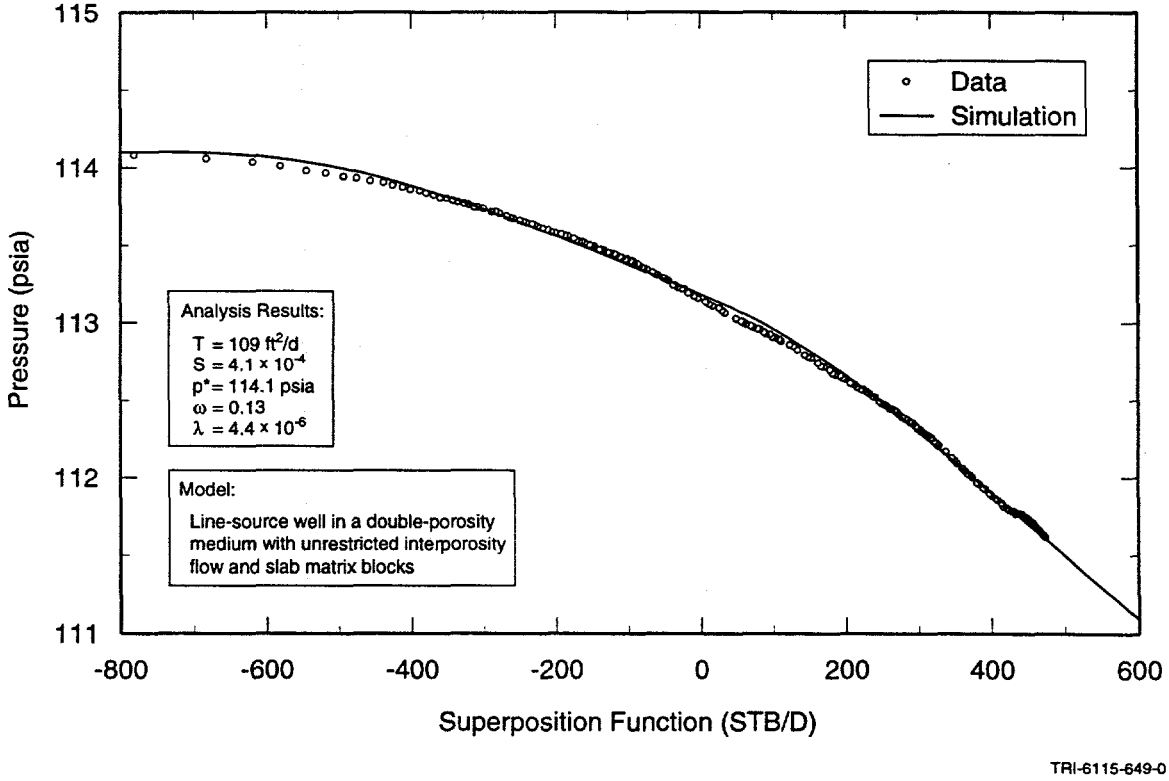

Figure A-26. Horner plot of H-9b drawdown data from test #1 with Interpret/2 simulation.

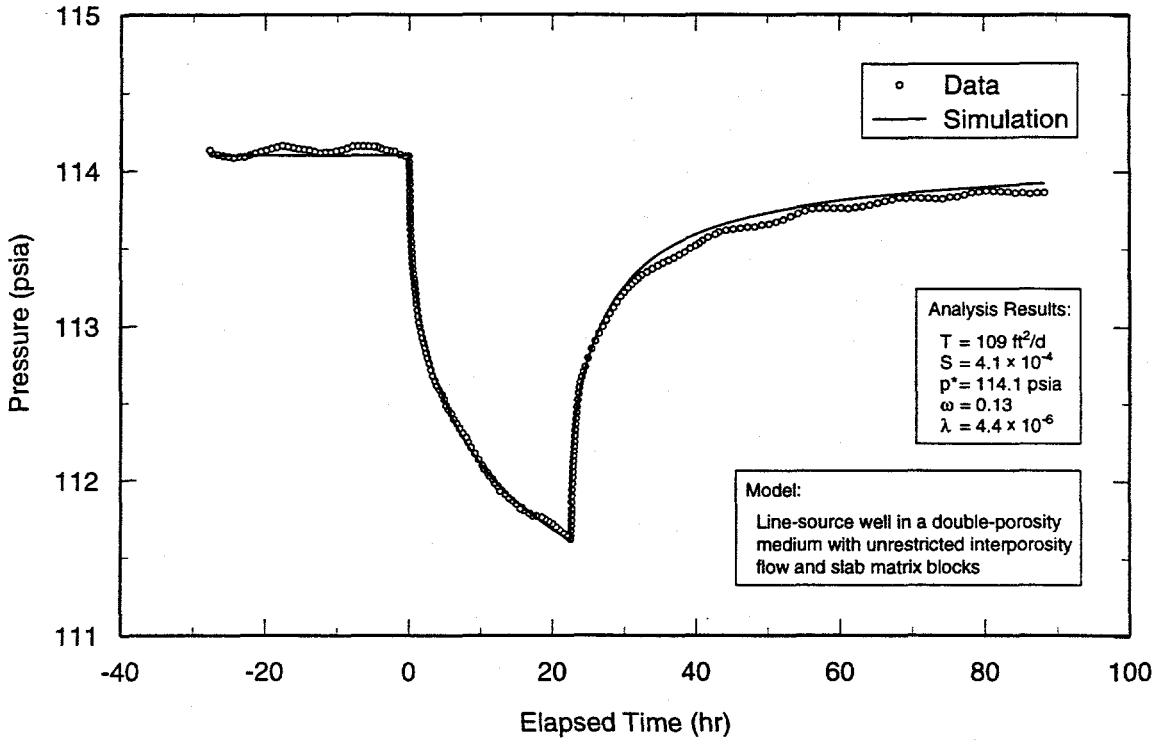

Figure A-27. Linear-linear plot of H-9b data from test #1 with Interpret/2 simulation derived from drawdown analysis.

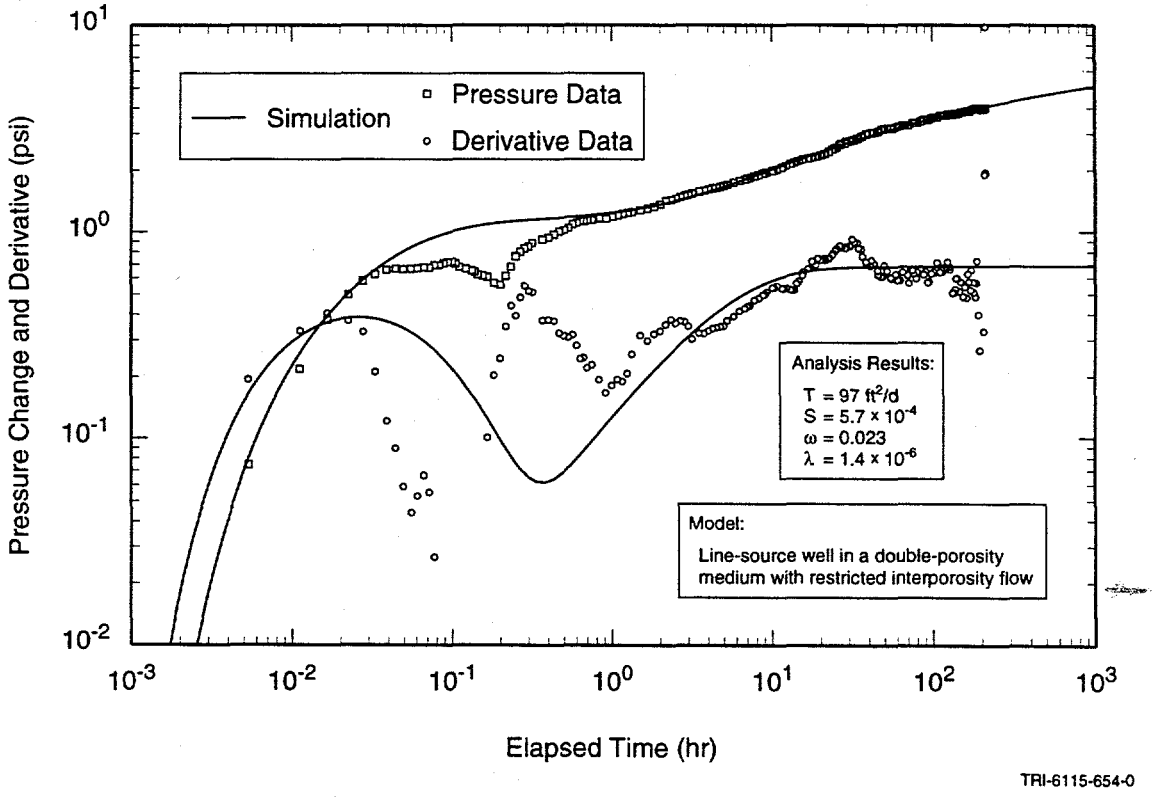

Figure A-28. Log-log plot of H-9a drawdown data from test #2 with Interpret/2 simulation.

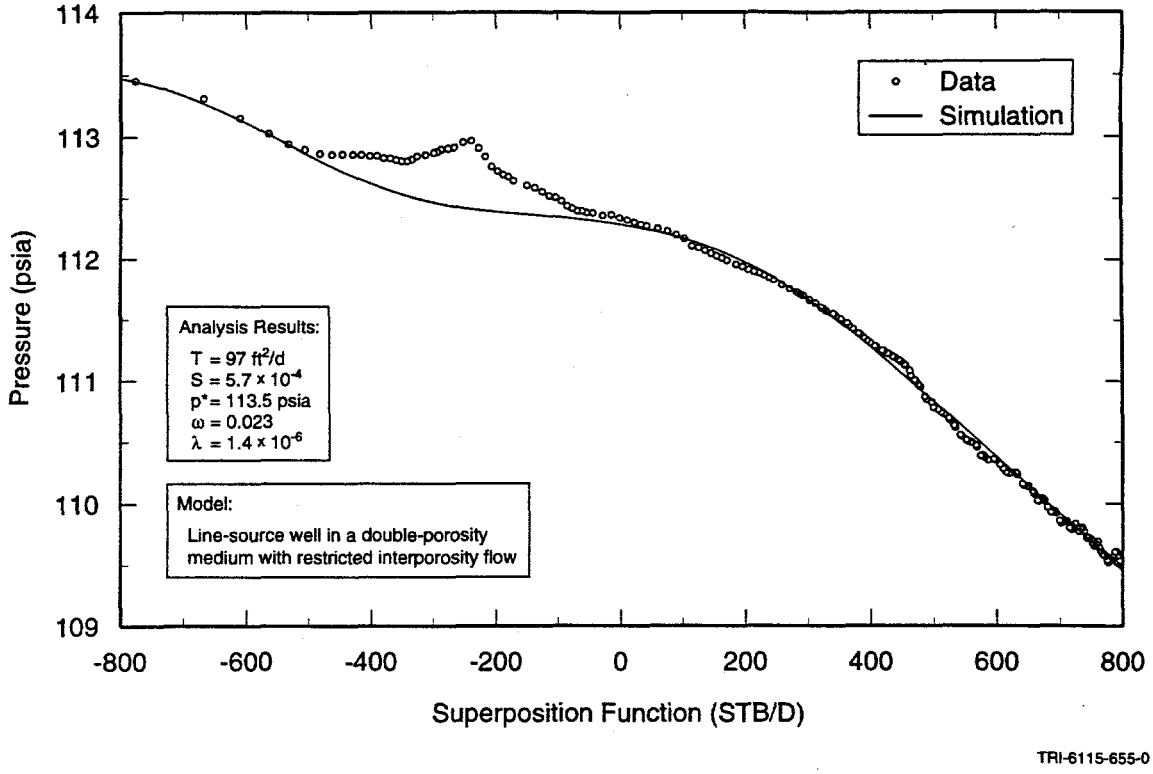

Figure A-29. Horner plot of H-9a drawdown data from test #2 with Interpret/2 simulation.

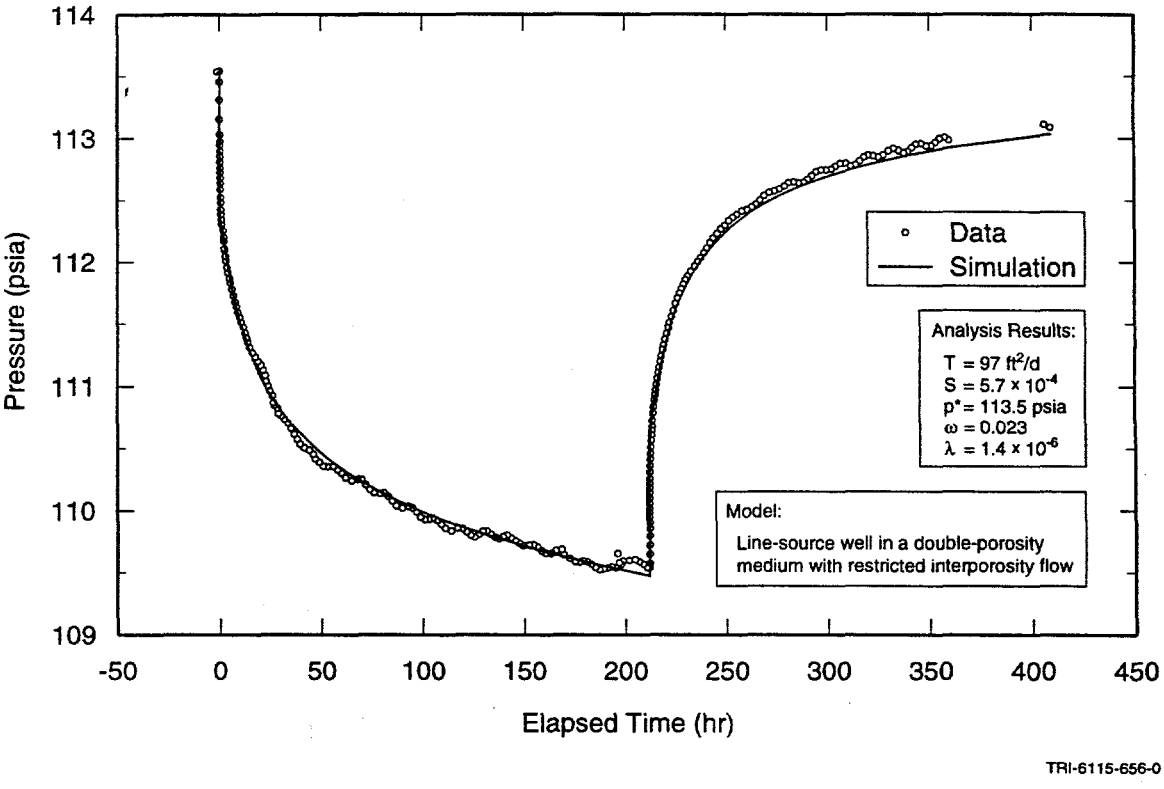

Figure A-30. Linear-linear plot of H-9a data from test #2 with Interpret/2 simulation derived from drawdown analysis.

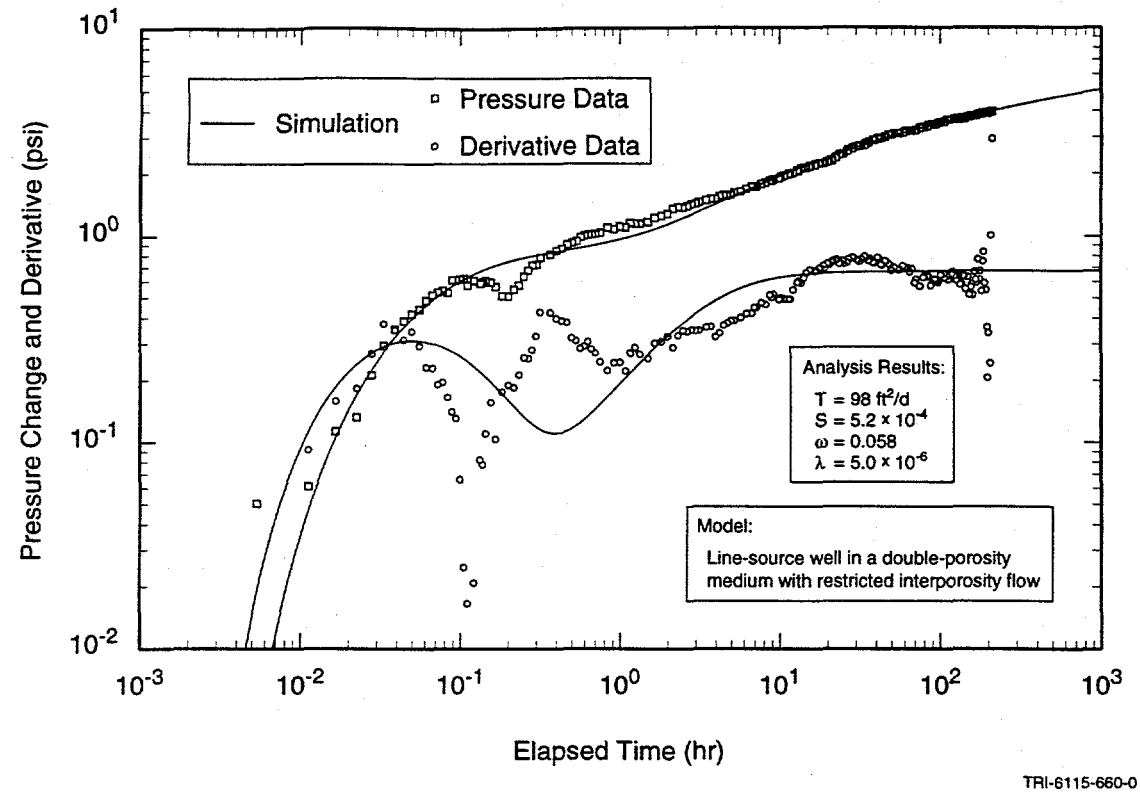

Figure A-31. Log-log plot of H-9c drawdown data from test #2 with Interpret/2 simulation.

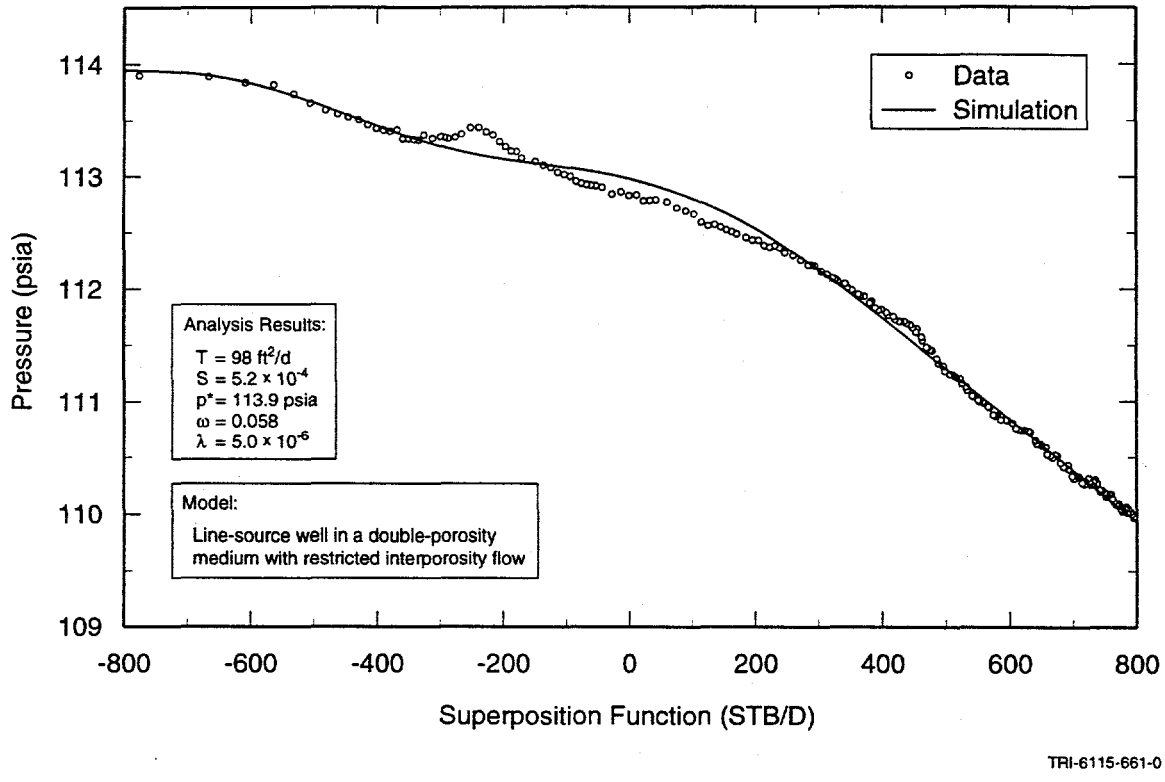

Figure A-32. Horner plot of H-9c drawdown data from test #2 with Interpret/2 simulation.

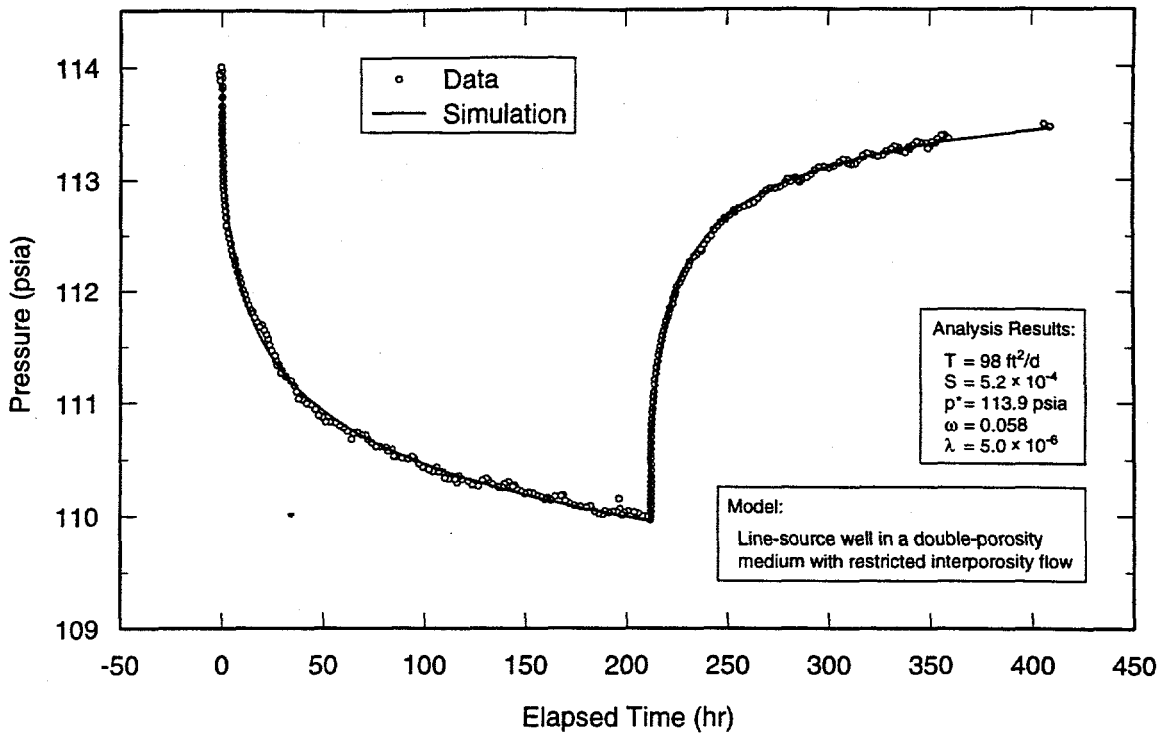

Figure A-33. Linear-linear plot of H-9c data from test #2 with Interpret/2 simulation derived from drawdown analysis.

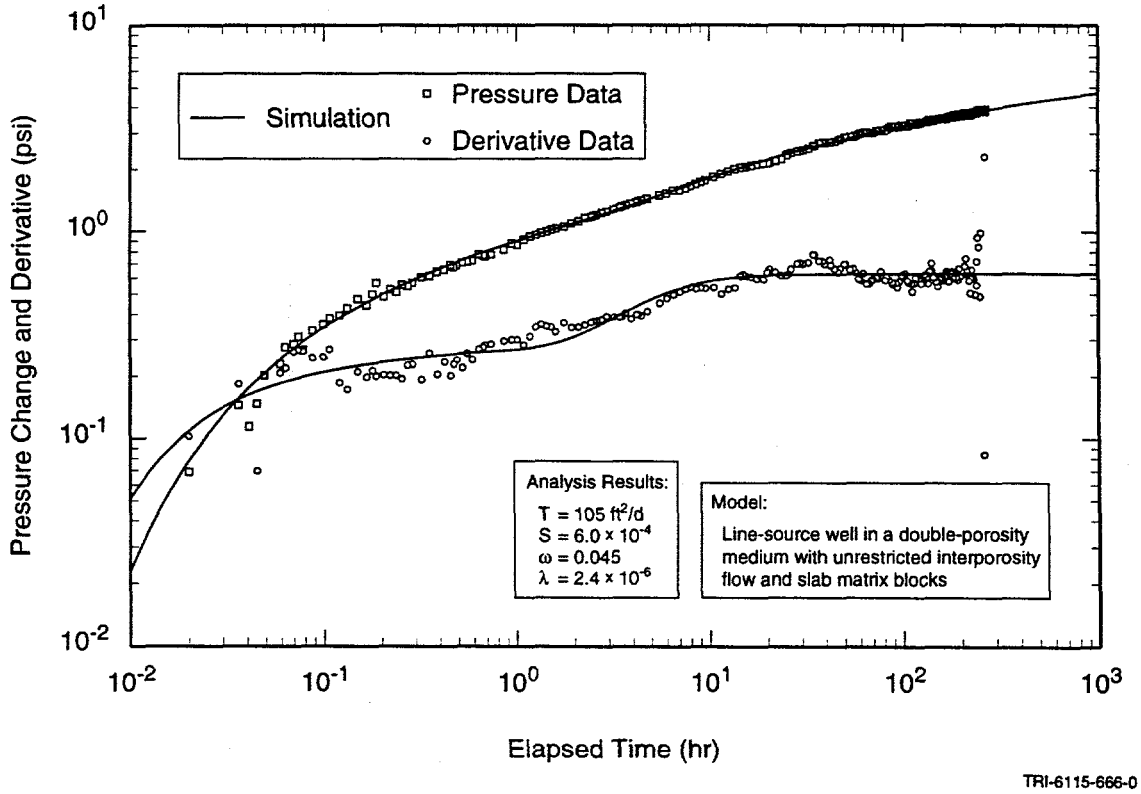

Figure A-34. Log-log plot of H-9a drawdown data from test #3 with Interpret/2 simulation.

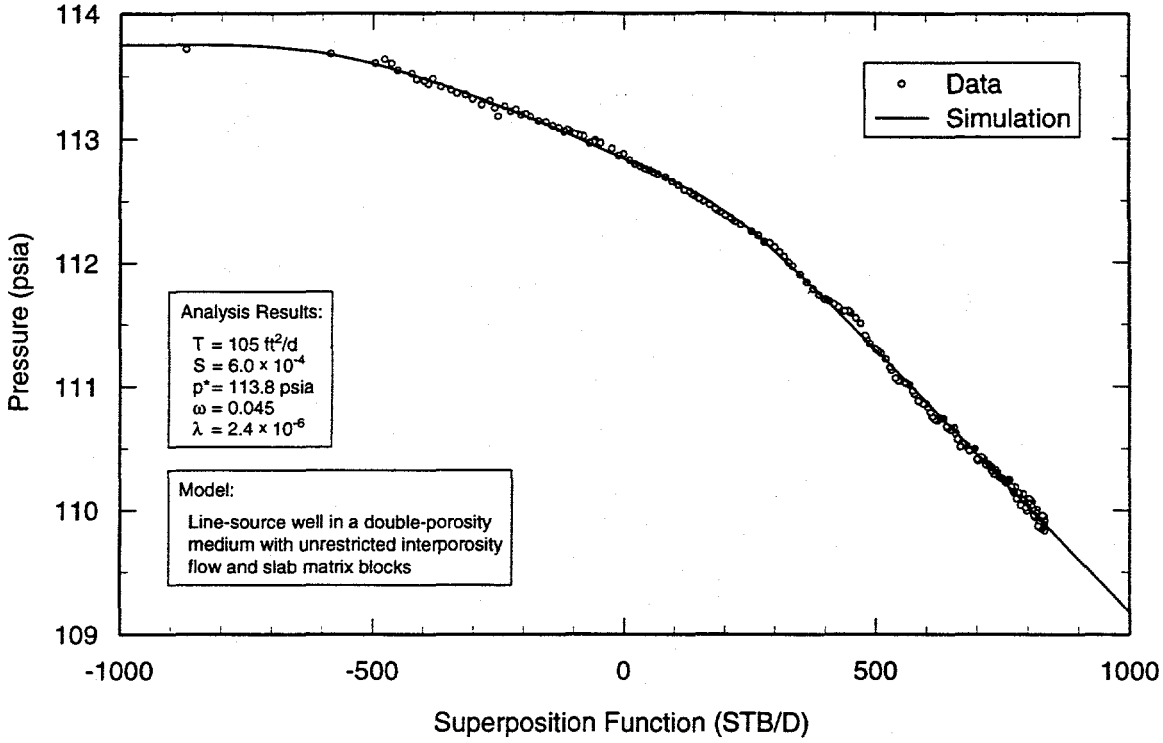

Figure A-35. Horner plot of H-9a drawdown data from test #3 with Interpret/2 simulation.

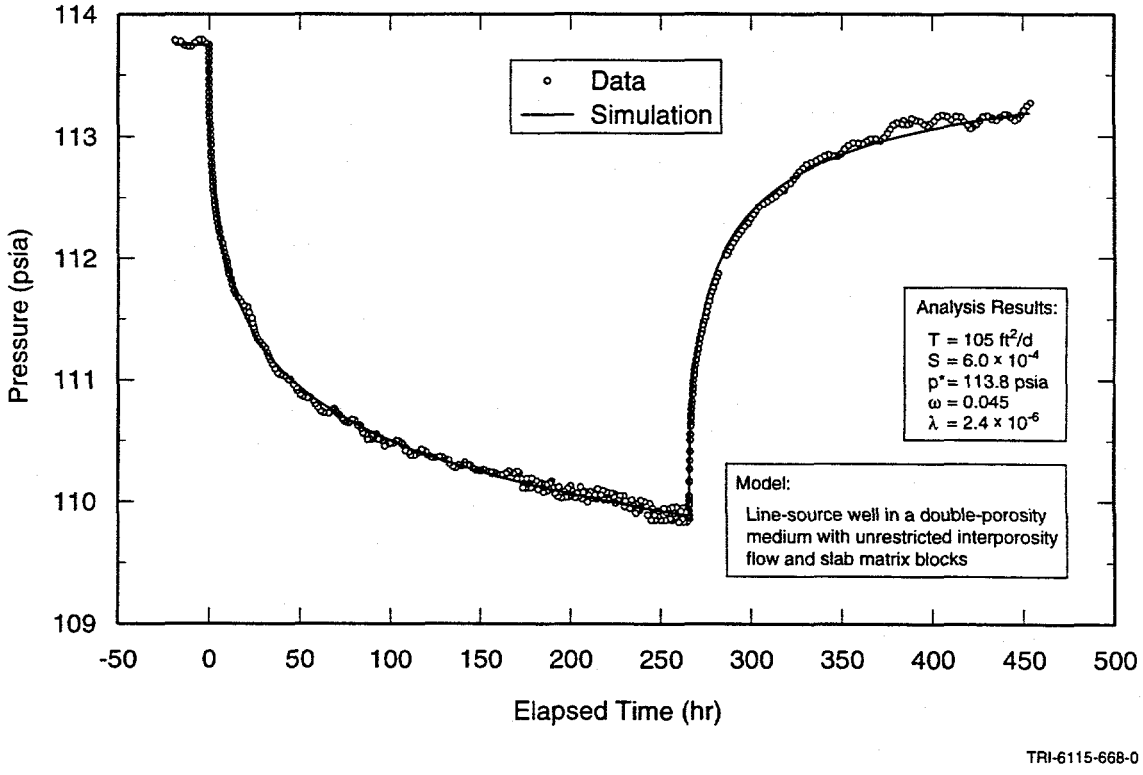

Figure A-36. Linear-linear plot of H-9a data from test #3 with Interpret/2 simulation derived from drawdown analysis.

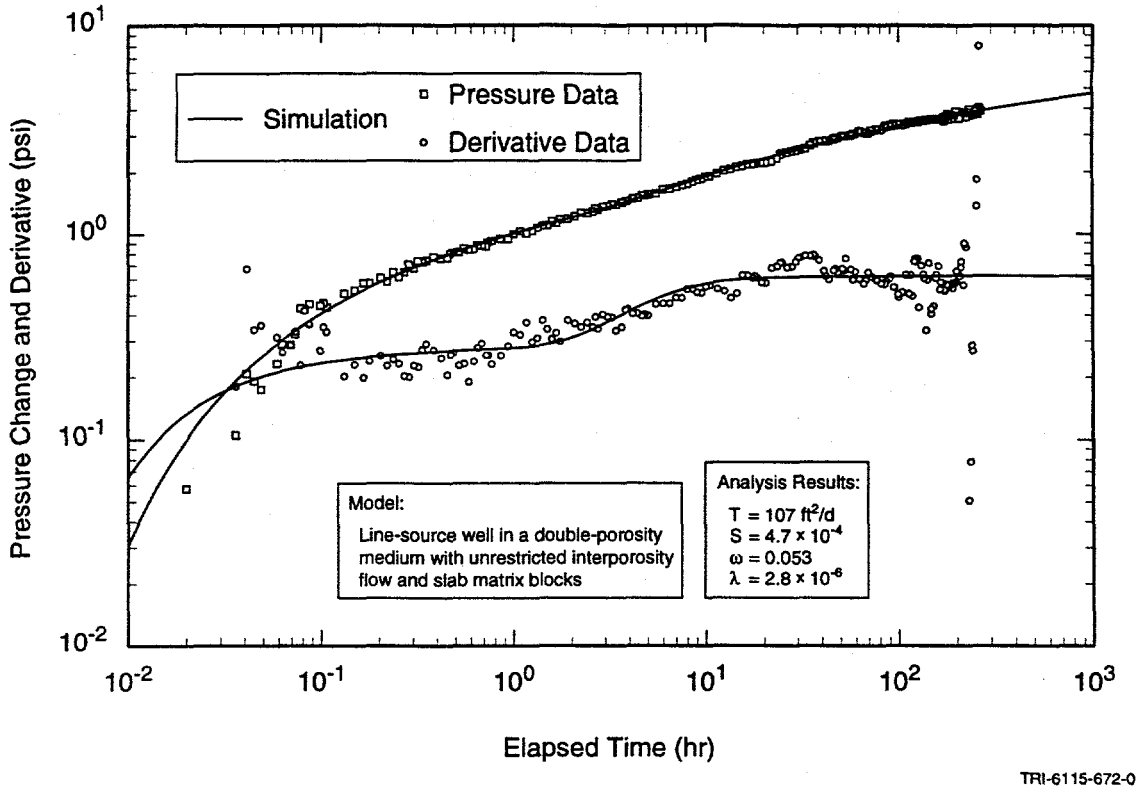

Figure A-37. Log-log plot of H-9b drawdown data from test #3 with Interpret/2 simulation.

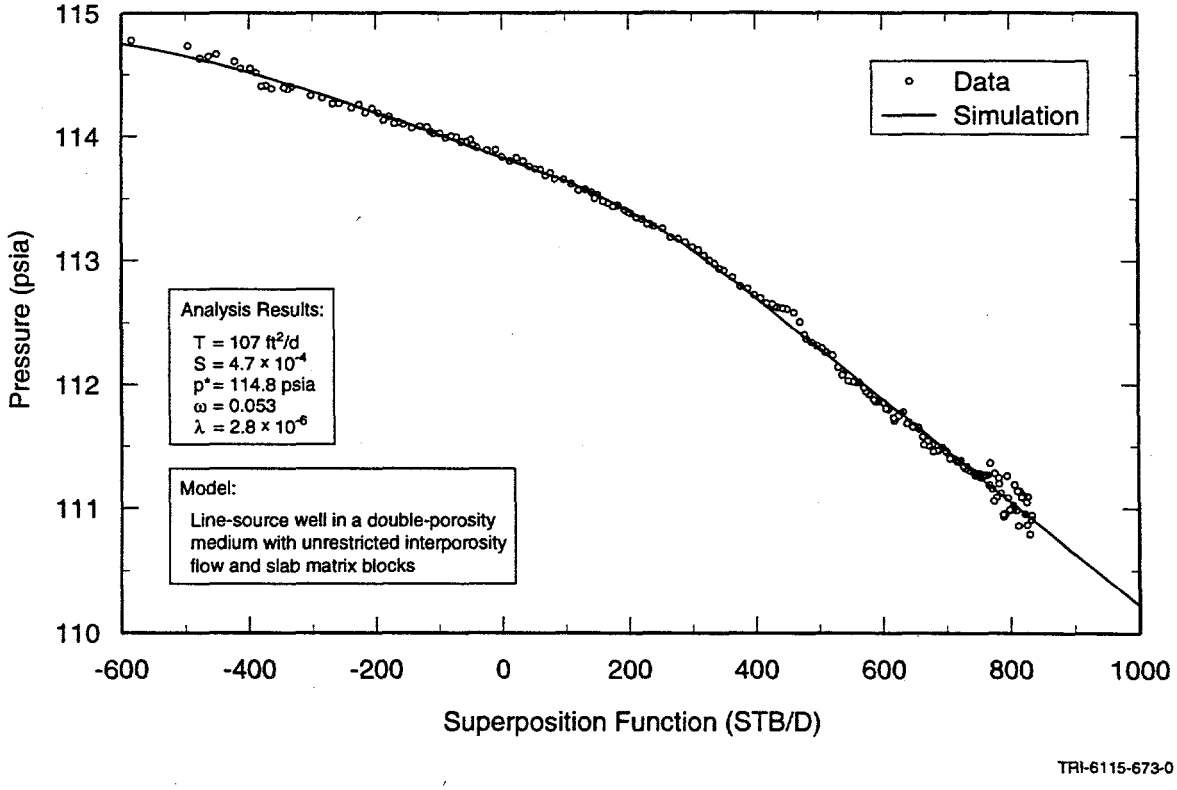

Figure A-38. Horner plot of H-9b drawdown data from test #3 with Interpret/2 simulation.

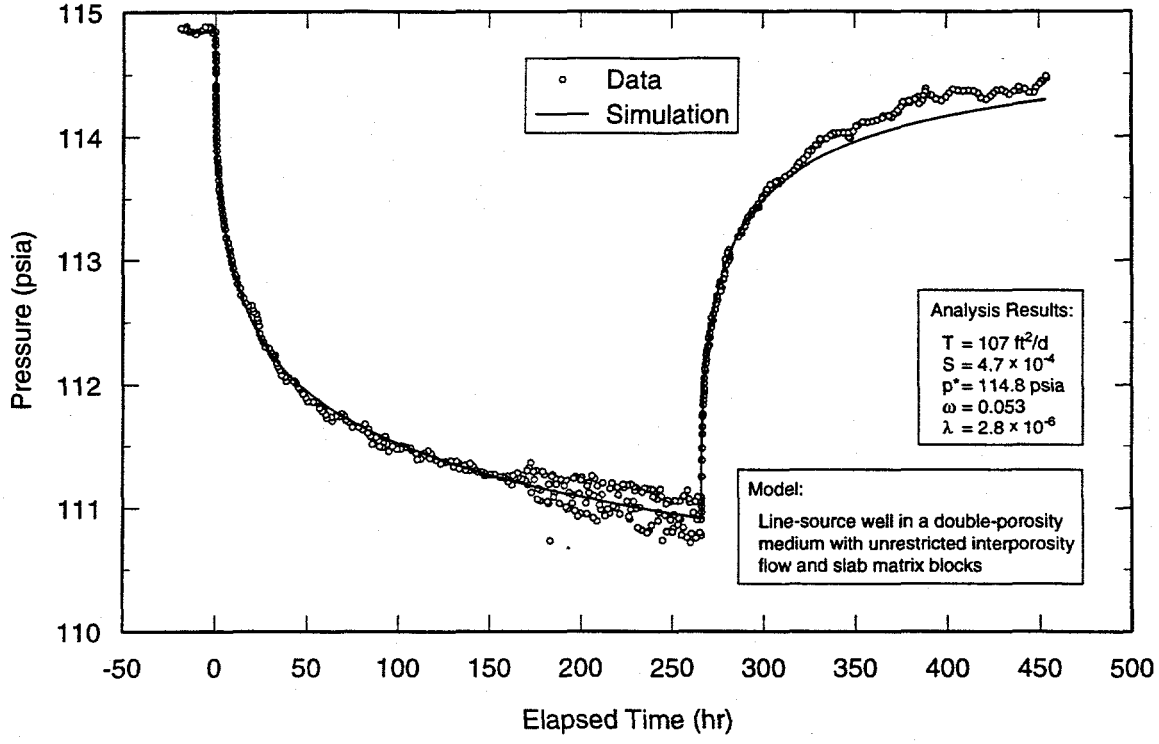

Figure A-39. Linear-linear plot of H-9b data from test #3 with Interpret/2 simulation derived from drawdown analysis.

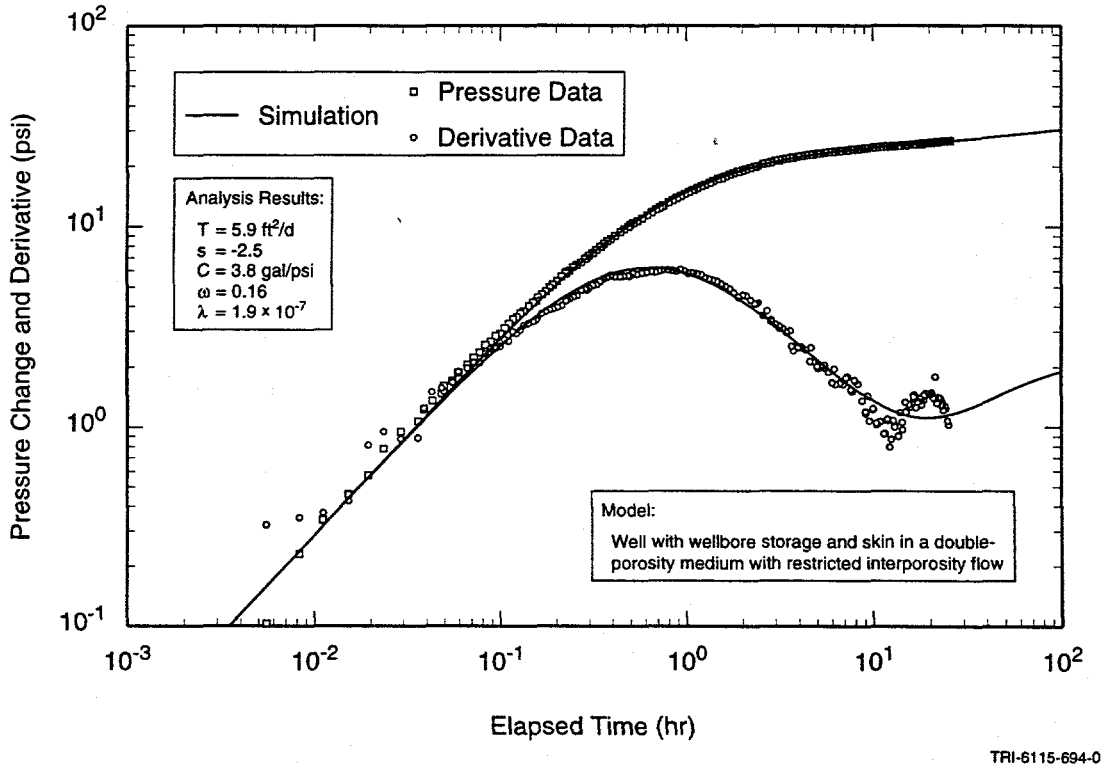

Figure A-40. Log-log plot of H-19b2 drawdown data from the second pumping period with Interpret/2 simulation.

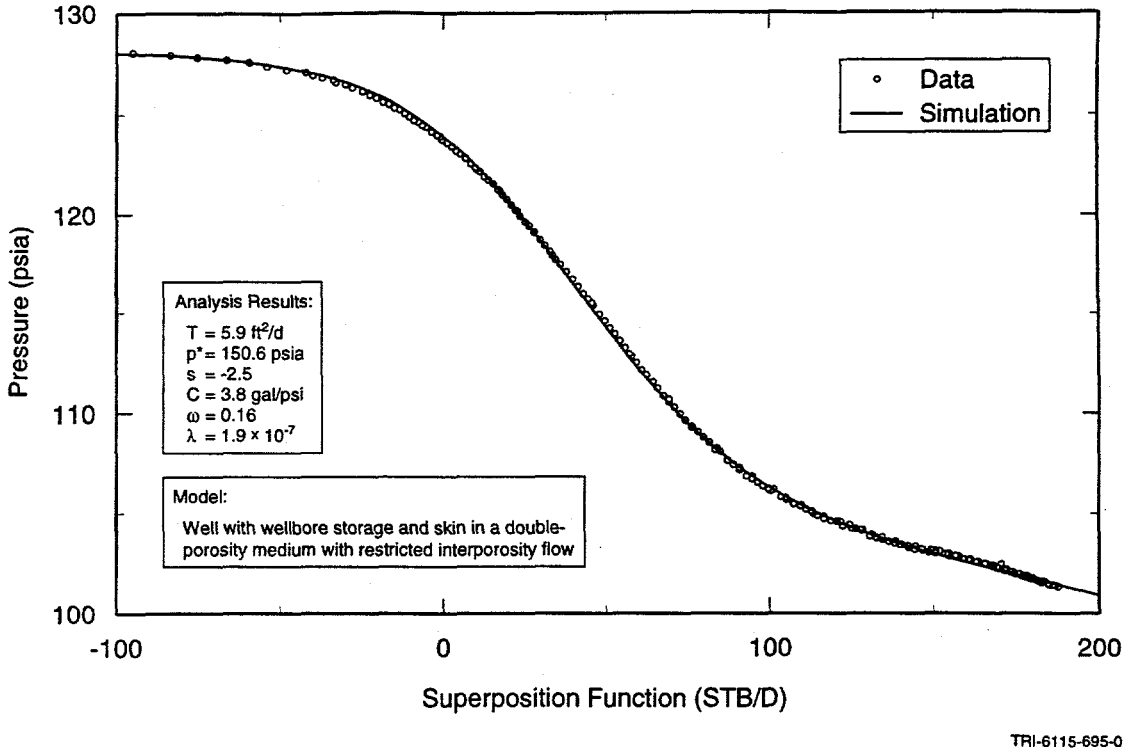

Figure A-41. Horner plot of H-19b2 drawdown data from the second pumping period with Interpret/2 simulation.

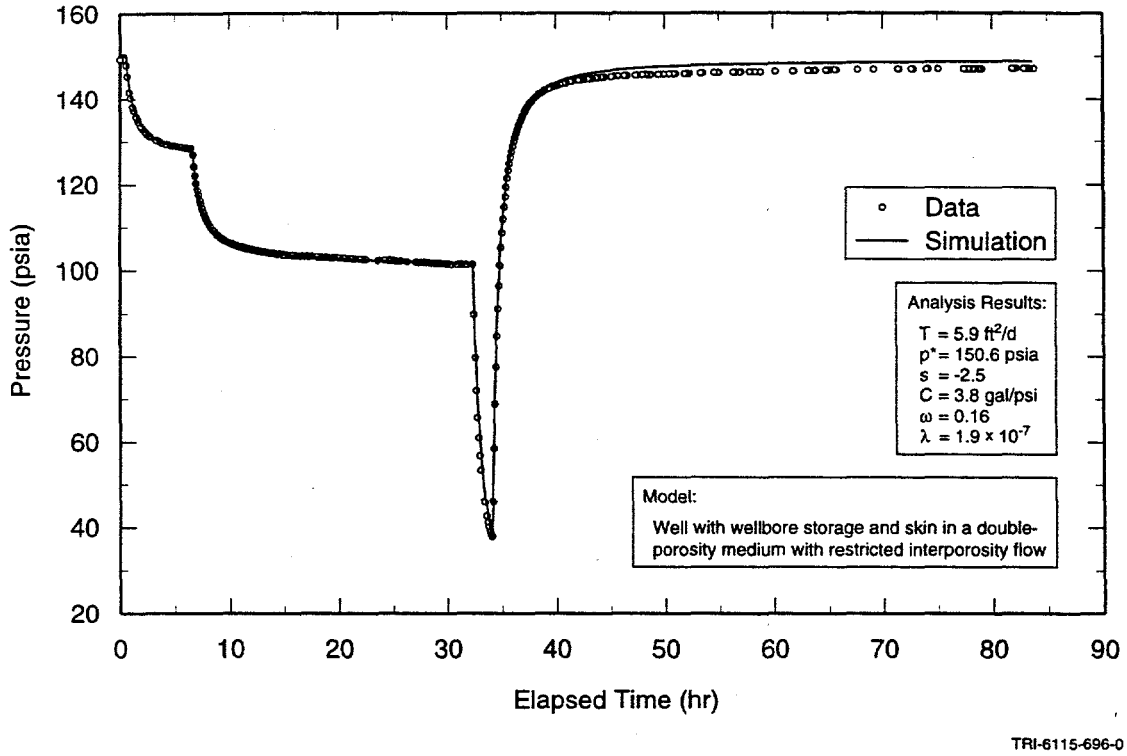

Figure A-42. Linear-linear plot of H-19b2 data with Interpret/2 simulation derived from analysis of drawdown data from the second pumping period.

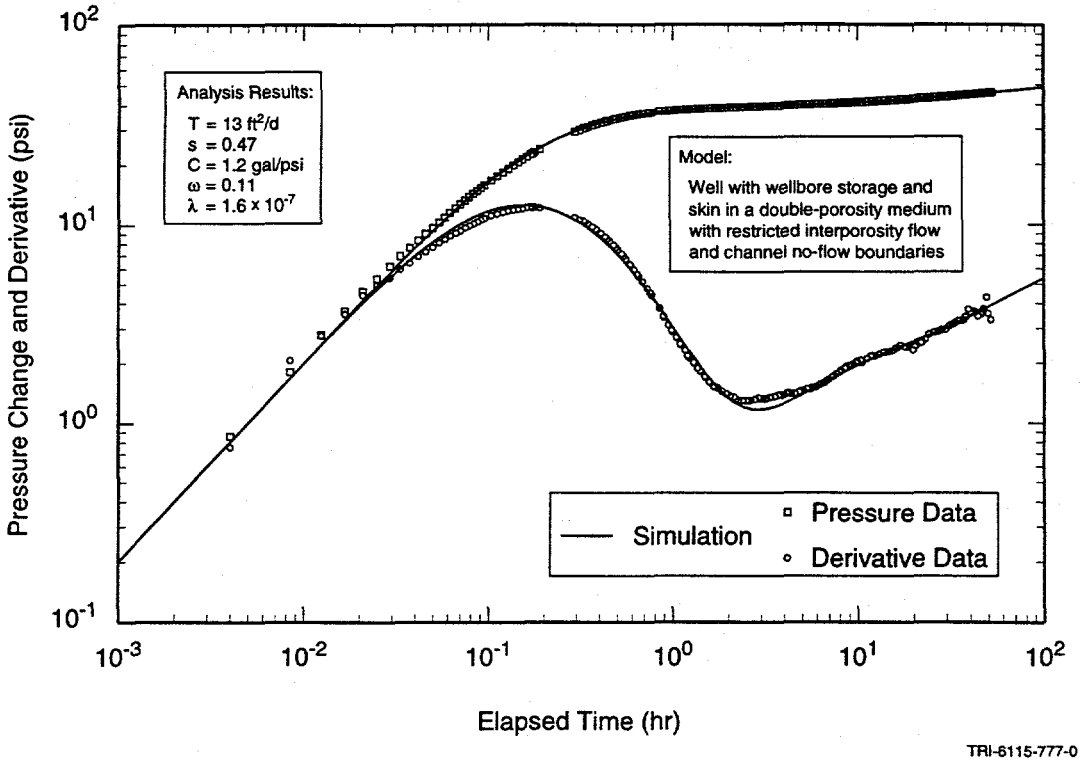

Figure A-43. Log-log plot of WQSP-4 drawdown data from the first pumping period with Interpret/2 simulation.

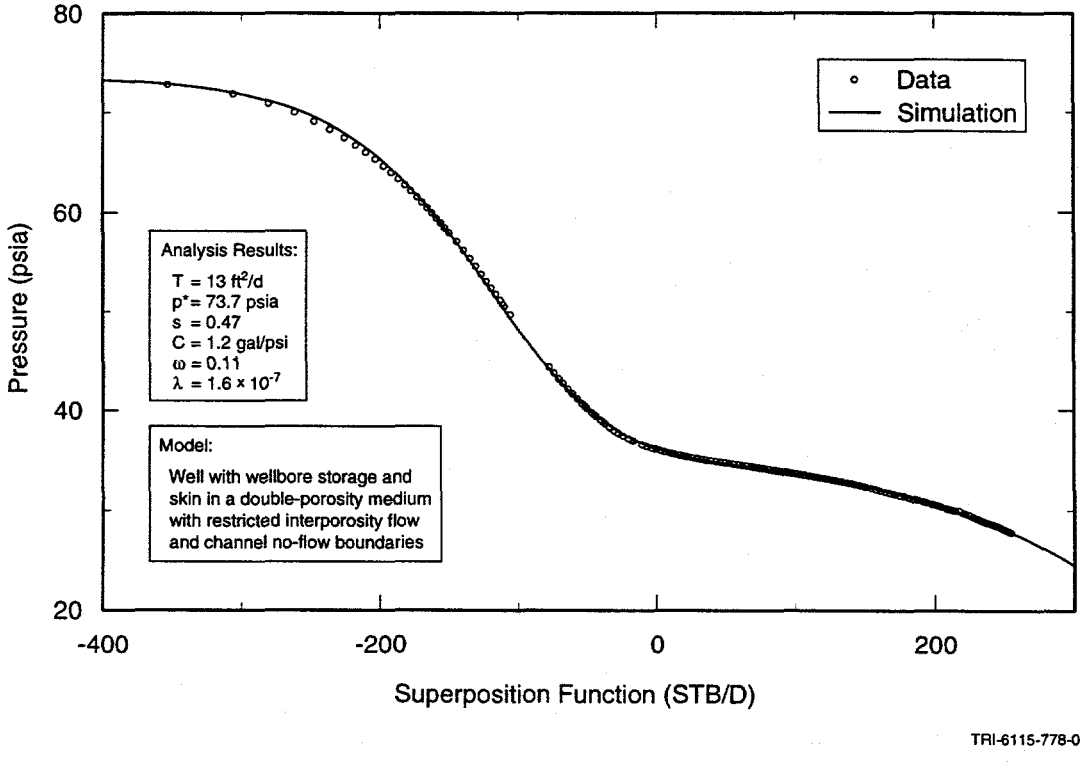

Figure A-44. Horner plot of WQSP-4 drawdown data from the first pumping period with Interpret/2 simulation.

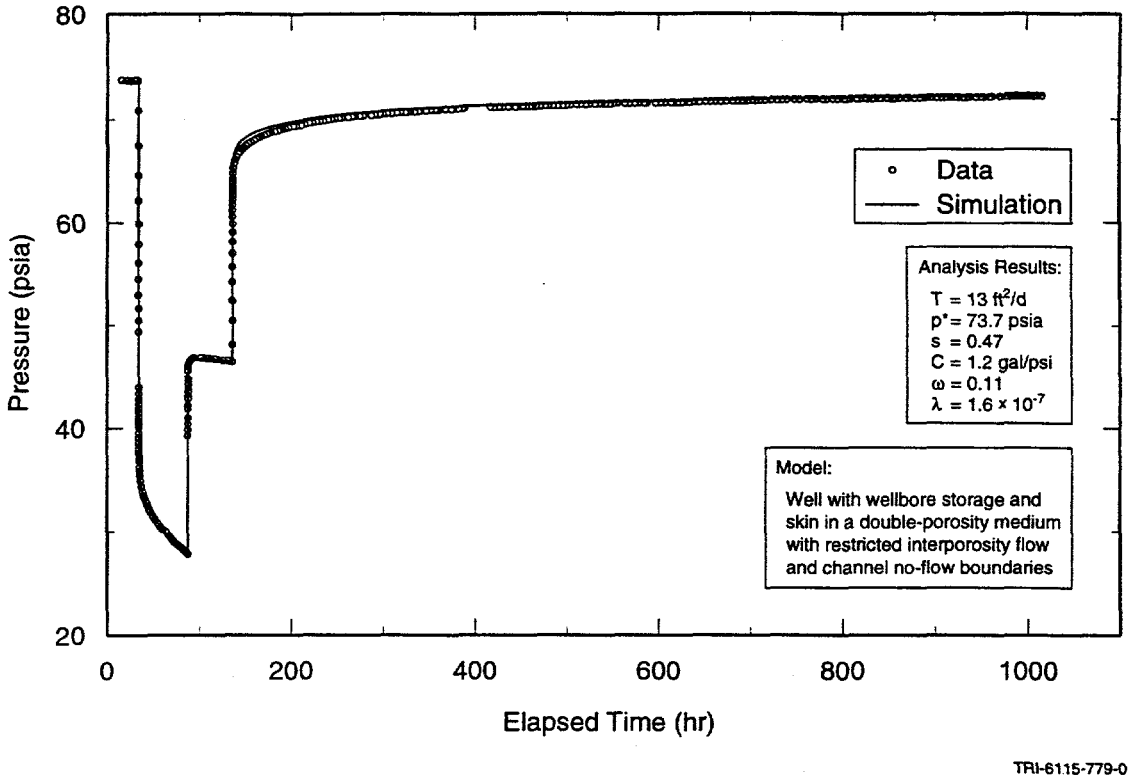

Figure A-45. Linear-linear plot of WQSP-4 data with Interpret/2 simulation derived from analysis of drawdown data from the first pumping period.

WIPP
UC721 - DISTRIBUTION LIST
SAND98-0049

Federal Agencies

US Department of Energy (4)
Office of Civilian Radioactive Waste Mgmt.
Attn: Deputy Director, RW-2
Acting Director, RW-10
Office of Human Resources & Admin.
Director, RW-30
Office of Program Mgmt. & Integ.
Director, RW-40
Office of Waste Accept., Stor., & Tran.
Forrestal Building
Washington, DC 20585

Yucca Mountain Site Characterization Office
Director, RW-3
Office of Quality Assurance
Attn: Project Director
P. O. Box 30307
North Las Vegas, NV 89036-0307

Yucca Mountain Site Characterization Office
Attn: L. E. Shephard
P.O. Box 30307
MS 523
North Las Vegas, NV 89036-0307

US Department of Energy
Research & Waste Management Division
Attn: Director
P.O. Box E
Oak Ridge, TN 37831

US Department of Energy (5)
Carlsbad Area Office
Attn: D. Galbraith
M. McFadden
R. Lark
J. A. Mewhinney
G. T. Basabilvazo
P.O. Box 3090
Carlsbad, NM 88221-3090

US Department of Energy
Office of Environmental Restoration and
Waste Management
Attn: M. Frei, EM-30
Forrestal Building
Washington, DC 20585-0002

US Department of Energy (3)
Office of Environmental Restoration and
Waste Management
Attn: J. Juri, EM-34, Trevion II
Washington, DC 20585-0002

US Department of Energy
Office of Environmental Restoration and
Waste Management
Attn: S. Schneider, EM-342, Trevion II
Washington, DC 20585-0002

US Department of Energy (2)
Office of Environment, Safety & Health
Attn: C. Borgstrom, EH-25
R. Pelletier, EH-231
Washington, DC 20585

US Department of Energy (2)
Idaho Operations Office
Fuel Processing & Waste Mgmt. Division
785 DOE Place
Idaho Falls, ID 83402

US Environmental Protection Agency (2)
Radiation Protection Programs
Attn: M. Oge
ANR-460
Washington, DC 20460

US Geological Survey
Water Resources Division
Attn: S. F. Richey
4501 Indian School Rd. NE, Suite 200
Albuquerque, NM 87110-3929

Boards

Defense Nuclear Facilities Safety Board
Attn: D. Winters
625 Indiana Ave. NW, Suite 700
Washington, DC 20004

Nuclear Waste Technical Review Board (2)
Attn: Chairman
J. L. Cohon
2300 Clarendon Blvd. Ste 1300
Arlington, VA 22201-3367

State Agencies

Attorney General of New Mexico
P.O. Drawer 1508
Santa Fe, NM 87504-1508

Environmental Evaluation Group (3)
Attn: Library
7007 Wyoming NE
Suite F-2
Albuquerque, NM 87109

NM Environment Department (3)
Secretary of the Environment
1190 St. Francis Drive
Santa Fe, NM 87503-0968

NM Bureau of Mines & Mineral Resources
Socorro, NM 87801

Laboratories/Corporations

Battelle Pacific Northwest Laboratories
Battelle Blvd.
Richland, WA 99352

Los Alamos National Laboratory
Attn: B. Erdal, INC-12
P.O. Box 1663
Los Alamos, NM 87544

Tech Reps, Inc. (3)
Attn: J. Chapman (1)
Loretta Robledo (2)
5000 Marble NE, Suite 222
Albuquerque, NM 87110

Westinghouse Electric Corporation (5)
Attn: Library
J. Epstein
J. Lee
R. Kehrman
R. G. Richardson
P.O. Box 2078
Carlsbad, NM 88221

S. Cohen & Associates
Attn: Bill Thurber
1355 Beverly Road
McLean, VA 22101

Golder Associates
Attn: T. W. Doe
4104 148th Avenue, NE
Redmond, WA 98052

Duke Engineering & Services, Inc. (9)
Attn: G. J. Ruskauff (5)
G. A. Freeze
D. A. Chace
P. S. Domski
R. M. Roberts
1650 University Blvd. NE. Suite 300
Albuquerque, NM 87102-1732

Duke Engineering and Services, Inc. (2)
Attn: J. F. Pickens
9111 Research Blvd.
Austin, TX 78758

Duke Engineering and Services, Inc.
Attn:. W. A. Stenrud
1012 W. Pierce, Suite A
Carlsbad, NM 88220

National Academy of Sciences
WIPP Panel

Tom Kiess (15)
Staff Study Director
GF456
2101 Constitution Ave.
Washington, DC 20418

Universities

University of New Mexico
Geology Department
Attn: Library
141 Northrop Hall
Albuquerque, NM 87131

University of Washington
College of Ocean & Fishery Sciences
Attn: G. R. Heath
583 Henderson Hall, HN-15
Seattle, WA 98195

New Mexico Tech
Department of Geoscience
Attn: J. Wilson
Socorro, NM 87801

Texas A&M University
Department of Geology
Attn: P. A. Domenico
College Station, TX 77843

University of Arizona
Department of Hydrology
Attn: S. P. Neuman
Tucson, AZ 85721

University of California
Lawrence Berkeley Laboratory
Earth Science Division
Attn: C. F. Tsang
1 Cyclotron Road
Berkeley, CA 94720

University of Kansas
Kansas Geological Survey
Attn: J. Butler
1930 Constant Ave.
Campus West
Lawrence, KS 66046

University of Wisconsin-Madison (2)
Department of Geology and Geophysics
Attn: M. P. Anderson
H. F. Wang
1215 Dayton St.
Madison, WI 53706

Libraries

Thomas Brannigan Library
Attn: D. Dresp
106 W. Hadley St.
Las Cruces, NM 88001

Government Publications Department
Zimmerman Library
University of New Mexico
Albuquerque, NM 87131

New Mexico Junior College
Pannell Library
Attn: R. Hill
Lovington Highway
Hobbs, NM 88240

New Mexico State Library
Attn: N. McCallan
325 Don Gaspar
Santa Fe, NM 87503

New Mexico Tech
Martin Speere Memorial Library
Campus Street
Socorro, NM 87810

WIPP Public Reading Room
Carlsbad Public Library
101 S. Halagueno St.
Carlsbad, NM 88220

Foreign Addresses

Atomic Energy of Canada, Ltd. (2)
Whiteshell Laboratories
Attn: B. Goodwin
C. C. Davison
Pinawa, Manitoba, R0E 1L0
CANADA

Environment Canada
National Water Research Institute
Canada Centre for Inland Waters
Attn: K. S. Novakowski
867 Lakeshore Road
P.O. Box 5050
Burlington, Ontario, L7R 4A6
CANADA

Francois Chenevier (2)
ANDRA
Parc de la Croix Blanche
1-7 rue Jean Monnet
92298 Chatenay-Malabry Cedex
FRANCE

Claude Sombret
Centre d'Etudes Nucleaires de la Vallee Rhone
CEN/VALRHO
S.D.H.A. B.P. 171
30205 Bagnols-Sur-Ceze
FRANCE

Commissariat a L'Energie Atomique
Attn: D. Alexandre
Centre d'Etudes de Cadarache
13108 Saint Paul Lez Durance Cedex
FRANCE

Bundesanstalt fur Geowissenschaften und
Rohstoffe (2)
Attn: M. Langer
K. Schelkes
Postfach 510 153
D-30631 Hannover
GERMANY

Bundesministerium fur Forschung und
Technologie
Postfach 200 706
5300 Bonn 2
GERMANY

WBI
Attn: W. Wittke
Henricistrasse 50
D-52072 Aachen
GERMANY

Institut fur Tieflagerung
Attn: K. Kuhn
Theodor-Heuss-Strasse 4
D-3300 Braunschweig
GERMANY

Gesellschaft fur Anlagen und Reaktorsicherheit
(GRS)
Attn: B. Baltes
Schwertnergasse 1
D-50667 Cologne
GERMANY

Shingo Tashiro
Japan Atomic Energy Research Institute
Tokai-Mura, Ibaraki-Ken, 319-11
JAPAN

Jaime Gomez-Hernandez
Dep. De Ingnieria Hidraulica y Mdio
Ambiente
Universidad Politenica de Valencia
46071 Valencia
SPAIN

Conterra AB
Attn: A. Winberg
Ogardesvagen 4
S-433 30 Partille
SWEDEN

GEOSIGMA AB
Attn:P. Anderson
P.O. Box 894
S-751 08 Uppsala
SWEDEN

Netherlands Energy Research Foundation ECN
Attn: J. Prij
3 Westerduinweg
P.O. Box 1
1755 ZG Petten
THE NETHERLANDS

Svensk Karnbransleforsorjning AB
Attn: F. Karlsson
Project KBS (Karnbranslesakerhet)
Box 5864
S-102 48 Stockholm
SWEDEN

Nationale Genossenschaft fur die Lagerung
Radioaktiver Abfalle (2)
Attn: S. Vomvoris
P. Zuidema
Hardstrasse 73
CH-5430 Wettingen
SWITZERLAND

AEA Technology
Attn: J. H. Rees
D5W/29 Culham Laboratory
Abington, Oxfordshire OX14 3DB
UNITED KINGDOM

AEA Technology
Attn: W. R. Rodwell
044/A31 Winfrith Technical Centre
Dorchester, Dorset DT2 8DH
UNITED KINGDOM

AEA Technology
Attn: J. E. Tinson
B4244 Harwell Laboratory
Didcot, Oxfordshire OX11 ORA
UNITED KINGDOM

Other

D. W. Powers
HC 12
Box 87
Anthony, TX 79821

Internal

MS	Org.	
0735	6115	P. B. Davies
0737	6831	E. J. Nowak
0737	6833	J. R. Tillerson
0779	6849	D. R. Anderson
0779	6848	H. N. Jow
0771	6800	M. Chu
0733	6832	J. T. Holmes
1395	6821	M. Marietta
0735	6115	R. L. Beauheim (5)
0735	6115	A. R. Lappin
0735	6115	L. C. Meigs
0735	6115	T. F. Corbet
0735	6115	R. M. Holt
0735	6115	S. J. Altman
0735	6115	S. A. McKenna
0735	6115	P.C. Reeves
0731	6811	K. Hart (2)
0731	4415	NWM Library (20)
9018	8940-2	Central Technical Files
0899	4916	Technical Library (2)
0619	12690	Review and Approval Desk, For DOE/OSTI (2)